The use of Precision Cut Lung Slices and Co-culture Modelling to Investigate the Effect of Human Rhinovirus on Cough and Airway Inflammation

Rebecca Jane Stinson

BSc (Hons) (Aberystwyth University)
MSc (Liverpool John Moores University)
PGCE (University of Hull)
Fellow of the Higher Education Academy

Thesis submitted for the Degree of Doctor of Philosophy (PhD)

The University of Hull and The University of York

Hull York Medical School

February 2020

Abstract

Human Rhinovirus (hRV) is a major cause of upper respiratory tract infections (URTIs) and is linked to lower respiratory tract infections (LRTIs) and airway diseases exacerbations. Cough, airway inflammation and hypersensation are common symptoms of hRV infections however, the mechanisms involved remain elusive. A promising hypothesis is neuromodulation, whereby stimulation of transient receptor potential channels (TRPV4) in airway epithelial cells release ATP, subsequently activating the purinoreceptor P2X3 on vagal afferent nerve fibres. Here it is hypothesised that hRV infection will alter expression of channels and receptors known to be involved in cough and airway inflammation, causing lung tissue to become hyperresponsive to cough and bronchoconstrictive agents.

A co-culture model of human airways using a lung epithelial cell line (A549 or Beas-2b) and astrocytes (1321N1 transfected with P2X3) to mimic neurones showed that activation of TRPV4 on lung epithelial cells led to ATP release which could evoke a measurable calcium influx into astrocytes. Additionally, A549 and Beas-2b cells responded differently to RV16 infection, with A549 cells exhibiting a reduced cytotoxicity, increased viability and proliferation compared to Beas-2b cells. Furthermore, RV16 infected *ex vivo* tissue showed limited impact on viability and cytotoxicity, reduced TEER measurements, increased bronchoconstriction and upregulated ICAM-1 protein expression. Finally, comparison of microfluidic devices to standard culture conditions demonstrated A549 cells could be cultured for 72 hours with similar rates of cell proliferation and viability, whilst PCLS could be cultured for 6 days with minimal impact on tissue viability or morphology.

Overall, findings suggest that the TRPV4–ATP–P2X3 neuromodulation theory may play a role in the mechanism of cough and supports observations indicating hRV causes URTIs more frequently than LRTIs. Furthermore, hRV infection of *ex vivo* tissue appears promising as a model that can replicate *in vivo* and *in vitro* observations. Whilst the microfluidic devices used to replicate elements of the aforementioned models provide a promising start to better recapitulating the *in vivo* environment.

Contents

List of Figures

List of Tables

Abbreviations

1N1 P2X3	1321N1 human brain astrocytoma cells transfected with a P2X3 receptor
1N1 WT	1321N1 human brain astrocytoma wild type cells
2D	Two dimensional
3D	Three dimensional
A549	A549 human lung epithelial cells
ACK	Ammonium-chloride-potassium
ALI	Air liquid interface
ANOVA	Analysis of variance
ATP	Adenosine triphosphate
Beas-2b	Beas-2b human bronchial epithelial cells
BCA	Bicinchoninic acid
BSA	Bovine serum albumin
CCD1	Cell culture device one
CCD2	Cell culture device two
CCD3	Cell culture device three
CCL17	Chemokine ligand 17
CDHR3	Human cadherin-related family member 3
cDNA	Complementary deoxyribonucleic acid
CF	Cystic fibrosis
CGRP	Calcitonin gene-related peptide
CNC	Computer numerical control
COPD	Chronic obstructive pulmonary disease
CO_2	Carbon dioxide
CTCF	Corrected total cell fluorescence
DEPC	Diethyl pyrocarbonate
dH_2O	Distilled water
DNA	Deoxyribonucleic acid
dNTP	Deoxyribonucleotide triphosphate
DMEM	Dulbecco's Modified Eagle Medium
DMSO	Dimethyl sulfoxide

dsRNA	Double stranded ribonucleic acid
DTT	Dithiothreitol
EC_{50}	Half maximal effective concentration
EDTA	Ethylenediaminetetraacetic acid
ENA-78	Epithelial-neutrophil activating peptide
ERS-2	Electrical resistance system 2
ETFE	Ethylene tetrafluoroethylene
FBS	Fetal bovine serum
GCSF	Granulocyte-colony stimulating factor
GM-CSF	Granulocyte-macrophage colony-stimulating factor
GPCR	G protein-coupled receptors
GRO	Growth-regulated oncogene
GRO-α	Growth-regulated oncogene alpha
GSK	GlaxoSmithKline
GSK101	GSK1016790a
H&E	Haematoxylin and eosin
H_2O_2	Hydrogen peroxide
HBSE	HEPES buffered saline with ethylenediaminetetraacetic acid
HBSS	Hank's balanced salt solution
HEPES	4-(2-hydroxyethyl)-1-piperazineethanesulfonic acid
HRP	Horseradish peroxidase
hRV	Human rhinovirus
hRV-A	Human rhinovirus species A
hRV-B	Human rhinovirus species B
hRV-C	Human rhinovirus species C
IC_{50}	Half maximal inhibitory concentration
ICAM-1	Intracellular adhesion molecule 1
ID	Internal diameter
IFN	Interferon
IGF-1	Insulin-like growth factor 1
IL	Interleukin
IL-1	Interleukin 1
IL-1α	Interleukin 1 alpha

IL-1β	Interleukin 1 beta
IL-2	Interleukin 2
IL-3	Interleukin 3
IL-4	Interleukin 4
IL-5	Interleukin 5
IL-6	Interleukin 6
IL-7	Interleukin 7
IL-8	Interleukin 8
IL-10	Interleukin 10
IL-12 p40/p70	Interleukin 12 homodimer p40/heterodimer p70
IL-13	Interleukin 13
IL-15	Interleukin 15
INT	Iodonitrotetrazolium
kbp	Kilobase pairs
KCl	Potassium chloride
kDa	Kilodalton
kHz	Kilohertz
LDH	Lactate dehydrogenase
LDLR	Low density lipoprotein receptors
LMP	Low melting point
LRTI	Lower respiratory tract infection
MBP	Major basic protein
MCh	Methacholine
MCP-1	Monocyte chemotactic protein 1
MCP-2	Monocyte chemotactic protein 2
MCP-3	Monocyte chemotactic protein 3
MCSF	Macrophage colony stimulating factor
MDC	Macrophage derived chemokine
MEM	Minimum essential medium
MDA-5	Myeloma differentiation antigen
$MgCl_2$	Magnesium chloride
MIG	Monokine induced by gamma interferon
MIP-1δ	Macrophage inflammatory protein 1 delta

MMP	Matrix metalloproteinase
MOI	Multiplicity of infection
mRNA	Messenger ribonucleic acid
Muc5AB	Mucin 5AB
Muc5AC	Mucin 5AC
NAD	Nicotinamide adenine dinucleotide
NADPH	Reduced nicotinamide adenine dinucleotide phosphate
NF-κB	Nuclear factor-kappa B
NHS	National Health Service
NKA	Neurokinin A
NKB	Neurokinin B
NLRX-1	Nod-like receptor X-1
NRT	No reverse transcriptase
OCT	Optimal cutting temperature compound
OD	Outer diameter
P2R	Purinergic P2 receptors
P2X3	Purinergic receptor 3
P2XR	Purinergic P2X receptors
P2YR	Purinergic G protein-coupled receptors
PBS	Phosphate buffered saline
PC	Polycarbonate
PCLS	Precision cut lung slices
PCR	Polymerase chain reaction
PDGF BB	Platelet derived growth factor BB
PDMS	Poly(dimethylsiloxane)
PEEK	Polyether ether ketone
PET	Polyethylene terephthalate
PFA	Paraformaldehyde
pfu	Plaque forming units
PGD_2	Prostaglandin D_2
PGE_2	Prostaglandin E_2
PI	Propidium iodide
PKR	Protein kinase R

PMMA	Poly(methylmethacrylate)
PMS	Phenazine methosulfate
PMSF	Phenylmethylsulfonyl fluoride
PRR	Pattern recognition receptors
PTFE	Polytetrafluoroethylene
PVDF	Polyvinylidene difluoride
qPCR	Quantitative real time polymerase chain reaction
RANTES	Regulated upon activation normal T cell expressed and secreted
RAR	Rapidly adapting receptors
RFU	Relative fluorescence units
RIG- I	Retinoic acid-inducible agent I
RNA	Ribonucleic acid
rpm	Revolutions per minute
ROS	Reactive oxygen species
RT-PCR	Reverse transcriptase polymer chain reaction
RV	Rhinovirus
RV16	Rhinovirus serotype 16
RV39	Rhinovirus serotype 39
SAR	Slowly adapting receptors
SCF	Stem cell factor
SDF-1	Stromal cell-derived factor 1
SEM	Standard error of the mean
SRB	Sulforhodamine B
ssRNA	Single stranded RNA
TAE	Tris-acetate-EDTA
TARC	Thymus and activation regulation cytokine
TBS	Tris-buffered saline
TBS-T	Tris-buffered saline with tween
TCA	Trichloroacetic acid
$TCID_{50}$	Median tissue culture infectious dose
TEER	Transepithelial electrical resistance
TEMED	Tetramethylethylenediamine
TGF-β1	Transforming growth factor beta 1

TLR3	Toll-like receptor 3
TNF-α	Tumour necrosis factor alpha
TNF-β	Tumour necrosis factor beta
TRP	Transient receptor potential
TRPA1	Transient receptor potential cation channel subfamily A (Ankyrin) member 1
TRPV1	Transient receptor potential cation channel subfamily V (Vanilloid) member 1
TRPV4	Transient receptor potential cation channel subfamily V member 4
TRPM8	Transient receptor potential cation channel subfamily M (Melastatin) member 8
URTI	Upper respiratory tract infection
UV	Ultraviolet
VEGF	Vascular endothelial growth factor
WST-1	Water soluble tetrazolium salt
ZO-1	Zona occludins 1

Thesis Associated Conference Abstracts

Stinson R.J., Morice A. H. and Sadofsky L. R. (2017). The use of co-culture to model the human airway *in vitro*. Poster session presented at: Allam Conference 2017, Hull.

Stinson R.J., Morice A. H. and Sadofsky L. R. (2018) Precision cut lung slices (PCLS): an alternative to *in vitro* modelling of the small airways. Poster session presented at: Allam Conference 2018, Hull.

Stinson R.J., Morice A. H. and Sadofsky L. R. (2018) Precision cut lung slices (PCLS): an alternative to *in vitro* modelling of the small airways. Poster session presented at: HYMS Conference 2018, Hull.

Stinson R.J., Morice A. H. and Sadofsky L. R. (2018) Precision cut lung slices (PCLS): an alternative to *in vitro* modelling of the small airways. Poster session presented at: British Association of Lung Research (BALR), Birmingham.

Stinson R.J., Morice A. H. and Sadofsky L. R. (2018) Calcium Signalling in Co-culture Models: a Promising Method for Modelling Cell-to-Cell Interactions in Acute and Chronic Cough. Oral presentation session presented at: British Thoracic Society (BTS), London. *Thorax*. **74** (supplement 4).

Stinson R.J., Morice A. H. and Sadofsky L. R. (2019) Calcium Signalling in Co-culture Models: a Promising Method for Modelling Cell-to-Cell Interactions in Acute and Chronic Cough. Oral presentation session presented at: Allam Conference 2019, Hull.

Acknowledgements

It is with great pleasure that I have the opportunity to thank so many individuals for their part in enabling me to achieve a lifelong dream of gaining a PhD. Firstly I would like to thank my supervisory team; Dr Laura Sadofsky, Professor Alyn Morice and Professor Nicole Pamme, for your guidance, words of wisdom, moments of inspiration and positivity towards my project even when I felt it was floundering. Special thanks go to Laura for providing me with such an amazing opportunity, for being my voice of reason and for our rambling conversations about the kids which have given much light relief when every experiment seemed to be failing. Thank you for believing in me.

I would also like to thank everyone else who has made even the smallest contribution along the way, the list is too extensive to name everyone. Extra thanks go to the Castle Hill Hospital Cardiothoracic team, especially Rob Bennett, Enosh Siraj and the numerous surgeons and nurses who have helped me to arrange and collect the tissue samples I required for my work. Special thanks go to the Daisy Lab members, particularly Respiratory Medicine who have provided immense support throughout this journey. To the Greenman and Hardman labs, thanks for your guidance on tissue work, microfluidics and the borrowing of much equipment along the way. To the technical staff thanks for answering all the random questions and always knowing just were the stuff I cannot find is located. To the microfluidic and chemical engineering teams, thank you for producing my microfluidic devices and helping make them work. To the CAM team, thank you for helping me settle into campus life so late in my research and helping my last few months run smoothly. Most importantly, thank you to the tissue donors who's generosity have made much of this research possible.

To my friends old and new, thank you for your understanding and patience. To Joanne and Kristina, my lifelong friends, thank you for being my normality when my PhD journey was driving me crazy. To Andy, Holly and Hayley, thank you for sharing this journey with me, your advice and random chats have brightened even the dullest of days. To Sam, I am forever in your debt, you made my last few months not only bearable but fun. I would never

have achieved quite as much as I did without your lab expertise, I cannot express my thanks enough. To Frankie, I am so pleased we got to experience the highs and lows of this journey together, it has been amazing and I look forward to many more years of friendship.

To my family, thank you for supporting me through this journey, dealing with the highs and lows in the only way you can, through sarcasm and laughter. To my sister Rachel, I am sorry I have been rather absent over the last three years, for which I apologise, I will visit more now I have finished. To my mum and dad, I could not have done this without you. You have always believed in my ability to achieve and facilitated it in whichever way you can. Thank you for your supportive comments even when you admitted you have no idea what I am talking about. Thank you for always being there to do the school run, bedtimes and late evening cover when I have not been able to. Thank you for your unconditional love and support, I could not have done it without you.

Finally, my thanks go to Chris and George. To Chris thank you for always being there, for listening to my ideas, for keeping me calm and for your help in funding my dream. Your support has been immeasurable and you have always believed in me even when I have not believed in myself. To George, so wise for one so young, thank you for trying to understand why I have been so busy and for dealing with missed weekends and evening with such maturity. Thank you for your never ending love and huggies, you have and always will brightened my every moment. I hope I have made you proud and have given you the desire and aspirations to achieve your dreams. I love you both more than words can express and I could not have done this without you.

So it is with great pleasure that I dedicate this thesis to my husband and son,

Chris and George.

Declaration

I confirm that this work is original and that if any passage(s) or diagram(s) have been copied from academic papers, books, the internet or any other sources these are clearly identified by the use of quotation marks and the reference(s) is fully cited. I certify that, other than where indicated, this is my own work and does not breach the regulations of HYMS, the University of Hull or the University of York regarding plagiarism or academic conduct in examinations. I have read the HYMS Code of Practice on Academic Misconduct, and state that this piece of work is my own and does not contain any unacknowledged work from any other sources.

1 Chapter 1: General Introduction

1.1 Human Rhinovirus

1.1.1 Discovery of Human Rhinovirus

Human rhinovirus (hRV) was initially isolated and identified in 1956 by two separate studies (Price, 1956; Pelon *et al*, 1957), being named JH by Price (1956) and GL 2060, then later ECHO 28 by Pelon *et al*, (1957; 1961). Both laboratories had identified a human respiratory virus which exhibited similar characteristics and whilst initially thought to have differing antigenic compositions, these differences were later attributed to varying serotypes (Gwaltney and Jordan 1964). Subsequent isolation of a number of differing serotypes led to the viruses isolated from common cold sufferers to be given a varied range of names due to subtle differences in characteristics. The resulting complexities led to intervention from "the Virus Subcommittee of the International Committee on the Nomenclature of Bacteria and Viruses" to enable clarification and classification of all viral isolates from the common cold to be named rhinovirus (Tyrrell and Chanock, 1963). The basic virology of hRV is now widely understood, with the virus classified as a member of the family *Picornaviridae* and the genus *Enterovirus*. hRV is a positive-sense, single stranded RNA (ssRNA) virus with a genome comprised of approximately 7.2kbp (Jacobs *et al*, 2013). Three species and over 100 serotypes of hRV have been identified, the species hRV-A comprises of 74 serotypes, hRV-B contains 25 serotypes and the more recently identified hRV-C consists of approximately 50 serotypes, with classification based on genomic similarities (Jacobs *et al*, 2013; Aponte *et al*, 2015) (Figure 1.1). Prevalence of hRV fluctuates throughout the year, with highest case numbers observed during the early stages of spring and autumn months (Fendrick *et al*, 2003).

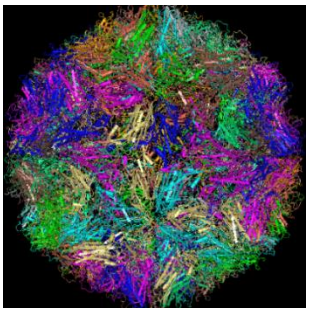
A.

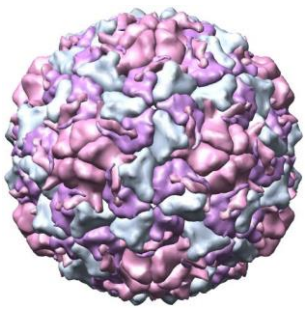
B.

Figure 1.1 Representative images of human Rhinovirus 16 showing protein coat structure at high resolution from NCBI's Molecular Modelling Database (NCBI MMDB, 2007) (**A**) and RCSB's Protein Data Bank (RCSB PDB, 2011) (**B**) (images adapted from Hadfield *et al*, 1997)

1.1.2 Epidemiology of Human Rhinovirus

hRV is responsible for a significant proportion of worldwide common cold infections and acute respiratory illnesses annually (Abdullah *et al*, 2013; Aponte *et al*, 2015), accounting for approximately 50% of all upper respiratory tract infections (URTIs) (Lee *et al*, 2012). Most adults under the age of 65 will suffer with 2 – 4 infections of hRV per annum (Nichol *et* al, 2005), whilst children experience 3 – 8 infections per year (Bertino, 2002) (Figure 1.2). Although the number of infections can be higher for individuals in regular close proximity to others such as those in schools, universities and nursery settings (Bertino, 2002; Nichol *et* al, 2005). hRV has long been recognised for its significant morbidity levels and thus the impact this has on lost productivity, work and school days and healthcare related costs (Fendrick *et al*, 2003; Nichol *et al*, 2005). However, the self-limiting nature and relatively short duration, median 7.4 days, of infection (Fendrick *et al*, 2003) originally classified hRV as a mild illness and minor pathogen (Tyrrell, 1965; Aponte *et al*, 2015).

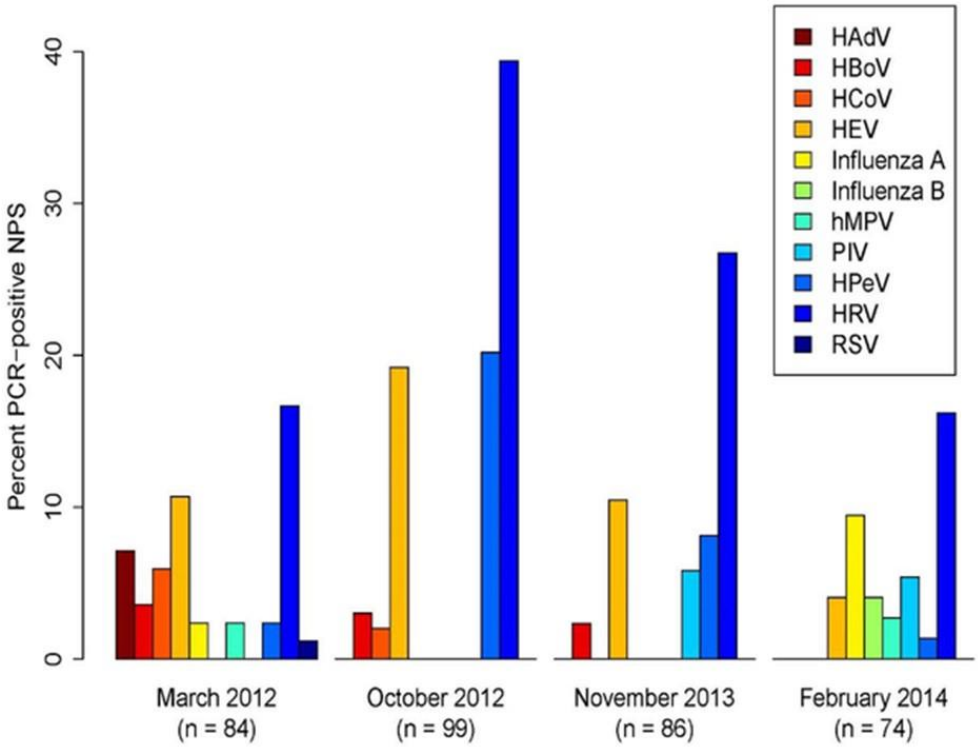

Figure 1.2 Variation in percentage of respiratory viruses detected in nasopharyngeal samples of children aged 1 to 6 years, during four separate visits to two day care facilities in Norway (image adapted from Moe *et al*, 2016).

Subsequent identification of hRV as a cause of lower respiratory tract infection (LRTIs) with the potential to hospitalise an individual with pre-existing respiratory illnesses has resulted in the recognition of hRV as a major pathogen in respiratory diseases (Papadopoulos and Johnston, 2000; Aponte *et al*, 2015). Furthermore, consideration of the importance of hRV in terms of its economic burden by Fendrick *et al* (2003) also recognised the significance of hRV as a major pathogen in mortality of the under-five population in developing countries where respiratory infections are the main cause of death. hRV has also been linked to exacerbations of pre-existing respiratory illnesses such as chronic obstructive pulmonary disease (COPD) (Figure 1.3), otitis media, chronic bronchitis, sinusitis, bronchiolitis in young children and fatal pneumonia in immunocompromised and elderly individuals (Griego *et al*, 2000; Jacobs *et al*, 2013). With around 40% of chronic bronchitis exacerbations (Zhu *et al*, 1996), up to 25% of COPD exacerbations (Kurai *et al*, 2013) and approximately 16% of bronchiolitis exacerbations (Mansbach and Carmargo, 2009) being accredited to hRV. hRV is also responsible for an estimated 50 – 80% of asthma exacerbations in adults and children (Yamaya *et al*, 1999; Griego *et al*, 2000; Message *et al*, 2008). Furthermore, the severity of the asthma exacerbations are influenced by the presence of hRV, with 40% of severe and 80% of mild attacks being linked to hRV infections (Ghildyal *et al*, 2005). Interestingly, hRV infections in early life has also been linked to an increased likelihood of developing asthma by school age, particularly in those with a pre-existing genetic risk (Rowe and Gill, 2015).

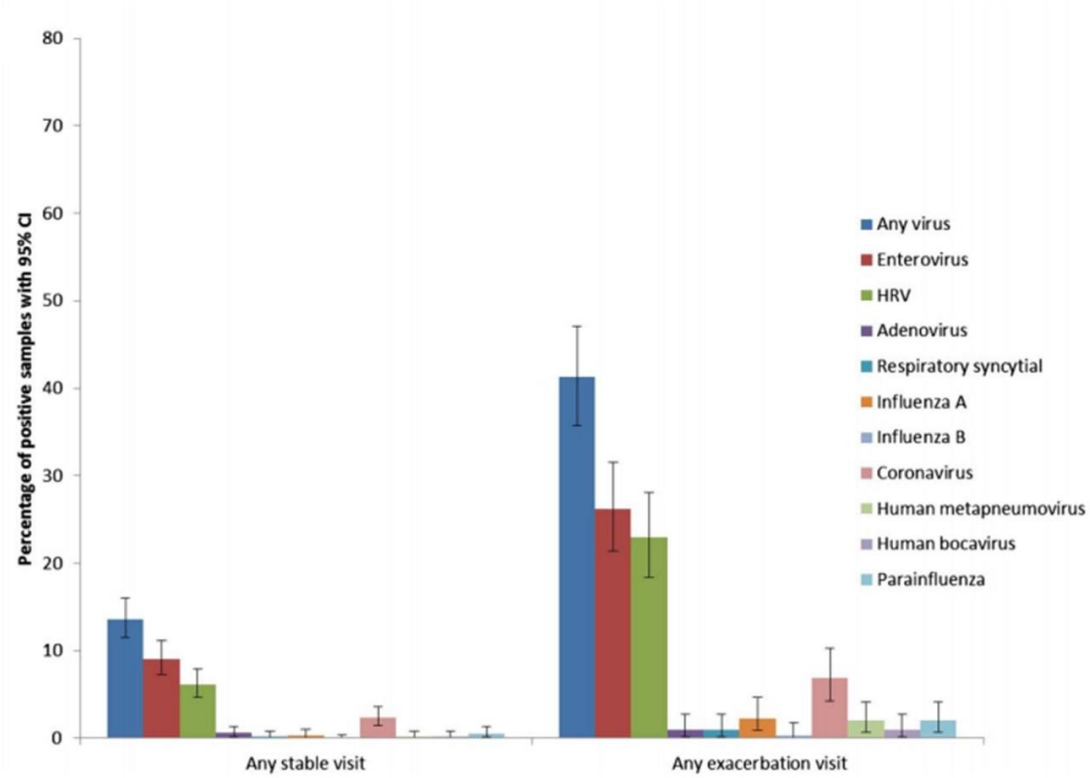

Figure 1.3 Percentage of sputum samples tested positive for various viruses during stable and exacerbations of COPD over a one year period (image adapted from Wilkinson *et al*, 2017).

1.1.3 Chronic Respiratory Disease Exacerbations due to Human Rhinovirus

The mechanisms that lead to exacerbation of asthma and other chronic lung diseases are not fully understood, particularly the hypersensitivity that occurs due to hRV infection (Abdullah *et al*, 2013), in part this incomplete understanding is due to the lack of suitable animal models which can be used to study different aspects of hRV pathogenesis (Newcomb *et al*, 2008). However, there is a likelihood that in those individuals with a pre-existing respiratory condition, such as COPD or asthma, the innate antiviral immune response is inadequate, making infection more likely and exacerbations more frequent (del Vecchio *et al*, 2015). Additionally, the potential co-infection with multiple respiratory pathogens appears to increase severity of these exacerbations and may factor in the level of hypersensitivity experienced (Aponte *et al*, 2015). Furthermore, the manifestation of more severe symptoms are apparent in LRTIs of hRV, as such these exacerbations could be a product of direct infection of the lower respiratory tract or equally a result of transmission of a URTI and a consequence of the cellular effect of the infection (Papadopoulos *et al*,

2000). Conversely, Newcomb *et* al, (2008) have suggested that lower respiratory tract inflammation may be a result of events that occur prior to viral replication, such as internalisation and attachment of the virus to respiratory epithelial cells, which elicit inflammatory responses, as opposed to a direct infection of the lower respiratory tract. Alternatively, the manifestation of more severe symptoms in asthmatics could be a direct consequence of the viral load in the epithelial cells of the respiratory tract. Epithelial cells of the primary bronchi have demonstrated an ability to replicate hRV more efficiently *in vitro* in cells taken from an asthmatic than those taken from a non-asthmatic. From these findings, it can be hypothesised that as the viral load increases, the extent of inflammation induced through infection also increases and symptoms become more severe (Message *et al*, 2008). On the contrary, *in vivo* studies of viral load in healthy individuals and those with asthma, under controlled conditions for infection and symptom observation, demonstrated that viral load in all individuals is similar and thus has limited impact on asthma exacerbation but does affect the inflammation response in general (Hammond *et al*, 2015). Given the extent of chronic respiratory disease exacerbations linked to hRV infection and the potential loss of work/school days and impact on healthcare provision, there is a need to enhance the understanding of the mechanisms, which are involved in the cough and airway inflammation response to this infection. Thus providing an opportunity to develop targeted therapy, which could be utilised to resolve the symptoms experienced in airway exacerbations due to hRV infection.

1.1.4 Human Rhinovirus Transmission

In healthy individuals the epithelial cells of the respiratory tract are the primary site for hRV infection (Griego *et al*, 2000), with the nasal mucosa also serving as another potential early infection site (Zhu *et al*, 1996; Ghildyal *et al*, 2005). Both infection sites are indicative of the mechanisms of transmission utilised by hRV, which includes direct contact, fomite contact and aerosol, thus nasal mucosa and airway epithelial cell colonisation ensures transmission between individuals is rapid and efficient (Jacobs *et al*, 2013). The production of excess mucus secretions and significant levels of inflammation in the nasal passages and lower airways are symptomatic of the majority of hRV infections, the increased production results in irritation and subsequently the more outwardly noticeable symptoms of cough and sneeze. These symptoms serve multiple purposes including prevention of aspiration in the

case of the cough (Eccles, 2005) and the onward transmission of the virus through both nasal and airway secretions (Dick *et al*, 1987). Additional cell types have also been identified as subsequent sites of infection with hRV, after primary infection of epithelial cells has occurred, secondary infection of these additional cell types, further increase the extent of inflammation and mucus production in the nasal passages and airways. The submucosal glands of the nasal passages can also be infected with hRV, given that these cells contain more goblet cells than the epithelial cells which line the airways, it is likely that infection of these cells will result in over secretion of mucus and the excessive production of nasal discharge (Yamaya *et al*, 1999). Whilst, fibroblast cells from human airways experimentally infected with hRV *in vitro*, subsequently produced inflammatory mediators, which may further contribute to the inflammatory response of the mucosal membranes (Ghildyal *et al*, 2005). Infection of the aforementioned cells culminates in the range of symptoms typically observed during hRV episodes, with mucus production resulting in sneeze, cough and nasal discharge and inflammation being responsible for symptoms including nasal congestion, watery eyes, cough and sinus pain (Eccles, 2005).

1.1.5 Human Rhinovirus Serotypes

In order for hRV to successfully infect a cell, the serotype of the virus must be considered as this factor determines the cellular receptors utilised by the virus to adhere and infiltrate the cell (Jacobs *et al*, 2013). Major group hRV serotypes (90% of hRV-A and hRV-B serotypes) use the receptor intracellular adhesion molecule – 1 (ICAM-1) to bind to the cell surface (Tomassini *et al*, 1989). Whilst, minor group hRV serotypes (10% of hRV-A and hRV-B serotypes) utilise low density lipoprotein receptors (LDLR) to adhere to the cell surface (Hofer *et al*, 1994) and hRV-C bind via human cadherin-related family member 3 (CDHR3) (Bochkov *et al*, 2015) (Figure 1.4).

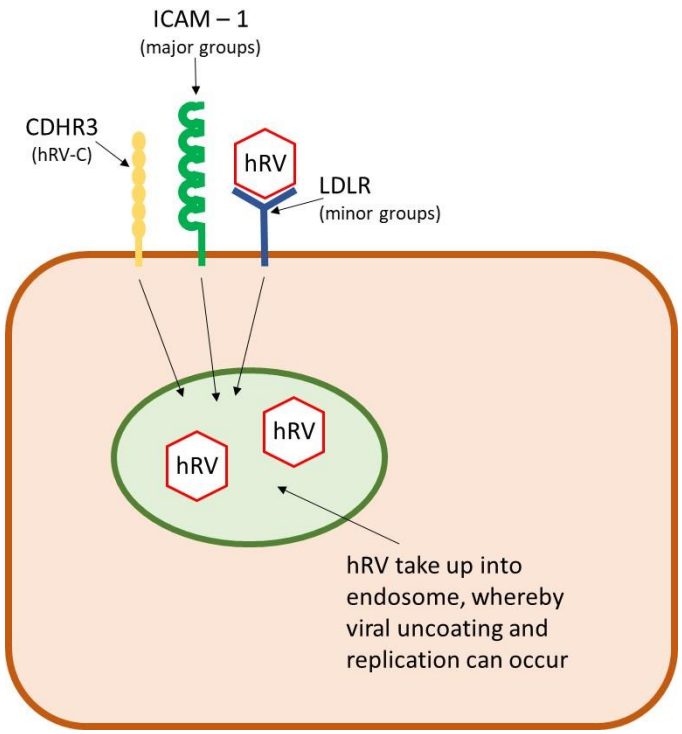

Figure 1.4 Binding of hRV to cell membrane receptors via three receptors. Major group serotypes bind to ICAM-1, minor group serotypes bind to LDLR and hRV-C serotypes bind to CDHR3. Once adhered to the host cell, hRV can infiltrate the cell via the use of endosome whereby viral uncoating and replication can commence (adapted from Jacobs *et al*, 2013).

The use of these specific cell receptors has made the study of hRV more problematic as they are absent from many animal models (Royston and Tapparel, 2016). ICAM-1 receptors used by hRV are found only in humans and chimpanzees, whilst LDLR are found in mice and humans. Given that only 10% of hRV serotypes belong in the minor group, the usefulness of murine models in hRV research are relatively limited (del Vecchio *et al*, 2015). Furthermore, hRV and other respiratory pathogens do not readily infect other animals, due to the high level of species specificity (del Vecchio *et al*, 2015) which has resulted in studies being predominately conducted *in vitro* via human cell culturing (Royston and Tapparel, 2016) or *in vivo* through the experimental infection of human volunteers (del Vecchio *et al*, 2015). Both methods have inherent problems insofar as *in vitro* methods can produce exaggerated effects when compared to *in vivo* measurements (Hammond *et al*, 2015). Whilst the management of experimentally infected individuals needs to be carefully controlled to remove the variables which can occur, such as the time from the onset of symptoms to the point of contact with healthcare provision, when natural and randomised

observations of the population are made (del Vecchio *et al*, 2015; Hammond *et al*, 2015). Whilst the aforementioned issues around *in vitro* and *in vivo* modelling applies to all hRV serotypes, hRV-C creates additional issues in terms of the study of this virus, insofar as hRV-C does not utilise the ICAM-1 and LDLR receptor for cell adherence. Binding of hRV-C to the host cell instead occurs via human cadherin-related family member 3 (CDHR3) (Bochkov *et al*, 2015). A variation which has prevented standard cell culture techniques being utilised for their identification and further study as this receptor is only expressed in differentiated airway epithelial cells, cultured at an air-liquid interface (ALI) (Bochkov and Gern, 2016).

1.1.6 Pathogenesis of Human Rhinovirus

As opposed to many other viruses, once cell adhesion and infection by hRV has occurred the extent of cellular damage observed is minimal (Griego *et al*, 2000). This means that the pathogenesis of hRV infections are a result of the host cell inflammatory response rather than the cytotoxic effect of the cell damage caused by the virus (Ghildyal *et al*, 2005). One of the most common symptoms of hRV infections caused by the pathogenesis of the virus is a cough. Subacute coughs lasting less than three weeks are typical of those observed in individuals suffering from hRV infections (Corne and Holgate, 1997) however, in some individuals a post infectious cough can last up to eight weeks before resolution of the symptoms occurs (Braman, 2006). Whilst in a smaller percentage of individuals, estimated at approximately 9 – 33% of the population (Spina and Page, 2013) the cough can become chronic and last significantly longer than eight weeks (Braman, 2006). However, the precise mechanism that elicits the cough response is still unclear. Thus, multiple potential causes of cough and associated airway inflammation have been proposed in an attempt to find the elusive mechanism(s), which cause this symptom in hRV infections (Atkinson *et al*, 2016). Involuntary cough reflex is mediated by vagal afferent nerves (Irwin *et al*, 2006), specifically non-myelinated bronchial C-fibres and myelinated rapidly adapting receptors (RAR) or Aδ-fibres (Morice *et al*, 2001), with slowly adapting receptors (SAR) hypothesised to be indirectly involved in the overall reflex mechanism (Grace *et al*, 2013). Furthermore, the efferent function of C-fibres is the release of tachykinins family members, neurokinin A (NKA), B (NKB) and substance P, which act on neurokinin receptors resulting in RAR stimulation, thus enhancing the cough reflex activation (El-Hashim and Amine, 2005). Tachykinins play a role in smooth muscle contraction and vasodilation, as such symptoms

exhibited in hRV infections could be attributed to the effects of these neuropeptides. In additional to potential bronchoconstriction, NKA and substance P are also thought to cause mucus secretion and increased vascular permeability (Joos *et al,* 1994), which eventually lead to localised oedema (Holzer, 1998) and stimulation of RAR due to this increased permeability (Bonham *et al*, 1996). C-fibres and RAR are also responsible for other airway reflexes including variations in breathing pattern, bronchoconstriction and mucus secretion (Bonham *et al*, 1996). The role of neuromodulation in airway inflammation is further supported through an increase in the reactivity in nerve fibres of asthmatics, chronic bronchitis and the elderly, which corresponds to the hyperresponsiveness observed in these individuals when exposed to respiratory infections such as hRV (Joos *et al*, 1994).

1.1.7 Airway Inflammation through Human Rhinovirus Infection

1.1.7.1 Innervation

Hypersensation of the airways due to innervation is linked to the upregulation of transient receptor potential (TRP) ion channels on sensory nerves. This includes the expression of TRP subfamily Vanilloid (V) member 1 (TRPV1), TRP member A1 (TRPA1) (Spina and Page, 2013), plus potential expression of TRP Melastatin 8 (TRPM8) and TRP subfamily V member 4 (TRPV4) in individuals with chronic pulmonary obstructive disease (COPD) and cystic fibrosis (CF) (Grace *et al* 2013). TRP ion channels are stimulated by various substances including bradykinins, reactive oxygen species (ROS), calcitonin gene-related peptide (CGRP), G protein-coupled receptors (GPCR) and tachykinins (Atkinson *et al*, 2016; Viana, 2016) (Figure 1.5). Although, not proven the role of TRP ion channels in hypersensitivity is hypothesised to be achieved through alteration in cellular response. Evidence for this hypothesis is derived from TRP ion channels acting as nociceptors on cellular membranes, hence changes in responsiveness result in receptors becoming hypersensitive leading to over activity, as seen in chronic cough patients' response to temperature changes (Morice, 2010).

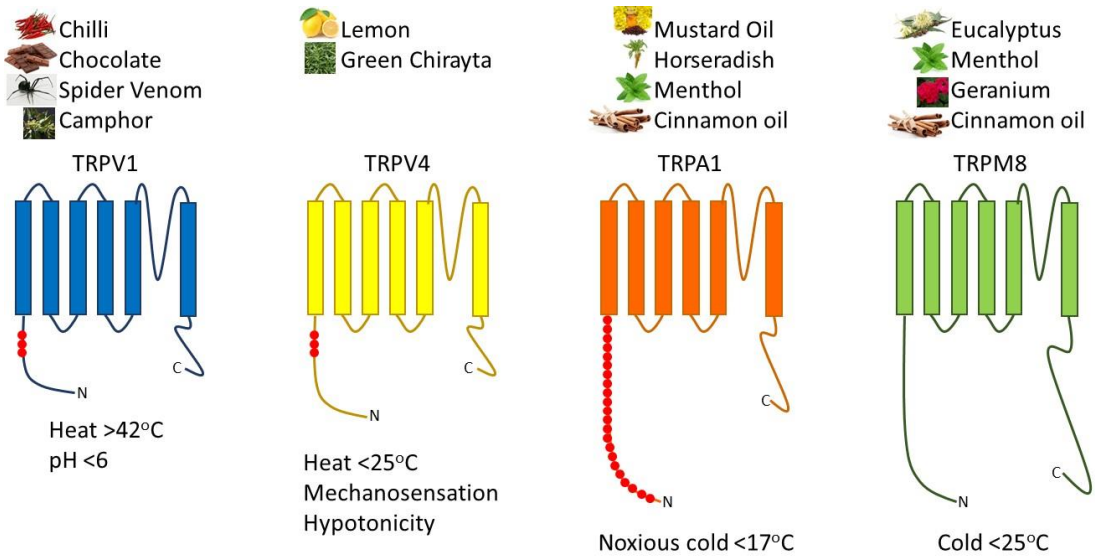

Figure 1.5 Structural representation of the various TRP channels involved in cough and airway inflammation. Common chemical stimuli shown above each TRP channel and other physical or mechanical stimuli shown below, whilst stimuli are specific to individual channels the activation of any channel leads to the release of ATP into the extracellular space (adapted from Blackshaw *et al*, 2010 and Belvisi *et al*, 2011).

Alternative receptors to TRP ion channels have also been identified as possible activators of cough reflex, namely the P2 purinergic receptors (P2R) on cell surfaces. Two families of P2R exist, known as P2XR or trans-cell membrane cationic channels and P2YR or trans-membrane domain G protein-coupled receptors, both of which play a role in the mediation of adenosine triphosphate (ATP) (Pelleg *et al*, 2016) (Figure 1.6).

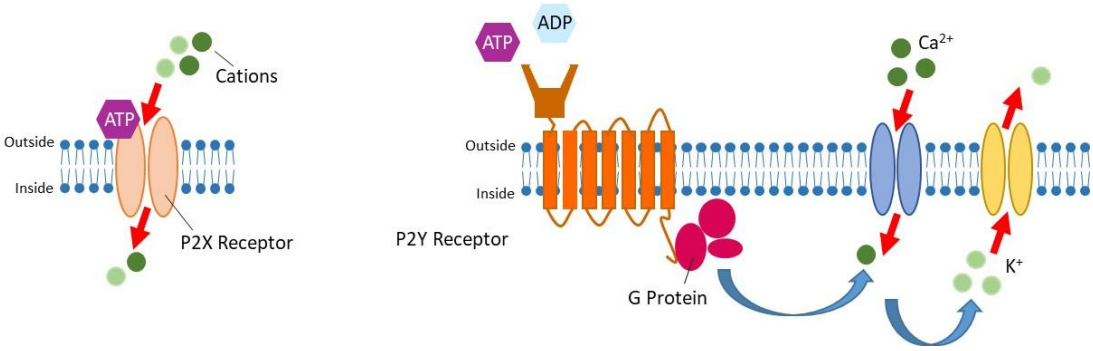

Figure 1.7 Structural representation of P2X and P2Y receptors identified as possible activators of cough reflex via stimulation with ATP (adapted from Franco-Bocanegra *et al*, 2019).

Specifically, the activation of P2X receptor by ATP stimulates C-fibres resulting in the initiation of the cough reflex (Kamei *et al*, 2005) and a marked increase in the level of bronchoconstriction (Pelleg *et al*, 2016). This mechanism results in the activation of P2X receptors, specifically P2X2 and P2X3, as a consequence of interactions between TRPV4 and P2X receptors, whereby TRPV4 releases ATP from the airway that subsequently stimulates P2X receptors and later Aδ-fibres resulting in bronchospasm and activation of cough reflex. However, ATP can elicit similar effects without activation of TRPV4 channels (Bonvini *et al*, 2016). The production of cytosolic ATP through cellular damage from high levels of the reactive oxygen species H_2O_2 in the airways (Lin *et al*, 2013; Taylor-Clark, 2016) and ATP production through airway cells including macrophages and epithelial cells, subsequently results in the independent activation of Aδ-fibres and C-fibres, causing bronchospasm and cough (Bonvini *et al*, 2016). There are marked differences between the management of extracellular ATP in healthy individuals and those with chronic pulmonary diseases, which may further explain the extent of inflammation observed within the small airways. The metabolism of extracellular ATP in healthy individuals is rapid and dependent on the use of ectoenzymes however, in asthmatics a decrease in the level of available ectoenzymes results in a reduction in the rate of ATP metabolism. This increased extracellular level is linked to sustained recruitment of neutrophils and macrophages, leading to the subsequent inflammation of the airways through the aforementioned pathway (Pelleg *et al*, 2016).

1.1.7.2 Bradykinins and CGRP

In addition to ATP the release of the proinflammatory mediator bradykinins is linked to bronchoconstriction, hyperresponsiveness in bronchi and plasma leakage, additionally this mediator also acts as a potent tussive agent and can indirectly stimulate TRPV1, thus further enhancing the cough reflex (de Oliveira *et al*, 2016). Whilst the role of CGRP is less clear, this sensory neuropeptide has been indicated as a bronchoconstrictive agent due to the chemoattractant properties toward immune cells, which subsequently results in an inflammatory effect (Le *et al*, 2014). CGRP has no direct effect on mucus secretion or plasma leakage (Dakhama *et al*, 2002), although this effect can occur due to the synergistic relationship between CGRP and other inflammatory mediators (Bonner *et al*, 2013). However, the colocalisation with substance P has been attributed to a bronchoprotective

effect, whereby CGRP inhibits the effects of substance P, reducing the extent of bronchoconstriction observed (Cadieux *et al*, 1999; Dakhama *et al*, 2002). Conversely, in individuals with existing airway diseases there is an upregulation of CGRP within the afferent nerves containing this neuropeptide (Groneberg *et al*, 2002). In asthmatics, this upregulation has been attributed to thymus and activation-regulated chemokine CCL17, which acts as a potent mediator to increase the dilatory effect of CGRP and thus plays a role in the pathogenesis of asthma and hyperresponsiveness of the airways (Bonner *et al*, 2013).

1.1.7.3 Reactive Oxygen Species

Reactive oxygen species (ROS) such as H_2O_2 can be generated due to oxidative stress as a result of the pathophysiological response to hRV infections, these affect different aspects of cellular defence mechanisms, including the activation of TRPA1 receptors (Andersson *et al*, 2008) and the destabilisation of epithelial tight junctions (Comstock *et al*, 2011). Generation of ROS is not a direct result of viral attachment or replication but is rather related to the extent of oxidative stress within cells (Kaul *et al*, 2000). However, whilst ROS can affect some aspects of cellular defence mechanisms it serves an important purpose in the innate immune system for destroying invading microorganisms (Comstock *et al*, 2011). Moreover, ROS has a role beyond interactions with TRP receptors in the mediation of airway inflammation, in the form of the disruption of the epithelial tight junctions (Comstock *et al*, 2011). hRV replication generates ROS through the electron transfer chain and reduced nicotinamide adenine dinucleotide phosphate (NADPH) oxidative enzyme in response to oxidative stress (Sajjan *et al*, 2008). The effectiveness of ROS is complemented by the generation of the replication intermediate double stranded ribonucleic acid (dsRNA), which has a similar mechanism to ROS in regards to barrier disruption. ROS and dsRNA aid in the disruption of epithelial barrier function through the induction of pattern recognition receptors (PRR) on airway epithelial cells. These include protein kinase R (PKR), Toll-like receptor 3 (TLR3), Nod-like receptor X-1 (NLRX-1), retinoic acid-inducible agent I (RIG-I) and myeloma differentiation antigen 5 (MDA-5) (Unger *et al*, 2014). Activation of PRR stimulates cytokine and chemokine production which results in airway inflammation and prolonged permeability in the mucosal membrane due to tight junction disassembly

(Rezaee *et al*, 2011), through the disruption of zona occludins 1 (ZO-1) and occludins within the membrane (Georas and Rezaee, 2014) (Figure 1.7).

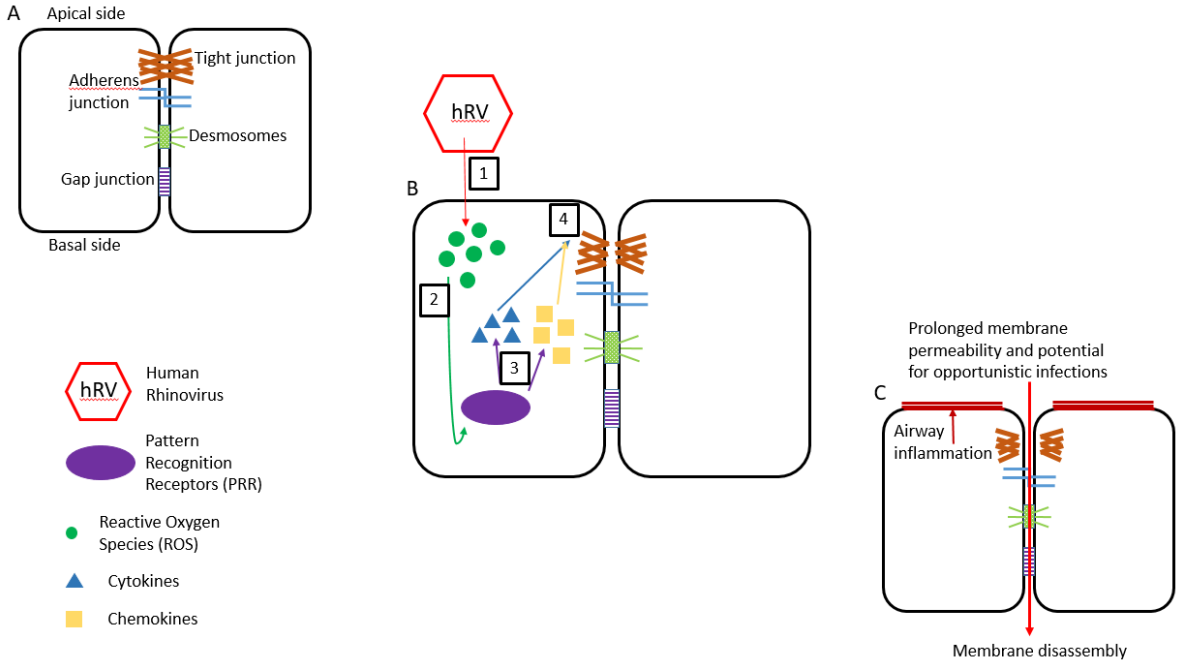

Figure 1.7 Healthy airway epithelial cells connected through tight junction, adherens junction, desmosomes and gap junction to create a barrier between inhaled particles and the blood stream (**A**). During hRV infection there is an upregulation of ROS generation (1), resulting in the activation of PRR within the cell (2) and the subsequent stimulation of cytokine and chemokine production (3), which disrupt tight junction assembly (4) (**B**). Leading to prolonged membrane permeability, increased potential for opportunistic infections and airway inflammation (**C**) (adapted from Atkinson *et al*, 2016).

Given that, epithelial cells lining the airway in healthy individuals create a barrier between inhaled particles and the blood stream, creating an effective part of the innate immune system, any disruption to this barrier has the potential to reduce efficiency of the immune system. There is increasing evidence in individuals with existing respiratory conditions that barrier function is disrupted (Rezaee *et al*, 2011), which may explain the severity of respiratory infections in these individuals. Furthermore, hRV may increase bacterial cell adhesion to and invasion of the epithelial airway cells, due to the aforementioned permeability, upregulation of ICAM-1 expression, reduced mucociliary clearance and

promotion of bacterial transmigration through the membrane. Thus enhancing the likelihood of coinfection with bacterial pathogens, particularly in individuals with existing respiratory diseases (Sajjan *et al*, 2008).

1.1.7.4 Cytokines and Mucin

The role of other proinflammatory mediators should not be underestimated in the pathophysiological effects of hRV infections. Proinflammatory cytokine and chemokine release due to hRV include interleukin (IL)-1, IL-6, IL-8, tumour necrosis factor (TNF)-α, interferon (IFN), granulocyte-macrophage colony-stimulating factor (GM-CSF) and RANTES (Griego *et al*, 2000). hRV infections result in the proliferation of cytokines, which appear to be dose dependent, with severity of infection increasing the extent of cytokines released (Kaul *et al,* 2000). Furthermore, the proliferation of cytokines is controlled by positive feedback mechanisms, through which the release of cytokine IL-8 results in oxidative stress and subsequent activation of nuclear factor-kappa B (NF-κB), which promotes expression of proinflammatory genes and upregulates further cytokine release (Bosco *et al*, 2016). Upregulation of NF-κB during hRV infection is implicated in the activation of various mucin genes (Shin *et al*, 2014). Muc5AC and Muc5AB are the two mucin genes responsible for increased mucus production in response to infection (Hewson *et al*, 2010). Whilst, mucus production is beneficial at the correct levels, excessive production can result in obstruction of the airways and increased inflammation, which can lead to exacerbations of symptoms in those individuals with existing respiratory conditions (Inoue *et al*, 2006; Zhu *et al*, 2009). Upregulation of cytokine expression results in the migration of leukocytes, specifically neutrophils, to the site of infection which, results in increased vascular permeability and subsequent leakage leading to the manifestation of hRV symptoms (Ghildyal *et al*, 2005). However, in individuals with existing airway diseases there is a dysregulation of some proinflammatory cytokines (Message *et al*, 2008; Jacobs *et al*, 2013). Which may add further credence to why these individuals have a reduced immune response to hRV infections and are subsequently at an increased risk of secondary infection (Stöckl *et al*, 1999).

1.1.7.5 Leukocytes

Further mediators in airway inflammation include leukotrienes, due to the potent effect on smooth muscle and vascular leakage these substances have been identified as potential bronchoconstrictive agents in airway inflammation (Hammarström, 1983). Furthermore, leukotrienes have also been identified in the recruitment of inflammatory cells, increased mucus secretion (Tamimi *et al*, 2012), airway oedema and bronchial hyperresponsiveness as a result of hRV infection. Leukotrienes are generated in response to hRV binding to ICAM-1 receptors and the upregulation of the synthesis of inflammatory mediators by leukocyte activity due to hRV infection (Seymour *et al*, 2002). However, leukocyte activity is not limited to leukotriene production, but are instead multifunctional. Eosinophils provide such an example of a leukocyte that plays a role beyond leukotriene production and includes the synthesis of several cytokines, which can be stored by the eosinophils ready for rapid activation, growth factors, chemokines and major basic protein (MBP) (Ravin and Loy, 2016). The release of these mediators is thought to be cytotoxic and thus responsible for some of the airway damage experienced in some chronic respiratory diseases, as levels of expression are markedly higher in these individuals (Pégorier *et al,* 2006) however, the role eosinophils play in healthy individual's airway inflammation during hRV infection is less clear (Atkinson *et al*, 2016). Conversely, neutrophil activity is also recognised as having an anti-inflammatory effect in hRV infections, through the release of prostaglandins and transforming growth factor (TGF)-β1 (Tang *et al,* 2016). Prostaglandins can have both a bronchoconstriction effect as seen with prostaglandin D_2 (PGD_2), whilst prostaglandin E_2 (PGE_2) has a protective effect due to its role in bronchodilation (Daham *et al*, 2014). In asthmatics however, there is an upregulation of PGD_2 binding to receptors, therefore resulting in the hyperresponsive effect that can be observed when inflammation is triggered by infection to allergen challenge (Farne *et al*, 2016). However, neutrophils alone are not responsible for the release of these mediators, instead it forms part their activity on monocytes (Tang *et al*, 2016), with mast cells, basophils and eosinophils also being capable of PGD_2 release (Farne *et al*, 2016). This idea is supported by the impaired innate immune response observed in asthmatic bronchial epithelial cells which had been cultured *in vitro* (Wark *et al*, 2005) and *ex vivo* (Johnston, 2005). Cells from asthmatics exposed to RV16 contained higher viral load but did not undergo apoptosis as early as cells from healthy individuals (Wark *et al*, 2005). Furthermore, endogenous production of TGF-β is also linked to innate immune system suppression in asthmatics. TGF-β appears to

increase susceptibility to hRV infection rather than limiting viral spread via apoptosis (Bedke *et al*, 2012). This delay in immune response is linked to prolonged and excessive narrowing of the airways as observed in asthma exacerbations (Johnston, 2005). Cross talk between the innate and adaptive immune system appears to be fundamental in the management of inflammation however, the entirety of this role is still unclear (Tang *et al*, 2016).

1.1.8 Modelling Human Rhinovirus Infections

1.1.8.1 In Vitro Modelling of Human Rhinovirus

Much of the current knowledge relating to hRV transmission and pathogenesis originates from the use of *in vitro* modelling, owing mainly to the limited range of animal models available. As a consequence, a range of *in vitro* models have been developed using a range of human derived cell lines which express the ICAM-1 binding site utilised in 90% of hRV serotypes (Xatzipsalti and Papadopoulos, 2007). Furthermore, the majority of cell lines used in respiratory research show evidence of cytopathic effect when infected with hRV, enabling morphological changes which occur as a result of infection to be easily observed (Jacobs *et al*, 2013). The most widely used cell lines originate from the upper and lower respiratory tract, frequently including alveolar type epithelial cells A549 and bronchial type epithelial cells Beas-2b, Calu-3 and 16HBE (Xatzipsalti and Papadopoulos, 2007; Zhu *et al*, 2010). However, human cell lines that originate from outside the respiratory tract are also utilised to culture hRV, including HeLa cells, embryonic lung fibroblast cells and embryonic kidney cells, as these provide models which compares favourably to human bronchial epithelial cells, demonstrating the benefit of utilising multiple cell lines to study hRV (Jacob *et al*, 2013). Cell lines are extensively used in respiratory research thanks to advantages such as being low cost, easy to culture, having increased longevity and less variability when compared to primary cells (Amineva *et al*, 2011). However, the immortalisation of primary cells to create cell lines has the potential to alter the expression of specific markers on the cells and thus the response observed. For example, the A549 cell line has a cancerous origin, thus whilst these cells represent a primary alveolar type II cell, the architecture, barrier properties and marker expression differs when compared to the primary cell types (Swain *et al*, 2010). In comparison, Beas-2b cells are non-cancerous in origin and retain wild type properties as cells are immortalised through infection with Ad12-SV40 virus (Park *et al*,

2015) nevertheless, this immortalisation process reduces the cells ability to differentiate into different epithelial cell types when compared to primary bronchial epithelial cells (Albright *et al*, 1990).

Whilst each cell line has its own distinct advantages for use within respiratory research, some respiratory cell lines better recapitulate the *in vivo* environment that other. For example, the Calu-3 cell lines is equally as well characterised as the A549 and Beas-2b cell lines however, when grown at an air liquid interface the cell differentiate into submucosal glands, secrete airway fluids and form tight junctions in a similar manner to primary cells (Zhu *et al*, 2010). Similarly, the HBE16 cell line grows effectively at an air liquid interface differentiating into polarised layers of microvilli and cilla, with the formation of tight junctions albeit to a lesser extent than Calu-3 cells (Ehrhardt *et al*, 2002; Forbes *et al*, 2003). Beas-2b cells have similarly been shown to differentiate in the presence of serum rather than in response to an air liquid interface (Stewart *et al*, 2012) nevertheless, Beas-2b cells also form tight junctions albeit to a lesser extent than the primary cells from which they were originally derived and in comparison to other bronchial cell lines (Forbes, 2000). Limited differentiation of A549 cells towards alveolar type II cell has been observed in long term culture in Hams F12 media when compared to DMEM (Cooper *et al*, 2016) however, although cells continue to express biochemical and morphological characteristics which are similar to primary alveolar cells, tight junction formation is reduced compared to *in vivo* (Srinivasan *et al*, 2015). Arguably, 16HBE and Calu-3 cell lines most closely represent the *in vivo* environment when primary cells are not available or feasible due to long term culture requirements however, A549 and Beas-2b cells continue to form a widely accepted, stable and reproducible airway models, being both cheap to culture and readily available (Srinivasan *et al*, 2015; Han *et al*, 2020). Furthermore, A549 and Beas-2b cells remain one of the most widely used and accepted model for the study of hRV (Greiller *et al*, 2019; Jang *et al*, 2006; Pang *et al*, 2017; Papi and Johnston, 1999; Zaheer and Proud, 2010). Thus, although limitations exist in regards to A549 and Beas-2b cells, extensive use of both cell lines as a model for hRV infection, alongside the maintained expression of biochemical and morphological characteristics similar to parent primary cells, provides reasonable justification for use as an airway model in subsequent research.

1.1.8.2 In Vivo Modelling of Human Rhinovirus

Although fewer *in vivo* models of hRV exist, the modelling which is currently utilised take two main forms, these being a limited number of animal models or controlled human infection (del Vecchio *et al*, 2015). When human respiratory viruses are considered as a whole, animal models predominately feature guinea pigs, ferrets, mice, hamsters and rats (Han *et al*, 2018). Although mouse models are typically the most frequently utilised animal model in respiratory research (Han *et al*, 2018), mouse models of *in vivo* infection with hRV have only arisen more recently with the advent of a transgenic mouse with ICAM-1 receptors (Bartlett *et al*, 2008). Prior to the development of this transgenic model, infection with hRV was only possible if minor group serotypes which bind to LDL receptors were utilised however, sustained viral replication was often not achievable (Yin and Lomax, 1986) or required passages to be alternated between mouse and human cells (Rasmussen and Racaniello, 2011). Given that minor group serotypes only account for 10% of hRV infections, mice models are not widely utilised in hRV *in vivo* modelling (del Vecchio *et al*, 2015), as such this more recently derived transgenic model which utilises the major group receptor ICAM-1 may enable more extensive use of animal models in hRV research (McLean, 2014). However, whilst a relevant mouse model now exist, many human respiratory viruses are not naturally pathogenic in mice, thus a higher inoculum of virus is required to infect the animal in comparison to *in vitro* modelling in human cell lines (Han *et al*, 2018).

In addition to the transgenic mouse model, cotton tail rats have also been suggested as a potential *in vivo* model. Infection of the rats with hRV serotypes 16 and 1B showed promising indications of pathological changes similar to the response observed in humans and a measureable viral load 48 hours post infection, which suggested viral replication may be occurring (Blanco *et al*, 2014). Similarly, infection of cotton rats with hRV serotype 14 showed detectable replication in both the upper and lower respiratory tract of the animal however, the inflammatory response was milder than that observed with hRV serotype 16 (Patel *et al*, 2017). This cotton rat model provide additional promise when compared to the transgenic mouse model as it requires no genetic manipulation being naturally semi-permissible to hRV (Blanco *et al*, 2014). Whilst ferrets, guinea pigs and hamsters have been utilised for the study of other respiratory viruses including enterovirus D, coronavirus and respiratory syncytial virus (Han *et al*, 2018), they lack the receptor specificity required for

hRV viral binding so cannot be used for the study of this virus (del Vecchio *et al*, 2015). However, guinea pigs also have relevance to the study of cough, alongside other animals such as cats and dogs. Unlike other rodents, guinea pigs elicit a measureable cough reflex regardless of state of consciousness and respond to tussive agents in a manner akin to the human response (Belvisi and Bolser, 2002). Beyond rodent models the other animals which exist for the study of hRV are non-human primates. Gibbons and chimpanzees have been utilised to test antiviral effectiveness as they share similar ICAM-1 receptors to humans, making them permissible to both minor and major group infections. However, chimpanzees lack observable clinical symptoms during infection, which when coupled with the high cost, impracticability and ethical restrictions for non-human primate research makes these *in vivo* animal models unrealistic for hRV research (Power *et al*, 2009).

With such a limited range of suitable animal models available for the study of hRV, alternative methods of *in vivo* studies take the form of human infections (del Vecchio *et al*, 2015). Randomised control trials of hRV infections in human subjects typically follow two main approaches, these being controlled inoculation of individuals with hRV (Harris and Gwaltney, 1996; Mosser *et al*, 2005; Proud *et al*, 2008; Mallia *et al*, 2012; Zhu *et al*, 2014; Turner *et al*, 2017) or the recruitment of individuals who are exhibiting respiratory infection symptoms due to naturally occurring infections (Jenner *et al*, 2007; Iwane *et al*, 2011; van der Zalm *et al*, 2011; Achten *et al*, 2017). Although the physiological relevance of such a model makes an ideal method to study hRV, disadvantages still exist. Both approaches utilise both healthy individuals and individuals with mild to moderate underlying respiratory conditions however, individuals with underlying respiratory conditions are more prone to exacerbation during hRV infections and thus require greater vigilance especially during the study (Roestenberg *et al*, 2018). Furthermore, careful management of infected individuals is required to reduce variability, such as the time from the onset of symptoms to the point at which contact with healthcare provision is made, this is especially important when natural infections are utilised (del Vecchio *et al*, 2015; Hammond *et al*, 2015). In additional the type of methods used to collect samples are often invasive, including methods such as nasal swabs, throat swabs, nasal lavage, airway epithelial cell brushing, bronchoalveolar lavage (BAL) samples and bronchial biopsies which are likely to cause discomfort to the participant (Mosser *et al*, 2005; Waris *et al*, 2013; Collins *et al*,

2014). Whilst, the number of suitable animal models available to study *in vivo* hRV infection is limited, the use of human infections overcomes this issue to some extent and although there are some limitations to consider when using these models, they provide a more physiologically relevant model than *in vitro* models can achieve. However, the opportunity to carry out such a cohort study is not always feasible, thus an alternative *ex vivo* model that can be widely utilised in a laboratory environment which combines elements of both *in vitro* and *in vivo* models would immensely benefit the study of hRV.

1.1.8.3 Precision Cut Lung Slices (PCLS) and Microfluidics for hRV Studies

Given the lack of suitable animal models for the study of hRV there is a need to develop a model that can utilise human tissue for the study of hRV and its role in cough and airway inflammation. The use of PCLS provides an opportunity to develop an *ex vivo* model which can more appropriately simulate the lung's response to hRV infection, as it enables lung parenchyma to be maintained thus providing a situation more akin to an *in vivo* model. The PCLS model removes some of the reliance on the use of controlled infections in human participants to study response or the use of traditional cell culture, which is limited to individual cell types, thus lacking the interactions observed between the multiple cell types found within the airway. However, whilst the use of PCLS reduces the burden on human participants and animal models alike, a benefit added to by the extensive number of usable tissue slices that can be collected from a single sample, its potential is limited by the viability of samples for prolonged time frames and the volume of reagents required to undertake any testing. The combination of PCLS and microfluidics provides an ideal platform to further increase viability through continuous perfusion of tissues, as observed *in vivo*, and reduced reagent consumption thanks to the small volumes required to perform standard immunoassays. Furthermore, the variation in microfluidic devices available also provides ample opportunities to study both tissue and individual cells from the airways in an extensive and varied manner. Thus providing the potentiation for the development of a range of models for hRV research that have previously not existed.

1.2 Precision Cut Lung Slices

1.2.1 Traditional Tissue Studies

Traditional methods of studying human tissue include the use of tissue and cell culturing, serology and microscopy, plus the use of molecular techniques in more recent decades (Houikian and Raoult, 2002) however, whilst each of these techniques has its own set of distinct advantages there are some issues that remain. For example, the disruption of tissue in order to isolate individual cells during cell culturing results in the loss of tissue architecture, thus impacting on how realistically cell-to-cell interactions occur (Grivel and Margolis, 2009). The use of *in vitro* techniques do allow for a level of simplicity that is not always achievable when dealing with *in vivo* models, similarly they are often cheaper and faster, which makes them a more viable option when working with human tissue (Neuhaus *et al*, 2013). Arguably, the influenza virus has a significant impact on global health, as such *in vitro* studies to identify a range of cellular mechanisms including those used by epithelial cells to absorb vaccines form an important role in developing a deeper understanding of the virus, its pathogenicity and potential therapeutic models. However, whilst the immune response that is elicited *in vitro* is effective against the virus, the effectiveness *in vivo* could differ hence the need for both models (Christensen *et al*, 2010). Furthermore, simplicity is not always beneficial, the complexity of cellular processes cannot always be effectively modelled *in vitro* thus there is a need for *in vivo* models to better demonstrate the mechanisms and interactions that take place within the tissue (Torisawa *et al*, 2014). The influenza virus once again provides evidence of the value of *in vivo* models, while simultaneously highlighting the issues surrounding the use of non-human models. Murine modelling of antiviral agents demonstrates the likelihood of effective use in humans however, mice lack the symptoms of infection thus other indicators have to be utilised to identify if successful infection has occurred. Conversely, ferrets exhibit symptoms of influenza in a similar manner to humans, also displaying a comparable level of complexity to human tissue when compared to murine models however, the husbandry of ferrets is more problematic than mice which potentially makes them a less viable option. As a result, multiple animal and non-human primate *in vivo* models are required to provide a comprehensive overview of the effectiveness of treatments in humans (Barnard, 2009).

1.2.2 Advantages of Precision Cut Lung Slices

To enable a more comprehensive understanding of the mechanisms and interactions utilised at a cellular level by respiratory pathogens, a model which combines both *in vitro* and *in vivo* techniques and procedures needed to be created. Such a model is provided by Precision Cut Lung Slices (PCLS), this *ex vivo* model provides the ability to observe cellular processes as expected during *in vitro* testing, whilst still allowing *in vivo* responses such as immunological reactions to be monitored (Neuhaus *et al*, 2013). PCLS as an *ex vivo* model provides a range of benefits over the use of more classical *in vitro* techniques. Potentially one of the most valuable advantages is the maintenance of the cellular architecture at a micromolecular level, which enables cell structures to respond as they would *in vivo* (Martin *et al*, 1996). This maintenance of cellular structures also provides increased flexibility as bronchial tubes of various sizes can be observed from different sections of lung tissue, enabling observations of a greater range of reactions to be made (Ressmeyer *et al*, 2006). PCLS is also advantageous due to the preservation of the lung parenchyma in the sampling method, which results in minimal changes to the elasticity of the lung tissue, thus making it comparable to *in vivo* responses (Alder *et al*, 1998). Furthermore, the methods used to create PCLS appears to have no adverse effect on the responsiveness of the airways, which remain similar to *in vivo* measurements. Additionally, limited narrowing of the airways is observed however, the re-inflation of lungs prior to slicing does cause some increase to airway area (Dandurand *et al*, 1993; Wohlsen *et al,* 2003). The preservation of responsiveness and minimal change to the airway size thus enables observations of bronchoconstriction to be measured *ex vivo* whilst providing results that would be expected if the same measurements were taken *in vivo* (Martin *et al*, 1996).

1.2.3 Challenges of Precision Cut Lung Slices

Although PCLS appears predominately to provide an effective method of sampling and observing mechanisms within lung tissue there are some challenges. Namely the need for the lung tissue to be free from incisions, disease and injury. Inflation of the lungs is achieved through the infusion of agarose gel into the airways, this ensures alveoli are expanded to near total lung capacity in order to support tissue structure (Fisher *et al*, 1994). As a result of needing to re-inflate the lung tissue, any incisions prevent full inflation, as the agarose tends to leak out before it has had the opportunity to fully gel (Fisher *et al*, 1994; Martin *et*

al, 1996). The issue of agarose leakage is problematic when sections of lung tissue are used, due to either impracticability relating to organ size or sample availability, as agarose leakage can be extensive making full inflation difficult and less reproducible (Vietmeier *et al*, 2007). Similarly, excessive mucus in the airways due to disease can also prevent complex expansion, as the agarose cannot fully infuse the lungs (Fisher *et al*, 1994; Martin *et al*, 1996). This could therefore limit the potential sample size depending on the reason for lung tissue removal. This being said, the issue is somewhat eradicated by the slicing technique used, multiple cores can be taken from one healthy lung, with each core being sliced into approximately 30 slices, thus several thousand slices can be created from a single healthy lung (Fisher *et al*, 1994; Wohlsen *et al*, 2003; Switalla *et al*, 2010). Slicing of the lung tissue can also cause some damage to the localised area (Ressmeyer *et al*, 2006), which can lead to pro-inflammatory responses (Neuhaus *et al*, 2013) and pre-contraction of the airways (Wohlsen *et al*, 2003). However, in order to limit adverse responses washing and regular changes of medium remove cellular debris and other cell mediators (Davidovich *et al*, 2013b), this processing ensures that cell marker levels are returned to pre-cutting levels within a couple of hours (Neuhaus *et al*, 2013). Additionally, inclusion of a suitable agonist into both the inflation agarose and washing medium can aid in the prevention of bronchoconstriction (Ressmeyer *et al*, 2006). The washing of slices in 37^{o}C medium after cutting, serves an additional purpose to remove excess agarose prior to further analysis (Paddenberg *et al*, 2014). However, examination of slices by microscopy indicate that agarose can remain in the airways after slicing and washing, which could potentially interfere with airway activity (Siminski *et al*, 1992; Sanderson *et al*, 2011). Conversely, the continued presence of agarose within the airways could prevent collapse throughout the duration of an experiment. Whilst having the additional benefit of providing a steady diffusion of nutrients to internal layers of tissue, when agarose is dissolved in suitable medium (Placke and Fisher, 1987). Irrespective of advantages and challenges of the re-inflation with and removal of agarose needs to be carefully managed if optimal tissue slices are to be produced.

1.2.4 Agarose Inflation

Whilst the end outcome of the PCLS process is the same, there are several variations in regards to the methods utilised to prepare the lung samples prior to slicing. The use of

agarose for inflation in itself is an important choice as the gel creates the support structure for the airways due to the viscosity of the solution, insofar as the agarose can infer a partial pressure on the airway ensuring it remains inflated throughout any further procedures (Sanderson, 2011). The exact method used to re-inflate the lung is typically similar between studies however, there appears to be differing opinions between authors in relation to the agarose concentrations, which can vary quite considerably. Henjakovic *et al* (2008a) suggest the use of a 0.75% agarose solution, whilst Lauenstein *et al* (2014) use a 1.5% agarose solution and Brown *et al* (2013) use differing concentrations of 2% and 3% in rat and human tissue respectively, the same concentrations utilised by van Rijt *et al* (2015) for mice (2%) and human (3%) tissue. Interestingly, Brown *et al* (2013) tissue preparation varied beyond the percentage of agarose used for inflation. Whilst both tissues where prepared in a similar manner prior to inflation the technique differed in that whole rat lungs were utilised allowing for inflation via the trachea, while human tissue received from a resection had to be inflated through injection into the tissue, demonstrating how the animal of origin may influence the process used. However, ranges between 0.5% and 4% have been utilised in some studies (Dandurand *et al*, 1993; Bergner and Sanderson, 2002a), with the predominate concentration being between 1.5 – 2%, suggesting that exact concentrations are not significant in preparation of the lung tissue but instead relate to later stages of the experimental method such as tissue slicing. Furthermore, excessive stiffness of the agarose, created by higher concentration solutions, could lead to unwanted trauma responses. A consequence of higher agarose concentrations is the potential of the stretch and recoil properties of the lung tissue to be affected, with the possible risk that over inflation may occur, due to the forces required to infuse the agarose (Sanderson, 2011). Conversely, the use of lower concentration agarose appears to have a potentially negative affect on the tissues' ability to maintain its *in* vivo shape and therefore its ability to recoil after contraction, resulting in the need for the addition of external supporting structures to maintain slice shape (Schlepütz *et al*, 2011; Rosner *et al*, 2014). Whilst the aforementioned concentrations have potential challenges, the use of 2% agarose does not result in excessive stretching of the lung tissue and is the equivalent to the stretch observed during breath holding *in vivo* (Dandurand *et al*, 1993; Brook *et al*, 2010), thus a concentration similar to this has become optimal for many studies (Table 1.1). As such the actual concentration of agarose used is entirely dependent on the nature of the experiment being conducted.

% Agarose Utilised	Total Number of Articles Using Concentration
1.5	10
1.75	1
2.0	19
3.0	3

Table 1.1: Variations in concentrations of agarose used in PCLS technique, total number of published articles on human PCLS (using search criteria "human precision cut lung slices" in given date range) for each given concentration from January 2008 – January 2018.

1.2.5 Inflation Agarose Formation

Similarly, variation also exist for the choice of solution used to dissolve the agarose prior to inflation however, when considered together they can broadly be grouped in to two categories of either cell/tissue culture medium or saline equilibrated buffer solutions, with the most predominate being DMEM and HBSS respectively. Osmolality of the solution is undeniably an important factor when considering the base solution of the inflation agarose, whereby the osmolality needs to be physiologically relevant. The use of either culture medium or buffer solutions ensures the inflation agarose is isotonic to the tissue, thus prevent damage to the tissue due to osmotic potential (Waymouth, 1970). Arguably, the use of culture media has the additional benefit of providing internal tissue layers with a continuous flow of nutrients (Placke and Fisher, 1987), which may increase tissue viability. However, multiple studies on maintenance of periodontal ligament after traumatic tooth loss demonstrate that HBSS outperforms culture media as a short term storage medium for 24 – 96 hours (Khinda *et al*, 2017). Whilst, the composition of HBSS and DMEM differ, the osmolality and pH ensure that tissue viability can be maintained for several days regardless of which solution is chosen to dissolve agarose.

1.2.6 Creating Lung Slices

The development of agarose filled lung tissue by Placke and Fisher (1987) subsequently followed by the development of lung slices of reproducible thickness by Stefaniak *et al* (1992) overcame the issue created by the large air spaces occupying the majority of the lung structure and extended the scope of study possible on this tissue (Parrish *et al*, 1995). Once prepared in the aforementioned manner, core samples can be taken, generally using

a modified method initially formulated to produce precision-cut liver slices, in which a turning cylinder slowly passes through the tissue to retrieve a core sample (Smith *et al*, 1986). These samples can then be sliced to uniform thickness using traditional tissue slicing methods. Warburg developed the original method utilised for tissue slicing in 1923 however, the technique used is somewhat laborious and potentially lacking in precision due to a razor blade being utilised for slicing. Developments in the field of neurobiology during the 1960s resulted in the need for an instrument that could form uniform cuts of tissue with minimal damage. The tissue slicer created by Krumdieck in 1980 removed the unwanted force applied by the operator when using a knife as done in traditional tissue slicing methods and enabled slices to be cut whilst submerged, which allowed for less desiccation, increased viability and greater temperature control (Krumdieck *et al*, 1980; Krumdieck, 2013). With the refinement in the processing of tissue slices, the accuracy and repeatability of slice production to within 5% thickness enabled precision-cut tissues slices to form a viable method of *in vitro* testing (Smith *et al*, 1985). Subsequently, updates made to the Krumdieck tissue slicer included an oscillating, mechanically controlled blade, which increased speed and reduced tissue damage further (Brendel *et al*, 1987).

1.2.7 Tissue Slicing Comparative Studies

Price *et al* (1998) compared the Krumdieck tissue slicer and the less complex, semi-automated Brendel Vitron tissue slicer (currently marketed as Vitron tissue slicer), to find no significant difference between the two instruments production of precision-cut liver slices, making them both viable choices for this procedure. Similarly, Zimmermann *et al* (2009) compared the Krumdieck tissue slicer to the more recently developed Leica VT1200 S Vibratome in the production of precision-cut liver slices. Although comparisons of tissue viability found no significant difference between the instruments, inconsistences in the variation of slice thickness was noticeable on the Krumdieck tissue slicers within a single sample and in both instruments when tissue slices from different species were directly compared. Furthermore, the Leica VT1200 S Vibratome has other advantages including, reduced slicing buffer volumes, finer slice thickness control, increased vertical vibration control to reduce tissue shearing and the ability to slice smaller samples than the Krumdieck tissue slicer. However, the slicing speed of the Leica VT1200 S Vibratome is slower and the whole instrument cannot be autoclaved so additional precautions have to

be taken to avoid contamination. The minimal difference between these instruments ensures both are viable options for the production of precision cut tissue slices however, depending on the tissue type the Leica VT1200 S Vibratome may produce slightly more reproducible slices (Zimmermann *et al,* 2009). Subsequent modifications of tissue slicing instruments had led to the development of the Compresstome^{TM} VF-300, which Abdelaal *et al* (2015) compared to the Technical Products International Vibratome 3000. The aforementioned Vibratome is directly comparable to the Leica Vibratome range, with variations in blade speed, amplitude and angle all being easily adjusted. Comparatively the Compresstome^{TM} VF-300 can cut faster than the Vibratome due to the additional support provided to the tissue sample, which enables higher blade speed rates to be utilised. Furthermore, the sample support tube provides greater stability to the tissue, allowing for larger sections and preventing the blade dislodging embedded tissue samples if fibrous tissue is encountered, a problem more frequently observed in the Vibratome. Although the Vibratome 3000 construction was deemed to be superior to the Compresstome^{TM} VF-300 and had the advantage of a blade reversing action, the Compresstome^{TM} VF-300 was identified as the more appropriate instrument for slicing fibrous tissue (Abdelaal *et al*, 2015), including lung tissue (Yim *et al*, 2013). As a result of refinements to the Krumdieck tissue slicer and the development of similar products, coupled with the minimal difference between each model, these automated tissues slicers have become the most reliable choice for the production of rapid and uniform precision-cut tissue slices (Table 1.2).

Tissue Slicer	**Total Number of Articles Using Each Tissue Slicer**
Krumdieck	19
Compresstome^{TM} VF-300	10
Hyrax V55	2
Leica VT1000S/VT1200S	2
Vitron	1

Table 1.2: Variations in tissue slicer used in PCLS technique, total number of published articles on human PCLS (using search criteria “human precision cut lung slices” in given date range) for each given tissue slicer from January 2008 – January 2018.

1.2.8 Slice Thickness

With a method in place to produce uniform tissue slices, subsequent development to the now widely, recognised PCLS method was the creation of uniform, reproducible and thin tissue slices. Prior to the development of precision-cut tissue slices and the production of consistently thin slices Dandurand *et al* (1993) has utilised lung slices with a thickness of 500 – 1000µm. However, these thicker slices resulted in some variations in response rate of bronchoconstriction and thus created a need for thinner, more precise slices when investigating *in vitro* bronchoconstriction (Martin *et al*, 1996). As a consequence of these variation, a study by Martin *et al* (1996) determined that an optimal thickness for a precision-cut tissue slice using a mechanical tissue slicer was approximately 250µm. However, this finding contradicts the optimal thickness suggested by Parrish *et al* (1995) of approximately 500µm and by Bach *et al* (1996) of approximately 500 – 700µm when considering the viability and potential practicality of a range of tissue slices. Furthermore, variations in tissue slice thickness are still apparent in more recent studies and range from 75µm to 500µm. The maximum slice thickness of approximately 500µm has been utilised in PCLS studies on rats, with lungs infused with 1% agarose solution (Alder *et al*, 1998), while Temann *et al* (2017) used human lung tissue slices of 600µm thickness, infused with 1.5% agarose to investigate inflammatory response. Whilst the minimum thickness of approximately 75µm has been utilised to conduct murine and rat PCLS, this confers an ability to study single cell responses however, 2% agarose concentration needs to be infused into the lungs to ensure sufficient stiffness (Bergner and Sanderson, 2002a; Brook *et al*, 2010). This being said the concentration of agarose alone does not necessarily appear to affect the potential to achieve thinner tissue slices. Morin *et al* (1999) and Tatler *et al* (2016) produced approximately 150µm thick slices after infusion of the lungs with 0.7% and 2% agarose solution respectively. However, these slices were cut with the tissue samples placed under ice-cold buffer for the entire duration of the slicing procedure, in order to maintain agarose hardness. This being said the Martin *et al* (1996) study has since influenced many PCLS studies and although the desired thickness of PCLS varies between studies, the most frequently used slice thickness is approximately 200 - 300µm, infused with an agarose concentration of 1.5 – 2% (Wohlsen *et al*, 2003; Brown *et al*, 2013; Davidovich *et al*, 2013b; Cairns *et al*, 2020) (Table 1.3).

Slice thickness (µm)	Author	Paper
200	Schlepütz *et al*, 2012	Neurally mediated airway constriction in human and other species: A comparative study using precision-cut lung slices (PCLS)
220	Zmora *et al*, 2017	Non-human primate orthologues of TMPRSS2 cleave and activate the influenza virus hemagglutinin
250	Cooper *et al*, 2008	Steroids completely reverse albuterol-induced β_2- adrenergic receptor tolerance in human small airways
	Switalla *et al*, 2010	Natural innate cytokine response to immunomodulators and adjuvants in human precision-cut lung slices
	Ressmeyer *et al*, 2010	Human airway contraction and formoterol-induced relaxation is determined by Ca^{2+} oscillations and Ca^{2+} sensitivity
	Cooper *et al*, 2011(a)	Formoterol and salmeterol induce a similar degree of β_2-adrenoceptor tolerance in human small airways but via different mechanisms
	Cooper *et al*, 2011(b)	C-027 Inhibits IgE-mediated passive sensitization bronchoconstriction and acts as a histamine and serotonin antagonist in human airways
	Banerjee *et al*, 2012	Trichostatin A abrogates airway constriction, but not inflammation, in murine and human asthma models
	Damera *et al*, 2012	An RGS4-mediated phenotypic switch of bronchial smooth muscle cells promotes fixed airway obstruction in asthma
	Lavoie *et al*, 2012	Dilatation of the constricted human airway by tidal expansion of lung parenchyma
	Seehase *et al*, 2012	LPS-induced lung inflammation in marmoset monkeys – an acute model for anti-inflammatory drug testing
	Davidovich *et al*, 2013a	Uses of remnant human lung tissue for mechanical stretch studies
	Neuhaus *et al*, 2013	Functional testing of an inhalable nanoparticle based Influenza vaccine using a human precision cut lung slice technique
	Lauenstein *et al*, 2014	Assessment of immunotoxicity induced by chemicals in human precision-cut lung slices (PCLS)
	Koziol-White *et al*, 2016a	Inhibition of spleen tyrosine kinase attenuates IgE-mediated airway contraction and mediator release in human precision cut lung slices
	Ojiaku *et al*, 2017	TGF-β1 evokes human airway smooth muscle cell shortening and hyperresponsiveness via Smad3
260 – 280	Sturton *et al*, 2008	Pharmacological characterization of indacaterol, a novel once daily inhaled β_2 adrenoceptor agonist, on small airways in human and rat precision-cut lung slices
250 – 300	Neuhaus *et al*, 2017	Assessment of long-term cultivated human precision-cut lung slices as an ex vivo system for evaluation of chronic cytotoxicity and functionality
300	Brown *et al*, 2013	A role for M_2 and M_3 muscarinic receptors in the contraction of rat and human small airways
	Sun *et al*, 2015	Immunostimulatory defective viral genomes from Respiratory Syncytial Virus promote a strong innate antiviral response during infection in mice and humans

	van Rijt *et al*, 2015	Protease-mediated release of chemotherapeutics from mesoporous silica nanoparticles to *ex vivo* human and mouse lung tumors
	Alsafadi *et al*, 2017	An ex vivo model to induce early fibrosis-like changes in human precision-cut lung slices
	Wujak *et al*, 2017	FXII promotes proteolytic processing of the LRP1 ectodomain
350	Robinett *et al*, 2014	Bitter taste receptor function in asthmatic and non- asthmatic human airway smooth muscle cells
	Carr *et al*, 2016	Interdicting G_q activation in airway disease by receptor-dependent and receptor-independent mechanisms
	Ghosh *et al*, 2016	Soluble guanylate cyclase as an alternative target for bronchodilator therapy in asthma
	Koziol-White *et al*, 2016b	Inhibition of PI3K promotes dilation of human small airways in a rho kinase-dependent manner
	Velalopoulou *et al*, 2017	Synthetic Secoisolariciresinol Diglucoside (LGM2605) Protects Human Lung in an Ex Vivo Model of Proton Radiation Damage
	Yoo *et al*, 2017	$G\alpha_{12}$ facilitates shortening in human airway smooth muscle by modulating phosphoinositide 3-kinase-mediated activation in a RhoA-dependent manner
400	Nave *et al*, 2008	Metabolism of ciclesonide in the upper and lower airways: review of available data
600	Temann *et al*, 2017	Evaluation of inflammatory and immune responses in long-term cultured human precision cut lung slices
750	An *et al*, 2012	TAS2R activation promotes airway smooth muscle relaxation despite β_2-adrenergic receptor tachyphylaxis

Table 1.3: Examples of published literature on human PCLS from January 2008 – January 2018, identifying variations in slice thickness used within each studies.

1.2.9 Slice Viability

Although no definitive slice thickness appears to exist, the necessity for a thin slice consistent with those used by a number of studies is based on the maintenance of slice viability. Slice thickness directly influences viability, as maintenance of cellular activity is dependent on the ability of oxygen to diffuse into the cells. Slices that are overly thick, may prevent cells in the middle layers receiving sufficient oxygen resulting in cell death. Whilst slices that are too thin, may have excessive numbers of damaged cells compared to viable cells, due to the disruption that occurs when slicing (Umachandran *et al*, 2004). Factors beyond slice thickness also affect viability, namely the need of the tissue slice to be maintained in suitable media for the duration of the study, to preserve the *in vivo* nature of the tissue slice. To increase viability daily changes of storage media are necessary, this increases viability to an average of 1 – 3 days (Ressmeyer *et al*, 2006), additionally the use

of roller culture can aid in the diffusion of oxygen further enhancing the longevity of the cells (Martin *et al*, 1996). However, with slices that are thinner than 250µm, separation of individual slices into a multi-well plate enable viability to be maintained with media change alone (Sanderson, 2011). Furthermore, the choice of medium used to store tissue slices can affect the viability of the tissue in culture. A comparison of 8 different types of commercially available media, demonstrated that MEM and M199 provided improved tissue viability, when measured through histological, morphological and DNA, RNA and protein level changes for an extended period of up to 28 days, with changes observed as early as 3 days in some mediums (Placke and Fisher, 1987). Measurement of viability can be conducted through numerous methods including measurements of lactate dehydrogenase leakage (Wohlsen *et al*, 2003), live/dead staining (Neuhaus *et al*, 2013) and thymine incorporation (Martin *et al*, 1996). Whilst viability of around 72 hours is generally achieved, longer periods of viability have been observed at approximately 5 days (Bergner and Sanderson, 2002b) although physiological changes occurred as a result of the extended storage (Sanderson, 2011). Furthermore, Rosner *et al* (2014) demonstrated that PCLS viability could be further extended through cryopreservation at -80^{o}C and subsequent storage in liquid nitrogen for a maximum of two weeks. When rapidly thawed in a 37^{o}C water bath the ensuing observations of airway contraction, cell death and the extent of ciliary beating appeared relatively unaffected compared to non-freeze thawed samples however, some minimal changes to metabolic activity was observed. Management of cryopreservation is vital for viability to be maintained. One potential consequence of cryopreservation is the formation of ice crystals within the intracellular matrix. As the cells and surrounding media are supercooled, the number of ice crystals which initially form in the media increase, this affects the osmotic potential of the media and results in water being drawn from the intracellular matrix causing the cells to dehydrate and become non-viable (de Graft and Koster, 2003). However, rate of cooling mediates this effect, in lung tissue a slower rate of cooling at approximately 1^{o}C per minute minimise crystal formation, whilst rates which fall either side of this, result in the formation of a large number of ice crystals (Rosner *et al*, 2014). Additionally, the use of the cryoprotectant dimethyl sulfoxide at a concentration of 10% inhibits ice crystal formation thus increasing likelihood of viability (Watson *et al*, 2016).

1.3 Microfluidics in Cell and Tissue Culturing

1.3.1 Principles of Microfluidics

The principle of microfluidics is the scaling of an assay onto an object that measures a few centimetres squared, developed in a manner to enable multiple repeats of an experiment to be conducted simultaneously and in identical conditions, thus the likelihood of erroneous results is reduced, increasing reproducibility and thus reliability of the measurements made (Weibel and Whitesides, 2006). As such the use of microfluidics for diagnostic assays would be to create a lab-on-a-chip that has the functionality to perform a complete range of assays potentially whilst a patient waits, thus recreating the total analysis system on a miniaturised scale (Tarn and Pamme, 2011). However, the use of microfluidics extends beyond the creation of devices that can replicate a range of diagnostic assays. A range of platforms have been designed to not only support the culturing of a single cell line or in some instances the co-culture of several cell lines but also more complex systems in the forms of tissues and organ (Dodson *et al*, 2015).

1.3.2 Microfluidic Device Design

Device design also influences the type of assays that can be conducted on any given device due to the type of material used for its creation. Predominately, microfluidic devices are constructed from the transparent polymer poly(dimethylsiloxane) (PDMS), as this flexible polymer enables a wide range of designs to be fabricated, including addition of other devices such as valves and pumps (Whitesides, 2006) (Table 1.4). PDMS also has advantages over glass and silicon devices in that it is more durable, less brittle, easier and quicker to fabricate and less expensive. Furthermore, silicon is opaque thus is inaccessible to the extensively used microscopy techniques of cell biology testing (Sackmann *et al*, 2014). Other complexities of fabricating glass and silicon chips is the difficulty in sealing channels and the semi-conductive properties of silicon make it unfeasible to use in electrophoresis type assays that rely on the use of electrical charge. Conversely, PDMS channels are relatively straightforward to seal, as is the bonding of layers (Duffy *et al*, 1998) and the channels hydrophobic nature can be altered to be more hydrophilic, enabling a greater range of assays to be performed (Sackmann *et al*, 2014). Whilst this ability to change channels to be more hydrophilic in nature aids loading of the device with fluids, exposure of the device to atmospheric conditions can cause the change to revert back to

hydrophobic affecting functionality (Eddings *et al*, 2008). However, storage of the device underwater can prolong the hydrophilic properties for around 7 days, alternatively increased stiffness of the PDMS membrane has similar effects and results in the device remaining hydrophilic for prolonged periods of approximately 21 days (Markov *et al*, 2014). As an elastomer PDMS has further advantages over glass and silicon, due to its flexibility, which provides potential to study the effects of sheer forces on cells (Huh *et al*, 2011) and consider organ level functions such as the cyclic mechanical strain experienced in breathing (Douville *et al*, 2011; Huh *et al*, 2012). Additionally, PDMS has a high permeability to gases therefore oxygen levels inside the device can be maintained at a sufficiently high enough level to ensure tissue viability, without the need for additional oxygen sources as seen in glass and silicon based devices (Huh *et al*, 2011). However, this permeability has the potential to be detrimental in cell culturing as small molecules dissolved in the culture media, could diffuse into the PDMS, altering concentrations of biologically or chemically active substances. Furthermore, the silica barrier used to give the microchannels the necessary hydrophilic properties is impermeable, therefore this could affect the amount of oxygen reaching the cell culture thus affecting longevity and viability of the cells (Markov *et al*, 2014). The extent of oxygen diffusion through the PDMS membrane can be further enhanced through an increased PDMS ratio in the polymer and air pressure (Lamberti *et al*, 2014). Given the advantageous properties of PDMS, this has become the logical choice for the development of microfluidic devices. As it provides the flexibility required to perform the varied range of tissue studies and assays needed for biological research. However, the extent of gas permeability of PDMS could be potentially problematic if gas concentrations within the device need maintaining at a specific level, such as considering how hypoxia affects cell response. Over time the percentage mix of gases inside and outside the device will begin to equilibrate towards atmospheric concentrations thus, could be of detriment if an experiment needs specific percentages of any given gas (Halldorsson *et al*, 2015). In these instances, the use of glass or similar non-permeable materials would be better suited to create a microfluidic device and needs some consideration when designing a device for biological research purposes. Thermoplastics provide scope for low cost alternatives to glass devices when PDMS is an unsuitable option. Commonly used thermoplastics include polycarbonate, poly(methylmethacrylate) (PMMA) and polystyrene. Each is significantly cheaper than both glass and PDMS and whilst the ease of fabrication is similar to that of PDMS, the flexibility afforded to PDMS is lacking in other thermoplastics. However, all are

optically transparent, thermally stable, solvent resistant, with the exception of polystyrene and biocompatible. Furthermore, lacking the gas permeability of PDMS they provide ideal candidates for fabrication of microfluidic devices when gas levels need managing within defined limits (Tsao, 2016).

Number of devices utilising material	**Material(s) used**
111	PDMS
12	Hydrogel (agarose, gelatine or collagen based)
9	PDMS + Glass
8	PMMA
7	Poly(ethylene glycol) (PEG)
5	Glass, Polystyrene (PS)
4	Silicone
3	PMMA + PDMS, Polycarbonate (PC)
2	Poly(Ɛ-caprolactone) (PCL), Cyclic olefin copolymer (COC) – TOPAS, Polysulfone, Sodium polyacrylate, PDMS + PC, Glass + PMMA, Resin
1	Polyurethane (PU), Paper, Photoresist, PC + PMMA, Poly(vinyl alcohol) (PVA), Thiol-ene polymer, Quartz substrate, Ostemer, Polyjet, Parafilm

Table 1.4: Examples of published literature on organ-on-a-chip microfluidic devices from January 2008 – August 2018, identifying variations in the material used to create microfluidic devices within each study.

1.3.3 Body-on-a-chip

The development of platforms, which have the capabilities of supporting tissue and organ equivalents represent a shift in *in vitro* culturing. Away from the use of single cell lines to a technique that is engineered to consider the physiological mechanisms of cells, not in isolation but in relation to each other, as would occur *in vivo* (van der Meer and van den Berg, 2012). With the success of tissue and organ-on-a-chip, the frontiers of microfluidics as a platform for biological research are pushed forwards to the consideration of whether a body-on-a-chip is feasible. Body-on-a-chip utilises multiple organ-on-a-chip devices, which are combined to create a device that parallels an entire system or body in which the order of the tissues or organs is physiologically correct and the fluid flow rates and forces experienced by cells is equivalent to those observed *in vivo* (Esch *et al*, 2014). Although,

the principle of body-on-a-chip appears novel, the idea that multiple cell types can be linked together in a single device has been attempted previously and forms the basis of some of the earliest work on biological based microfluidics devices (Baker, 2011). This initial development by Sin *et al* (2001) created an etched silicon device which linked together intestinal, liver and fat cells, termed animal-on-a-chip, which endeavoured to predict the pharmacokinetics of drugs as they passed through the tissues (Sung *et al*, 2010; Baker, 2011). Subsequently, Sonntag *et al* (2010) created a chip comprising of multi-micro-organoids that supported cultures of brain, bone marrow and liver however, in this instance the organs did not interact, as fluid did not flow between chambers. Whilst, Imura *et al* (2010) created a device which contained cell cultures of liver, intestine and breast cancer to evaluate drug interactions, in a manner similar to the work by Sin *et al* (2001). The aforementioned studies indicate that a potential for body-on-a-chip exists, which may have a role to play in not only better understanding cell-to-cell interaction, but more importantly perhaps, pharmacokinetics and pharmacodynamics which could be utilised in drug development. Furthermore, integration of body-on-a-chip and lab-on-a-chip could increase the viability of point-of-care diagnostics (van der Meer and van den Berg, 2012).

1.3.4 Advantages of Microfluidics – Reagents

Microfluidics overcomes the problems faced with more traditional techniques thanks to a range of features that cannot be achieved in more traditional cell culture methods. One of the predominant features which provides such benefit is the size of the structures in use. Whilst traditional methods utilise multi-well microtiter plates that over the assays duration use relatively large volumes of reagents and cellular matter (Luo *et al*, 2008). The channels in microfluidic chips are typically 10 – 100µm in size (McDonald *et al*, 2000) and utilise fluid volumes of 10^{-9} to 10^{-18} litres (Whitesides 2006; Henares *et al*, 2008). Furthermore, the advantage of using less reagent is the reduction in both waste and cost of the overall assay (McDonald *et al*, 2000). This design therefore creates a large surface area to volume ratio, which subsequently increases the rate of diffusion and thus reduces the length of time taken to complete an analysis (Henares *et al*, 2008). The design of the microfluidic system also provides a greater level of control over the reagents utilised. With small sample volumes the potential for uncontrolled mixing is reduced and occurs only as a result of diffusion (Chiu *et al*, 2017). This control is achieved as the movement of reagents through

the microfluidic system is via laminar flow, with the dominant force being the viscosity of the reagent (Henares *et al*, 2008). This results in a low Reynolds number, which consequently causes a reduction in the extent of turbulent forces, thus preventing excessive uncontrolled mixing and increasing precision within the experiment (Stone *et al*, 2004; Weibel and Whitesides, 2006) (Figure 1.8). The reduction in size enables experimental throughput to be increased at no additional cost, similarly the quantity of biological tissue required is also decreased thus both factors improve the amount of data which can be collected in comparison to more traditional techniques (Zambon *et al*, 2015).

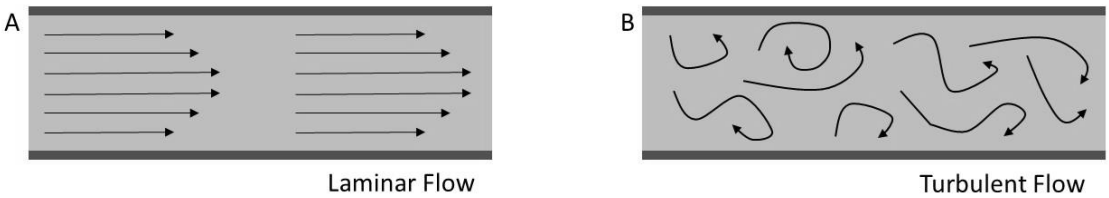

Figure 1.8 Laminar flow within a microfluidic system, flow achieved due to a low Reynolds number, enabling controlled mixing to occur via diffusion only (**A**). Turbulent flow within a microfluidic system, showing evidence of uncontrolled mixing and reduced precision within an experiment (**B**).

1.3.5 Challenges of Microfluidics – Reagents

The precision and control afforded by the development of microfluidic devices has potential connotations for many fields of study, in particular is the use of these devices within drug development however, the practicalities of using small sample volumes can hamper the usefulness of devices. Reduced reagent volumes and cell counts can influence the detection sensitivity of an assay, as there is a potential for pharmacological activity to alter and the effective concentration of a drug to change thus the outcome of a clinical trial may differ significantly to the data collected *in vitro* (Esch *et al*, 2015). Furthermore, the reduced scale of assays in microfluidic devices means that comparisons of results from a study, with previously published data of a similar study using conventional techniques, is problematic due to the variations in the data collected. The performance of traditional assays on microfluidic devices may also be hampered by availability of equipment that is able to accurately deliver volumes in the nanolitre range, compared to the conventional

microlitre volumes, potentially resulting in wastage of remaining reagents (Duncombe *et al*, 2015). Reduced reagent volumes also poses a problem with drying of samples, as evaporation of media becomes more apparent when smaller volumes and gas permeable chips, such as poly(dimethylsiloxane) (PDMS), are utilised. Evaporation of media has the potential to alter the osmolarity and pH, which invariably could result in cell death. However, the use of continuous media flow through the device can overcome this issue effectively (Halldorsson *et al*, 2015).

1.3.6 Advantages of Microfluidics – Cellular Environment

This miniaturisation has other benefits for microfluidic device design as they can be created in a manner that recapitulates the environment of a tissue *in vivo* which traditional techniques cannot emulate (Esch *et al*, 2015) and in doing so overcomes some of the disadvantages of traditional culture methods. Traditional 2-dimensional (2D) cell cultures have advantages insofar as they generate vast quantities of generally inexpensive data however, this relative simplicity of cells cultured in a single monolayer means that cultures cannot support more complex tissue specific functions nor provide accurate representation of the manner in which drug interactions may occur (Bhatia and Ingber, 2014; Esch *et al*, 2015). Furthermore, cells *in vivo* tend to grow in 3-dimensions (3D) therefore multiple cell types are arranged alongside each other, which give rise to cell-to-cell interactions and spatial orientations which are not achievable in traditional 2D cell culture (Dawson *et al*, 2016b). To create a more realistic representation of the spatial orientation of cell *in vivo*, 3D culturing has been utilised. Cultures grown on hydrogels, extracellular matrix gels and spheroids aim to mimic the interactions between cells however, they lack the functionality observed *in vivo* due to lack of blood flow. Therefore interactions with cells outside those being cultured and often create difficulties in sample collection for analysis (Huh *et al*, 2010; Bhatia and Ingber, 2014; Dawson *et al*, 2016b). With these issues in mind, *ex vivo* tissue cultures have been trialled as alternatives to traditional 2D and 3D cultures. Whilst this maintains tissue architecture, the removal of related vasculature often results in early cell death and reduced viability therefore making its usefulness in disease or drug modelling less viable. However, the slice thickness generated as a result of precision cut tissue procedures does alleviate some viability issues as nutrient delivery can be maintained by continuous perfusion of culture media (Astolfi *et al*, 2016). Microfluidics provides a

mechanism to overcome these difficulties insofar as cells can be grown not only in 3D, through the use of membranes coated in extracellular matrix, as done in traditional 3D cell culturing, but multiple layers of cells can be grown with chambers or channels separated by porous membranes (Huh *et al*, 2010). This creates an environment that has the ability to replicate the same microarchitecture as the tissue, allows for the interaction between tissues as seen *in vivo* and provides similar biochemical and mechanical stimuli (Esch *et al*, 2015).

1.3.7 Microfluidics Extending Viability of Tissue Culture

The importance of maintaining tissue architecture and cell-to-cell interactions forms only a subsection of the capabilities of a microfluidic device. Further beneficial features of microfluidic devices include the continuous flow of reagents through the microfluidic system via a capillary vessel network, enabling these devices to replicate the natural environment of the cell or tissue under investigation, for example, thus these devices enable the perfusion rate *in vivo* to be mimicked *in vitro* (Shaw *et al*, 2011). Additionally, the inclusion of immune cells in the fluid flowing through the system provides an opportunity to observe the inflammatory response and action of neutrophils, due to an artificial bacterial infection, in manner that would be expected *in vivo* (Huh *et al*, 2010). Furthermore, the continuous flow also overcomes the issue of the potential build-up of waste and unused nutrients observed in traditional cell culturing (Kim *et al*, 2006) and aids in the prevention of early necrosis in the most central sections of the tissue (Zambon *et al*, 2015). In effect creating a mechanism of extracellular fluid management *in vitro* that is similar to the process of homeostasis that would normally occur *in vivo* (Kim *et al*, 2007). The potential to manage nutrient and waste levels *in vitro* within similar ranges to those observed *in vivo*, may enable tissue biopsies to remain viable on the microfluidic device for extended periods, thus giving greater flexibility for analysis (Shaw *et al*, 2011). Hattersley *et al* (2008) and van Midwoud *et al* (2009) demonstrated the use of precision-cut liver slices on a microfluidics platform could remain viable for a minimum of 24 hours, with Hattersley *et al* (2008) suggesting potential viability of approximately 70 hours. When analysed on the microfluidic device using traditional test methods for toxicology, metabolism and absorption, the results produced were comparable to those collected from multi-well plate analysis methods (Hattersley *et al*, 2008). Subsequently, tissue viability on a microfluidic

device has shown to extend beyond 3 days, Torisawa *et al* (2016) have utilised microfluidic devices to culture bone marrow, with cell viability after 4 to 7 days remaining similar to that observed using the typical culturing methods. Whilst Astolfi *et al* (2016) have maintained micro-dissected tumours samples viability for 8 days without tissue perfusion. Whilst extending viability provides additional time to study drug interactions within a tissue, this is often still insufficient to gain a full understanding of the effects of the compound being tested (Astolfi *et al*, 2016) (Table 1.5). However, given the limitations of using animal models for drug development, such as cost, length of time required to conduct trials and often suitability of the animal models utilised (Huh *et al*, 2010), microfluidic devices could provide a mechanism for long term cell and tissue culture and as a direct effect reducing the cost of pharmaceutical development.

Species/Tissue Utilised	**Time in Culture**	**Author**	**Paper**
Human head and neck squamous cell carcinoma (HNSCC)	48 hours	Bower *et al*, 2017	Maintenance of head and neck tumor on chip gateway to personalized treatment
	70 hours	Hattersley *et al*, 2012	A microfluidic system for testing the responses of head and neck squamous cell carcinoma tissue biopsies to treatment with chemotherapy drugs
	15 days	Carr *et al*, 2014	Analysis of radiation-induced cell death in HNSCC and rat liver maintained in microfluidic devices
Human heart	3 days	Qiao *et al*, 2018	Multiparametric slice culture platform for the investigation of human cardiac tissue physiology
Human pancreatic islets	150 min	Leoni *et al*, 2010	Functional MRI characterization of isolated human islet activation
Human ovary	8 days	Astolfi *et al*, 2016	Micro-dissected tumor tissues on chip an ex vivo method for drug testing and personalized therapy
Human ectocervix, endometrium, liver, fallopian tubes and ovaries	28 days	Xiao *et al*, 2017	A microfluidic culture model of the human reproductive tract and 28-day menstral cycle
Human skin	14 days	Wagner *et al*, 2013	A dynamic multi organ chip for long term cultivation and substance testing proven by 3D human liver and skin tissue co-culture
	28 days	Maschmeyer *et al*, 2015	A four-organ-chip for interconnected long-term co-culture of human

			intestine, liver, skin and kidney equivalents
Rat heart	3.5 hours	Cheah *et al*, 2010	Microfluidic perfusion system for maintaining viable heart tissue with real-time electrochemical monitoring of ROS
Rat liver	24 hours	van Midwoud *et al*, 2009	Microfluidic biochip for the perfusion of precision cut rat liver slices for metabolism and toxicology studies
	70 hours	Hattersley *et al*, 2008	Development of a microfluidic device for the maintenance and interrogation of viable tissue biopsies
	15 days	Carr *et al*, 2014	Analysis of radiation-induced cell death in HNSCC and rat liver maintained in microfluidic devices
Rat pancreatic islets	5 hours	Rountree *et al*, 2016	BaroFuse, a novel pressure-driven, adjustable-throughput perfusion system for tissue maintenance and assessment
Mouse adrenal gland	24 hours	Tedjo *et al*, 2018	Electrochemical biosensor system using a CMOS microelectrode array provides high spatially and temporally resolved images
Mouse aorta	24 hours	Wang *et al*, 2012	Polydimethylsiloxane embedded mouse aorta ex vivo perfusion model proof-of-concept study focusing on atherosclerosis
Mouse brain	90 min	Mauleon *et al*, 2013	Enhanced loading of Fura-2AM calcium indicator dye in adult rodent brain slices via a microfluidic oxygenator
	8 hours	Blake *et al*, 2010	A microfluidic brain slice perfusion chamber for multisite recording using penetrating electrodes
	5 days	Rambani *et al*, 2009	Culturing thick brain slices An interstitial 3D microperfusion system for enhanced viability
Mouse heart	3 days	Qiao *et al*, 2018	Multiparametric slice culture platform for the investigation of human cardiac tissue physiology
Mouse liver	5 hours	Rountree *et al*, 2016	BaroFuse, a novel pressure-driven, adjustable-throughput perfusion system for tissue maintenance and assessment
Mouse lymph node	3 hours	Catterton *et al*, 2018	User-defined local stimulation of live tissue through a movable microfluidic port
Mouse ovary and prostate	8 days	Astolfi *et al*, 2016	Micro-dissected tumor tissues on chip an ex vivo method for drug testing and personalized therapy

Mouse ectocervix, endometrium, liver, fallopian tubes and ovaries	28 days	Xiao *et al*, 2017	A microfluidic culture model of the human reproductive tract and 28-day menstral cycle
Mouse small intestine	1 – 5 days	Yissachar *et al*, 2017	An intestinal organ culture system uncovers a role for the nervous system in microbe-immune crosstalk
Dog and cat ovary	2 – 4 days	Nagashima *et al*, 2018	Evaluation of an ovary-on-a-chip in large mammalian models species specificity and influence of follicle isolation status

Table 1.5: Examples of published literature on tissue viability/culture time in microfluidic devices from January 2008 – January 2018, identifying variations in culture time and the types of tissue and species of origin used within each studies.

1.3.8 Recreating Cellular Interactions through Microfluidics

Microfluidic device development provides a suitable platform for more complex studies of tissue interactions not only between cells but also in relation to other mechanical and biochemical stimuli. The principles of organ-on-chips incorporate microenvironmental stimuli that are based on the functionality expressed by the organ in question. Using these principles, functional models of kidney, blood vessels, lung, liver, heart, retina, skin, intestine and pancreatic tissue have been successfully engineered on a miniature scale for use in microfluidic devices (van der Meer and van den Berg, 2012). Detailed herein is a brief overview of some of the engineered devices that are utilised to study the tissue and organ level functions. Tissue tumour biopsies embedded in microfluidic devices have demonstrated how small samples, particularly of rare tumours, can be optimised to enable parallel testing of multiple pharmaceutical compounds, thus effectively extending the number of compounds which may be identified as suitable for clinical trials (Astolfi *et al*, 2016). Pancreatic islets of Langerhans cultured on microfluidic devices, have been shown to survive for longer when compared to traditional cell culture and hold the potential for islet viability to be tested prior to transplantation as a mechanism to treat Type 1 diabetes (Silva *et al*, 2013). Skin biopsies cultured on microfluidic devices in an *ex vivo* manner have the possibility to maintain underlying skin architecture, in a manner unachievable *in vitro*, thus they provided an opportunity to create a model which better represents the *in vivo* nature of skin reactivity (Atac *et al*, 2013). Lymph node slices cultured *ex vivo* on

microfluidic devices overcome the simplicity of cell culture and complexity of *in vivo* testing by providing a mechanism to study functionality of specific areas of a lymph node, which are otherwise inaccessible. Thus providing potential areas within the lymph node that could be directly targeted for the treatment of inflammatory diseases (Ross *et al*, 2017). The creation of a microfluidic device with multiple access points to study e*x vivo* retina modelling utilising whole mice retinas, provided a new model which could precisely target specific areas of the tissue and effectively localise delivery of reagents. Subsequently this could be utilised in the study of innervation within ocular diseases whereby, specific nerves could be targeted (Dodson *et al*, 2015). Intestinal tissues cultured in microfluidic devices have utilised both *ex vivo* techniques via tissue slices and *in vitro* methods using 3D culture. *Ex vivo* modelling enabled nutrient flow and blood to be modelled on alternate sides of the device that can then be utilised to investigate intestinal disorders and therapies (Dawson *et al*, 2016a). Whilst *in vitro* growth of intestinal epithelial cells subjected to cyclic mechanical stress as experienced *in vivo* elongated and differentiated into villi, a process not observed in static cell culture, thus better recapitulating the environment of the intestine and providing a potential model to recreate intestinal diseases for subsequent therapy development (Kim *et al*, 2012; Kim and Ingber, 2013). The use of mechanical forces that replicate the shear force and cyclic strain within a microfluidic device, are beneficial in a range of organ models beyond the intestinal tract. For example, the use of whole mouse olfactory arteries with intact musculature attached reversibly to a microfluidic device, whilst being maintained in near *in vivo* conditions of temperature and pressure have been utilised to consider the role of calcium on vascular tone. However, the development of the aforementioned method has implication beyond the study of vascular tone, providing potential for vascular remodelling research and the study of vascular structure and function at both cellular and organ level (Yasotharan *et al*, 2015).

1.3.9 Recreating Respiratory Environments through Microfluidics

Similarly, research on lung tissue has extended to consider the role of mechanical forces on the models developed, although this has not been utilised in all lung studies. Benam *et al* (2015) lined a microchannel with lung epithelial cells exposed to air and media flow to create an air-liquid interface, the impact of the related sheer forces resulted in the differentiation of cells to form functioning cilia and associated cell types. This effect

replicated in both healthy and diseased cell lines, provides the potential to study inflammatory response of respiratory diseases in relation to changes inside the airways. The recapitulation of small airway response to cigarette smoke further supports the importance of creating a model that combines the breathing patterns observed *in vivo*, when simulating conditions *in vitro*. The introduction of an air liquid interface and a clinically relevant inhalation pattern, generates similar shear forces to those observed *in vivo*, resulting in the differentiation of airway epithelial cells into pseudostratified ciliated airway epithelial cells, which mimic those found in human airways. The ability to maintain the air liquid interface provided a better environment to observe the effects of cigarette chemicals on ciliary action and reduced the extent of variability in the observations made when cells are immersed in medium (Benam *et al*, 2016). Using a similarly designed device Huh *et al* (2007) demonstrated that the characteristic crackle observed as a sign in respiratory diseases occurs due to the combination of the formation, propagation and subsequent rupturing of a liquid plug in an occluded airway prior to the reopening of the airway. Furthermore, repetitive propagation and rupturing of liquid plugs resulted in cellular damage due to mechanical stress caused by the forward movement of the liquid plug. Evidence of mechanical stress generated in this manner could thus be associated with the cellular injury observed in respiratory diseases, potentially resulting in further aggravation and inflammation of the affected airways. Tavana *et al* (2011) subsequently confirmed this latter idea, with further investigation identifying the potential use of surfactants as a therapy to reduce lung damage. Breathing motion, replicated on a microfluidic device has been utilised to investigate pulmonary oedema and the effect of alveolar leakage on oxygen transportation.

Observations from the use of cyclic mechanical strain, to replicate breathing pattern and equivalent volume, identified this type of sheer force led to the activation of transient receptor potential cation channel subfamily V member 4 (TRPV4 ion channels). TRPV4 ion channels have been implicated in vascular leakage in lung tissue, thus identifying a potential target for therapeutic agents in the management of pulmonary oedema (Huh *et al*, 2012). Additionally, cyclic mechanical strain, has also being utilised to demonstrate that ventilation induced lung injury incurred as a direct result of mechanical ventilation in acute respiratory disease syndrome, is not as a direct result of the cyclic stretch caused by the

ventilation process. Whilst, lung injury due to ventilation has been precluded, this method could provide potential options for the development of new ventilation strategies (Douville *et al*, 2011). Utilising the aforementioned models Stucki *et al* (2015) have eliminated some of the issues related to accurately managing the pressure changes induced by the cyclic mechanical action generated in previous models, by designing a device comprised of a membrane to represent an alveoli epithelial monolayer and a second membrane to represent the diaphragm. In this device, the pressure exerted on the alveoli membrane is recreated through diaphragm movements in a manner more akin to *in vivo* respiration, as opposed to physical stretch being applied to the alveoli membrane. Furthermore, the study showed the importance of mechanical stress in increasing permeability of the alveoli epithelia layer, the level of inflammatory marker IL-8 released and extent of metabolic activity (Stucki *et al*, 2015). Given the capabilities of microfluidic devices to support a range of tissue and cell types in various formats, the potential of microfluidics as a platform for biological research is extensive and provides multiple opportunities for the creation of relevant human models on which pharmaceutical compounds can be tested prior to clinical trials (Tian *et al*, 2019).

1.4 Microfluidics in Immunological Assays

1.4.1 Disadvantages of Current Immunological Assays

Immunological assays have been in widespread use since the 1960s as a method of performing a range of analytical techniques for basic sciences, clinical and pharmaceutical need (Henares *et al*, 2008). Although, traditional immunological assays provide a range of clinically useful diagnostic tests, there are often complex and lengthy procedures involved before any useful diagnostics can take place. As a result, these assays have not been suitable for utilisation for point-of-care diagnostics in a clinical setting (Bhattacharyya and Klapperich, 2007). Additionally, the use of assays *in vitro* do not truly represent the processes that are occurring *in vivo* (Kim *et al*, 2007). Such disadvantages have resulted in the long-term investment and development in the miniaturisation of assays, to make point-of-care diagnostics more viable and to reduce cost of testing. Miniaturisation and creation of total chemical analysis systems in the early 1990s became the predecessor of the current research in microfluidics (Manz *et al*, 1992).

1.4.2 Utilisation of Microfluidic Devices for Assays

Microfluidic devices have functionality outside cell and tissue culturing, that provide potential for not only the creation of *ex vivo* models for pharmaceutical development but also provide the scope for personalised care through diagnostic at the point-of-care, using immunological assays. The current range of microfluidic devices available for this purpose are based on the use of either heterogeneous or homogeneous immunological assays (Ng *et al*, 2010). Microfluidics predominately utilises heterogeneous assays, which take the form of traditional immunological assays albeit on a miniaturised scale (Shaw *et* al, 2011). One variation of heterogeneous assay utilises the wall of the channel through the immobilisation of the antibody onto this aspect of the microfluidic device. Subsequent introduction of the sample into the microfluidic device then enables the immobilised antibodies to bind the antigens in the sample and the reaction to occur in the same manner as a traditional assay (Baldini *et al*, 2009; Yang *et al*, 2009; Tarn and Pamme, 2011). In order to perform the aforementioned assays, mechanisms to immobilise functional particles, typically antibodies, on to the wall or other solid surfaces in microfluidic devices need to be utilised. The methods most commonly utilised include passive absorption on to the surface of the device and the more complex but equally effective use of covalent bonding. Both are effective however, the strength of the bonds formed between the functional particle and the device surface are directly influenced by the chemistry of the material used for the device (Barbosa and Reis, 2017). To overcome immobilisation issues, alternative heterogeneous methods have been created, these use other solid objects, such as bead or pillars, within the channel to create a similar affect to wall-based assays, by trapping particles that can then be utilised in the reaction (Erickson and Li, 2004). Methods include the use of a physical barrier within the channel that allows functional particles to be trapped and then exposed to antigens and antibodies for reactions to be observed (Pereira *et al*, 2010). Alternatively, a barrier can be generated for example by a microvortex to selectively sort particles by size, with the optimal size being retained by the vortex action and unnecessary particles being stripped by washing (Sollier *et al*, 2014). Further options include the use of either magnetic or non-magnetic microbeads coated in an antibody, these are later immobilised within the microfluidic device so that reaction with the desired protein occurs (Ng *et al*, 2010).

1.4.3 Continuous Flow in Microfluidics

Less static methods are also utilised within microfluidic devices, for example exposure of the functional particle to a continuous flow of reagents (Hofmann *et al*, 2002), whilst the functional particle is manipulated and held in place through various methods such as magnetism, acoustic bubbles and electrical fields (Chen *et al*, 2016). An advantage which continuous flow confers is the removal of the inefficient nature of more traditional assays, such as the speed of binding due to limited replenishment of reagents (Hofmann *et al*, 2002), which can still exist even when traditional assays are scaled down for a microfluidic platform (Tarn and Pamme, 2011). Furthermore, continual flow provides additional advantages in that it is possible to simultaneously run a number of different assays on a single device. This is due to the design of the microfluidic platform with multiple channels coupled with the constant exchange of reagents and the range of assays available in this format. Having the option to multiplex assays reduces analysis time and thus makes it a more viable option as a point-of-care diagnostic tool (Henares *et al*, 2008; Mok *et al*, 2014). The use of continuous flow provides an opportunity to combine targeted delivery of a reagent, continual perfusion of a tissue and observation of an immunological assay. A microfluidic device comprised of three layers of chambers and channels, designed to study lymph node tissue provides an example of the combinations of different types of functionality provided by microfluidic devices. In the aforementioned device, a lymph node tissue slice is incorporated into a holding chamber under continuous perfusion of medium, the second and third layers then enabled localised chemical stimulation and observation via immunofluorescence (Ross *et al*, 2017), thus beginning to merge the differing functionalities of microfluidic devices.

1.4.4 Digital and Droplet Microfluidics

Other modification of immunological assay includes the use of digital and droplet microfluidics, electrostatic forces and pressurised flow to manipulate reagents and functional particles enabling assays to be conducted (Ng *et* al, 2010). Digital and droplet microfluidics utilise electrodes to manipulate droplets containing functional particles and reagents together to enable the assay to occur within a combined droplet (Guo *et al*, 2012). Once combined droplets are incubated as per the assay procedure, sorted based on relevant selection criteria and then broken to recover the content for subsequent analysis

as necessary (Mazutis *et al*, 2013). Droplet microfluidics has potential beyond the use of immunological assays, through the combination of 3D cell culture techniques and microfluidics to manipulate and culture cells within a droplet. Tumour cells held in alginate droplets have the capability to form spheroids that can subsequently be trapped within a microsieve and exposed to chemicals such as, pharmaceutical agents in order to analyse the toxicology of these compounds against the selected tumour cells (Yu *et al*, 2010). The use of droplet microfluidics to culture spheroids has additional advantages insofar as cells can be kept viable for a number of days on the device to enable a range of analysis to be conducted. Subsequently, after analysis has been completed on chip, disruption of the droplet can take place, resulting in the dissociation of cells within the spheroid, enabling them to be analysed off chip, through methods such as flow cytometry (Patra *et al*, 2016). Electrostatic forces enable reagent flow to be controlled via an electric field, in a manner similar to electrophoresis thus providing an ability to manage flow rate however, the properties of analytes have to be considered as these can lead to excessive heating and negatively affect the assay. Whilst, pressure flow systems use either positive pressure or vacuums to drive reagents through the device, this is more beneficial than electrostatic flow, as in pressure flow systems the effect of analyte properties is negligible (Ng *et al*, 2010). Of the aforementioned methods, digital and droplet microfluidics and continuous flow provide the greatest scope for the development of point-of-care diagnostics, as they remove the elongated reagent change and wash times observed in the wall-based and trapped particle assays, thus increasing speed of analysis and usefulness within clinical diagnosis (Tarn and Pamme, 2011). Additionally, the small volumes of reagents not only reduce costs but also the extent of background noise and the total surface area available for reactions is significantly increased, thus providing a beneficial platform to perform a range of immunoassays on (Guo *et al*, 2012).

1.4.5 Homogenous Assays in Microfluidics

The variation of homogeneous assays used in microfluidics is more limited as the nature of the assay being carried out in solution means they can have lower sensitivity than heterogeneous assays, this therefore often necessitates that reagent concentrations are increased prior to the assay being run (Lin *et al*, 2010). This has the potential to be problematic during pharmaceutical development, as alterations to pharmacological activity

could have negative connotations when pharmaceutical compounds are tested in clinical trials (Esch *et al*, 2015), thus these effects need to be negated if these devices are to be widely utilised. However, homogenous assays offer some benefits over heterogeneous assays in that they are better suited to electrophoresis based assays and offer a greater potential for multiplexing (Lin *et al*, 2010). For example, capillary electrophoresis enables bound and unbound antibodies in solution to be differentiated by molecular weight and electrophoretic properties (Ng *et al*, 2010). Whilst fluorescence assays enable the visual detection of protein interactions as they occur in solution. Furthermore, with fluorescence assays there is the additional benefit that reagent volumes can be reduced to level unachievable in standard microtiter plate analysis as the effects of evaporation is less pronounced in miniaturised assays. However, other constraints need to be considered such as the complexities of simultaneously screening droplets and the nature of reagent delivery which invariably makes the use of these assays more complex (Cheow *et al*, 2014).

1.5 Working Hypothesis

The role of TRP channels and P2X receptors in acute cough in response to respiratory tract infections is not fully understood. Current evidence indicates that the TRPV4 – ATP – P2X3 pathway may play a role in the activation of cough, with blockage of P2X3 receptors reducing cough frequency in chronic cough patients. However, the exact mechanism still remains elusive, thus a part of this thesis will be focused on the development of a model which could be utilised to investigate this interaction *in* vitro. In addition, infection with human rhinovirus (hRV) is linked to not only acute cough but also airway inflammation and hypersensitivity. However, the mechanisms that lead to hypersensitivity are still unclear due to the lack of suitable animal models which can be used to study different aspects of hRV pathogenesis, thus there is a need to develop a model which combines both *in vitro* and *in vivo* techniques and procedures. The use of human PCLS therefore provides an opportunity to create a human lung model which more appropriately represents the *in vivo* environment, whilst allowing *in vitro* testing to be conducted, thus this forms the second part of this thesis. The overall hypothesis is hRV infection will alter expression of channels and receptors which are known to be involved in cough and airway inflammation, causing lung tissue to become hyperresponsive to cough and bronchoconstrictive agents. This thesis will focus on the development of three models (*in vitro* co-culture, *ex vivo* PCLS and microfluidic devices to encompass the two aforementioned models) which can be used to characterise the role of hRV in cough and airway inflammation.

1.6 Aims

1. Optimise a co-culture model utilising A549 or Beas-2b and 1321N1 P2X3 cell lines to investigate interactions between the cell lines
2. Investigate the effect of human rhinovirus 16 (RV16) on A549 and Beas-2b cell lines on cell cytotoxicity and viability
3. Optimise the use of PCLS technique on human lung tissue and determine maximum culture period PCLS remains viability
4. Investigate the effect that RV16 infection has on cough and airway inflammation through the use of the PCLS model
5. Create a lung-on-a-chip model which utilises PCLS and cell culture

2 Chapter 2: Optimisation of a Human Cellular Model of the Airways to Study Human Rhinovirus Infection

2.1 Introduction

As a major causative agent of the common cold, hRV infections are instigated in approximately 50% of URTIs (Lee *et al*, 2012) and have been shown to play a role in both LTRIs (Papadopoulos and Johnston, 2000; Aponte *et al*, 2015) and exacerbations of underlying respiratory conditions (Griego *et al*, 2000; Jacobs *et al*, 2013). Whilst typically self-limiting and short lived, hRV has long been recognised for its significant morbidity levels in both adults and children. As such the economic burden of hRV infections is substantial, specifically in terms of healthcare costs and loss of productivity (Fendrick *et al*, 2003; Nichol *et al*, 2005). However, for some individuals symptoms do not resolve quickly and the most common symptom of hRV infection, a cough, can persist beyond eight weeks and become chronic (Braman, 2006). This being said, the precise mechanism that elicits the cough response is still unclear. Multiple causes of cough and associated airway inflammation have been proposed in an attempt to find the elusive mechanism(s), which cause this symptom in hRV infections (Atkinson *et al*, 2016). A potential step in the cough mechanism pathway could be via neuromodulation, whereby P2X receptors respond to ATP released by TRPV4 receptors, leading to downstream activation of afferent nerves fibres (Song and Morice, 2017). The role of P2X receptors have been further implicated in the cough mechanism pathway through a phase II clinical trial, which demonstrated a 75% reduction in daytime cough frequency in patients prescribed a P2X3 antagonist (Abdulqawi *et al*, 2015).

Given the noticeable interest in the study of the TRPV4 – ATP – P2X3 pathway and its role in the cough mechanism, this chapter aims to optimise a co-culture calcium signalling model utilising airway epithelial cells and astrocytes transfected with P2X3, to mimic neurones, to investigate interactions between the different receptors expressed on these cell lines. Whilst not investigated here, the long term aim of this model is to utilise the method to study the interactions of TRPV4 and P2X3 in hRV post-viral cough. Thus, this chapter also aims to investigate the effect of RV16 on cell cytotoxicity and viability in airway epithelial cells. This will provide a baseline to for the human PCLS model discussed in chapter 3 and for future study of the post-viral cough using the co-culture model.

2.2 Methods

2.2.1 Cell Lines

2.2.1.1 1321N1 P2X3

1321N1 human brain astrocytoma cells, transfected with a P2X3 receptor, henceforth referred to as 1N1 P2X3 cells, gifted from Dr Samuel Fountain (University of East Anglia), were cultured in 75cm^2 Cellstar® cell culture flasks (Griener Bio-one, Gloucestershire, UK) with 10ml of Dulbecco Modified Eagle Medium (DMEM) (Lonzo, Fisher Scientific, Leicestershire, UK) containing 10% fetal bovine serum (FBS) (Gibco, Leicestershire, UK), penicillin (100U/ml) – streptomycin (100µg/ml) (Fisher Scientific) and 2mM L-Glutamine (Gibco), henceforth referred to as complete DMEM. In additional to the complete DMEM cells were cultured with the antibiotic supplement puromycin dihydrochloride (1µg/ml) (Sigma-Aldrich, Dorset, UK) to ensure only cells carrying the conferred antibiotic resistance gene introduced during transfection were retained throughout the culture process (Bothwell *et al*, 2018). Cells were used between passages 10 – 50.

2.2.1.2 1321N1 Wild Type (WT)

1321N1 human brain astrocytoma cells, henceforth referred to as 1N1 WT cells, gifted from Dr Samuel Fountain (University of East Anglia). Cells were cultured in 75cm^2 Cellstar® cell culture flasks with 10ml of complete DMEM. Cells were used between passages 10 – 50.

2.2.1.3 A549 Cell Line

A549 human lung epithelial cells were purchased from Public Health England. Cells were cultured in 75cm^2 Cellstar® cell culture flasks with 10ml of complete DMEM. Cells were used between passages 10 – 50.

2.2.1.4 Beas-2b

Beas-2b human bronchial epithelial cells were purchased from Public Health England. Cells were cultured in 75cm^2 Cell+ cell culture flasks (Sarstedt, Leicestershire, UK) with 10ml of serum free LHC-9 Medium (Fisher Scientific) to maintain the cells in their undifferentiated

state. Cells were differentiated through the addition of 10% FBS in the media, differentiated cells were cultured in 10ml of complete DMEM in 75cm^2 Cellstar® cell culture flasks. Cells were used between passages 10 – 50.

2.2.1.5 HeLa Ohio

HeLa Ohio human cervix carcinoma cells were purchased from Public Health England. Cells were cultured in 75cm^2 Cellstar® cell culture flasks with 10ml of complete DMEM. Cells were used between passages 10 – 50.

2.2.1.6 Kwik-Diff™ Staining for Normal Cell Morphology

Normal cellular morphology of 1N1 P2X3, Beas-2b and A549 cells was shown using a differential staining kit (Shandon™ Kwik-Diff™, Fisher Scientific). Cells were seeded in 6 well plates (Greiner Bio-one) at a seeding density of 5x10^5 cells in 2ml of complete DMEM and cultured for 24 hours to reach approximately 80% confluency. To enabling staining of the cells, media was completely removed, the cells were washed 3 times with 1ml of 1x phosphate buffered saline (PBS) (Fisher Scientific) and the excess removed from the well. Cells were fixed with 1ml of Kwik-Diff™ reagent 1 (methanol) for 10 minutes, the excess removed and the well dried. Cells were stained with 1ml of Kwik-Diff™ reagent 2 (eosin) for 10 minutes and counterstained with 1ml of Kwik-Diff™ reagent 3 (methylene blue) for 10 seconds, the excess was removed and the well dried between each step. Finally cells were washed with 1ml of distilled water (dH_2O) until all excess stain was removed and left to completely dry prior to imaging using light microscopy.

2.2.2 Culturing of Cell Lines

2.2.2.1 Reviving Frozen Cell Lines

Cells were stored in the gas phase of liquid nitrogen until required. When needed cells were rapidly thawed at 37°C and seeded into 75cm^2 flasks containing 9ml complete DMEM, plus additional supplements as required, at a seeding density of 20,000cells/cm^2. Prior to seeding Beas-2b cells at 20,000cells/cm^2, thawed cells were transferred to a centrifuge

tube with 5ml of warmed serum free LHC-9 media, centrifuged at 150x g for 3 minutes, the supernatant discarded and the cell pellet resuspended in 10ml of serum free LHC-9 media. Cells were incubated at 37°C in 5% CO_2 until 70 – 80% confluent.

2.2.2.2 Sub-culturing of Confluent Cell Lines

Confluent cells were washed with 5ml of sterile 1x PBS, aspirated and incubated at 37°C with 2ml of HEPES buffered saline with ethylenediaminetetraacetic acid (EDTA) (HBSE) (see appendix A1). 1N1 WT, 1N1 P2X3 and HeLa Ohio cells were incubated for a period of 2 minutes until no cells remained adhered to the flask. A549 cells were incubated for 10 minutes due to the cells being more strongly adhered thus requiring longer to dissociate from the flask. Dissociated cells were aspirated from the flask and 3ml of complete DMEM added to quench the HBSE. Cell suspensions were centrifuged at 300x g for 5 minutes, the supernatant discarded and the cell pellet resuspended in 1ml of complete DMEM, cell count was determined by haemocytometry (see 2.2.2.3). For Beas-2b cells, the above protocol was followed with complete DMEM being substituted for serum free LHC-9 media for undifferentiated cells, for all Beas-2b experiments 5ml of HBSE and a 10 minute incubation was utilised, the HBSE was neutralised with 10ml of LHC-9 or DMEM prior to a centrifugation step of 300x g for 5 minutes.

2.2.2.3 Cell Counting and Viability

Cell suspensions were mixed with 0.4% Trypan Blue solution (Fisher Scientific) at a 1:1 ratio and applied to a haemocytometer. Cells were visualised by light microscopy with cell viability being determined by presence or absence of cytoplasmic staining, unviable cells stain blue whilst viable cells remain unstained as membrane integrity ensure the dye is excluded from the cells (Strober, 2015). Cell counts were determined by counting the number of viable and unviable cells in 5 independent 1mm x 1mm x 0.1mm squares on the haemocytometer. An average of the 5 squares was taken, this was multiplied by 2 to account for the Trypan Blue dilution and subsequently converted to give number of cells/ml by multiplying by $1x10^4$. Once viable cell count was determined further dilutions were made using complete DMEM to provide a suitable cell counts for passaging of cell lines or suitable seeding densities for assays.

2.2.2.4 Storage of frozen cell lines

Cell lines with the exception of Beas-2b cells were frozen down at a density of $2x10^6$ in FBS and 10% dimethylsulfoxide (DMSO) (Fisher Scientific) using an isopropanol chamber (Fisher Scientific), with a temperature decrease rate of 1°C per hour. Cells were left at -80°C overnight before transfer to gas phase liquid nitrogen for long term storage. Beas-2b cells were frozen in the same manner however, the freezing media used comprised of a 1:1 ratio of fresh LHC-9 media and conditioned LHC-9 media with 10% DMSO. Conditioned LHC-9 media was collected between 24 – 48 hours after passaging of Beas-2b cells, centrifuged at 150x g for 5 minutes and the supernatant filtered using a 0.22µm filter (Fisher Scientific) before storing at -20°C for later use.

2.2.3 Methods for Characterisation of Cell Lines via Western Blot

2.2.3.1 Preparation of Cell Lysates for Western Blotting

A549 and Beas-2b were grown to near confluency in a $75cm^2$ flask and washed twice with ice cold 1x PBS to remove traces of complete DMEM. To each flask 1.5ml of ice cold 1x lysis buffer containing 1mM phenylmethylsulfonyl fluoride (PMSF) (Sigma-Aldrich) was added and incubated for 5 minutes on ice. Cells were scraped off the bottom of the flask and transferred to a 1.5ml centrifuge tube on ice. The lysate was sonicated at 24kHz using an UP200S ultrasonic processor (Hielscher, Teltow, Germany) for 30 seconds at 0.5 pulse cycle, 70% amplitude, chilled on ice and centrifuged for 10 minutes at 14,000x g maintained at 4°C throughout. Supernatant was retained and stored at -20°C until required.

2.2.3.2 Bicinchoninic Acid (BCA) Assay for Protein Quantification of Cell Lysates

Cell lysates were assayed to determine the protein concentration (μgml^{-1}) using a BCA assay (Fisher Scientific). To enable protein concentrations in cell lysates to be calculated a serial dilution of bovine serum albumin (BSA) (Fisher Scientific) in cell lysis buffer was performed to create protein standards between $2mgml^{-1}$ – $15.625\mu gml^{-1}$. 25µl of cell lysate, protein standard or lysis buffer as an absorbance blank was added to duplicate wells of a clear, flat bottomed 96 well plate (Sarstedt), to which 200µl of BCA working solution (50:1 ratio of BCA solution to copper sulphate) was added. The plate was mixed, incubated in the dark at

37°C for 30 minutes and absorbance was measured on a Tecan Infinite M200 multimode plate reader (Tecan Group Limited, Männedorf, Switzerland) at 562nm, each value was adjusted to account for the absorbance blank. Using the absorbance values generated from the serial dilution a standard curve was generated and used to determine the protein concentrations in the cell lysates. Cell lysates were diluted in 4x Laemmli buffer (see appendix A2) to given identical final protein concentrations. To reduce and denature the proteins in the cell lysates the samples were heated to 90°C for 8 minutes, cooled, centrifuged at 14000x g for 2 minutes and used either immediately or stored at -20°C for later use.

2.2.3.3 Sodium Dodecyl Sulphate Polyacrylamide Gel Electrophoresis (SDS-PAGE)

Cell lysates, positive controls and an EZ-Run™ prestained protein ladder (Fisher Scientific) were loaded into wells at a concentration of 50µg of protein and separated using a 10% SDS-polyacrylamide gel made in house (Table 2.1). Gels were run vertically in Bio-Rad electrophoresis units (Bio-Rad, Hertfordshire, UK), using 1x running buffer (see appendix A2) at 120V for 90 – 120 minutes until the dye front reached the bottom of the gel.

	3% Stacking Gel		**10% Resolving Gel**
H_2O	2.435ml	**H_2O**	3.2ml
30% Acrylamide	935µl	**30% Acrylamide**	2.65ml
Buffer 2 (see appendix A2)	935µl	**Buffer 1 (see appendix A2)**	2ml
10% APS	37.5µl	**10% APS**	37.5µl
TEMED	5µl	**TEMED**	2.65µl

Table 2.1 Reagent and volume per gel used to produce SDS-polyacrylamide gels for western blot analysis of cell lysates.

2.2.3.4 Transfer and Blocking

Proteins were transferred from the SDS-polyacrylamide gel to a midi sandwich polyvinylidene fluoride (PVDF) membrane (Bio-Rad) using a Trans-Blot® Turbo Transfer system (Bio-Rad) at 25V for 10 minutes. PVDF membranes were air dried for 1 hour,

reactivated with methanol for 10 minutes, rinsed with dH_2O and then blocked in 5% fat free milk solution made in tris-buffered saline with 0.1% tween (TBS-T 0.1%) for 1 hour.

2.2.3.5 Probing and Visualising

After blocking the PVDF membranes were incubated with primary antibodies (Table 2.2) made in TBS-T (0.1%) overnight at 4^{o}C, in the dark with gentle agitation on a seesaw rocker (Stuart^{TM}, Fisher Scientific) throughout. After removal of the primary antibodies, PVDF membranes were washed three times for 5 minutes in TBS-T (0.1%) in the dark with gentle agitation. Fluorescent secondary antibodies (Table 2.3) in TBS-T (0.1%) were applied to the PVDF membranes and incubated for 1 hour in the dark with gentle agitation followed by three washes for 5 minutes in TBS-T (0.1%) in the dark with gentle agitation. PVDF membranes were rinsed with tris-buffered saline (TBS) (see appendix A2) and visualised with Li-cor Odyssey CLx (Li-cor, Nebraska, USA) using manufacturer pre-set channel setting at 700 and 800nm wavelengths. PVDF membranes were probed a second time for remaining targets using the method outlined above.

Antibody	**Protein Size**	**Dilution**	**Animal Raised In**	**1st/2nd Probe**	**Supplier**
P2X3	55kDa	1:500	Mouse	1st	Santa Cruz Biotechnologies Inc. (Wembley, UK)
α-Tubulin	55kDa				
TRPV4	100kDa		Rabbit	2nd	Abcam (Cambridge, UK)

Table 2.2 Details of primary antibodies utilised in western blot to probe for desired targets in A549 and Beas-2b cell lines as part of the characterisation process.

Antibody	**Dilution**	**Animal Raised In**	**Supplier**
Anti-Mouse	1:15000	Goat	Li-cor
Anti-Rabbit			

Table 2.3 Details of secondary antibodies utilised in western blot to fluorescently visualise primary antibodies bound to desired targets in A549 and Beas-2b cell lines as part of the characterisation process.

2.2.4 Methods for Characterisation of Cell Lines via RNA Extraction

2.2.4.1 RNA Extraction from Cell Lines

A549 and Beas-2b were grown to near confluency in a 75cm^2 flask and washed once with ice cold 1x PBS to remove traces of complete DMEM. The PBS was aspirated, replaced with 1ml of Trizol (Fisher Scientific), the flask scraped briefly and the cell lysate transferred to a 1.5ml centrifuge tube. The tube was left to sit at room temperature for 5 minutes prior to the addition of 250µl chloroform (Sigma Aldrich), shaken vigorously for 15 seconds and left to sit for a further 5 minutes at room temperature. The lysate was centrifuged at 10,000rpm for 5 minutes and the aqueous phase transferred to a clean 1.5ml centrifuge tube. To this 550µl of isopropanol (Sigma Aldrich) was added, left to sit for 5 minutes, centrifuged at 14,000rpm for 20 minutes and placed on ice for the remainder of the procedure. The isopropanol was decanted and 1ml of 75% ethanol (Fisher Scientific) in diethylpyrocarbonate (DEPC) treated H_2O (Fisher Scientific) added, the pellet gently washed and centrifuged at 9500rpm for 5 minutes. The ethanol was decanted and the pellet air dried until a small meniscus of ethanol remained. The RNA pellet was resuspended in 40µl of DEPC treated H_2O and retained on ice for immediate preparation for cDNA synthesis.

2.2.4.2 Measurement of RNA Quantity in Sample

RNA concentrations in cell lysates were measured using a Thermo Fisher NanoDrop Lite Spectrophotometer (Fisher Scientific) at 260nm. Sample purity was established by obtaining a 260/280 ratio, with ideal ratio being >1.8 and lower suggesting partial degradation (Fleige and Pfaffl, 2006). Prior to obtaining RNA concentration 2µl of DEPC treated H_2O was applied to the optical measurement surface to obtain a blank measurement. The same volume of cell lysate was applied to the optical measurement surface to obtain a final RNA concentration in ng/µl and a 260/280 ratio.

2.2.4.3 cDNA Synthesis from RNA

Extracted RNA was converted to cDNA (>2µg) for further analysis using RevertAid Reverse Transcriptase (Fisher Scientific). Reagents were added to 0.2ml PCR tubes in the order

specified in table 2.4, with a variable volume of RNA to ensure the quantity of cDNA required was obtained. Additionally, control tubes were also made without RevertAid Reverse Transcriptase. cDNA was produced using the thermal cycling conditions specified in table 2.5.

Reagent	**Volume**	**Final Concentration**
Template RNA	-	2µg
Random hexamer primers	1µl	-
Nuclease-free H_2O	<14.5µl	-
10mM deoxynucleoside triphosphate (dNTP) mix	1µl	10mM
5x reaction buffer (50mM Dithiothreitol (DTT), 250mM Tris-HCl (pH8.3), 20mM $MgCl_2$, 250mM KCl)	4µl	-
RiboLock RNase inhibitor	0.5µl	200U/µl
RevertAid reverse transcriptase	1µl	200U/µl
Total	25µl	-

Table 2.4 Reagents utilised to synthesis cDNA from RNA isolated from A549 and Beas-2b cell lines as part of characterisation process.

Process	**Temperature (°C)**	**Time (min)**
Activation	-	-
Anneal	50	30
Extension	85	5

Table 2.5 Thermal cycling conditions used to synthesis cDNA.

2.2.4.4 Reverse Transcription Polymerase Chain Reaction (RT-PCR)

cDNA was amplified using the primers specified in table 2.6 alongside DreamTaq DNA polymerase (Fisher Scientific). The primers were designed in house, using NCBI primer-BLAST with specific requirement of melting temperature 50 – 60°C, GC<60% and intron spanning (Atkinson, 2019) Reagents were added to 0.2ml PCR tubes in the order specified in table 2.7, using varying volumes of cDNA (2µg) to enable amplification of the required gene sequence. Additionally, control tubes were also made without DreamTaq DNA polymerase. Amplification was achieved using the thermal cycling conditions specified in table 2.8.

Primer	Direction	Sequence	Designed
TRPV4	Forward	5'-CTGAGACCCTCCCTGGACTA-3'	In house (Atkinson, 2020)
	Reverse	5'-GAGAAGACACTGCTTGCTCAGA-3'	
P2X3	Forward	5'-ACCATCGGGATCATCAACCG-3'	In house (Atkinson, 2020)
	Reverse	5'-CATGATGGGCGTTTCCACTG-3'	
β-Actin	Forward	5'-CGTGGGCCGCCCTAGGCACCA-3'	Ramachandran, Morice and Compton, 2006
	Reverse	5'-TTGGCCTTAGGGTTCAGGGGG-5'	

Table 2.6 Primers utilised in RT-PCR to amplify cDNA synthesised from A549 and Beas-2b cells as part of the characterisation process.

Reagent	Volume	Final Concentration
Template cDNA	0.5 – 20.375µl	2µg
Nuclease-free H_2O	<20.375µl	-
Forward primer	0.5µl	-
Reverse primer	0.5µl	-
10mM dNTP mix	0.5µl	10mM
10x DreamTaq green reaction buffer (manufacturers formula containing 20mM $MgCl_2$)	2.5µl	
DreamTaq DNA polymerase	0.125µl	5U/µl
Total	25µl	-

Table 2.7 Reagents utilised in RT-PCR to amplify cDNA synthesised from A549 and Beas-2b cell lines as part of characterisation process.

Stage	Step	Number of Cycles	Temperature (°C)	Time (sec)
	Preheat lid	-	105	-
1	Initial denaturation	1	95	180
2	Denaturation	35	95	30
	Annealing		55	30
	Extension		72	60
3	Final Extension	1	72	600
	Hold	-	10	∞

Table 2.8 Thermal cycling conditions used in RT-PCR to amplify cDNA.

2.2.4.5 Agarose Gel Electrophoresis

A 1.3% agarose gel was made using 1x Tris-acetate-EDTA (TAE) buffer (see appendix A1) and stained with Midori Green DNA stain (Geneflow, Litchfield, UK) at a 1:10 stain to sample ratio. Amplified cDNA, negative controls and a 1kb DNA ladder were loaded into the agarose gel under 1x TAE buffer and electrophoresed at 110V for approximately 45 minutes. The gel was visualised under blue LED light (wavelength 460 – 490nm) on a Molecular Imager VersaDoc™ MP 4000 (Bio-Rad).

2.2.5 Assays Utilising Cell Lines

2.2.5.1 Calcium Signalling Single Cell Lines

Calcium signalling was conducted using the Invitrogen™ Molecular Probes™ Fluo-4 Direct™ Calcium Assay Kit (Fisher Scientific). For single cell line cultures, cells were grown to 80 – 90% confluency (as per manufacturer's instructions) in 200µl of phenol red free, complete DMEM (Gibco) in flat, black, clear bottomed 96 well plates (Griener Bio-one). Once confluent, 150µl of media was removed from the wells, 50µl of assay mix (made to manufacturer's instruction, with the addition of 200µl of probenecid added per 10ml of assay mixture) was added to each well and the plate incubated for a total of 60 minutes (30 minutes at 37°C and 30 minutes at room temperature) in the dark. Cells were stimulated with the desired agonist or antagonist diluted in phenol red free media (time varied depending on experiment) and the relative fluorescence measured at 485nm excitation and 535nm emission on a Perkin Elmer Victor X3 multimode plate reader (Perkin Elmer, Buckinghamshire, UK) every second for 120 seconds. The cells were subsequently exposed to 2µM A23187 Calcium Ionophore (Sigma-Aldrich) diluted in 1x Hank's buffered saline solution (HBSS) (Gibco) to achieve a measurement of maximal relative fluorescence over a 120 second period. Data was presented as a percentage response rate to agonist, calculated based on the maximal response to A23187 using the following equation:

$$[(Ca^{2+})_i] = \frac{\Delta RFU_{agonist}}{\Delta RFU_{A23187}} \times 100$$

Measurements of each conditions were run in triplicate on a three separate occasions to enable statistical analysis to be conducted.

2.2.5.2 Calcium Signalling Mixed Culture

This method was used alongside the co-culture method to enable further consideration of the TRPV4 – ATP – P2X3 pathway. The rationale for utilising this method alongside the co-culture method to was see if there was any difference in the extent of calcium signalling measured. The aim of this method was to identify whether stimulating A549 or Beas-2b cells with the TRPV4 agonist GSK101 to release ATP, could in turn stimulate 1N1 P2X3 cells, thus creating a larger calcium signalling response than when cells cultured as individual cell lines. For this reason cells were cultured either individually (as single cell lines) or in the same well (mixed culture of airway epithelial cells and astrocyte cells), with identical seeding densities utilised in both individual and mixed wells. Owing to similar doubling times (22, 24 and 26 hours for A549, 1N1 P2X3 and Beas-2b cells respectively), all cell lines were seeded at the same initial seeding density for 52 hours until approximately 80 – 90% confluency was achieved in mixed wells. Lower levels of confluency were evident in wells were cell lines had been cultured individually as a consequence of the use of same seeding densities throughout, this subsequently enabled calcium signalling response rates in single cell cultures to be combined to identify if any additive effect could be identified when cell lines were grown together.

Calcium signalling was conducted as outlined in 2.2.5.1 with mixed cell lines cultured in a single well. Equal seeding densities of A549 or Beas-2b cells and 1N1 P2X3 cells were seeded in flat, black, clear bottomed 96 well plates in 200µl of phenol red free, complete DMEM and grown to 80 – 90% confluency (as per manufacturer's instructions for calcium signalling assay kit) over a 52 hour period. Seeding equal densities ensured an approximately 1:1 ratio of A549 or Beas-2b to 1N1 P2X3 cells were achieved in each well. Cells were with stimulated with the TRPV4 agonist GSK1016790a (henceforth referred to as GSK101) (Sigma Aldrich) at varying concentration and the relative fluorescence measured as previously described.

2.2.5.3 ATP Assay Single Cell Lines

Measurements of ATP were made using the Invitrogen™ Molecular Probes™ ATP Determination Kit (A22066). Cells were grown to 80 – 90% confluency in clear, flat

bottomed 96 well plates prior to stimulation with the desired agonist. Prior to measuring samples, a standard curve was created for each individual experiment due to variations in level of luminescence measured. To create a standard curve 10µl of known ATP concentrations, ranging from 0.1nM to 3000nM was added to 100µl of assay mixture (made to manufacturer's instructions) in a white, flat bottomed 96 well plate (Greiner Bio-one). Measurements of luminescence were made at wavelength 560nm using a Perkin Elmer Victor X3 multimode plate reader three times, the background readings deducted and average values plotted as a standard curve (Figure 2.1). The production of a standard curve enabled luminescence values measured during the ATP assay on cells to be converted into an ATP concentration, using the value given for the gradient of the slope of the graph.

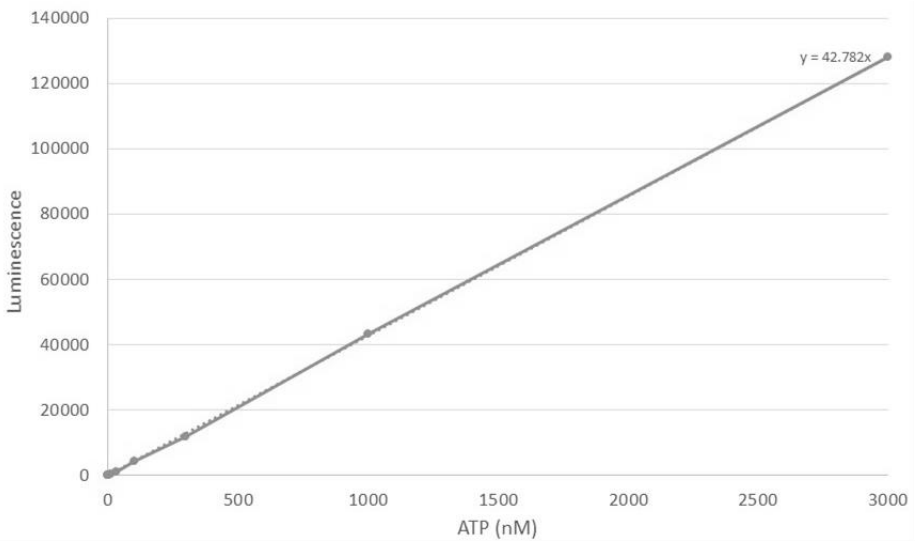

Figure 2.1 An example standard curve produced using the ATP Determination Kit

To measure extracellular ATP released from the A549 and Beas-2b cells lines 100µl of complete DMEM was left on the cells, to which 100µl of the TRPV4 agonist GSK101 in complete DMEM was added at the desired concentration to stimulate the cells, a 10µl supernatant sample was taken immediately and then at 60 second intervals for a period of 10 minutes, with the luminescence value in each well read in triplicate and adjusted for the background luminescence. Luminescence values were converted to ATP values by dividing the value measured by the plate reader by the value given by the gradient of the slope. Measurements were taken from either duplicate or triplicate wells on three separate occasions to enable statistical analysis to be conducted.

2.2.6 Measurements of Tight Junction Formation

2.2.6.1 Transepithelial Electrical Resistance (TEER) Measurements

TEER measurements were taken of A549, Beas-2b and 1N1 P2X3 cells cultured on 24 well hanging inserts (Thincert™) with 0.4µm pore size and transparent polyethylene terephthalate (PET) membrane (Greiner Bio-one) over a period of 14 days for A549 and 1N1 P2X3 cells and for up to 35 days for Beas-2b cells, with media changes taking place every 48 – 72 hours. Cells were seeded at an initial density of $5x10^4$ on the apical surface of the membrane (Figure 2.2a) with 200µl of complete DMEM in the insert and 600µl of complete DMEM in the well. These volumes were increased to 500µl of complete DMEM in the insert and 1000µl of complete DMEM in the well for Beas-2b cells to allow for successful measurements.

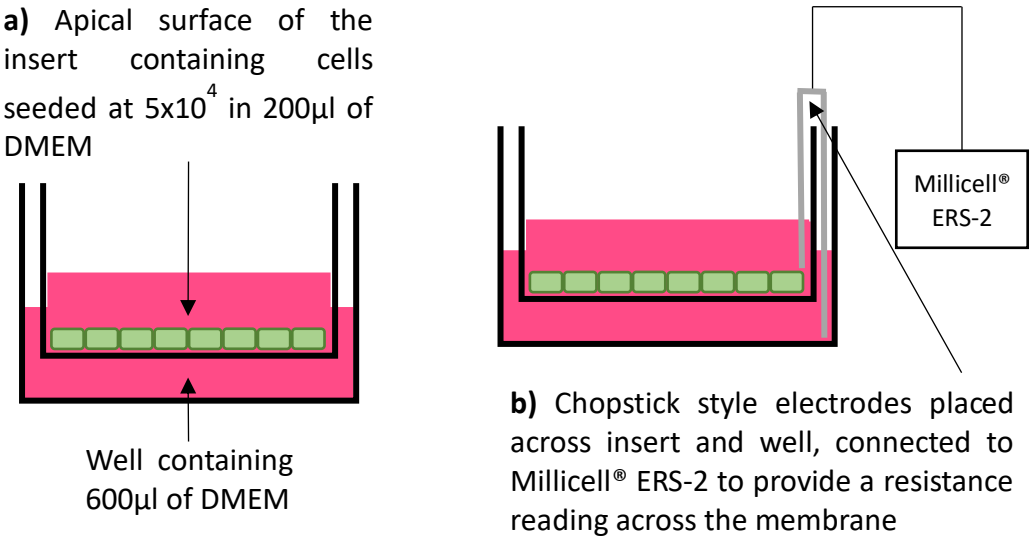

Figure 2.2 Representation of the cell culture arrangement used for the measurement of electrical resistance across the membrane (**A**) and the positioning of the chopstick style electrodes used to measure electrical resistance across the membrane (**B**).

Cells were left for 24 hours to completely adhere and enable them to complete one cell cycle (Bible and Kaufmann, 1996; Haniu *et al*, 2013). Before commencing any resistance readings a number of steps were taken to reduce variations in resistance measurements across the membrane. The diameter of the membrane can increase the likelihood of

fluctuations in readings, with larger diameters (>24mm) preventing uniform distributed of current across the membrane (Srinivasan *et al*, 2015), thus by using 24 well Thincerts™ the diameter was reduced to approximately 10mm therefore aiding in the stability of reading. In addition, the cells and media were allowed to adjust to room temperature for approximately 30 minutes to reduce any variation in the resistance due to temperature fluctuations (Srinivasan *et al*, 2015). TEER measurements were taken using a Millicell® Electrical Resistance System (ERS-2) (Merck Millipore, Hertfordshire, UK), the electrode was placed with the longer arm inside the well and the short arm inside the insert away from the wall of the well (Figure 2.2b). The resistance measurement was allowed to stabilise before repeating the process in a further two positions around the well. Measurements were taken using a blank insert containing the same volumes of complete media, warmed to room temperature. Blank values were averaged, subtracted from each of the average values from cell containing wells and multiplied by the surface area of the insert to give resistance in $\Omega.cm^2$. The entire process was repeated every 24 hours thereafter for the entire culture period. The above process was repeated for A549 and Beas-2b cells with the introduction of an air-liquid interface (ALI) after 72 or 96 hours respectively by complete removal of the media contained within the insert, this length of time ensured cells had sufficient time to form a confluent monolayer. In order to take a resistance measurement, pre-warmed media was reapplied onto the cells for 10 minutes prior to sampling, giving sufficient time for cells to stabilise and ensuring an accurate measurement could be taken. Measurements were taken from triplicate wells on three separate occasions to enable statistical analysis to be conducted.

2.2.6.2 Fluorescein Exclusion Assay

A549 cells were seeded on 6 well Thincert™, 0.4µm pore size, transparent PET membrane (Griener Bio-one) at a density of $5x10^5$ cells and cultured over a period of 7 days, with media changes every 72 hours. For Beas-2b cells the culture period was extended to 14 days with media changes every 48 hours and included the introduction of an ALI after 4 days in culture. Based on TEER values previously recorded time points of 4 days, 7 days and 14 days were chosen to measure the extent of fluorescein movement across the membrane, similarly these measurements influenced the time points chosen to introduce an ALI. To remove any excess autofluorescence created through the use of complete DMEM (Babcock *et al*, 2004),

fluorescein solution was made in 1x PBS and the media in the well was replaced with 3ml of 1x PBS when working with A549 cells. For Beas-2b cells the fluorescein solution was made in phenol red free DMEM and complete DMEM in the wells was similarly substituted, this change prevent cells from detaching from the membrane as observed when using 1x PBS and reduced the autofluorescence created by the presence of phenol red in the complete DMEM (Ettinger and Wittmann, 2014). At the end of each culture period 1.5ml of 0.01mg/ml of fluorescein solution (fluorescein sodium salt, Sigma-Aldrich) was added to the insert and incubated at 37^{o}C, 5% CO_2 for 120 minutes. 100µl samples of supernatant were taken in triplicate from each well at 30 and 120 minutes, relative fluorescent intensity was measured at 485nm excitation and 535nm emission on a Perkin Elmer Victor X3 multimode plate reader using flat, black, clear bottomed 96 well plates. Background fluorescence values (i.e. 0mg/ml fluorescein) were subtracted from the recorded values and the percentage fluorescein exclusion calculated as a percentage of the maximum fluorescein leakage through a blank membrane, using the following calculation;

$$\%FL = [(m-y)/z]*100$$

Were %FL is fluorescein leakage, m is mean fluorescence intensity of concentration involved, y is the mean minimum (0%) leakage and z is the mean maximum (100%) leakage.

The standard curve for fluorescein was created using concentrations of fluorescein from 0mg/ml to 1mg/ml, 100µl of each concentration was sampled and fluorescence readings measured in triplicate and averaged, values were plotted to produce a standard curve enabling leaked fluorescein concentration to be calculated (Figure 2.3).

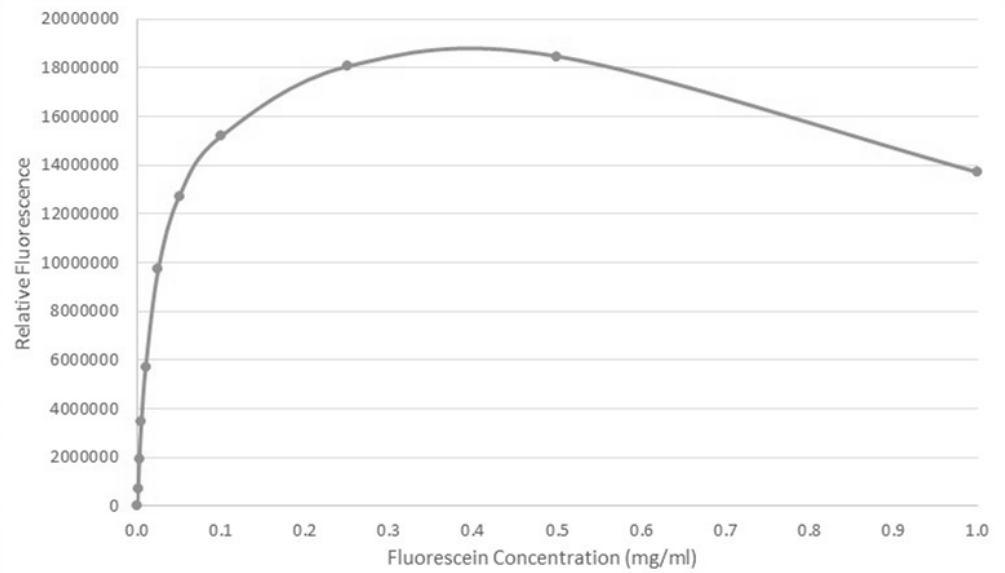

Figure 2.3 An example standard curve of relative fluorescence at varying concentrations of fluorescein.

2.2.7 Co-Culture

2.2.7.1 Optimised Co-Culture Method

Following the optimisation steps outline 2.3.6.1 subsequent co-culture experiments were set up using the following protocol. A549 or Beas-2b cells were seeded at a density of $1x10^5$ in a maximum of 200µl of complete DMEM on the basal surface of an invert 24 well Thincert™ and left to adhere at room temperature in a sterile category 2 laminar flow hood for 30 – 120 minutes. Thincerts™ were subsequently returned to the correct orientation and placed in a clear, flat bottomed 24 well plate with 1ml of complete DMEM. 1N1 P2X3 or 1N1 WT cells were then seeded on the apical side of the membrane at $5x10^4$ in a maximum of 300µl of complete DMEM and incubated at 37°C, 5% CO_2 for 4 or 7 days with media changes taking place every 3 days.

Alternatively, 1N1 P2X3 or 1N1 WT cells were seeded at $1x10^5$ in 1ml of complete DMEM into the bottom of a 24 well, clear bottom, black plate and A549 or Beas-2b cells were seeded on the apical surface of a Thincert™ at $5x10^4$ in 300µl of complete DMEM. Cells were incubated at 37°C, 5% CO_2 for 4 or 7 days with media changes taking place every 3 days.

2.2.7.2 Co-Culture ATP Analysis

Measurements of ATP were made in a similar manner to the single cell culture method with the Invitrogen™ Molecular Probes™ ATP Determination Kit using 100µl of assay mixture and 10µl of cell supernatant. As previously described (see 2.2.5.3) a standard curve was created for each individual experiment using known concentrations of ATP prior to any stimulation of cells by agonists. Measurements of luminescence were made at wavelength 560nm using a Perkin Elmer Victor X3 multimode plate reader, three times and average values plotted as a standard curve.

A549 or Beas-2b cells were seeded at $1x10^6$ on either the apical or basal surface of a 6 well Thincert™ membrane as described in the co-culture method (see 2.2.7.1). Cells were cultured for 7 days at which point ATP measurements were taken to assess the extent of ATP which could pass through the membrane and potentially interact with other cells. The cells were stimulated through the addition of equal volumes of double concentrated TRPV4 agonist GSK101 (final concentration 100nM) to the volume of complete media in either the apical or basal chamber of the Thincert™ dependant on cell orientation. A 10µl supernatant sample was taken immediately and then at 60 second intervals for a period of 10 minutes, from both the apical and basal chamber, with the luminescence value in each well read in triplicate. Luminescence values were converted to ATP values as previously described (see 2.2.5.3). Measurements were taken from duplicate wells on three separate occasions to enable statistical analysis to be conducted.

2.2.7.3 Co-Culture Calcium Signalling

Calcium signalling was conducted using the Invitrogen™ Molecular Probes™ Fluo-4 Direct™ Calcium Assay Kit with relative fluorescence measured at 485nm excitation and 535nm emission on a Perkin Elmer Victor X3 multimode plate reader every second for 600 seconds. Co-cultures of desired cell lines were grown to confluency as described previous (see 2.2.7.1) and where necessary 24 well Thincerts™ were transferred from clear, flat-bottomed 24 well plates to black, clear bottomed 24 well plates to enable fluorescent measurements to be made. For 1N1 P2X3 cells grown in the bottom of the well 300µl of phenol red free DMEM was left in the wells, 300µl of assay mix (made as described

previously, see 2.2.5.1) was added to each well and the plate incubated for a total of 60 minutes (30 minutes at 37°C and 30 minutes at room temperature) in the dark. In instances when inhibition of P2X3 receptor was investigated, either 300µl of the P2X3 antagonist NF110 (Santa Cruz Biotechnology Inc.) or an additional 300µl of phenol red free DMEM was added to the well and incubated at room temperature for 30 minutes prior to stimulation of cells in the upper chamber. A549 cells were stimulated in the upper chamber with 200µl of the TRPV4 agonist GSK101 (100nM final concentration) and the fluorescence intensity measured from the bottom of the plate at a height of 13mm from the bottom (this distance after optimisation gave the least variable results and the fluorescence intensity was neither too bright nor dim for the plate reader to measure). The 1N1 P2X3 cells were then exposed to 300µl of 2µM A23187 Calcium Ionophore to achieve a measurement of maximal relative fluorescence over a 120 second period. The same process was repeated for the alternative arrangement of cells on the insert however, in this orientation volumes were reduced to 100µl of media, 100µl of assay mix, 100µl of NF110 or phenol red free DMEM and 100µl of calcium ionophore when working with the 1N1 P2X3 cells and A549 cells were stimulated with a total of 500µl of GSK101 (100nM final concentration). Measurements were taken from triplicate wells on a three separate occasions to enable statistical analysis to be conducted.

2.2.8 Rhinovirus Culture

2.2.8.1 Determination of $TCID_{50}$ Rhinovirus

The median tissue culture infectious dose ($TCID_{50}$) (Gern *et al*, 2019) of human Rhinovirus 16 (RV16) was calculated via an endpoint dilution assay. Undiluted stock RV16 (gifted from Dr Michael Edwards, Imperial College London) was diluted to 10^{-7} via 7 ten-fold dilutions, with thorough mixing between each dilution step, 50µl of each dilution was added to 8 replicate wells of a clear, flat bottom 96 well plate and 2 wells left without virus to act as controls (Figure 2.4) in duplicate plates.

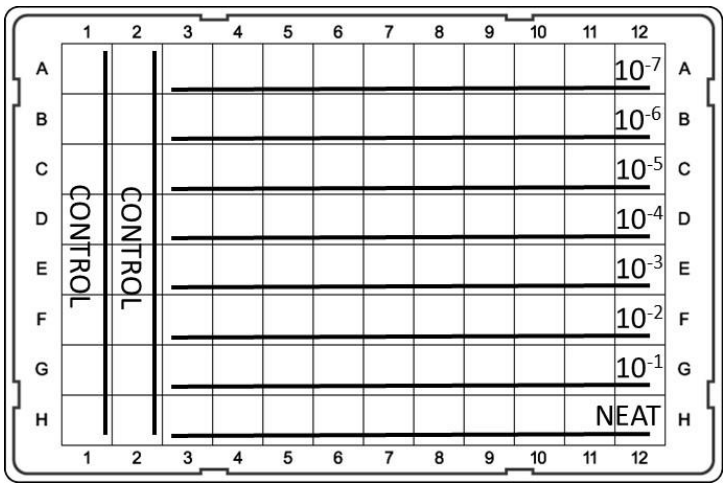

Figure 2.4 $TCID_{50}$ endpoint dilution assay plate arrangement.

Hela Ohio cells were counted as outlined previously (see 2.2.2.3) and diluted to a final concentration of $5x10^4$cells/ml in infection DMEM (DMEM with 4% FBS, 2mM L-Glutamine). 150µl of the final cell suspension was added to each well and incubated at 37°C, 5% CO_2 for 72 hours. The cytopathic effect of RV16, determined by the extent of monolayer integrity (Papi *et al*, 2001), was checked every 24 hours and recorded at 48 and 72 hours by scoring wells as positive or negative if cytopathic effect was evident or absent respectively. Cytopathic effect was determined by the evidence of cell rounding and sloughing in individual wells. Wells were scored as 0 if negative for cytopathic effect and 0.125 if positive, giving a range between a maximum of 1 if all wells were positive and 0 if all wells were negative. The sum of all dilutions were used for subsequent calculations of $TCID_{50}$ using the Reed and Muench method (Ramakrishnan, 2016) providing the dilution at which 50% of cells survive.

The $TCID_{50}$ value calculated was subsequently converted to a $TCID_{50}$/ml which was used to calculate the equivalent plaque forming units (pfu) per millilitre using the formula:

$$pfu/ml = TCID_{50}/ml * 0.7$$

The pfu/ml value can then be utilised to enable the volume of virus required to deliver a multiplicity of infection (MOI) of 1 to be calculated using the formula:

$$MOI = \text{number of cells} \div pfu/ml$$

Where MOI refers to the number of infectious virions per cell (Shabram and Aguilar-Cordova, 2000). The MOI can then be adjusted for specific experiments to ensure infection is as physiologically relevant as possible.

2.2.8.2 Propagation of Rhinovirus Stock

Hela Ohio cells were seeded in four 175cm^2 Corning® cell culture flasks (Sigma Aldrich) at a density of 5x10^6 and incubated at 37^{o}C, 5% CO_2 for 48 hour period until just confluent. When confluent each flask was washed twice with infection DMEM (DMEM with 2% FBS, 2mM L-Glutamine) prior to the addition of 7.5ml of infection DMEM and 5ml of seed RV16 stock. Flasks were incubated at room temperature with gentle agitation on a gyro-rocker (Stuart^{TM}) at 15rpm for 1 hour, to ensure even distribute and improved viral binding. After incubation a further 12.5ml infection DMEM was added to each flask and the flasks transferred to an incubator at 37^{o}C, 5% CO_2 for 24 hours or until a cytopathic effect of 80-90% was observed. Once the desired cytopathic effect was observed, cells were dislodged from the flask, the media pooled in 50ml centrifuge tubes and frozen overnight at -80^{o}C. The media was subsequently thawed at room temperature, refrozen at -80^{o}C for a minimum of 1 hour before repeat thawing, the freeze/thaw cycle was repeated again to ensure Hela Ohio cells had lysed. After the final freeze/thaw cycle the media was centrifuged at 4000rpm for 15 minutes to pellet the cell debris, the supernatant containing the virus decanted and frozen at -80^{o}C in preparation for the second growth round. To further increase the volume of viral stock, the aforementioned process was repeated using twenty 175cm^2 flasks, generating a total of 500ml of virus stock. After the last centrifuge step the supernatant was sterilised using a 0.2µm Corning® disposable vacuum filter (Fisher Scientific), aliquoted and stored at -80^{o}C.

2.2.8.3 Rhinovirus Infection of Cell Lines

A549 and Beas-2b cells were seeded at the required density for the desired experiment and incubated at 37^{o}C, 5% CO_2 for 26 hours. The required volume of RV16 needed to infect the cell monolayer at a MOI of 1 was calculated using the $TCID_{50}$ from previous endpoint dilution assay and the number of cells present after the 26 hour incubation period (based on a doubling time of 22 and 26 hours for A549 and Beas-2b cells respectively). Each well

to be infected was completely emptied of media and the required volume of RV16 (thawed from -80°C in a 37°C water bath) was added to each well. The plate was incubated at room temperature and gently agitated on a gyro-rocker at 15rpm for 1 hour. The monolayer was subsequently washed twice with 1x PBS and the required volume of infection DMEM (plate size dependent) was added to each well prior to incubation at 37°C, 5% CO_2 until needed.

2.2.8.4 Preparing Rhinovirus Controls

Rhinovirus controls with a MOI of 1 were created by ultraviolet (UV) inactivation or ultrafiltration, for sham infection which mirrored the conditions of a RV16 infection. For UV inactivation, RV16 was placed in an open 100ml glass beaker on ice and UV irradiated for 30 minutes at 1200µJ/cm^2 using a CL-1000L ultraviolet crosslinker (Ultra-violet Products (UVP) Ltd, Cambridge, UK). UV crosslinking results in the formation of covalent links between interacting viral RNA and/or proteins (Poria and Ray, 2017). Whilst this renders the virus non-infectious, ICAM-1 receptor sites are retained thus interaction with the receptor is still possible (Johnston *et al*, 1998). Whilst for ultrafiltration, RV16 was placed in a 20ml Sartorius™ Vivaspin™ 20 Centrifugal Concentrator (Fisher Scientific) with a 30kDa molecular mass cut-off, centrifuged at 12,000x g for 12 minutes and the filtrate collected. This process enables the removal of viral particles and viral RNA however, smaller molecules such as cytokines are retained. Therefore any response measured is a result of soluble products rather than viral activity (Papi and Johnston, 1999). Once inactivated cells were treated as per the RV16 infection procedure (see 2.2.8.3).

2.2.8.5 Demonstrating Infectivity of Rhinovirus Infection in Cell Culture

To confirm successful infection of cells, a modified endpoint dilution assay was conducted utilising the cell culture effluent from A549 and Beas-2b cells, 48 hours post infection. Hela Ohio cells were seeded at a density of 5x10^4cells/ml in a clear, flat bottom, 96 well plate in complete DMEM and incubated at 37°C, 5% CO_2 for 24 hours. After 24 hours incubation, media was completely aspirated from all wells and replaced with 150µl of infection DMEM. Undiluted cell culture effluent from RV16 and ultrafiltered RV16 treated cells was diluted to 10^{-7} via 7 ten-fold dilutions, 50µl of each dilution was added to 8 replicate wells of a clear, flat bottom 96 well plate and 2 wells left without virus to act as controls (Figure 2.5).

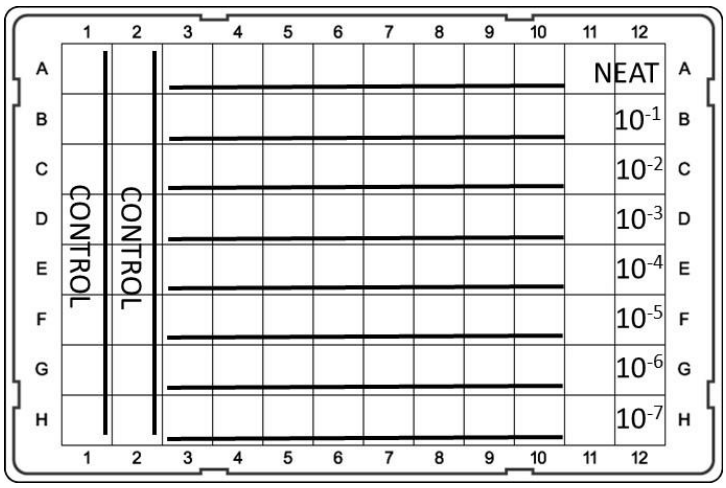

Figure 2.5 Modified endpoint dilution assay plate arrangement to demonstrate successful infection of A549 and Beas-2b cells with RV16 or ultrafiltered RV16.

Wells were checked for cytopathic effect by the evidence of cell rounding and sloughing in individual wells every 24 hours until this became apparent or for a maximum of 5 days if no infection was present.

2.2.9 Methods of Assessing Effect of Rhinovirus Infection in Cell Culture

2.2.9.1 Rhinovirus Infection for Fluorescein Exclusion Assay

A549 and Beas-2b cells were seeded on 6 well Thincert™, 0.4µm pore size, transparent PET membrane at a density of $2.5x10^5$ cells and incubated at 37°C, 5% CO_2 for 4 days. After the initial 96 hour incubation period, cells were infected at a MOI of 1 with the required volume of RV16, UV inactivated RV16 or infection DMEM (basal control) in duplicate wells, using the method outlined in 2.2.8.3 and 2.2.8.4. After the 1 hour incubation period the wells were washed twice with 1x PBS, infection DMEM refreshed in the apical chamber and the plates incubated at 37°C, 5% CO_2 for a further 7 days, with media (using complete DMEM) changes every 48-72 hours. After the 7 day culture period fluorescein leakage across the membrane was measured using the method outlined in 2.2.6.2 with some minor modifications. These modifications being the use of phenol red free complete DMEM for both cells lines, triplicate sample of supernatant taken at the 120 minutes time point only and plate measurements taken on a Tecan Infinite M200 multimode plate reader.

2.2.9.2 Rhinovirus Infection for TEER Measurements

A549 and Beas-2b cells were seeded on 24 well Thincert™, 0.4μm pore size, transparent PET membrane at a density of $5x10^4$ cells and incubated at 37°C, 5% CO_2 for 96 hours using the method outlined in 2.2.6.1. After the initial 96 hour incubation period, cells were infected at a MOI of 1 with the required volume of RV16, UV inactivated RV16 or infection DMEM (basal control) in duplicate wells, using the method outlined in 2.2.8.3 and 2.2.8.4. After the 1 hour incubation period the wells were washed twice with 1x PBS, infection DMEM refreshed in the apical chambers and the plates incubated at 37°C, 5% CO_2, with media (using complete DMEM) changes every 48 – 72 hours for the duration of the culture period. To identify if the presence of an ALI had any influence on TEER measurements post-infection, duplicate wells of Beas-2b cells had an ALI introduced at 96 hours immediately after infection in the manner outlined in 2.2.6.1. Initial TEER measurements were taken in triplicate from each well, 24 hours post seeding using the method outlined in 2.2.6.1 and subsequently every 24 hours thereafter for the entire culture period.

2.2.9.3 Rhinovirus Infection for Zymography and Lactate Dehydrogenase (LDH) Analysis

A549 and Beas-2b cells were seeded in clear 24 well plate at a density of $1x10^5$ cells and incubated at 37°C, 5% CO_2 for 24 hours. After the initial 24 hour incubation period, cells were infected at a MOI of 1 with the required volume of RV16, ultrafiltrated RV16 or infection DMEM (basal control) in triplicate wells, using the method outlined in 2.2.8.3 and 2.2.8.4. After the 1 hour incubation period the wells were washed twice with 1x PBS, infection DMEM replenished in each well and the plates incubated at 37°C, 5% CO_2 for a further 7 days. DMEM was completely aspirated and replenished at 24, 48, 72 and 168 hours post infection, with effluent collected stored at 4°C for LDH analysis to help ensure that LDH levels not deteriorate (Greiff and Kelly, 1966; Jacobs *et al*, 1986) or -80°C for analysis by zymography.

2.2.9.4 Rhinovirus Infection for Sulforhodamine B (SRB) and LDH

A549 and Beas-2b cells were seeded at varying densities depending on the length of time cells remained in culture post infection, in clear 24 well plate (Sarstedt) and incubated at

37°C, 5% CO_2 for 24 hours. This produced a reverse time course which resulted in final seeding densities of $2x10^5$ in all wells at the point of infection. Cells were infected 24, 48, 72 or 168 hours post seeding at a MOI of 1 with the required volume of RV16, ultrafiltrated RV16 or infection DMEM (basal control) in quadruplicate wells, using the method outlined in 2.2.8.3 and 2.2.8.4. After the 1 hour incubation period the wells were washed twice with 1x PBS, infection DMEM replenished in each well and the plates incubated at 37°C, 5% CO_2 for a further 24, 48, 72 or 168 hours, with media changes every 48 – 72 hours with complete DMEM.

2.2.9.5 Rhinovirus Infection for Water Soluble Tetrazolium salt (WST-1) Cell Proliferation Assay

A549 and Beas-2b cells were seeded in clear 96 well plate to produce a reverse time course which resulted in final seeding densities of $2.5x10^4$ at the point of infection and incubated at 37°C, 5% CO_2 for 24 hours. Cells were infected 24, 48, 72 or 168 hours post seeding at a MOI of 1 with the required volume of RV16, ultrafiltrated RV16 or infection DMEM (basal control) in triplicate wells, using the method outlined in 2.2.8.3 and 2.2.8.4. After the 1 hour incubation period the wells were washed twice with 1x PBS, infection DMEM replenished in each well and the plates incubated at 37°C, 5% CO_2 for a further 24, 48, 72 or 168 hours, with media changes every 48 – 72 hours with complete DMEM.

2.2.9.6 Zymography for Assessment of Matrix Metalloproteinases (MMP) Upregulation

Undiluted cell culture effluent (8µl) collected as outlined in 2.2.9.4 were mixed with 5x non-reducing buffer (2µl) (see appendix A3) and EZ-Run™ prestained protein ladder were loaded into wells and separated using a 7.5% acrylamide gel containing gelatine (4mg/ml) made in house (Table 2.9). Gels were run vertically in Bio-Rad electrophoresis units, using 1x running buffer (see appendix A3) at 150V for 45 – 60 minutes until the dye front reached the bottom of the gel.

	3% Stacking Gel		7.5% Separating Gel
0.5M Tris (pH 6.8)	1.25ml	**1.5M Tris (pH 8.8)**	2ml
30% Acrylamide	670µl	**30% Acrylamide**	2ml
H_2O	3.075ml	**H_2O**	2ml
		Gelatine (4mg/ml)	2ml
10% SDS	50µl	**10% SDS**	80µl
10% APS	50µl	**10% APS**	80µl
TEMED	10µl	**TEMED**	10µl

Table 2.9 Reagent and volume per gel used to produce zymography gels for MMP analysis of cell lines post-infection with RV16.

The gel was washed twice for 30 minutes with washing buffer (see appendix A3), rinsed in incubation buffer (see appendix A3) for 10 minutes with gentle agitation on a gyro-rocker and incubated in fresh incubation buffer at 37°C for 24 hours. The gel was subsequently stained with staining solution (see appendix A3) for 45 minutes, rinsed with dH_2O to remove excess staining solution and destained in destaining solution (see appendix A3) until clear bands could be seen (approximately 60 minutes). The gel was imaged using white light on a ChemiDoc™ XRS+ System (Bio-Rad).

2.2.9.7 LDH Assay

For cells infected using the method outline in 2.2.9.3, lysed cell supernatant and effluent collected from media changes for cells infected with RV16 were measured for LDH levels, using a modified OPS Diagnostic LDH assay protocol, as an indication of cytotoxicity. LDH is released from cells when membranes lyse during cell death, thus providing a predictor for cell health and measure of cytotoxicity (Fotakis and Timbrell, 2006). Effluent from triplicate wells was completely aspirated every 24 hours for the first 72 hours and then after 168 hours, with wells being replenished with fresh complete DMEM at each stage. Sample of effluent were retained at 24, 48, 72 and 168 hour time points post infection, thus each effluent sample represented the previous 24 hour time period of cell growth for the first 72 hours and then the remainder of the culture period. Effluent from each time point was pooled, centrifuged at 10,000x g for 5 minutes, the supernatant collected and stored at 4°C for a maximum of 7 days prior to use to limit the extent of LDH degradation in the sample (Houle *et al*, 2015). Cells were lysed 168 hours post infection in 500µl of completed DMEM

containing 50µl of 10% (v/v) lysis buffer (lysis buffer is comprised of 10% Triton X-100, (Fisher Scientific) in dH_2O), incubated at 37°C, 5% CO_2 for 45 minutes and effluent processed as outlined below. Similarly for cells infected using the method outline in 2.2.9.4, lysed cell supernatant for cells infected with RV16 were measured for LDH levels. Duplicate wells of cells were lysed at 24, 48, 72 and 168 hours post infection in 500µl of completed DMEM containing 50µl of 10% (v/v) lysis buffer (Triton X-100), incubated at 37°C, 5% CO_2 for 45 minutes and effluent processed as outlined below.

To complete the assay 50µl 200mM Tris buffer (see appendix A1), 50µl 50mM Lithium Lactate (Fisher Scientific) and 50µl of LDH assay mixture (see appendix A1) were added to a clear, flat bottomed 96 well plates. To this 50µl of cell effluent or lysed cell supernatant was added in duplicate and incubated at room temperature for 15 minutes. Due to the presence of phenol red in the complete DMEM, a media blank measurement was also taken to account for the absorbance due to the media. Additionally a positive control using 1% BSA and a negative control using distilled water were also measured. Absorbance was measured on a Tecan Infinite M200 multimode plate reader at 490 and 690nm, each effluent value was adjusted to account for the media blank.

2.2.9.8 SRB Assay

A549 and Beas-2b cells grown and infected in triplicate wells as outlined in 2.2.8.3 and 2.2.8.4 were fixed with 1ml of ice cold (4°C) 25% trichloroacetic acid (TCA) (Sigma-Aldrich) on ice for 1 hour, washed 4 times with distilled water, the supernatant discarded and the plate dried. Fixed cells were stained using 250µl of 0.4% sulforhodamine B in 1% acetic acid (both Sigma-Aldrich) per well for 30 minutes at room temperature, excess stain removed, the wells washed 4 times with 1% acetic acid, the supernatant discarded and the plate dried. Subsequently the stain was dissolved in 500µl 10mM Tris base (Fisher Scientific) at pH10 on a gyro-rocker for 5 minutes to ensure even distribution of the stain across the well. Absorbance was measured on a Tecan Infinite M200 multimode plate reader at 540nm, with 21 points measured per well.

2.2.9.9 WST-1 Cell Proliferation Assay

A549 and Beas-2b cells were grown and infected in triplicated wells as outlined in 2.2.8.3 and 2.2.8.4, media was aspirated from each well to leave 100µl, to which 10µl of WST-1 reagent (Roche, Fisher Scientific) was added. Due to the presence of phenol red in the complete DMEM, a media blank measurement was also taken to account for difference in absorbance. Plates were incubated in the dark at 37^{o}C for 30 minutes and absorbance measured on a Tecan Infinite M200 multimode plate reader at 420nm, all values were adjusted to account for the media blank.

2.2.10 Statistical Analysis

Unless otherwise stated, all data is presented as the mean of three independent replicates of an experiment plus/minus the standard error of the mean (±S.E.M). All data was analysed using GraphPad Prism 8.0.2 software. Data was checked for normality visually using the widely utilised quantile-quantile (Q-Q) plot and statistically using a Shapiro-Wilk test (Razali and Wah, 2011). Statistical analysis was performed where data was appropriate using a combination of two and one-way analysis of variance (ANOVA) followed by Tukey post hoc test for multiple comparison, paired and unpaired t-tests. Data which contained multiple time points was analysed with multiple t-tests utilising the Holm-Sidák method for corrections of multiple comparisons. Where appropriate, the individual test conducted is stated in each figure legend. Statistical significance was determined by a P value of less than 0.05, exact P values are stated were appropriate.

2.3 Results

2.3.1 Normal Morphology of Cell Lines

To demonstrate the normal morphology of cell lines used in experiments, cells were stained using Kwik-Diff^{TM} staining kit and cells viewed under a light microscope at 100x and 400x magnification (Figure 2.6). Normal morphology of 1321N1 human brain astrocytoma cells transfected with P2X3 showed neurone morphology of bipolar cells which interlinked with each other (Public Health England, 2016). Whilst A549 human alveolar epithelial cells showed the typical monolayer formation of basal epithelial type II alveolar cells (Public

Health England, 2012). Similarly, Beas-2b human bronchial epithelial cells having been differentiated through the introduction of 10% FBS grown in a monolayer typical of bronchial epithelial cells (Public Health England, ND).

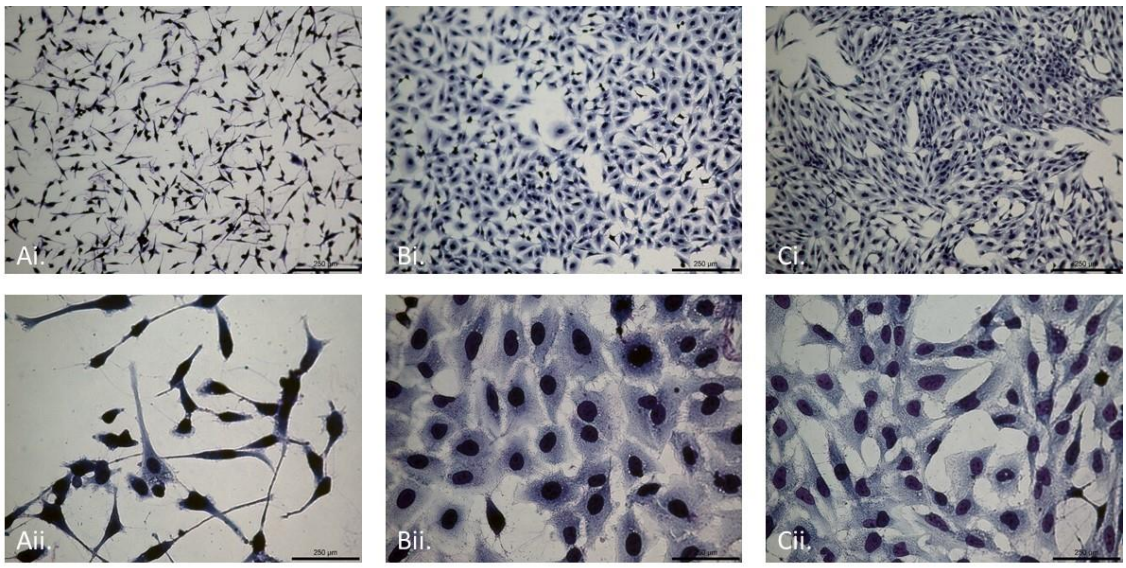

Figure 2.6 Ai – Aii represents 1321N1 human brain astrocytoma cells transfected with P2X3 viewed at 100x magnification (**Ai**) and 400x magnification (**Aii**). **Bi – Bii** represents A549 human lung epithelial cells viewed at 100x magnification (**Bi**) and 400x magnification (**Bii**). **Ci – Cii** represents Beas-2b human bronchial epithelial cells viewed at 100x magnification (**Ci**) and 400x magnification (**Cii**). Images represents three independent experiments (n=3).

2.3.2 Characterisation of A549 and Beas-2b Cells

Due to the difficulty of maintaining *in vitro* cultures of primary respiratory epithelial cell lines, immortalised cell lines such as A549 and Beas-2b cells are widely used models for the study of lung diseases and as such can be considered a representative cell type in the study of respiratory infection, cough and airway inflammation (Hillyer *et al*, 2018). Arguably the use of these cell lines enables both URTIs and LRTIs to be considered due to their placement within the respiratory tract, making them suitable models for subsequent experiments. Whilst these cell lines are extensively used, before conducting further functional analysis both cell lines were characterised to identify whether the physiologically relevant TRP receptor (TRPV4) was present and the P2X receptor (P2X3) which is hypothesised to interact with TRPV4 is absent.

2.3.2.1 Airway Epithelial Cell Lines Express TRPV4 but not P2X3 mRNA

Unstimulated A549 and Beas-2b were grown to near confluency and RNA isolated and amplified using TRPV4, P2X3, and β-actin primers using the method outline in 2.2.4 both with and without the presence of reverse transcriptase as a negative control. A549 cells were positive for expression of TRPV4 and the positive loading control β-actin. The expression of P2X3 was inconclusive due to the presence of a low level positive result in one of the three experiments (Figure 2.7a). Similarly, Beas-2b cells were positive for expression of TRPV4 and the positive loading control β-actin, whilst being negative for P2X3 expression (Figure 2.7b).

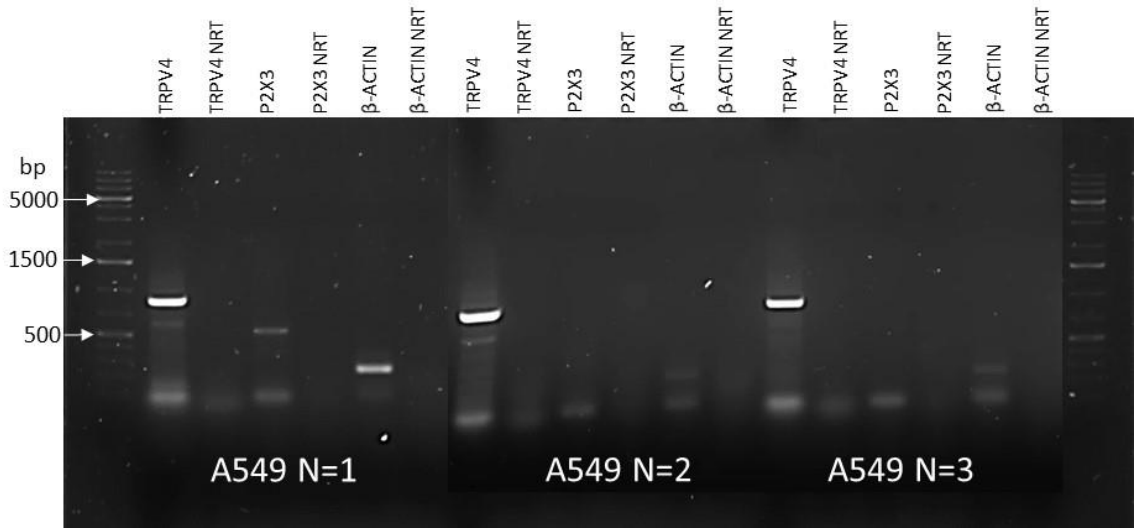

Figure 2.7a Endogenous mRNA expression of TRPV4 and P2X3 in A549 cell line, shown by endpoint RT-PCR agarose gel products. Expression of TRPV4 (882bp), P2X3 (432bp) and loading control β-actin (242bp) represented with presence of reverse transcriptase (TRPV4, P2X3 and β-actin) and without reverse transcriptase (TRPV4 NRT, P2X3 NRT and β-actin NRT). Data represents three independent experiments (n=3).

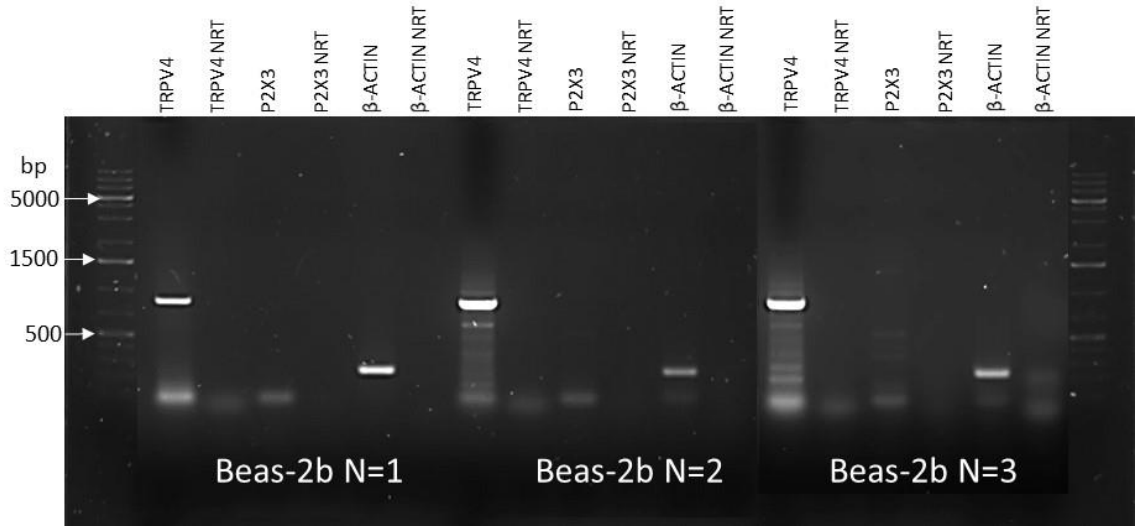

Figure 2.7b Endogenous mRNA expression of TRPV4 and P2X3 in Beas-2b cell line, shown by endpoint RT-PCR agarose gel products. Expression of TRPV4 (882bp), P2X3 (432bp) and loading control β-actin (242bp) represented with presence of reverse transcriptase (TRPV4, P2X3 and β-actin) and without reverse transcriptase (TRPV4 NRT, P2X3 NRT and β-actin NRT). Data represents three independent experiments (n=3).

2.3.2.2 Airway Epithelial Cell Lines Express TRPV4 but not P2X3 Protein

To further confirm the presence of TRP channels and P2X3 receptors in A549 and Beas-2b cell lines, western blot analysis was conducted on unstimulated cell lysates using the method outlined in 2.2.3 with antibodies that had previously been optimised for use. A549 showed positive expression for TRPV4 and the loading control α-tubulin, whilst being negative for P2X3 expression (Figure 2.8a). Similarly, Beas-2b showed positive expression for TRPV4 and the loading control α-tubulin, whilst being negative for P2X3 expression (Figure 2.8b).

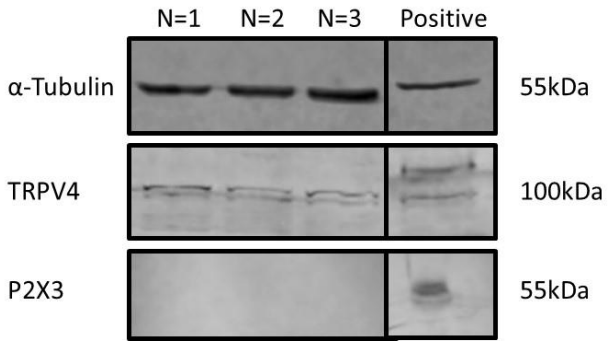

Figure 2.8a Western blot analysis to show protein expression of TRPV4 and P2X3 in A549 cell line. Membranes were loaded with 50µg of protein from A549 whole cell lysates and positive controls for TRPV4 and P2X3 expression (whole cell lysates from HEK293 cells transcribed with TRPV4 and 1321N1 cells transcribed with P2X3 respectively). Membranes were probed with anti-TRPV4 primary antibody for expression TRPV4, anti-P2X3 primary antibody for expression P2X3 and anti-α-tubulin primary antibody for expression α-tubulin used as a loading control (expected molecular weights 100kDa, 55kDa and 55 kDa respectively). All antibodies were used at a concentration of 1:500. Data represents three independent experiments (n=3).

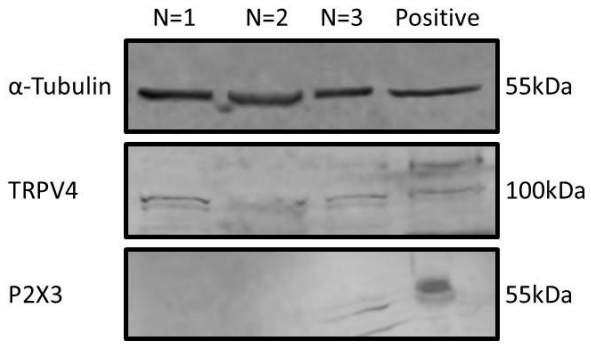

Figure 2.8b Western blot analysis to show protein expression of TRPV4 and P2X3 in Beas-2b cell line. Membranes were loaded with 50µg of protein from Beas-2b whole cell lysates and positive controls for TRPV4 and P2X3 expression (whole cell lysates from HEK293 cells transcribed with TRPV4 and 1321N1 cells transcribed with P2X3 respectively). Membranes were probed with anti-TRPV4 primary antibody for expression TRPV4, anti-P2X3 primary antibody for expression P2X3 and anti-α-tubulin primary antibody for expression α-tubulin used as a loading control (expected molecular weights 100kDa, 55kDa and 55 kDa respectively). All antibodies were used at a concentration of 1:500. Data represents three independent experiments (n=3).

2.3.3 Functional Analysis of TRPV4 Receptor

2.3.3.1 Airway Epithelial Cell Lines Released ATP when Stimulated with TRPV4 Agonist

To confirm the TRPV4 – ATP – P2X3 pathway existed in the airway epithelial cell lines, functional analysis of A549 and Beas-2b cells was performed. Both wild type Beas-2b and A549 cells express TRPV4 receptors (see 2.3.2) thus when stimulated with the TRPV4 agonist GSK101 the cells released ATP. However, the optimum concentration required for consistent ATP release needed to be determined for use in subsequent experimental procedures. To ascertain the amount of extracellular ATP which could be released by A549 and Beas-2b cells, cells were stimulated with varying concentrations of TRPV4 receptor agonist GSK101 and the extracellular ATP measured as outlined in 2.2.5.3.

A549 cells demonstrated increasing release of extracellular ATP with increasing concentrations of GSK101. The addition of 0nM GSK101 (vehicle control, complete DMEM only) resulted in a minimal ATP release as a consequence of mechanosensation of TRPV4 receptors when any solution is added to the cells (Brierley *et al*, 2008). There was no significant difference ($P>0.05$) between the increasing concentrations of GSK101 and the measureable amount of extracellular ATP however, there was a significant difference between 300nM GSK101 and 0nM ($P<0.05$) (Figure 2.9).

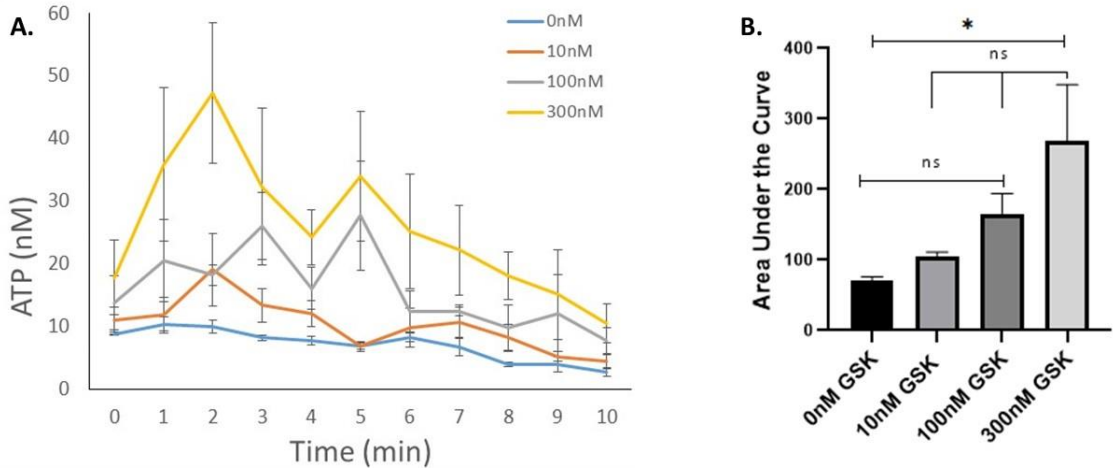

Figure 2.9 Extracellular ATP released by A549 cells after stimulation with TRPV4 agonist GSK101 at concentrations ranging from 0nM to 300nM over a duration of 10 minutes post stimulation (**A**). Area under curve analysis of A549 extracellular ATP release after exposure to aforementioned conditions (**B**). Results are displayed as mean ± SEM (n=3). Statistical analysis was conducted using a one-way ANOVA with multiple comparison by Tukey analysis. $P<0.05^{*}$

Similarly, Beas-2b cells demonstrated increasing release of extracellular ATP with increasing concentrations of GSK101 however, the amount of extracellular ATP released was lower when compared to A549 cells. The addition of 0nM GSK101 (vehicle control, complete DMEM only) again resulted in a minimal ATP release as a consequence of mechanosensation of TRPV4 receptors. Likewise, there was no significant difference ($P>0.05$) between the increasing concentrations of GSK101 and the measureable amount of extracellular ATP however, there was a significant difference between 300nM GSK101 and 0nM ($P<0.05$) (Figure 2.10).

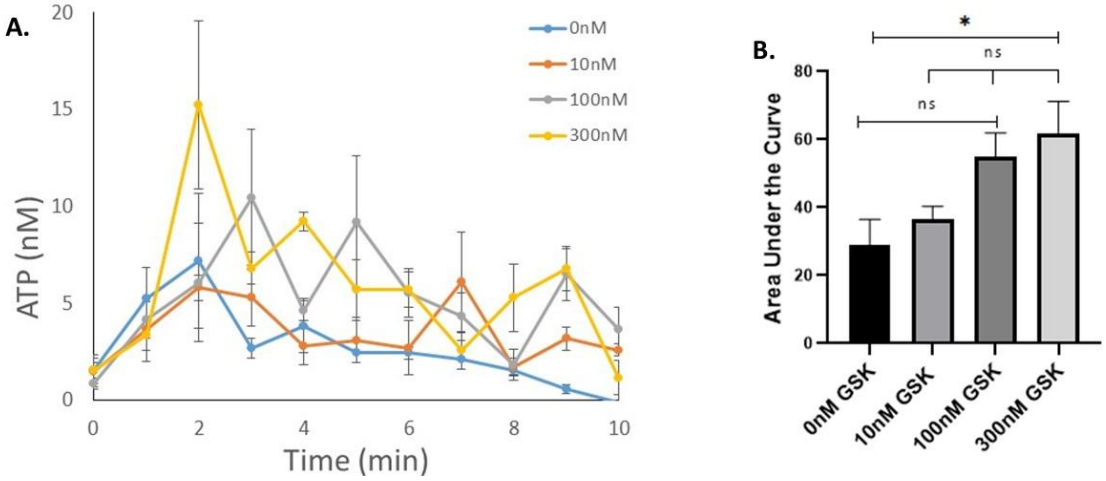

Figure 2.10 Extracellular ATP released by Beas-2b cells after stimulation with TRPV4 agonist GSK101 at concentrations ranging from 0nM to 300nM over a duration of 10 minutes post stimulation (**A**). Area under curve analysis of Beas-2b extracellular ATP release after exposure to aforementioned conditions (**B**). Results are displayed as mean ± SEM (n=3). Statistical analysis was conducted using a one-way ANOVA with multiple comparison by Tukey analysis. $P<0.05^{*}$

2.3.3.2 ATP is Metabolised by A549 Cell Line

To demonstrate the rapid metabolism of extracellular ATP by ectoATPases on cell surfaces (Lazarowski *et al*, 2000), A549 cells were spiked with known concentrations of ATP, effluent collected and luminescence measured over a 5 minute period, these luminescence values were subsequently converted to equivalent ATP values. When compared to the standard curve values of ATP there was a reduction in the amount of ATP measured when applied to A549 cells at all time points and for all concentrations above 10nM (n=3), thus accounting for the rapid decay in the measured amount of ATP in other assays (Figure 2.11).

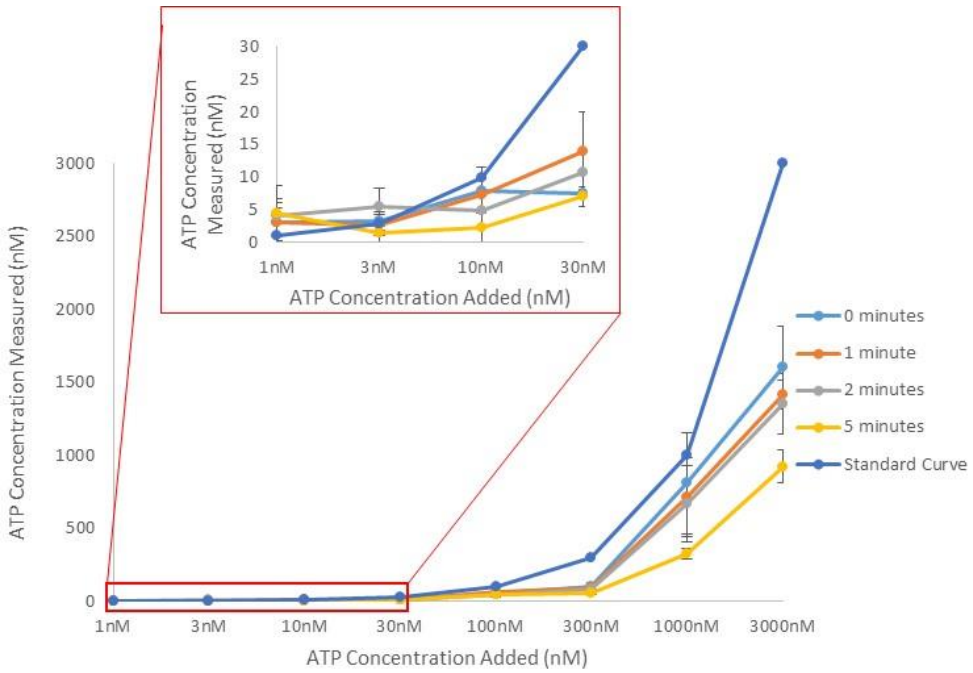

Figure 2.11 Extracellular ATP metabolism by A549 cells after spiking cells with known ATP concentrations over a duration of 5 minutes. Results are displayed as mean ± SEM (n=3).

2.3.3.3 Optimised Seeding Density for Calcium Signalling in A549 Cell Line

To identify the optimal seeding density to utilise for calcium signalling experiments A549 cells were seeded at varying densities and cultured for 24 hours prior to conducting the calcium signalling assay described in 2.2.5.1. When seeded at 5000 or 10000 cells/well (96 well plate with 0.32cm^2 surface area) there was no significant difference between the responses measured however, when seeding density was increased to 50000 cells/well there was a significant increase in the measured response when compared to 5000 ($P<0.005$) and 10000 ($P<0.01$). Similarly, when seeding density was increased to 100000 cells/well there was a significant increase in the measured response when compared to all other seeding densities ($P<0.001$) (Figure 2.12). Thus based on this increased response a seeding density of 100000 cells/well was utilised for all further 96 well plate format calcium signalling experiments.

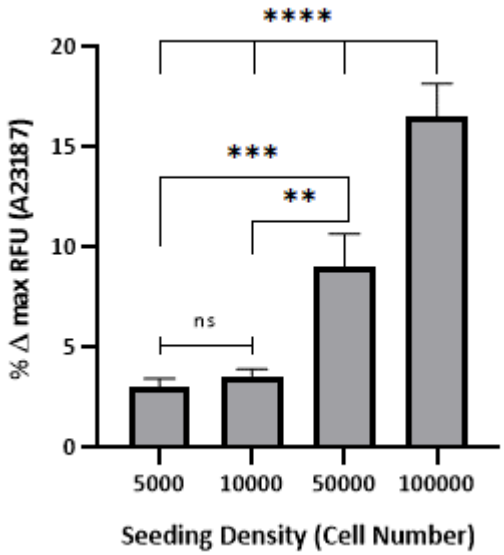

Figure 2.12 Calcium signalling response measured in A549 cell line showing the impact of variation in seeding density when subsequently stimulated with TRPV4 agonist GSK101 (100nM). Responses were measured as a percentage of maximum response to control, calcium ionophore A23187. Results are displayed as mean ± SEM (n=4). Statistical analysis was conducted using a two-way ANOVA with multiple comparison by Tukey analysis. $P<0.01^{**}$, $P<0.005^{***}$, $P<0.001^{****}$

2.3.3.4 Airway Epithelial Cell Lines Express Functional TRPV4

To continue investigating whether the TRPV4 – ATP – P2X3 pathway is involved in the mechanism of cough, further functional analysis of A549 and Beas-2b cells was performed using intracellular calcium signalling. Having shown both wild type Beas-2b and A549 cells express TRPV4 receptors (see 2.3.2) activation of the TRPV4 receptors with the agonist GSK101 could be measured by the resulting calcium flux as outlined in 2.2.5.1. To determine the optimum concentration required for a consistent response a dose response curve was conducted on A549, Beas-2b and 1N1 P2X3 cells.

A549 and Beas-2b cells demonstrated a functionally positive response to GSK101, enabling a calculation of an EC_{50} value of 413nM (Figure 2.13a) and 116nM (as calculated by AAT Bioquest Quest Graph™ EC50 Calculator) (Figure 2.13b) respectively. Whilst 1N1 P2X3 cells demonstrated no obvious positive response across a range of concentrations, resulting in

an EC_{50} value of 1183nM (Figure 2.13c). Based on these observation, the previous ATP analysis and existing literature, an optimum concentration of 100nM GSK101 would be used in subsequent experiments, as this provided more consistent results across all analysis whilst, not activating 1N1 P2X3 to any noticeable extent.

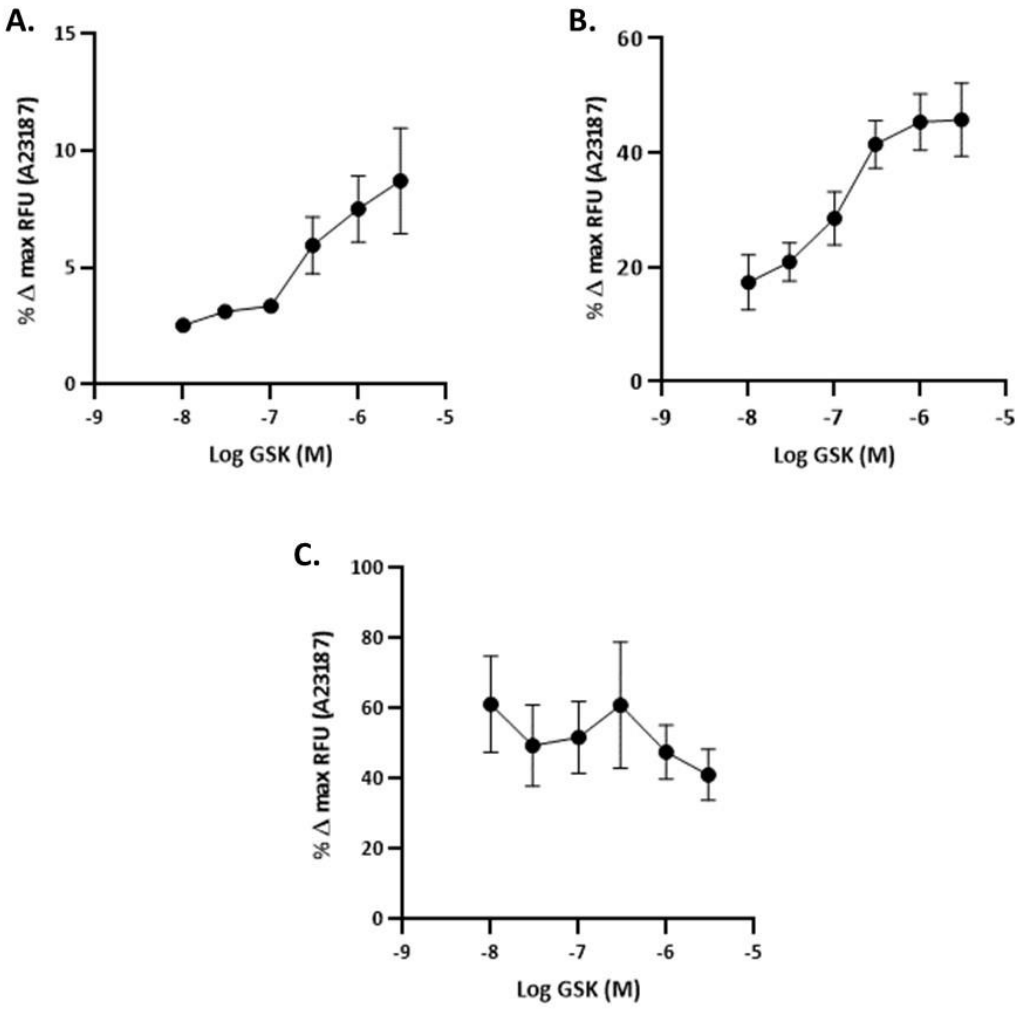

Figure 2.13 Dose response curve of A549 (**A**), Beas-2b (**B**) and 1N1 P2X3 (**C**) cell lines when stimulated with TRPV4 agonist GSK101. Responses measured as a percentage of maximum response to control, calcium ionophore A23187. Results are displayed as mean ± SEM (n=3). A549 EC_{50} = 413nM, Beas-2b EC_{50} = 116nM, 1N1 P2X3 EC_{50} = 1183nM

The calculation of accurate half maximal effective concentration (EC_{50}) values for dose responses typically produce sigmoidal shaped (S-shaped) curves, which are smooth and symmetrical in nature (Liang *et al*, 2015). Whilst no S-shaped curve was expected for 1N1

P2X3 cells (Figure 2.13c), as this cell line does not express TRPV4 receptors, a clear S-shaped curve should have been observed for both A549 and Beas-2b cells. The Beas-2b cells produced a near S-shaped curve when stimulated with GSK101 (Figure 2.13b) however, the A549 response fits less closely to this expected norm (Figure 2.13a). The lack of the S-shaped curve is probably due to having an insufficient range of concentrations to ensure the upper plateau is reached. Furthermore, the averaging of data across multiple replicates may have impacted the overall shape of the curve. The disadvantage of using an incomplete concentration range is that the estimation of the EC_{50} is likely to be altered (Jiang and Kopp-Schneider, 2015). However, due to time and cost constraints, further analysis to extend the concentration range used was not practicable. It is also worth noting the varied range of GSK101 concentrations which are utilised within the existing literature, which ranges from 1nM to 1µM (Jin *et al*, 2011; Zhao *et al*, 2014; Behringer and Segal, 2015; Mihara *et al*, 2018; Bonvini *et al*, 2020; Solari *et al*, 2020). When EC_{50} values are considered Jin *et al* (2011) identify an EC_{50} of 3.3nM and a 10nM concentration being near maximal, conversely, Zhao *et al* (2014) identified an EC_{50} of 18.1nM with a concentration of 100nM being near maximal, whilst Bonvini *et al* (2020) utilise 100nM as a submaximal concentration, suggesting a higher EC_{50}. Given this variation, the EC_{50} value generated through experimentation with the Beas-2b cell lines is close to the Bonvini *et al* (2020), submaximal value of 100nM and although the A549 value is noticeably higher at 413nM, the final chosen concentration of 100nM is aligned to the ranges used within the existing literature which utilises this TRPV4 agonist.

2.3.3.5 Airway Epithelial Cell Lines Express Functional TRPV4 which can be Inhibited with TRPV4 Antagonist

To support the positive TRPV4 functional analysis of A549 and Beas-2b cells, TRPV4 receptors activity was blocked using a TRPV4 antagonist. Cells were treated with 10µM of the TRPV4 antagonist HC-067047 for 30 minutes prior to stimulation with the EC_{50} of GSK101 (100nM) and the resulting calcium flux measured. Similarly, to show that 1N1 P2X3 cells were not negatively affected by the application of the antagonist, the cells were treated in the same manner as above prior to stimulation with the EC_{50} of ATP (P2X3 agonist, 400nM) as outlined in 2.2.5.1.

A549 cells demonstrated no change (P>0.05) in intracellular calcium response when treated with HC-067047 prior to GSK101 application compared to GSK101 alone (Figure 2.14a), whilst Beas-2b cells demonstrated a significant reduction in intracellular calcium flux when treated with HC-067047 prior to GSK101 application (P<0.005) compared to GSK101 alone (Figure 2.14b). 1N1 P2X3 cells demonstrated no significant change (P>0.05) in intracellular calcium response when treated with HC-067047 prior to ATP application compared to ATP alone (Figure 2.14c).

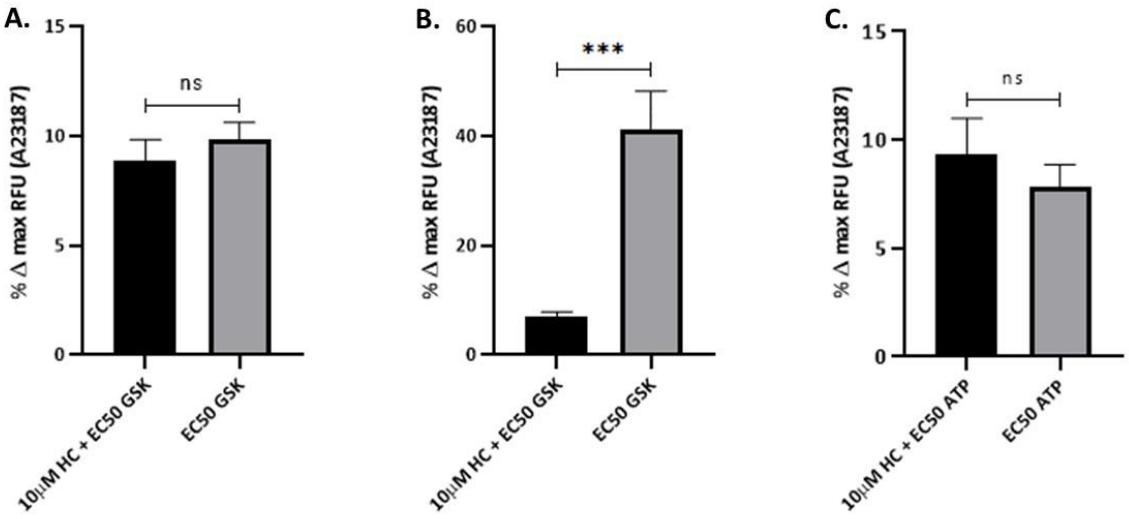

Figure 2.14 Calcium signalling response measured in A549 (**A**) and Beas-2b (**B**) cell lines after incubation with either TRPV4 antagonist HC-067047 or complete DMEM for 30 minutes prior to stimulation with the EC_{50} concentration of TRPV4 agonist GSK101 (100nM). Calcium signalling response measured in 1N1 P2X3 (**C**) cell line after incubation with either TRPV4 antagonist HC-067047 or complete DMEM for 30 minutes prior to stimulation with the EC_{50} concentration of P2X3 agonist ATP (400nM). Responses were measured as a percentage of maximum response to control, calcium ionophore A23187. Results are displayed as mean ± SEM (n=3). Statistical analysis was conducted using an unpaired t-test. $P<0.005^{***}$

2.3.4 Functional Analysis of P2X3 Receptor

2.3.4.1 Transfected Astrocyte Cell Line Expresses Function P2X3

In order to consider the latter end of the TRPV4 – ATP – P2X3 pathway, functional analysis of 1N1 P2X3 cells was performed using intracellular calcium signalling. Activation of the P2X3 receptors with the agonist ATP resulted in intracellular calcium release from the cells which was measured as outlined in 2.2.5.1. To determine the optimum concentration required for a consistent response a dose response curve was conducted on 1N1 P2X3, A549 and Beas-2b cells.

1N1 P2X3 cells demonstrated a functionally positive response to ATP, enabling a calculation of an EC_{50} value of 419nM (Figure 2.15a). Whilst A549 and Beas-2b cells demonstrated relatively steady responses across the lower range of concentrations, with a observable peak in response rate at 3000nM ATP, this resulted in an EC_{50} value of 1592nM (Figure 2.15b) and 4310nM (as calculated by AAT Bioquest Quest Graph™ EC50 Calculator) (Figure 2.15c) for A549 and Beas-2b respectively. Based on these observation and existing literature, an optimum concentration of 400nM ATP was used in subsequent experiments, as this provided consistent results whilst, not activating A549 and Beas-2b cells to any noticeable extent.

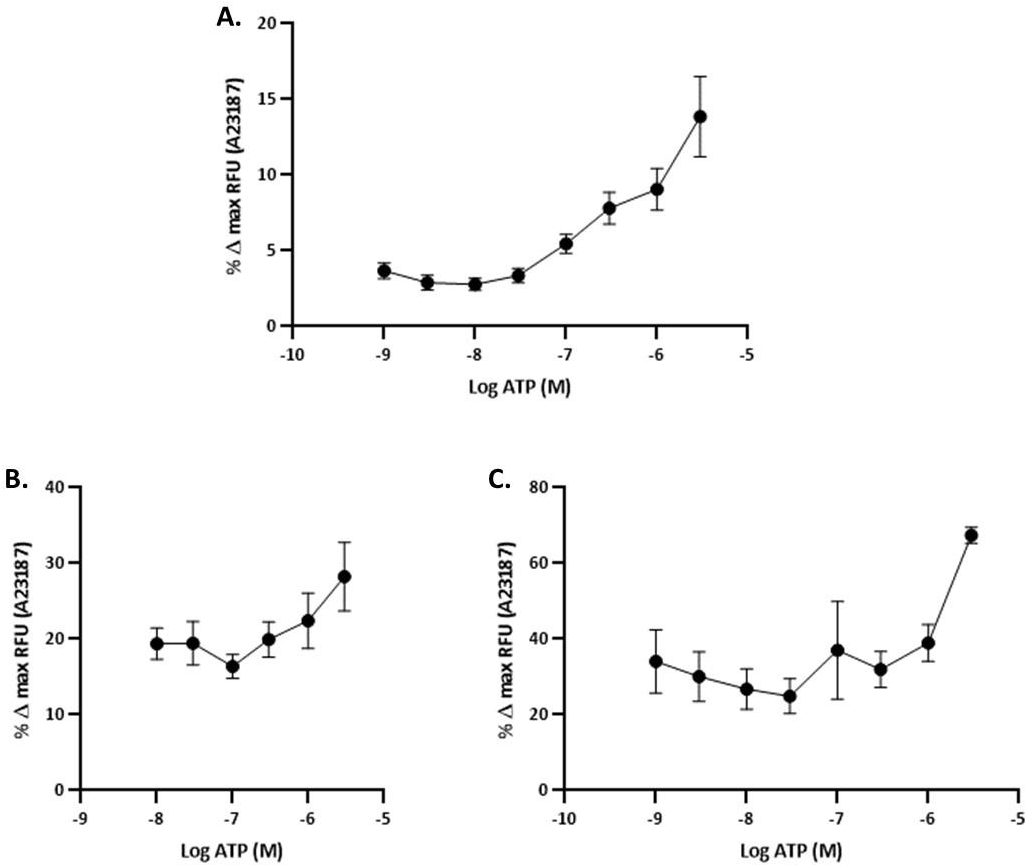

Figure 2.15 Dose response curve of 1N1 P2X3 (**A**), A549 (**B**) and Beas-2b (**C**) cell lines when stimulated with P2X3 agonist ATP. Responses measured as a percentage of maximum response to control, calcium ionophore A23187. Results are displayed as mean ± SEM (n=3). EC_{50} = 419nM, A549 EC_{50} = 1592nM, Beas-2b EC_{50} = 4310nM

2.3.4.2 Transfected Astrocyte Cell Line Expresses Functional P2X3 but is not Inhibited with P2X3 Antagonist

To support the positive P2X3 functional analysis of 1N1 P2X3 cells, an attempt was made to block P2X3 receptor activity by using a P2X3 antagonist. 1N1 P2X3 cells were subjected to a dose response curve with varying concentrations of the P2X3 antagonist NF110 for 15 minutes prior to stimulation with the EC_{50} of ATP (400nM) and the resulting calcium flux measured. Similarly, to show that A549 and Beas-2b cells were not negatively affected by the application of the antagonist, the cells were treated with a high dose of NF110 (300nM) in the same manner as above prior to stimulation with the EC_{50} of GSK (100nM) as outlined in 2.2.5.1.

The dose response curve produced as a consequence of treatment of 1N1 P2X3 cells with NF110 prior to EC_{50} ATP application enabled an IC_{50} of 24nM to be calculated (Figure 2.16a). However, when compared to the control (DMEM replacing NF110) all concentrations showed an increase in calcium flux rather than the expected reduction due to the antagonist effect (Figure 2.16b).

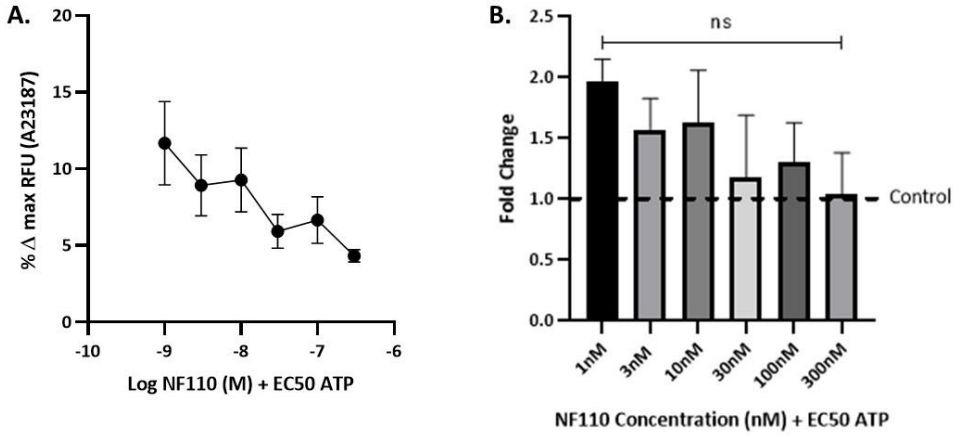

Figure 2.16 Dose response curve of 1N1 P2X3 cell line when incubated with P2X3 antagonist NF110 for 15 minutes prior to stimulation with P2X3 agonist ATP at the EC_{50} concentration (419nM), IC_{50} = 24nM (**A**). Response at increasing NF110 concentration shown as fold change against positive control (EC_{50} ATP) (**B**). Responses measured as a percentage of maximum response to control, calcium ionophore A23187. Results are displayed as mean ± SEM (n=3). Statistical analysis was conducted using a one-way ANOVA with multiple comparison by Tukey analysis.

A549 cells demonstrated a minimal increase (P>0.05) in intracellular calcium response when treated with NF110 prior to GSK101 application compared to GSK101 alone (Figure 2.17a), whilst Beas-2b cells demonstrated no change in intracellular calcium flux when treated with NF110 prior to GSK101 application (P>0.05) compared to GSK101 alone (Figure 2.17b). In light of the fact that no observable inhibitory effect occurred when NF110 was applied to 1N1 P2X3 cells and due to time constraints preventing further concentrations being tested to identify whether any inhibitory effect could be achieved, a concentration of 300nM NF110 was used in subsequent experiments, as this reduced the calcium flux to

the same level as the control whilst, not affecting A549 and Beas-2b cells to any noticeable extent.

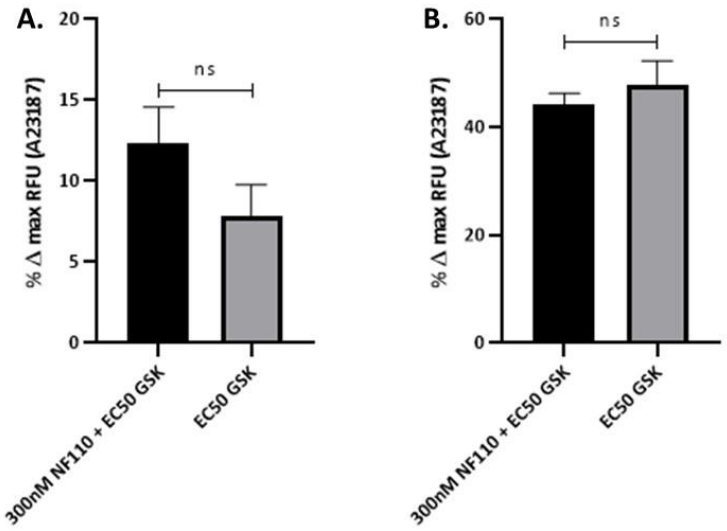

Figure 2.17 Calcium signalling response measured in A549 (**A**) and Beas-2b (**B**) cell lines after incubation with either P2X3 antagonist NF110 or complete DMEM for 15 minutes prior to stimulation with the EC_{50} concentration of TRPV4 agonist GSK101 (100nM). Responses were measured as a percentage of maximum response to control, calcium ionophore A23187. Results are displayed as mean ± SEM (n=3). Statistical analysis was conducted using an unpaired t-test.

2.3.4.3 Wild Type Astrocyte Cell Line is not Activated by ATP

To further confirm the presence of a functional P2X3 receptor, 1N1 P2X3 and wild type 1N1 cells were treated with the P2X3 agonist ATP at varying concentration and the resulting calcium flux measured using the method outlined in 2.2.5.1. As previously shown and replicated again here, 1N1 P2X3 cells demonstrate a functionally positive response to ATP, whilst wild type 1N1 cells which lack the P2X3 receptor showed no functional response to ATP at any concentration ($P<0.05$) (Figure 2.18).

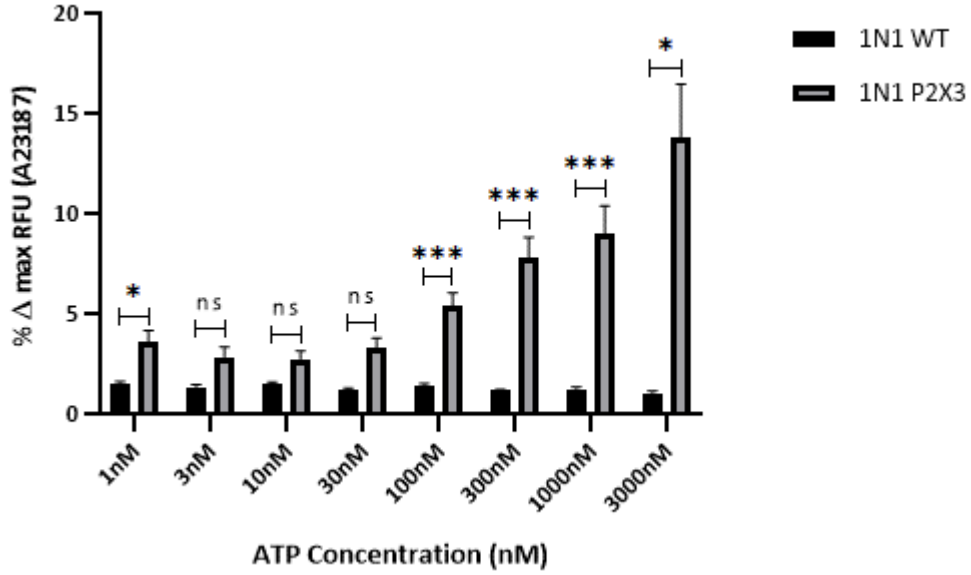

Figure 2.18 Calcium signalling response measured in 1N1 WT and 1N1 P2X3 cell lines stimulated with P2X3 agonist ATP. Responses measured as a percentage of maximum response to control, calcium ionophore A23187. Results are displayed as mean ± SEM (n=3). Statistical analysis was conducted using a multiple t-tests using the Holm-Sidák method. $P<0.05^{*}$, $P<0.005^{***}$

2.3.5 Assessment of Tight Junction Formation

To better understand the monolayer formation of the cell lines of interest in preparation for subsequent experiments using co-culture techniques and Rhinovirus (RV) infection, an assessment of the formation of tight junctions and the extent of membrane leakage was performed to identify the optimum time points for infecting cells and conducting co-culture calcium signalling.

2.3.5.1 TEER Measurements Revealed Limited Tight Junction Formation in Airway Epithelial Cell Lines but not Transfected Astrocytes

The first method used to assess the formation of tight junctions in A549, Beas-2b and 1N1 P2X3 cell lines was TEER measurements using the method outlined in 2.2.6.1. A549 cells cultured without the presence of an air-liquid interface (ALI) demonstrated a gradual increase in resistance measurements over the first 120 hours post seeding, at which point

the measurements plateaued before finally decreasing as cells began to die at around 250 hours post seeding. Similarly, when an ALI is introduced to the A549 cells, peak measurements were seen at 120 hours and with decreasing measurements noticeable around 250 hours furthermore, there was little difference between the resistance measurements and point at which cell death began (Figure 2.19).

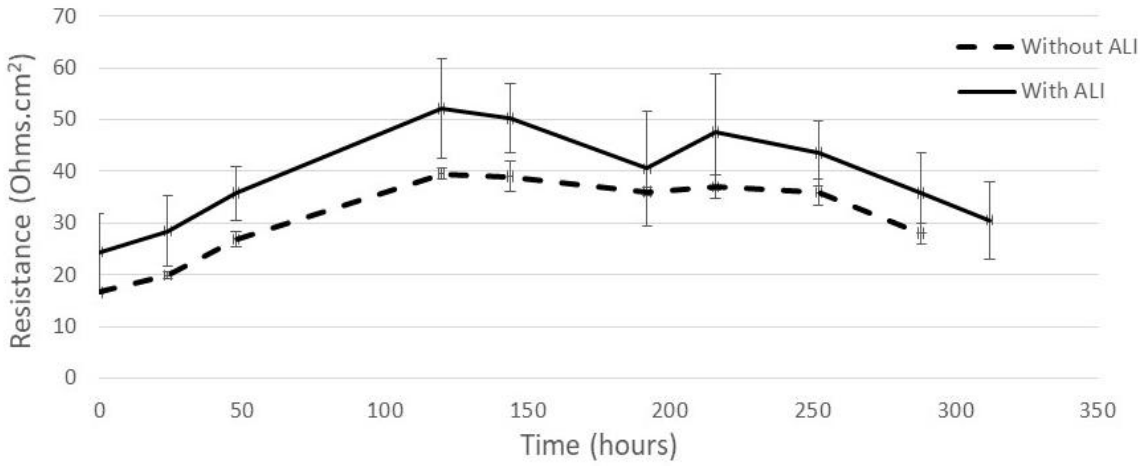

Figure 2.19 TEER measurements from a confluent monolayer of A549 cells, taken from 24h post seeding for a total of 14 days where an ALI was present this was introduced after 72 hours. Results are displayed as mean ± SEM (n=3).

Beas-2b cells cultured without the presence of an ALI demonstrated a gradual increase in resistance measurements over the first 250 hours post seeding, at which point the measurements plateaued before decreasing as cell death began at around 400 hours post seeding, with the resistance readings returning to original measurements after 700 hours in culture. Conversely, when an ALI was introduced to the Beas-2b cells resistance measurements continued to increase for an extended time period with peak measurements occurring at 500 hours, before rapidly decreasing as cells could no longer be maintained from 600 hours onwards before finally returning to initial resistance measurements at 850 hours (Figure 2.20).

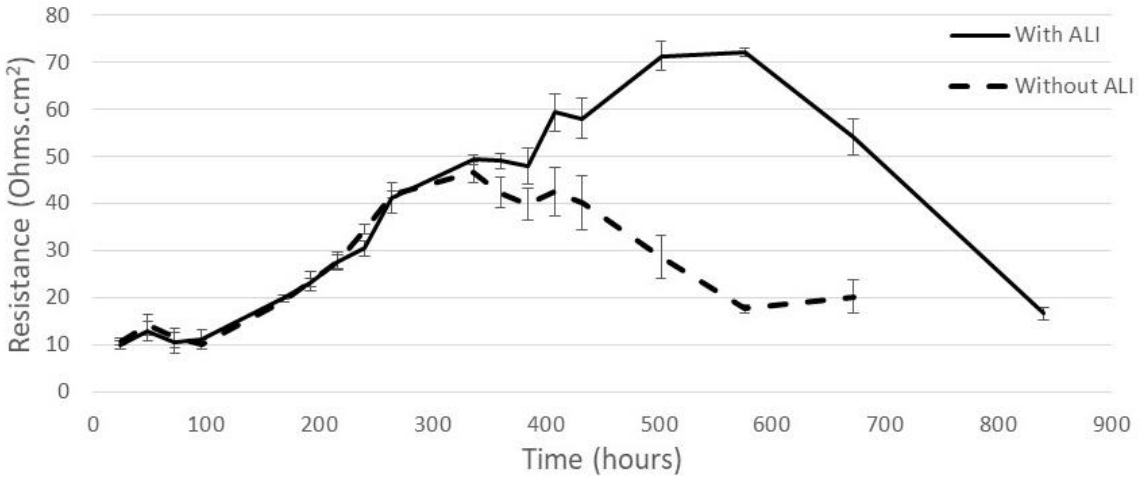

Figure 2.20 TEER measurements from a confluent monolayer of Beas-2b cells, taken from 24h post seeding for a maximum of 35 days, where an ALI was present this was introduced after 96 hours. Results are displayed as mean ± SEM (n=3).

Based on the A549 and Beas-2b resistant measurements, any RV infections conducted to investigate impact on tight junction formation were conducted after 96 hours in culture. Whilst co-culture calcium signalling were conducted after cells had been in culture for 7 days as in both cases this ensured tight junctions had started to form and cell density was sufficiently high to enable calcium flux to be measured.

1N1 P2X3 cells did not form a monolayer in the same manner as epithelial cells (Figure 2.6) which was reflected in the resistance measurements recorded over the duration of the culture period whereby the typical increase, plateau and decrease in measurement was absent and instead an erratic range of measurements were observed (Figure 2.21). Thus, although this cell line was utilised in co-culture experiments, time points for calcium signalling was based on the measurements made in A549 and Beas-2b cells.

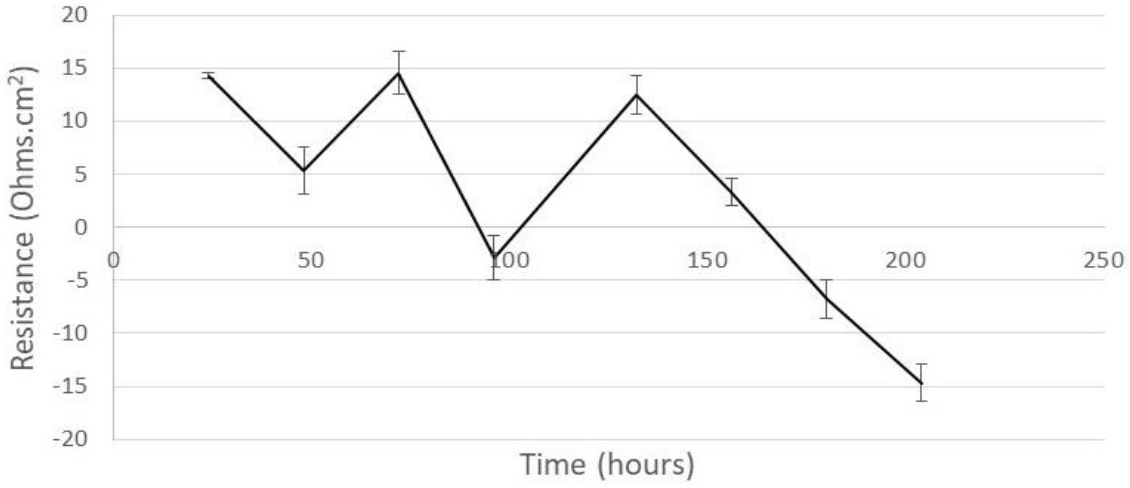

Figure 2.21 TEER measurements from a confluent monolayer of 1N1 P2X3 cells, taken from 24h post seeding for a total of 14 days. Results are displayed as mean ± SEM (n=3).

2.3.5.2 Fluorescein Exclusion Measurements Revealed Limited Tight Junction Formation in Airway Epithelial Cell Lines

To support the findings from the TEER measurements regarding the point at which tight junctions are strongest, a fluorescein exclusion assay was performed on A549 and Beas-2b cells to demonstrate the extent of leakage through the monolayer using the method outlined in 2.2.6.2. The extent of fluorescein leakage seen in A549 cells was lower after 7 days in culture compared to after 4 days in culture ($P>0.05$), whilst the extent of leakage also increased when sampled at 2 hours after fluorescein application compared to 30 minutes (Figure 2.22).

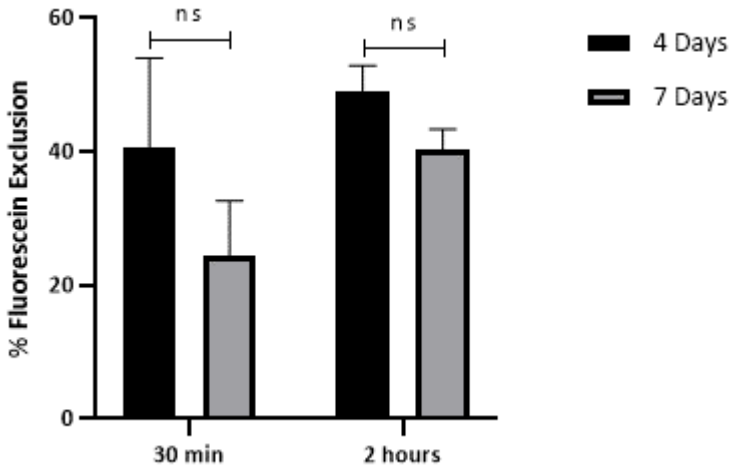

Figure 2.22 Percentage fluorescein exclusion (sampled after 30 minutes and 2 hours incubation with fluorescein solution) through a confluent monolayer of A549 cells, 4 and 7 days post seeding. Fluorescein exclusion was calculated as a percentage of the maximum fluorescein leakage through a blank membrane, relative fluorescent intensity was measured at 485nm excitation and 535nm emission, accounting for media blank. Results are displayed as mean ± SEM (n=3). Statistical analysis was conducted via multiple t-test using the Holm-Sidák method.

The extent of fluorescein leakage in Beas-2b cells when sampled after 2 hours progressively reduced as time in culture was extended, there was a non-significant reduction in fluorescein leakage between 4 and 7 days in culture and between 7 and 14 days in culture ($P>0.05$), whilst there was a significant reduction in fluorescein leakage between 4 and 14 days in culture ($P<0.01$), with the lowest percentage leakage measured after 14 days in culture. The extent of leakage also slightly decreased when sampled at 2 hours compared to 30 minutes (Figure 2.23).

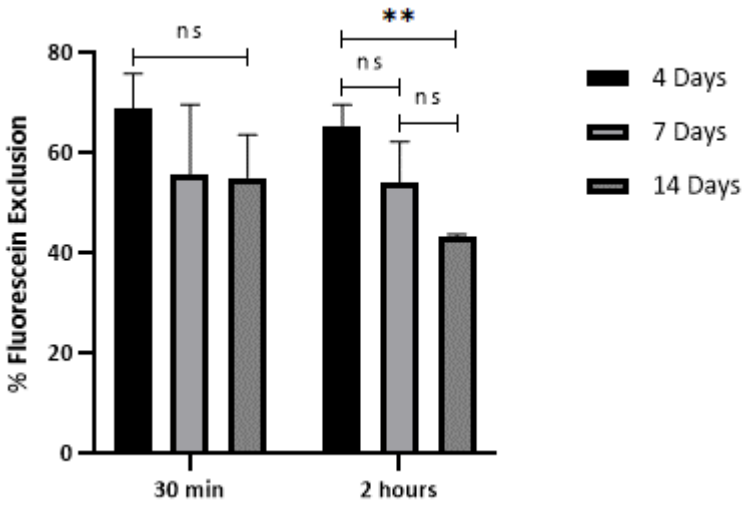

Figure 2.23 Percentage fluorescein exclusion (sampled after 30 minutes and 2 hours incubation with fluorescein solution) through a confluent monolayer of Beas-2b cells, 4, 7 and 14 days post seeding. Fluorescein exclusion was calculated as a percentage of the maximum fluorescein leakage through a blank membrane, relative fluorescent intensity was measured at 485nm excitation and 535nm emission, accounting for media blank. Results are displayed as mean ± SEM (n=3). Statistical analysis was conducted via multiple t-tests using the Holm-Sidák method. $P<0.01^{**}$

When an ALI was introduced to the Beas-2b cells cultured for 14 days, the extent of fluorescein leakage with an ALI was higher than without an ALI when sampled at 30 minutes ($P>0.05$). However, when sampled at 2 hours there was a significant increase in the fluorescein leakage in the presence of an ALI compared to no ALI ($P<0.01$) (Figure 2.24). The increase in fluorescein leakage observed in the presence of an ALI is a reflection on the monolayer becoming partially detached from Thincert™ during the incubation period between the 30 minutes and 2 hour sampling times. Based on this observation an ALI was not introduced when using this method for subsequent experiments with RV infection. Furthermore, based on the A549 and Beas-2b fluorescein leakage measurements coupled with the previous TEER measurements any RV infections conducted to investigate impact on tight junction formation was conducted after 7 days in culture.

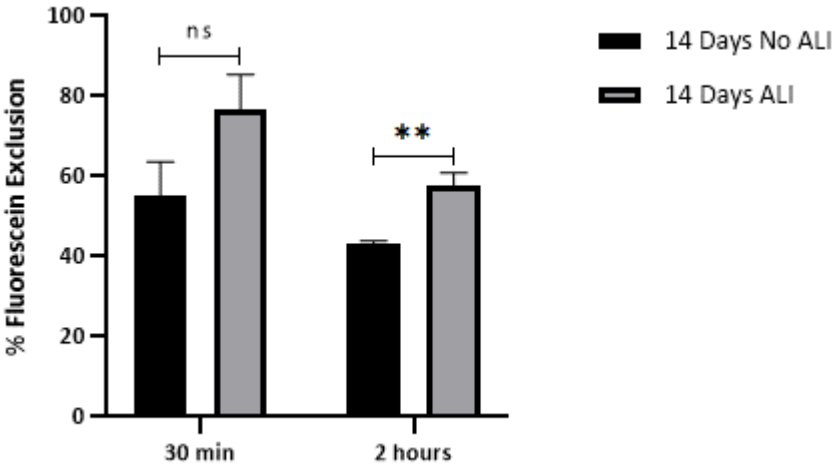

Figure 2.24 Percentage fluorescein exclusion (sampled after 30 minutes and 2 hours incubation with fluorescein solution)through a confluent monolayer of Beas-2b cells, 14 days post seeding with and without the introduction of an ALI after 4 days in culture. Fluorescein exclusion was calculated as a percentage of the maximum fluorescein leakage through a blank membrane, relative fluorescent intensity was measured at 485nm excitation and 535nm emission, accounting for media blank. Results are displayed as mean ± SEM (n=3). Statistical analysis was conducted via multiple t-test with multiple comparisons using the Holm-Sidák method. $P<0.01^{**}$

2.3.6 TRPV4 – ATP – P2X3 Pathway Interaction

Having shown that A549 and Beas-2b cells had positive expression of TRPV4 which produced a measureable response to the TRPV4 agonist GSK101 and 1N1 P2X3 cells had a positive functional response to the P2X3 agonist ATP, the next stage of investigation was to attempt to identify if there was any interaction between the cell lines using the hypothesised TRPV4 – ATP – P2X3 pathway.

2.3.6.1 Co-Culture Optimisation

A549, Beas-2b, 1N1 WT and 1N1 P2X3 cells were cultured using a hanging insert in a manner which ensured the cells were not in direct contact with each other but could be used to measure cell-to-cell interactions. Initially, 6 well transparent PET membrane Thincert™, 0.4µm pore size, were inverted, covered with a 50ml centrifuge tube (Fisher

Scientific) with the cone removed and placed on a 100mm petri dish (Fisher Scientific). 1N1 P2X3 cells were seeded on the basal surface of the Thincert™ at a density of $1x10^6$ in a total of 2ml of complete DMEM and left to adhere for 48 hours at 37°C, 5% CO_2. After 48 hours the Thincert™ was placed in a 6 well plate in the correct orientation with 2ml of fresh media, A549 cells were subsequently seeded on the apical surface of the Thincert™ at a density of $1x10^6$ in a total of 2ml of complete DMEM and left to adhere for 48 hours at 37°C, 5% CO_2 (Figure 2.25). This method was based on work conducted by Simintiras *et al* (2017) and whilst this method worked in principle, on replication the design had two main flaws, firstly the plates quickly became contaminated with fungal growth due to the length of time spent outside the confines of a sterile plate in the incubator. To resolve this problem the method was modified so the 1N1 P2X3 cells were left to adhere for 2 hours at 37°C, 5% CO_2 however, this still resulted in contamination with fungal growth. Secondly, the media used to seed the 1N1 P2X3 cells slowly leaked away from the Thincert™ over the duration of the incubation period resulting in the cells drying and subsequently dying. The change to a 2 hour incubation period was also insufficient to prevent the leakage of the media from the tube, thus the alternative method outlined below was devised.

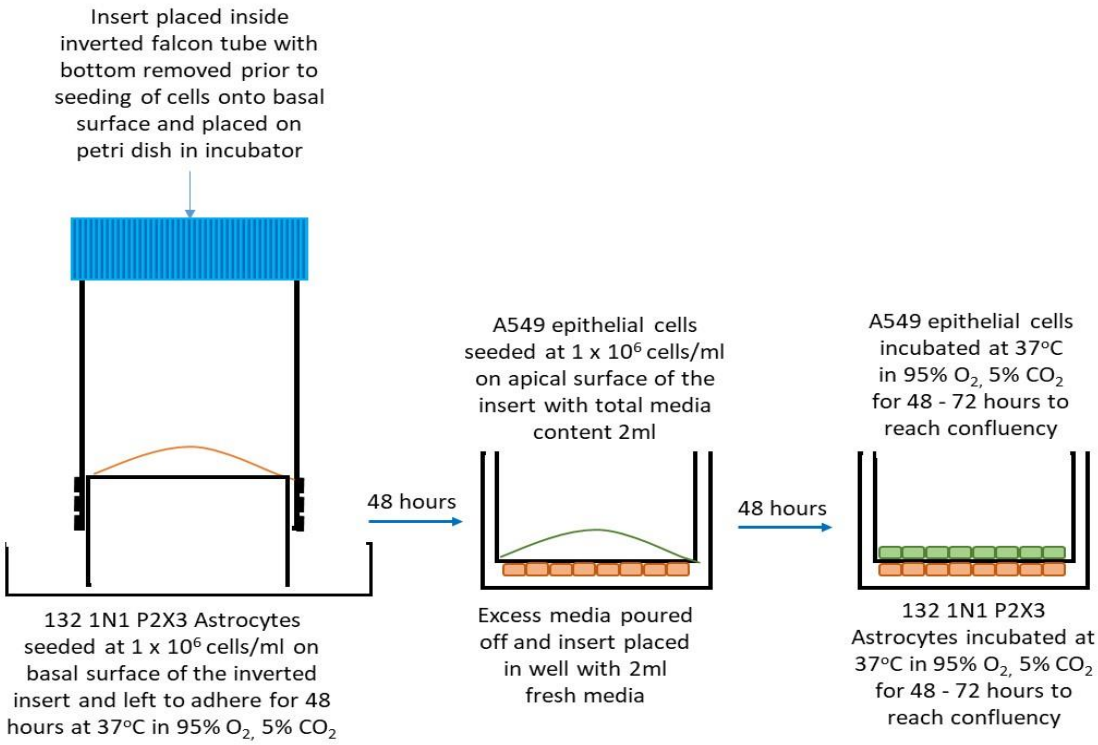

Figure 2.25 Representation of the method used to create the initial cell culture arrangement used for the co-culture experiments.

To overcome the issue of media leakage and fungal contamination, cells were cultured on both the apical and basal surfaces of 24 well transparent PET membrane Thincert™, 0.4µm pore size (Greiner Bio-one), at an initial seeding density of $5x10^4$. The change from 6 well to 24 well Thincert™ enabled the calcium signalling method described in 2.2.5.1 to be developed as the black wall, clear bottom plates were only available in the 24 well format and required a smaller volume of reagents making the optimisation process more cost effective. Initially 1N1 P2X3 cells were seeded on the basal surface of the membrane and A549 cells on the apical surface however, while this orientation was effective for cellular growth, the use of this arrangement was ineffective for calcium signalling assays thus modification were made to enable the cells to take up the dye required to conduct the assay.

Subsequent co-culture experiments were performed with A549 or Beas-2b cells on the basal surface of the membrane and 1N1 P2X3 or 1N1 WT cells on the apical surface (Figure 2.26). To enable cells to be seeded on the basal surface of the membrane, the Thincert™ was inverted and A549 or Beas-2b cells seeded at $1x10^5$ in a maximum of 200µl of complete DMEM. This small volume of media ensured the cells did not overflow the edge of the Thincert™ whilst providing a relatively complete coverage of the entire membrane surface, while the increased seeding density accommodated the loss of cells due to non-adherence. The seeded Thincert™ remained inverted in a sterile category 2 laminar flow hood (Esco Gb Ltd, Barnsley, UK) for a minimum of 30 minutes for A549 cells and 2 hours for Beas-2b cells prior to being returned to the correct orientation and placed in 1ml of complete DMEM in a 24 well, clear, flat-bottomed plate (Sarstedt). 1N1 P2X3 or 1N1 WT cells were then seeded on the apical side of the membrane at $5x10^4$ in a maximum of 300µl of complete DMEM. Cells were incubated at 37°C, 5% CO_2 for 4 or 7 days, depending on the experimental procedure being followed ensuring cells were confluent and had fully covered the membrane.

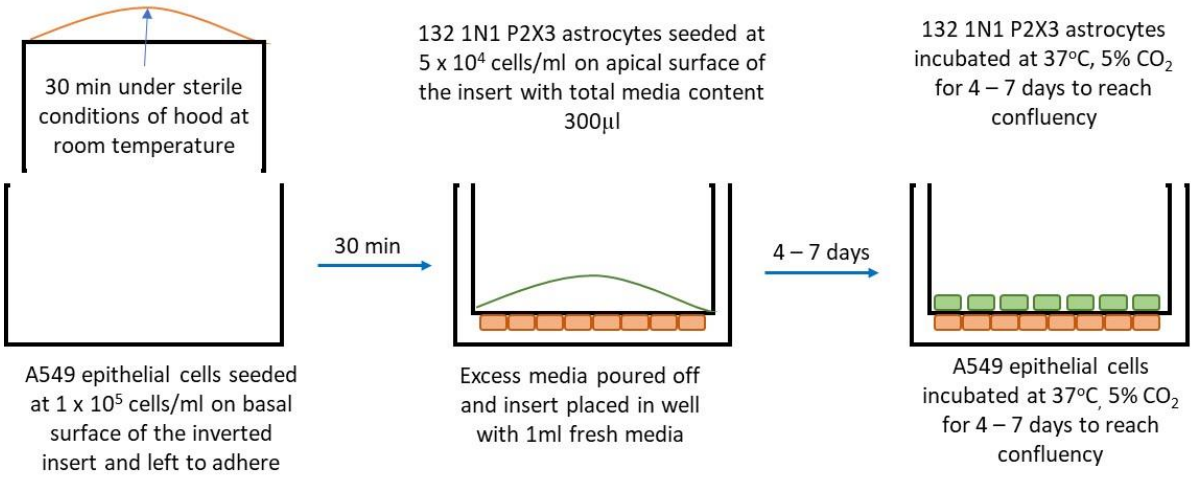

Figure 2.26 Representation of the method used to create the cell culture arrangement used for the co-culture experiments.

To provide further options for subsequent experimental procedures an alternative format was created which although removed the contact directly across the membrane, still ensured that the cells were in close proximity to each other thus providing a similar extent of cell-to-cell interactions. In the alternative format 1N1 P2X3 or 1N1 WT cells were seeded at $1x10^5$ in 1ml of complete DMEM into the bottom of a 24 well, clear bottom, black plate (Greiner Bio-one) and A549 or Beas-2b cells were seeded on the apical surface of a Thincert™ at $5x10^4$ in 300µl of complete DMEM (Figure 2.27). Cells were incubated at 37°C, 5% CO_2 for 4 or 7 days depending on the experimental procedure being following and ensuring cells reached confluency before use.

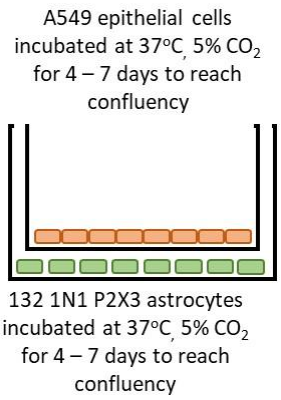

Figure 2.27 Representation of the alternative method used to create the cell culture arrangement used for the co-culture experiments.

2.3.6.2 Low Concentrations of ATP Crossed the Permeable PET Membrane in Co-culture Model

The size of an ATP molecule is approximately 0.7nm (Azarashvili *et al*, 2011), thus theoretically ATP should be able to pass through the 0.4µm pores of the Thincerts™. To ascertain the extent of ATP which crossed the membrane A549 and Beas-2b cells were cultured on Thincerts™ for 7 days and stimulated with GSK101 using the method outlined in 2.2.7.3 and ATP flow measured from both an apical and basal perspective.

When A549 cells were cultured on the apical aspect of the Thincert™ the amount of ATP measured when a sample was collected from directly above the cells shows a pattern similar to that observed in 2.3.3.2. However, when the sample collected from the well was considered the amount of ATP measured was considerably lower and lacking the equivalent peaks in ATP released (Figure 2.28a). When the orientation of the cells was changed to culture A549 cells on the basal aspect of the Thincert™ the amount of ATP measured when a sample was collected from directly below the cells showed a pattern similar to that observed in 2.3.3.2 albeit at a lower ATP level. Similarly, when the sample collected from the well was considered the amount of ATP measured was considerably lower however, in this instance exhibited equivalent peaks at the same time points as those observed in direct relation to the cells (Figure 2.28b).

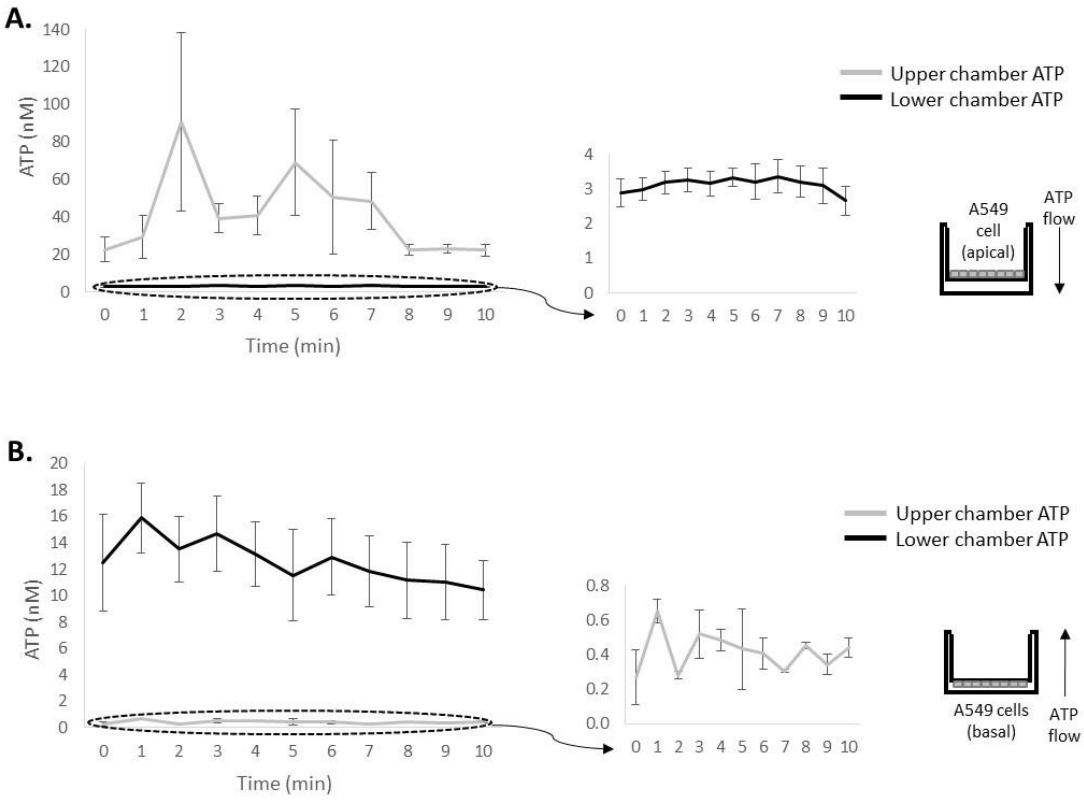

Figure 2.28 Ability of extracellular ATP released by A549 cells to cross a permeable membrane after stimulation with 100nM TRPV4 agonist GSK101. ATP was measured directly above the monolayer (represented by largest ATP values) and across the opposing side of the Thincert™ (represented by circled line and exploded graph), over a duration of 10 minutes post stimulation. Both variations of the dual culture method were utilised to measure the extent of ATP crossing the membrane, A549 cells were cultured on either the apical aspect of the Thincert™ (**A**) or the basal aspect of the Thincert™ (**B**). Results are displayed as mean ± SEM (n=3).

When Beas-2b cells are cultured on the apical aspect of the Thincert™ the amount of ATP measured when a sample was collected from directly above the cells showed a pattern similar to that observed in 2.3.3.2. However, when the sample collected from the well was considered the amount of ATP measured was considerably lower and lacked the equivalent peaks in ATP released (Figure 2.29a). When the orientation of the cells was changed to culture A549 cells on the basal aspect of the Thincert™ the amount of ATP measured when a sample was collected from directly below the cells showed a pattern similar to that observed in 2.3.3.2. Similarly, when the sample collected from the well was considered the

amount of ATP measured was considerably lower and lacked the equivalent peaks in ATP released (Figure 2.29b).

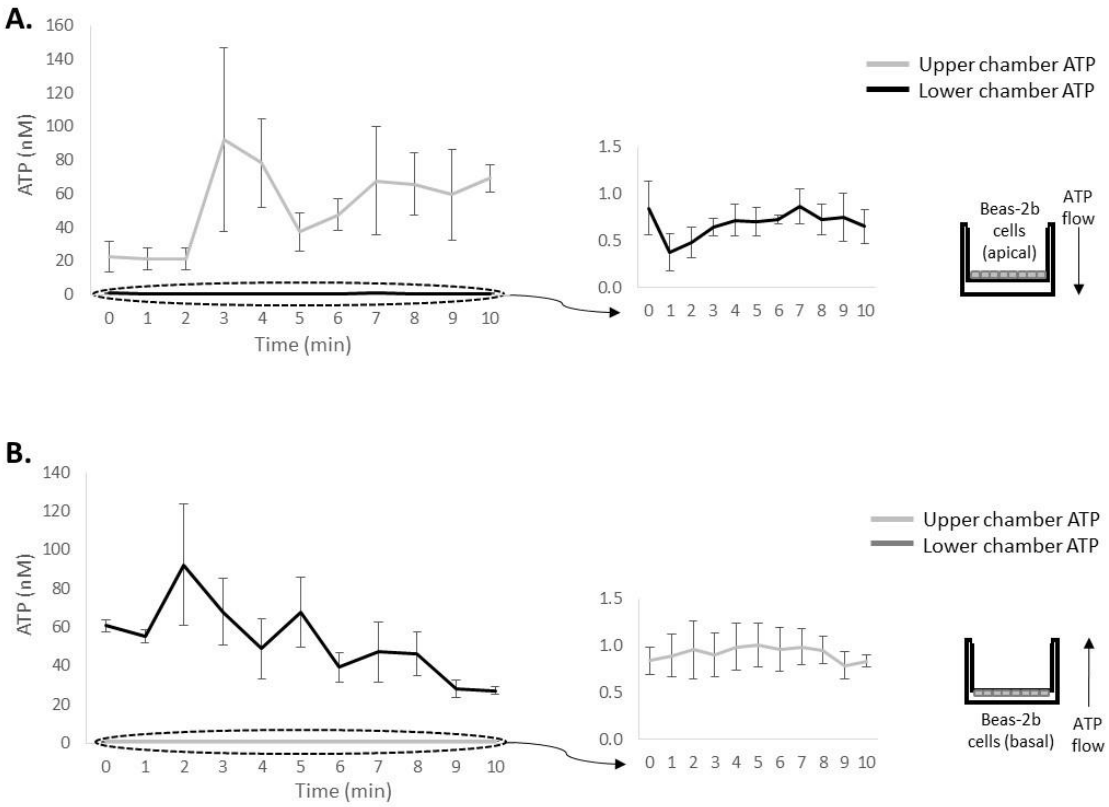

Figure 2.29 Ability of extracellular ATP released by Beas-2b cells to cross a permeable membrane after stimulation with 100nM TRPV4 agonist GSK101. ATP was measured directly above the monolayer (represented by largest ATP values) and across the opposing side of the Thincert™ (represented by circled line and exploded graph), over a duration of 10 minutes post stimulation. Both variations of the dual culture method were utilised to measure the extent of ATP crossing the membrane, Beas-2b cells were cultured on either the apical aspect of the Thincert™ (**A**) or the basal aspect of the Thincert™ (**B**). Results are displayed as mean ± SEM (n=3).

2.3.6.3 Calcium Signalling can be Induced in Astrocyte Cell Line Following Activation of TRPV4 in Airway Epithelial Cells in a Co-Culture Model

To continue investigating whether there was any interaction between TRPV4 and P2X3 receptors, either A549 or Beas-2b cells were co-cultured on a Thincert™ with 1N1 P2X3

cells on the opposing aspect of the Thincert™, additionally A549 cells were also co-cultured with 1N1 WT cells which did not express the P2X3 receptor. 1N1 P2X3 were also treated with either EC_{50} NF110 (300nM) or complete DMEM for 15 minutes prior to stimulation of A549 or Beas-2b cells with EC_{50} GSK101 (100nM), measurements were taken from the chamber containing the 1N1 P2X3/1N1 WT cells using the optimised method outlined in 2.2.7.3.

When A549 cells were cultured on the basal aspect of the membrane and 1N1 P2X3/1N1 WT cells were co-cultured on the apical aspect of the Thincert™ membrane, there was a significant reduction in the percentage response to control ($P<0.01$) between 1N1 P2X3 cells treated with EC_{50} NF110 compared to without NF110 treatment at both 600 and 120 seconds. When the response between 1N1 P2X3 without treatment with EC_{50} NF110 and 1N1 WT cells are compared there was a non-significant reduction at 600 seconds ($P>0.05$) however, when a response was measured at 120 seconds the reduction is significantly different ($P<0.01$) (Figure 2.30a).

When A549 cells were cultured on the apical aspect of the Thincert™ membrane and 1N1 P2X3/1N1 WT cells were cultured in the bottom of a 24 well, there was no change in the percentage response to control between 1N1 P2X3 cells treated with EC_{50} NF110 or 1N1 WT cells compared to 1N1 P2X3 cells without NF110 treatment at 600 seconds ($P>0.05$). When responses were measured at 120 seconds there was also no change between 1N1 P2X3 with and without NF110 treatment ($P>0.05$) however, there was a significant reduction between 1N1 P2X3 cells without NF110 treatment and 1N1 WT cells ($P<0.05$) (Figure 2.30b).

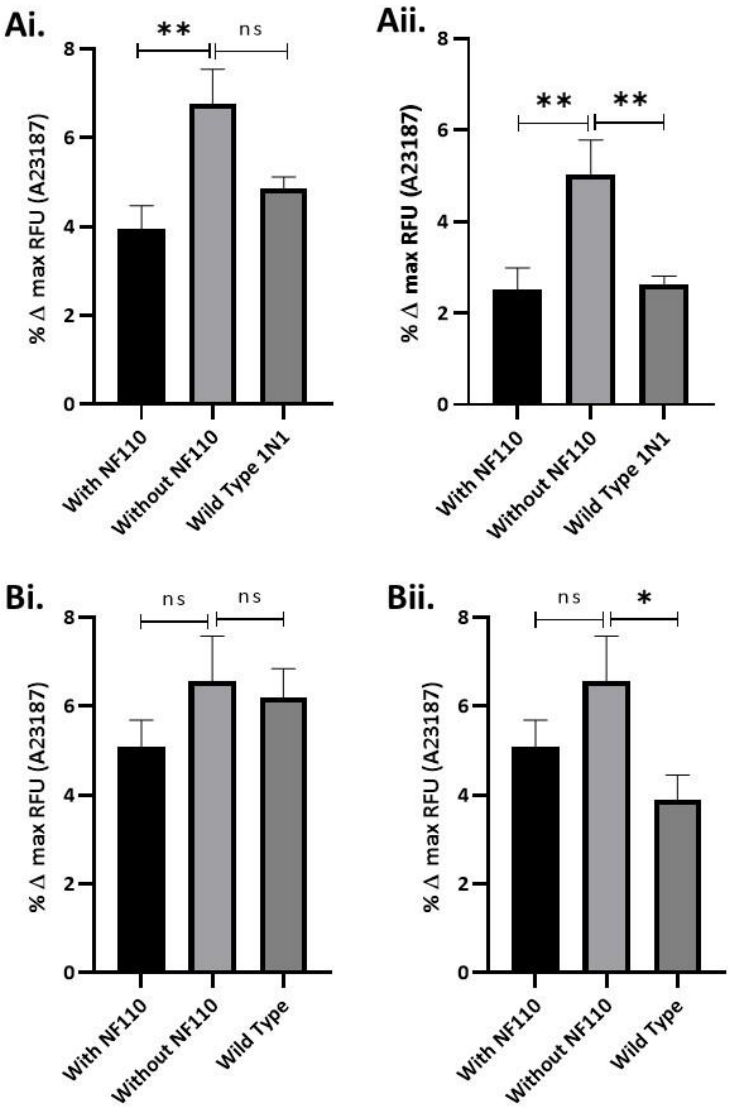

Figure 2.30 Calcium signalling response measured in 1N1 P2X3 and wild type (WT) 1N1 cell lines after stimulation of A549 (on the opposing side of a Thincert^{TM}) with TRPV4 agonist GSK101. P2X3 antagonist NF110 was also applied to 1N1 P2X3 cells. A549 cells were cultured on the basal aspect of the membrane, whilst 1N1 P2X3/1N1 cells were cultured on the apical aspect of the membrane and response recorded for 600 seconds (**Ai**) or 120 seconds (**Aii**). Alternatively A549 cells were cultured on the apical aspect of the membrane, whilst 1N1 P2X3/1N1 cells were cultured in the bottom of a 24 well plate and response recorded for 600 seconds (**Bi**) or 120 seconds (**Bii**). Responses were measured as a percentage of maximum response to control, calcium ionophore A23187. Results are displayed as mean ± SEM (n=3). Statistical analysis was conducted using a one-way ANOVA with multiple comparison by Tukey analysis. $P<0.05^{*}$, $P<0.01^{**}$

When Beas-2b cells are cultured in either orientation there was no significant difference in the percentage response to control between 1N1 P2X3 cells treated with EC_{50} NF110 compared to 1N1 P2X3 cells without NF110 treatment at both 600 and 120 seconds (P>0.05) (Figure 2.31).

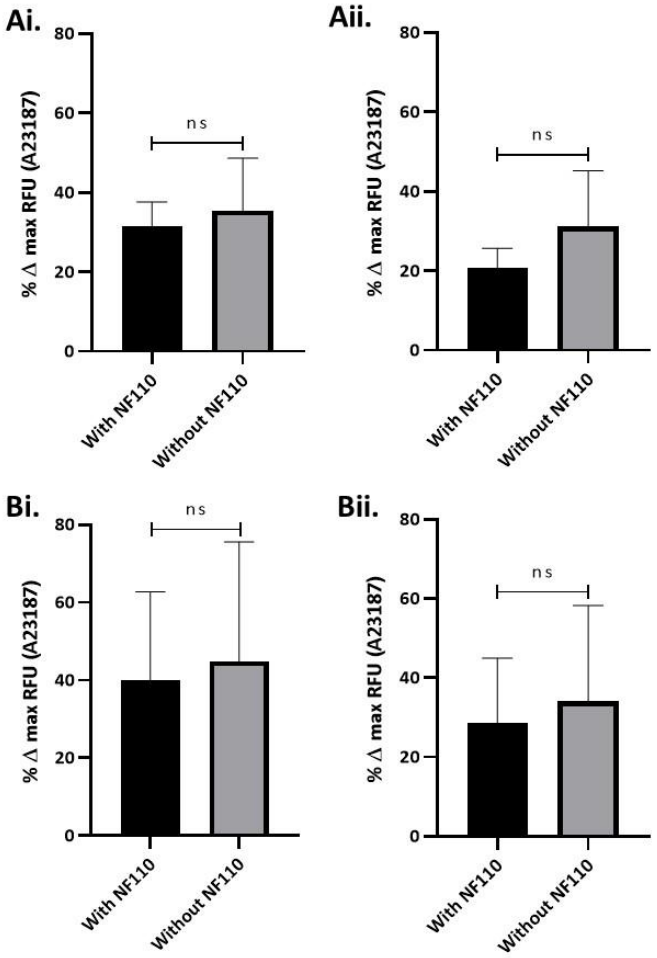

Figure 2.31 Calcium signalling response measured in 1N1 P2X3 cell line after stimulation of Beas-2b (on the opposing side of a Thincert™) with TRPV4 agonist GSK101. P2X3 antagonist NF110 was also applied to 1N1 P2X3 cells. Beas-2b cells were cultured on the basal aspect of the membrane, whilst 1N1 P2X3 cells were cultured on the apical aspect of the membrane and response recorded for 600 seconds (**Ai**) or 120 seconds (**Aii**). Alternatively Beas-2b cells were cultured on the apical aspect of the membrane, whilst 1N1 P2X3 cells were cultured in the bottom of a 24 well plate and response recorded for 600 seconds (**Bi**) or 120 seconds (**Bii**). Responses were measured as a percentage of maximum response to control, calcium ionophore A23187. Results are displayed as mean ± SEM (n=3). Statistical analysis was conducted using an unpaired t-test.

2.3.6.4 Airway Epithelial and Astrocyte Cell Lines Distribute Evenly in a Mixed Culture Model

To show that cells lines grown in mixed culture for 48 hours continue to demonstrate normal morphology and are evenly distributed throughout the culture plate, cells were stained using Kwik-Diff™ staining kit and cells viewed under a light microscope at 100x and 400x magnification. After 48 hours in culture, normal morphology of A549, Beas-2b and 1N1 P2X3 was still observed and cells appeared to be relatively evenly distributed throughout the imaged area with both epithelial and neuronal cells growing within the same culture area (Figure 2.32).

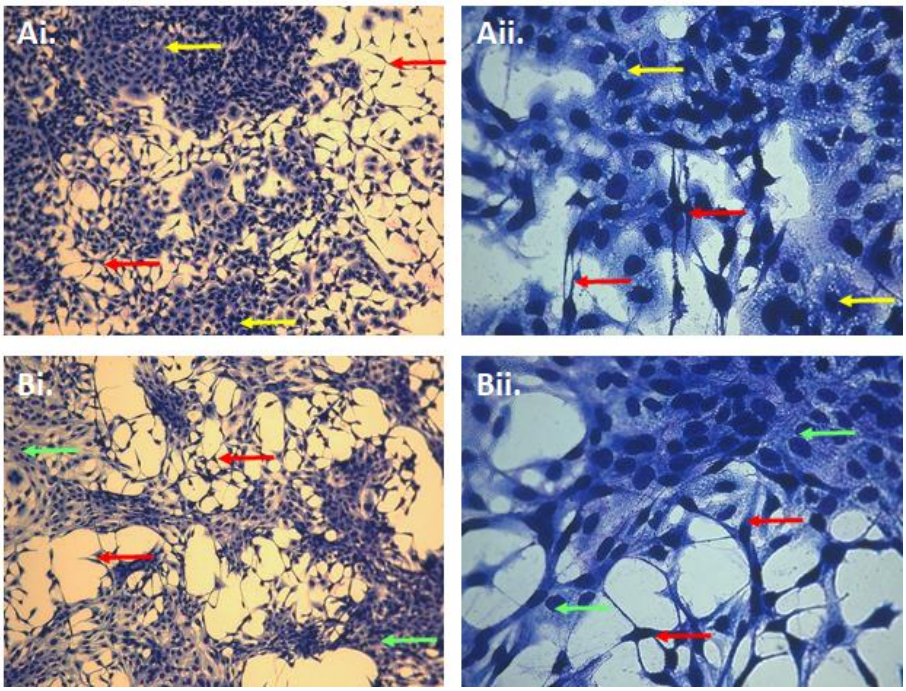

Figure 2.32 Ai – Aii represents A549 human lung epithelial cells and 1321N1 human brain astrocytoma cells transfected with P2X3 cultured together over a 48 hour time period, viewed at 100x magnification (**Ai**) and 400x magnification (**Aii**). **Bi – Bii** represents Beas-2b human bronchial epithelial cells and 1321N1 human brain astrocytoma cells transfected with P2X3 cultured together over a 48 hour time period, viewed at 100x magnification (**Bi**) and 400x magnification (**Bii**). Arrows indicate 1N1 P2X3 cells (red), A549 cells (yellow) and Beas-2b cells (green). Images represents three independent experiments (n=3).

2.3.6.5 Calcium Signalling can be Induced in Astrocyte Cell Line Following Activation of TRPV4 in Airway Epithelial Cells in a Mixed Culture Model

To support the results from the co-culture calcium signalling experiments and to further investigate whether there was any interaction between TRPV4 and P2X3 receptors. A549, Beas-2b and 1N1 P2X3 cells were cultured either individually (as single cell lines) or in the same well, with identical seeding densities utilised in both individual and mixed wells. Owing to similar doubling times (22, 24 and 26 hours for A549, 1N1 P2X3 and Beas-2b cells respectively), all cell lines were seeded at the same initial seeding density for 52 hours until approximately 90% confluency was achieved in mixed wells. Lower levels of confluency were evident in wells were cell lines had been cultured individually as a consequence of the use of same seeding densities throughout, this subsequently enabled calcium signalling response rates in single cell cultures to be combined to identify if any additive effect could be identified when cell lines were grown together. A549 or Beas-2b and 1N1 P2X3 cells were stimulated with varying concentrations of GSK101 and in one instance treated with EC_{50} NF110 (300nM) for 15 minutes prior to stimulation with EC_{50} GSK101 (100nM) using the optimised method outlined in 2.2.5.2. It should be noted that the application of 0nM GSK101, represented the application of phenol red free DMEM without any agonist, this allowed the extent of mechanosensation caused by the application of the DMEM to the A549 or Beas-2b cells to be shown and considered alongside the responses measured due to the application of the TRPV4 agonist.

The percentage response to control was calculated for A549 and 1N1 P2X3 cells cultured individually and the two values added together to give a total percentage response. When this combined response was compared to the percentage response to control for A549 and 1N1 P2X3 cells cultured in the same well there was no significant difference between the observed values ($P>0.05$). It should be noted however, that when EC_{50} NF110 (300nM) is applied to the mixed cultured there was a reduction in percentage response, although non-significantly. Similarly, when a higher concentration of GSK101 was utilised (300nM) there was also a non-significant increase in response for cells grown in a mixed culture compared to those grown individually (Figure 2.33).

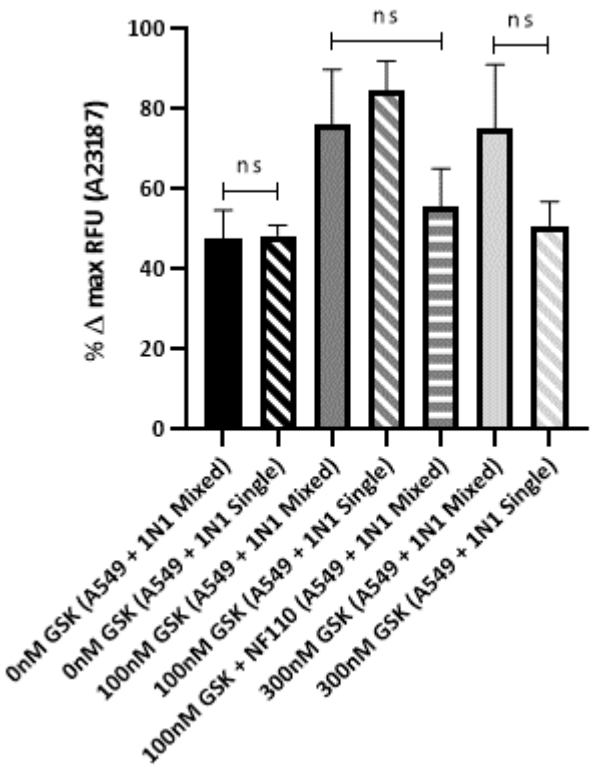

Figure 2.33 Calcium signalling response measured in A549 and 1N1 P2X3 cell lines stimulated with TRPV4 agonist GSK101. Cells were cultured both separately (values combined for graph, identified as 'single' on axis label) and mixed. P2X3 antagonist NF110 was also utilised in the mixed culture method. Responses measured as a percentage of maximum response to control, calcium ionophore A23187. Results are displayed as mean ± SEM (n=6). Statistical analysis was conducted using a one-way ANOVA with multiple comparison by Tukey analysis.

The percentage response to control was calculated for Beas-2b and 1N1 P2X3 cells cultured individually and the two values added together to give a total percentage response. When this combined response was compared to the percentage response to control for Beas-2b and 1N1 P2X3 cells cultured in the same well there was no significant difference between the observed values ($P>0.05$). It should be noted however, that when EC_{50} NF110 (300nM) was applied to the mixed cultured there was a non-significant reduction in percentage response (Figure 2.34).

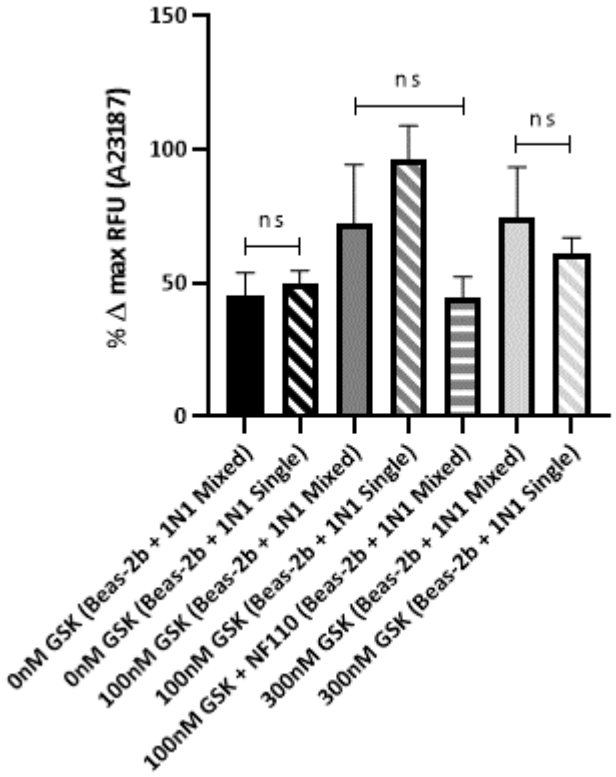

Figure 2.34 Calcium signalling response measured in Beas-2b and 1N1 P2X3 cell lines stimulated with TRPV4 agonist GSK101. Cells were cultured both separately (values combined for graph, single) and mixed. P2X3 antagonist NF110 was also utilised in the mixed culture method. Responses measured as a percentage of maximum response to control, calcium ionophore A23187. Results are displayed as mean ± SEM (n=6). Statistical analysis was conducted using a one-way ANOVA with multiple comparison by Tukey analysis.

2.3.7 Measuring the Impact of Rhinovirus Infection

Having demonstrated the functional responses of A549 and Beas-2b cell lines in basal conditions the cells were subsequently infected with human Rhinovirus serotype 16 (RV16). This enabled comparisons in cellular response between RV infection (RV16), sham infection (ultrafiltered RV16) or basal conditions to be considered.

2.3.7.1 Human Rhinovirus can Infect Airway Epithelial Cell Lines

To confirm successful infection of A549 and Beas-2b cells with RV16 samples of cell supernatant were taken from cells infected with RV16 or ultrafiltered RV16, 48 hours post infection. After conducting seven 10-fold dilutions, cell supernatant was applied to Hela Ohio cells, incubated and scored after 4 days (see 2.2.8.5).

Confirmation of successful infection of A549 cells was evident after the completion of the modified endpoint dilution assay. When scored, Hela Ohio cells treated with RV16 supernatant from A549 cells at dilutions below 10^{-1} were alive, whilst those treated with more concentrated supernatants were dead. Conversely, when ultrafiltered RV16 supernatant from A549 cells was applied at any concentration to Hela Ohio cells all cells survived (Figure 2.35). This can be further supported through the microscopy images which show cell death, evident through rounding and sloughing, in Hela Ohio cells treated with undiluted RV16 supernatant from A549 cells. Whilst those cells which were treated with either diluted RV16 supernatant or any concentration of ultrafiltrated RV16 supernatant look similar in appearance to basal (control) cells (Figure 2.36).

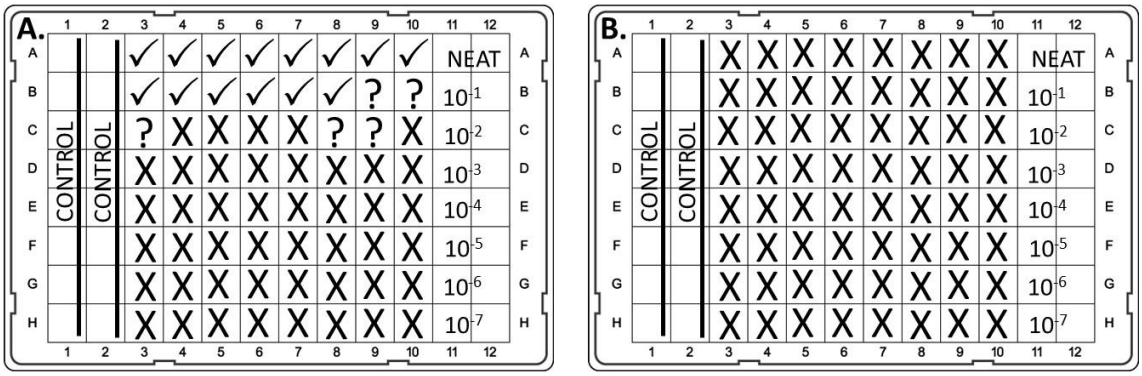

Figure 2.35 Hela Ohio cells subjected to a modified endpoint dilution assay scored 4 days post application of A549 cell supernatant from cell infected for 48 hours with RV16 (**A**) and cells treated for 48 hours with ultrafiltered RV16 (**B**). Images represents three independent experiments (n=3).

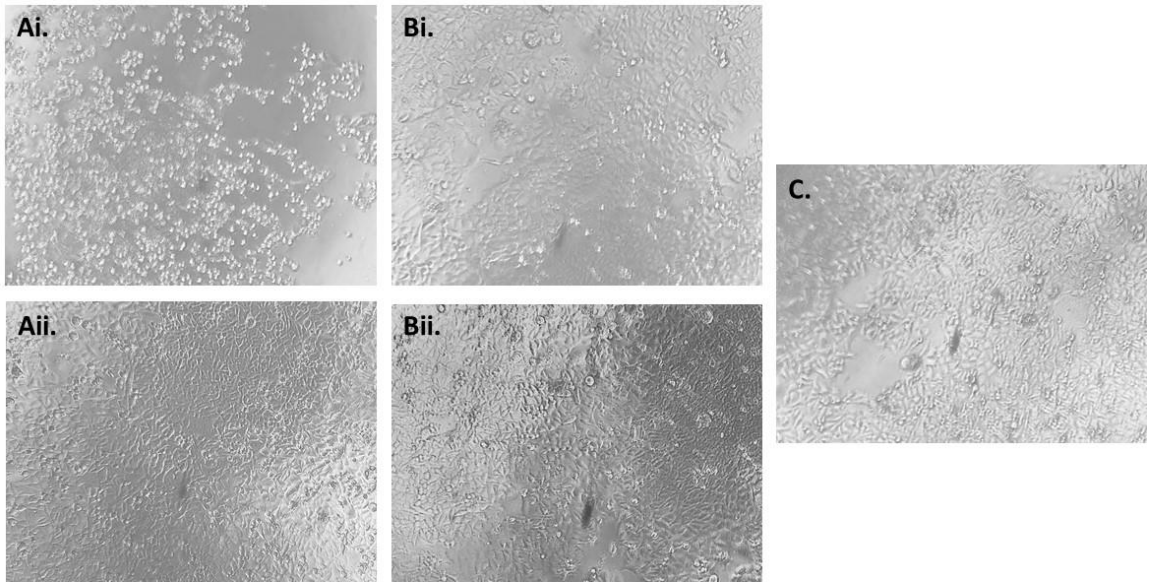

Figure 2.36 Hela Ohio cells viewed at 100x magnification, 4 days post application of A549 cell supernatant from cell infected for 48 hours with RV16 (**Ai – Aii**) and cells treated for 48 hours with ultrafiltered RV16 (**Bi – Bii**). Supernatant was applied undiluted (**Ai** and **Bi**) or after a 10^{-3} dilution (**Aii** and **Bii**), **C** represents Hela Ohio cells cultured for 4 days in control conditions. Images represents three independent experiments (n=3).

Confirmation of successful infection of Beas-2b cells was evident after the completion of the modified endpoint dilution assay. When scored, Hela Ohio cells treated with RV16 supernatant from Beas-2b cells at dilutions below 10^{-3} were alive, whilst those treated with more concentrated supernatants were dead. Similarly, when ultrafiltered RV16 supernatant from Beas-2b cells was applied to Hela Ohio cells at dilutions below 10^{-1} were alive, whilst those treated with more concentrated supernatants were dead. (Figure 2.37). This can be further supported through the microscopy images which show cell death, evident through rounding and sloughing, in Hela Ohio cells treated with undiluted RV16 and ultrafiltered RV16 supernatant from Beas-2b cells. Whilst those cells which were treated with either diluted RV16 or ultrafiltered RV16 supernatant look similar in appearance to basal cells (Figure 2.38).

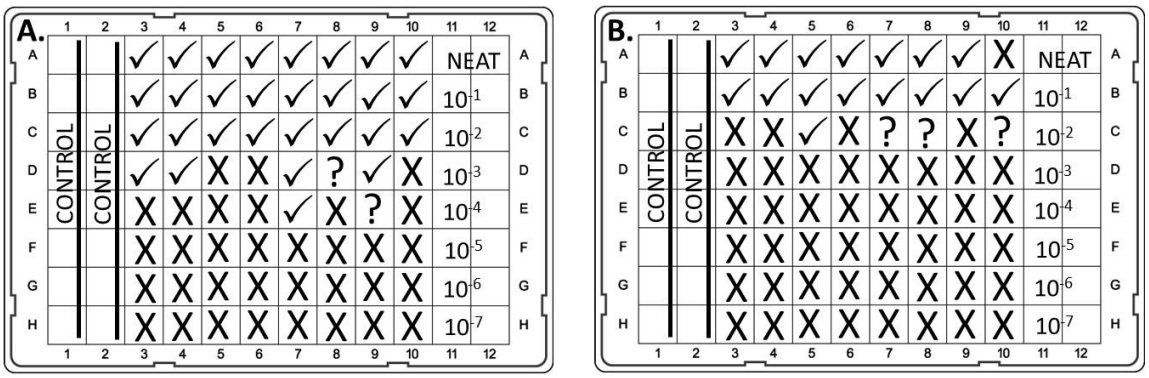

Figure 2.37 Hela Ohio cells subjected to a modified endpoint dilution assay scored 4 days post application of Beas-2b cell supernatant from cell infected for 48 hours with RV16 (**A**) and cells treated for 48 hours with ultrafiltered RV16 (**B**). Images represents three independent experiments (n=3).

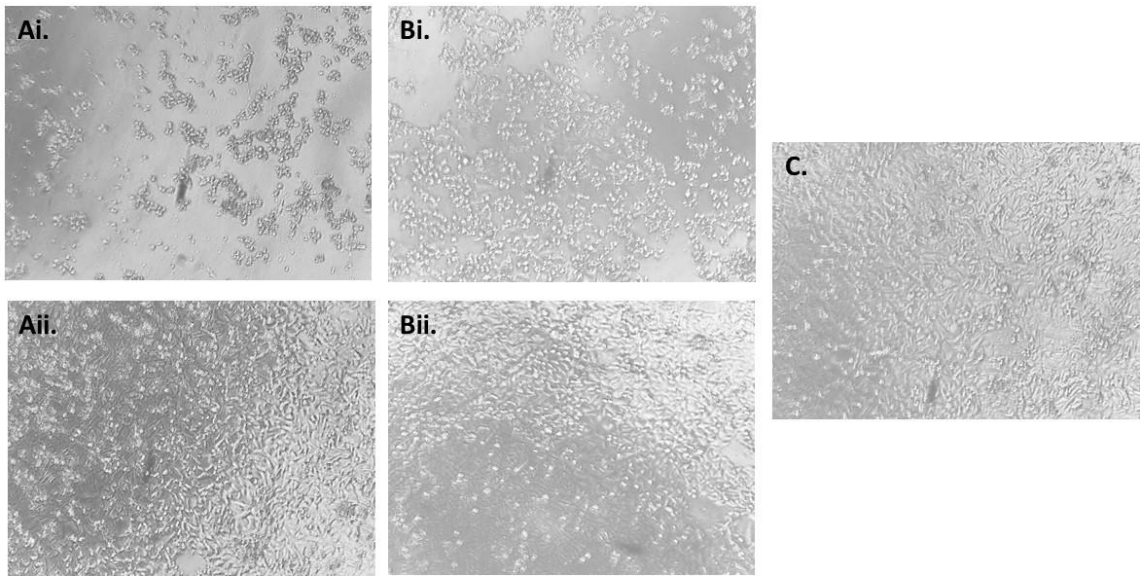

Figure 2.38 Hela Ohio cells viewed at 100x magnification, 4 days post application of Beas-2b cell supernatant from cell infected for 48 hours with RV16 (**Ai – Aii**) and cells treated for 48 hours with ultrafiltered RV16 (**Bi – Bii**). Supernatant was applied undiluted (**Ai** and **Bi**) or after a 10^{-3} dilution (**Aii** and **Bii**), **C** represents Hela Ohio cells cultured for 4 days in control conditions. Images represents three independent experiments (n=3).

2.3.7.2 Exposing DMEM to UV may Cause Release of Cytotoxic Compounds

During early RV16 experiments (including the TEER experiment outlined below) it became apparent that when RV16 was UV inactivated, the cells it was subsequently used to treat died very rapidly. In order to rectify the problem and to account for some of the data collected as a consequence, RV16 and complete DMEM was UV inactivated for 30 minutes at varying intensities (1200µJ/cm^2 or 12000µJ/cm^2) and in vessels made of different materials with different surface areas (60mm polystyrene culture dish, 100mm polystyrene petri dish or a 50ml glass beaker). The UV inactivated RV16 was applied to a confluent monolayer of Hela Ohio cells and monitored for cell death over a 4 day period.

UV inactivation of RV16 in a polystyrene vessel regardless of surface area or UV intensity resulted in cell death of treated Hela Ohio, this can be supported through the microscopy images which show evidence of the rounding and sloughing seen when Hela Ohio cells die. Similarly, when RV16 is UV inactivated in a glass vessel at both intensities Hela Ohio cells predominately underwent cell death however, at the lower intensity (1200µJ/cm^2) some cells survived as seen in some areas of the microscopy image (Figure 2.39).

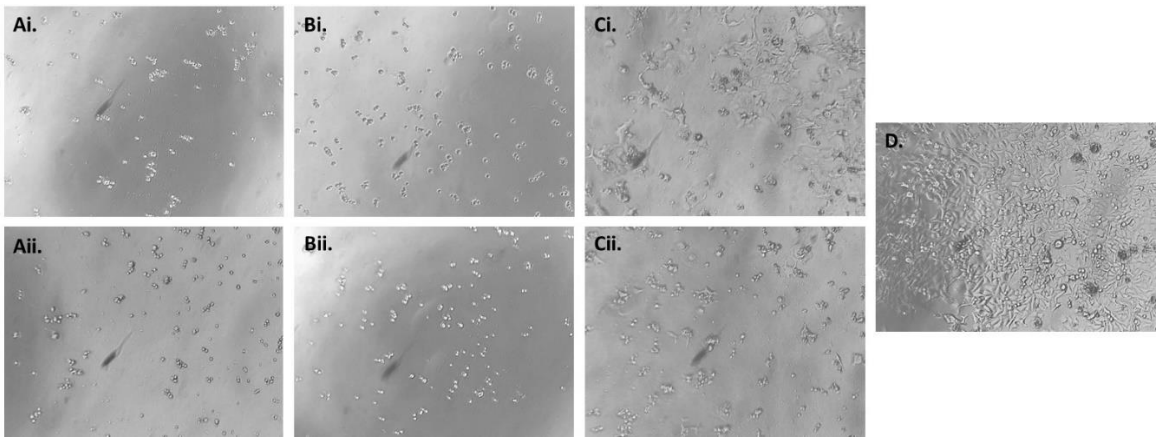

Figure 2.39 Represents Hela Ohio cells viewed at 100x magnification, 4 days post application of UV inactivated RV16. Inactivation was for 30 minutes at 1200µJ/cm^2 (**Ai – Ci**) and 12000µJ/cm^2 (**Aii – Cii**), in either a sterile 60mm culture dish (**Ai – Aii**), a sterile 100mm petri dish (**Bi – Bii**) or a sterile glass beaker (**Ci – Cii**). **D** represents Hela Ohio cells cultured for 4 days in control conditions. Images represents three independent experiments (n=3).

UV treatment of complete DMEM in a polystyrene vessel regardless of surface area or UV intensity resulted in cell death of treated Hela Ohio, this can be supported through the microscopy images which show evidence of the rounding and sloughing seen when Hela Ohio cells die. Conversely, when complete DMEM is UV treated in a glass vessel at both intensities, there is a reduction in the extent of cell death observed and areas of cell survival can be seen in some areas of the microscopy image (Figure 2.40). As a consequence of this observation further experiments would be performed using ultrafiltered RV16 which did not elicit the same effect on the cells it was applied to.

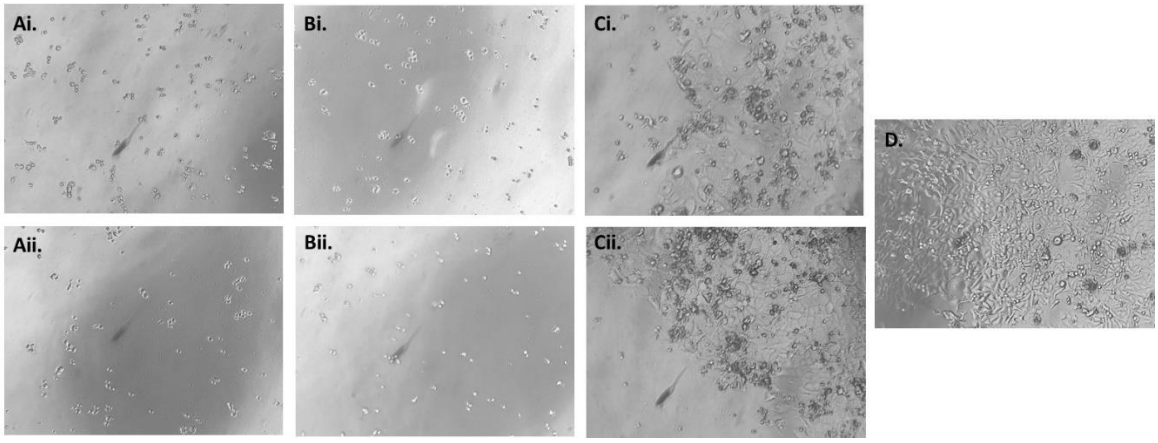

Figure 2.40 Represents Hela Ohio cells viewed at 100x magnification, 4 days post application of UV treated DMEM. Treatment was for 30 minutes at 1200µJ/cm^2 (**Ai – Ci**) and 12000µJ/cm^2 (**Aii – Cii**), in either a sterile 60mm culture dish (**Ai – Aii**), a sterile 100mm petri dish (**Bi – Bii**) or a sterile glass beaker (**Ci – Cii**). **D** represents Hela Ohio cells cultured for 4 days in control conditions. Images represents three independent experiments (n=3).

2.3.7.3 Human Rhinovirus Infection does not Significantly Alter Tight Junction Formation Using TEER Measurements

To assess whether infection of A549 and Beas-2b cell lines with RV16 affected the formation of tight junctions, TEER measurements were taken over a period of 840 hours or until cells detached from the Thincert^{TM} using the method outlined in 2.2.9.2. A549 cells cultured without the presence of an ALI demonstrated a gradual increase in resistance measurements over the first 96 hours post seeding, at which point the cells were infected with RV16 or treated with UV inactivated RV16 or complete DMEM (basal conditions). Post

infection, measurements continued to rise in all conditions until approximately 250 hours, at which point measurements fell slightly before plateauing and finally decreasing as cells began to die at around 600 hours post seeding. The TEER measurements for all conditions remained closely aligned until the point of infection, at this time point the resistance measurements obtained for RV16 and UV inactivated RV16 deviated from basal measurements which were consistently higher. This observation was supported with the area under the curve values which showed no significant difference in area under the curve ($P>0.05$) for RV16 and UV inactivated RV16 compared to basal condition (Figure 2.41).

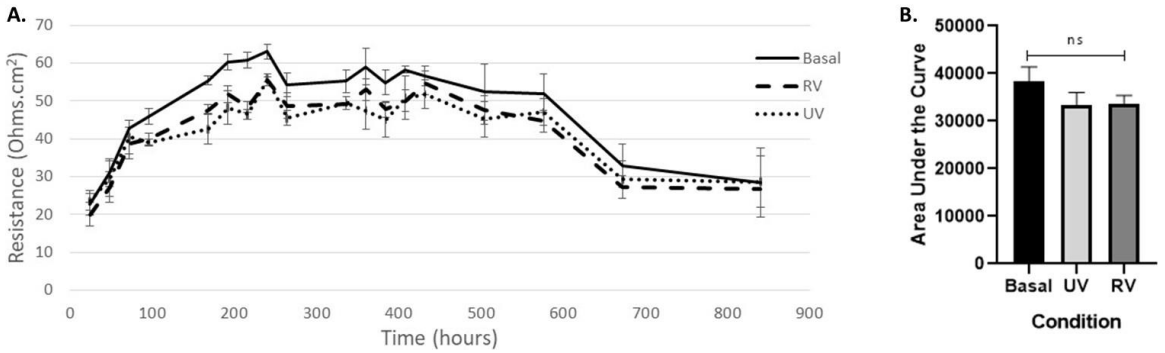

Figure 2.41 TEER measurements from a confluent monolayer of A549 cells, taken 96h pre-exposure and subsequently until 840h post exposure to RV16, ultrafiltered RV16 or basal conditions (**A**). Area under curve analysis of A549 TEER measurements after exposure to aforementioned conditions (**B**). Results are displayed as mean ± SEM (n=3). Statistical analysis was conducted using a one-way ANOVA with multiple comparison by Tukey analysis.

Beas-2b cells cultured without the presence of an ALI demonstrated a gradual increase in resistance measurements over the first 96 hours post seeding, at which point the cells were infected with RV16 or treated with UV inactivated RV16 or complete DMEM (basal conditions). Post infection, measurements continued to rise in all conditions until approximately 250 hours, at which point measurement began to fall, plateauing temporarily at 500 hours and finally returning to baseline measurements as cells began to die at around 650 hours post seeding. The TEER measurements for all conditions remained closely aligned until the point of infection, at this time point the resistance measurements obtained for UV inactivated RV16 deviated from RV16 and basal measurements which were

consistently higher. This observation was supported with the area under the curve values which showed no significant difference between all conditions (P>0.05) (Figure 2.42).

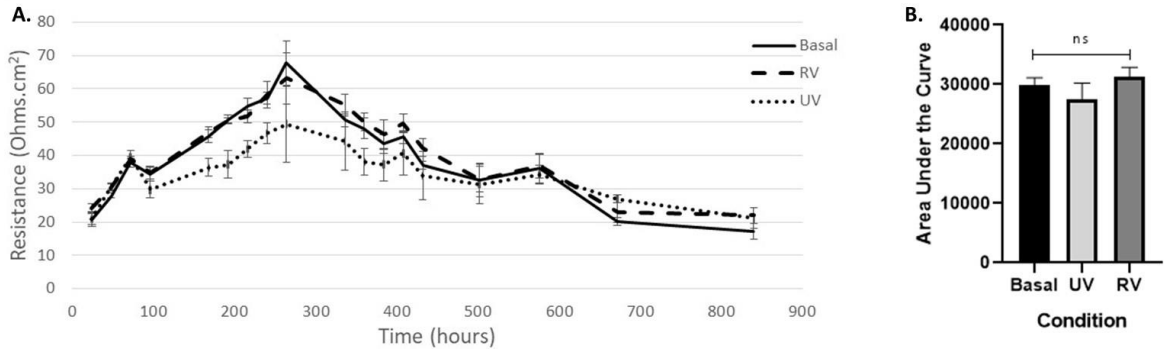

Figure 2.42 TEER measurements from a confluent monolayer of Beas-2b cells, taken 96h pre-exposure and subsequently until 840h post exposure to RV16, ultrafiltered RV16 or basal conditions. Area under curve analysis of Beas-2b TEER measurements after exposure to aforementioned conditions (**B**). Results are displayed as mean ± SEM (n=3). Statistical analysis was conducted using a one-way ANOVA with multiple comparison by Tukey analysis.

Beas-2b cells cultured with an ALI demonstrated a gradual increase in resistance measurements over the first 96 hours post seeding, at which point an ALI was introduced and the cells were infected with RV16 or treated with UV inactivated RV16 or complete DMEM (basal conditions). Post infection, measurements continued to rise in all conditions until approximately 300 hours, at which point measurements plateaued until 500 hours at which point measurements began to fall as cells began to die. The TEER measurements for all conditions remained closely aligned until the point of infection, at this time point the resistance measurements obtained for RV16 and UV inactivated RV16 deviated from basal measurements which are typically higher through the majority of the culture period. This observation was supported with the area under the curve values which showed no difference in area for RV16 compared to basal and a non-significant reduction in area for UV inactivated RV16 compared to both RV16 and basal condition (P>0.05) (Figure 2.43).

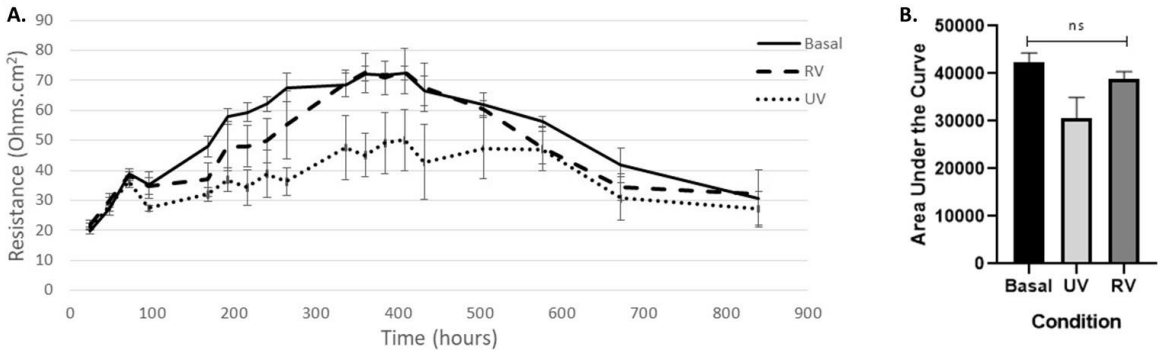

Figure 2.43 TEER measurements from a confluent monolayer of Beas-2b cells in the present of an air-liquid interface (introduced at 96h), taken 96h pre-exposure and subsequently until 840h post exposure to RV16, ultrafiltered RV16 or basal conditions. Area under curve analysis of Beas-2b TEER measurements after exposure to aforementioned conditions (**B**). Results are displayed as mean ± SEM (n=3). Statistical analysis was conducted using a one-way ANOVA with multiple comparison by Tukey analysis.

2.3.7.4 Human Rhinovirus Infection does not Significantly Alter Tight Junction Formation Using Fluorescein Exclusion Measurements

To support the findings from the TEER measurements in assessing changes to tight junction formation due to RV16 infection, a fluorescein exclusion assay was performed on A549 and Beas-2b cells to demonstrate the extent of leakage through the monolayer using the method outlined in 2.2.9.1. The extent of fluorescein leakage seen in A549 cells infected with RV16 and cultured for 7 days was not significantly different to the leakage measured in ultrafiltered RV16 and basal conditions ($P>0.05$) (Figure 2.44).

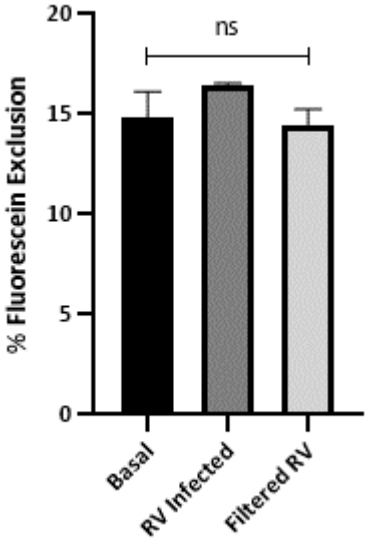

Figure 2.44 Percentage fluorescein exclusion through a confluent monolayer of A549 cells, 7 days post exposure to RV16, ultrafiltered RV16 or basal conditions. Fluorescein exclusion was calculated as a percentage of the maximum fluorescein leakage through a blank membrane, relative fluorescent intensity was measured at 485nm excitation and 535nm emission, accounting for media blank. Results are displayed as mean ± SEM (n=3). Statistical analysis was conducted using a one-way ANOVA with multiple comparison by Tukey analysis.

Similarly, the extent of fluorescein leakage seen in Beas-2b cells infected with RV16 and cultured for 7 days was not significantly different to the leakage measured in ultrafiltered RV16 and basal conditions ($P>0.05$) (Figure 2.45).

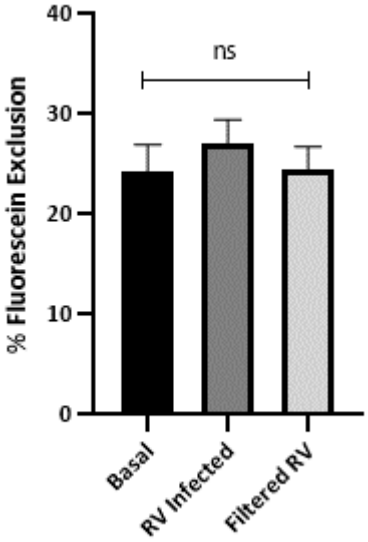

Figure 2.45 Percentage fluorescein exclusion through a confluent monolayer of Beas-2b cells, 7 days post exposure to RV16, ultrafiltered RV16 or basal conditions. Fluorescein exclusion was calculated as a percentage of the maximum fluorescein leakage through a blank membrane, relative fluorescent intensity was measured at 485nm excitation and 535nm emission, accounting for media blank. Results are displayed as mean ± SEM (n=3). Statistical analysis was conducted using a one-way ANOVA with multiple comparison by Tukey analysis.

2.3.7.5 Human Rhinovirus had Limited Impact on MMP Activity

Upregulation of proinflammatory mediators is well documented in hRV infections, including the upregulation of matrix metalloproteinase-2 (MMP-2) and matrix metalloproteinase-9 (MMP-9) (Wang *et al*, 2009). Classified as gelatinases, MMP-2 and MMP-9 are responsible for extracellular matrix protein degradation and consequently is involved in inflammation pathways (Shimokawa *et al*, 2002).

To identify whether any upregulation in MMP-2 and MMP-9 could be measured in response to RV16, A549 and Beas-2b cells were infected with RV16 and the supernatant collected between 24 and 168 hours. Subsequently, the supernatant was electrophoresed through a 7.5% acrylamide gel containing 4mg/ml gelatine, the gels stained and imaged as described in 2.2.9.6. Bands on the gel were analysed with densitometry using ImageJ software, the

relative density was calculated and compared as a fold change to the basal conditions (Figure 2.46a; Figure 2.47a).

Analysis of A549 cell supernatant showed there was an increase in MMP-2 activity for both RV16 infected and ultrafiltered RV16 treated cells compared to basal at all time point however, overall there was no significant difference in MMP-2 activity for RV16 infected and ultrafiltered RV16 treated conditions compared to basal at any point over the culture period ($P>0.05$). Similarly, there was an increase in MMP-9 activity for RV16 infected cells compared to all other conditions at 24 to 72 hours however, overall there was no significant difference in MMP-9 activity for RV16 infected and ultrafiltered RV16 treated conditions compared to basal at any point over the culture period ($P>0.05$) (Figure 2.46b).

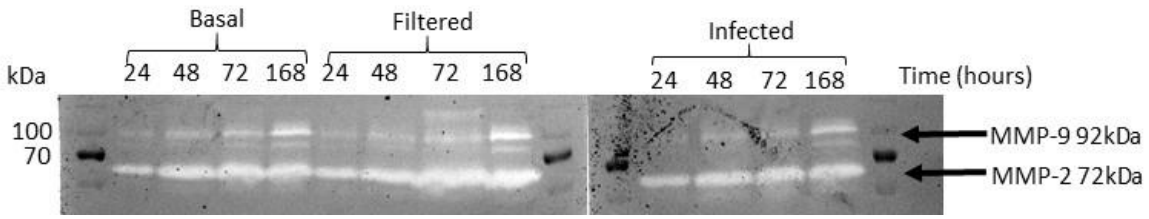

Figure 2.46a Zymograph to show MMP activity in A549 cell line, 24 – 168h post exposure to RV16, ultrafiltered RV16 or basal conditions. Cell culture supernatant was analysed for MMP-2 (72kDa) and MMP-9 (92kDa) activity. Representative image of three independent experiments (n=3).

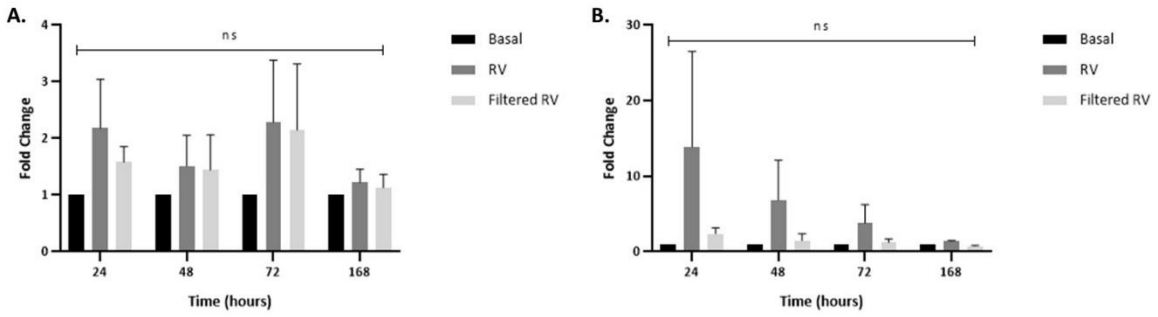

Figure 2.46b Densitometry analysis of zymographs to show MMP activity in A549 cell line, 24 – 168h post exposure to RV16, ultrafiltered RV16 or basal conditions. MMP activity in A549 cells presented as fold change from basal control for MMP-2 (**A**) and MMP-9 (**B**). Bands on the gel were analysed with densitometry using ImageJ software, the relative density was calculated and compared as a fold change to the basal conditions. Results are displayed as mean ± SEM (n=3). Statistical analysis was conducted using a two-way ANOVA with multiple comparison by Tukey analysis.

Analysis of Beas-2b cell supernatant showed there was no significant difference in MMP-2 activity in RV16 infected and ultrafiltered RV16 treated conditions compared to basal at any point over the culture period (P>0.05). Similarly, analysis of MMP-9 no significant difference in activity in RV16 infected and ultrafiltered RV16 treated conditions compared to basal at any time point over the culture period (P>0.05) (Figure 2.47b).

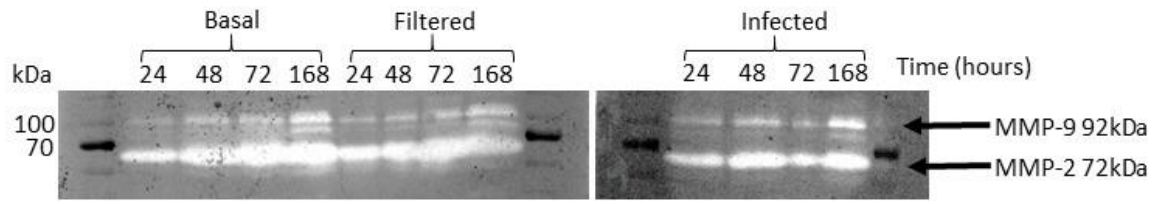

Figure 2.47a Zymograph to show MMP activity in Beas-2b cell line, 24 – 168h post exposure to RV16, ultrafiltered RV16 or basal conditions. Cell culture supernatant was analysed for MMP-2 (72kDa) and MMP-9 (92kDa) activity. Representative image of three independent experiments (n=3).

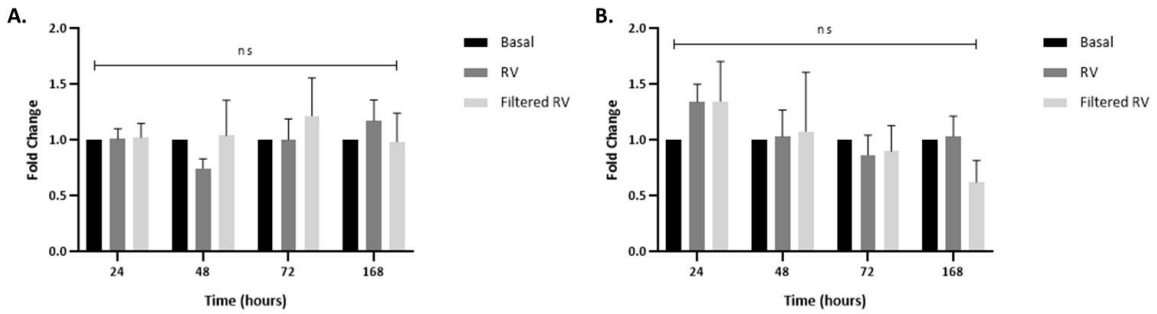

Figure 2.47b Densitometry analysis of zymographs to show MMP activity in Beas-2b cell line, 24 – 168h post exposure to RV16, ultrafiltered RV16 or basal conditions. MMP activity in Beas-2b cells presented as fold change from basal control for MMP-2 (**A**) and MMP-9 (**B**). Bands on the gel were analysed with densitometry using ImageJ software, the relative density was calculated and compared as a fold change to the basal conditions. Results are displayed as mean ± SEM (n=3). Statistical analysis was conducted using a two-way ANOVA with multiple comparison by Tukey analysis.

2.3.7.6 Human Rhinovirus Increases Cytotoxicity in Beas-2b but not A549 Cells

The extent of cellular cytotoxicity in A549 and Beas-2b cells infected with RV16 was determined by measuring the level of LDH in effluent collected during the 7 day culture period and after complete lysis of the cells at the end of the culture period as described in 2.2.9.7. When comparing the effluent there was no significant difference ($P>0.05$) between the amount of LDH released by A549 cells after any treatment at 24, 48 and 72 hours. After 168 hours in culture there was significantly more LDH released from A549 cells in basal conditions compared to those treated with RV16 ($P<0.01$) and ultrafiltered RV16 ($P<0.05$), whilst there was no significant difference between the LDH released by A549 cells treated with RV16 or ultrafiltered RV16 ($P>0.05$). After complete lysis of cells there was no significant difference between LDH released from A549 cells treated with RV16 and basal conditions ($P>0.05$) however, there was a reduction in LDH released from A549 treated with ultrafiltered RV16 compared to basal conditions ($P<0.05$) (Figure 2.48).

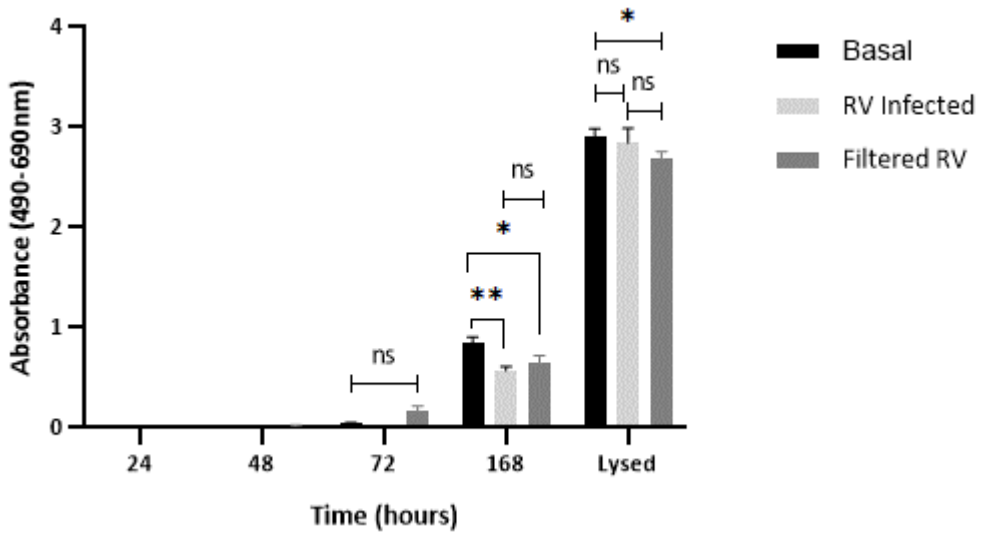

Figure 2.48 LDH analysis of A549 cells, 24 – 168h post exposure to RV16, ultrafiltered RV16 or basal conditions and after complete lysis 168h post exposure. LDH measurements were based on absorbance reading (490 – 690nm) accounting for media blank. Results are displayed as mean ± SEM (n=3). Statistical analysis was conducted using a two-way ANOVA with multiple comparison by Tukey analysis. $P<0.05^{*}$, $P<0.01^{**}$

When comparing the effluent there was no significant difference ($P>0.05$) between the amount of LDH released by Beas-2b cells after any treatment at 24, 48 and 72 hours. After 168 hours in culture there was significantly more LDH released from Beas-2b cells treated with ultrafiltered RV16 and in basal conditions compared to those treated with RV16 ($P<0.05$), whilst there was no significant difference between ultrafiltered RV16 and basal conditions ($P>0.05$). After complete lysis of cells there was a significant reduction in the amount of LDH released from Beas-2b cells treated with RV16 compared to cells treated with ultrafiltered RV16 and in basal conditions ($P<0.001$) however, there was no significant difference between ultrafiltered RV16 and basal conditions ($P>0.05$) (Figure 2.49).

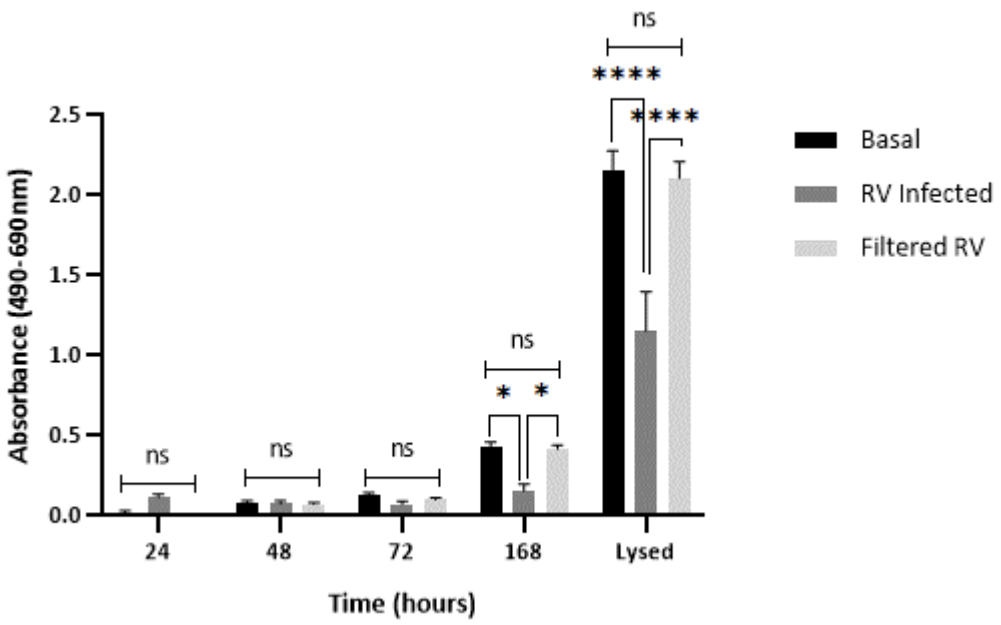

Figure 2.49 LDH analysis of Beas-2b cells, 24 – 168h post exposure to RV16, ultrafiltered RV16 or basal conditions and after complete lysis 168h post exposure. LDH measurements were based on absorbance reading (490 – 690nm) accounting for media blank. Results are displayed as mean ± SEM (n=3). Statistical analysis was conducted using a two-way ANOVA with multiple comparison by Tukey analysis. $P<0.05^{*}$, $P<0.001^{****}$

2.3.7.7 Human Rhinovirus Increases Cytotoxicity in Beas-2b but not A549 Cells in Lysed Cells

To further support the findings from the LDH time course, a reverse time course was performed as described in 2.2.9.4 to show the extent of cellular cytotoxicity in lysed A549 and Beas-2b cells infected with RV16 at varying time points post infection to determine at which time point changes in levels of LDH occurred using the method described in 2.2.9.7. After complete lysis of cells there was no significant difference between LDH released from A549 cells treated with RV16, ultrafiltered RV16 or basal conditions at any time point post infection ($P>0.05$) (Figure 2.50).

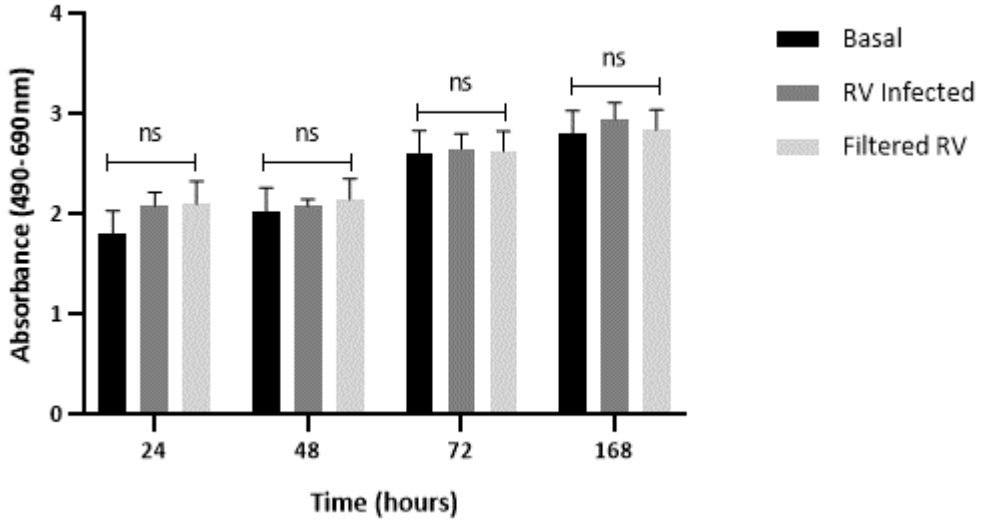

Figure 2.50 LDH analysis of A549 cells, lysed 24 – 168h post exposure to RV16, ultrafiltered RV16 or basal conditions. LDH measurements were based on absorbance reading (490 – 690nm) accounting for media blank. Results are displayed as mean ± SEM (n=3). Statistical analysis was conducted using a two-way ANOVA with multiple comparison by Tukey analysis.

After complete lysis of cells there was no significant difference between LDH released from Beas-2b cells treated with RV16, ultrafiltered RV16 or basal conditions at 24 and 48 hours post infection ($P>0.05$). However, at 72 and 168 hours post infection there was significant reduction in the amount of LDH released from Beas-2b cells treated with RV16 compared to cells treated with ultrafiltered RV16 and in basal conditions ($P<0.001$) however, there was no significant difference between ultrafiltered RV16 and basal conditions ($P>0.05$) (Figure 2.51).

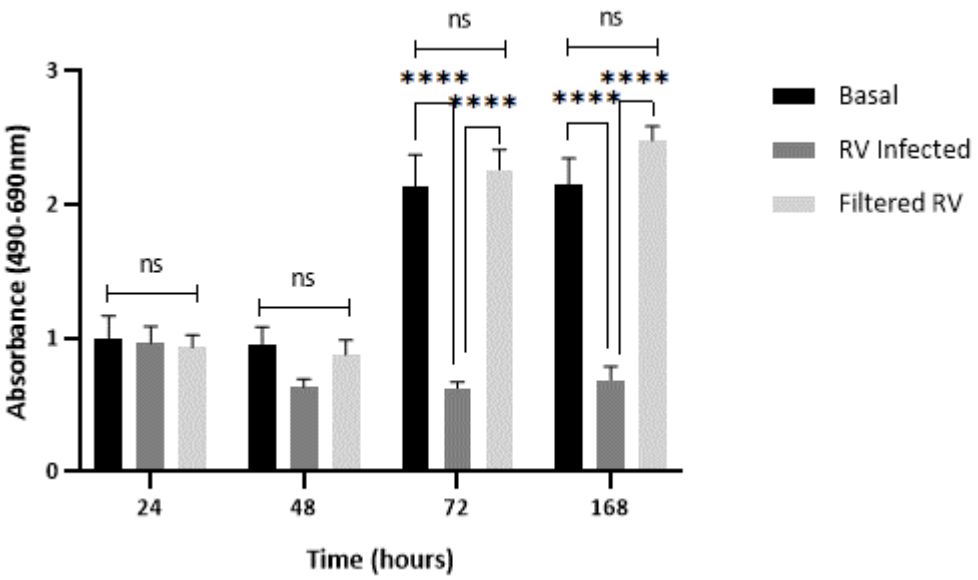

Figure 2.51 LDH analysis of Beas-2b cells, lysed 24 – 168h post exposure to RV16, ultrafiltered RV16 or basal conditions. LDH measurements were based on absorbance reading (490 – 690nm) accounting for media blank. Results are displayed as mean ± SEM (n=3). Statistical analysis was conducted using a two-way ANOVA with multiple comparison by Tukey analysis. $P<0.001^{****}$

2.3.7.8 Human Rhinovirus Decreases Cell Mass in Beas-2b but not A549 Cells

To further support the findings from the LDH reverse time course, a SRB assay (using a reverse time course) was performed to show the change in cell density of A549 and Beas-2b cells infected with RV16 at varying time points post infection, using the method described in 2.2.9.8. After converting absorbance values to fold change values, representing equivalent cell mass, there was no significant difference in the cell mass of A549 cells treated with RV16, ultrafiltered RV16 or basal conditions at any time point post infection ($P>0.05$) with the except of 24 hours post seeding, where there was a slight reduction in ultrafiltered RV16 cell mass compared to basal and RV16 ($P<0.05$) (Figure 2.52).

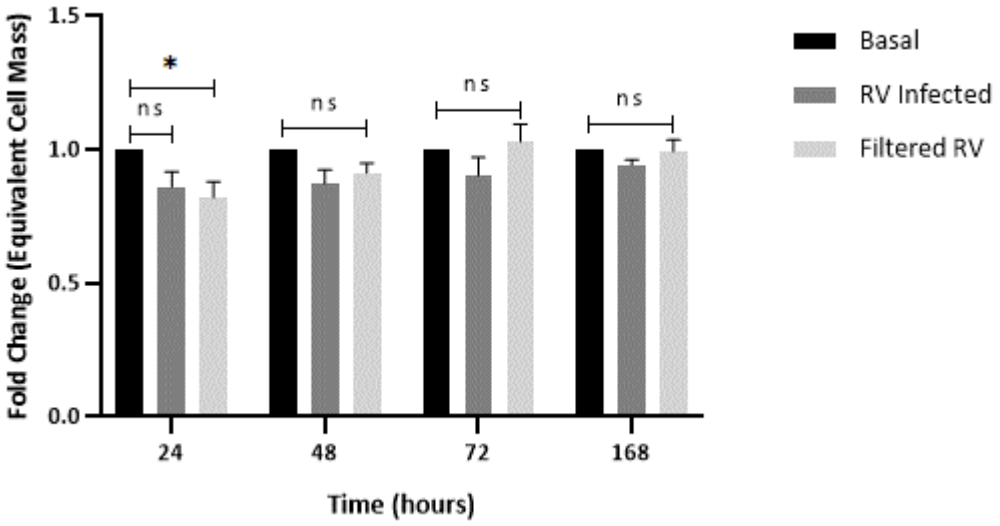

Figure 2.52 SRB analysis of A549 cells 24 – 168h post exposure to RV16, ultrafiltered RV16 or basal conditions. SRB measurements were based on absorbance reading (540nm) and converted to fold change, representing equivalent cell mass. Results are displayed as mean ± SEM (n=3). Statistical analysis was conducted using a two-way ANOVA with multiple comparison by Tukey analysis. $P<0.05^{*}$

After converting absorbance values to fold change values, representing equivalent cell mass, there was no significant difference in the cell viability of Beas-2b cells treated with RV16, ultrafiltered RV16 or basal conditions at 24 hours post infection ($P>0.05$). However, at 48, 72 and 168 hours post infection there was a significant reduction in the cell mass of Beas-2b cells treated with RV16 compared to cells treated with ultrafiltered RV16 ($P<0.01$ at 48h, $P<0.001$ at 72 and $P<0.005$ 168h) and in basal conditions ($P<0.05$ at 48h, $P<0.005$ at 72 and 168h) however, there is no significant difference between ultrafiltered RV16 and basal conditions at any time point ($P>0.05$) (Figure 2.53).

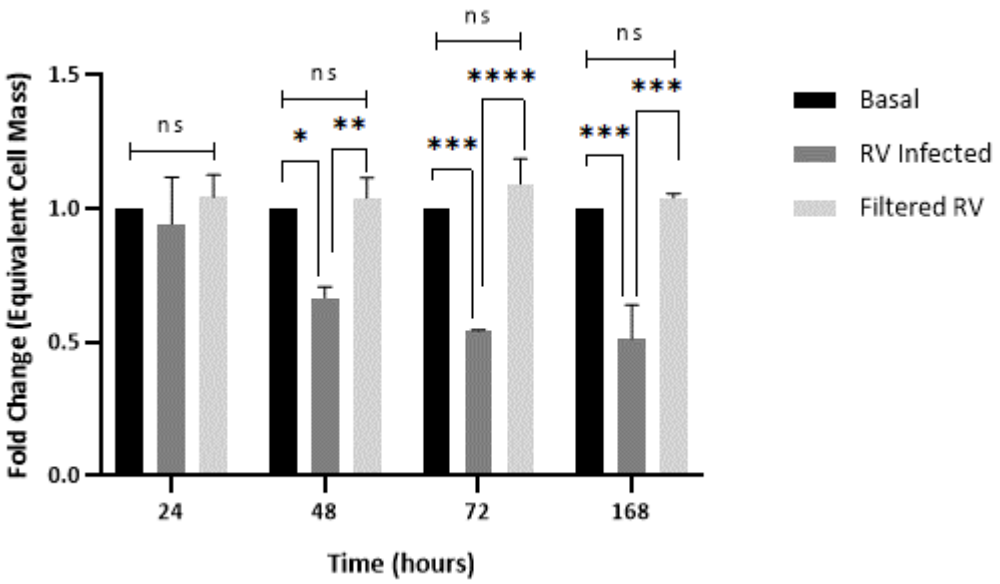

Figure 2.53 SRB analysis of Beas-2b cells 24 – 168h post exposure to RV16, ultrafiltered RV16 or basal conditions. SRB measurements were based on absorbance reading (540nm) and converted to fold change, representing equivalent cell mass. Results are displayed as mean ± SEM (n=3). Statistical analysis was conducted using a two-way ANOVA with multiple comparison by Tukey analysis. $P<0.05^{*}$, $P<0.001^{**}$, $P<0.005^{***}$, $P<0.001^{****}$

2.3.7.9 Human Rhinovirus does not Affect Cell Proliferation in Airway Epithelial Cells

To aid clarification of the findings from LDH cytotoxicity and SRB cell viability assays a WST-1 assay was conducted to identify whether observed differences were a consequence of cell proliferation or due to other factors. A WST-1 assay was performed using a reverse time course to show the extent of cell proliferation of A549 and Beas-2b cells infected with RV16 at varying time points post infection, using the method described in 2.2.9.9. Analysis of A549 cells shows there was no significant difference in cell proliferation of A549 cells treated with RV16, ultrafiltered RV16 or basal conditions at any time point post infection ($P>0.05$) (Figure 2.54).

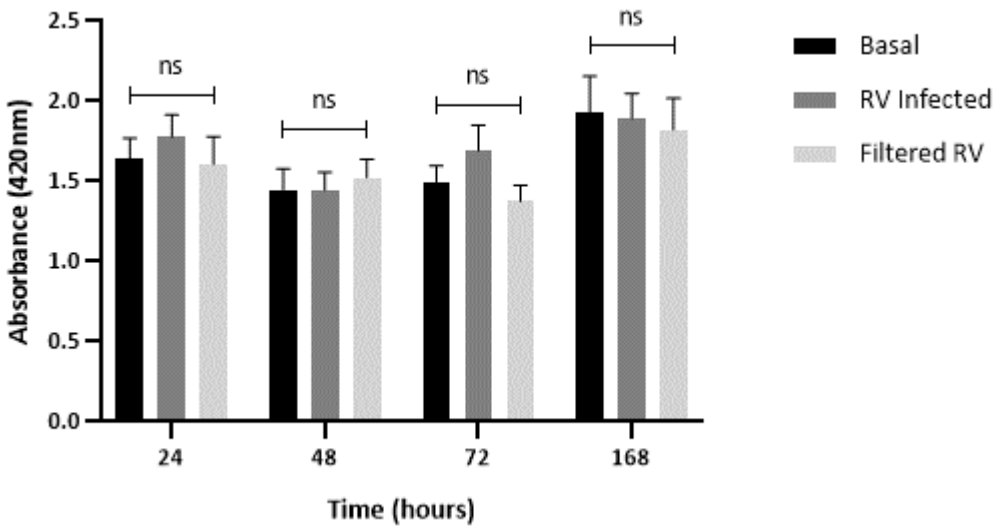

Figure 2.54 WST-1 analysis showing tetrazolium salt conversion by A549 cells 24 – 168h post exposure to RV16, ultrafiltered RV16 or basal conditions. WST-1 measurements were based on absorbance reading (420nm) accounting for media blank. Results are displayed as mean ± SEM (n=3). Statistical analysis was conducted using a two-way ANOVA with multiple comparison by Tukey analysis.

Analysis of Beas-2b cells shows there was no significant difference in cell proliferation of Beas-2b cells treated with RV16, ultrafiltered RV16 or basal conditions at any time point post infection ($P>0.05$), with the exception of 24 hours whereby there was a significant increase in cell proliferation between a basal condition and Beas-2b cells treated with ultrafiltered RV16 ($P<0.05$) (Figure 2.55).

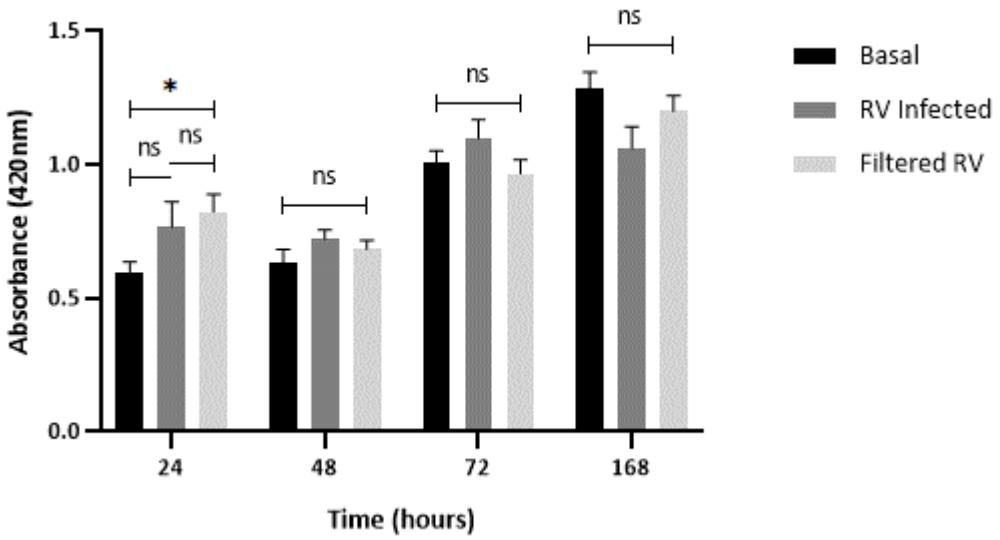

Figure 2.55 WST-1 analysis showing tetrazolium salt conversion by Beas-2b cells 24 – 168h post exposure to RV16, ultrafiltered RV16 or basal conditions. WST-1 measurements were based on absorbance reading (420nm) accounting for media blank. Results are displayed as mean ± SEM (n=3). Statistical analysis was conducted using a two-way ANOVA with multiple comparison by Tukey analysis. $P<0.05^{*}$

2.4 Discussion

2.4.1 TRPV4 – ATP – P2X3 Interaction Potential Pathway for Cough Mechanism

Whilst the mechanism involved in cough is not fully understood, neuromodulation via P2Y and P2X receptors in response to ATP released by TRPV4 receptors have been indicated as a potential step in the cough mechanism pathway (Song and Morice, 2017). The role of P2X receptors, specifically P2X3, in this pathway have previously been implicated in a phase II clinical trial using the P2X3 antagonist AF-219 (now MK-7264, generic name Gefapixant) which showed a 75% reduction in daytime cough frequency in patients prescribed 600mg AF-219 twice daily compared to placebo (Abdulqawi *et al*, 2015). Thus in an attempt to gain further insight into the pathway involved in the cough mechanism A549 and Beas-2b cells were used for modelling cell types found in the respiratory system, whilst 1N1 P2X3 cells were used to model the nerve cell type found in close proximity to the airways.

Prior to conducting any experiments with dual cultures, individual cell lines were characterised and functional activity confirmed. To enable good response rates to be achieved in all experiments, optimal seeding density for A549 cells was determined at $1x10^6$ per well in a 96 well plate. This seeding density was then translated to cells per mm^2 so that equivalent densities could be used in all subsequent experiments regardless of multi-plate size. Furthermore, given that all cell lines used replicate at a similar rate, this seeding density could be used for all cell lines ensuring consistency across each experiment. RT-PCR data demonstrated both A549 and Beas-2b cells expressed TRPV4 as shown in existing literature (Henry *et al*, 2016), whilst no P2X3 expression was observed in Beas-2b cells a minimal level of expression was observed in A549 cells. TPRV4 protein expression was subsequently confirmed via western blot analysis of the cell lines, whilst no evidence of P2X3 protein expression was seen. Functional activity of TRPV4 receptors was determined through ATP release analysis and calcium signalling using the TRPV4 agonist GSK101, with results supporting the western blot findings, demonstrating functional TRPV4 response and no P2X3 response unless very high concentration of agonist were utilised. This response may indicate the low level expression of P2X7 receptors in airway epithelial cells, which are stimulated by ATP in the same manner as P2X3 receptors and could potentially explain this observation (Takai *et al*, 2014). Similarly, when TRPV4 antagonist HC-067047 was applied to A549 and Beas-2b cells the calcium signalling response observed on the application of GSK101 could be attenuated effectively in Beas-2b cells but less effectively in A549 however, overall this demonstrated the correct receptor was being activated when the agonist was applied. It should be noted however, that the effectiveness of GSK101 is not consistent across studies, with response time and rates vary greatly between existing studies (Jin *et al*, 2011; Zhang *et al*, 2012; Bonvini *et al*, 2016) but given that other TRPV4 agonist lack specificity (Thorneloe *et al*, 2008) this remained the most suitable option once optimal concentrations had been identified. The 1N1 P2X3 transfected cell line was similarly characterised for functional activity via calcium signalling using the P2X3 receptor agonist, ATP, no functional response to TRPV4 activity was observed when GSK101 was applied. Furthermore, the P2X3 response could not be suppressed to any extent with the application of the P2X3 antagonist NF110, thus making it impossible to demonstrate ATP was activating the desired receptor. Although the P2X3 antagonist was on the whole completely ineffective, there is a lack of alternatives available for commercial purchase, with this being the most selective but lacking potency (Bölcskei and Farkas, 2014), thus this

became the only viable option available for use in attempting to attenuate the P2X3 response.

Alongside characterisation of the cell lines it was also imperative to determine optimal culture conditions to create a viable co-culture model. For this reason TEER measurements and fluorescein exclusion assays were performed to identify the length of time cells needed in culture to form a confluent monolayer with tight junctions. Both the fluorescein exclusion assay and TEER measurements demonstrated that A549 and Beas-2b cells form tight junctions within 7 days and continue to maintain a confluent monolayer for up to 4 weeks. However, the maximum resistance measurements taken were approximately 70-80Ω.cm^2, which is considerably lower than the maximum which can be obtained in some cell lines (Srinivasan *et al*, 2015). Furthermore, after 7 or 14 days in culture for A549 or Beas-2b respectively, there was still 40-50% leakage of fluorescein across the Thincert™ membrane. These low resistance measurements and continuous leakage are a reflection of the difference between primary epithelial cells and cell lines, whereby cell lines display many of the physiological features of the equivalent primary cells but lack function, as such cell lines do not form strong tight junctions and retain a certain degree of leakiness in comparison to primary cells (Mathias *et al*, 2002; Srinivasan *et al*, 2015). Although the culturing of Beas-2b cells in the presence of an ALI had also been considered, the prolonged culture of Beas-2b cells in this manner resulted in cells detaching from the Thincert™ making subsequent experimentation difficult. This aspect of the research requires further development as Beas-2b cells have been shown to have some limited capacity to differentiate in the presence of an ALI however, Stewart *et al* (2012) demonstrated that Beas-2b cells do not perform well in the presence of ALI, reporting low TEER measurements, limited differentiation and poor expression of markers of epithelial differentiation. This being said, as a model the presence of an ALI would better reflect the anatomical arrangement of the cells *in vivo* and may have produced data which is more in line with the observations made *in vivo* particularly were RV16 infection is concerned. In direct comparison, although 1N1 P2X3 cells form a confluent monolayer, the bipolar structure of the cells means gaps exist through the monolayer preventing TEER measurements being made, thus decisions around culture periods in preparation for co-culture calcium signalling were based on the observations relating to A549 and Beas-2b cells. With this in mind, 7

days was chosen as the optimum time point after seeding to conduct co-culture calcium signalling, as this ensured cell monolayers and tight junctions has adequately formed.

After determining optimum culture periods, seeding densities and agonist/antagonist concentrations A549 and Beas-2b cells were cultured using the co-culture method without the presence of 1N1 P2X3 cells to determine if ATP could successfully pass across the Thincert™. Theoretically, given the size of an ATP molecule it should successfully have passed across the Thincert™ in either direction however, this experiment demonstrated that whilst a consistently high level of ATP could be measured directly next to the cells in culture, only a small amount of ATP passed across the Thincert™ regardless of which surface cells were cultured on or the cell line stimulated. There are two potential reasons for this very low movement of ATP. Firstly, the presence of ectoATPases on the cell surface, resulting in the rapid metabolism of ATP released by the cells before it can pass across the membrane (Durnin *et al*, 2016), explaining the higher concentrations measured directly adjacent to the cells compared to the lower concentration measured in the opposing chamber. Secondly, ATP is negatively charged therefore this may affect its ability to pass through the pores of the Thincerts™ and may reflect the low concentrations measured in the opposite chamber to the stimulated cells (Azarashvili *et al*, 2011). Although, only low concentrations of ATP passed through the Thincert™, previous single cell culture calcium signalling showed that 1N1 P2X3 cells could respond to ATP concentrations in the nanomolar range, thus some response should still be measureable using the co-culture method.

Having shown ATP can cross the Thincert™ membrane in either orientation, albeit to a limited extent, cells were subsequently cultured on both sides of the membrane and the co-culture calcium signalling method optimised for reagent volume and instrument read height prior to further experimentation. When co-culturing calcium signalling was conducted with A549 cells on the basal aspect on the membrane a reduction in response rate was measured when 1N1 P2X3 cells were treated with NF110 or when alternatively 1N1 WT cells were used. Similarly, when A549 cells were cultured on the apical aspect of the membrane there was also a reduction in the response rate compared to 1N1 P2X3 or

1N1 WT cells. Conversely, when the same experiments were repeated with Beas-2b cells, no change in response was observed. Although the response rates measured were relatively small, especially when considering the A549 cells and not significant in all cases, if these response rates are triangulated back to the measured calcium signalling response of 1N1 P2X3 to ATP and the ATP concentrations which were previously shown to cross the membrane, would suggest that this method of studying cell to cell interaction is viable. Furthermore, the observed reduction in response rate when NF110 or wild type cells lacking P2X3 receptors were utilised, continue to support this as a model for studying interactions as the antagonist is applied to only cells which carry the P2X3 receptor thus blocking the activation of these receptor by the extracellular ATP released by A549 or Beas-2b cells.

To further support the observations of the co-culture model, a mixed culture calcium signalling model was utilised. Prior to conducting any calcium signalling, seeding densities and culture periods were optimised for a mixed culture of A549 or Beas-2b with 1N1 P2X3. This optimisation showed that both cell lines could be seeded at the same densities as they were replicating at a similar rate, that cells were evenly distributed across the well and a near confluent monolayer (grown to 90% confluency as per the manufacturer's instructions for the calcium signalling assay) had formed 48 hours post seeding. Where cell lines had been cultured individually, lower levels of confluency were evident as a consequence of the use of same seeding densities throughout, this subsequently enabled calcium signalling response rates in single cell cultures to be combined to identify if any additive effect could be identified when compared to cell lines were grown together. Utilising these observations, the mixed culture method showed that when the highest concentration of GSK101 (300nM) was applied to a mixed cultured of either A549 or Beas-2b with 1N1 P2X3 cells there was an additive effect, whereby the response rate increased very slightly compared to when single cell lines were treated with the same concentration of GSK101. Furthermore, the application of NF110 showed a reduction in response rate suggesting in this instant the activation of P2X3 receptors had been blocked by the application of the antagonist, thus the ATP released by the A549 or Beas-2b cells is less effective at activating the receptors. However, given the lack reduction in calcium signalling response observed when only 1N1 P2X3 cells were treated with NF110, makes it difficult to ascertain whether

this albeit non-significant reduction was a due to the application of the P2X3 antagonist or rather the results of some unknown effect.

Given the aforementioned observations relating to the co-culture method it would suggest that the hypothesised TPRV4 – ATP – P2X3 pathway has the potential to be part of the mechanism involved in cough. Work with single cell lines has shown TRPV4 activation results in the release of extracellular ATP, whilst stimulation of P2X3 with ATP results in intracellular calcium flux, thus by placing two cell lines which contain these receptors in close proximity interaction between the receptors should be possible. This is the premise of the co-culture method whereby activation of TPRV4 receptors in A549 or Beas-2b cells by GSK101 results in ATP release which subsequently activates the P2X3 receptors in 1N1 cells. The results of the co-culture method and mixed culture methods suggest that these interactions occur and reduced response rate after application of NF110 to block the P2X3 receptor further support this observation. However, the question regarding whether the TRPV4 – ATP – P2X3 pathway plays a major or minor role in the cough activation pathway cannot be answered *in vitro* and needs further study *in vivo*.

The development of this co-culture calcium signalling model has enabled the TRPV4 – ATP – P2X3 pathway to be further investigated and with some minor modification could be utilised to investigate similar pathways between other cell lines. However, there are a number of limitations which need to be addressed in order to make the model more effective. Firstly, limitations pertaining to the Thincert^{TM} need to be considered, this includes the pore size of the Thincert^{TM} membrane at 0.4µm, which although large enough for ATP molecules to pass through, would probably benefit from being increased to help ATP pass across the membranes without being so large that small cells could pass through. Additionally, the material the membrane is made of may need to be further considered as this may help overcome the potential effect that the negative charge of the ATP has on its ability to pass across the membrane. Secondly, the agonists and antagonists being utilised, although specific, are relatively inconsistent which is reflected in the observed responses when then applied to cells. Whilst changing to more specific and consistent agonists and antagonists would be the most ideally resolution, the lack of choice available means that

further tailoring optimal concentrations to the experimental conditions is the only method which could be employed to enhance future research. Finally, it would be worth considering a method of altering the amount of ATP release by TRPV4 receptors. Whilst the antagonist HC-067047 could be utilised to reduce ATP release, the observed results of this antagonist are not always consistent, thus identifying and trialling an alternative method to block ATP release by TRPV4 receptors would help to further confirm the observation made regarding the TRPV4 – ATP – P2X3 pathway. Alternatively, rather than trying to limit ATP release, reducing the impact of ectoATPases could be considered as a method to increase the extent of extracellular ATP available to cross the membrane and activate the P2X3 receptors.

It is also worth considering the cell lines that have been utilised throughout this stage of the research. Although A549 cells are a widely used model in respiratory research as they retain some of the characteristics of primary alveolar type II cells (Swain *et al*, 2010) however, alveolar cells are not implicated in cough thus are less akin to the *in vivo* response. In response to this Beas-2b cells were also utilised, which similarly are also a widely accepted respiratory model. Beas-2b cells being immortalised from normal primary bronchial cells (Stewart *et al*, 2012) retain phenotypic features of the primary cell type and benefit from being non-malignant unlike A549 cells (Zhao and Klimecki, 2015), furthermore bronchial cells could be implicated in a cough so in this instance may be a more realistic model than A549 cell. To further extend the developed models, the use of cell lines from the oro- or laryngopharynx region of the respiratory tract may be beneficial as these cells may also play a role in cough *in vivo*. Whilst the use of primary cells in this model would be the ultimate ideal, the difficulty in obtaining and maintaining sufficient cells coupled with the variability between donors make this unfeasible, thus the use of established cell lines continue to form the best option for future development of this model.

Although further development is required to refine this newly developed co-culture calcium signalling model, the response rates measured when triangulated with single cell line calcium signalling and ATP assays, suggest that the co-culture responses are representative of the stimulation of TRPV4 causing ATP release by A549/Beas-2b cells and

the calcium flux observed when 1N1 P2X3 receptors are activated with the agonist ATP. Suggesting that direct interactions between cell receptors can be measured when grown in close proximity via the co-culture methods, using a calcium signalling method traditionally reserved for use with single cell cultures.

2.4.2 Cell Viability of Rhinovirus-16 Infected Cells Differs Between Cell Lines

The long term aim of the co-culture calcium signalling model is to apply to model to the study of post-viral cough. Cough forms one of the most common symptoms in hRV infections however, the exact mechanism still remains elusive (Dicpinigaitis *et al*, 2014) thus further understanding of this mechanism would be desirable and may aid in the identification of potential therapeutic targets for cough suppression. Additionally, given that elements of this research are focussed on the infection of PCLS, which due to the lack of current research is a somewhat unknown entity, the infection of the aforementioned cell lines forms an ideal starting point. In an attempt to gather some baseline measurements relating to infection, A549 and Beas-2b cell lines were initially used to investigate cellular changes in response to infection. Both cell lines are permissible to RV16 infection and are a widely accepted model for the study of respiratory infection (Rider *et al*, 2013), thus these cell lines made an ideal choice for this study.

Prior to conducting any experiments regarding cellular response, it was necessary to show that both cell lines could be successfully infected. Collection of cell supernatant 48 hours post infection and subsequent application to Hela Ohio cells (chosen due to being highly permissible to hRV infection with an observable cytopathic effect (Came *et al*, 1976)), using the viral titre method, confirmed that RV16 was actively replicating in the A549 and Beas-2b cells. However, what became apparent during these initial infectivity checks was the negative effect that UV inactivated RV16 was having on the A549 and Beas-2b cells. When RV16 was inactivated by UV to create a sham infection, the application of the inactivated virus to A549 and Beas-2b cells appeared to cause a cytotoxic effect. To determine the potential cause of the unexpected cytotoxic effect, RV16 and DMEM were UV inactivated in polystyrene culture dishes of different surface areas and in a glass beaker. It became apparent that the UV was reacting with the plastic, resulting in the release of cytotoxic

chemicals (Mutou *et al*, 2006), as when applied to Hela Ohio cells the cytopathic effect was apparent in not only the UV inactivated RV16 but also the DMEM from the plastic culture dishes, whilst RV16 and DMEM inactivated in a glass beaker produce a much reduced cytopathic effect, particularly in the case of DMEM. Based on these observations, future experiments with the exception of TEER measurements, were conducted with sham infections created using ultrafiltered RV16 as this did not have the same pronounced cytopathic effect. It should be noted that although creating a sham infection is important to enable viral effect to be compared to basal in an effective manner, neither UV inactivated or ultrafiltered treated virus will produce negative results as both result in cytokine release from treated cells, albeit reduced by at least 50% compared to basal (Johnston *et al*, 1998; Papi and Johnston, 1999). When UV inactivated virus is considered cytokine release occurs as a result of the inactivated virus still being present intact and able to bind to ICAM-1 receptors (Johnston *et al*, 1998), whilst ultrafiltration removes viral particles and RNA however, small molecules such as cytokines are not removed which consequently leads to further cytokine release (Papi and Johnston, 1999), thus regardless of the method used to create the sham infection, some positive response may be observed when compared to basal.

It has previously been shown that TEER measurements reduce in response to hRV infection, due to the mechanism of the infection weakening the tight junctions (Lopez-Souza *et al*, 2004; 2009). This observation was made in the A549 cells which showed a slight reduction in TEER measurements. Similarly, when Beas-2b cells were cultured with an ALI there was also a slight reduction in TEER measurements. The same observation is not apparent in Beas-2b without an ALI, which may reflect the difference between *in vitro* and *in vivo* physiology of the cells. The maximum TEER measurements were in line with those measured without RV16 infection and continued to reflect the weak tight junction formation in these cell lines. With this in mind it is difficult to conclude whether the infection is the sole cause of the reduction in TEER, especially due to the aforementioned issue relating to the use of UV inactivated RV16. To support the TEER observations a fluorescein exclusion assay was performed, with the sham infection created by ultrafiltered RV16 rather than UV inactivated RV16. In both A549 and Beas-2b cells there was a slight increase in leakage of RV16 infected cells compared to basal and sham infection, which

were similar. This increased fluorescein leakage suggests that the tight junctions which are formed, albeit weak to begin with, display further weakening in response to RV16 infection and similarly coincide with the observed changes in TEER measurements.

To identify whether there was any changes in proinflammatory response to RV16 infection, MMP-2 and MMP-9 upregulation was considered, as increasing levels are linked to extracellular matrix degradation and the inflammation pathway (Shimokawa *et al*, 2002) and subsequently may relate to the weakening of tight junctions (Cauwe *et al*, 2007). In A549 cells there was evidence of an upregulation of MMP-9 to a minimal extent over the course of a 7 day infection with RV16. When MMP-2 was considered there was no increase in activity over the course of the infection for either RV16 and sham infection at any time points. Conversely, there was a slight increase in activity of MMP-9 over the course of the experiment however, RV16 activity remained higher than both sham infection and basal, but differences decreased over time, with the highest increase being observed at 24 hours. In Beas-2b cells the observations were similar however, there no change in either MMP-2 or MMP-9 activity for RV16 over the entire duration of the time course, although a very slight increase in MMP-9 activity was observed at 24 hours post infection for both RV16 and sham infection. MMP-9 expression has been shown to be of importance in the lungs, including bronchial epithelial cells, with upregulation occurring as a consequence of a suitable stimulus (Gualano *et al*, 2006). This upregulation in bronchial cells explains the observations in the Beas-2b cells and may go some way to explain the A549 response, as MMP-9 upregulation occurs after infection with respiratory syncytial virus and is linked to cell to cell spread of the virus (Gualano *et al*, 2006). Furthermore, peak MMP-9 activity in BAL samples was also detected at 7 to 14 days post infection (Gualano *et al*, 2006), which given that samples were not taken beyond 7 days may explain why not observable changes are seen in either cell line. This limited changes in MMP activity supports previous findings of upregulation of MMP-9 in hRV infected airway cells *in vitro* (Tacon *et al*, 2010) and suggests that the dysregulation of the tight junctions observed through the reduction in TEER measurements and increased fluorescein leakage may be a direct consequence of the observed increase in MMP activity and thus the extracellular matrix degradation this can result in.

To investigate the cytotoxic effect of RV16 infection, the LDH release of A549 and Beas-2b cells over 7 days was considered. A549 cells showed a reduction in LDH release to the supernatant in RV16 infected cells and sham infection when compared to basal however, after complete lysis a similar change was not observed, this would suggest that there is a slight increase in cytotoxicity in infected cells compared to basal. Conversely, Beas-2b cells showed a significant reduction in LDH released into the supernatant at 168 hours and after complete cell lysis for RV16 infection compared to sham infection and basal. The reduction in LDH from lysed cells would suggest an increased extent of cytotoxicity, as the characteristic spike in LDH release after lysis indicates cells are viable, as LDH is only released once cell membranes are lysed (Fotakis and Timbrell, 2006). However, there is no corresponding increase in LDH supernatant at 168 hours, which would be expected if cell death was occurring prior to lysis, rather there is also a decrease in LDH for RV16 infection at this time point. Instead of suggesting increased cytotoxicity, this sudden reduction in LDH release may indicate there is another potential change in cellular response.

To support the LDH time course data, cells were infected for varying durations prior to lysis and LDH analysis. In this method, A549 cells showed no change in LDH release at all time points for RV16 infection, as shown in the time course experiment. Conversely, Beas-2b showed a significant LDH reduction for RV16 infection compared to sham infection and basal at all time points except 24 hours and 48 hours, although the latter still showed a reduction. This supports the idea of increased cytotoxicity however, it does not explain the lack of LDH release in the supernatant, as in lysed cells the LDH released is lower in RV16 infections across numerous time points. In an attempt to determine the reason for the observable difference in cytotoxicity a SRB assay was conducted in the same manner as the LDH assay. Given that SRB binds to all cells present in a culture, it can be used as an approximation of cell mass and number (Orellana and Kasinski, 2016). When A549 cells were considered there was a similar pattern to the LDH data, where there was a very slight reduction in cell mass for RV16 infected cells at all time points with the exception of ultrafiltered RV16 against basal at 24 hours, which is likely to be related to slower replication in some wells due to the position on the plate. In Beas-2b cells there was a significant reduction in RV16 infected cell mass compared to basal and ultrafiltered RV16 at all time points beyond 24 hours. This reduction in cell mass indicates that rather than

RV16 having just a cytotoxic effect it is potentially effecting cell number, mass and/or growth within 48 hours of infection. To provide further clarification regarding the effect RV16 was having on the cells, a WST-1 cell proliferation assay was performed. A549 cells continued to show no significant difference in proliferation rate when RV16 infected cells were compared to either basal or sham infection. Similarly, Beas-2b cells showed no significant difference in proliferation rate at any time point with the exception of basal cells at 24 hours which is likely to be the aforementioned issue relating to well position. There was however, a slight reduction in proliferation at 168 hours in RV16 infected cells compared to basal and ultrafiltered RV16. These observations suggest that the cells are proliferating at a similar rate regardless of infection, thus the reduction in cell mass may be due to a mixture of cytotoxicity and cell size rather than number alone. This may also account for the difference in the extent of LDH measured, as reduction in cell number or size could account for the total LDH released into the supernatant or in response to lysis being lower. These observations are in line with the theory that hRV causes only minimal cellular damage once adhered to a cell (Griego *et al*, 2000) and that the pathogenesis of hRV is a result of host cell inflammatory response as opposed to a cytolytic effect on infected cells *in vivo* (Ghildyal *et al*, 2005). Furthermore, Lötzerich *et al* (2018) demonstrated that hRV infections can suppress both apoptosis and programmed necrosis in infected cells, with cell death potentially occurring via a caspase-independent pathway. The presence of a caspase-independent cell death pathway in infected cells may also explain the lack of proliferation observed even when there are apparent high levels of cytotoxicity after infection (Roumane *et al*, 2018) however, further research is required to confirm this observation.

Whilst, this data collectively is somewhat inconclusive and has consequently resulted in the creation of more questions regarding the way in which hRV affects cellular activity, it has provided a basis on which to develop the PCLS infection protocol. Furthermore, the models used here have three main limitations that need addressing. Firstly, there is a noticeable difference in response between A549 and Beas-2b cells which is likely a reflection on the cell type, position in the airways and mode of immortalisation. Given the lower respiratory tract infections with hRV are relatively infrequent and are predominantly observed in individuals with underlying respiratory diseases (Hayden, 2004), it is not necessarily

unsurprising that the A549 cells appear to have only a minimal response to RV16 infection. Conversely, the Beas-2b bronchial cell type is more akin to the cells which would be exposed to an upper respiratory tract infection with hRV, which may explain the differences in response post infection. This being said, the type of tissue received for PCLS is predominately comprised of terminal regions of bronchi and alveoli, thus having both cell types as a model seems a reasonable decision to have made. In addition the accessibility of primary bronchial cells is limited, as previously discussed, makes these cell line models a suitable and viable alternative. Secondly, the MOI of 1 chosen for all experiments could potentially be a limiting factor in the results, as it is difficult to determine the number of virions that infect each cell *in vivo* (Lopez-Souza *et al*, 2009). Thus at one virion per cell, this could be either an over or under estimation of the extent of infective particles during a hRV infection, which means the responses measured may not be a true representation of the *in vivo* response. This being said, using an MOI of 1 is a widely accepted value (Johnston *et al*, 1998; Papadopoulos *et al*, 2000; Oliver *et al*, 2008; Lötzerich *et al*, 2018) and at approximately one virion per cell this made the most logical MOI value to utilise. Finally, whilst the problems which arose as a consequence of UV inactivation were rectified, the use of ultrafiltered RV16 still resulted in a response in some experiments. Ultrafiltration of RV16 removes the active viral particle however, due to size restraints of the filters used soluble factors, such as cytokines, are not completely removed and can therefore cause an inflammatory response (Papi and Johnston, 1999) which may explain the increased MMP activity observed as this forms part of the inflammatory pathway.

Alongside the aforementioned limitations, it is also worth considering the impact that the chosen statistical analysis may have had on the data collected, as for some data sets the visual representation of the data appears to show clear effect (for example figure 2.33 and 2.34) but when P values are considered no significant difference is recorded. Predominately, statistical analysis was performed using a combination of two and one-way ANOVA followed by Tukey post hoc test for multiple comparison, paired and unpaired t-tests or in the case of data which contained multiple time points, multiple t-tests utilising the Holm-Sidák method for corrections of multiple comparisons. The aforementioned analytical methods were chosen based not only on whether data was normally distributed but also the robustness of the test being utilised.

Although, data was checked for normality visually using the widely utilised quantile-quantile (Q-Q) plot and statistically using a Shapiro-Wilk test, with the latter test method chosen as it is considered to be more powerful than other available normality tests (Razali and Wah, 2011). It should be noted that the power of this test remains low when sample sizes are small and performance is reduced when sample sizes of less than 30 are analysed by this test (Razali and Wah, 2011). Whilst the majority of the data collected was normally distributed, in a few instances tests for normality were not met, this being said, whilst normal distribution is strived for, it is often not achievable (Blanca *et al*, 2018). Furthermore, the n number in this chapter does not exceed 6, thus the performance of the Sharipo-Wilks test is likely to have been reduced (Razali and Wah, 2011) and so may not accurately represent the distribution of the data collected. As such other methods for conducting statistical analysis on the data were considered including alternatives for ANOVA such as Kruskal-Wallis and Welch tests or Mann-Whitney tests to replace t-tests (Tomarken and Serlin, 1986; Hart, 2001). Absence of normality and unequal variances can lead to the level of significance being distorted when using ANOVAs, as such the use of the Welch and Kruskal-Wallis tests aim to control for errors pertaining to non-normality and unequal variances (van Hecke, 2012; Jan and Shieh, 2014). However, it should be noted that non-normality has little impact on significance values when variances are equal, although the power of the test does decrease (van Hecke, 2012). Furthermore, although the Kruskal-Wallis and Welch tests provide suitable alternatives to an ANOVA, these often do not perform as well, especially when sample sizes are small and equal (Lantz, 2013), which is applicable in the data collected throughout this chapter were the n number does not exceed 6. Thus the use of ANOVAs for statistical analysis was a logical choice, as it is robust enough to manage assumptions regarding distribution and variance not being met (Black *et al*, 2010; Schmider *et al*, 2010).

As with the use of ANOVAs, t-tests also rely on data meeting a series of assumptions including normal distribution and equal sample sizes (Fagerland, 2012). Thus the presence of some non-normally distributed data, presented an opportunity to consider alternative tests. The Mann-Whitney test is a widely accepted non-parametric alternative to a t-test, which considers both the mean and median, thus being less specific, as opposed to testing only mean as is done in a t-test (Fagerland, 2012). The advantage of using the Mann-

Whitney test is that it makes fewer assumptions regarding distribution of data, thus overcomes the issues relating to non-normally distributed data (Rochon *et al*, 2012). Furthermore, the use of non-parametric tests such as the Mann-Whitney test are often suited to smaller sample sizes (Rochon *et al*, 2012) however, this is contradicted in other literature which indicates that t-tests can be performed on smaller sample sizes (for example with the n number as low as 4) compared to a Mann-Whitney test (for example with a minimum n number of 8) (Fay and Proschan, 2010). This being said, Mann-Whitney and t-tests have similar power unless data distribution is skewed to a large extent or has multimodal distribution. Similarly, unequal variances or sample sizes has limited impact on the power of either test (de Winter and Dodou, 2010) and where direct comparison of mean values is the desirable measure to use, then a t-test performs more efficiently than a Mann-Whitney test (Fay and Proschan, 2010). Furthermore, if data only slightly deviates away from normal distribution, then the use of a t-test is still valid (Rochon *et al*, 2012). These aforementioned factors alongside the Sharipo-Wilk P value and Q-Q plots obtained for non-normally distributed data, suggested data did not deviate widely from normal distribution ensuring a t-test is robust enough to analyse the data collected.

For data which was analysed via multiple t-tests or ANOVAs, the post hoc and multiple comparison tests applied to the data analysis were based on the recommendations made by the GraphPad software. The use of multiple comparison tests adjust the probability of incorrectly rejecting the null hypothesis, thus reducing the risk of type I errors (Sinclair *et al*, 2013; Dinno, 2015). Such errors can occur as a result of conducting multiple t-tests between groups of interest rather than utilising an ANOVA, as this method could inflate the risk of making a type I error, therefore employing multiple comparison analysis overcomes this problem (McHugh, 2011). Various multiple comparison for t-tests exist, including Bonferroni, Sidák, Holm, and Holm-Sidák, with the latter being the most powerful adjustment (Dinno, 2015), which influenced the decision to use this particular test. Similar variability in options exist for ANOVAs and include Dunnett, Bonferroni, Dunn, Bonferroni-Dunn and Tukey however, of these, Tukey has the greatest power whilst not being negatively affected if test assumptions are not met (Jaccard *et al*, 1984). There are two main factors which aided in the decision to use Tukey post hoc analysis on completion of the ANOVAs. Firstly, equal sample sizes were used for each experiment which were suitable

for use alongside Tukey analysis. Secondly, in this instance Tukey is more suitable than the Dunnett method as whilst this method allows comparison to the control group, it does not allow comparison between other groups (Lee and Lee, 2018), a factor which needed considering here to enable multiple groups to be compared to one another, alongside a control. A disadvantage of using multiple comparisons is that with each comparison the risk of drawing wrong conclusions about the significance increases (Gelman *et al*, 2012). However, by utilising multiple comparisons the overall significance level can be controlled and allows for comparison between multiple groups, which cannot be achieved by performing an ANOVA alone, thus the use of multiple comparisons enables more information to be gathered from the analysis of the data presented (McHugh, 2011; Lee and Lee, 2018). Thus, although the tests utilised to undertaken statistical analysis are robust enough to deal with data not meeting some assumptions, the small sample sizes in all experiments is likely to be a limitation whereby outliers in the results may noticeably affect the mean and/or standard deviation (Mishra *et al*, 2019). As such this may go some way to explain why visual representation of some data appears to show clear effect but when P values are considered no significant difference is recorded.

Finally, although the co-culture signalling model could not be utilised here to investigate the role of hRV in post-viral cough, this data demonstrates that there is a difference in response to infection between alveolar cells (A549) and bronchial cells (Beas-2b), which reflects the differences in cell type and position within the airways and the likelihood of infection with hRV. Whilst A549 cells show little change in response to infection, Beas-2b cells show an increase in cytotoxicity, decrease in cell mass and no change in proliferation rate as time after infection progresses, suggesting that cell growth (in terms of overall size of single cells) but not number is potentially affected and that hRV has a cytotoxic effect. Furthermore, there is an increase in fluorescein leakage and decrease in TEER measurements, which suggests that there is a reduction in tight junction integrity, albeit it only a small one. Which when coupled with the minor changes seen in MMP activity may be a consequence of extracellular matrix degradations, which ultimately could aid in the opportunistic bacterial infections that are observed in some hRV infections (Sajjan *et al*, 2008).

3 Chapter 3: Optimisation of a Human Tissue Model of the Airways to Study Human Rhinovirus Infection

3.1 Introduction

The use of PCLS in respiratory research provides an opportunity to conduct *in vitro* techniques and procedures whilst retaining *in vivo* responses (Neuhaus *et al*, 2013), owing to the maintenance of cellular architecture and preservation of lung parenchyma (Martin *et al*, 1996; Alder *et al*, 1998). However, whilst the technique is widely used, there is a lack of consistence regarding the optimal slice thickness and longevity of PCLS in culture, with 200 - 300µm being the most frequently used thickness (Sturton *et al*, 2008; Schlepütz *et al*, 2012; Bai *et al*, 2016; Alsafadi *et al*, 2017; Zmora *et al*, 2017) for culture periods of approximately 3 days (Bergner and Sanderson, 2002b; Wohlsen *et al*, 2003; Ressmeyer *et al*, 2006; Neuhaus *et al*, 2013). As a result of this observation this chapter aims to optimise the use of PCLS technique and in doing so try to determine whether an optimal thickness and maximum culture period for viability can be established.

Owing to the maintenance of the lung parenchyma, architecture and responsiveness, PCLS forms an ideal model to study the effect of hRV infection on human tissue as it better recapitulates the *in vivo* environment (Martin *et al*, 1996). Similarly, the use of *ex vivo* tissue provides a greater level of complexity than *in vitro* experiments, whilst removing the difficulties faces when conducting *in vivo* research (Torisawa *et al*, 2014). Given the lack of suitable animal models which can be used to study different aspects of hRV pathogenesis (Newcomb *et al*, 2008) there is a need to develop a model that can utilise human tissue for the study of hRV and its role in cough and airway inflammation. This is particularly true for the mechanisms leading to airway inflammation, hypersensitivity and exacerbation of underlying respiratory conditions, which are currently not fully understood (Abdullah *et al*, 2013). Thus, this chapter also aims to investigate the effect that RV16 infection has on cough and airway inflammation through the optimisation and use of a PCLS infection model.

3.2 Methods

3.2.1 Optimised PCLS Process

3.2.1.1 Lung Tissue Inflation and Preparation for Slicing

Excess human lung tissue (ethics number 12/SC/0474) was received from cardiothoracic surgical procedures, (predominately lung resection surgery) at Castle Hill Hospital, Hull University Teaching Hospitals NHS Trust weighing between 2 – 8g. Where donors were undergoing resection for lung cancer, tissue was received from tumour margins and thus considered to be normal tissue. Tissue was transported from the operating theatre in Krebs-Henseleit buffer at pH7.4, gassed with 95% O_2, 5% CO_2 to the laboratory on ice within 30 minutes of removal from the donor. Initial gross weight of the sample was taken to enable a sufficient volume of low melting point (LMP) agarose (Fisher Scientific) to be used for the inflation process. Where necessary the sample was washed with DMEM containing 10% FBS, penicillin (100U/ml) – streptomycin (100µg/ml), 2mM L-Glutamine and Amphotericin B (2.5 µg/ml) (Gibco), henceforth referred to as tissue DMEM, to remove excess blood prior to inflation. Tissue was infused with 3% LMP agarose in tissue DMEM on ice, using 3 – 4ml/g, via a 19G needle until the tissue was firmly inflated. Inflated tissue was rested on ice for 30 minutes to ensure agarose was firm prior to removal of the visceral pleura from the tissue surface and sectioning of tissue into pieces of $10mm^3$. These pieces of tissue were subsequently embedded in 7% LMP agarose in 1x PBS and stored on ice at 4°C for 2 – 3 hours prior to slicing. Small off cuts of tissue were utilised for initial lysed LDH measurements, viability via trypan blue exclusion, preservation for sectioning and explants for lung fibroblast growth.

3.2.1.2 Lung Tissue Slicing

After 2 – 3 hours at 4°C embedded tissue was trimmed to remove excess agarose and adhered to the Leica Vibratome VT1200S (Leica Biosystems, Milton Keynes, UK) specimen plate using cyanoacrylate. The sample was left to adhere fully, placed in the buffer tray and completed submerged in cold (4°C) sterile 1x PBS. The buffer tray was surrounded by ice and the instrument light source switched off to help maintain the reduced PBS temperature and retain the firmness of the agarose. Tissue was sliced using stainless steel double edged razor blades (after trying multiple brands, Wilkinson Sword produced the cleanest and

most consistent tissue slices thus were used throughout), at various thicknesses from 300 – 1000µm, depending on experimental requirement, using a blade feed rate of 0.1 – 0.3mms^{-1} and an amplitude of 2.25mm. Tissue slices were collected from the buffer tray immediately post slicing, placed in fresh 1x PBS and using a 6 or 8mm biopsy punch (Selles Medical, Hull, UK) a tissue disc was taken, biopsied tissue slices were placed in 12 well plates (Sarstedt) with 500µl of tissue DMEM. Individual tissue slices were weighed to enable comparison of data per milligram of tissue prior to incubation at 37^{o}C, 5% CO_2 for a maximum of 7 days. Media was changed on tissue slices 2 hours post slicing and every 24 hours thereafter, with all tissue effluent stored at 4^{o}C until processed.

3.2.1.3 Lung Tissue Lump Collection

Alongside PCLS small tissue lumps were also collected as an alternative for some infection experiments as the physiological structure of the lung tissue remains similar to the excess tissue initially extracted from the donor (Nicholas *et al*, 2015). Additionally, the use of tissue lumps enabled tissue which inflated or sliced poorly to be utilised more effectively thus reducing unnecessary waste. Tissue lumps were collected both pre and post inflation to allow for comparison of LDH cytotoxicity and viability via trypan blue exclusion. Tissue lumps of 2 – 3mm^3 were taken from various positions off larger pieces of excess tissue remaining after inflated tissue had be prepared for tissue slicing or from tissue collected prior to inflation. Tissue lumps were placed in 48 well plates (Sarstedt) with 500µl of tissue DMEM. Individual tissue lumps were weighed to enable comparison of data per milligram of tissue prior to incubation at 37^{o}C, 5% CO_2 for a maximum of 7 days. Media was changed on tissue lumps 2 hours post slicing and every 24 hours thereafter, with all tissue effluent stored at 4^{o}C until processed.

3.2.1.4 Weighing Lung Tissue Slices and Tissue Lumps

Prior to weighing tissue slices, PCLS and tissue lumps were placed briefly on filter paper and turned to remove as much excess tissue DMEM from all surfaces of the tissue as possible. Removal of the excess moisture provided a final mass that represented the lung tissue and inflation agarose, thus ensuring that when later analysis was conducted measurements represented the effect on the PCLS or tissue lump only. Whilst removal of excess moisture

could easily be achieved, this was not true of the agarose which was retained in the tissue, thus the final mass of any inflated tissue also included the weight of the agarose. It is not possible to account for the exact amount of agarose in any individual PCLS or tissue lump, as this varies not only between each PCLS or lump taken but also between each donor. Whilst, the retained agarose is inert and unlikely to have any impact on the tissue viability and thus raw measurements made (Ulrich *et al*, 2011), agarose retention will impact on any analysis were values are calculated per milligram of tissue. This increase in mass as a result of retained agarose means that the values recorded per milligram of tissue will be lower than if no agarose was present, as the overall mass of inflated PCLS or tissue lump is greater than uninflated tissue. Given the removal of agarose from the tissue is not possible it is worth considering the impact of this addition mass when any analysis is conducted.

3.2.2 Processing and Analysing Human Tissue for Assessing Viability

3.2.2.1 Tissue Lysis

Tissue was lysed after a given number of days in culture to enable LDH values to be determined. Tissue was minced into pieces of 1 – 2mm before being placed into a 1.5ml microcentrifuge tube with 500µl of tissue DMEM for further homogenisation with a micropestle (Fisher Scientific). 50µl of 10% (v/v) lysis buffer (Triton X-100) was added to the homogenised tissue and incubated at 37^{o}C, 5% CO_2 for 24 hours. Supernatant was subsequently decanted and stored at 4^{o}C for short term use and -80^{o}C for long term use.

3.2.2.2 LDH Assay

For each experimental condition to be measured via LDH, PCLS and lump tissue were cultured in duplicate (for example at 300µm, 500µm, 700µm and 1000µm thickness), thus the following method is applicable to each individual sample, with data averaged for each condition using the method discussed below. Lysed tissue samples and effluent collect from media changes for tissue were measured for LDH levels, using a modified OPS Diagnostic LDH assay protocol, as an indication of cytotoxicity. Effluent samples were collected 2 hours post inflation and subsequently every 24 hours and stored at 4^{o}C for a maximum of 7 days. To collect effluent, tissue DMEM was completely aspirated and replenished with fresh

tissue DMEM, as such each LDH absorbance value represents the data from the previous 24 hours, with the exception of the initial 2 hour data point. Lysed tissue supernatant was collected after homogenised tissue had been lysed for 24 hours (see 3.2.2.1). To complete the assay LDH assay mixture (see 2.2.9.7) was added to a clear, flat bottomed 96 well plates, to which 50µl of each tissue effluent or lysed tissue supernatant was added in duplicate and incubated at room temperature for 15 minutes. Due to the presence of phenol red in the tissue DMEM, a media blank measurement was also taken to account for the absorbance due to the media. Additionally a positive control using 1% BSA and a negative control using distilled water were also measured. Absorbance was measured on a Thermo Scientific™ Multiskan™ FC Microplate Photometer (Fisher Scientific) or Tecan Infinite M200 multimode plate reader at 490 and 690nm, each tissue effluent value was adjusted to account for the media blank and normalised per milligram of tissue, giving a value of relative absorbance per milligram.

LDH absorbance values were calculated using the following method:

The absorbance for a media blank was taken in duplicate wells on every LDH plate run, to account for the presence of phenol red in the tissue DMEM, this was then averaged. For example;

Media Blank 1	**Media Blank 2**	**Average Media Blank**
0.344	0.384	0.364

Duplicate measurements for each effluent or lysed tissue sample were taken, therefore two wells of data accounted for each tissue sample. For each well the raw absorbance data was adjusted for the media blank. For example;

	Raw Absorbance	**Average Media Blank**	**Adjusted Absorbance**
Well 1	0.793	0.364	0.429
Well 2	0.773	0.364	0.409

The adjusted absorbance value for each effluent or lysed tissue sample was subsequently averaged. For example;

Well 1 Adjusted Absorbance	Well 2 Adjusted Absorbance	Averaged Adjusted Absorbance
0.429	0.409	0.419

This value was then divided by the mass of the relevant PCLS or lump tissue sample in milligrams. For example;

Average Adjusted Absorbance	Mass of PCLS (mg)	Average Absorbance (per mg)
0.419	40.7	0.0103

Owing to duplicate PCLS or lump tissue samples being taken per condition the average absorbance for each condition was also calculated to give a single data point ±S.E.M. The example;

Average Absorbance (per mg) PCLS 1	Average Absorbance (per mg) PCLS 2	Average Absorbance (per mg) for condition
0.0103	0.0256	0.0176 ± 0.0054

This gave a final absorbance value of 0.0176 ± 0.0054 for a 300µm PCLS at 2 hours post slicing (this value represents a single donor).

3.2.2.3 Tissue Dissociation

Tissue was dissociated to achieve a single cell suspension which could be used to assess viability and determine approximate cell counts to enable suitable RV16 viral load to be delivered to lump tissue and PCLS. Tissue was minced into pieces of 1 – 2mm with the addition of 4µl type IV collagenase (working concentration 2mg/ml) and 8µl dispase II (both Gibco) (working concentration 0.4%) to help start the enzymatic digestion of connective tissue. Tissue was subsequently placed in 200µl of tissue DMEM and incubated at 37^{o}C, 5% CO_2 on a tube rotator (Miltenyi Biotech, Surrey, UK) at 20rpm for 2 hours. On removal from the incubator 300µl of tissue DMEM was added to the tissue and the mixture was rapidly

pipetted 5 – 6 times with a P1000 pipette (Gilson, Bedfordshire, UK) to help further disaggregate cells. This mixture was discharged onto a 70µm cell strainer (Fisher Scientific) pre-wetted with 1ml of 1x PBS and effluent collected in a 50ml centrifuge tube (Fisher Scientific). A subsequent 500µl of tissue DMEM was used to wash the microcentrifuge tube to maximise cell retrieval before discharge onto the cell strainer. A further 4ml of 1x PBS was used to wash the cell strainer to ensure all dissociated cells had been collected. The cell suspension was centrifuged at 600x g for 5 minutes at 4^{o}C, the supernatant was discarded and the cell pellet resuspended in 1ml of tissue DMEM. Prior to counting the number of viable and unviable cells in the dissociated tissue, a 50µl cell suspension sample was added to 50µl of ammonium-chloride-potassium (ACK) lysis buffer (Fisher Scientific) to remove red blood cells and facilitate the counting of other cells. This dilution was accounted for in subsequent calculation of viability and cell count.

3.2.2.4 Calculating Tissue Viability

Cell suspensions from dissociated tissue were mixed with 0.4% Trypan Blue solution at a 1:1 ratio and applied to a haemocytometer. Cells were visualised by light microscopy with cell viability being determined by presence or absence of cytoplasmic staining, unviable cells stain blue whilst viable cells remain unstained. Cell counts were determined by counting the number of viable and unviable cells in 5 independent 1mm x 1mm x 0.1mm squares on the haemocytometer. An average of the 5 squares was taken, this was multiplied by 2 to account for the ACK lysis buffer dilution and by a further 2 to account for the Trypan Blue dilution. The final value of both the viable and unviable cells was converted to give number of cells/ml by multiplying by $1x10^4$. To calculate the viability of the tissue the number of viable cells was divided by the total number of cells (viable plus unviable) and converted into a percentage.

3.2.3 Live Tissue Analysis

3.2.3.1 Imaging of Live PCLS on Stereo Microscope

PCLS of varying thickness (300 – 1000µm) were temporarily mounted on a glass microscope slide and imaged at x10 magnification, x1 zoom using a Zeiss SteREO Discovery.V8

microscope (Carl Zeiss Ltd, Cambridge, UK) after a culture period of 1, 5 and 7 days post slicing. Multiple images were taken using Zeiss AxioVision software (Carl Zeiss Ltd) and stitched together (using Autostitch software produced by the University of British Columbia) to provide a complete image of the PCLS allowing for observations of changes in gross morphology over the culture period.

3.2.3.2 Measuring Bronchoconstriction

700µm PCLS were placed in 6 well plates with 1000µl of tissue DMEM and observed at x10 magnification, x1 zoom using a Zeiss SteREO Discovery.V8 microscope to enable a small bronchiole to be identified for bronchoconstriction measurements. Baseline measurements of bronchiole diameter and circumference where possible, were taken using Zeiss AxioVision software, after which 10µl of 100mM methacholine (MCh) (final working concentration 1mM) a potent bronchoconstrictive agent (Ressmeyer *et al*, 2010) was added directly above the bronchiole position within the PCLS. Images and measurement of the bronchioles were taken immediately after the addition of MCh, every 60 seconds for the first 5 minutes and subsequently every 5 minutes for a total of 30 minutes. The same process was repeated using a final working concentration of 10µM histamine applied directly above the bronchiole position. With images taken immediately after addition, then every 60 seconds for 5 minutes and subsequently at 10 minutes, by which time the bronchiole had returned to baseline measurements.

3.2.3.3 TEER Measurements of PCLS

To reduce fluctuations in resistance readings (see 2.2.6.1) and in order to maintain consistence between *in vitro* and *ex vivo* TEER measurements, the same size Thincert™ were utilised in all experiment and thus influenced the maximum diameter of the PCLS utilised. The diameter of the 24 well Thincert™ membrane were approximately 7mm, to ensure the PCLS completely covered the membrane a 8mm diameter biopsy punch was used as this created the tissue slice which fitted tightly in the well and covered the entire membrane. PCLS were not adhered to the membrane thus reducing the risk of damage to either the membrane or the tissue, in addition, the chosen diameter and thickness ensured the PCLS settled flat on the membrane and any air bubbles could be removed from under

the PCLS by applying gentle pressure ensuring the entire PCLS was in contact with the membrane whilst TEER measurements were taken. Triplicate 8mm diameter, 1000µm PCLS were placed in 12 well plates with 500µl of tissue DMEM for 24 hours post slicing to allow pro-inflammatory mediators released due to slicing to decrease. PCLS were subsequently transferred to a 24 well Thincert^{TM}, 0.4µm pore size, transparent PET membrane containing 200µl tissue DMEM in the apical chamber and 500µl complete media in the basal chamber and incubated at 37^{o}C, 5% CO_2 for the duration of the measurement period. Initial TEER measurements were taken in triplicate from each well, 24 hours post slicing using the method outlined in 2.2.6.1 and subsequently every 24 hours thereafter for a maximum of 168 hours.

3.2.4 Preserving PCLS for Sectioning and Analysis

3.2.4.1 Snap Freezing PCLS and Lump Tissue

PCLS between 300 – 700µm thicknesses and small lumps of lung tissue were embedded in optimal cutting temperature compound (OCT) (Fisher Scientific) and immersed in pre-cooled 2-methylbutane (Sigma Aldrich). Both were held in liquid nitrogen for 1 – 2 minutes, until tissue was completely frozen. Frozen tissue specimens were transferred to -80^{o}C for long term storage.

3.2.4.2 Cryosectioning of PCLS and Lump Tissue

Snap frozen PCLS and small lumps of tissue were sectioned at 10µm using a Leica CM1100 Cryostat (Leica Biosystems). Sections were mounted on Thermo Scientific™ SuperFrost Plus™ Adhesion slides (Fisher Scientific), allowed to dry for 20 – 30 minutes and stored at -20^{o}C for future staining.

3.2.4.3 Haematoxylin and Eosin (H&E) Staining of Frozen PCLS Sections

Sectioned frozen tissue was stained using H&E to show the basic histology of the tissue after culture periods of 0 – 7 days. To fix and permeabilise the tissue prior to staining, sections were submerged in ice cold acetone, left for 10 minutes at -20^{o}C and washed for

1 minute under cold running water (Gelderblom *et al*, 1992). Sections were placed in Haematoxylin (Sigma Aldrich) for 30s, rinsed with cold water twice to remove excess stain and the presence of staining checked using light microscopy. Sections were counter stained with 2% Eosin Y in H_2O (Sigma Aldrich) for 10 minutes, rinsed twice with cold water and checked for the presence of staining, further counter staining for 1 minute intervals was carried out as necessary. Sections were dehydrated by submerging microscope slides in increasing ethanol concentrations of 70%, 90% and 100% for a period of 1 minute per concentration. Stained and dehydrated tissue sections were subsequently cleared by placing in Histoclear II (Scientific Laboratory Supplies Ltd (SLS), Nottingham, UK) for 1 minute and repeating 3 times. Slides were dried and coverslips mounted using Histomount (Fisher Scientific) in preparation for imaging via light microscopy.

3.2.5 Rhinovirus Culture in PCLS and Lump Tissue

3.2.5.1 Optimised Rhinovirus Infection of PCLS and Lump Tissue

Small inflated tissue lumps and 8mm diameter 500µm PCLS were prepared as outlined in 3.2.1.2 and 3.2.1.3 and incubated overnight at 37°C, 5% CO_2 to allow for any pro-inflammatory markers which have been released due to inflation and slicing to subside. After overnight incubation the required volume of RV16 needed to infect the tissue at a MOI of 0.025 was calculated using the $TCID_{50}$ from previous endpoint dilution assay (outlined in 2.2.8.1) and the predicted number of cells present in each individual tissue sample (outlined in 3.3.7), added to each well and the final volume made to 500µl with infection DMEM. The plate was incubated at room temperature and gently agitated on a gyro-rocker at 15rpm for 2 hours. The tissue was subsequently washed once with 1x PBS and 500µl of infection DMEM added to each well prior to incubation at 37°C, 5% CO_2.

3.2.6 Assessing Effectiveness of Rhinovirus Infection in PCLS and Lump Tissue

3.2.6.1 Viral Replication Confirmation from PCLS and Lump Tissue

Hela Ohio cells were seeded at a density of $5x10^4$cells/ml in a clear, flat bottom, 96 well plate in complete DMEM and incubated at 37°C, 5% CO_2 for 24 hours. After 24 hours complete DMEM was aspirated from all wells and replaced with 150µl of infection DMEM.

To confirm successful infection of tissue, 50µl of post-infection tissue effluent from tissue exposed to RV16, ultrafiltered RV16 and basal conditions was added to triplicate wells containing the Hela Ohio cells, with 2 wells per row left as controls (Figure 3.1).

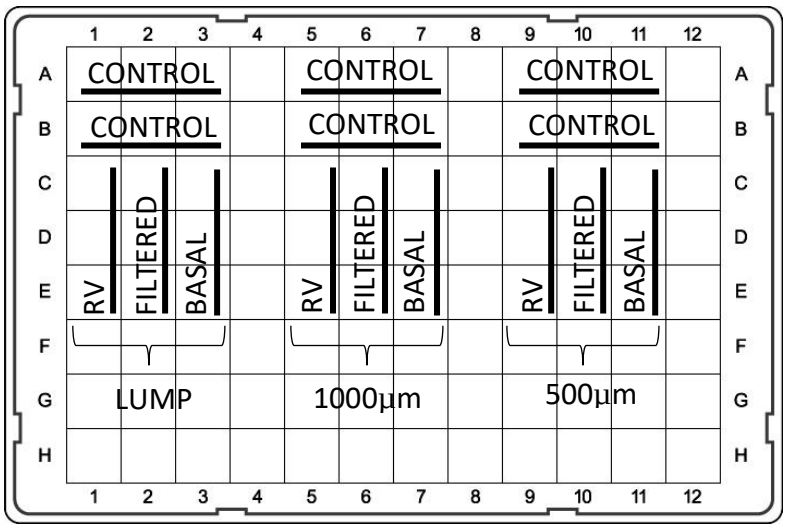

Figure 3.1 Example tissue infection confirmation plate arrangement.

Wells were checked for cytopathic effect by the evidence of Hela Ohio cell rounding and sloughing in individual wells every 24 hours until this became apparent or for a maximum of 5 days if no infection was present.

3.2.6.2 LDH Assay Post Rhinovirus Infection

LDH assay was conducted as outlined in 3.2.2.2 with minor modifications due to infection of tissue with rhinovirus. Effluent samples from tissue designated as basal, RV16 treated or ultrafiltered RV16 treated were collected at 2 and 24 hours post inflation/pre rhinovirus infection, and subsequently every 24 hours post infection for a maximum of 5 days post infection and stored at 4^{o}C. To collect effluent, tissue DMEM was completely aspirated and replenished with fresh tissue DMEM, thus each LDH absorbance value represents the data from the previous 24 hours, with the exception of the initial 2 hour data point. Tissue was lysed as outlined in 3.2.2.1 and assayed as outlined in 3.2.2.2, absorbance was measured on a Tecan Infinite M200 multimode plate reader at 490 and 690nm all values were

adjusted to account for the media blank and normalised per milligram of tissue, giving a value of relative absorbance per milligram, using the method outlined in 3.2.2.2.

3.2.6.3 CytoTox-Glo™ Cytotoxic Assay Post Rhinovirus Infection

The remaining effluent and lysed tissue samples after LDH analysis (see 3.2.6.2) which had been designated as basal or RV16 treated was pooled at each time point and measured for dead-cell protease activity as an indication of dead cell number. Dead-cell protease activity was measured using the CytoTox-Glo™ Cytotoxic Assay (Promega, Southampton, UK) which utilises the interaction between the luminogenic substrate alanyl-alanyl-phenylalanyl-aminoluciferin and the dead cell protease released through cell membrane lysis to provide an indication of the extent of cell death. 25µl of each tissue effluent or lysed tissue supernatant was added to duplicate well, to which 25µl of CytoTox-Glo™ assay reagent was added before briefly mixing on an orbital shaker and incubating in the dark at room temperature for 15 minutes. Due to the presence of phenol red in the tissue DMEM, a media blank measurement was also taken to account for any auto-luminescence due to the media. Measurements of luminescence were made at wavelength 560nm using a Tecan Infinite M200 multimode plate reader. Each tissue effluent value was adjusted to account for the media blank and normalised per milligram of tissue, giving a value of relative luminescence per milligram.

3.2.6.4 WST-1 Cell Proliferation Assay Post Rhinovirus Infection

Basal, RV16 treated or ultrafiltered RV16 treated small tissue lumps, 8mm diameter 500µm and 1000µm PCLS were collected 5 days post infection and transferred to clear 24 well, flat bottom plates. 250µl of tissue DMEM was added to each well, to which 25µl of WST-1 reagent was added. Due to the presence of phenol red in the tissue DMEM, a media blank measurement was also taken to account for difference in absorbance. Plates were incubated in the dark at 37°C for 120 minutes, the tissue discarded and absorbance measured on a Tecan Infinite M200 multimode plate reader at 420nm, with 21 points measured per well. All values were adjusted to account for the media blank and normalised per milligram of tissue, giving a value of relative absorbance per milligram.

3.2.6.5 Calculating Tissue Viability Post Rhinovirus Infection

Tissue viability was calculated using the method outlined in 3.2.2.4 for basal, RV16 treated or ultrafiltered RV16 treated tissue 5 days post infection, after dissociating of the tissue in the manner outline in 3.2.2.3. The final value of both the viable and unviable cells was converted to give number of cells/ml by multiplying by $1x10^4$. To calculate the viability of the tissue the number of viable cells was divided by the total number of cells (viable plus unviable) and converted into a percentage.

3.2.6.6 Zymography for Assessment of MMP Upregulation

Undiluted tissue culture effluent (8µl) collected post infection as outlined in 3.2.6.2 were pooled, mixed with 5x non-reducing buffer (2µl), loaded into wells alongside EZ-Run™ prestained protein ladder and separated using a 7.5% acrylamide gel containing gelatine (4mg/ml) made in house (Table 2.9). Gels were run, stained, destained and imaged using the procedure outlined in 2.2.9.6

3.2.6.7 TEER Measurements of PCLS Post Rhinovirus Infection

Triplicate 8mm diameter, 1000µm PCLS were placed in 12 well plates with 500µl of tissue DMEM for 24 hours post slicing to allow pro-inflammatory mediators release due to slicing to decrease. PCLS were subsequently transferred to a 24 well Thincert™ with 0.4µm pore size and transparent PET membrane containing 200µl tissue DMEM in the apical chamber and 500µl tissue media in the basal chamber for the duration of the measurement period. Initial TEER measurements were taken in triplicate from each well, 24 hours post slicing using the method outlined in 2.2.6.1. After which, PCLS were infected at a MOI of 0.025, the required volume of RV16, ultrafiltered RV16 or infection DMEM (basal control) was applied to duplicate wells and the volume made up to 500µl using the method outlined in 3.2.5.1. After the 2 hour incubation period the wells were washed once with 1x PBS, infection DMEM refreshed in each well and the plates incubated at 37°C, 5% CO_2. TEER measurements were subsequently taken every 24 hours thereafter for a maximum of 6 days post infection, with media (using tissue DMEM) changes every 24 hours.

3.2.6.8 Bronchoconstriction Measurements Post Rhinovirus Infection

Basal, RV16 treated or ultrafiltered RV16 treated 700µm PCLS 5 days post infection were placed in 6 well plates with 1000µl of tissue DMEM and observed at x10 magnification, x1 zoom using a Zeiss SteREO Discovery.V8 microscope to identified suitable bronchioles for bronchoconstriction measurements. Baseline bronchiole diameter measurements were taken using Zeiss AxioVision software, after which the tissue DMEM was removed and replaced with 1000µl of 10µM histamine applied directly above the bronchiole position. Images were taken immediately after addition, then every 60 seconds for 5 minutes and subsequently at 10 minutes.

3.2.6.9 Cytokine Array

Human cytokine antibody array membranes (Abcam) were placed printed side up in the manufacturer provided 8 well plate and blocked with 2ml of 1x blocking buffer for 30 minutes at room temperature. Effluent samples from 500µm PCLS designated as basal or RV16 treated were collected at 24, 60, 96 and 120 hours post infection, centrifuged to remove cell debris and pooled to give a single sample. Pooled samples were created by pooling the effluent from 2 PCLS per condition, 200µl of effluent was collected per time point from each PCLS, pooled and gently mixed to generate a total of approximately 1.6ml of effluent per condition. 1x blocking buffer was aspirated, replaced with 1ml of undiluted effluent and incubated at 4^{o}C overnight. Membranes were transferred to 100mm square petri dishes (Sarstedt), 20ml of wash buffer I applied and a large volume wash conducted for 45 minutes at room temperature with gentle agitation on a gyro-rocker. Membranes were transferred back to the 8 well plate and washed 3 times with 2ml of wash buffer I for 5 minutes at room temperature with gentle agitation, this process was subsequently repeated with wash buffer II in the same manner. Wash buffer II was completely aspirated, replaced with 1ml of 1x biotin-conjugated anti-cytokines and incubated at 4^{o}C overnight. After overnight incubation, 1x biotin-conjugated anti-cytokines was aspirated and the 3 wash steps with wash buffer I and wash buffer II were repeated as previously described. Wash buffer II was completely aspirated, replaced with 2ml of 1x horseradish peroxidase (HRP)-conjugated streptavidin and incubated at 4^{o}C overnight. After overnight incubation, 1x HRP-conjugated streptavidin was aspirated and the 3 wash steps with wash buffer I and

wash buffer II were repeated as previously described. Membranes were transferred printed side up to filter paper to absorb excess wash buffer and then placed on a plastic sheet. To each membrane 500µl of detection buffer mixture (1:1 mix of detection buffer C and detection buffer D) was applied, incubated at room temperature for 2 minutes and a second plastic sheet placed on top of the membrane ensuring all air bubbles were removed. The membranes were imaged on a Li-cor C-Digit® Blot Scanner (Li-cor) and analysed via densitometry using ImageJ software, with all dots adjusted to account for negative control and normalised against positive control dots.

3.2.7 Assessing Effectiveness of Rhinovirus Infection in PCLS and Lump Tissue via Western Blot Analysis

3.2.7.1 Preparation of Tissue Lysates for Western Blotting Post Rhinovirus Infection

Basal, RV16 treated or ultrafiltered RV16 treated small tissue lumps and 500µm PCLS were collected 5 days post infection and washed twice with ice cold 1x PBS to remove traces of tissue DMEM. Tissue samples were placed in a 1.5ml microcentrifuge tube containing 1ml of ice cold 1x lysis buffer containing 1mM PMSF, homogenised on ice and sonicated twice at 24kHz using an UP200S ultrasonic processor for 30 seconds at 0.5 pulse cycle, 70% amplitude, with 30 seconds cooling on ice between each cycle. Tissue lysates were centrifuged for 15 minutes at 14,000x g maintained at 4^{o}C throughout, supernatant retained and stored at -20^{o}C until used.

3.2.7.2 BCA Assay for Protein Quantification from Tissue Lysates

Protein concentrations in tissue lysates were calculated using the method outlined in 2.2.3.2 and samples prepared accordingly. For lysates that required non-denaturing conditions (ICAM-1), tissue lysates were diluted in 5x non-reducing buffer (see appendix A2) to equalise final protein concentrations and either used immediately or stored at -20^{o}C for later use.

3.2.7.3 Sodium Dodecyl Sulphate Polyacrylamide Gel Electrophoresis (SDS-PAGE)

Tissue lysates were loaded and run using the method outlined in 2.2.3.3 with some minor modification. Due to ICAM-1 requiring non-denaturing conditions, samples which had been prepared in 5x non-reducing buffer were loaded on a separate gel and run separately in 1x running buffer at 120V for 90 – 120 minutes until the dye front had reached the bottom of the gel.

3.2.7.4 Transfer and Blocking

Transfer and blocking was carried out using the method outlined in 2.2.3.4.

3.2.7.5 Probing and Visualising

Probing and visualisation was carried out in the same manner as the method outlined in 2.2.3.5 with modification to the primary (Table 3.1a, 3.1b and 3.1c) and secondary antibodies (Table 3.2) used for the target proteins.

Antibody	Protein Size	Dilution	Animal Raised In	1st/2nd Probe	Supplier
P2X3	55kDa	1:500	Mouse	1st	Santa Cruz
α-Tubulin	55kDa				
MUC5AC	130kDa			2nd	Abcam
TRPV4	100kDa		Rabbit		

Table 3.1a Details of primary antibodies utilised to probe for desired targets in 500µm PCLS post-infection with RV16, using reducing conditions.

Antibody	Protein Size	Dilution	Animal Raised In	1st/2nd Probe	Supplier
P2X3	55kDa	1:500	Mouse	2nd	Santa Cruz
α-Tubulin	55kDa				
MUC5AC	130kDa			1st	Abcam
TRPV4	100kDa		Rabbit		

Table 3.1b Details of primary antibodies utilised to probe for desired targets in tissue lumps post-infection with RV16, using reducing conditions.

Antibody	Protein Size	Dilution	Animal Raised In	1st/2nd Probe	Supplier
ICAM-1	90kDa	1:500	Mouse	1st	Abcam
α-Tubulin	55kDa			2nd	Santa Cruz

Table 3.1c Details of primary antibodies utilised to probe for desired targets in 500µm PCLS and tissue lumps post-infection with RV16, using non-reducing conditions.

Antibody	Dilution	Animal Raised In	Supplier
Anti-Mouse	1:15000	Goat	Li-cor
Anti-Rabbit			

Table 3.2 Details of secondary antibodies utilised to fluorescently visualise primary antibodies bound to desired targets 500µm PCLS and tissue lumps post-infection with RV16.

3.2.7.6 Western Blot Analysis

Quantification of western blot bands was conducted via densitometry using ImageJ software. All bands were adjusted to account for background noise and normalised to the reference protein α-Tubulin (Gallo-Oller *et al*, 2018). Data was presented as a fold change against basal values.

3.2.8 Assessing Effectiveness of Rhinovirus Infection in PCLS and Lump Tissue via RNA Extraction and Analysis

3.2.8.1 RNA Extraction from Tissue Post Rhinovirus Infection

Basal, RV16 treated or ultrafiltered RV16 treated small tissue lumps were collected 5 days post infection and washed once with ice cold 1x PBS to remove traces of tissue DMEM. The washed tissue was transferred to a 1.5ml centrifuge tube, covered with 1ml of Trizol and homogenised with scissors and a micropestle. The tube was left to sit at room temperature for 5 minutes prior to the addition of 250µl chloroform, shaken vigorously for 15 seconds and left to sit for a further 5 minutes at room temperature. The tissue lysate was centrifuged at 10,000rpm for 5 minutes and the aqueous phase transferred to a clean 1.5ml microcentrifuge tube. To this 550µl of isopropanol (Sigma Aldrich) was added, left to sit for 5 minutes, centrifuged at 14,000rpm for 20 minutes and placed on ice for the remainder of

the procedure. The isopropanol was decanted and 1ml of 75% ethanol in DEPC treated H_2O added, the pellet gently washed and centrifuged at 9500rpm for 5 minutes. The ethanol was decant and the pellet air dried until a small meniscus of ethanol remained. The RNA pellet was resuspended in 25µl of DEPC treated H_2O and retained on ice for immediate preparation for cDNA synthesis.

3.2.8.2 RNA Extraction from Tissue Culture Effluent Post Rhinovirus Infection

Basal, RV16 treated or ultrafiltered RV16 treated tissue effluent was collected 5 days post infection, pooled and centrifuged at 12,000rpm for 5 minutes. 500µl of supernatant was transferred to clean a 1.5ml microcentrifuge tube to which 1ml of Trizol was added, all subsequent steps were performed as outlined in 3.2.8.1.

3.2.8.3 Measurement of RNA Quantity in Sample

RNA concentrations in tissue lysates and concentrated effluent were measured using a Thermo Fisher NanoDrop Lite Spectrophotometer at 260nm following the method outlined in 2.2.4.2.

3.2.8.4 cDNA synthesis from RNA

Extracted RNA from tissue and effluent was converted to cDNA (2µg) for further analysis using the method outlined in 2.2.4.3.

3.2.8.5 RT-PCR

cDNA synthesised from lump tissue lysates were amplified using the primers specified in table 3.3 following the method and thermal cycling conditions outlined in 2.2.4.4.

Primer	Direction	Sequence	Designed
TRPV4	Forward	5'-CTGAGACCCTCCCTGGACTA-3'	In house (Atkinson, 2020)
	Reverse	5'-GAGAAGACACTGCTTGCTCAGA-3'	
P2X3	Forward	5'-ACCATCGGGATCATCAACCG-3'	In house (Atkinson, 2020)
	Reverse	5'-CATGATGGGCGTTTCCACTG-3'	
β-Actin	Forward	5'-CGTGGGCCGCCCTAGGCACCA-3'	Ramachandran, Morice and Compton, 2006
	Reverse	5'-TTGGCCTTAGGGTTCAGGGGG-5'	

Table 3.3 Primers utilised to amplify cDNA synthesised from tissue lumps PCLS post-infection with RV16.

3.2.8.6 Agarose Gel Electrophoresis

A 1.3% agarose gel was made and electrophoresed using the method outlined in 2.1.4.5.

3.2.8.7 Quantitative Real Time Polymerase Chain Reaction (qPCR) to Determine Viral Load

cDNA synthesised from concentrated tissue effluent (tissue lumps, 500µm and 1000µm PCLS) and tissue lump lysate collected 5 days post-infection with RV16, ultrafiltered RV16 and basal conditions, was amplified using RV16 specific primer sequences provided in a Primerdesign genesig kit for human Rhinovirus 16 (Primerdesign Ltd, Chandler's Ford, UK) alongside TaqMan® Advance Master Mix (Fisher Scientific). Reagents were added to 0.2ml ultra clear qPCR tubes in the order specified in table 3.4, using varying volumes of cDNA (200ng) to enable amplification of the required gene sequence. Additionally, negative controls were also made, either without cDNA or using no reverse transcriptase samples from 3.2.8.4 in place of cDNA. A serial dilution of positive controls (2 – $2x10^5$ copy number, provided as part of the aforementioned kit) was also performed to provide a standard curve, thus enabling quantification of viral load in samples to be calculated. Amplification was performed on an Applied Biosciences™ StepOnePlus™ Real Time PCR system (Fisher Scientific) achieved using the thermal cycling conditions specified in table 3.5.

Reagent	Volume	Final Concentration
TaqMan advance master mix	10µl	-
Primer mix	1µl	-
Template cDNA	-	200ng
Nuclease-free water	<9µl	-
Total	20µl	-

Table 3.4 Reagents utilised in qPCR to amplify RV16 cDNA synthesised from tissue lumps and concentrated tissue effluent (tissue lumps, 500µm and 1000µm PCLS) post-infection with RV16.

Stage	Step	Number of Cycles	Temperature (°C)	Time (sec)
1	Uracil-N-glycosylase incubation	1	50	180
2	Polymerase activation	1	95	20
3	Denaturation	40	95	1
	Anneal/extend		60	20
	Hold	-	10	∞

Table 3.5 Thermal cycling conditions used to amplify RV16 cDNA in qPCR.

3.2.9 Statistical Analysis

Unless otherwise stated, all data is presented as the mean of three independent replicates of an experiment plus/minus the standard error of the mean (±S.E.M). All data was analysed using GraphPad Prism 8.0.2 software. Data was checked for normality visually using the widely utilised Q-Q plot and statistically using a Shapiro-Wilk test. Statistical analysis was performed where data was appropriate using a combination of two and one-way analysis of variance (ANOVA) followed by Tukey post hoc test for multiple comparison, paired and unpaired t-tests. Data which contained multiple time points was analysed with multiple t-tests utilising the Holm-Sidák method for corrections of multiple comparisons. Where appropriate, the individual test conducted is stated in each figure legend. Statistical significance was determined by a P value of less than 0.05, exact P values are stated were appropriate.

3.2.10 Representation of Biological and Technical Repeats

For each experiment conducted the number of biological and technical repeats was shown to provide further clarity. Where n number is donated for any given experiment, it was expressed as both N and n. Whereby N represents the number of donor samples (biological repeats) and n represents the total number of PCLS and/or small tissue lumps used per donor in each experiment (technical repeats).

3.3 Results

3.3.1 Optimisation of PCLS

PCLS is a widely used technique to study aspects of lung anatomy and physiology however, the method used to create lung slices varies between studies. Variations include the percentage concentration of agarose for inflation (Henjakovic *et al,* 2008a; Brown *et al,* 2013; Lauenstein *et al,* 2014), the solvent used to dissolve the agarose (Waymouth, 1970; Placke and Fisher, 1987), the thickness of the slice produced (An *et al*, 2012; Schlepütz *et al*, 2012; Sun *et al*, 2015; Ghosh *et al*, 2016; Ojiaku *et al*, 2017; Temann *et al*, 2017) and the choice of tissue slicer utilised (Price *et al,* 1998; Zimmermann *et al,* 2009; Abdelaal *et al,* 2015). As such the techniques needed to be optimised for the equipment available to the group.

All lungs used during the optimisation process were porcine, sourced from a local butchers and originating from the normal slaughter process, as excess tissue. The use of porcine tissue prevented wastage of valuable human lung tissue, which could be utilised by the group for other research. Furthermore, the quantity of lung tissue available through the local butchers was greater than that available through cardiothoracic surgical procedures at Castle Hill Hospital, Hull University Teaching Hospitals NHS Trust, which provided sufficient opportunities to trial various methods of creating multiple, identical slices. Murine lungs were considered as a potential alternative for optimising the procedure however, the difference in size and slight variations in structure made porcine lungs a more viable option, as these provided a closer analogy to human lung tissue (O'Neill *et al*, 2013).

3.3.1.1 Agarose Solution for Inflation

A review of the existing literature identified several variations in the solvent utilised to create the agarose solution for the inflation process. These variations could be grouped into two categories of tissue culture medium or saline equilibrated buffer solutions (Waymouth, 1970; Placke and Fisher, 1987). Based on current literature and considering the volumes that would be required in the initial stages, a sterile HEPES – Ringer buffer solution at pH7.4 was chosen over tissue culture media, to ensure tissue viability whilst limiting wastage of more valuable resources. However, whilst this buffer represents one example of physiological saline solutions, the creation of the buffer is relatively time consuming given the volumes required during the optimisation of the inflation and slicing procedures. After consideration of the various types of saline available, later stages of the optimisation process moved to the use of 1x PBS. PBS is an isotonic solution buffered to pH7.4, widely used in laboratory research, which provides a suitable alternative for use in the inflation process as the pH is physiologically appropriate and the osmolality will not affect the tonicity of the cells within the lung tissue (Martin *et al*, 2006). Furthermore, the production of 1x PBS is less error prone and cheaper than HEPES – Ringer buffer and was used during all slicing to bathe the tissue, preventing overheating and reducing friction. Given the change to 1x PBS had no obvious effect on the tissue, this solution was utilised to conduct the remainder of the optimisation. Whilst, the use of 1x PBS was suitable for the optimisation process, the lack of nutrients supplied by PBS to the tissue meant that to enable tissue viability to be extended for as long as possible, tissue DMEM containing 10% FBS, penicillin (100U/ml) – streptomycin (100µg/ml), 2mM L-Glutamine and Amphotericin B (2.5 µg/ml), would be used to aid delivery of nutrients to the cells when human tissue samples were utilised (Placke and Fisher, 1987).

3.3.1.2 Percentage Agarose for Inflation

Literature surrounding PCLS points to the use of LMP agarose to inflate the lung tissues (Fisher *et al*, 1994; Wohlsen *et al*, 2003; Switalla *et al*, 2010; Sanderson, 2011). LMP agarose melts at approximately 65^{o}C which consequently reduces the temperature at which it gels. LMP agarose has a gelling point of approximately 26^{o}C which allows for infusion into the tissue at around 37^{o}C thus this process can be completed without causing damage to the

tissue (Martin *et al*, 2008). However, the percentage of agarose utilised to inflate the tissue to near terminal capacity, varies between different studies, ranging from 0.5% to 4%. With such variability, the middle of the range was selected to try the initial attempts of inflating the tissue, as this would make it easier to identify where the tissue had been inflated by the agarose due to the firmer texture once solidified. The use of 2% agarose created a firm inflation however, initial attempts were hampered by establishing the optimal method for keeping the agarose at around 40^{o}C to prevent premature gelling of the solution. Ultimately, the best method for ensuring the agarose remained molten was to suspend a flask of agarose in a 40^{o}C water bath as this maintained the optimum viscosity for inflation, as opposed to a 37^{o}C incubator which had a tendency to cause premature gelling of the agarose before inflation could be completed. 1.5% agarose was subsequently trialled for its suitability however, when the inflated lung tissue was sectioned into smaller pieces the tissue was too soft and as a result did not remain sufficiently inflated to be sliced. Although, a firmer inflation was achieved using 2% agarose, a similar issue was experienced when slicing the inflated tissue, thus a higher concentration of agarose, of 3%, was trialled (based on personal communications with GlaxoSmithKline (GSK)). This concentration resulted in a firmer, more stable inflation, which could be sectioned into smaller pieces to allow preparation for slicing to occur. The success of this concentration has resulted in all subsequent samples being inflated using 3% agarose.

3.3.1.3 Inflation Technique

Many of the methods outlined in the literature utilise murine models for PCLS, therefore the inflation of the tissue can be conducted via insertion of a cannula into the trachea and whole lungs are thus inflated (Henjakovic *et al*, 2008a; Tatler *et al*, 2016) (Figure 3.2a). However, the porcine lungs utilised in optimisation were whole, having a total lung capacity of approximately 1100 – 1500ml (Protti *et al*, 2015). This made it unfeasible to inflate whole lungs completely, due to the volume of agarose required and the potential for premature solidification of the agarose in the airways, rather than the alveoli, due to the distance the agarose had to travel. To overcome this problem, the porcine lungs were sectioned into smaller pieces of approximately 5 – 10g, this enabled larger airways to be removed, which hinder the inflation process, whilst also ensuring the tissue samples were more representative of pieces received from surgical resections (Figure 3.2b). Sectioning of the

tissue prior to inflation caused some inherent problems, as typically there were several open ended airways, which leaked agarose as inflation occurred. Performing the inflation procedure on ice overcame some of the leakage problems, as this allowed the agarose to gel quickly, creating a seal around the outside of the tissue preventing further leakage and allowed complete inflation to occur. It became evident during sectioning that the distal sections of the lung tissue inflated poorly, due to the termination of bronchioles more proximally in the tissue and the difficulty in forcing sufficient agarose into the alveoli, as such although these aspects of the lung could be inflated they were not always ideal for use in the PCLS process.

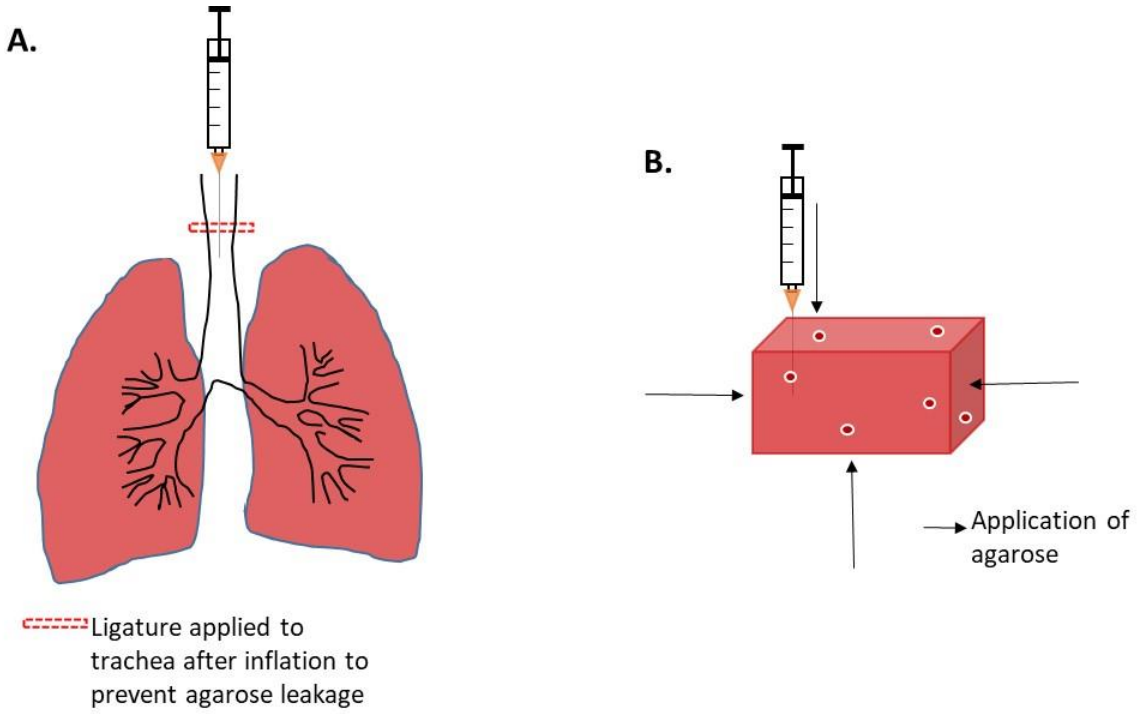

Figure 3.2 Inflation of intact murine lungs via perfusion of agarose through the trachea until both lungs are firmly inflated. Whilst agarose solidifies, leakage is prevented through the closure of the trachea after inflation with a suitable ligature (**A**). Inflation of smaller sections of porcine/human lung via repeated injection of agarose over all exposed surfaces of the tissue, until tissue is firmly inflated. Agarose leakages is unavoidable but can be slowed by performing on ice (**B**).

Identification of the optimal agarose concentration enabled ideal volumes of agarose per gram of tissue to be determined. Initially, inflation was attempted by slowly delivering around 1 – 2ml per gram of agarose to a piece of tissue. This produced inflated tissue however, when slicing was attempted the tissue was overly soft and did not retain its structure. As a result, 3 – 4ml per gram was trialled (based on personal communications with GSK) which produced a more rigid inflation that maintained its shape when sliced. During the identification of the optimum agarose volume to utilise, the process of inflating the tissue was also perfected. This included using a larger gauge needle of ≥19G (1.1mm diameter) which provided sufficient agarose delivery whilst being less prone to blocking as the agarose cooled and began to gel, when compared to smaller gauge needles and has subsequently become the preferred option for all inflations. Additionally, the maximum syringe size used for agarose delivery was 2ml, as this reduced the volume which could be delivered at once. This reduced the likelihood of large boluses of agarose forming, which had occurred when using 5ml syringes, thus preventing over expansion of lung vasculature and damage to surrounding tissue. Delivery of approximately 500µl of agarose, slowly, as the needle was drawn out of the tissue, enabled firm inflation without the formation of large boluses of agarose, thus providing usable sections of lung tissue. This was determined initially by adding food colouring to the agarose solution, so that it became obvious what path the agarose had taken through the tissue (Figure 3.3), thus enabling developments in the technique to be observed, problems to be rectified and optimum volumes of agarose to be assessed.

Figure 3.3 Section of porcine lung tissue before inflation (**A**), after inflation (**B**) and after slicing through the inflated tissue (**C**). Agarose (coloured black for ease of identification) is visible throughout **B** and **C** showing complete inflation and perfusion of the tissue.

3.3.1.4 Tissue Slicing Technique

Based on previous studies an optimal slice thickness of 200 – 250µm was identified and aimed for in the creation of the initial slices (Schlepütz *et al*, 2012; Neuhaus *et al*, 2013; Bai *et al*, 2016; Zmora *et al*, 2017). Tissue slicing was conducted on a Leica Vibratome VT1200S with vibrocheck, which enabled calibration of the z-axis alongside management of the blade amplitude, feed rate and slice thickness. The design of the vibratome meant that the 5 – 10g pieces of tissue were too large to be sliced in one piece. Various methods described the removal of tissues cores of 8 – 10mm in diameter (Fisher *et al*, 1994; Wohlsen *et al*, 2003; Switalla *et al*, 2010) however, when the technique was attempted using a sharpened cork borer, the tissue did not core cleanly but was instead macerated and became unusable. Based on repeated failure of removing tissue cores, an alternative solution was derived in which cubes of tissues approximately 15mm^3 were taken for slicing, that could then be made uniform in diameter through the use of a biopsy punch. The tissue cube size was later reduced to around 10mm^3 due to issues with the vibratome design which resulted in the tissue sample repeatedly becoming detached from the sample specimen plate, to which it was glued, as the pressure from the action of the cutting blade forced the larger tissue samples off the specimen plate. The pleural membrane on porcine lungs, as in humans, is fibrous (Rogers *et al*, 2008), causing the cutting blade to drag on the sample rather than cutting cleanly. This resulted in either the slice not being taken, the sample becoming unstuck or the tissue being pulled from the embedding agarose. To overcome this issue, the pleural membrane was removed after inflation but before slicing, which reduced the extent of fibrous tissue and aided in the slicing process.

The vibratome lacks any form of tissue sample holder, which created the aforementioned issues of sample adherence creating a further disadvantage of providing no stability to the sample being sliced. The nature of lung tissue meant that although relatively firm, due to the addition of agarose, the spongy texture of the tissue remains, thus the samples lack rigidity and do not slice with ease. As a result, there was a necessity to embed the sample in 7% LMP agarose to provide the vibratome cutting blade with a denser material in which to stabilise the initial cutting action (Figure 3.4). Attempts to slice the tissue when not embedded but supported by a piece of cork, provided some alleviation of the stability issues however, the vibratome still failed to cut uniform or sufficient numbers of slices. The

pressure created by the cutting blade when samples were not embedded also resulted in the tissue becoming deformed, which resulted in wedge shaped slices or tissue being pushed beyond the set cutting field, before slipping under the blade edge.

Figure 3.4 Porcine tissue sections of approximately 10mm^3 embedded in 7% agarose in preparation for slicing on the Leica Vibratome

The optimum length of time required for embedding agarose to fully solidify was determined through the ease of slicing and the number of slices achieved. All inflation was carried out at room temperature on ice, to promote rapid gelling of the agarose in the tissue, inflated tissue then remained on ice for a further 30 minutes to ensure complete solidification of inflation agarose whilst the embedding agarose was prepared. Once embedded, samples were then left initially at room temperature to solidify for 30 minutes however, whilst this did provide some additional stability for slicing further rigidity was required. Based on this observation embedded samples were placed in varying conditions (Table 3.6) to identify the optimum temperature and time for storage whilst embedding agarose fully solidified.

Storage Condition	**Storage Times (hours : minutes)**			
4°C on ice	1:00	1:30	3:00	4:00
4°C	3:00	18:00		
23°C on ice	3:00			
23°C	0:30	3:00		
-20°C	3:00			

Table 3.6 Embedded tissue samples storage conditions trialled during optimisation

Of the storage options in table 3.6, the optimum arrangement was to store samples at 4°C on ice for a minimum of 90 minutes, with extended periods having little impact on the total number of usable slices obtained. This length of time ensured the agarose in both the tissue and surrounding it was firmed and sliced easier, whilst not causing any cellular damage to the tissue. At room temperature or 4°C the samples were not firm enough, unless left overnight at 4°C, whilst at -20°C the embedding agarose froze and then fractured on thawing, whilst the tissue became less firm, potentially due to cellular damage.

3.3.1.5 Slice Thickness Varies Depending on Subsequent Assay

Recognition of the need to embed samples enabled slices to be produced more consistently, initially at 1000µm, but through refinement of the process slices became thinner at 700µm, 500µm, 300µm and 250µm. In terms of producing larger numbers of useable slices, 300 – 500µm was the optimum thickness achievable on the vibratome, depending on tissue quality, as below this at either 200 or 250µm slices were not produced consistently, with partial slices being a reoccurring issue. However, the variations observed in the literature predominantly support a thickness of 200 – 300µm (Sturton *et al*, 2008; Schlepütz *et al*, 2012; Bai *et al*, 2016; Alsafadi *et al*, 2017; Zmora *et al*, 2017; Cairns *et al*, 2020), which means that although 300µm is on the upper end of this range, it falls within a suitable range for viability purposes. Observation of the slices under a light microscope provided evidence that individual cells and lung structures were more clearly definable in the thinner slices (300µm) rather than the thicker slices (≥500µm) (Figure 3.5). Clearly defined structures visible under a light microscope, specifically the Zeiss SteREO Discovery.V8 microscope, were of importance to the overall study to enable analysis of bronchoconstriction in response to exposure to a range of chemicals stimuli e.g. cytokines.

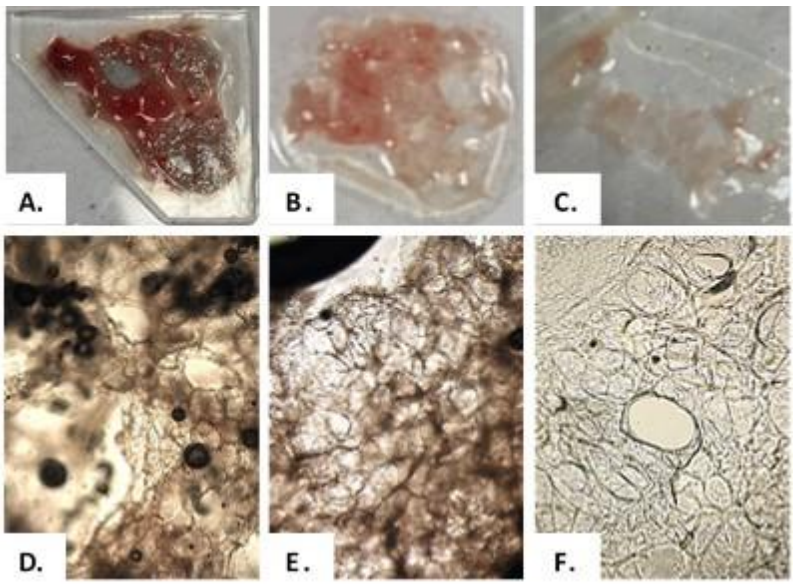

Figure 3.5 A – C represent tissue slices produced on the Leica Vibratome at 500µm (**A**), 300µm (**B**) and 200µm (**C**) thicknesses. **D – F** represent tissue slices at 500µm (**D**), 300µm (**E**) and 200µm (**F**) thicknesses viewed under a light microscope at 100x magnification.

However, initial attempts to measure bronchoconstriction in 300µm thick tissue slices were complicated by the difficulty of handling the relatively fragile slices and the adherence of the tissue slices to a culture plate to prevent them moving around the plate when bronchoconstrictive agents were applied. The adherence of the tissue slices to the culture plate had two main problems; firstly the tissue in contact with the adhesive, once cured, becomes hard making that area unusable for any measurements. Secondly, tissue slices had to be taken out of tissue DMEM to be adhered to the culture plate, whilst this in itself was not problematic due to the short duration required for the adhesive to cure, the reapplication of tissue DMEM often resulted in tissue becoming unstuck and making the procedure somewhat futile. As a consequence of the aforementioned problems, a decision had to be made relating to the optimal thickness to use for any future bronchoconstriction measurements. Thus, although 300µm thick slices provided more clearly identifiable structures, the delicate nature of the slices made it difficult to place and maintain tissue slices in a suitable orientation without being adhered to a surface. As a result 700µm were trialled and proved to be more substantial and effective for use in bronchoconstriction measurements, being noticeable more robust when transferred between culture plates, whilst the additional weight of the thicker slices also removed the need to adhere tissue to the culture plate as the tendency to move under the application of the bronchoconstrictive

agents was less pronounced and did not negatively affect the positioning of the slice under the microscope. Furthermore, the use of a Zeiss SteREO Discovery.V8 microscope also negated some of the issues relating to imaging thicker tissue slices, as the wide field of view and large working distance enabled clear images of the tissue slice surface including prominent airways to be observed without the need for resolution of internal structures, thus aiding in the decision to use 700µm PCLS for all future bronchoconstriction measurements.

The actual thickness required depended on the experiment being conducted however, there was a need to utilise a range of slice thickness from 300 – 1000µm. Therefore these needed to be replicated with minimal variation. To consistently achieve these thinner slices, the amplitude and blade feed rate needed adjusting, one of the main problems associated with slicing lung tissue is the fibrous nature of the pleural membrane and cartilage rings forming the airways. Increasing the amplitude of the blade to 2.25mm and reducing the blade feed rate to 0.1 – 0.3mms^{-1}, made reproduction of thinner slices possible. However, the blade feed rate was variable depending on the extent to which the tissue could be inflated, with less inflated or more fibrous tissue requiring a slower blade feed rate. Given the reproducibility of slices using the aforementioned settings, all future work generally utilised these values, with variations made depending on tissue quality.

3.3.1.6 Agarose Cannot Easily be Removed from PCLS

After producing tissue slices numerous studies immerse the tissue slices in 37^{o}C buffer or media, either with or without oxygen perfusion, for several hours to remove the agarose from the slices (Wohlsen *et al,* 2003; Paddenberg *et al*, 2014; Herbert *et al*, 2017). Given that LMP agarose has a melting point of around 65^{o}C, the likelihood of agarose being removed from the tissue slice by immersing in media at 37^{o}C seems unlikely. In an attempt to identify whether this process worked 12 slices of tissue were immersed for 18 hours in tissue DMEM at 37^{o}C with 5% CO_2. Light microscopy images were taken before and after the slices had been immersed and compared to see if the agarose had been removed. From the images it was apparent that the agarose remains *in situ* after immersing, although slices are softened and more flexible. Evidence of cut marks on the agarose are noticeable in a

number of slices and agarose bubbles are found in all slices both before and after immersion thus, immersing the slices in media does not removed the agarose (Figure 3.6).

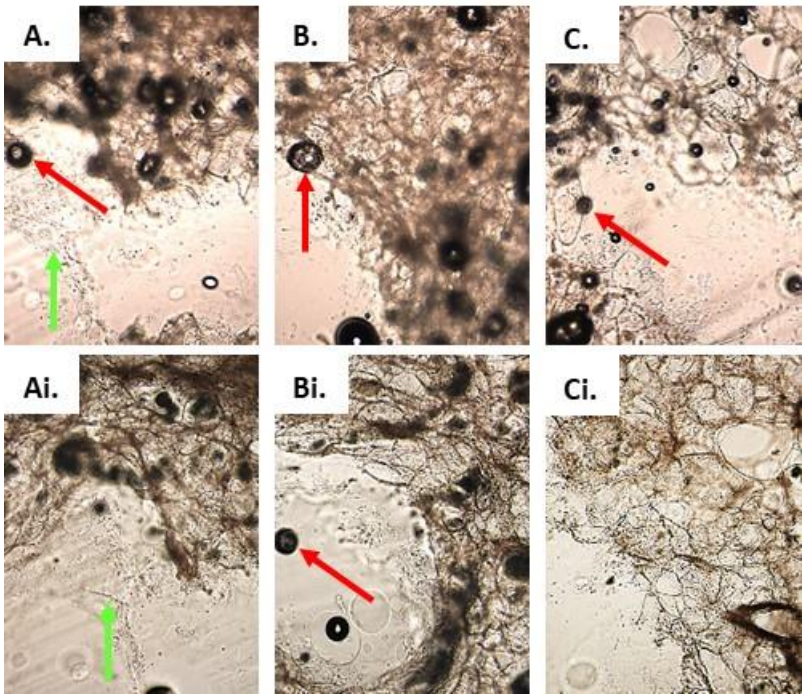

Figure 3.6 A – C represent tissue slices of 300µm thicknesses viewed under a light microscope at 100x magnification immediately after slicing. **Ai – Ci** represent the same tissue viewed under a light microscope at 100x magnification after immersion in DMEM for 18 hours. Arrows indicate agarose bubbles (red) and cut marks on the agarose (green). Representative images of multiple PCLS taken (N=1, n=12).

However, in the first instance the tissue was submerged in a multi-well plate, thus remaining static for the duration of the immersion. In order to assess whether agarose could be removed via gentle agitation, tissue slices were subjected to various methods of agitation for a period of 2 hours prior to an overnight incubation of 21 hours at 37°C with 5% CO_2. A total of 12 tissue slices, 4 slices per method, were utilised and exposed to the following conditions: 1. Tissue slices were incubated at 37°C in a multi-well plate, the media surrounding the tissue was changed every 30 minutes for the first hour and then after an additional hour. 2. Tissue slices were placed in 10ml of media in a 50ml centrifuge tube, this was floated in a stirring water bath, at 37°C before transfer to fresh media in a multi-well plate overnight. 3. Tissue slices were placed in 10ml of media in a 50ml centrifuge tube,

this was rotated on tube rotator in an incubator at 37°C, before transfer to fresh media in a multi-well plate overnight. Comparison of light microscopy images before and after immersion indicate no change in the presence of agarose within the airway however, the images appear to have fewer agarose bubbles and debris on the slices. The most noticeable improvement appeared to be in the slices that had repeated media changes, although all samples appeared to have benefitted from a media change (Figure 3.7). As such, it would be beneficial to change the media surrounding the tissue a minimum of once, at around 2 hours, after slicing has taken place and where possible multiple media changes should take place. Media changes act to remove debris, loose agarose and provide the added benefit of removing any inflammatory markers that may have arisen through the slicing process (Davidovich *et al*, 2013a).

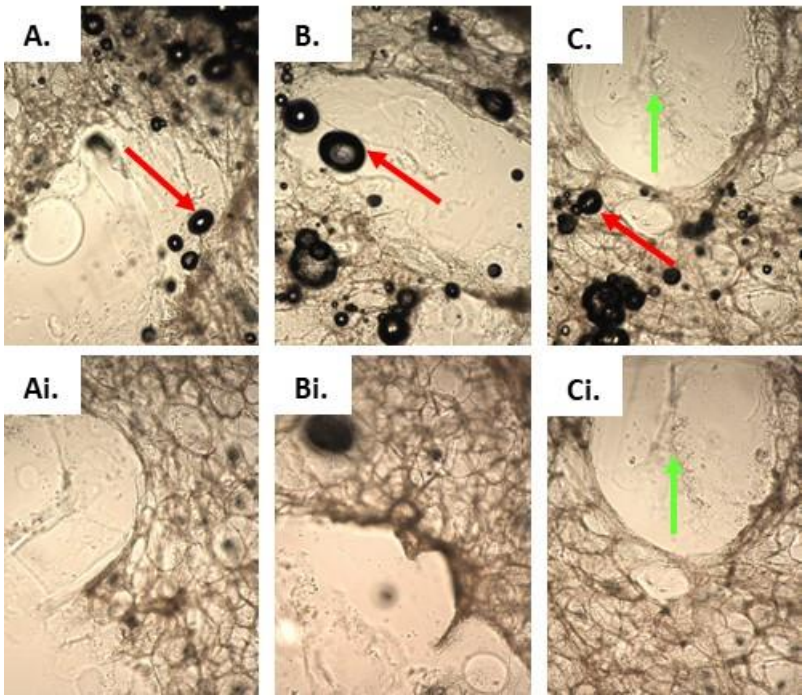

Figure 3.7 Tissue slices of 300µm thicknesses viewed under a light microscope at 100x magnification before (**A – C**) and after (**Ai – Ci**) exposed to various submersion conditions including: 2 hours of media changes (**Ai**). 2 hours submerged in media and agitated through flotation in a stirring water bath at 37°C (**Bi**). 2 hours submerged in media and agitated via rotation on a tube rotator in an incubator at 37°C (**Ci**), each slice was subsequently placed in fresh media for 21 hours. Arrows indicate agarose bubbles (red) and cut marks on the agarose (green). Representative images of multiple PCLS taken (N=1, n=12).

Based on the aforementioned findings, it is questionable whether the agarose removal indicated in some research (Wohlsen *et al,* 2003; Paddenberg *et al*, 2014; Herbert *et al*, 2017) has actually occurred or whether it is assumed to have occurred. This being said, the continued presence of agarose in the tissue appears to have no obvious impact on any findings within current literature. Furthermore, the inflation process aims to create an *ex vivo* environment equivalent to near total lung capacity ensuring airways remain open during any experimental process which when coupled with the limited rigidity afforded to the tissue by the agarose should ensure lung physiology remains unaltered and akin to the *in vivo* environment.

3.3.1.7 Slices Remain Viable for up to 7 Days

The length of time a tissue slice, remains viable is a subject of debate within the literature, with 72 hours being the typical period of viability (Bergner and Sanderson, 2002b; Wohlsen *et al*, 2003; Ressmeyer *et al*, 2006). As such, a method for assessing the viability of tissue slices was required in order to identify the extent to which tissue can be utilised before apoptosis and necrosis become too pronounce to make experimentation possible. However, the action of producing a tissue slice has inherent problems relating to viability of the slice, namely the friction and heat generated through the slicing process. This is likely to cause some damage to the outer most layers of the lung tissue, as such these cells will release pro-inflammatory markers and may begin the process of apoptosis (Levy and Harvey, 1974; Umachandran *et al*, 2004). Given this early damage to the tissue, an assessment of the baseline level of cellular damage was taken, alongside other measurement taken throughout the duration of the experiment. However, this initial assessment needed to ensure that no further tissue damage occurred and so requires the effluent levels of cellular markers to be assessed rather than the levels found within the tissues, thus limiting the choice of assays that can be run, should measurements need to be taken at specific time points during the culture period. This factor directly influenced the first choice of assay utilised to assess viability, with LDH being the first measure used. The Pierce LDH Cytotoxicity Assay (Thermo Scientific, Leicestershire, UK) was used to measure the level of LDH released from the cells at various time points over the duration of 7 days. This included measurements after 2 hours, when media was changed to remove any debris and then at 24 hour time points for the duration of the incubation, after 7 days

the tissue was completely lysed through homogenisation and the addition of lysis buffer to indicate the total amount of LDH remaining in the tissue after lysis (Figure 3.8).

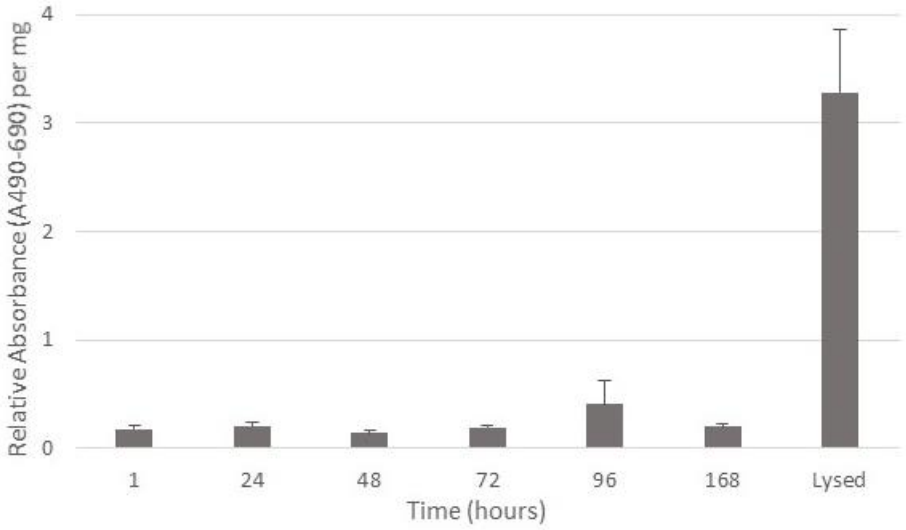

Figure 3.8 LDH release profile of 10mm^2, 300µm PCLS from porcine lung tissue 168 hours post slicing. LDH measurements were based on absorbance reading (490 – 690nm) accounting for media blank and normalised per milligram of tissue, after PCLS was completely lysed. Results are displayed as mean ± SEM (N=2, n=6).

Figure 3.8 shows the extent of LDH measured in the effluent collection over the duration of the experiment and clearly indicates low levels of LDH directly after slicing and a sharp increase after treatment with lysis buffer. However, whilst this initial data is as expected there were inherent issues with the protocol used, which needed rectifying to identify the optimum method for assessing cellular damage by this method. Namely, the complete change of media at each collection point, which would ensure that the levels of LDH recorded were a representation of the previous 24 hours rather than a collection of the LDH released through the duration of the incubation. Sanderson (2011) and Ressmeyer *et al* (2006) suggest that daily media changes will extend the viability of slices, thus better representing the levels of LDH at any given time point, whilst benefitting the overall viability of the tissue slices and increasing the range of measurements that can be made due to the larger volumes of effluent that would be available. Additionally, there was no increase in the level of LDH at the initial time point as expected due to damage caused during slicing.

In this instance, this could be due to the length of time the slices remained in the slicing buffer due to the tissue slicing poorly, which resulted in an extend time period to gain the required number of slices. In cases when the tissue does not slice with ease, it may be beneficial to place tissue slices into fresh media whilst slicing continues, to prevent the loss of LDH and other pro-inflammatory markers in the slicing buffer. Finally, it needs noting that there is a need to weigh individual tissue slices, as although tissue slices are identical in size, the extent of fibrous tissue, blood vessels and agarose is variable and so results in different weights of tissue. By collecting individual slice mass, it enabled calculation of LDH per microgram, providing a comparative level of LDH across various sections of tissue as values were normalised based on weight. This initial data suggested that the tissue was viable for the 7 days it was in culture however, LDH can underestimate the number of dead cells present (Smith *et al*, 2011) as cell membranes have to rupture to enable LDH leakage to occur, which happens when cells are necrotic or nearing the end of apoptosis (Diemert *et al*, 2012). As such, the tissue in this instance could be undergoing apoptosis but contain intact membranes preventing LDH leakage resulting in lower levels of LDH being recorded. Samples were stored for a maximum of 5 days at 4^{o}C prior to measuring the extent of LDH in the effluent, this helped to ensure that the level of LDH did not deteriorate, as both storage temperature and time are linked to LDH stability in stored samples (Greiff and Kelly, 1966; Jacobs *et al*, 1986).

Based on the aforementioned observations an optimised protocol for tissue inflation and slicing was finalised as outlined in 3.2.1. The optimised method utilised 2 – 3ml of 3% LMP agarose per gram of tissue, inflated on ice and allowed to solidify. Tissue was subsequently sectioned into pieces of approximately 10mm^3, embedded in 7% LMP agarose and chilled for 90 minutes. Embedded tissue pieces were sliced at between 300 – 1000µm, placed in 500µl tissue DMEM and incubated at 37^{o}C, 5% CO_2. Although optimisation was conducted on porcine tissue, all work conducted post optimisation was performed on human tissue samples. Thus any discussion from 3.3.2 onwards relates to the use of human tissue received from cardiothoracic surgical procedures as outlined in 3.2.1.1.

3.3.2 Morphological Assessment of Healthy PCLS and Lump Tissue

3.3.2.1 Gross Morphology of Tissue Shows Little Change Over a 7 Day Culture Period

To determine whether the gross morphology of PCLS changed over the 7 day culture period, PCLS of various thicknesses (300µm, 500µm, 700µm and 1000µm) were sliced as outlined in 3.2.1.2 and cultured for a total of 7 days with images being taken after 1, 5 and 7 days post slicing at 10x magnification, 1x zoom on a Zeiss SteREO Discovery.V8 microscope and images stitched together as outlined in 3.2.3.1. Based on the stitched images there appeared to be little change in the gross morphology at any time point during the culture period or for any PCLS thickness. However, there was some change in colour of the PCLS at 7 days post slicing for all thicknesses with the exception of 300µm (Figure 3.9).

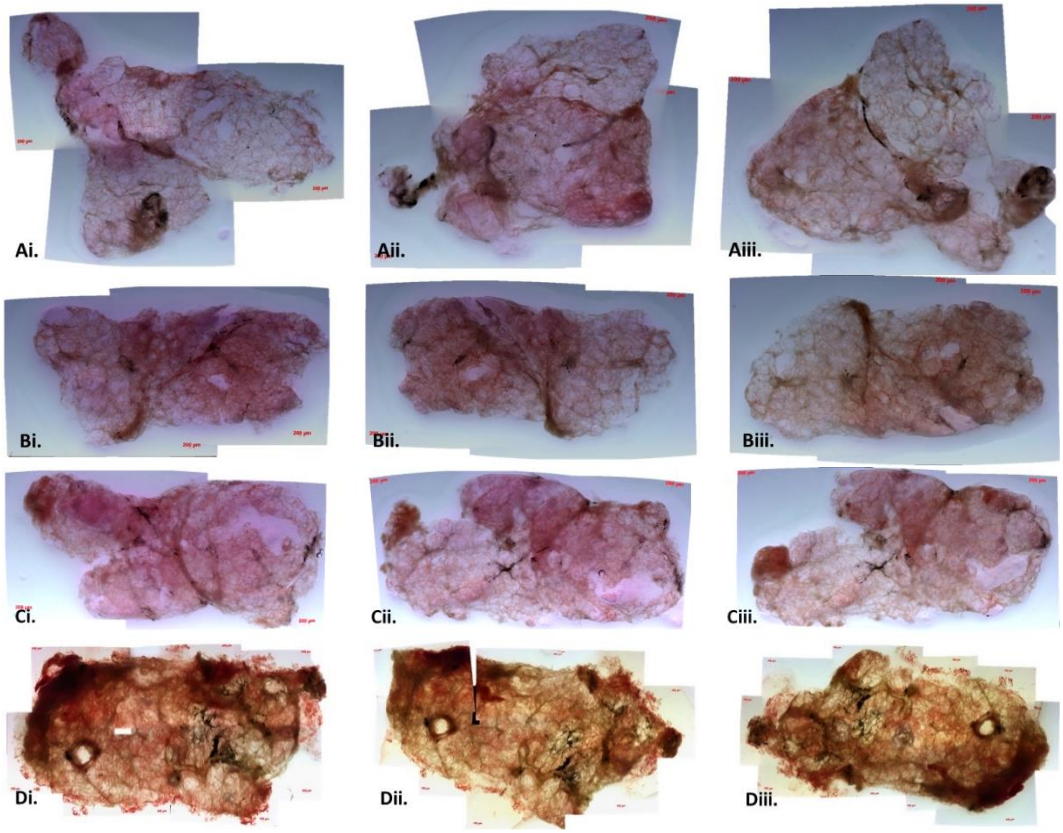

Figure 3.9 Gross morphology of varying thickness PCLS at 1, 5 and 7 days post slicing, viewed in multiple sections at 10x magnification, 1x zoom on a Zeiss SteREO Discovery.V8 microscope and images stitched together. PCLS thicknesses displayed; 300µm (**Ai – Aiii**), 500µm (**Bi – Biii**), 700µm (**Ci – Ciii**), 1000µm (**Di – Diii**) at 1 day (**Ai – Di**), 5 days (**Aii – Dii**) and 7 days (**Aiii – Diii**) post slicing. Images represents three independent experiments (N=3, n=4).

3.3.2.2 Cellular Morphology of Tissue Shows Little Change Over a 7 Day Culture Period

To determine whether the cellular morphology of PCLS changed over the 7 day culture period, PCLS of various thicknesses (300µm, 500µm, 700µm and 1000µm) were sliced as outlined in 3.2.1.2. Day 0 PCLS were either immediately preserved for later sectioning (using snap freezing 3.2.4.1) or cultured for 1, 5 or 7 days. After the desired number of days in culture, PCLS were preserved as outlined above, 8µm cryosections (3.2.4.2) taken and stained with H&E (3.2.4.3) prior to imaging on a light microscope at x100 magnification.

Based on the images taken of cryosectioned PCLS, there appeared to be little change in the cellular morphology at any time point during the culture period or for any PCLS thickness. However, as time progressed the membranes of some cells appeared to be less intact around the edge of some alveoli, this is most noticeable at 7 days and in 700µm thick PCLS compared to other thicknesses (indicated by yellow arrow). The type of tissue received from cardiothoracic surgery is apparent in these sections, as the structure present is predominately alveolar sacs (indicated by white arrows) and the lung parenchyma (indicated by red arrows). Furthermore, the retention of agarose within the tissue also appears to be evident as this can be seen in some of the alveolar spaces however, it should be mentioned that this could be mucus which is often found in damaged or diseased lung tissue (indicated by black arrows) (Fisher *et al*, 1994; Martin *et al*, 1996) (Figure 3.10).

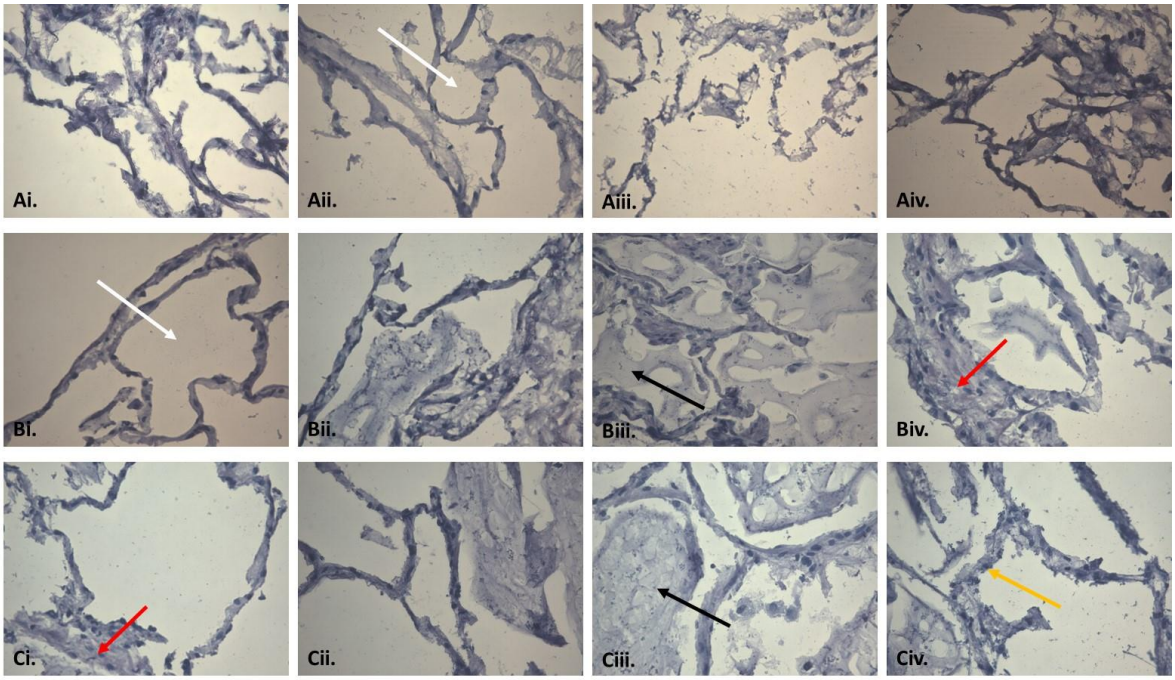

Figure 3.10 Microscopy images (x400 magnification) of H&E stained cryosections of varying thickness PCLS at 0, 1, 5 and 7 days post slicing. PCLS thicknesses displayed; 300µm (**Ai – Aiv**), 500µm (**Bi – Biv**) and 700µm (**Ci – Civ**) at 0 days (**Ai – Ci**), 1 day (**Aii – Cii**), 5 days (**Aiii – Ciii**) and 7 days (**Aiv – Civ**) post slicing. Arrows indicate alveolar sacs (white) lung parenchyma (red), presence of agarose or mucus (black) and membrane damage (yellow). Images represents three independent experiments (N=3, n=12).

3.3.3 Healthy Tissue Lactate Dehydrogenase (LDH) Cytotoxicity Analysis

Prior to undertaking the rhinovirus infection of PCLS it was necessary to determine the length of time PCLS would remain viable in culture and identify the optimum PCLS thickness. Maximum and minimum PCLS thickness was also considered, as one thickness would not have suit all experiments, thus it was necessary to form a wide view of how healthy tissue responded in culture before infection was considered.

3.3.3.1 LDH Confirms Human PCLS Remained Viable Over a 7 Day Culture Period

To determine the length of time PCLS remained viable in culture, the extent of cellular cytotoxicity was determined by measuring the level of LDH in lysed tissue after 24, 120 and 168 hours in culture utilising PCLS of various thicknesses. When all PCLS thicknesses were

considered after 120 and 168 hours in culture there was no significant difference (P>0.05) between the LDH released for any PCLS thickness. With the exception of 1000µm which had no significant differences in LDH release at any time point (P>0.05), there was a significant increase in LDH release between 24 hours and 120 hours (P<0.001 for 300µm, P<0.005 for 500µm and P<0.01 for 300µm), a similar significant increase in LDH release between 24 hours and 168 hours for all PCLS thicknesses (P<0.001) (Figure 3.11).

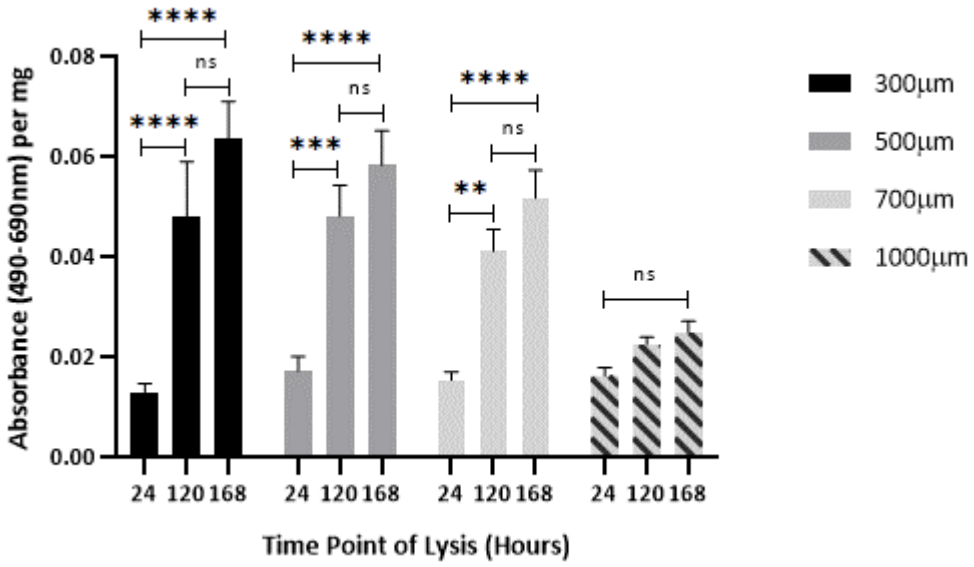

Figure 3.11 LDH analysis of 10mm^2 PCLS of varying thicknesses at 24, 120 and 168 hours post slicing. LDH measurements were based on absorbance reading (490 – 690nm) accounting for media blank and normalised per milligram of tissue, after PCLS was completely lysed. Results are displayed as mean ± SEM (N=6, n=24). Statistical analysis was conducted using a two-way ANOVA with multiple comparison by Tukey analysis. P<0.01**, P<0.005***, P<0.001****

3.3.3.2 Slice Thickness (Below 1000µm) does not Affect Human PCLS Viability

To determine whether there was any difference in viability between PCLS of 300µm to 1000µm over the length of the culture period, the extent of cellular cytotoxicity was determined by measuring the level of LDH in tissue culture effluent collected between 2 and 168 hours and in lysed tissue after 24, 120 and 168 hours in culture. When all PCLS thicknesses were considered after 24 hours in culture there was no significant difference

(P>0.05) between the LDH released into the cell culture effluent or after lysis for any PCLS thickness. However, it should be noted that although there was a slight increase between the LDH measured in the effluent and in the lysed tissue, there was no characteristic spike in LDH release after lysis at this time point (Figure 3.12).

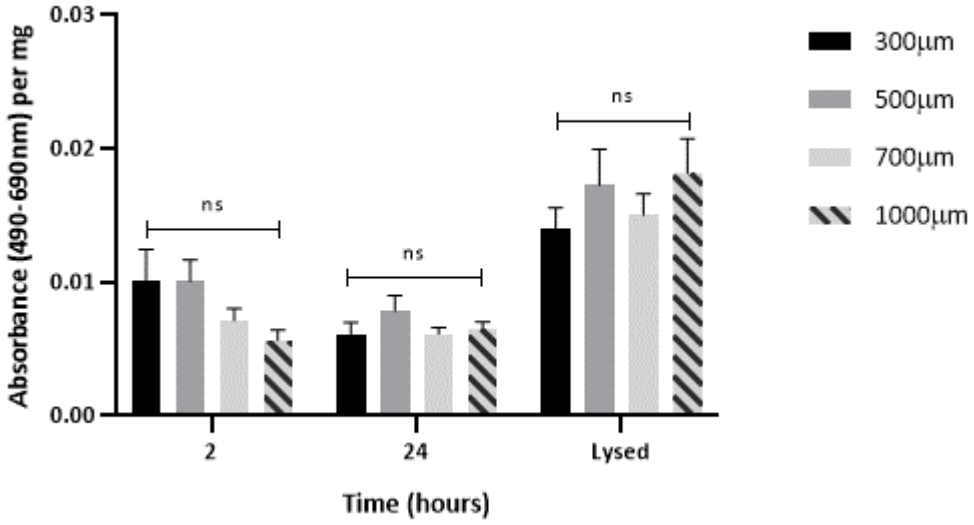

Figure 3.12 LDH analysis of 10mm^2 PCLS of varying thicknesses at 24 hours post slicing. LDH measurements were based on absorbance reading (490 – 690nm) accounting for media blank and normalised per milligram of tissue, for effluent collected at 2 and 24 hours during culture period and after PCLS was completely lysed. Results are displayed as mean ± SEM (N=6, n=8). Statistical analysis was conducted using a two-way ANOVA with multiple comparison by Tukey analysis.

When all PCLS thicknesses were considered after 120 hours in culture there was no significant difference (P>0.05) between the LDH released into the tissue culture effluent for any PCLS thickness. When the lysed tissue LDH release was compared there was no significant difference between 300µm, 500µm and 700µm (P>0.05). Similarly, there was no significant difference between 700µm and 1000µm (P>0.05) however, there is a significant increase in the LDH released by both 300µm and 500µm compared to that released by 1000µm PCLS slices (P<0.01). Here, the characteristic spike in LDH release after lysis is evident for all PCLS thicknesses indicating the tissue was viable at the end of the culture period (Figure 3.13).

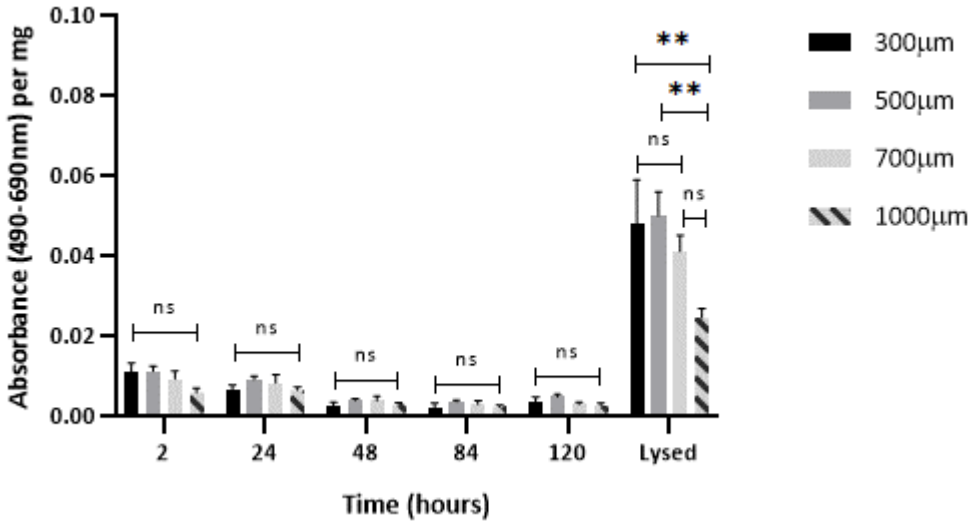

Figure 3.13 LDH analysis of 10mm^2 PCLS of varying thicknesses at 120 hours post slicing. LDH measurements were based on absorbance reading (490 – 690nm) accounting for media blank and normalised per milligram of tissue, for effluent collected between 2 and 120 hours during culture period and after PCLS was completely lysed. Results are displayed as mean ± SEM (N=6, n=8). Statistical analysis was conducted using a two-way ANOVA with multiple comparison by Tukey analysis. P<0.01**

When all PCLS thicknesses were considered after 168 hours in culture there was no significant difference (P>0.05) between the LDH released into the tissue culture effluent for any PCLS thickness. When the lysed tissue LDH release was compared there was no significant difference between 300µm, 500µm and 700µm (P>0.05). However, there was a significant increase in the LDH released by both 300µm, 500µm (both P<0.001) and 700µm (P<0.005) compared to that released by 1000µm PCLS slices. Again, the characteristic spike in LDH release after lysis is present for all PCLS thicknesses indicating tissue was viable at the end of the culture period (Figure 3.14).

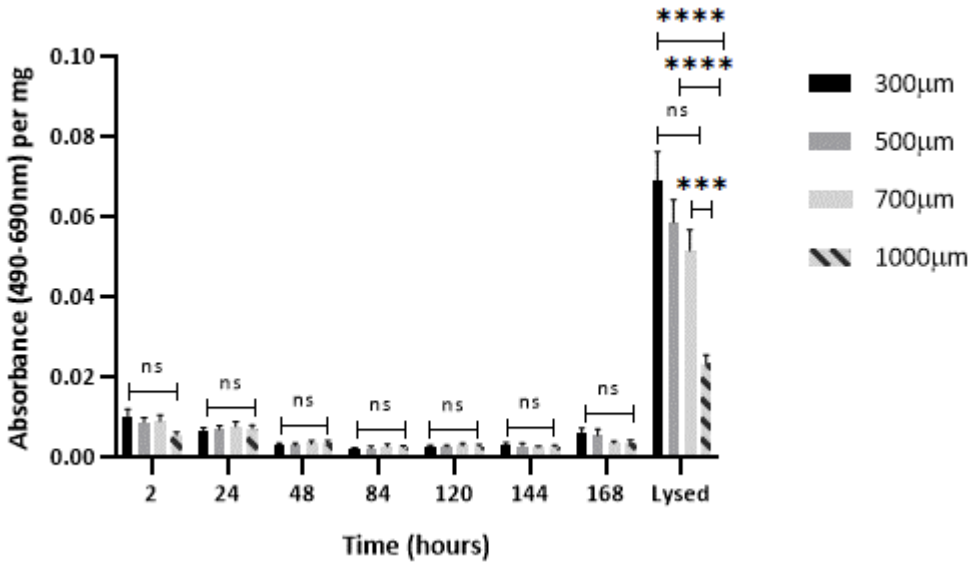

Figure 3.14 LDH analysis of 10mm^2 PCLS of varying thicknesses at 168 hours post slicing. LDH measurements were based on absorbance reading (490 – 690nm) accounting for media blank and normalised per milligram of tissue, for effluent collected between 2 and 168 hours during culture period and after PCLS was completely lysed. Results are displayed as mean ± SEM (N=6, n=8). Statistical analysis was conducted using a two-way ANOVA with multiple comparison by Tukey analysis. P<0.005***, P<0.001****

3.3.3.3 LDH Confirms Human Inflated Lump Tissue Remains Viable Over a 7 Day Culture Period

As an alternative to PCLS for infection, small tissue lumps of 2 – 3mm^3 were prepared from inflated tissue and used to determine the length of time viability could be maintained in culture. The extent of cellular cytotoxicity was determined by measuring the level of LDH in tissue culture effluent collected between 2 and 168 hours and in lysed tissue after 24, 120 and 168 hours in culture. The LDH released into the tissue effluent followed a similar pattern regardless of the length of time the tissue lumps were in culture. Observable spikes in LDH were seen after the initial sectioning of the tissue lumps at 2 hours, followed by a drop at 24 hours and a subsequent stabilising of LDH release. Post lysis the characteristic spike in LDH release is observable at all time points (Figure 3.15).

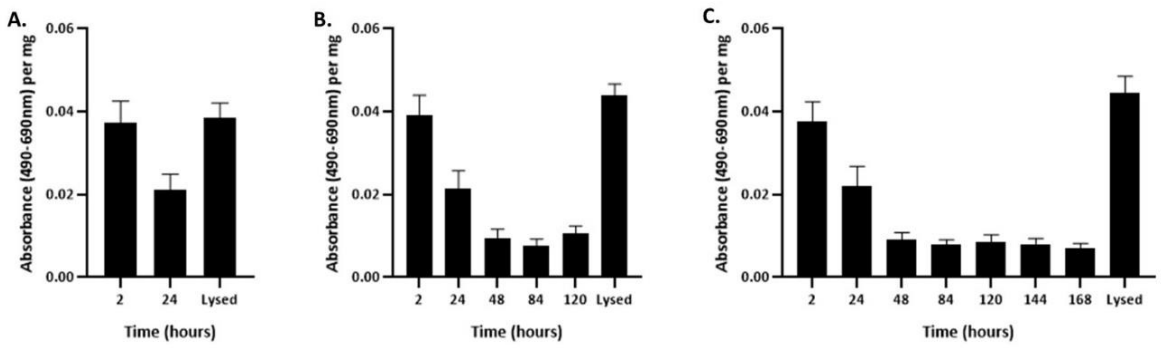

Figure 3.15 LDH analysis of 2 – 3mm^3 inflated tissue lumps at 24 (**A**), 120 (**B**) and 168 hours (**C**) post sectioning. LDH measurements were based on absorbance reading (490 – 690nm) accounting for media blank and normalised per milligram of tissue, for effluent collected between 2 and 168 hours during culture period and after tissue lumps were completely lysed. Results are displayed as mean ± SEM (N=5, n=9).

When all time points for lysed inflated tissue lumps were compared there was no significant difference (P>0.05) between the LDH released at 24, 120 or 168 hours (Figure 3.16).

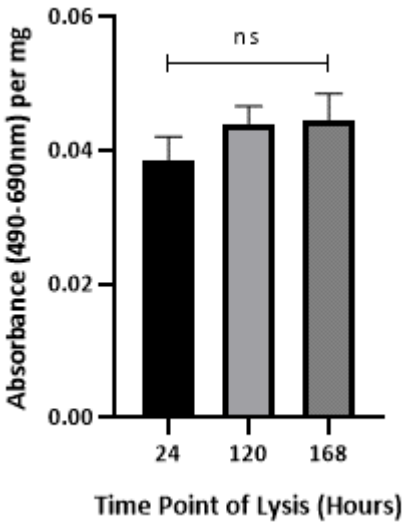

Figure 3.16 LDH analysis of 2 – 3mm^3 inflated tissue lumps at 24, 120 and 168 hours post sectioning. LDH measurements were based on absorbance reading (490 – 690nm) accounting for media blank and normalised per milligram of tissue, after tissue lumps were completely lysed. Results are displayed as mean ± SEM (N=5, n=9). Statistical analysis was conducted using a one-way ANOVA with multiple comparison by Tukey analysis.

3.3.3.4 LDH Confirms Human Uninflated Lump Tissue Remains Viable Over a 7 Day Culture Period

To identify if inflating the lung tissue had any impact on the extent of LDH released from the tissue, small tissue lumps of 2 – 3mm^3 were prepared from uninflated tissue and used to determine the length of time viability could be maintained in culture. The extent of cellular cytotoxicity was determined by measuring the level of LDH in tissue culture effluent collected between 2 and 168 hours and in lysed tissue after 24, 120 and 168 hours in culture. The LDH released into the tissue effluent followed a similar pattern regardless of the length of time the tissue lumps were in culture. Observable spikes in LDH were seen after the initial sectioning of the tissue lumps at 2 hours, followed by a drop at 24 hours and a subsequent stabilising of LDH release. Post lysis the characteristic spike in LDH release is observable at all time point (Figure 3.17).

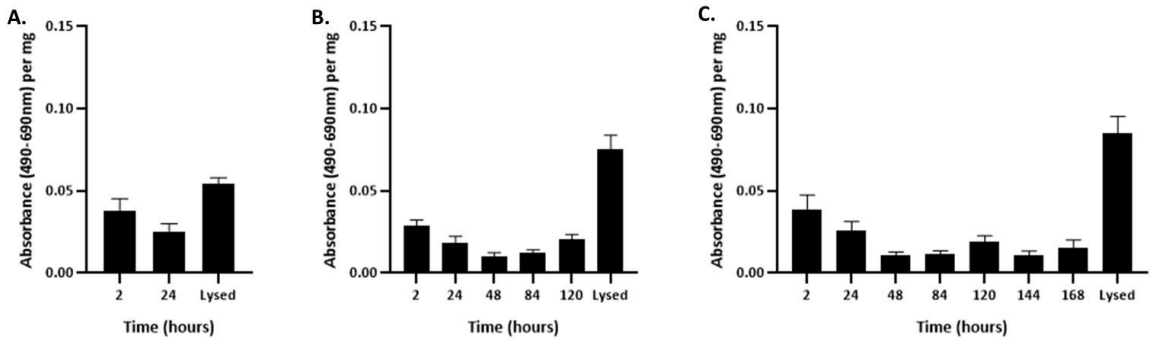

Figure 3.17 LDH analysis of 2 – 3mm^3 uninflated tissue lumps at 24 (**A**), 120 (**B**) and 168 hours (**C**) post sectioning. LDH measurements were based on absorbance reading (490 – 690nm) accounting for media blank and normalised per milligram of tissue, for effluent collected between 2 and 168 hours during culture period and after tissue lumps were completely lysed. Results are displayed as mean ± SEM (N=3, n=9).

When all time points for lysed inflated tissue lumps were compared there was no significant difference between the LDH released at 24 and 120 hours or 120 and 168 hours ($P>0.05$) however, there was a significant increase in LDH released by tissue after 168 hours in culture compared to 24 hours ($P<0.05$) (Figure 3.18).

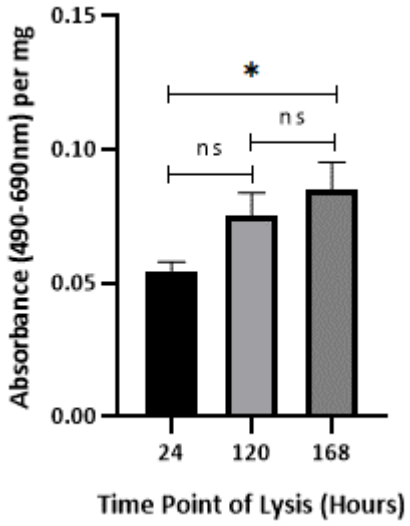

Figure 3.18 LDH analysis of 2 – 3mm^3 uninflated tissue lumps at 24, 120 and 168 hours post sectioning. LDH measurements were based on absorbance reading (490 – 690nm) accounting for media blank and normalised per milligram of tissue, after tissue lumps were completely lysed. Results are displayed as mean ± SEM (N=3, n=9). Statistical analysis was conducted using a one-way ANOVA with multiple comparison by Tukey analysis. P<0.05*

3.3.3.5 Both Human PCLS and Inflated Lump Tissue have Similar Viability

Both inflated tissue lumps and PCLS of varying thicknesses appeared to be viable in culture for up to 168 hours, thus a direct comparison of the LDH released from lysed tissue was conducted to determine if any difference in viability existed. The extent of cellular cytotoxicity determined by measuring the level of LDH in lysed tissue after 24, 120 and 168 hours in culture was compared. The statistical analysis conducted in 3.3.3.2 and presented in figure 3.12, 3.13 and 3.14 is not represented on this graph for clarity. When all PCLS thicknesses were considered at 24 hours there was a significant increase in LDH released from lysed tissue lumps compared to all PCLS thicknesses (P<0.01). At 120 hours there was no significant difference in the LDH released from lysed tissue lumps compared to PCLS of 300µm, 500µm and 700µm (P>0.05), whilst there was a significant increase in LDH released by lysed tissue lumps compared to 1000µm PCLS (P<0.05). After 168 hours in culture there was no significant difference in the LDH released from lysed tissue lumps compared to PCLS of 500µm and 700µm (P>0.05), whilst there was a significant increase in LDH released by lysed tissue lumps compared to 300µm (P<0.005) and 1000µm PCLS (P<0.01) (Figure 3.19).

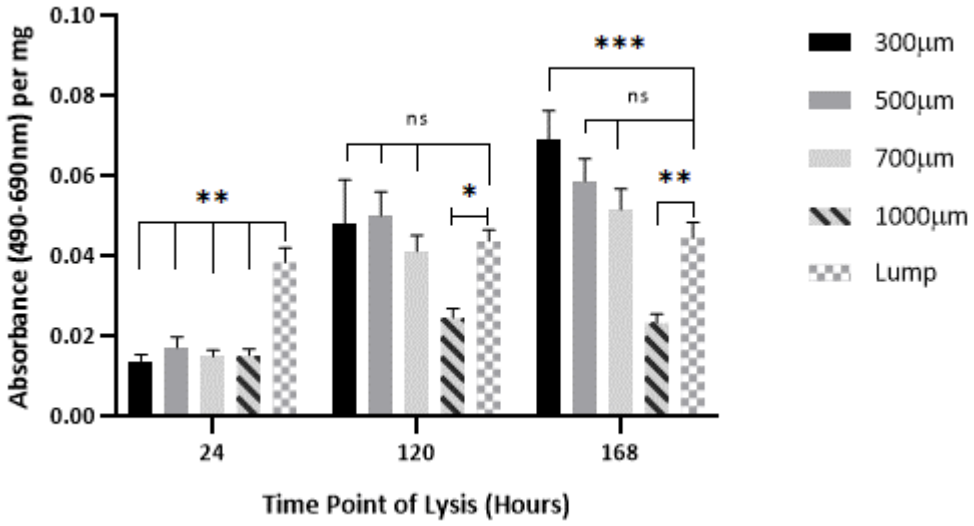

Figure 3.19 LDH analysis comparison of 10mm^2 PCLS of varying thicknesses and 2 – 3mm^3 inflated tissue lumps at 24, 120 and 168 hours post slicing. LDH measurements were based on absorbance reading (490 – 690nm) accounting for media blank and normalised per milligram of tissue, after PCLS was completely lysed. Results are displayed as mean ± SEM (N=5, n=33). Statistical analysis was conducted using a two-way ANOVA with multiple comparison by Tukey analysis. P<0.05*, P<0.01**, P<0.005***

3.3.3.6 Uninflated Lump Tissue Remains Significantly More Viable Than Inflated Lump Tissue

Both inflated and uninflated tissue lumps appeared to be viable in culture for up to 168 hours, thus a direct comparison of the LDH released from lysed tissue was conducted to determine if any difference in viability existed. The extent of cellular cytotoxicity determined by measuring the level of LDH in lysed tissue after 24, 120 and 168 hours in culture was compared. When both inflated and uninflated lumps are considered at 24 hours there was a significant increase in LDH released from lysed uninflated tissue lumps compared to inflated tissue lumps (P<0.01). At 120 hours there was a significant increase in LDH released from lysed uninflated tissue lumps compared to inflated tissue lumps (P<0.005). At 168 hours there was a significant increase in LDH released from lysed uninflated tissue lumps compared to inflated tissue lumps (P<0.005) (Figure 3.20).

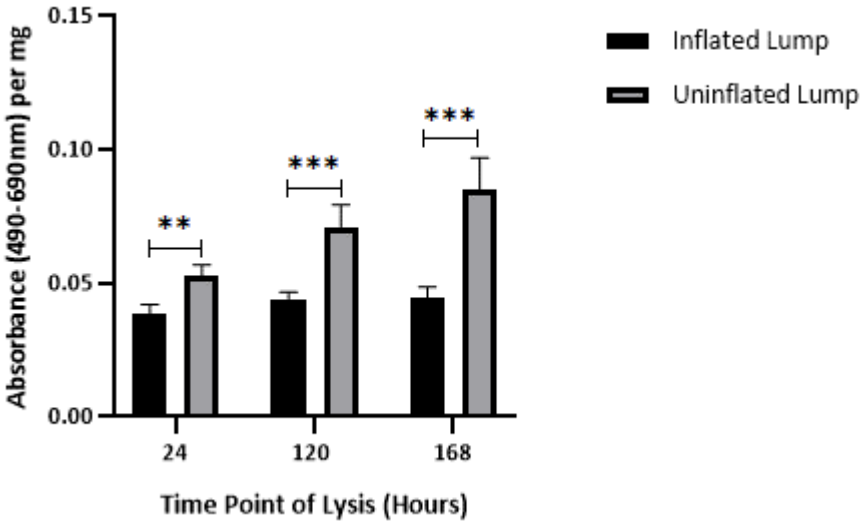

Figure 3.20 LDH analysis comparison of 2 – 3mm^3 inflated and uninflated tissue lumps at 24, 120 and 168 hours post slicing. LDH measurements were based on absorbance reading (490 – 690nm) accounting for media blank and normalised per milligram of tissue, after PCLS was completely lysed. Results are displayed as mean ± SEM (N=5, n=18). Statistical analysis was conducted via multiple t-tests using the Holm-Sidák method. P<0.01**, P<0.005***

3.3.4 Healthy Tissue Trypan Blue Exclusion Viability Analysis

To support the findings from the LDH analysis, healthy tissue viability was also assessed through the use of trypan blue exclusion after tissue had been dissociated into single cell suspensions.

3.3.4.1 Trypan Blue Exclusion Confirms Slice Thickness does not Affect Human PCLS Viability Over a 7 Day Culture Period

Trypan blue exclusion assay was utilised to further determine whether there was any difference in viability between PCLS of 300µm to 1000µm over the length of the culture period, using the method outlined in 3.2.2.3 and 3.2.2.4. When all PCLS thicknesses were considered there was no significant difference in percentage viability of any thickness at initial dissociation (0 hours) or after 24 hours in culture (P>0.05). After a 120 hours in culture there was no significant difference in viability between 300µm, 500µm or 700µm

PCLS (P>0.05), similarly no significant difference in viability existed between 500µm, 700µm or 1000µm PCLS (P>0.05) however, there was a significant reduction in viability at 120 hours for 300µm PCLS compared to 1000µm PCLS (P<0.05). After a 168 hours in culture there was no significant difference in viability between 300µm and 500µm PCLS (P>0.05), similarly no significant difference in viability exists between 500µm, 700µm or 1000µm PCLS (P>0.05) however, there was a significant reduction in viability at 168 hours for 300µm PCLS compared to both 700µm and 1000µm PCLS (P<0.05) (Figure 3.21).

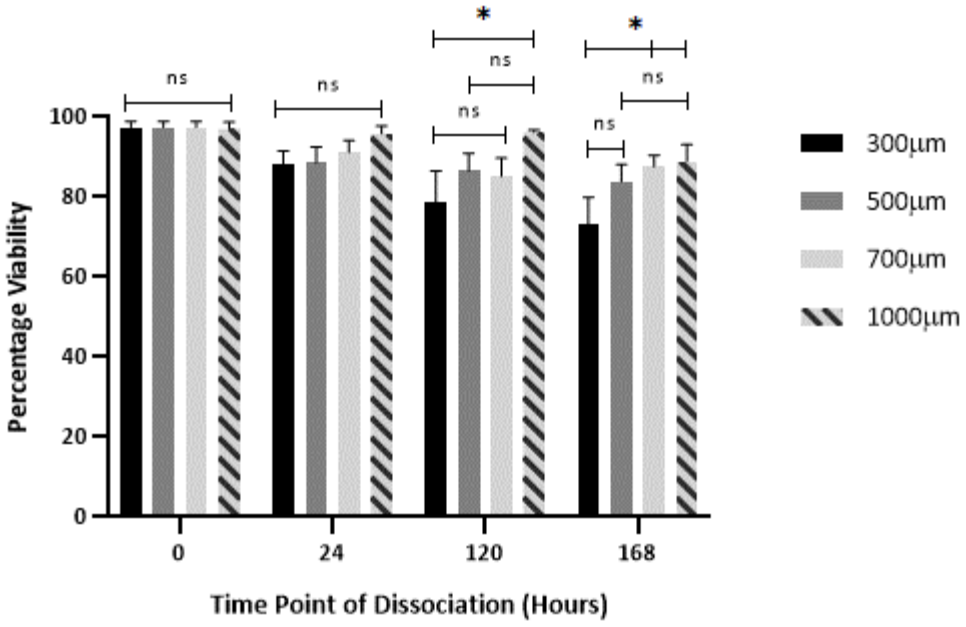

Figure 3.21 Trypan blue exclusion assay to show percentage viability of 10mm^2 PCLS of varying thicknesses at 0, 24, 120 and 168 hours post slicing. Viability calculation were based on the number of live (unstained) cells as a percentage of the total (live, unstained plus dead, stained) cells. Results are displayed as mean ± SEM (N=5, n=16). Statistical analysis was conducted using a two-way ANOVA with multiple comparison by Tukey analysis. P<0.05*

3.3.4.2 Trypan Blue Exclusion Confirms Human Inflated Lump Tissue Remained Viable Over a 7 Day Culture Period

Trypan blue exclusion assay was utilised to further determine whether there was any difference in viability of small tissue lumps of 2 – 3mm^3 over the length of the culture period,

using the method outlined in 3.2.2.3 and 3.2.2.4. Compared to the percentage viability calculated at 0 hours there was no significant difference between the viability at 24 and 168 hours (P>0.05) however, there was a significant reduction in viability at 120 hours compared to the initial viability (P<0.01). Similarly, there was no significant difference in viability between 24 hours and 168 hours or 120 hours and 168 hours (P>0.05) however, there was a significant reduction in viability at 120 hours compared to 24 hours (P<0.01) (Figure 3.22).

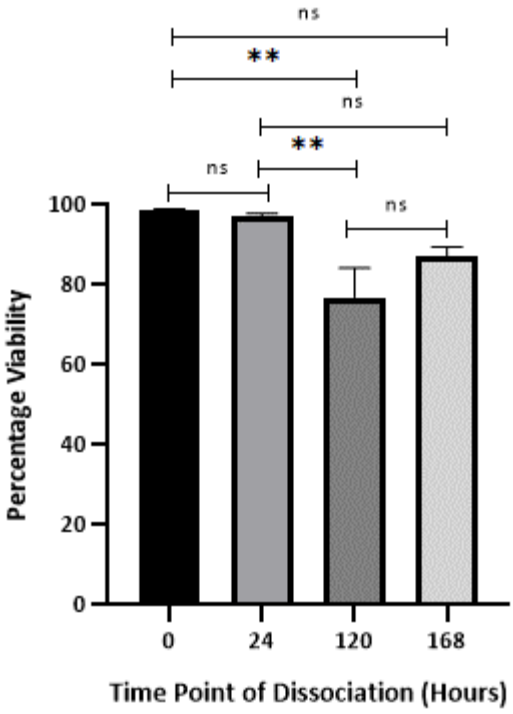

Figure 3.22 Trypan blue exclusion assay to show percentage viability of 2 – 3mm^3 inflated tissue lumps at 0, 24, 120 and 168 hours post sectioning. Viability calculation were based on the number of live (unstained) cells as a percentage of the total (live, unstained plus dead, stained) cells. Results are displayed as mean ± SEM (N=6, n=4). Statistical analysis was conducted using a one-way ANOVA with multiple comparison by Tukey analysis. P<0.01**

3.3.4.3 Trypan Blue Exclusion Confirms Human Uninflated Lump Tissue Remained Viable Over a 7 Day Culture Period

Trypan blue exclusion assay was utilised to further determine whether there was any difference in viability of small uninflated tissue lumps of 2 – 3mm^3 over the length of the culture period, using the method outlined in 3.2.2.3 and 3.2.2.4. When all time points were compared there was no significant difference between the percentage viability of the tissue as time progresses (P>0.05) (Figure 3.23).

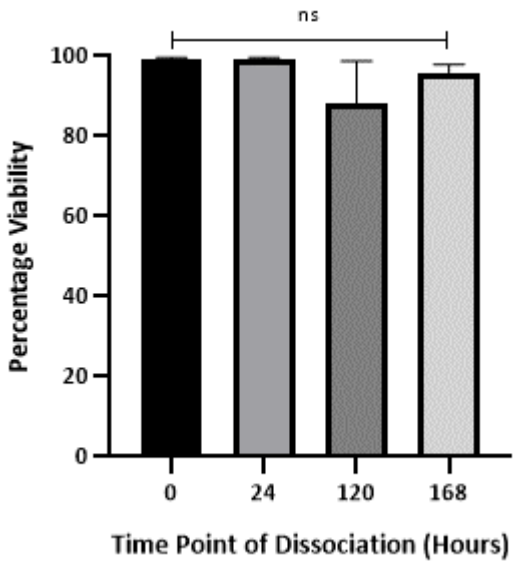

Figure 3.23 Trypan blue exclusion assay to show percentage viability of 2 – 3mm^3 uninflated tissue lumps at 0, 24, 120 and 168 hours post sectioning. Viability calculation were based on the number of live (unstained) cells as a percentage of the total (live, unstained plus dead, stained) cells. Results are displayed as mean ± SEM (N=3, n=4). Statistical analysis was conducted using a one-way ANOVA with multiple comparison by Tukey analysis.

3.3.4.4 Both Human PCLS and Inflated Lump Tissue have Similar Viability

Based on both the LDH and trypan blue viability data, inflated tissue lumps and PCLS of varying thicknesses appear to be viable in culture for up to 168 hours, thus a direct comparison of percentage viability was conducted to determine if any difference in viability existed. The statistical analysis conducted in 3.3.4.1 and presented in figure 3.21 is not represented on this graph for clarity. When all PCLS thicknesses were considered at 0, 24

and 168 hours there was no significant different in the percentage viability between tissue lumps compared to all PCLS thicknesses (P>0.05). At 120 hours there was no significant difference in percentage viability of tissue lumps compared to PCLS of 300µm, 500µm and 700µm (P>0.05) however, there was a significant decrease in percentage viability of tissue lumps compared to 1000µm PCLS (P<0.05) (Figure 3.24).

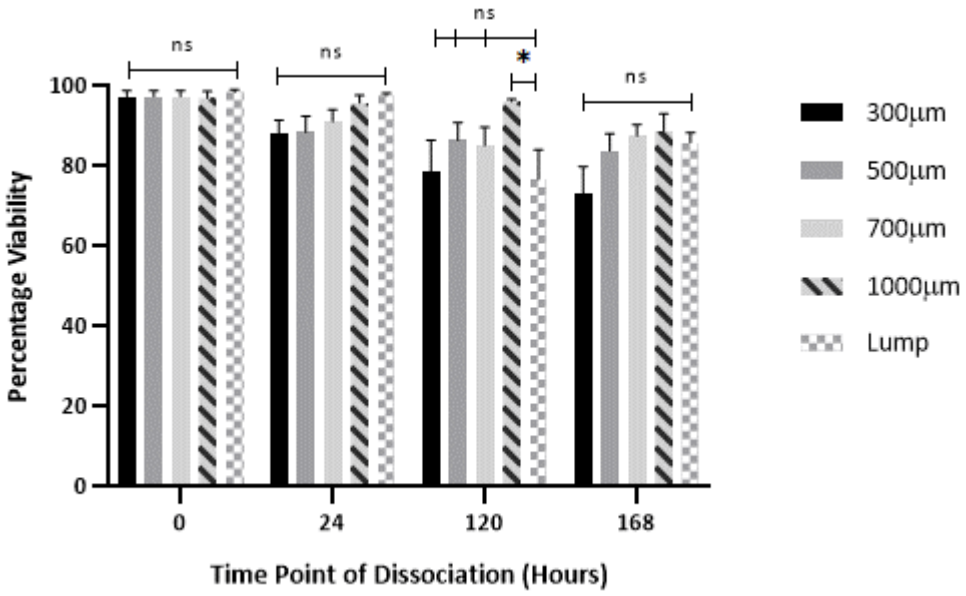

Figure 3.24 Trypan blue exclusion assay comparison to show percentage viability of 10mm^2 PCLS of varying thicknesses and 2 – 3mm^3 inflated tissue lumps at 0, 24, 120 and 168 hours post slicing. Viability calculation were based on the number of live (unstained) cells as a percentage of the total (live, unstained plus dead, stained) cells. Results are displayed as mean ± SEM (N=5, n=20). Statistical analysis was conducted using a one-way ANOVA with multiple comparison by Tukey analysis. P<0.05*

3.3.4.5 Both Uninflated Lump Tissue and Inflated Lump Tissue have Similar Viability

Based on both LDH and trypan blue exclusion data inflated and uninflated tissue lumps appear to be viable in culture for up to 168 hours, thus a direct comparison percentage viability for both types of tissue lumps was conducted. When both inflated and uninflated lumps were considered there was no significant different in percentage viability between either type of tissue lump at any time point (P>0.05) (Figure 3.25).

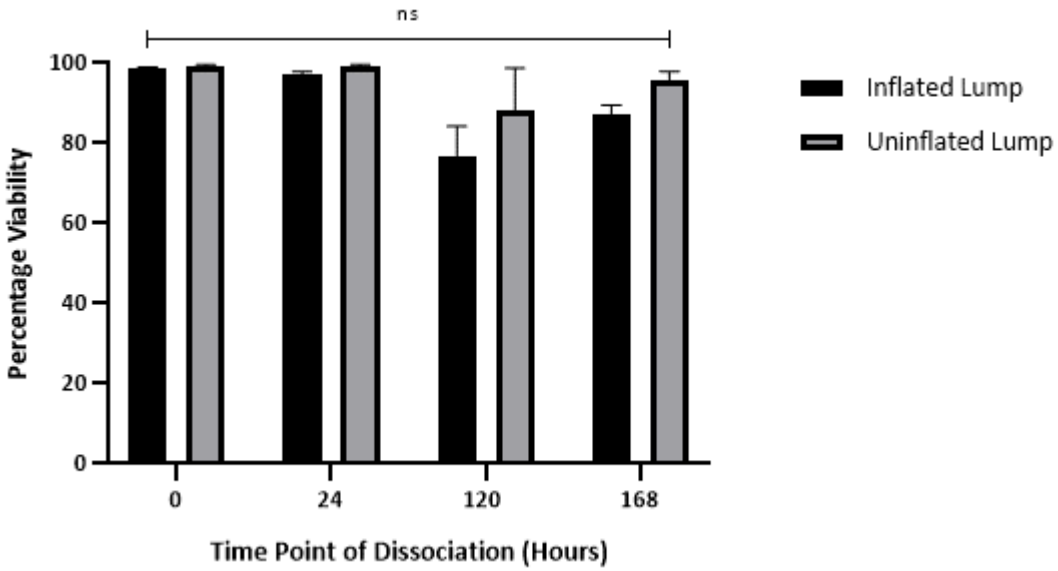

Figure 3.25 Trypan blue exclusion assay comparison to show percentage viability of comparison of 2 – 3mm^3 inflated and uninflated tissue lumps at 0, 24, 120 and 168 hours post slicing. Viability calculation were based on the number of live (unstained) cells as a percentage of the total (live, unstained plus dead, stained) cells. Results are displayed as mean ± SEM (N=3, n=8). Statistical analysis was conducted via multiple t-tests using Holm-Sidák method.

3.3.5 TEER Measurements in Human PCLS Reduce Over Time

To further identify methods which could be utilised to determine whether PCLS changed throughout the culture period, TEER measurements were made at 24 to 48 hour intervals over the duration of the 7 days culture period using the method outlined in 3.1.3.3. PCLS were allowed to equilibrate for 24 hours post slicing to allow pro-inflammatory markers released in response to cell damage from slicing to reduce and stabilise, in line with the previously observed LDH data. Initial TEER measurements at 24 hours were approximately 32Ω.cm^2 falling sharply over the first 24 hours in culture before plateauing to some extent before falling again to the lowest recorded value at 168 hours as cell death becomes widespread (Figure 3.26).

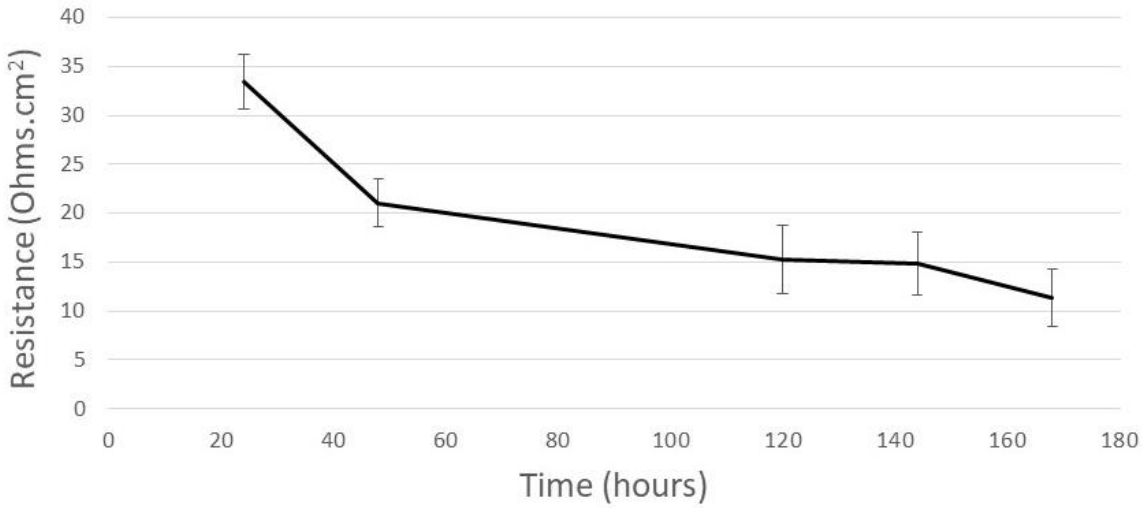

Figure 3.26 TEER measurements from healthy 8mm diameter 1000µm PCLS, taken from 24h post slicing for a total of 6 days. Results are displayed as mean ± SEM (N=5, n=3).

3.3.6 Histamine Induces Bronchoconstriction in Human PCLS

To demonstrate whether bronchoconstriction measurements could be successfully observed prior to infection with RV16, 700µm PCLS were treated with either 1mM methacholine or 10µM histamine and the effect on bronchoconstriction of bronchioles measured every minute for 5 minutes and subsequently at 5 minute intervals for a total of 10 to 15 minutes. Measurements were taken at x10 magnification, x1 zoom using a Zeiss SteREO Discovery.V8 microscope, as outlined in 3.2.3.2. Application of 1mM methacholine to the PCLS caused progressive bronchoconstriction over the 15 minute observation period. After treatment there was a 19.6% percentage decrease in bronchiole diameter from baseline measurements to the smallest measured diameter at 10 minutes there was however, no recovery in bronchiole size over the observation period (Figure 3.27).

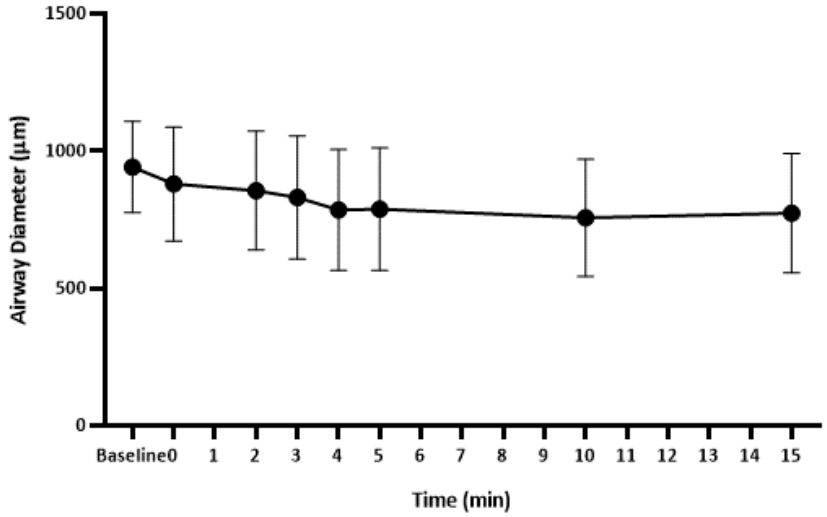

Figure 3.27 Bronchoconstriction measurements in bronchioles of 700µm PCLS treated with 1mM methacholine. Measurements taken every minute for 5 minutes and subsequently at 5 minute intervals at x10 magnification, x1 zoom using a Zeiss SteREO Discovery.V8 microscope. Results are displayed as mean ± SEM (N=2, n=2).

Application of 10µM histamine to the PCLS causes progressive bronchoconstriction over the 10 minute observation period. After treatment there was a 32.1% percentage decrease in bronchiole diameter from baseline measurements to the smallest measured diameter at 2 minutes, upon reaching the smallest diameter measure there was a steady recovery in bronchiole size over the observation period (Figure 3.28). Evidence of the reduction in bronchiole diameter and subsequent recovery is shown in the representative images taken after the application of histamine to the PCLS (Figure 3.29).

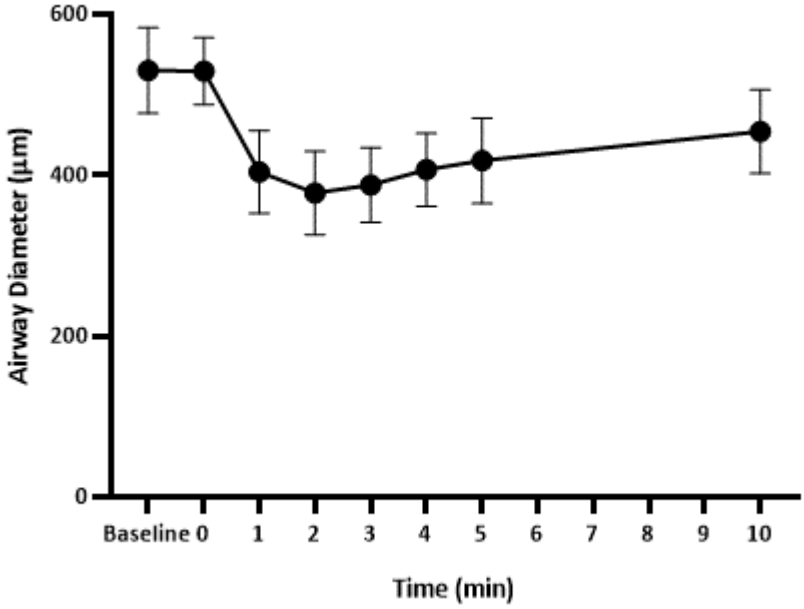

Figure 3.28 Bronchoconstriction measurements in bronchioles of 700µm PCLS treated with 10µM histamine. Measurements taken every minute for 5 minutes and subsequently at 5 minute intervals at x10 magnification, x1 zoom using a Zeiss SteREO Discovery.V8 microscope. Results are displayed as mean ± SEM of 6 PCLS replicates (N=1, n=6).

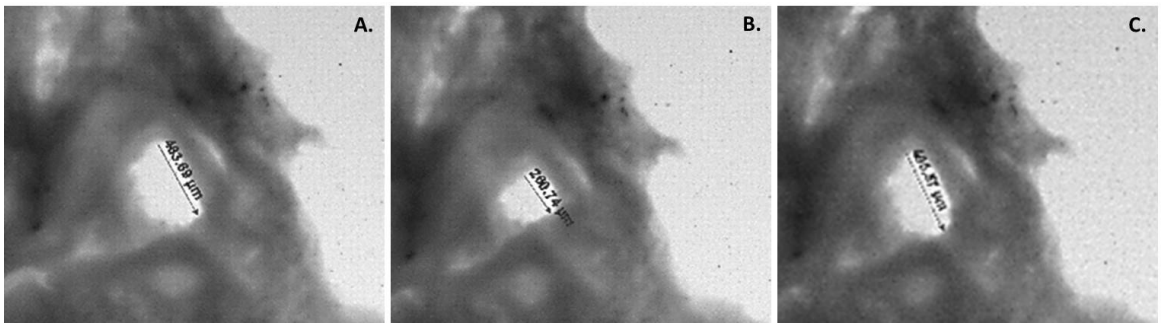

Figure 3.29 Bronchoconstriction measurements in bronchioles of 700µm PCLS treated with 10µM histamine. Representative images of 6 PCLS slices (N=1, n=6) showing measurements taken on initial application of histamine (**A**), 2 minutes after application (**B**) and 10 minutes post applications (**C**). All images taken x10 magnification, x1 zoom using a Zeiss SteREO Discovery.V8 microscope and subsequently cropped and expanded to clearly show airway of interest. Measurements read (**A**) 483.89µm, (**B**) 260.74µm and (**C**) 495.37µm.

3.3.7 Optimisation of Rhinovirus Infection of PCLS and Lump Tissue

Small inflated tissue lumps and 500µm PCLS were prepared as outlined in 3.2.1.2 and 3.2.1.3 and incubated overnight at 37°C, 5% CO_2 to allow for any pro-inflammatory markers which had been released due to inflation and slicing to subside. Prior to attempting infection, excess tissue samples were dissociated (see 3.2.2.3) and the number of cells per milligram of tissue calculated. By using this value and the individual mass of each tissue lump or slice, it was possible to produce an indication of the number of cells present in each tissue lump or slice to be infected. Although it is not possible to identify different cell types through this method, it gives an approximation to work with.

Based on the MOI of 1 utilised in cell culture infection, the volume of RV16 required was calculated however, using this MOI the volume required per piece of tissue was larger than the working volume of the well, therefore the MOI was reduced to 0.1 and 0.01 and the volumes recalculated. With a MOI of 0.1 the volume still remained too large for the well, whilst 0.01 was too small to provide sufficient coverage of the tissue by media during the incubation period. Thus for the first attempt at infection, an MOI of 0.025 was determined (based on the aforementioned conditions) which provided sufficient media to cover the tissue. Whilst, the volume and the extent of coverage of the tissue helped to determine the optimal MOI to use, consultation of current literature provided further guidance around suitable ranges that are deemed physiologically relevant. Although, Kennedy *et al* (2018) utilised a MOI of approximately 0.001 ($TCID_{50}$ 3000/ml) to infect PCLS with RV39, the limited examples of *ex vivo* human PCLS being infected with hRV, required *in vitro* studies to be considered in determining the final MOI. The MOIs utilised *in vitro* for infections with RV16 range from 10 (Brockman-Schneider *et al*, 2014), through 4 (Oliver *et al*, 2006) to 0.03 (Kuo *et al*, 2011). Given this variation, determining a single physiologically relevant MOI was not possible, thus falling between the aforementioned *in vitro* and *ex vivo* MOIs, the chosen MOI of 0.025 seemed a reasonable starting point. Furthermore, it could be argued that the RV16 will only infect airway epithelial cells expressing ICAM-1 receptors rather than other cells present in the tissue (Paine *et al*, 1994), thus increasing the MOI is unlikely to cause increased rate of infection (Nicholas *et al*, 2015) although the time the tissue was exposed to the unbound virus may have some impact.

The second consideration on the first attempt at infection was the length of time the tissue needed to be incubated with the RV16. Kennedy *et al* (2018) used an incubation period of 4 hours to infect human PCLS with RV39, thus this influenced the chosen maximum incubation time of 4 hours which was used alongside 1 and 2 hours incubation periods. Tissue was incubated at room temperature, on a gyro-rocker, with RV16 or ultrafiltered RV16 for 1, 2 or 4 hours, whilst basal tissue was maintained under 500µl of tissue DMEM for the duration of the incubation period. After the incubation period tissue was washed once with 1x PBS and 500µl of infection DMEM added to each well. Tissue was incubated at 37^{o}C, 5% CO_2 for a further 6 days with media changes (using tissue DMEM) every 24 hours.

Upon analysis of the preliminary LDH levels (Figure 3.30), it became apparent that there was little difference between the chosen time points, which may be a reflection on the higher MOI used when compared to the Kennedy *et al* (2018). Given the lack of variation between time points the middle of the range was chosen to give sufficient time for the virus to bind with the cells for all future experiments.

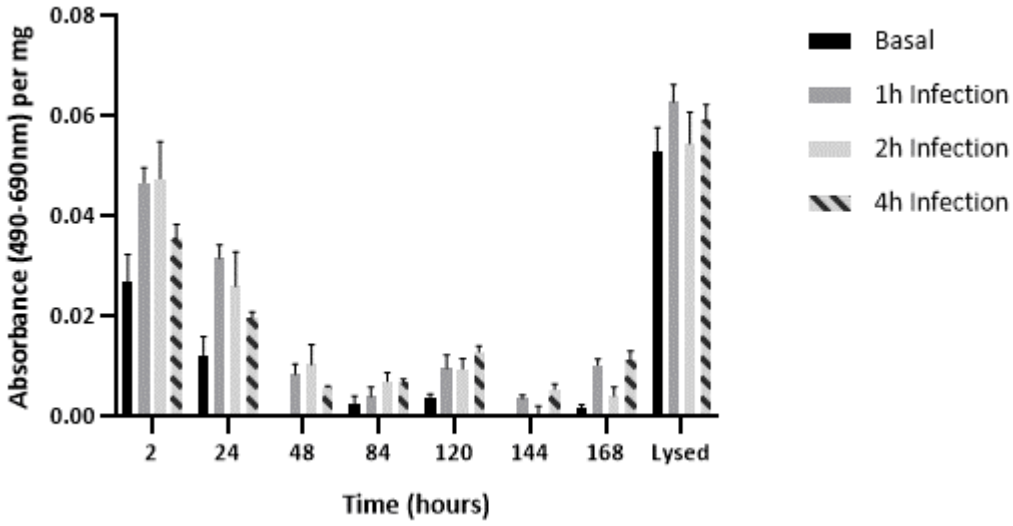

Figure 3.30 Preliminary LDH data comparing incubation times for tissue lumps with RV16 against basal conditions. Results are displayed as mean ± SEM of 3 tissue lump replicates per condition (N=1, n=12).

To identify whether the MOI used altered the amount of cytotoxicity measured, an MOI of 0.025, 0.01 and 0.0025 was used to infect the tissue. With the lower MOI there was insufficient media to cover the tissue for the duration of the 2 hour incubation period, to compensate for this and to prevent tissue dehydrating additional infection DMEM to a total volume of 500µl, was added to each well. Analysis of the LDH data generated from this test similarly showed little different between the MOI used however, based on the observation that there was reduced LDH release from the 0.0025 and 0.025 MOI, thus suggesting increased cytotoxicity (Figure 3.31). In order to maximise the chance to achieving successful infection and observable outcome, whilst providing effective coverage of the tissue samples a MOI of 0.025 was used for future experiments.

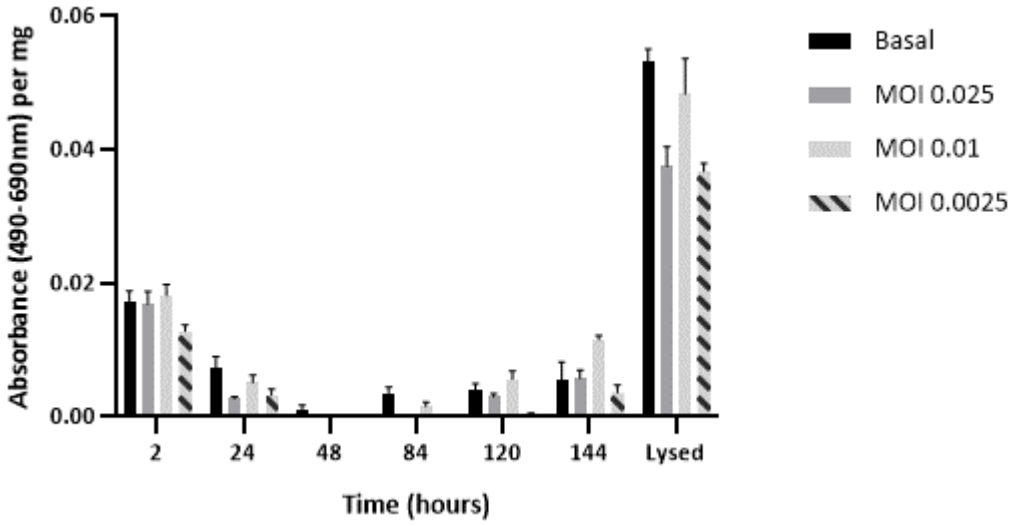

Figure 3.31 Preliminary LDH data comparing differing MOI of RV16 used to infect tissue lumps against basal conditions. Results are displayed as mean ± SEM of 3 tissue lumps replicates per condition (N=1, n=12).

3.3.8 Confirmation of Rhinovirus Infection in Human PCLS and Lump Tissue

3.3.8.1 Hela Ohio Cell Line Infection with Human PCLS Supernatant Confirmed Human Rhinovirus Tissue Infection

To confirm successful infection of PCLS with RV16, samples of tissue effluent were taken from PCLS (varying thicknesses) and lump tissue infected with RV16 or ultrafiltered RV16,

48 hours post infection and applied to Hela Ohio cells, incubated and scored after 5 days (see 3.2.6.1).

Initially various MOIs were utilised to identify the lowest value which could be used, whilst still allowing for successful infection. When scored, Hela Ohio cells treated with tissue effluent from RV16 infected lump tissue there was clear evidence of infection at an MOI of 0.025 as all Hela Ohio cells show evidence of cell rounding and sloughing. At lower MOI there was sporadic evidence of cell rounding and sloughing, but this was not evident in all cases with many cells still being alive. Similarly, when tissue effluent from ultrafiltered RV16 treated lump tissue and basal tissue effluent was applied to Hela Ohio cells, they typically showed no evidence of cell rounding and sloughing. The same observations were also made when tissue effluent is taken from 1000µm PCLS infected with RV16, ultrafiltered RV16 and in basal conditions at a MOI of 0.025 (Figure 3.32). Based on these observations the most consistent infection occurred when a MOI of 0.025 was used, thus this MOI was determined to as the most effective and was utilised in all subsequent experiments.

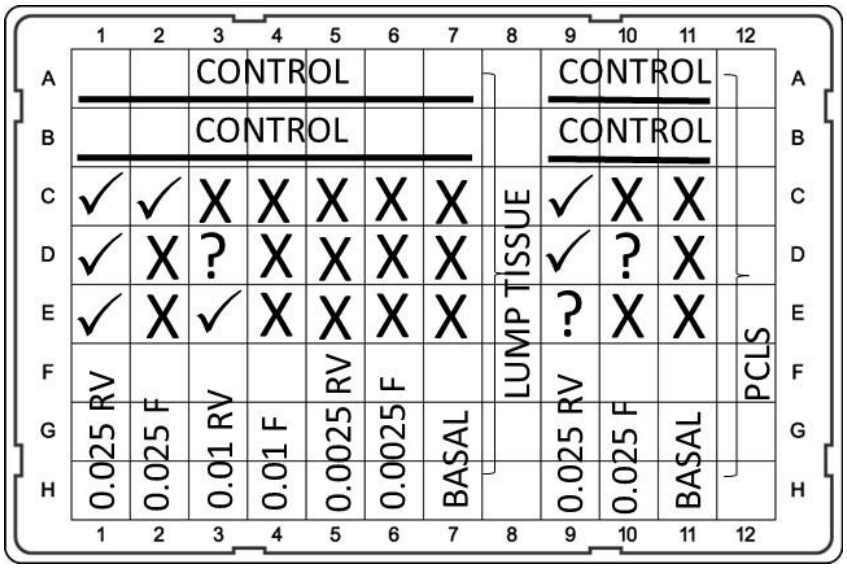

Figure 3.32 Representative plate of Hela Ohio cells subjected to a modified endpoint dilution assay scored 5 days post application of PCLS and lump tissue effluent from tissue infected for 48 hours with various MOIs of RV16, ultrafiltered RV16 or subjected to basal conditions (N=1, n=10).

Having confirmed that using a MOI of 0.025 has the most consistent effect in terms of tissue infection, subsequent experiments utilised this MOI. The representative modified titre plate shown below (Figure 3.33) shows that lump tissue and various thickness PCLS could be successfully infected with RV16 due to the evidence of cell rounding and sloughing in all wells containing Hela Ohio cells treated with tissue effluent. Furthermore, when tissue effluent was applied to Hela Ohio cells from tissue exposed to ultrafiltered RV16 and basal conditions there was no evidence of cell rounding and sloughing, indicating there was no active replication of hRV in the tissue and that evidence of infection was solely due to the *ex vivo* infection process. This can be further supported through the microscopy images which showed cell death, evident through rounding and sloughing, in Hela Ohio cells treated with undiluted tissue effluent from RV16 infected tissue. Whilst in contrast, those cells which were treated with either tissue effluent from ultrafiltrated RV16 tor basal treated tissue looks similar in appearance to control cells (Figure 3.34).

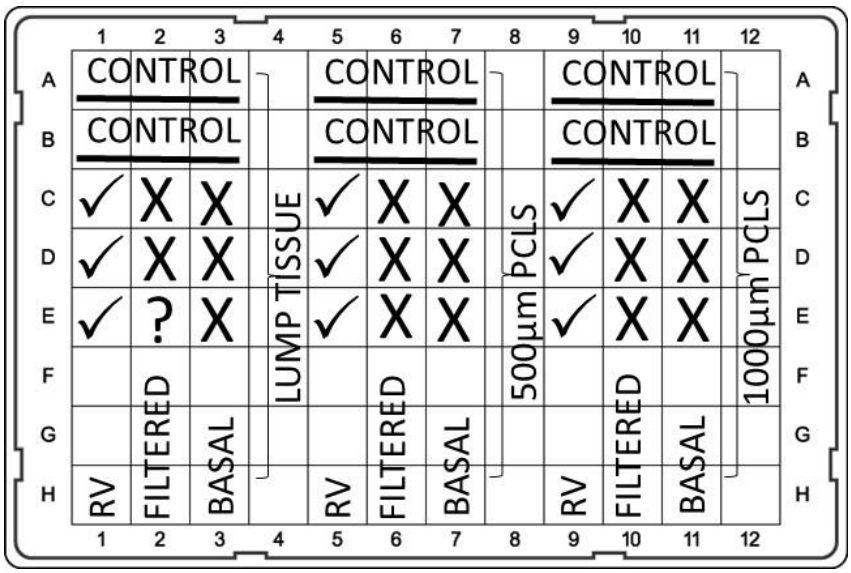

Figure 3.33 Representative plate of Hela Ohio cells subjected to a modified endpoint dilution assay scored 5 days post application of tissue effluent from lump tissue, 500µm and 1000µm PCLS infected for 48 hours with RV16, ultrafiltered RV16 or subjected to basal conditions. Data represents five independent experiments (N=5, n=9).

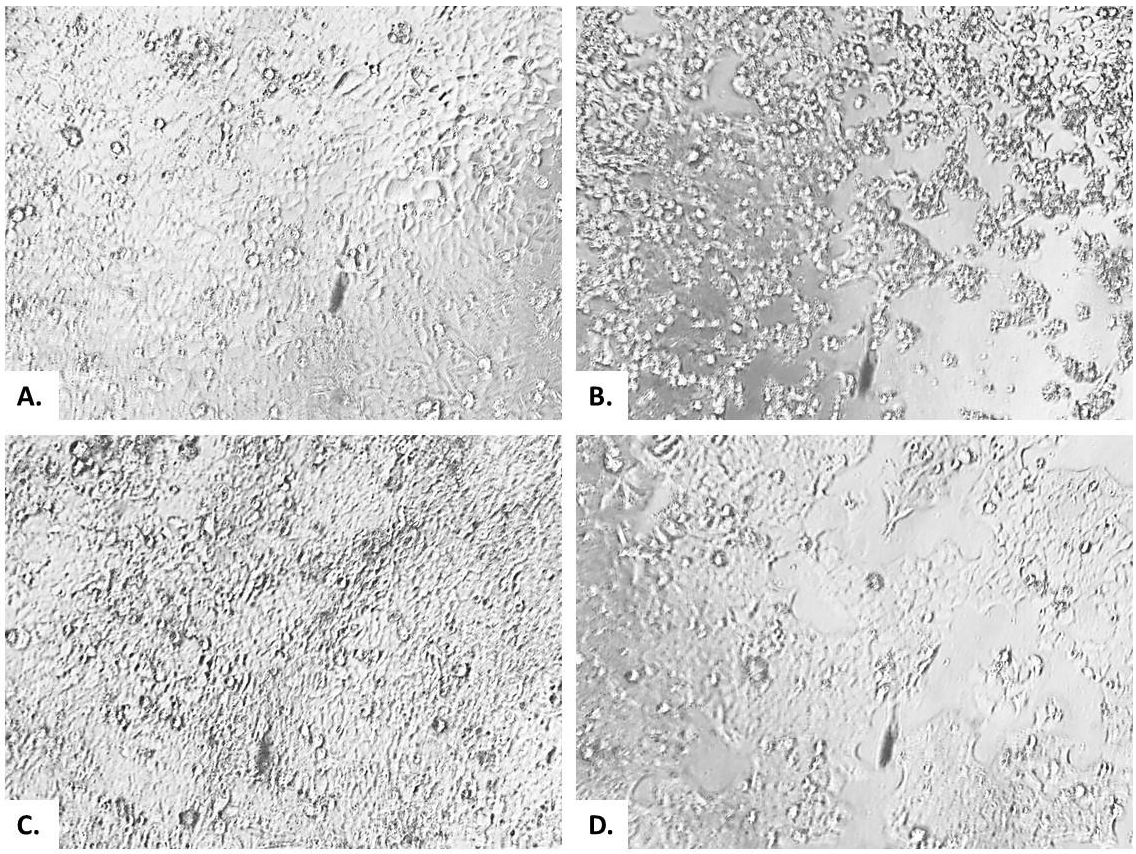

Figure 3.34 Representative images of Hela Ohio cells viewed at 100x magnification after 5 days in culture in control conditions (**A**) and 5 days post application of tissue effluent from 1000µm PCLS infected for 48 hours with RV16 (**B**), with ultrafiltered RV16 (**C**) and in basal conditions (**C**). Data represents five independent experiments (N=5, n=3).

3.3.8.2 Human PCLS Infection was Confirmed via qPCR Analysis

To confirm the observations made in the viral titre plates using tissue effluent qPCR was conducted on concentrated tissue effluent (tissue lumps, 500µm and 1000µm PCLS) and lump tissue lysates collected 5 days post infection with RV16, ultrafiltered RV16 and basal conditions. qPCR was carried out as outline in 3.2.8.7 and a standard curve produced to enable quantification of viral load in the samples to be calculated. Tissue effluent collected from 1000µm PCLS gave a measureable viral load copy number averaging 1271 in RV16 infected tissue whilst ultrafiltered RV16 and basal conditions produced undeterminable values. Similarly, tissue effluent collected from lump tissue gave a measureable viral load copy number averaging 8246 in RV16 infected tissue whilst ultrafiltered RV16 and basal conditions produced undeterminable values. Indicating successful infection of the tissue had occurred as any unbound viral particles are washed away after the 2 hour incubation

period, thus only actively replicating virus is present in tissue effluent. Although, titre plates showed evidence of successful infection of 500µm PCLS, when tissue effluent collected from 500µm PCLS was processed no determinable values could be measured in any conditions. The same undeterminable values were also observed when lump tissue lysates were processed for all condition (Table 3.7). No RT replicates were also carried out for all conditions and tissue variants, with all conditions showing undeterminable values (data not shown).

Tissue Condition	**Source of Viral RNA**	**Copy Number**		
		RV16 Treated	**Ultrafiltered RV16 Treated**	**Basal Conditions**
1000µm PCLS (N=1)	Effluent	992	Undetermined	Undetermined
1000µm PCLS (N=2)		1550	Undetermined	Undetermined
500µm PCLS (N=1)		Undetermined	Undetermined	Undetermined
Lump (N=1)		15320	Undetermined	Undetermined
Lump (N=2)		1172	Undetermined	Undetermined
Lump (N=1)	Tissue	Undetermined	Undetermined	Undetermined
Lump (N=2)		Undetermined	Undetermined	Undetermined

Table 3.7 Viral load copy number determined via qPCR in concentrated tissue effluent (tissue lumps, 500µm and 1000µm PCLS) and lump tissue lysates collected 5 days post infection with RV16, ultrafiltered RV16 and basal conditions.

3.3.9 LDH Cytotoxicity Analysis Post Rhinovirus Infection

3.3.9.1 Rhinovirus Infection of Human PCLS was not Cytotoxic when Measured by LDH Assay

Having shown that PCLS could be successfully infected with RV16, the extent of cytotoxicity was next considered. To determine whether infection of PCLS had any impact on the LDH release during a 6 day culture period and after complete tissue lysis. PCLS of 500 and 1000µm thicknesses were prepared and infected for 2 hours with RV16 (MOI 0.025), treated with ultrafiltered RV16 or maintained in basal conditions. The extent of cellular cytotoxicity was determined by measuring the level of LDH in tissue culture effluent collected between 2 and 144 hours and in lysed tissue. In 500µm PCLS the LDH released into the tissue effluent followed a similar pattern of low level LDH release in all conditions

throughout the culture period. After lysis there was an observable spike in LDH for all conditions, with no significant increase in the amount of LDH released by RV16 and ultrafiltered RV16 treated tissue compared to basal (P>0.05) (Figure 3.35).

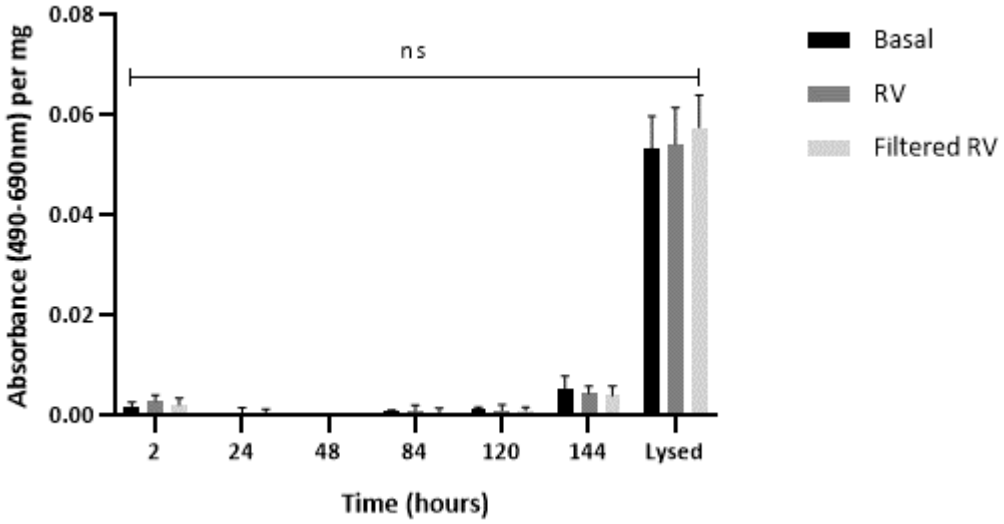

Figure 3.35 LDH analysis of 500µm PCLS infected with RV16, ultrafiltered RV16 and in basal conditions. LDH measurements were based on absorbance reading (490 – 690nm) accounting for media blank and normalised per milligram of tissue, for effluent collected between 2 and 144 hours during culture period and after PCLS was completely lysed. Results are displayed as mean ± SEM (N=4, n=6). Statistical analysis was conducted using a two-way ANOVA with multiple comparison by Tukey analysis.

Similarly, in 1000µm PCLS the LDH released into the tissue effluent followed a similar pattern of low level LDH release in all condition throughout the culture period. After lysis there was an observable spike in LDH for all conditions, with no significant increase in the amount of LDH released by RV16 and ultrafiltered RV16 treated tissue compared to basal (P>0.05) (Figure 3.36).

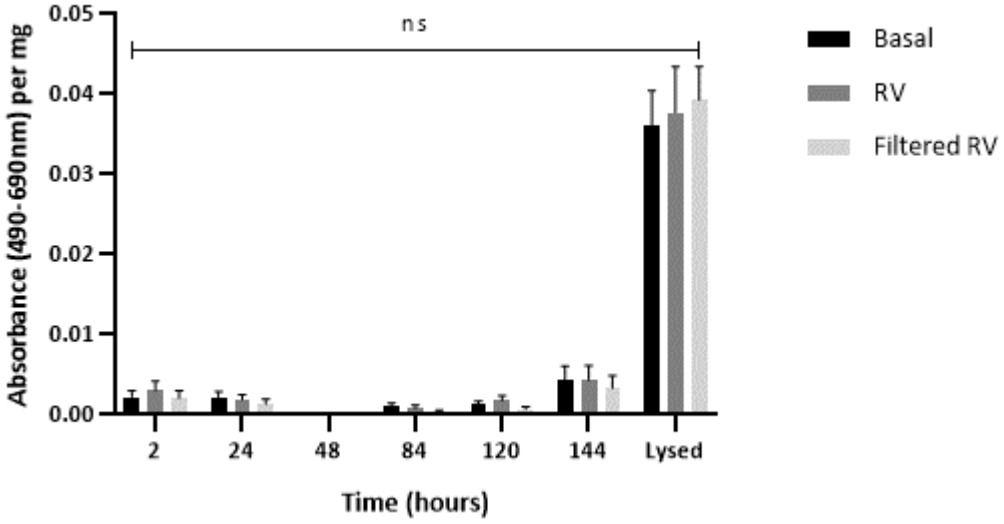

Figure 3.36 LDH analysis of 1000µm PCLS infected with RV16, ultrafiltered RV16 and in basal conditions. LDH measurements were based on absorbance reading (490 – 690nm) accounting for media blank and normalised per milligram of tissue, for effluent collected between 2 and 144 hours during culture period and after PCLS was completely lysed. Results are displayed as mean ± SEM (N=3, n=6). Statistical analysis was conducted using a two-way ANOVA with multiple comparison by Tukey analysis.

3.3.9.2 Rhinovirus Infection of Human Lump Tissue was not Cytotoxic when Measured by LDH Assay

Having shown there was no difference between the LDH released by PCLS after infection with RV16, the same process was repeated on small tissue lumps of 2 – 3mm^3 having previously shown tissue lump viability was similar to PCLS. Small tissue lumps of 2 – 3mm^3 were prepared and infected for 2 hours with RV16 (MOI 0.025), treated with ultrafiltered RV16 or maintained in basal conditions. The extent of cellular cytotoxicity was determined by measuring the level of LDH in tissue culture effluent collected between 2 and 144 hours and in lysed tissue. The LDH released into the tissue effluent followed a similar pattern to those previously observed with an increased level of LDH released at 2 and 24 hours before reducing and stabilising throughout the remaining culture period in all conditions. After lysis there was an observable spike in LDH for all conditions, with no significant difference in amount of LDH released by ultrafiltered RV16 treated tissue compared to basal ($P>0.05$), similarly there was no difference between RV16 and ultrafiltered RV16 LDH release ($P>0.05$)

however, there was a significant reduction in LDH released from lysed tissue infected with RV16 compared to those maintained in basal conditions (P<0.05) (Figure 3.37).

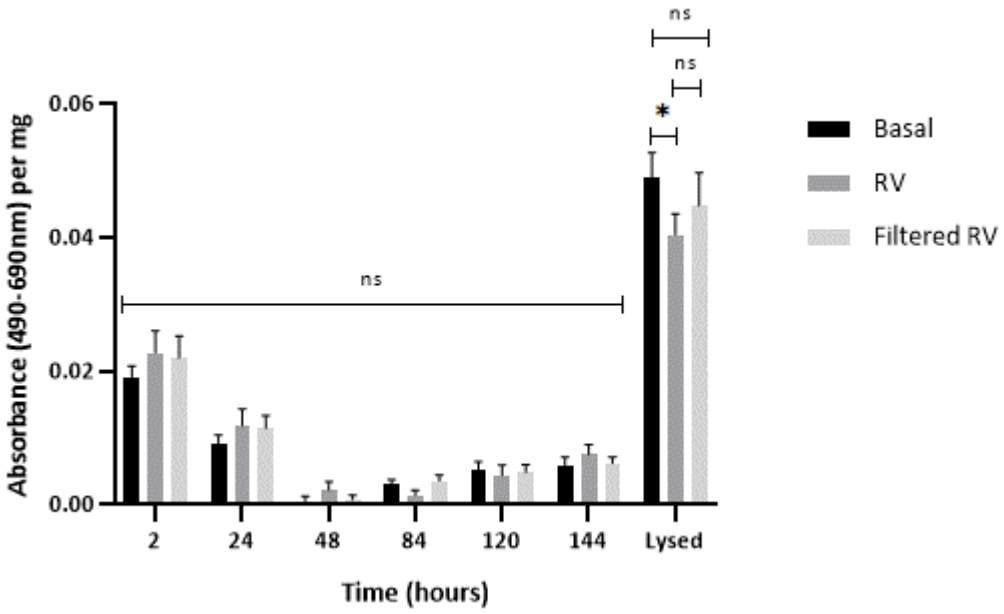

Figure 3.37 LDH analysis of 2 – 3mm^3 lump tissue infected with RV16, ultrafiltered RV16 and in basal conditions. LDH measurements were based on absorbance reading (490 – 690nm) accounting for media blank and normalised per milligram of tissue, for effluent collected between 2 and 144 hours during culture period and after complete lysis of lump tissue. Results are displayed as mean ± SEM (N=6, n=9). Statistical analysis was conducted using a two-way ANOVA with multiple comparison by Tukey analysis. P<0.05*

3.3.10 Trypan Blue Exclusion Viability Analysis Post Rhinovirus Infection

3.3.10.1 Viability does not Change Following Rhinovirus Infection of Human PCLS

To confirm the LDH findings, a trypan blue exclusion assay was utilised to show the extent of tissue viability after RV16 infection. PCLS of 500 and 1000µm thicknesses were prepared and infected for 2 hours with RV16 (MOI 0.025), treated with ultrafiltered RV16 or maintained in basal conditions. After 6 days in culture, the equivalent to 5 days post infection, tissue was dissociated using the method outlined in 3.2.2.3. In 500µm PCLS there was no significant difference in the percentage viability between any condition however,

there appears to be a reduction in percentage viability in RV16 infected tissue compared to ultrafiltered RV16 treated and basal tissue (P>0.05) (Figure 3.38).

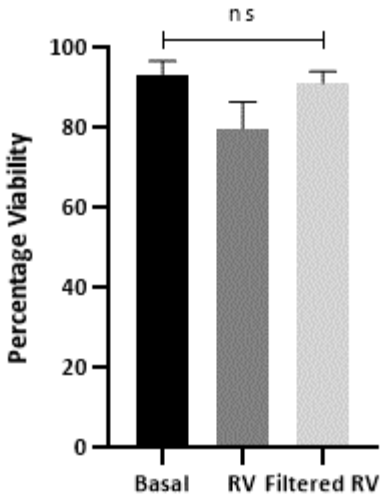

Figure 3.38 Trypan blue exclusion assay to show percentage viability of 500µm PCLS infected with RV16, ultrafiltered RV16 and in basal conditions. Viability calculations were based on the number of live (unstained) cells as a percentage of the total (live, unstained plus dead, stained) cells. Results are displayed as mean ± SEM (N=3, n=3). Statistical analysis was conducted using a one-way ANOVA with multiple comparison by Tukey analysis.

Due to only completing two replicates of the trypan blue exclusion assay with 1000µm PCLS it was not possible to conduct statistical analysis. However, observation of the presented date shows there was a reduction in percentage viability in RV16 infected tissue compared to ultrafiltered RV16 treated and basal tissue (Figure 3.39).

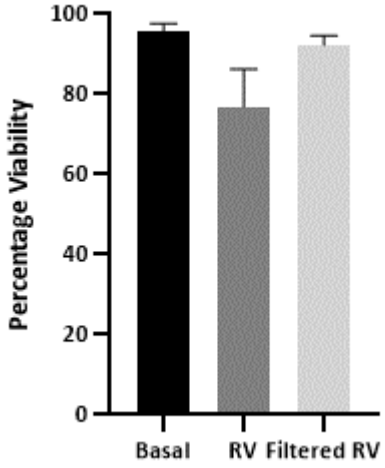

Figure 3.39 Trypan blue exclusion assay to show percentage viability of 1000µm PCLS infected with RV16, ultrafiltered RV16 and in basal conditions. Viability calculations were based on the number of live (unstained) cells as a percentage of the total (live, unstained plus dead, stained) cells. Results are displayed as mean ± SEM (N=2, n=3). Statistical analysis could not be conducted due to insufficient data.

3.3.10.2 Viability does not Change Following Rhinovirus Infection of Human Lump Tissue

To confirm the LDH findings in lump tissue, a trypan blue exclusion assay was utilised to show the extent of tissue viability after RV16 infection. Small tissue lumps of 2 – 3mm^3 were prepared and infected for 2 hours with RV16 (MOI 0.025), treated with ultrafiltered RV16 or maintained in basal conditions. After 6 days in culture, the equivalent to 5 days post infection, tissue was dissociated using the method outlined in 3.2.2.3. There was no significant difference in the percentage viability between any condition however, there was a reduction in percentage viability in RV16 infected tissue compared to ultrafiltered RV16 treated and basal tissue ($P>0.05$) (Figure 3.40).

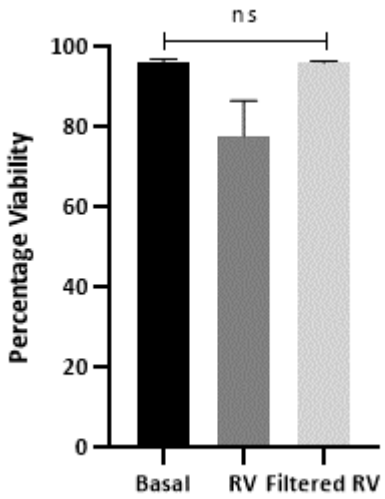

Figure 3.40 Trypan blue exclusion assay to show percentage viability of 2 – 3mm^3 tissue lumps infected with RV16, ultrafiltered RV16 and in basal conditions. Viability calculations were based on the number of live (unstained) cells as a percentage of the total (live, unstained plus dead, stained) cells. Results are displayed as mean ± SEM (N=6, n=3). Statistical analysis was conducted using a one-way ANOVA with multiple comparison by Tukey analysis.

3.3.11 CytoToxGlo™ Cytotoxicity Analysis Post Rhinovirus Infection

3.3.11.1 Dead Cell Protease Release Significantly Increased After Lysis Following Rhinovirus Infection of Human PCLS

To further enhance and support the cytotoxicity findings from the LDH assay, a dead cell protease assay was undertaken as outlined in 3.2.6.3. PCLS of 500µm thickness was prepared and infected for 2 hours with RV16 (MOI 0.025) or maintained in basal conditions and cultured for a total of 6 days. The extent of dead cell protease activity was determined by measuring the amount of luminescence from pooled tissue culture effluent collected between 2 and 144 hours and in pooled lysed tissue. The pattern observed in the extent of luminescence from tissue effluent is similar to that seen in the LDH assay (see 3.3.9.1) with low levels of dead cell protease activity in both conditions throughout the culture period, with no significant difference in activity at any time point (P>0.05). After lysis there was an observable spike in dead cell protease activity for both conditions, with a significant

increase in the amount of dead cell protease released by RV16 compared to basal (P<0.05) (Figure 3.41).

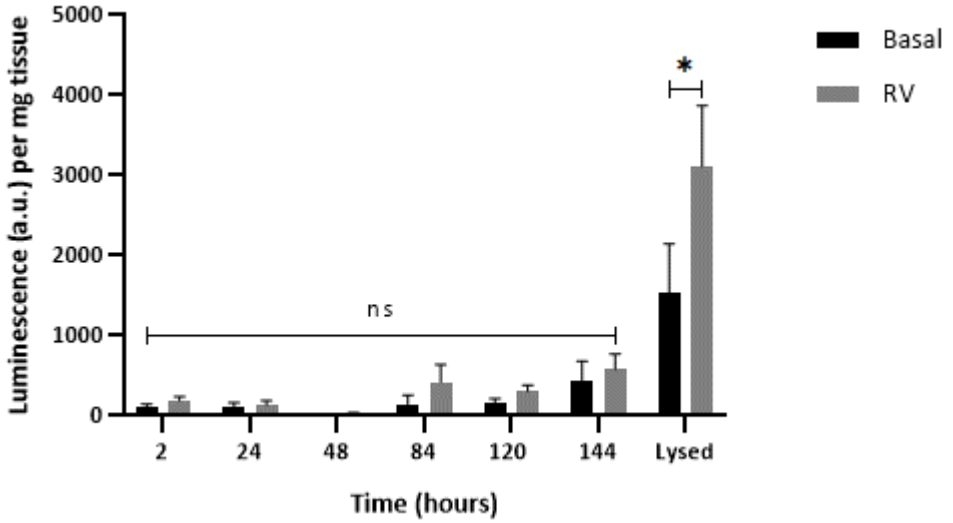

Figure 3.41 Dead cell protease analysis of 500µm PCLS infected with RV16, ultrafiltered RV16 and in basal conditions. Dead cell protease activity measurements were based on luminescence reading accounting for media blank and normalised per milligram of tissue, for effluent collected between 2 and 144 hours during culture period and after PCLS was completely lysed. Results are displayed as mean ± SEM (N=3, n=4). Statistical analysis was conducted using a two-way ANOVA with multiple comparison by Tukey analysis. P<0.05*

3.3.11.2 Dead Cell Protease Release does not Change Following Rhinovirus Infection of Human Lump Tissue

To further support the cytotoxicity findings from the LDH assay for small lump tissue, a dead cell protease assay was undertaken as outlined in 3.2.6.3. 2 – 3mm^3 lump tissue was prepared and infected for 2 hours with RV16 (MOI 0.025) or maintained in basal conditions and cultured for a total of 6 days. The extent of dead cell protease activity was determined by measuring the amount of luminescence from pooled tissue culture effluent collected between 2 and 144 hours and in pooled lysed tissue. The pattern observed in the extent of luminescence from tissue effluent is similar to that seen in the LDH assay (see 3.3.9.2) with an increased level of dead cell protease activity in both conditions at 2 and 24 hours before

stabilising throughout the remainder of the culture period, with no significant difference in activity at any time point (P>0.05). After lysis there was an observable spike in dead cell protease activity for both conditions, with a non-significant but increased amount of dead cell protease released by RV16 compared to basal (P>0.05) (Figure 3.42).

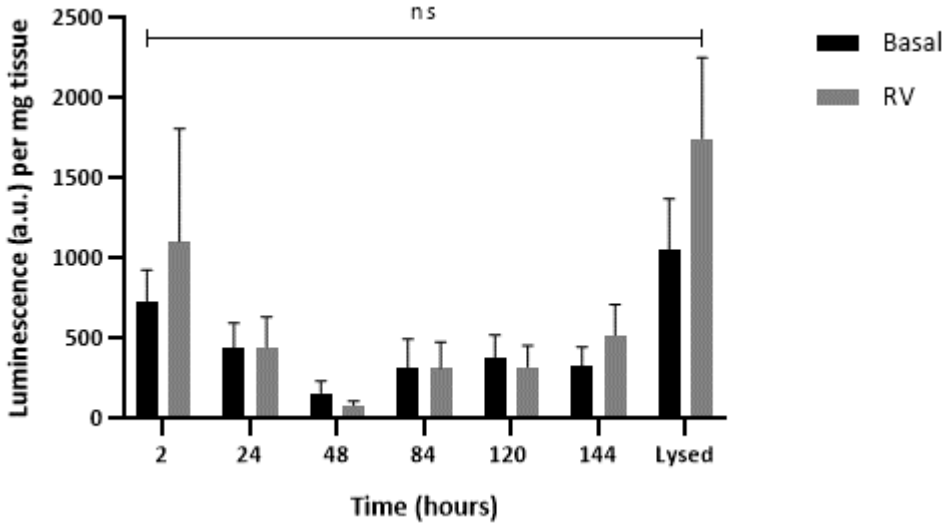

Figure 3.42 Dead cell protease analysis of 2 – 3mm^3 tissue lumps infected with RV16, ultrafiltered RV16 and in basal conditions. Dead cell protease activity measurements were based on luminescence reading accounting for media blank and normalised per milligram of tissue, for effluent collected between 2 and 144 hours during culture period and after complete lysis of tissue lumps. Results are displayed as mean ± SEM (N=4, n=4). Statistical analysis was conducted using a two-way ANOVA with multiple comparison by Tukey analysis.

3.3.12 WST-1 Cell Proliferation Analysis Post Rhinovirus Infection

3.3.12.1 Tetrazolium Salt Conversion does not Change Following Rhinovirus Infection of Human PCLS

To provide further confirmation of the LDH and CytoToxGlo™ results for PCLS, a WST-1 cell proliferation analysis was performed as outlined in 3.2.6.4 as a method of showing the extent of cell viability, as the conversion of tetrazolium salt to formazan by mitochondrial dehydrogenase can only occur in viable cells (Adan *et al*, 2016). PCLS of 500 and 1000µm

thicknesses were prepared and infected for 2 hours with RV16 (MOI 0.025), ultrafiltered RV16 treated or maintained in basal conditions and cultured for a total of 6 days. The extent of tetrazolium salt conversion was determined by measuring the absorbance in tissue effluent sampled after 2 hours incubation with the WST-1 reagent in duplicate PCLS per condition. In 500µm PCLS there was no significant change in conversion of tetrazolium salt by RV16 infected PCLS compared to PCLS treated with ultrafiltered RV16 or in basal conditions (P>0.05) (Figure 3.43).

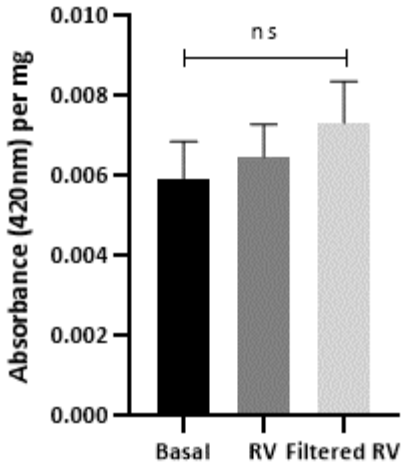

Figure 3.43 WST-1 analysis showing tetrazolium salt conversion by 500µm PCLS after infection with RV16, ultrafiltered RV16 or in basal conditions. WST-1 measurements were based on absorbance reading (420nm) accounting for media blank and normalised per milligram of tissue. Results are displayed as mean ± SEM (N=3, n=6). Statistical analysis was conducted using a one-way ANOVA with multiple comparison by Tukey analysis.

In 1000µm PCLS there was no significant change in conversion of tetrazolium salt by RV16 infected PCLS compared to both basal conditions and ultrafiltrated RV16 treated PCLS (P>0.05) (Figure 3.44).

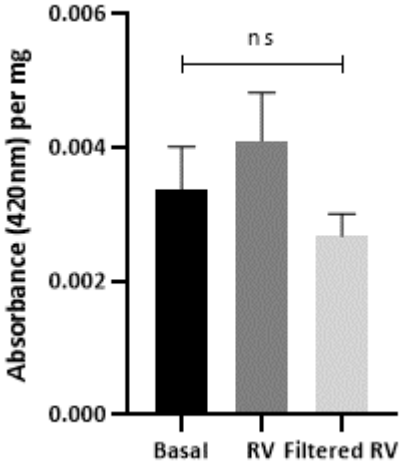

Figure 3.44 WST-1 analysis showing tetrazolium salt conversion by 1000µm PCLS after infection with RV16, ultrafiltered RV16 or in basal conditions. WST-1 measurements were based on absorbance reading (420nm) accounting for media blank and normalised per milligram of tissue. Results are displayed as mean ± SEM (N=3, n=6). Statistical analysis was conducted using a one-way ANOVA with multiple comparison by Tukey analysis.

1000µm PCLS that were used for TEER measurements for a total of 7 days post slicing (see 3.3.14) were also utilised in a WST-1 cell proliferation analysis to determine if a similar pattern in tissue viability could be observed after an additional day in culture. The 1000µm PCLS from TEER showed no significant change in conversion of tetrazolium salt by RV16 infected PCLS compared to both basal conditions and ultrafiltered RV16 treated PCLS ($P>0.05$) (Figure 3.45).

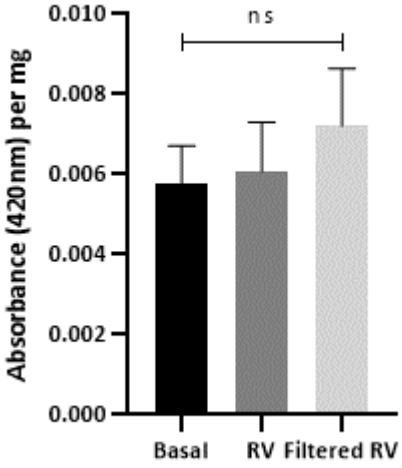

Figure 3.45 WST-1 analysis showing tetrazolium salt conversion by 1000µm PCLS after infection with RV16, ultrafiltered RV16 or in basal conditions. WST-1 measurements were based on absorbance reading (420nm) accounting for media blank and normalised per milligram of tissue. Results are displayed as mean ± SEM (N=3, n=6). Statistical analysis was conducted using a one-way ANOVA with multiple comparison by Tukey analysis.

3.3.12.2 Tetrazolium Salt Conversion does not Change Following Rhinovirus Infection of Human Lump Tissue

For further confirmation of the LDH and CytoToxGlo results for small lump tissue, a WST-1 cell proliferation analysis was performed as outlined in 3.2.6.4 as a method of showing the extent of cell viability. 2 – 3mm^3 lump tissue was prepared and infected for 2 hours with RV16 (MOI 0.025), ultrafiltered RV16 treated or maintained in basal conditions and cultured for a total of 6 days. The extent of tetrazolium salt conversion was determined by measuring the absorbance in tissue effluent sampled after 2 hours incubation with the WST-1 reagent in duplicate lump tissue per condition. These results show no significant increase in conversion of tetrazolium salt by lump tissue in basal conditions compared to both RV16 infected and ultrafiltered RV16 treated lump tissue ($P>0.05$) (Figure 3.46).

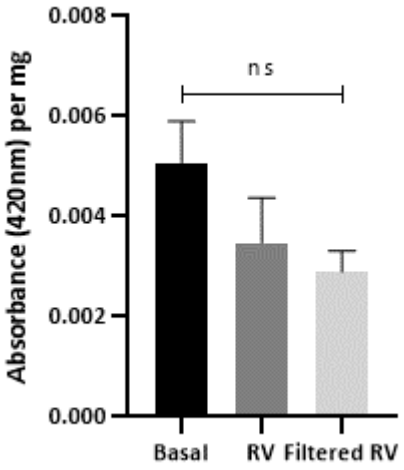

Figure 3.46 WST-1 analysis showing tetrazolium salt conversion by 2 – 3mm^3 lump tissue after infection with RV16, ultrafiltered RV16 or in basal conditions. WST-1 measurements were based on absorbance reading (420nm) accounting for media blank and normalised per milligram of tissue. Results are displayed as mean ± SEM (N=3, n=6). Statistical analysis was conducted using a one-way ANOVA with multiple comparison by Tukey analysis.

3.3.13 TEER Measurements are not Significantly Altered in Response to Human Rhinovirus Infection

Having shown some slight differences in TEER measurements arise when A549 and Beas-2b cell lines were infected with RV16 (see 2.3.7.3) and that TEER measurements could be made on 1000µm PCLS (see 3.3.5) the two ideas were combined to determine whether TEER measurements of tissue slices were altered in response to RV16 infection. An initial TEER measurement was taken 24 hours post slicing, prior to infection, subsequent TEER measurements were taken over the remaining period of 168 hours using the method outlined in 3.2.6.7. PCLS in basal conditions showed a relatively stable range of TEER measurements throughout the culture period until the 144 hours at which point readings fell. Similarly, after an initial increase 24 hours post treatment with ultrafiltered RV16 the readings for these slices fell slightly and stabilise over the duration of the culture period. In contrast, PCLS infected with RV16 show a sustained reduction in TEER measurements throughout the entire culture period. This observation is supported with the area under the curve values which interestingly show a non-significant reduction in area for RV16 compared to both ultrafiltered RV16 and basal conditions (P>0.05) (Figure 3.47).

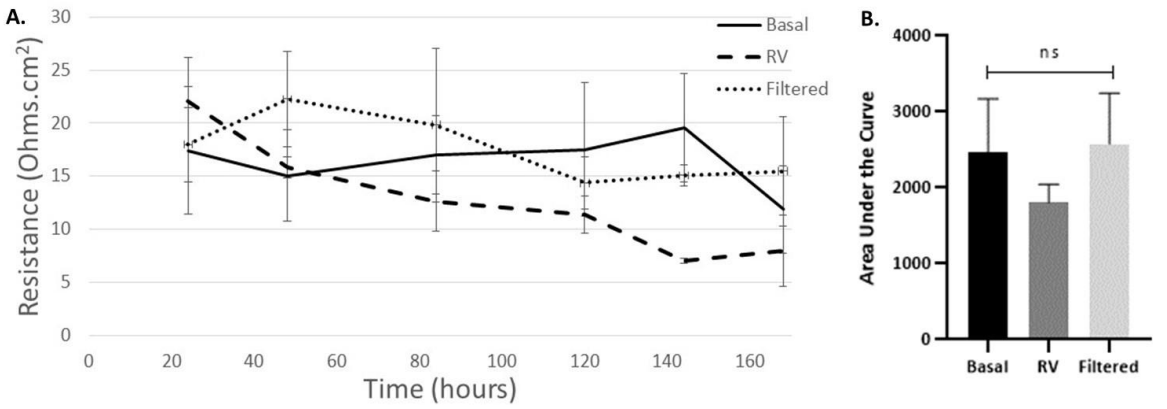

Figure 3.47 TEER measurements from 1000µm PCLS taken 24h post slicing and subsequently until 168h post exposure to RV16, ultrafiltered RV16 or basal conditions (**A**). Area under curve analysis of TEER measurements after exposure to aforementioned conditions (**B**). Results are displayed as mean ± SEM (N=3, n=6). Statistical analysis was conducted using a one-way ANOVA with multiple comparison by Tukey analysis.

3.3.14 Zymography for Assessment of MMP Upregulation Post Rhinovirus Infection

3.3.14.1 Human Rhinovirus had Limited Impact on MMP Activity in Human PCLS

Although no significant changes were observed in terms of the upregulation of MMP-2 and MMP-9 in A549 and Beas-2b cell lines (see 2.3.7.5), the same process was replicated using tissue supernatant collected from 500µm PCLS between 24 and 120 hours post infection with RV16 or after treatment with ultrafiltered RV16 or basal conditions, to identify whether any changes could be identified in tissue samples. Subsequently, the supernatant was electrophoresed through a 7.5% acrylamide gel containing 4mg/ml gelatine, the gels stained and imaged as described in 3.2.6.6 (Figure 3.48). Bands on the gel were analysed with densitometry using ImageJ software, the relative density was calculated and compared as a fold change to the basal conditions.

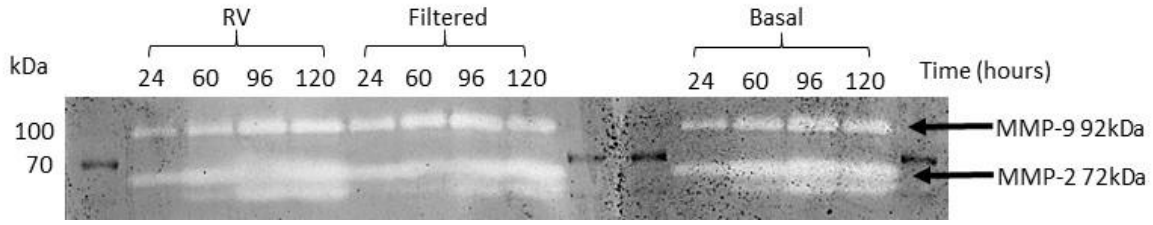

Figure 3.48 Zymograph to show MMP activity in 500µm PCLS, 24 – 120 hours post exposure to RV16, ultrafiltered RV16 or basal conditions. Tissue culture supernatant was analysed for MMP-2 (72kDa) and MMP-9 (92kDa) activity. Representative image of three independent experiments (N=3, n=6).

Analysis of 500µm PCLS tissue supernatants showed a very slight decrease in MMP-2 activity for RV16 compared to basal at 24 and 60 hours however, overall there was no significant difference in fold change against basal conditions for MMP-2 in either RV16 infected or ultrafiltered RV16 treated conditions at any time point over the culture period (P>0.05). Similarly, analysis of MMP-9 showed there was no significant difference in fold change against basal conditions for MMP-9 in either RV16 infected and ultrafiltered RV16 treated conditions at any time point over the culture period (P>0.05) (Figure 3.49).

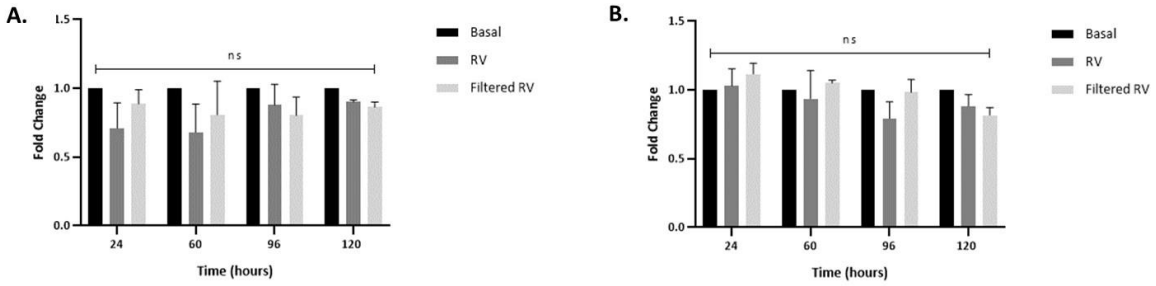

Figure 3.49 Densitometry analysis of zymographs to show MMP activity in 500µm PCLS, 24 – 120 hours post exposure to RV16, ultrafiltered RV16 or basal conditions. MMP activity in 500µm PCLS presented as fold change from basal control for MMP-2 (**A**) and MMP-9 (**B**) respectively. Bands on the gel were analysed with densitometry using ImageJ software, the relative density was calculated and compared as a fold change to the basal conditions. Results are displayed as mean ± SEM (N=3, n=6). Statistical analysis was conducted using a two-way ANOVA with multiple comparison by Tukey analysis.

3.3.14.2 Human Rhinovirus had Limited Impact on MMP Activity in Human Lump Tissue

Having shown MMP activity could be measured in 500µm PCLS the same process was replicated using tissue supernatants collected from 2 – 3mm^3 lump tissue between 24 and 120 hours post infection with RV16 or after treatment with ultrafiltered RV16 or basal conditions. Subsequently, the supernatant was electrophoresed through a 7.5% acrylamide gel containing 4mg/ml gelatine, the gels stained and imaged as described in 3.2.6.6 (Figure 3.50). Bands on the gel were analysed with densitometry using ImageJ software, the relative density was calculated and compared as a fold change to the basal conditions.

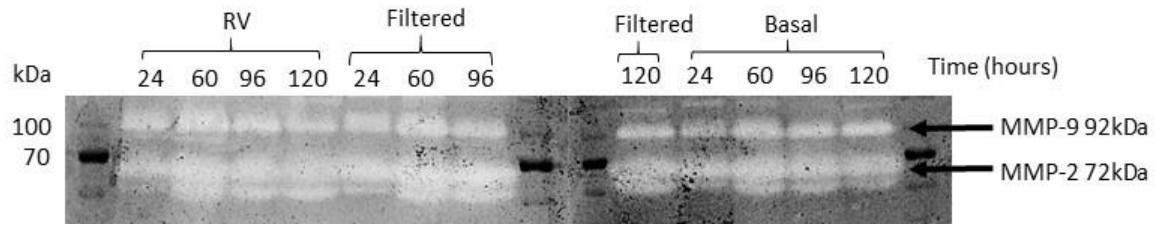

Figure 3.50 Zymograph to show MMP activity in 2 – 3mm^3 lump tissue, 24 – 120 hours post exposure to RV16, ultrafiltered RV16 or basal conditions. Tissue culture supernatant was analysed for MMP-2 (72kDa) and MMP-9 (92kDa) activity. Representative image of three independent experiments (N=3, n=6).

Analysis of lump tissue supernatant showed there was a very slight reduction in MMP-2 activity for RV16 infected conditions compared basal for all time points after 24 hours post infection however, overall there was no significant difference in fold change against basal conditions for MMP-2 in either RV16 infected or ultrafiltered RV16 treated conditions at any time point over the culture period ($P>0.05$). Similarly, analysis of MMP-9 showed a very slight reduction in activity for RV16 infected conditions compared basal for all time points after 24 hours post infection however, overall there was no significant difference in fold change against basal conditions for MMP-9 in either RV16 infected and ultrafiltered RV16 treated conditions at any time point over the culture period ($P>0.05$) (Figure 3.51).

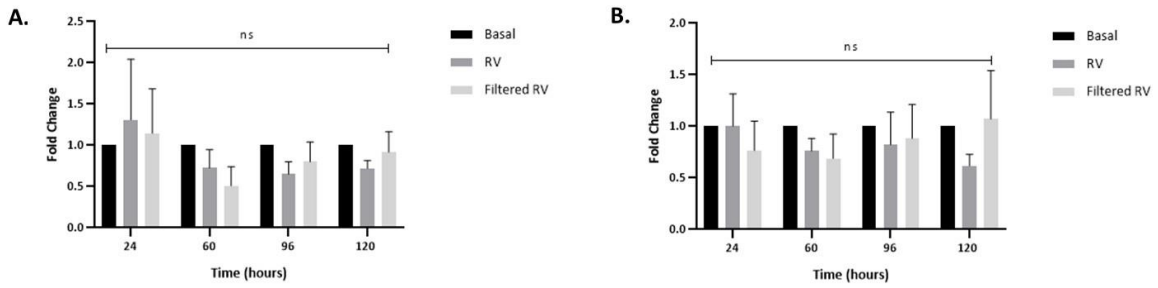

Figure 3.51 Densitometry analysis of zymograph to show MMP activity in 2 – 3mm^3 lump tissue, 24 – 120 hours post exposure to RV16, ultrafiltered RV16 or basal conditions. MMP activity in 2 – 3mm^3 lump tissue presented as fold change from basal control for MMP-2 (**A**) and MMP-9 (**B**) respectively. Bands on the gel were analysed with densitometry using ImageJ software, the relative density was calculated and compared as a fold change to the basal conditions. Results are displayed as mean ± SEM (N=3, n=6). Statistical analysis was conducted using a two-way ANOVA with multiple comparison by Tukey analysis.

3.3.15 Human Rhinovirus Infection does not Alter the Extent of Bronchoconstriction Measured in Human PCLS

To determine whether bronchoconstriction measurements were altered as a consequence of infection with RV16, ultrafiltered RV16 treatment or basal conditions, 700µm PCLS were treated with 10µM histamine 120 hours post infection and the effect on bronchoconstriction of bronchioles measured every minute for 5 minutes and subsequently at 5 minute intervals for a total of 10 minutes. Measurements were taken at x10 magnification, x1 zoom using a Zeiss SteREO Discovery.V8 microscope, as outlined in 3.2.6.8. Application of histamine to PCLS from any conditions causes bronchoconstriction to occur to a minimal extent over the 10 minute observation period however, no recovery in bronchiole size occurred over the observation period (Figure 3.52a). Due to insufficient replicates of the bronchoconstriction experiment statistical analysis could not be conducted however, the following observations can be made. When the extent of bronchoconstriction was considered as a percentage change, there was a greater level of constriction in ultrafiltered RV16 treated PCLS (22.16%) and RV16 PCLS (32.33%) compared to basal (12.61%) (Figure 3.52b). Similarly, when the extent of bronchoconstriction was considered as a fold change against basal there was approximately 1.5 fold increase in bronchoconstriction in RV16 infected and ultrafiltered RV16 treated PCLS compared to

basal (Figure 3.52c). Evidence of the reduction in bronchiole diameter was shown in the representative images taken after the application of histamine to the PCLS (Figure 3.53).

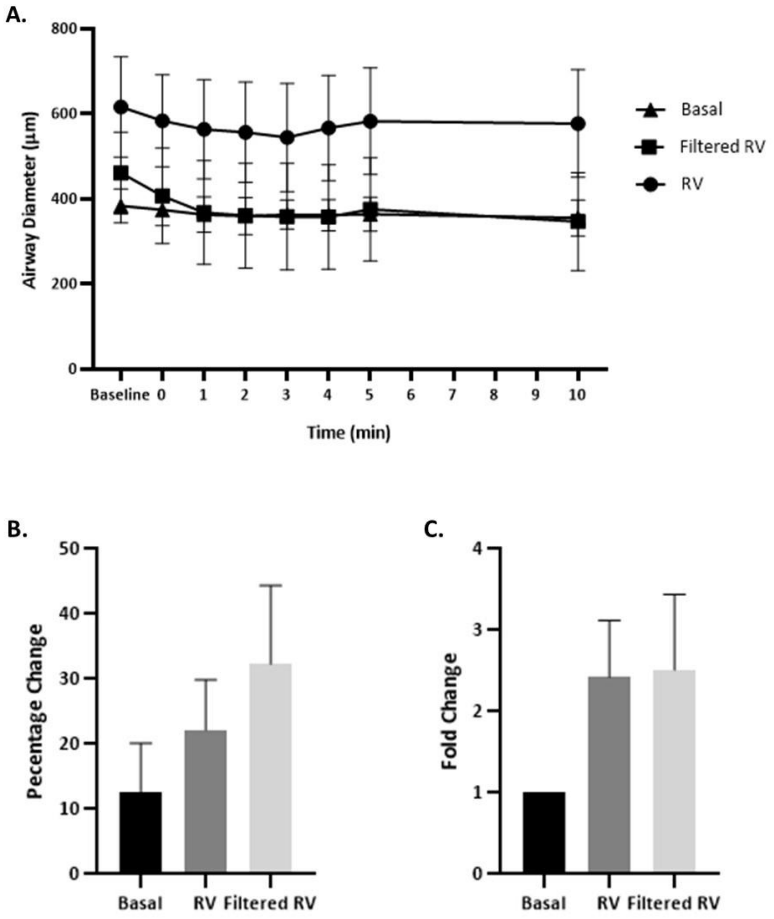

Figure 3.52 Bronchoconstriction measurements in bronchioles of 700µm PCLS treated with 10µM histamine 120 hours post infection with RV16, filtered RV16 or in basal conditions. Measurements taken every minute for 5 minutes and subsequently at 5 minute intervals at x10 magnification, x1 zoom using a Zeiss SteREO Discovery.V8 microscope (**A**), presented as maximum percentage change from baseline measurement for each condition (**B**) and as fold change against basal (**C**). Results are displayed as mean ± SEM of 2 separate bronchioles from 2 PCLS replicates per condition (N=1, n=6). Statistical analysis could not be conducted due to insufficient replicates of the experiment.

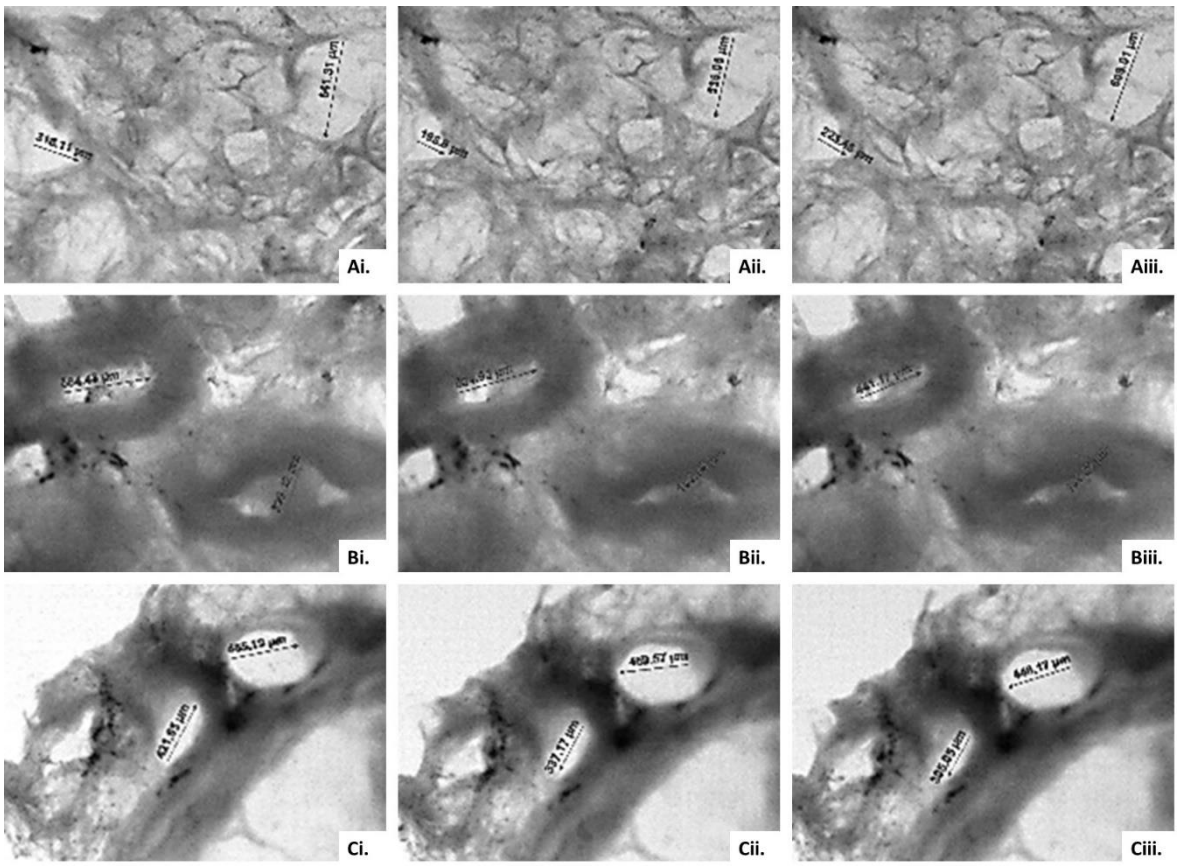

Figure 3.53 Bronchoconstriction measurements in bronchioles of 700µm PCLS treated with 10µM histamine 120 hours post infection with RV16 (**Ai – Aiii**), filtered RV16 (**Bi – Biii**) and in basal conditions (**Ci – Ciii**). Representative images of 2 separate bronchioles from 2 PCLS replicates per condition (N=1, n=6) showing measurements taken on initial application of histamine (**Ai – Ci**), 2 minutes after application (**Aii – Cii**) and 10 minutes post applications (**Aiii – Ciii**). All images taken x10 magnification, x1 zoom using a Zeiss SteREO Discovery.V8 microscope and subsequently cropped and expanded to clearly show airway of interest. Measurements read (**Ai**) 318.11µm and 641.31µm, (**Aii**) 198.80µm and 536.06µm, (**Aiii**) 223.48µm and 609.01µm, (**Bi**) 339.12µm and 584.43µm, (**Bii**) 150.75µm and 534.93µm, (**Biii**) 165.52µm and 441.17µm, (**Ci**) 421.65µm and 465.19µm, (**Cii**) 337.17µm and 459.57µm and (**Ciii**) 305.05µm and 448.17µm.

3.3.16 Cytokine Array Analysis Revealed Human Rhinovirus Infection Altered Expression of Some Proinflammatory Mediators

Existing studies regarding the effects of hRV on cytokine release have shown that a number of proinflammatory cytokines including IL-1, IL-6, IL-8, TNF-α, IFN, GM-CSF, RANTES and

TGF-β1 are upregulated in response to an infection *in vitro* and *in vivo* (Griego *et al*, 2000; Tang *et al,* 2016). To determine whether a similar response can be measured *ex vivo* a cytokine array membrane pre-spotted with 42 human cytokine antibodies was treated with pooled supernatant collected from 500µm PCLS between 24 and 120 hours post infection with RV16 or basal conditions. Subsequently, cytokine array membranes were treated as outlined in 3.2.6.9, with imaging of the cytokine array enabled through treatment with HRP-conjugated streptavidin (Figure 3.54; Table 3.8). Cytokine array membranes were imaged using a Li-cor C-Digit® Blot Scanner. Dots on the membranes were analysed with densitometry using ImageJ software, the integrated density was calculated, adjusted for background and normalised against a one of the positive control spots (randomly selected). Subsequently integrated density was compared as a fold change to the basal conditions.

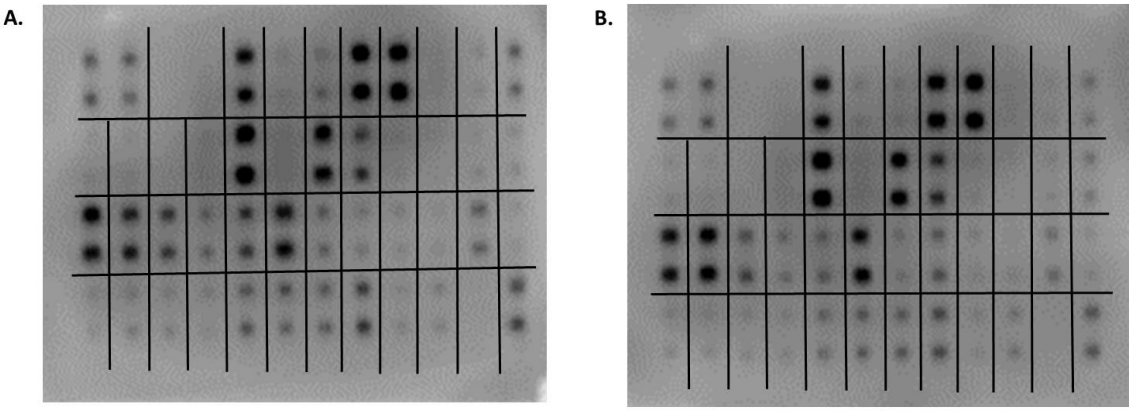

Figure 3.54 Cytokine array membrane to showing cytokine activity in pooled supernatant from 500µm PCLS, collected 24 – 120 hours post exposure to RV16 (**A**) or basal conditions (**B**). Representative image of two independent experiments (N=2, n=4).

	A	B	C	D	E	F	G	H	I	J	K	L
1	Pos	Pos	Neg	Neg	ENA-78	GCSF	GM-CSF	GRO	GRO-α	I-309	IL-1α	IL-1β
2	Pos	Pos	Neg	Neg	ENA-78	GCSF	GM-CSF	GRO	GRO-α	I-309	IL-1α	IL-1β
3	IL-2	IL-3	IL-4	IL-5	IL-6	IL-7	IL-8	IL-10	IL-12 p40/p70	IL-13	IL-15	INF-γ
4	IL-2	IL-3	IL-4	IL-5	IL-6	IL-7	IL-8	IL-10	IL-12 p40/p70	IL-13	IL-15	INF-γ
5	MCP-1	MCP-2	MCP-3	MCSF	MDC	MIG	MIP-1δ	RANTES	SCF	SDF-1	TARC	TGF-β1
6	MCP-1	MCP-2	MCP-3	MCSF	MDC	MIG	MIP-1δ	RANTES	SCF	SDF-1	TARC	TGF-β1
7	TNF-α	TNF-β	EGF	IGF-1	Angiogenin	Oncostatin M	Thrombopoietin	VEGF	PDGF BB	Leptin	Neg	Pos
8	TNF-α	TNF-β	EGF	IGF-1	Angiogenin	Oncostatin M	Thrombopoietin	VEGF	PDGF BB	Leptin	Neg	Pos

Table 3.8 Tissue culture supernatant was analysed for 42 human cytokine antibodies outlined above, these correspond to the lines shown on the images in figure 3.55.

Due to the large amount of data that was generated from the cytokine array, the fold change values were grouped together to make any changes easier to identify. The measurements collected for basal were set to a fold change of 1.0 to allow for virally infected sampled to be compared to basal (Flaherty *et al*, 2019). Using this as a baseline, values of greater than 1 were considered to show an upregulation of any given cytokine, whilst a value of less than 1 were considered to represent a down regulation of any given cytokine (Yu *et al*, 2019). Using these values alone would have produced groups containing a large number of cytokines, with the exception of no change, therefore smaller ranges were utilised to give a clear indication of which cytokines had shown the most change against basal. Given the very small changes which were observed, a range of 0.2 fold change between each group was utilised, rather than whole numbers which were utilised in other studies where larger changes were observed (Chandran *et al*, 2017; Lu *et al*, 2020), thus enabling data to be presented in a manner which was easier to interpret than if each fold change value was listed.

Whilst it was not possible to determine whether the up or down regulation of a cytokine in response to infection with RV16 was significant due to insufficient replicates, based on the density of the dots there appeared to be some variation in activity between 500µm PCLS tissue supernatant infected with RV16 compared to basal (Figure 3.55). Based on fold change values, there was an upregulation in IL-6, MCP-3, MCSF, TARC, TGF-β1 and IGF-1 in RV16 infected supernatant compared to basal. Whilst there was no change in TNF-β, Thrombopoietin and Leptin. All other cytokine responses appear to be downregulated to a limited extent however, in the case of a number of cytokines there was less than a 0.2 fold change in RV16 responses compared to basal, which arguably could also be consider as showing no change (Figure 3.56; Table 3.9).

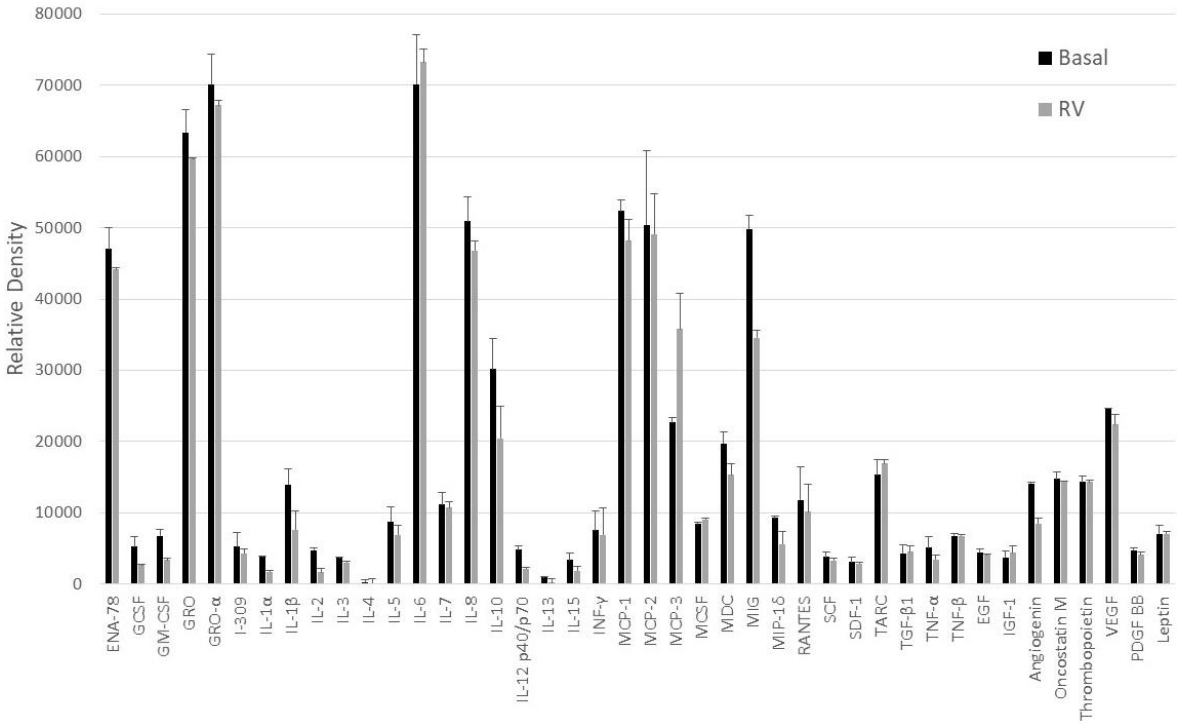

Figure 3.55 Densitometry analysis of cytokine array in pooled supernatant collected from 500µm PCLS, 24 – 120 hours post exposure to RV16 or basal conditions. Integrated density curve was calculated using ImageJ, adjusted to account for the background and normalised against a randomly selected positive control dot. Results are displayed as mean ± SEM (N=2, n=4). Statistical analysis could not be conducted due to insufficient replicates of the experiment.

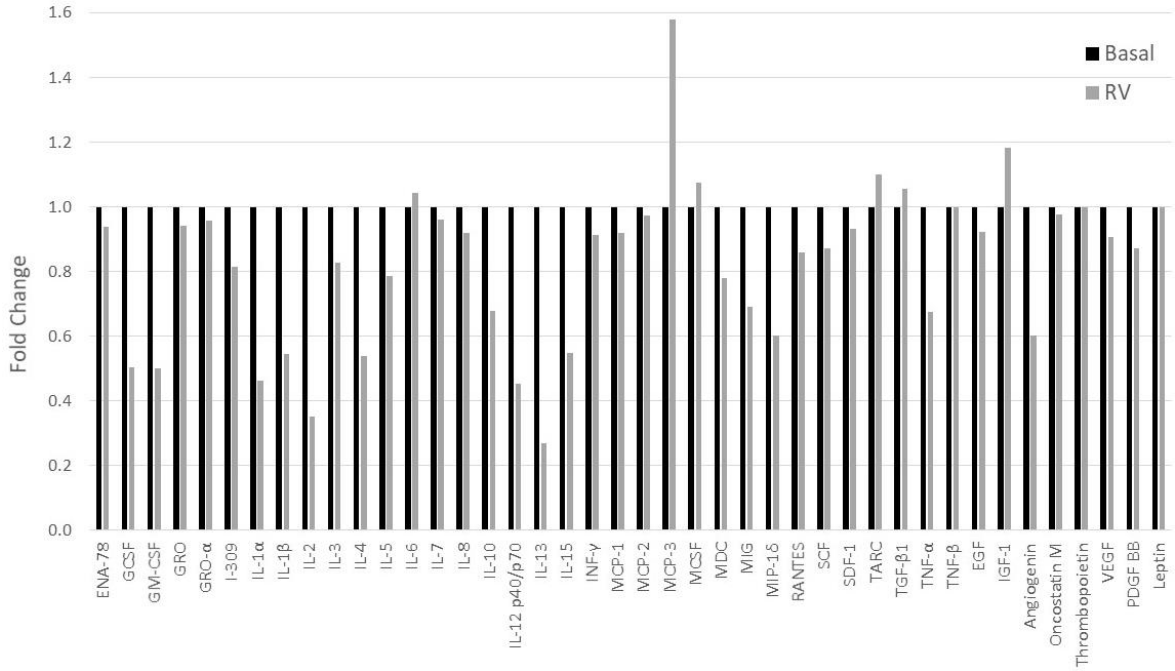

Figure 3.56 Fold change from basal control to show difference in density of cytokines in pooled supernatant collected from 500µm PCLS, 24 – 120 hours post exposure to RV16 or basal conditions. Integrated density curve was calculated using ImageJ, adjusted to account for the background, normalised against a randomly selected positive control dot and fold change calculated against changes in basal conditions. Statistical analysis could not be conducted due to insufficient replicates of the experiment.

Fold Change	Cytokine
1.21 and over	MCP-3
1.01 – 1.20	IL-6, MCSF, TARC, TGF-β1, IGF-1
1.00 (no change)	TNF-β, Thrombopoietin, Leptin
0.80 – 0.99	ENA-78, GRO, GRO-α, I-309, IL-3, IL-7, IL-8, INF-γ, MCP-1, MCP-2, RANTES, SCF, SDF-1, EGF, Oncostatin M, VEGF, PDGF BB
0.60 – 0.79	IL-5, IL-10, MDC, MIG, MIP-1δ, Angiogenin
0.40 – 0.59	GCSF, GM-CSF, IL-1α, IL-1β, IL-4, IL-12 p40/p70, IL-15, TNF-α
0.39 and below	IL-2, IL-13

Table 3.9 Cytokines grouped based on observable fold change against basal, with fold change represented as no change (1.00), upregulation (≥1.01) or downregulation (≤0.99) in cytokine activity.

3.3.17 Western Blot Analysis

3.3.17.1 Rhinovirus Infection does not Significantly Increased ICAM-1 or TRPV4 Protein Expression in Human PCLS

To identify whether there were any changes in global protein expression of TRPV4 and ICAM-1 after *ex vivo* infection, whole tissue lysates were isolated from 500µm PCLS, 120 post exposure to RV16, ultrafiltered RV16 or in basal conditions. Lysates were collected and western blot analysis conducted as outlined in 3.2.7 and probed for global protein expression of TRPV4, ICAM-1 and the loading control α-tubulin (Figure 3.57).

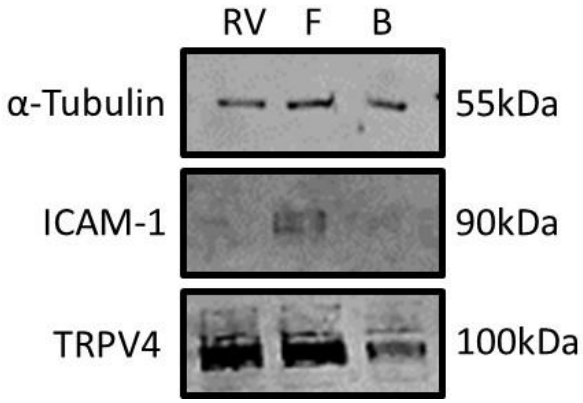

Figure 3.57 Western blot analysis to show protein expression of TRPV4, ICAM-1 and α-tubulin in 500µm PCLS, 120 hours post exposure to RV16, ultrafiltered RV16 or basal conditions, conditions represented on image as RV, F and B respectively. Membranes were loaded with 50µg of protein from whole tissue lysates. Membranes were probed for expression of TRPV4 with anti-TRPV4 antibody, ICAM-1 with anti-ICAM-1 antibody and α-tubulin as a loading control with anti-α-tubulin (expected molecular weights 100kDa, 90kDa and 55kDa respectively). All antibodies were used at a concentration of 1:500. Data represents three independent experiments (N=3, n=3).

Densitometry analysis of the western blots, after normalisation against the loading control showed no significant difference in protein expression of either ICAM-1 or TRPV4 post RV16 infection or post treatment with ultrafiltered RV16 compared to basal ($P>0.05$). This being said, although not significant there appears to be some increase in TRPV4 protein expression in RV16 infected tissue lysates compared to both basal and ultrafiltered RV16

treated tissue lysates. A similar increase in protein expression was also observed for ICAM-1 in both RV16 infected and ultrafiltered RV16 treated tissue lysates compared to basal (Figure 3.58).

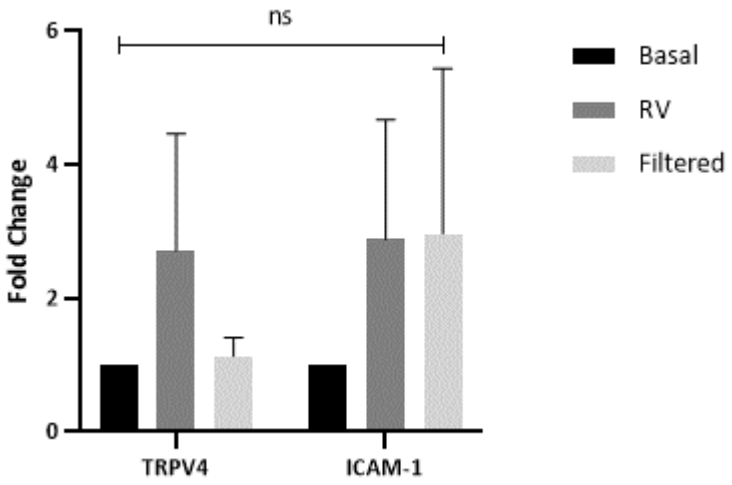

Figure 3.58 Densitometry analysis of western blots showing changes in protein expression of TRPV4 and ICAM-1 in whole tissue lysates of 500µm PCLS, 120 hours post exposure to RV16, ultrafiltered RV16 or basal conditions. Changes in protein expression were normalised against the loading control α-tubulin and presented as fold change from basal control. Results are displayed as mean ± SEM (N=3, n=3). Statistical analysis was conducted using a two-way ANOVA with multiple comparison by Tukey analysis.

3.3.17.2 Rhinovirus Infection does not Significantly Increased ICAM-1, P2X3, Muc5AC or TRPV4 Protein Expression in Human Lump Tissue

Having shown some variation in protein expression of TRPV4 and ICAM-1 in 500µm PCLS the same process was replicated using whole tissue lysates isolated from 2 – 3mm^3 lump tissue, 120 post exposure to RV16, ultrafiltered RV16 or in basal conditions. Lysates were collected and western blot analysis conducted as outlined in 3.1.7 and probed for global protein expression of TRPV4, P2X3, ICAM-1, Muc5AC and the loading control α-tubulin (Figure 3.59).

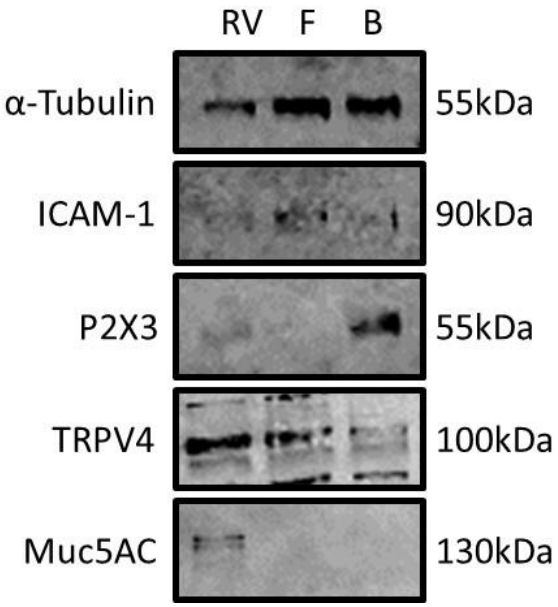

Figure 3.59 Western blot analysis to show protein expression of TRPV4, P2X3 ICAM-1 and Muc5AC in 2 – 3mm^3 lump tissue, 120 hours post exposure to RV16, ultrafiltered RV16 or basal conditions, conditions represented on image as RV, F and B respectively. Membranes were loaded with 50µg of protein from whole tissue lysates. Membranes were probed for expression of TRPV4 with anti-TRPV4 antibody, P2X3 with anti-P2X3 antibody, ICAM-1 with anti-ICAM-1 antibody, Muc5AC with anti-Muc5AC antibody and α-tubulin as a loading control with anti-α-tubulin (expected molecular weights 100kDa, 55kDa, 90kDa 130kDa and 55kDa respectively). All antibodies were used at a concentration of 1:500. Data represents three independent experiments (N=3, n=3).

Densitometry analysis of the western blots, after normalisation against the loading control showed no significant difference in protein expression of TRPV4, P2X3, ICAM-1 or Muc5AC post RV16 infection or post treatment with ultrafiltered RV16 compared to basal ($P>0.05$). Whilst, not significant there was an increase in both TRPV4 and Muc5AC protein expression in RV16 infected tissue lysates compared to both basal and ultrafiltered RV16 treated tissue lysates. Similarly, there was an increase in protein expression of ICAM-1 in both RV16 infected and ultrafiltered RV16 treated tissue lysates compared to basal. Conversely, there was a very slight decrease in P2X3 protein expression in both RV16 infected and ultrafiltered RV16 treated tissue lysates compared to basal (Figure 3.60).

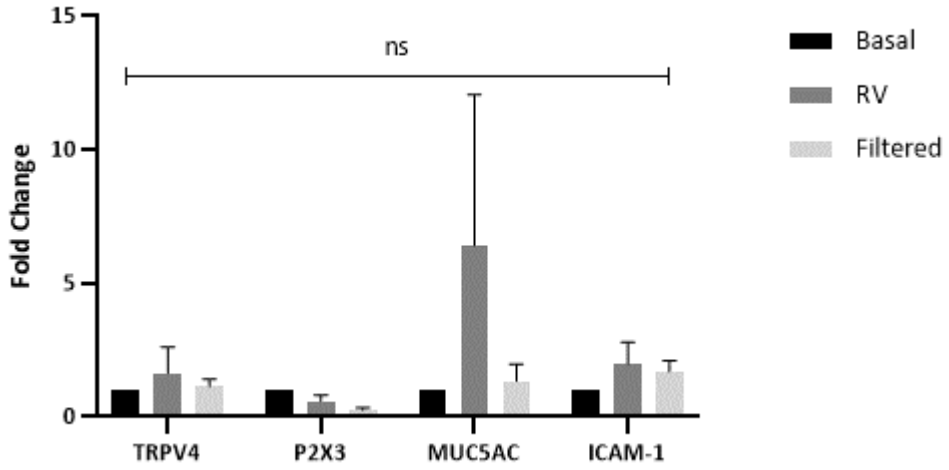

Figure 3.60 Densitometry analysis of western blots showing changes in protein expression of TRPV4, P2X3 ICAM-1 and Muc5AC in whole tissue lysates of 2 – 3mm^3 lump tissue, 120 hours post exposure to RV16, ultrafiltered RV16 or basal conditions. Changes in protein expression were normalised against the loading control α-tubulin and presented as fold change from basal control. Results are displayed as mean ± SEM (N=3, n=3). Statistical analysis was conducted using a two-way ANOVA with multiple comparison by Tukey analysis.

3.4 Discussion

3.4.1 PCLS Thickness has Limited Impact on Viability

Existing studies which utilise PCLS as a model typically maintain slices for around 72 hours, although in some instances this time is extended (see 1.1.9). Similarly, the optimum PCLS thickness specified in many studies varies widely, with the 200 – 300µm range being most extensively used (see 1.1.8 and table 1.3). However, due to the practicalities of infecting the PCLS with RV16 having an extended time frame beyond the 72 hour window would make the procedure more feasible. Furthermore, the RV16 infections of A549 and Beas-2b cells showed more noticeable changes after culture periods of around 7 days (see 2.3.7). Due to these observations identifying the length of time PCLS could be maintained as viable and the optimum thicknesses to use formed the first focal point of this chapter.

To determine the optimal PCLS thickness and viability for both PCLS and lump tissue, various methods were utilised to ensure similar observations were made across a range of various measures. The gross morphology images taken of individuals PCLS over a 7 day culture period showed little change in morphology when any thickness was considered however, there were some observable colour changes, with tissue becoming darker at 7 days post slicing for all but the 300µm slices. This being said, it is difficult to produce a highly magnified image of these slices due to the nature of the microscope used, which limits the amount of detail that can be observed. Furthermore, whilst this method allows the same slices to be imaged multiple times during the culture period, the transportation of the slices between the incubator and microscopy suite prevents identical positioning of the slices being achieved at each time point which further hampers any changes being observed with ease. Given the limited changes observed in the gross morphology, the cellular morphology was also considered through the use of H&E staining. Using cryopreserved tissue sections, tissue was retrieved immediately after slicing and then at intervals over a 7 day culture period. This showed little difference in the cellular structure at any time point for 300 and 500µm thicknesses but with some loss of structural integrity of the cells and connective tissue after 7 days in 700 and 1000µm thick PCLS, an observation also made by Neuhaus *et al* (2017). These images support the observations of the gross morphology although the sectioning technique requires further development to improve the final quality of the sections. Additionally, these sections also show persistence of agarose within the alveolar spaces and larger airways/blood vessels although, an alternative cause of these large areas of non-cellular material could be mucus which is often present in diseased or damaged tissue (Fisher *et al*, 1994; Martin *et al*, 1996). To identify this non-cellular material further immunohistochemistry processing using Muc5AC and Muc5B antibodies could determine if the material is mucus or agarose.

To support observations around the morphology of PCLS, LDH assays were performed utilising the same conditions to investigate the extent of cytotoxicity at different stages in the culture period. When the extent of cytotoxicity and thus viability over the seven day period is considered there was no difference between the amount of LDH released at 120 or 168 hours post slicing at any thickness however, there was a significant difference between 24 hours and 120 or 168 hours. When PCLS thicknesses were compared at

different time points, there was no difference in LDH released from any thickness of lysed tissue after 24 hours in culture however, as time in culture increases the amount of LDH released by 1000µm PCLS is noticeably reduced compared to all other thicknesses of PCLS, indicating an increased level of cytotoxicity and thus reduced viability in 1000µm PCLS compared to other thicknesses. It should be noted that the LDH released at 24 hours was lower in all thicknesses compared to 120 or 168 hours. This contradicts expected findings which would suggest that the more LDH releases after lysis is indicative of cells being more viable (Fotakis and Timbrell, 2006). Given that tissue viability should decrease over time the LDH release post lysis should also decrease, thus the increased LDH release may be a reflection of the deteriorating tissue quality resulting in more effective and complete lysis of the tissue to release stored LDH from viable but also potentially apoptotic cells, as LDH is typically used to show extent of necrotic cells due to LDH being released in response to membranes rupture (Maes *et al*, 2015). This being said, consistently lower release of LDH by 1000µm PCLS compared to other thicknesses would suggest that this thickness was less viable for further studies and although the findings for 24 hours are somewhat perplexing, the lack of variability between 300, 500 and 700µm PCLS after 120 or 168 hours suggest that any thickness can be utilised and the decision should be based on the experimental need. Furthermore, the spike in LDH after lysis at 120 or 168 hours suggests that the tissue remains viable and thus provides suitable longevity of the tissue for subsequent infection and measurement of effect.

As an alternative to PCLS, small 2 – 3mm^3 tissue lumps were also utilised, as the lack of slicing helps to retains some of the lung parenchyma and typical structure of the lower respiratory tract. When LDH released from lysed tissue at 24, 120 and 168 hours was considered for inflated lump tissue there was no difference at any time point. Interestingly, there is some increase in LDH release as time progresses however, this was not as exaggerated as the differences seen in the PCLS. Similarly, when uninflated lumps are considered there is no difference at 120 and 168 hours however, there was a significantly reduced LDH release at 24 hours compared to 168 hours. When compared to PCLS, inflated lumps appeared more viable at 24 hours compared to any PCLS thickness whilst there was no difference in viability at 120 hours with the exception of 1000µm PCLS. At 168 hours there was no difference in viability when 500 and 700µm PCLS were considered however,

inflated lump tissue appeared less viable than 300µm and more viable than 1000µm PCLS. These observations suggest that inflated lump tissue provides a viable alternative to PCLS for later experimentation with RV16. When uninflated lumps were compared to inflated lumps, the uninflated tissue appears significantly more viable at 24, 120 and 168 hours than the inflated tissue. This may be a reflection of the inflation process causing some minimal damage to the tissue, which may have an impact on the long term viability or alternatively may be due to the retained agarose which not only makes complete lysis more difficult but also increases the final weight of the tissue lump. This increased tissue mass could potentially be reflected in a reduced absorbance per milligram of tissue, as a similar amount of LDH is likely to be released by the tissue, but the increased weight would thus reduce the value per milligram as the inflated tissue weighs more than the uninflated tissue. Whilst uninflated tissue would also provide a suitable alternative, the benefits of inflating the tissue include restoring lungs to a state more akin to the *in vivo* environment (Dandurand *et al*, 1993; Brook *et al*, 2010) and enables tissue slicing to be conducted which provides good surface area availability for exposure to test compounds thus making inflation prior to sectioning into lumps or slicing the better option for future experiments.

To confirm LDH findings PCLS viability was also calculated using trypan blue exclusion assay. When 500, 700 and 1000µm PCLS were considered at each time point there was no difference in viability although it did progressively decline as time in culture increases. Whilst viability of 300µm PCLS showed the most noticeable decrease from baseline over the duration of the culture period. This reduction in viability demonstrates that tissue slowly deteriorates over the culture period but that it does not fall much below 80% in all thicknesses and thus supports the findings of the LDH assay which indicated tissue was still viable after a 7 day period. Interestingly the lowest viability is seen in the thinnest PCLS which contradicts previous studies which suggests viability is enhanced due to better nutrient exchange in thinner PCLS (Umachandran *et al*, 2004), the reason for such an observation is unclear and may be a reflection on the difficulty of obtaining PCLS of 300µm, subsequently causing more damage to the tissue and reducing the long term viability of the tissue. Similarly, when inflated tissue lumps are considered viability is maintained above 80% for the duration of the culture period. Curiously, there is a drop in viability at 120 hours before increasing again slightly at 168 hours. The relatively high viability supports the LDH

data and the decrease in viability at 120 hours may reflect differences in tissue samples and the position collected from the larger sample. The uninflated lump tissue also shows maintained viability over the 7 day culture period with minimal decrease over time. Interestingly, the same drop in viability is seen at 120 hours which again may reflect the position of collection from the larger sample or alternatively may be the result of a single donor with a lower overall viability that has subsequently affected the data in a negative manner. When inflated lump tissue is compared to PCLS there is no difference in viability with the exception of 120 hours compared to 1000µm, which is in line with the previous discussion about the noticeable decrease in viability. Similarly, when inflated and uninflated tissue is compared there is no difference in viability over the culture period. The trypan blue exclusion data supports the LDH, further suggesting that there is little difference between various thicknesses of PCLS or lump tissue, thus any thickness could be utilised and the optimal thickness depends on the experiment being undertaken rather than solely on the long term viability of the tissue.

Having demonstrated that there is little difference in cytotoxicity and viability depending on the thickness of the tissue slice, alternative methods of showing changes to the PCLS were also utilised. Use of TEER over a 7 day culture period showed a decrease in resistance measurements through the duration of the culture period which may reflect a reduction in tissue integrity. Whilst the TEER measurements show a decrease over the duration of the culture period, whether these values represent any specific effect needs to be considered. The measurements recorded are noticeably lower than those taken in chapter 2 when cell lines were utilised, with a maximum of approximately $32\Omega.cm^2$ recorded for tissue compared to approximately $50\Omega.cm^2$ and $70\Omega.cm^2$ for A549 and Beas-2b cells respectively. Although these values are adjusted to account for the presence of the membrane, which provides a certain degree of resistance, the low values would suggest that the values do no truly represent the resistance within the tissue. Furthermore, the structure of the lung tissue, with the presence of numerous airways (as shown through gross morphology and histology images) means that the tissue is unlikely to cover the membrane completely, instead there will be gaps across the entire surface. In addition the agarose which infiltrates the airways may also add to the total resistance (Pomfret *et al*, 2013). This being said, the resistance does decrease over the culture period, so may reflect some changes to the tissue

quality. However, equally it may reflect the loss of agarose through media changes or changes to the position of the tissue on the membrane owing to the PCLS not being adhered. Further development of this method would be beneficial if it is to be used more effectively to measure tissue integrity.

Finally to further show that tissue is viable after processing and reacts to potent bronchoconstrictive agents in a manner akin to the *in vivo* environment tissue was treated with methacholine or histamine. When PCLS were exposed to methacholine a small amount of bronchoconstriction was observed however, when PCLS were exposed to histamine, bronchioles constrict by approximately 30% demonstrating tissue remains viable after slicing and the *ex vivo* response to the bronchoconstrictive agent is similar to the response observed *in vivo* (Kowal *et al*, 2017). Furthermore, the observed bronchoconstriction after treatment of PCLS with histamine supports observations by Wohlsen *et al* (2003) and Ressmeyer *et al* (2010) who noted constrictions of up to 40% and 50% of initial airway area respectively, thus suggesting the bronchoconstriction observed is akin to the *in vivo* response.

Given the observations around the viability of PCLS it seems reasonable to suggest that experimental periods of up to 7 days is feasible without any significant impact on tissue viability, supporting observations made by Neuhaus *et al* (2017) and to some extent Placke and Fisher (1987). Furthermore, the data indicates that there is little difference between the varying thicknesses of PCLS. Thus whilst 300 and 500µm PCLS has the least variability in relation to LDH data, the trypan blue data indicates that 700 and 1000µm PCLS can also be utilised in relevant experiments. For example 700µm PCLS are better suited to conducting bronchoconstriction measurements as they are more resilient, less fragile and easier to handle, making positioning of the PCLS to take measurements more effective and reliable, for similar reasons the use of 1000µm PCLS provide a good basis for TEER experiments. Thus based on the aforementioned observations 500µm PCLS were chosen as the optimum thickness for the majority of experiments, with 700µm PCLS being utilised for bronchoconstriction measurements and 1000µm PCLS used in TEER analysis. Although, the chosen optimum thickness is greater than many other studies which utilised 200 –

300µm (Sturton *et al*, 2008; Schlepütz *et al*, 2012; Bai *et al*, 2016; Alsafadi *et al*, 2017; Zmora *et al*, 2017), other studies have utilised thicknesses between 400 – 750µm (Nave *et al*, 2008; An *et al*, 2012; Temann *et al*, 2017), suggesting the deviation from the more commonly used thicknesses is not completely unprecedented. Finally it should also be noted that small lump tissue provided LDH and trypan blue data which was comparable to PCLS data, thus small lump tissue was also utilised in subsequent experiments to provide an alternative method of investigating the impact of RV16 infection on the tissue.

3.4.2 Infection of PCLS and Lump Tissue with RV16 has a Minimal Effect on Cytotoxicity, Bronchoconstriction and Cytokine Release.

Due to the lack of literature relating to the infection of human lung tissue *ex vivo* with RV16 the infection procedure required optimisation prior to making any subsequent measurements. Based on initial observations using LDH and factors relating to methodological issues, an optimum MOI of 0.025 was determined and appeared to have the most noticeable effect on the tissue viability. Whilst, the chosen MOI was higher than that used by Kennedy *et al* (2018) when infecting *ex vivo* PCLS with RV39, other *in vitro* studies with RV16 utilise MOIs of 0.03 – 0.04 (Oliver *et al*, 2006; Kuo *et al*, 2011) which is comparable to the MOI used in this study and thus could be considered physiologically relevant. To confirm successful infections of PCLS and lump tissue, modified titre plates were performed initially with variable MOIs, which supported the chosen MOI of 0.025, as lower MOIs caused less consistent infections. Subsequent infections of all PCLS thicknesses and lump tissue showed evidence of viral replication, as application of tissue effluent to Hela Ohio cells showed evidence of cell rounding and sloughing when collected from infected tissue whilst effluent from tissue exposed to sham infection (ultrafiltered RV16) or retained in basal conditions had little impact on the growth of Hela Ohio cells.

To further support the successful infection of the tissue observed in the titre plates, qPCR was utilised on concentrated tissue effluent and tissue lysates to quantify a viral load. This confirmed that actively replicating virus could be measured in 1000µm PCLS and lump tissue effluent but not in 500µm PCLS tissue effluent. Lack of measureable viral load in the 500µm PCLS may be due to the copy number being too low to determine rather than an

absence of replicating virus, as titre plates suggested that replicating virus was being released into the effluent. Similarly, no viral load was detectable in the tissue lysates, the reason for this is less clear and may have a number of explanations including damage to viral RNA during the production of tissue lysates, poor RNA extraction overall, the presence of agarose reducing the successful RNA extraction or the very high level of cellular RNA could have reduced the effectiveness of the process, especially given the success seen in the tissue effluent. The variability of viral load particularly in the lump tissue effluent is also noteworthy as the large variation may be due to the number of susceptible cells to RV16 in one piece of tissue compared to another due to the manner in which the tissue is collected from a larger tissue sample. Whilst, these differences are evident, overall the infection appears successful due to the presence of viral RNA in tissue effluent from infected tissue while sham infection and basal conditions show no evidence of viral RNA.

Having shown tissue can be successfully infected, the cytotoxic effect of RV16 on tissue was considered through numerous measures. Initially LDH was chosen to investigate any cytotoxic effect induced by RV16 infection. When 500 and 1000µm PCLS were considered there was no difference in LDH release in any condition however, when lump tissue was analysed there was a significant reduction in the LDH released from RV16 infected tissue compared to either sham infection or basal conditions, suggesting that the RV16 infection was having a cytotoxic effect on the lump tissue resulting in a decreased viability. To further support these findings, a trypan blue exclusion assay was conducted. As with the LDH findings, there was no significant change in viability however, there was a slight reduction in viability of infected 500 and 1000µm PCLS compared to sham infection and basal, similarly a small reduction was also seen in lump tissue. Interestingly, when the total cell count (post tissue dissociation) was considered there was a reduction in the number of cells per milligram of tissue in infected tissue compared to sham infection and basal tissue (data not shown), which would suggest that whilst there is only a minimal reduction in viability of infected tissue, but also that total cell count may have some role to play, an observation which was also made in Beas-2b cells infected with RV16 (see 2.4.2).

Although LDH and trypan blue exclusion analysis showed similar findings and indicated that RV16 had limited impact on cytotoxicity and tissue viability, further measures were also taken in an attempt to confirm these findings. As an alternative to LDH analysis, CytoToxGlo™ assay was performed as a measure of cytotoxicity based on dead cell protease release. The CytoToxGlo™ assay is considered to be more sensitive than LDH due to measurements being made through luminescence rather than fluorescence, thus reducing likelihood of background interference (Cho *et al*, 2008). Due to insufficient reagent availability only tissue effluent collected from basal and infected tissue could be utilised. When 500µm PCLS are considered there was a no difference in dead cell protease in infected tissue effluent compared to basal. However, after lysis there was a significant increase in dead cell protease released from infected tissue compared to basal. Similarly, when lump tissue was considered there was no significant difference in dead cell protease released into the effluent over time or post lysis between the two conditions although, it should be noted that there was a slight increase in dead cell protease release post lysis by infected tissue compared to basal. The increase in dead cell protease released by infected tissue compared to basal would indicate that the virus is having a cytotoxic effect on the tissue resulting in decreased membrane integrity thus supporting some of the observations made in the LDH and trypan blue findings.

To further support the previous cytotoxicity measurements a WST-1 cell proliferation assay was conducted. When 500µm, 1000µm PCLS and lump tissue were considered there was no change in the conversion of tetrazolium salts in infected tissue compared to sham infected and basal conditions. It should be noted however, that with the exception of the lump tissue data, there tends to be an increased conversion of tetrazolium salts by infected and sham infected PCLS compared to basal. This observation would suggest increased tissue viability in infected and sham infected tissue compared to basal. The reason for these observations is not wholly clear however, Lötzerich *et al* (2018) have shown that hRV can delay apoptosis and necrosis which may explain the increased tetrazolium conversion as a consequence of infected cells not reaching the cytolytic stage thus remaining metabolically active. Furthermore, viral infection can lead to remodelling of host cell metabolism during replication (Thaker *et al*, 2019) which may also lead to the increased activity measured in this instance. Interestingly, when lump tissue is compared there is a decrease in tetrazolium

conversion in infected tissue compared to basal. This is in line with dead cell protease findings which also present a reduction in tissue viability. Given the consistency between the findings of multiple assays the differences observed between PCLS and lump tissue would suggest that the reduced processing of the lump tissue compared to the PCLS may influence the way in which the RV16 effects the tissue. Collectively all of the cytotoxicity and viability data indicates that RV16 has little impact on the viability of the tissue however, this is not wholly unsurprising given that *in vivo* studies have shown limited cytolytic effect (Ghildyal *et al*, 2005), as such this combined data would continue to support the theory that hRV causes only minimal cellular damage once adhered to a cell (Griego *et al*, 2000).

Although the combined cytotoxicity data indicates that RV16 has little impact on the viability of the tissue and as such findings are relatively consistent across all assays, it is worth considering the limitations of each assay and any impact this may have. Each viability assay has its own set of limitations which influenced the decision to conduct a wide range of tests to gain as much insight as possible about tissue viability. Although the trypan blue data is on the whole supportive of the LDH observations, it should be noted that the values obtained after several days in culture remain near to 100% viable. This seems somewhat unlikely as the tissue will begin to deteriorate once removed from the donor (Inci, 2017). The reason for such observations could be due to a multitude of factors including the various elements of the assay design and the presence of retained agarose. When the assay method is considered the first limitation relates to the dissociation process. During the process of optimising the dissociation, the tissue was left for varying periods of time including overnight for approximately 16 hours, this resulted in almost 0% viability, as the enzymes used to breakdown the collagen and connective tissues also damaged the cells (Reichard and Asosingh, 2018). Thus a shorter time frame was chosen however, this risked the tissue not fully dissociating as lung tissue is very fibrous (Reichard and Asosingh, 2018; Rogers *et al*, 2008), therefore the viability recorded may not accurately represent the viability of the tissue as some cells may not have been extracted from the PCLS or tissue lumps. Furthermore, the presence of retained agarose also hampered the dissociation process, as although the tissue was homogenised to release as many cells as possible, the mixture produced was still very gelatinous and may have resulted in cells being retained in this mixture rather than passing through the cell strainer during the wash stages, which

means dead cells are as equally likely to be left behind as live cells. This being said, the inert nature of the agarose is unlikely to have much effect on the tissue viability (Ulrich *et al*, 2011) and owing to the fact it cannot pass through the cell strainer, it should have no bearing on the actual assay itself. Whilst the trypan blue assay is easy to conduct, the dye is toxic to mammalian cells, thus the length of time a sample can be left in contact with the dye needs to be limited so as not to negatively affect results (Piccinini *et al*, 2017). Once bound to dead cells the differentiation between what constitutes a stained and unstained cells in somewhat subjective, relying on the interpretation of the user (Katsares *et al*, 2009). Moreover, the dissociation has a tendency to create small tissue fragments which owing to the presence of proteins may bind with the trypan blue which can subsequently be difficult to distinguish from cells (Piccinini *et al*, 2017), as such these factor have the potential to make final viability estimations quite inaccurate. Given the potential for variability and inaccuracy, the use of other measures of viability alongside trypan blue should be considered. To overcome some of the subjectivity relating to the use of the trypan blue assay, additional methods could be used such as live/dead staining. This method utilises calcein AM to stain live cells and ethidium homodimer-1 to stain dead cells, thus when used alongside a dead control to allow images to be normalised, may give a clearer indication of the extent of cell death which had occurred (Sanfilippo *et al*, 2011). Both trypan blue staining and live/dead staining have the drawback of only being able to distinguish between live or dead cells, thus the extent of apoptotic cells within the tissue is not discernible, leading to an assumption being made based solely on necrotic cells. To address this limitation, identification of apoptotic cells through staining with Annexin V and necrotic cells through staining with PI would be beneficial to determine if any differences arise when all stages of cell death are considered (Rieger *et al*, 2011). However, as the pathogenesis of hRV is not a result of cytolytic effect (Ghildyal *et al*, 2005) and hRV infection can result in the suppression of both apoptosis and necrosis, with cell death occurring via a caspase-independent pathway (Lötzerich *et al*, 2018), thus the methods discussed above may still be insufficient to explain changes that are occurring at a cellular level. Thus although some differences are observed, the mechanisms involved needs further investigation.

As with trypan blue staining, LDH, WST-1 and CytoToxGlo™ assays also have limitations to consider. As with trypan blue, retained agarose affects the lysis process in both LDH and

CytoToxGlo™ assays. Whilst this is perhaps less problematic owing to cells being ruptured to obtain cell content rather than needing to be retained, the addition of a lysis buffer to a homogenised tissue sample creates a gelatinous mixture which often is difficult to sample from, thus the amount of LDH or dead cell protease which is present in the sample may be an underestimation of the total amount present in the tissue. Furthermore, the LDH assay also has a tendency to underestimate the extent of cell death, as cells have to be far enough through the process of apoptosis to have damaged cell membranes and thus able to release LDH (Smith *et al*, 2011). Similarly, the WST-1 assay also have some disadvantages, such as long incubation periods, cell toxicity and limited sensitivity (Adan *et al*, 2016) however, it can be used on whole tissues slices rather than requiring the lysis step (Lauenstein *et al*, 2014), thus overcoming the issues around the retained agarose creating a gelatinous mixture which is difficult to sample from. In comparison the CytoToxGlo™ assay is considered more sensitive than the LDH and WST-1 assays owing to the use of luminescence rather than absorbance (Cho *et al*, 2008) however, faces the same issues regarding tissue lysis. This being said, the increased sensitivity which it provides makes it a valuable addition to cytotoxicity and viability studies. The range of limitations which exist for each viability assay was the driving factor for utilising a wide range of assay, as this aided in confirming any observations made regarding the effect of RV16 on viability or cytotoxicity with *ex vivo* tissue samples.

Dysregulation of tight junctions in response to hRV infection have been shown to occur in *in vitro* cell culture experiments (Lopez-Souza *et al*, 2004; 2009). Thus to identify if similar effects could be measured post infection of PCLS with RV16, tight junction and tissue integrity was assessed through the use of TEER measurements. The TEER measurements taken in 1000µm PCLS showed no significant difference in resistance measurements in infected tissue compared to basal and sham infection, although a very slight reduction in resistance for infected tissue can be observed throughout the 7 day culture period. This observation suggests that there is little change in tissue integrity in response to hRV infection, as such it is unclear from this experiment whether any change in resistance is solely owing to the tight junction integrity reducing or due to the pathogenesis of the infection. Furthermore, the aforementioned discussion regarding the histological structure of the lung tissue and the impact this may have on the TEER measurements also needs to

be considered here, as the observed changes could potentially reflect the differences in the extent of airway between each PCLS taken rather than being a virus specific effect. However, if any of the observed changes are a consequence of virus effect it is potentially due to the upregulation of ROS, leading to the destabilisation of epithelial tight junctions (Comstock *et al*, 2011) rather than any cytolytic effect, as this is typically not observed in infected cells *in vivo* (Ghildyal *et al*, 2005) thus supporting the theory that hRV causes only minimal cellular damage once adhered to a cell (Griego *et al*, 2000). Given the limitations of this method, further development is required. In addition to fully determine whether tight junction integrity is reduced, staining the PCLS for changes to occludins, claudins and tight junction protein would help to visually represent any changes in expression, overcoming the limitations discussed regarding retain agarose and airway structure, thus enabling a more conclusive reason for the aforementioned observations to be formed.

Having shown there are no clear changes to tissue integrity the next stage of investigation was to consider whether there was any change in proinflammatory response post infection. As previously shown in chapter 2, upregulation of MMP-2 and MMP-9 are linked to the inflammatory pathway and extracellular matrix degradation (Shimokawa *et al*, 2002) and potential tight junction weakening (Cauwe *et al*, 2007), with A549 and Beas-2b cells demonstrating that RV16 infection caused some slight changes in MMP-2 and MMP-9 expression. Thus a similar approach was taken with 500µm PCLS and lump tissue to identify if any changes could be observed. When PCLS tissue was considered there was no change in either MMP-2 or MMP-9 activity over time in all conditions. When lump tissue was considered the response was also similar, with no change in either MMP-2 or MMP-9 activity over time. However, in both 500µm PCLS and lump tissue there appears to be a slight reduction in MMP-2 and MMP-9 activity for infected tissue compared to sham infection and basal for all time points except 24 hours post infection. The lack of upregulation post infection with RV16 contradicts some of observations made in A549 and Beas-2b cells and those made in previous studies (Shimokawa *et al*, 2002; Cauwe *et al*, 2007), which makes forming a conclusion difficult. The reason behind the lack of change in expression post infection may reflect the length of time post infection being insufficient. As peak MMP-9 activity in BAL samples was detected between 7 to 14 days (Gualano *et al*, 2006) as opposed to the 5 days used here. Furthermore, the tissue collected is typically

from the terminal edge of a lobe and is predominately alveolar tissue. Thus the cell type infected may not truly reflect the cells which are infected in an upper respiratory tract infection and which have previously been linked to upregulation of MMP-9 (Gualano *et al*, 2006). The reason for tissue removal may also influence the MMP activity, with MMP-2 and MMP-9 expression in cancerous lung tissue being higher than in normal tissue (Merchant *et al*, 2017). Given that the predominant reason for lung resection is to remove cancerous tissue and although tumour margin is received, thus being deemed healthy, there is likely to be a global increase in MMP expression which may explain the high levels measured in basal tissue and the lack of upregulation observed post infection.

Bronchoconstriction is linked to numerous proinflammatory mediators released as a consequence of hRV infection (Joos *et al*, 1994; Bonham *et al*, 1996; Dakam *et al*, 2014; de Oliveira *et al*, 2016; Pelleg *et al*, 2016), thus to identify if the extent of bronchoconstriction changed post infection with RV16, 700µm PCLS were challenged with histamine. When compared to basal, PCLS treated with RV16 or sham infection demonstrated an increase in bronchoconstriction. Although these initial observations are promising, the lack of replicates makes it difficult to form any definitive conclusion about the effects of RV infection on bronchoconstriction. Furthermore, the response observed in the sham infection suggests that the observed response may not be solely a result of the viral infection. The increased bronchoconstriction response post RV infection may be due to the proinflammatory mediators released by the tissue in response to infection (Joos *et al*, 1994; Bonham *et al*, 1996; Dakam *et al*, 2014; de Oliveira *et al*, 2016; Pelleg *et al*, 2016). Whilst, the increased bronchoconstriction observed in the sham infection may be a consequence of the proinflammatory response caused by the cytokines still present in the retained filtrate, as although the ultrafiltration of RV16 to create a sham infection removes viral particles and viral RNA, smaller molecules such as cytokines can be retained (Papi and Johnston, 1999), thus explaining why similar increases are not seen in basal conditions. Although, differences were observed between RV16 infected and basal tissue, it is worth considering whether the persistence of agarose within the PCLS had the potential to restrict the extent to which the bronchioles can constrict in response to the application of histamine. The use of agarose is important in creating an *ex vivo* environment which recapitulates the *in vivo* environment, whereby inflation causes lungs to stretch to near

total lung capacity as observed during breath holding and maintains open airways during experimental procedures (Dandurand *et al*, 1993; Brook *et al*, 2010). As such, although agarose is retained in the PCLS and could potentially restrict bronchoconstriction, the low concentration used during the inflation process provided only limited rigidity to the tissue, thus whilst the impact of the agarose should hopefully be negligible, the full extent of the role it plays in bronchoconstriction is not completely clear.

To further explore the effects of hRV infection, a human cytokine array was utilised in an attempt to provide an overview of the cytokines and chemokines which are up or down regulated in response to RV16 infection on 500µm PCLS. A small degree of upregulation was seen in the case of IL-6, macrophage colony stimulating factor (MCSF), thymus and activation regulation cytokine (TARC), TGF-β1, insulin-like growth factor-1 (IGF-1) and monocyte chemotactic protein-3 (MCP-3) for RV16 infected tissue compare to basal. The upregulation of IL-6 is extensively documented in hRV infections and is linked to the host response and symptoms during infection due to its role in the regulation of pulmonary inflammation and mucosal antibody response (Zhu *et al*, 1996). Furthermore, IL-6 can factor in elimination of the virus (Kennedy *et al*, 2012) through the activation of T cells, stimulation of B cell differentiation and the production of antibodies (Subauste *et al*, 1995). The upregulation seen in response to RV16 infection of tissue may thus be a reflection on the tissue activating these responses in order to deal with the infection. MCSF as a cytokine is responsible for increasing anti-microbial actions of macrophages, with an early increase in MCSF concentrations seen during inflammation (Fixe and Praloran, 1998), which explains the upregulation seen in response to RV16 infection of tissue. TARC upregulation leads to the recruitment of Th2 cells during airway infection as part of the cytokine cascade, specifically IL-3 and IL-4 (Nonaka *et al*, 2010), which explains the observed upregulation of TARC in RV16 infection and may go some way to explain why no change was observed in IL-3 and IL-4, if the infection has not progressed sufficiently to cause the recruitment of T-helper type 2 (Th2) cells and the subsequent release of further cytokines. The upregulation of TGF-β1 is linked to anti-inflammatory action of neutrophils during hRV infection (Tang *et al*, 2016), furthermore, TGF-β is also linked to the potential promotion of hRV replication as a consequence of innate immune system suppression (Bedke *et al*, 2012), which supports the observed upregulation. IGF-1 is linked to the modulation of the immune

response and proinflammatory pathways (Wolters *et al*, 2017), which may explain the upregulation observed here. Finally, MCP-3 upregulation may be a consequence of the RV infection leading to the release of the chemokine to stimulate eosinophil recruitment (Xatzipsalti and Papadopoulos, 2007). In the case of these upregulated cytokines and chemokines only IL-6 and TGF-β1 were expected based on previous studies (Griego *et al*, 2000; Tang *et al*, 2016) however, the others noted are also potentially linked to later stages of the cytokine cascade and may reflect samples being collected too soon after infection. Furthermore, the slight downregulation or no change in expression observed in other cytokines including TNF-β, IL-1α, IL-10, GM-CSF and RANTES which are known to be involved in the proinflammatory response to hRV infection (Griego *et al*, 2000; Tang *et al*, 2016), could also be due to the infection not having progressed for sufficiently long enough to cause the expected upregulation. Whilst, a number of immune cells including neutrophils, macrophages, dendritic cells and T cells are retained in PCLS (Lyons-Cohen *et al*, 2017), the recruitment of cells which circulate in the blood during the inflammatory response cannot be replicated in this model (Henjakovic *et al*, 2008b), thus the absence of these cells may prevent the upregulation of some cytokines. As mentioned in previous aspects of the discussion the higher levels of cytokines and chemokines measured in basal tissue could be a reflection on the general health of the tissue due to the presence of underlying respiratory disease such as cancer (Staal-van den Brekel *et al*, 1995) and COPD (Kang *et al*, 2012).

It should be noted that due to insufficient replicates statistical analysis could not be performed, thus firm conclusions are difficult to form and further replicates would help to continue the development of the current observations. The limited number of replicates and lack of ultrafiltered virus control are both noteworthy limitations in this particular analysis of RV16 effect on *ex vivo* tissue. Due to financial constraints, a total of four membranes could be purchased, whilst this would have enabled a single replicate of RV16 infected, ultrafiltered RV16 treated and basal tissue to be conducted, it was deemed more appropriate to replicate RV16 and basal conditions twice, to increase the likelihood of identifying any changes (Biau *et al*, 2008). The lack of an ultrafiltered virus control means there is a risk that effects which are caused as a consequence of the virus binding to the ICAM-1 receptor on cells alone, rather than due to the presence of any cytokines and small

molecules in the culture media, which may have arisen during propagation of the virus, may be missed (McClain *et al*, 2016). However, because ultrafiltration does not remove small molecules such as cytokines but only viral particles and viral RNA, some of the observed changes seen the viral sample may have also been mirrored in the sample exposed to the ultrafiltered virus control (Papi and Johnston, 1999). Whilst, the use of an ultrafiltered virus control may cause some increase production of cytokines compared to basal, it would be beneficial to include sham infection samples alongside the RV16 treated and basal samples to give a more balanced view of the effect of RV16 on the cytokine release in *ex vivo* tissue. In addition, expansion of the cytokines array data though the use of ELISAs would give increased specificity and a clearer image of the inflammatory response of hRV infections *ex vivo*.

Alongside the assessment of viability and changes to cytokine and chemokine activity, changes in global protein expression was also considered through western blot analysis. When 500µm PCLS was considered there was no significant difference in TRPV4 or ICAM-1 expression in RV infected tissue lysates compared to basal and sham infection. Owing to large S.E.M in the data, any potential for significant data is lost however, it is worth considering why any small difference which can be observed in the data may have occurred. The slight increase in TRPV4 expression may reflect the mechanism of infection whereby hRV depletes calcium stores to aid in viral replication. Thus given the role of TRP channels in calcium flux across the membrane may explain the slight increase in expression in order to facilitate the viral replication process (Chen *et al*, 2020). Similarly, there is a slight increase in ICAM-1 protein expression in RV infected and sham infected tissue lysates compared to basal. As a member of the major group serotypes of hRV, RV16 uses ICAM-1 to bind to the cell surface (Papi and Johnston, 1999), thus the upregulation of the protein may aid in the spreading of hRV within the respiratory tract and contribute to the inflammatory response (Grünberg *et al*, 2000). Given soluble factors can be retained after ultrafiltration of RV16 to create a sham infection, the similar increase seen in ICAM-1 expression may be a result of these factors interacting with the tissue as seen in other experiments. A number of studies on airway epithelial cells have demonstrated an upregulation in ICAM-1 in response to hRV infection. Suggesting ICAM-1 upregulation increases susceptibility of surrounding cells to hRV binding enhancing spread, whilst also

being related to the pathogenesis of infection, leading to cytokine production and subsequent inflammation (Terajima *et al*, 1997; Yamaya *et al*, 1999; Grünberg *et al*, 2000; Othumpangat *et al*, 2012). Similarly, Shukla *et al* (2017), demonstrated in fixed human tissue that individuals with obstructive airway disease had an increased expression of ICAM-1 compared to individuals without obstructive airway disease, which may explain the increased susceptibility to hRV infections in these individuals. Additionally Winther *et al* (2002), demonstrated increased ICAM-1 expression in nasal epithelial cells and nasal lavage fluid collected from healthy individuals up to 5 days after controlled infection with hRV. Thus, the ICAM-1 upregulation observed in *ex vivo* human tissue, is in line with previous *in vitro* and *in vivo* finding further supporting the role this receptor plays in hRV binding and spread within the respiratory tract. Although probed for, there was no observable bands with P2X3 and Muc5AC antibodies, thus no conclusions can be drawn in relation to this.

When lump tissue lysates were considered, there was a similar observation of a no significant change in protein expression for TRPV4, ICAM-1, P2X3 and Muc5AC in RV infected tissue lysate compared to sham infection and basal. The same issue regarding S.E.M is also apparent in this data set, thus similar observations can be made for lump tissue lysate samples. As with PCLS lysate samples, there appears to be a slight upregulation in TPRV4 and ICAM-1, in addition a similar upregulation in Muc5AC in RV infected tissue lysate compared to sham infection and basal can also be observed. It should be noted, as with other data, that the Muc5AC data set has a large S.E.M which is potentially a consequence of poor α-tubulin loading control expression and the presence of a band in only one replicate makes drawing a definitive conclusion difficult. This being said, an upregulation in Muc5AC expression is linked to the increased mucus production observed as a symptom of a hRV infection, partly due to its importance in mucociliary clearance (Zhu *et al*, 2009) but also potentially as a consequence of the increased epithelial cell permeability (Inoue *et al*, 2006), thus this observed upregulation may reflect these changes. The inconsistences between donors may be a result of underlying comorbidities as excessive mucus production is observed in asthmatics (Groneberg *et al*, 2002) and in COPD sufferers (Inoue *et al*, 2006) however, any comorbidities are not known for individual donors, thus this may explain the increased protein expression in some but not all replicates. P2X3 protein expression shows a very small downregulation in hRV infected and sham infection

compared to basal. As with Muc5AC expression the presence of bands are only clearly seen in a single replicate, making the formation of any conclusion difficult. Cells containing P2X3 receptor have been shown to be present in rodent lungs (Adriaensen *et al*, 2015) however, the presence of P2X3 receptors in human lungs is less clear. This being said, various P2X receptors have been identified in human primary cells isolated from bronchial epithelial of cystic fibrosis donor and tracheal epithelial of non-cystic fibrosis donors (Taylor *et al*, 1999). Furthermore, histological studies of human airway innervation suggests similarities to guinea pig morphology which are used more extensively in airway studies (West *et al*, 2015), thus the expression of P2X3 sensory nerves is possible in human lung tissue, with increased expression seen in a number of respiratory diseases including COPD (Bonvini and Belvisi, 2017). The difference in expression observed between replicates, as with Muc5AC expression, may reflect variation in donors and presence of comorbidities. However, given the lack of consistency in the data and no existing data regarding P2X3 expression changes in human lung tissue in response to hRV infection, it is difficult to determine if this downregulation is a direct consequence of the infection or due to inherent problems with the antibodies used and the poor α-tubulin loading control. Interestingly, the highest expression of P2X3 and Muc5AS were observed in the same donor sample, further supporting the potential for donor comorbidities affecting the outcome of an experiment.

Finally to further support changes to protein expression, RT-PCR was also conducted to identify if similar patterns of gene expression could be detected in mRNA post exposure to RV16 in lump tissue. All replicates were negative for TRPV4 and P2X3 expression in any condition, similarly with the exception of a very low level positive response in a single basal tissue sample, all replicates were negative for the loading control β-actin. The failure to amplify β-actin would suggest an issue with the RNA extraction process resulting in RNA degradation, even when NanoDrop values suggested high RNA concentrations, as the same primers were utilised in chapter 2 RT-PCR successfully. It would be beneficial to replicate this experiment again after further optimisation to identify whether any changes to the aforementioned gene expression can be observed.

A noteworthy limitation throughout this chapter which needs to be addressed is that in general experiments have a low N number (biological replicates) which in some instances has prevented some statistical analysis being conducted. A total of 21 tissue samples were received, weighing between approximately 1.1g and 7.4g, with the majority having a gross uninflated mass of approximately 2g. Although a reasonable number of samples were received, the quality of the sample varied between donors, which impacted the number of PCLS and tissues lumps which could be generated from each donor sample. However, to enable a suitable number of technical replicates (represented by n number) for each time point and condition to be performed, and to allow for the range of assay employed, the resulting N number per experiment was reduced. Conducting a larger number of experiments has the disadvantage of creating low N numbers and consequently may have impacted the likelihood of data being significant (Biau *et al*, 2008). Increasing the N number may have altered some of the observations made within the data, especially were there appears to be an effect but no significant difference is measured (for example figure 3.40 and 3.46). In addition reducing the number of experiments performed would have enabled higher N numbers to be achieved however, given that the infection of PCLS and lump tissue with RV16 is a technique that has not been performed previously, attempting to identify whether the infection had been successful and optimising the methods used took precedent and utilised the majority of the available tissue. Whilst increasing the N number would have been of immense benefit, it is not always feasible owing to a number of reasons. These reasons included the length of time it took to process the tissue and the length of time tissue was cultured for, which made it difficult to finish processing one sample and start processing the next sample on the same day, therefore samples had to be staggered were possible to allow for assays to be completed. Furthermore, the variation in sample size and quality resulted in variations in the amount of PCLS and lump tissue that could be generated, thus this influenced the total number of experiments which could be performed per donor and could only be determined once initial processing had occurred, limiting the amount of advanced planning which could be conducted. In addition, tissues samples were not always available and several weeks or months could pass without any samples, thus the final N number was impacted by not only the available tissue but also the time constraints applied to the research. Given this low N number and the large S.E.M. observed in many assays, the majority of data typically shows little or no significance. As such it was necessary to discuss trends in the data whereby, small changes have been explored in

relation to existing studies however, without additional replicates it is not possible to say with certainty whether the changes observed are either significant or an accurate representation of how RV16 infections effect the tissue.

Alongside the impact that a small N number may have on the data collected, there is also a need to consider the choices made in regards to the statistical analysis utilised in this chapter. As with some of the data in chapter 2, the visual representation of some data in chapter 3 appears to show clear effect (for example figure 3.40 and 3.46) but when P values are consider no significant difference is recorded. Data was checked for normality visually using the widely utilised Q-Q plot and statistically using a Shapiro-Wilk test, whilst statistical analysis was performed using a combination of two and one-way ANOVA followed by Tukey post hoc test for multiple comparison, paired and unpaired t-tests or multiple t-tests utilising the Holm-Sidák method for corrections of multiple comparisons, were multiple time points needed comparing. The aforementioned analytical methods were chosen based not only on whether data was normally distributed but also the robustness of the test being utilised, with the justification for the chosen tests being determined by the discussion conducted in chapter 2 (see 2.4.2). Whilst the majority of the data collected was normally distributed, in a few instances tests for normality were not met, this being said, whilst normal distribution is strived for, it is often not achievable (Blanca *et al*, 2018). Furthermore, the number of biological replicates in this chapter does not exceed 6 and the number of technical replicates does not exceed 18, thus the performance of the Sharipo-Wilks test is likely to have been reduced as the sample size is below 30 (Razali and Wah, 2011) and so may not accurately represent the distribution of the data collected. Although the tests utilised to undertaken statistical analysis are robust enough to deal with data not meeting some assumptions, the small sample sizes in all experiments is likely to be a limitation whereby outliers in the results may noticeably affect the mean and/or standard deviation (Mishra *et al*, 2019). It is also worth considering that there is likely to be a large amount of variation between donor samples and any comorbidities are unknown. These variations are likely to be the reason for outliers occurring within the data and may go some way to explain why visual representation of some data appears to show clear effect, but when P values are consider no significant difference is recorded.

Although, this data collectively is somewhat inconclusive, the results suggest that the manner in which hRV infections interact with human tissue *ex vivo* shows some similarities in responses to previous *in vitro* cell based studies however, further questions need addressing to better understand the mechanisms which are involved in these interactions. A result of the aforementioned inconsistences, is the formation of a number of limitations relating to this model which need to be addressed to improve the overall meaning of this data. Firstly, is the variations observed between donors and the problem this creates in regards to analysis, leading to large standard deviations. Due to the nature of the tissue collection process, the reduction in variation is impossible, instead increasing the number of replicates would help to improve the reliability of the findings. In addition, collection of comorbidity information relating to underlying respiratory diseases could also help determine whether anomalies in the data are a direct consequence of the underlying diseases. However, this would depend on whether appropriate amendments could be made to the ethics approval held. Secondly, due to the limited number of samples received either insufficient replicates or lack of optimisation of methods was a problem. Methods such as RNA extraction, cytokine array analysis and bronchoconstriction are prime examples of areas which need development to enable further conclusions to be drawn. Secondly, whether the virus penetrates the full depth of the PCLS and lump tissue should also be considered as a potential limitation in this study. Whilst data shows that tissue remains viable throughout the culture period regardless of thickness, it is harder to determine whether this has any impact on the infective capabilities of RV16 or if the presence of agarose affects the virus' ability to bind to cells. This being said, PCLS and lung tissue explant models using other respiratory viruses have shown that a range of cell types including, alveolar and bronchial epithelial cells, ciliated cells and adjacent submucosal cells throughout the tissue could be successfully infected (Booth *et al*, 2004; Punyadarsaniya *et al*, 2011; Weinheimer *et al*, 2012: Hocke *et al*, 2013; Bryson *et al*, 2020). This would suggest that the presence of agarose has little impact on viral replication, as the process used to create PCLS is typically similar between studies. In addition the inert nature of agarose means it will not interact with the virus in any away (Ulrich *et al*, 2011) and given that nutrients can diffuse into and out of the agarose, the virus may also be able to pass through without any impedance (Placke and Fisher, 1987). In this study whether this extent of infection has occurred is not clear, the presence of viral RNA in tissue supernatant and the cell death observed in Hela cell titre plate demonstrates that the virus is actively replicating

in the tissue, as all excess virus is washed off after the initial incubation period, as such any virus detected in the supernatant is release from the tissue. However, this alone does not show whether the tissue is infected throughout or just on the surface cells. Fixing, sectioning and staining tissue with an anti-RV16 antibody (Mosser *et al*, 2002; Goris *et al*, 2009) may aid in the process of determining whether the virus had penetrated through multiple layers of cell, infecting not only the outer surfaces but also the middle of the tissue. Finally, the other limitation which needs some consideration is the length of time tissue is cultured for post infection with RV16. Although the 5 day period resulted in some changes, these are often slight and it is questionable whether extending or reducing the culture period would be beneficial in order to produce a more noticeable response. Replication of the previously discussed experiments utilising various end points would help to identify at what stage during the infective period optimal measurements can be made.

Although the data has a number of limitations and inconsistences, overall the data demonstrates that the changes previously observed *in vitro* can to some extent be replicated in a model that is more akin to the *in vivo* environment. Collectively, when the viability data from LDH, CytoToxGlo^{TM}, trypan blue and WST-1 assay is considered, it is evident that the extent of cytotoxicity caused by RV16 infection is minimal however, some reduction in viability is measureable in some instances, most noticeably when using dead cell protease activity as a measure. The minimal amount of cytotoxicity and thus limited change in viability, is in line with the *in vitro* observations made in chapter 2 and other cell based studies (Schroth *et al*, 1999; Inoue *et al*, 2006; Wark *et al*, 2009; Kicic *et al*, 2016; Etemadi *et al*, 2017). These observations are also in line with *in vivo* studies which have shown hRV has a limited cytolytic effect on cells (Ghildyal *et al*, 2005) and causes only minimal cellular damage once adhered to a cell (Griego *et al*, 2000). When proinflammatory response is considered, there is evidence of a slight upregulation of some cytokines and chemokines which are involved in the hRV infection response. Similarly, when global protein expression slight upregulation of receptors involved in hRV infection is also observed. However, these observations should be considered with a degree of uncertainty owing to a lack of replicates and inconsistencies in the data, as such it would be beneficial to conduct further optimisation to provide additional clarity and enable conclusions to be drawn. Although collectively the data adds little to the existing knowledge of the

mechanisms involved in hRV infections, it shows that *ex vivo* tissue prepared as either PCLS or small tissue lumps can be successfully infected with RV16. As such, whilst further developments of methods used to investigate the effect of hRV are required, this model provides a suitable alternative to existing animal and cellular models which is more akin to the *in vivo* environment.

4 Chapter 4: Optimisation of Microfluidic Devices for Airway Epithelial Cells and Human Tissue Culture

4.1 Introduction

The use of microfluidics in the study of respiratory diseases is predominately focused on the use of 2D and 3D cell culture to replicate the environment of the lung. Microfluidics aims to recreate the *in vivo* environment using *in vitro* conditions, thus providing a better recapitulation of the respiratory tract than can be achieved using more traditional cell culture techniques (Esch *et al*, 2015). Traditional 2D cell cultures provide advantages such as generating vast quantities of data however, the relative simplicity of a single monolayer means complex tissue specific functions may not be accurately represented (Bhatia and Ingber, 2014; Esch *et al*, 2015). Comparatively 3D cell cultures provide a more realistic representation of the spatial orientation of cells and cell-to-cell interactions observed *in vivo* however, the same functionality cannot be achieved due to lack of blood flow and interactions with cells outside those being cultured (Huh *et al*, 2010; Bhatia and Ingber, 2014; Dawson *et al*, 2016b). The ability to create more realistic representations of spatial orientation of cells makes the employment of microfluidic in the creation of cell culture respiratory models particularly beneficial, as not only can cells be used to line microchannels in a manner akin to the airways, but air-liquid interfaces can be created as media can be flowed under the cells, mimicking the blood flow seen *in vivo* (Huh *et al*, 2007; 2012; Tavana *et al*, 2011; Benam *et al*, 2015; 2016). Furthermore, microfluidic systems allow for continuous perfusion of cells or tissue in a manner akin to the *in vivo* environment. Thus reducing the potential accumulation of waste and unused nutrients, aiding in the prevention of early necrosis and extending the longevity of the culture period beyond that seen when utilising traditional culture techniques (Kim *et al*, 2006; Hattersley *et al*, 2008; Shaw *et al*, 2011; Zambon *et al*, 2015; Torisawa *et al*, 2016).

Given the capabilities of microfluidic devices to support a range of tissue and cell types in various formats, the potential of microfluidics as a platform for biological research is extensive and provides multiple opportunities for the creation of relevant human models on which pharmaceutical compounds can be tested prior to clinical trials (Tian *et al*, 2019). Based on these observation this chapter aims to create two lung-on-a-chip models which can support cell culture and PCLS, with the long term of intention of replicating the work conducted in chapter 2 and 3 on a miniaturised scale, with extended culture period and hopefully at a higher throughput than can be achieved using traditional culture methods.

4.2 Methods

4.2.1 Cell Culture Microfluidic Device Optimisation

4.2.1.1 Optimisation of Cell Culture Device Overview

Three iterations of a microfluidic device were trailed as part of the optimisation of the co-culture methods on a microfluidic device. All microfluidic devices for use in cell culture were designed and manufactured by Dr Alex Iles (Department of Chemistry, University of Hull). The initial design incorporated a glass and polydimethylsiloxane (PDMS) device outlined in 4.2.1.2 (referred to as cell culture device one (CCD1)), the second poly(methyl methacrylate) (PMMA) device outlined in 4.2.1.3 (referred to as cell culture device two (CCD2)) and the third polycarbonate (PC) device outlined in 4.2.1.4 (referred to as cell culture device three (CCD3)). The process of making modifications to the devices enabled problems to be mitigated for, thus increasing the effectiveness of each device as a method of culturing cell lines.

4.2.1.2 Cell Culture Device Iteration One

CCD1 was designed and manufactured by Dr Alex Iles (Department of Chemistry, University of Hull) for use in cell culture. The device was comprised of two identical sides which were separated by a 15mm x 15mm, 12µm thick, 0.4µm pore size, transparent PET membrane (Sabeu, Germany). Each side was comprised of two elements, a glass outer layer and PDMS inner layer. The glass layer measuring 30mm x 30mm x 3mm was milled using a CNC machine, to create a hexagon chamber measuring 8mm x 6mm x 100µm. Each glass layer was served with a 1.6mm inlet and outlet, which were permanently bonded with epoxy resin to a 200µl pipette tip, cut to fit the inlet/outlet, to serve the different cell lines grown on both surfaces of the membrane. Each PDMS layer was created using a PC mould, milled on a CNC machine, the PDMS layer measured 30mm x 30mm x 3mm, with a 9mm hole punched into the centre to allow complete DMEM to pool over the top of the membrane (Figure 4.1).

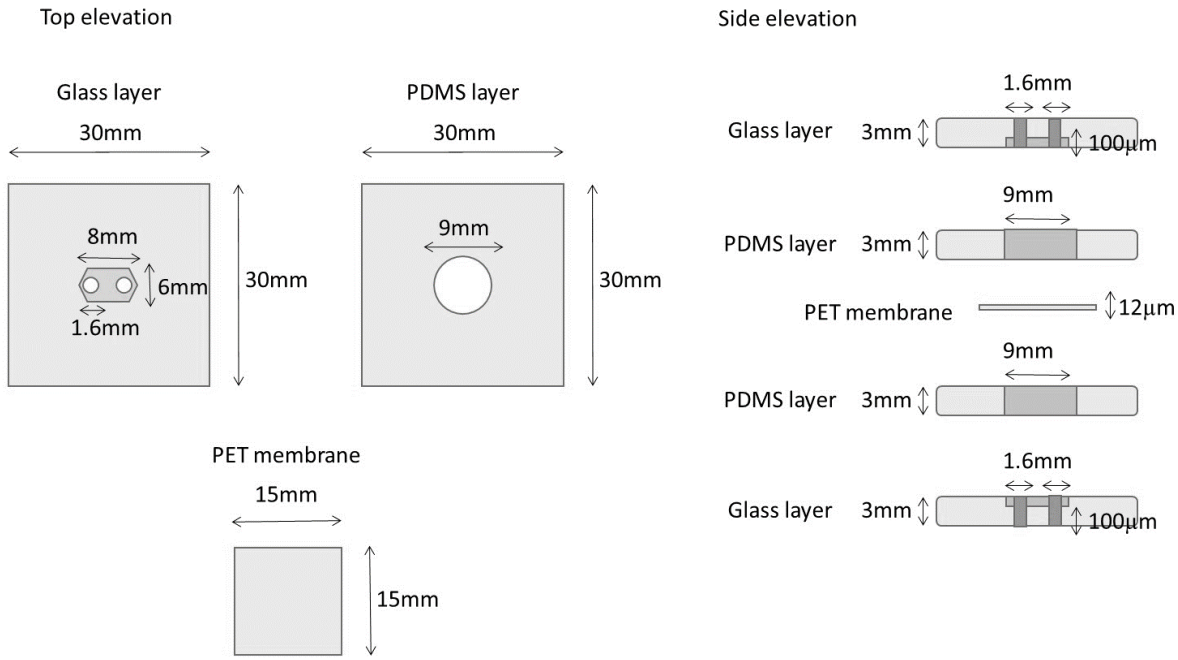

Figure 4.1. Cell culture device one schematic showing the top and side elevations of the main glass and PDMS body of the device and PET membrane used for a cell culture surface.

Fluid was delivered/collected from the device through ethylene tetrafluoroethylene (EFTE) Teflez® tubing (1.6mm outer diameter (OD), 0.5mm inner diameter (ID)) (Kinesis, Cambridgeshire, UK), connected to the device by permanently bonding with epoxy resin to the inlet/outlet fittings. Direction of complete DMEM flow was via the inlet in the glass layer, pooling and passing across the membrane via the chamber in the PDMS layer, before being collected via the outlet in the glass layer (Figure 4.2). When constructed the device was held together by binder clips and temporarily bonded with nail varnish to help create a seal around the device. Nail varnish was chosen over cyanoacrylate as this was prone to seeping into the membrane and being toxic to the cells, it also provided a temporary fixation that enabled repeated usage of the same device which was difficult to achieve with other adhesives.

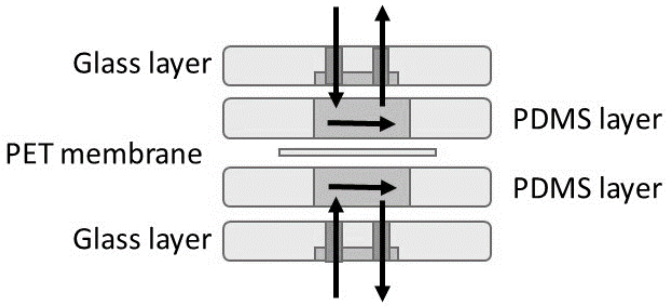

Figure 4.2 Direction of the fluid flow through the glass and PDMS layers of cell culture device one. Fluid flow depicted by arrows, complete DMEM flows into device via inlet, passes across the PET membrane before flowing out via the outlet.

The membrane and PDMS layer were temporarily bonded together 24 hours prior to use enabling the fixative to completely dry and any solvents evaporate. Cells were seeded in a manner similar to the co-culture method described previously (see 2.2.7.1). Briefly the PDMS/membrane layer was placed in a 60mm culture dish (Fisher Scientific) with 7ml of completed DMEM, the upper surface of the membrane was seeded with $3x10^4$ A549 cells in 200µl of complete DMEM. The seeding density used was calculated based on the surface area ($63mm^2$) of the available membrane and volume of the chamber ($190mm^3$) in comparison to that of various multi-well plates. Membranes were subsequently incubated at 37°C, 5% CO_2 for 2 hours to allow cells to adhere (Figure 4.3a). The membrane was then rotated and 1N1 P2X3 cells were seeded at the same density and manner as the A549 cells on the opposite surface of the membrane. After a further 2 hours incubation an additional 1ml of complete DMEM was added to the top layer of the membrane to ensure the cells remained submerged for the duration of the culture period. The membrane was incubated overnight prior to transfer to CCD1 to ensure cells had fully adhered, thus reducing the likelihood of removal due to the shear forces generated by the continuous perfusion of the device.

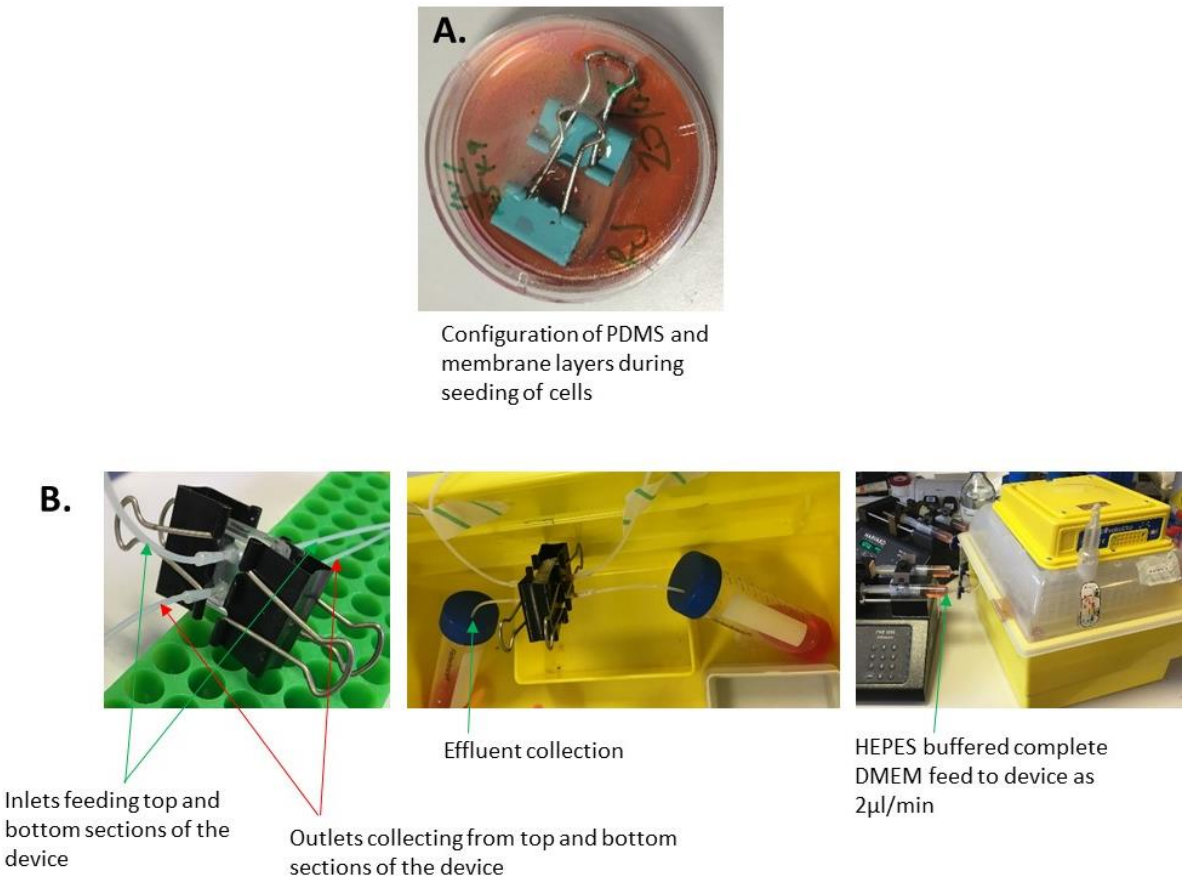

Figure 4.3 Microfluidic cell culture device one showing configuration of PDMS and PET membrane layers of the device during the process of seeding cell lines onto the membrane **(A)** and from left to right; the fully constructed device, the effluent collection arrangement and arrangement on infusion syringe pump **(B)**.

After overnight incubation the glass layers of the device were secured and the two chambers manually perfused to ensure the cells remained covered in the complete DMEM whilst the device was transferred to the egg incubator. Cells were incubated in a darkened, humidified egg incubator at 37°C. The device was perfused using a Harvard Apparatus PHD Ultra infuse/withdraw syringe pump (Harvard Apparatus, Cambridgeshire, UK) through individual inlets via ethylene tetrafluoroethylene (EFTE) Teflez® tubing (1.6mm outer diameter (OD), 0.5mm inner diameter (ID)) (Kinesis) at a rate of 2µl/min with HEPES buffered complete DMEM, this ensured sufficient replenishment of nutrients whilst not creating too much shear stress (Figure 4.3b). Although not required for further analysis at the optimisation stage, effluent was collected from individual outlets at 24 hour time points over the 72 hour culture period. To check cell viability both on and off the device and to

ensure the cell lines could successfully be cultured on the membrane, the PDMS/membrane layer was cultured in standard culture condition in a 37°C, 5% CO_2 incubator for 72 hours, thus enabling a direct comparison between the methods used.

One of the main issues with this device was the likelihood of leakages due to the method used to construct the device. There were times during the culture period when the membrane was completely devoid of media, therefore causing cell death. Additionally, the device design resulted in bubble formation within the PDMS chamber, directly next to the membrane when being placed in the culture dish. Whilst every effort was made to remove the air bubble additional ones often formed as the device moved around during transfer to/from the incubator and whilst being perfused. The presence of these air bubbles hindered cellular growth due to the absence of nutrients in areas of the membrane were the bubble persisted, thus preventing good coverage of the membrane by cells.

4.2.1.3 Cell Culture Device Iteration Two

As a response to the aforementioned issues a new design was produced in the form of a PMMA microfluidic device. CCD2 was designed with the same aim of being able to culture two different cell lines on opposing sides of a membrane however, this device was more securely held together to provide better perfusion and optimise cell growth. CCD2 was designed and manufactured by Dr Alex Iles (Department of Chemistry, University of Hull) for use in cell culture. The device comprised of two identical PMMA sides measuring 80mm x 50mm x 10mm milled using a CNC machine and drilled in four corners to enable the device to be sealed. Each half comprised of a 3mm diameter inlet and outlet tapering to 0.8mm at the fluid delivery/collection point and a milled central chamber approximately 25mm x 10mm x 0.2mm, surrounded by a 1mm deep channel to hold a silicone O-ring to improve the seal between the two halves. Cells were cultured on 12µm thick, 0.4µm pore size, transparent PET membrane which was solvent bonded with chloroform to a PMMA wafer. The PMMA wafer was laser cut measuring approximately 25mm x 10mm x 0.3mm with a central hole measuring approximately 15mm x 7mm. The wafer was secured in the central chamber (200µm depth per side) which was sealed with O-rings and screws to minimise leakages from the cell culture area (Figure 4.4).

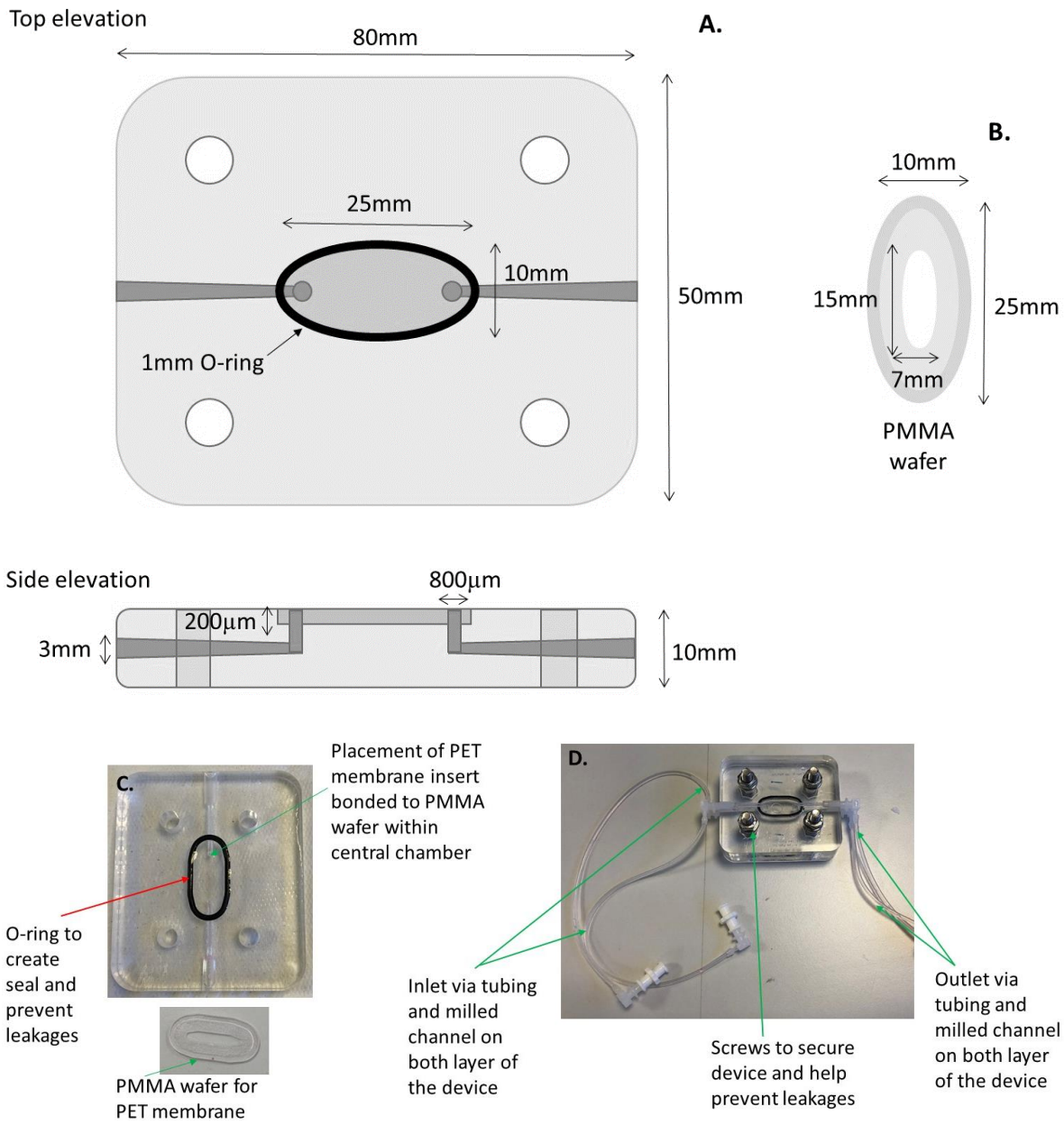

Figure 4.4 Cell culture device two schematic showing the top and side elevations of the main PMMA body of the device **(A)** and the PMMA wafer for use as a cell culture surface **(B)**. Images represent one half of cell culture device two with PMMA wafer **(C)** and constructed device **(D)**.

Fluid was delivered/collected from the device through platinum cured tubing (2.4mm OD, 0.8mm ID) (Advanced Fluid Solutions, Essex, UK), connected to the device by a polypropylene push fit elbow luer connector (Thistle Scientific, Glasgow, UK). Direction of complete DMEM flow was via the inlet in either layer, passing across either the top or

bottom of the membrane through the milled central chamber, before being collected via the outlet in either layer (Figure 4.5).

Figure 4.5 Direction of the fluid flow through the main PMMA body of cell culture device two. Fluid flow depicted by arrows, complete DMEM flows into device via inlet, passes over the PET membrane via the milled central chamber before flowing out via the outlet.

As with CCD1 the surface area of the membrane was calculated and compared to the surface areas of multi well plates to help determine a suitable seeding density for the cell lines being used. The surface area of the membrane being 75mm^2 and the volume being 15mm^3. The wafer was placed in 500µl of complete DMEM to ensure cells had sufficient media without immersing the wafer which would have prevented cells from adhering to the membrane. A549 cells were seeded at an initial density of 2x10^5 and incubated at 37°C, 5% CO_2 for 4 hours to allow cells to adhere. This cell line was seeded first as it is proliferates faster than the 1N1 P2X3 cell line, has stronger adherence and forms a complete monolayer. Similarly, the seeding density was relatively high to account for potential lost due to overspill from the edge of the wafer during transfer to the incubator. After incubation the wafer was rotated and placed in 1ml of complete media. 1N1 P2X3 cells were seeded onto the opposite side of the membrane at an initial density of 1x10^5 and incubated at 37°C, 5% CO_2 for 18 hours to allow cells to adhere. The lower seeding density utilised for the 1N1 P2X3 cells reflects the indentation formed in the centre of the wafer which prevented cells from being lost from the membrane during transfer to the incubator. After overnight incubation, the wafer was transferred to the central chamber of the device, secured and manually perfused. The device was placed in a darken, humidified egg incubator, at 37°C and perfused at a rate of 2µl/min with HEPES buffered complete DMEM through the two inlets feeding the apical and basal surfaces of the membrane, similarly effluent was collected via two outlets. This design ensured separation of cell lines and media could be maintained throughout the entire culture period (Figure 4.6). To check cell viability both on and off the device, the PMMA wafer/membrane layer was cultured in standard culture

condition in a 37°C, 5% CO_2 incubator for 72 hours, thus enabling a direct comparison between the methods used.

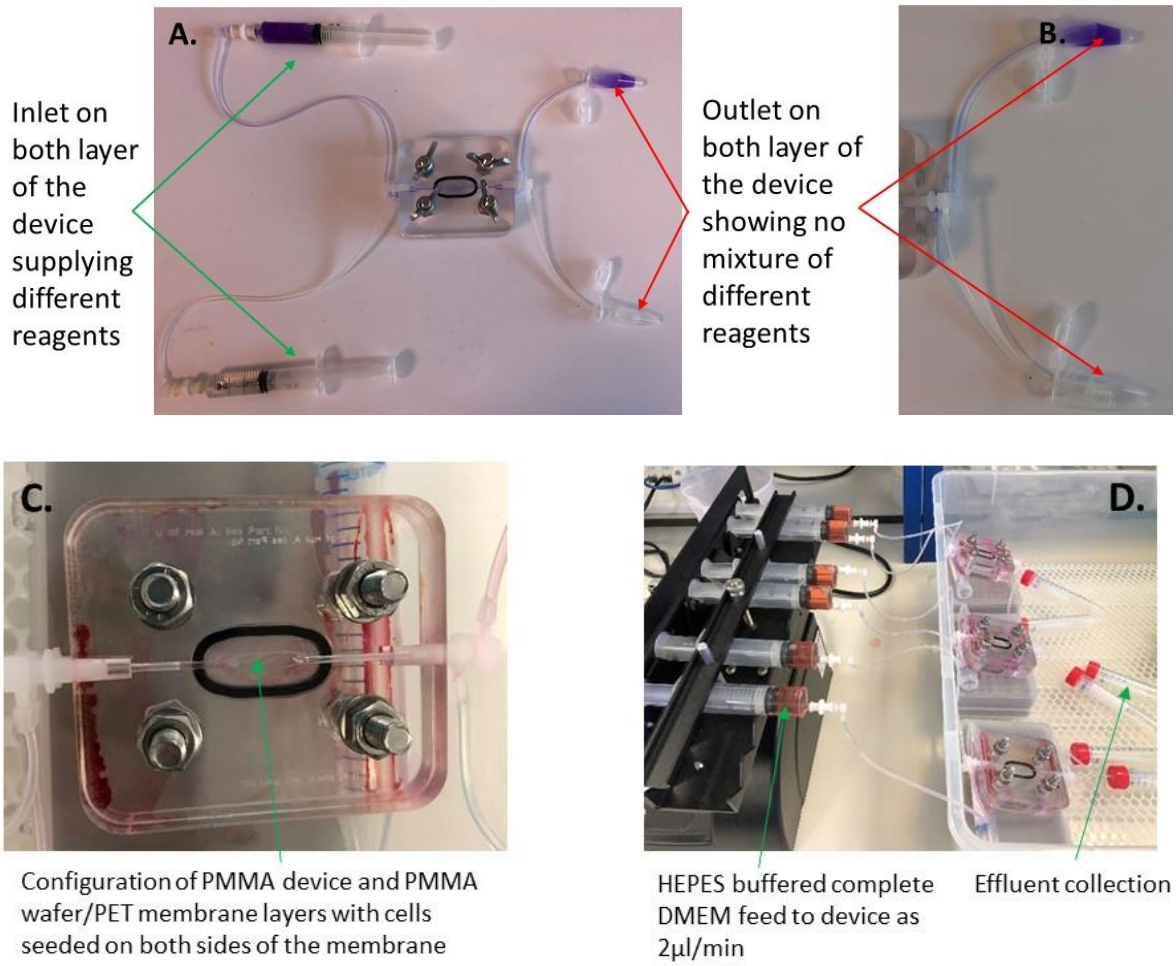

Figure 4.6 Microfluidic cell culture device two configuration showing the complete device showing separate inlets and outlet supplying different reagents to opposing sides of the membrane **(A)**, effluent collected at outlets showing no mixing of reagents through the device **(B)**, the fully configured device with media perfused central chamber containing membrane/wafer seeded with cells **(C)** and arrangement on infusion syringe pump with separate effluent collection from both sides of the membrane **(D)**.

Three issues became apparent during the optimisation of CCD2, these being the leakage of media from the inlets of the device, problems with sterilising the device and the sheer force generated due to the position of the inlets over the membrane. The degree of leakage seen in each repeated use of the device varied, thus when less leakage occurs cell growth was

evident but reduced compared to cells grown off device for comparison, whilst increased leakage resulted in cell death due to lack of perfusion during the culture period (Figure 4.7). Much of this leakage arose from an inability to firmly secure the push fit elbow luer connector (Thistle Scientific) used for the attachment of tubing to the device, to overcome this problem polytetrafluoroethylene (PTFE) tape was wrapped around the connector which succeeded in minimising leakages.

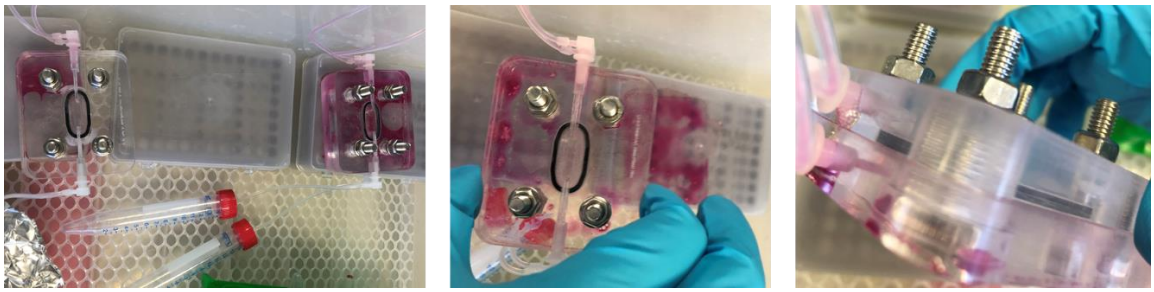

Figure 4.7 Microfluidic cell culture device two configuration showing extent of leakage from the device, most noticeable from the inlet channels, resulting in the pooling of complete DMEM under the device during the culture period.

Sterilising the device was problematic due to being unable to autoclave PMMA as it is unable to withstand the high temperatures used in the process (Münker *et al*, 2018). As an alternative to this, the device could be cleaned by wiping flat surfaces and perfusing channels with 70% ethanol however, if allowed to soak overnight in the ethanol the device is damaged by the solvent, causing it to swell resulting in cracks and crazing at the surface (Higuchi, 2015). This made securing the device via the screws difficult due to the tightness of the fitting in the milled channels and subsequently caused more cracking due to overtightening and stress across the surface. The inability to thoroughly clean the device thus increased the risk of infection to the cells being grown within the device and potentially effecting the outcome of any further analysis.

The final issue stemmed from the position of the inlets and outlets over the wafer and the resulting shear forces this generated. After the 72 hour culture period the membranes were removed from the device and compared to those cultured in the incubator by staining cells

with Kwik Diff™ staining solution. This comparison showed the uneven cell growth across the membrane removed from the device compared to those cultured in the incubator. This sporadic growth was most noticeable directly below the inlet and outlet position, suggesting that the shear stress generated by the perfusion was sloughing the cells off the membrane preventing the formation of a confluent monolayer. Whilst trying to address this problem only A549 cells were grown on the membrane and left overnight to adhere to try to reduce the likelihood of being sheared off the membrane, additionally the flow rate was lowered to 1µl/min to further reduce the extent of shear stress within the device.

4.2.1.4 Cell Culture Device Iteration Three

In response to the issues experience with CCD2, a third design of a polycarbonate (PC) microfluidic device was tested. CCD3 was designed and manufactured by Dr Alex Iles (Department of Chemistry, University of Hull) for use in cell culture. The device comprised of two identical PC sides measuring 80mm x 50mm x 10mm milled using a CNC machine and drilled in four corners to enable the device to be sealed. Each half comprised of a 3mm diameter inlet and outlet tapering to 0.8mm at the fluid delivery/collection point and a milled central chamber approximately 25mm x 10mm x 0.5mm, surrounded by a 1mm deep channel to hold a silicone O-ring to improve the seal between the two halves. Cells were cultured on 12µm thick, 0.4µm pore size, transparent PET membrane which was solvent bonded with chloroform to a PMMA wafer. The PMMA wafer was laser cut measuring approximately 25mm x 10mm x 0.3mm with a central hole measuring approximately 11mm x 5mm. The wafer was secured in the central chamber (500µm depth per side) which was sealed with O-rings and screws to minimise leakages from the cell culture area (Figure 4.8).

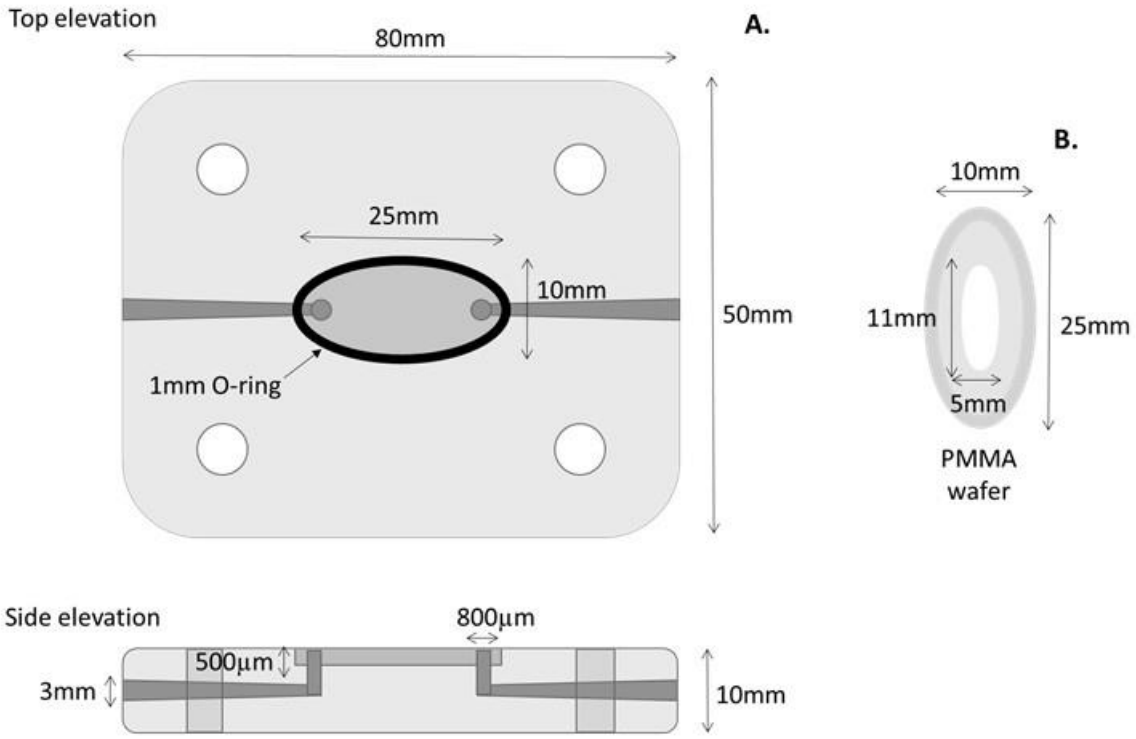

Figure 4.8 Cell culture device three schematic showing the top and side elevations of the main PC body of the device **(A)** and the PMMA wafer for use as a cell culture surface **(B)**.

Fluid was delivered/collected from the device through platinum cured tubing (2.4mm OD, 0.8mm ID) (Advanced Fluid Solutions), connected to the device by a polypropylene push fit elbow luer connector (Thistle Scientific) wrapped in PTFE tape to create a secure fitting. Direction of complete DMEM flow was via the inlet in either layer, passing across either the top or bottom of the membrane through the milled central chamber, before being collected via the outlet in either layer (Figure 4.9).

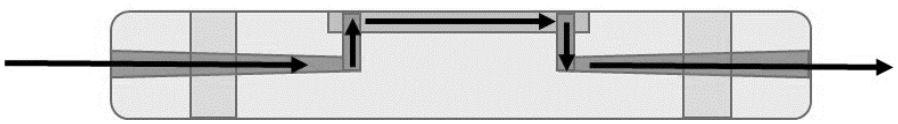

Figure 4.9 Direction of the fluid flow through the main PC body of cell culture device three. Fluid flow depicted by arrows, complete DMEM flows into device via inlet, passes over the PET membrane via the milled central chamber before flowing out via the outlet.

CCD3 was identical to CCD2 in terms of design with the exception of being made of PC which allowed the device to be autoclaved resolving the issue related to cleaning and the depth of the central chamber which was increased from 200µm to 500µm to allow for a larger of volume of complete DMEM to perfuse the system at any given time. However, the main difference was the design of the PMMA wafer, the working area of the wafer was reduced to ensure the inlets and outlets were no longer positioned directly over the useable are of the membrane (Figure 4.10). By making this slight change it ensured perfusion was maintained but the shear stress generated by this process did not cause cells to be sloughed away from the membrane, thus allowing cells to grow more consistently and evenly across the membrane. Additionally, by maintaining a reduced flow rate of 1µl/min, using a single cell line and continuing to wrap PFTE tape around the inlet/outlet push fit connectors allowed for a device which functioned more effectively than the previous two iterations.

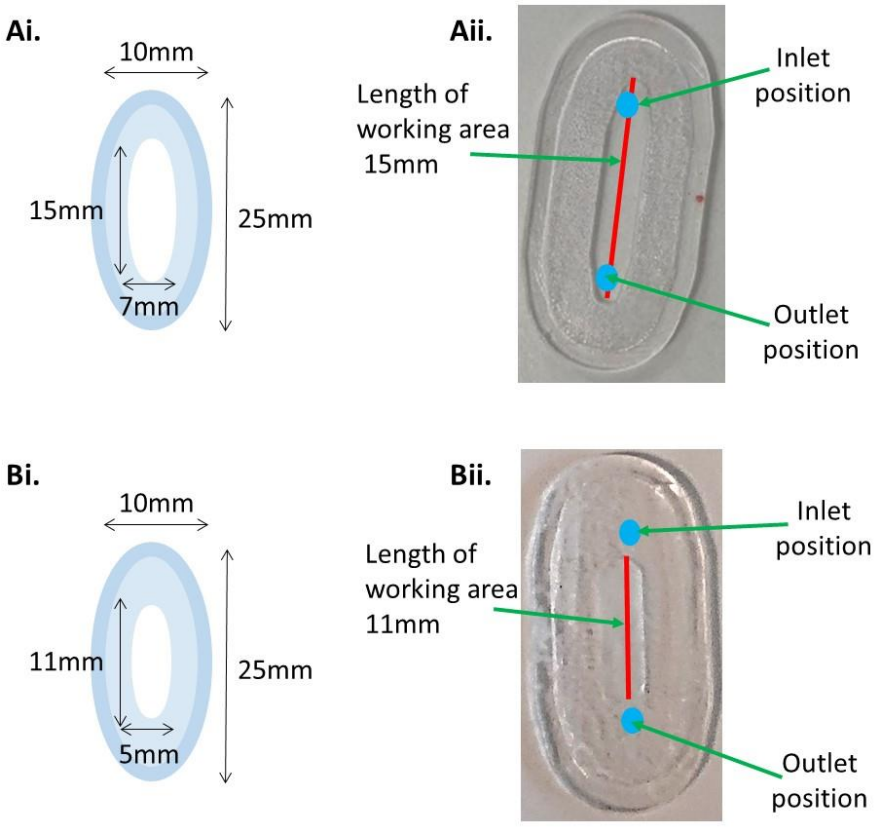

Figure 4.10 PMMA wafer variations in cell culture device two **(Ai)** and three **(Bi)** showing the position of the inlets and outlets in relation to the working area of the membrane of cell culture device two **(Aii)** and three **(Bii)**.

4.2.2 Cell Culture Microfluidic Device Design

4.2.2.1 Optimised Device Design for Cell Culture

A microfluidic device was designed and manufactured by Dr Alex Iles (Department of Chemistry, University of Hull) for use in cell culture. The device comprised of two identical PC sides measuring 80mm x 50mm x 10mm milled using a CNC machine and drilled in four corners to enable the device to be sealed. Each half comprised of a 3mm diameter inlet and outlet tapering to 0.8mm at the fluid delivery/collection point and a milled central chamber approximately 25mm x 10mm x 0.5mm, surrounded by a 1mm deep channel to hold a silicone O-ring to improve the seal between the two halves (Figure 4.11a). To provide a cell culture surface a PMMA wafer was laser cut measuring approximately 25mm x 10mm x 0.3mm with a central hole measuring approximately 11mm x 5mm. To provide a cell culture surface a 12µm thick, 0.4µm pore, transparent PET membrane was cut to fit the wafer and chloroform bonded to the rough surface of the wafer (Figure 4.11b).

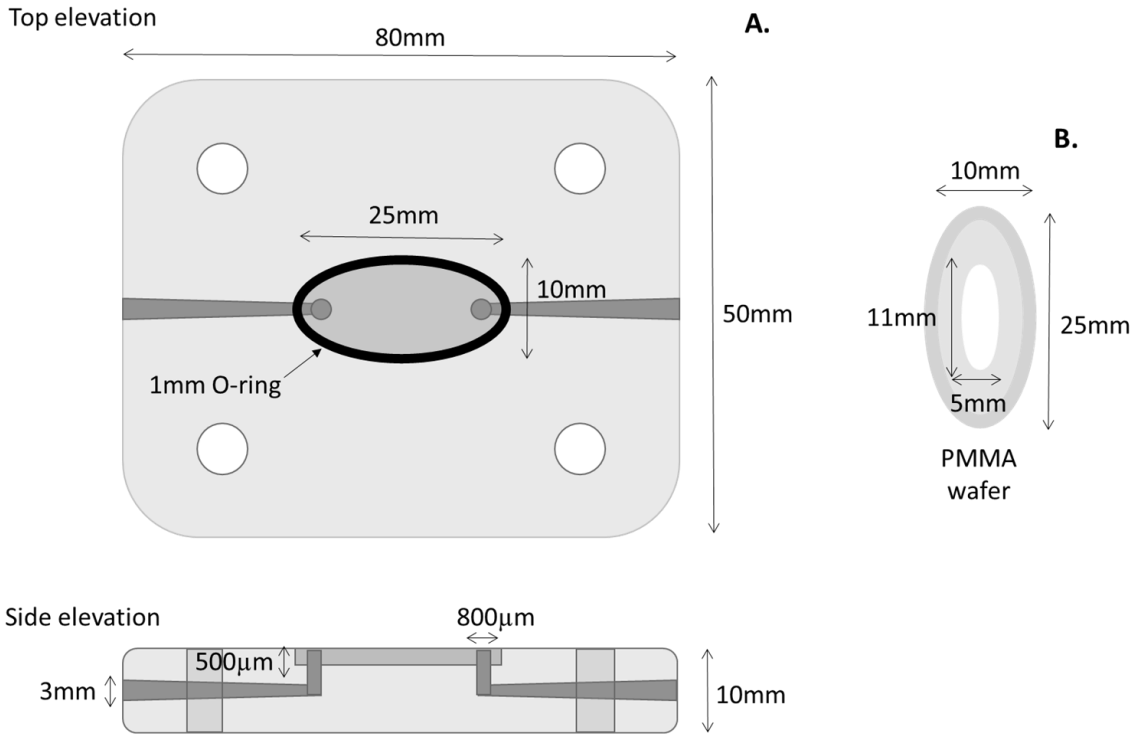

Figure 4.11 Optimised cell culture microfluidic device schematic showing the top and side elevations of the main PC body of the device **(A)** and the PMMA wafer for use as a cell culture surface **(B)**.

Fluid was delivered/collected from the device through platinum cured tubing (2.4mm OD, 0.8mm ID), connected to the device by a polypropylene push fit elbow luer connector, wrapped with PTFE tape to ensure a secure fit. Direction of complete DMEM flow was via the inlet in either layer, passing across either the top or bottom of the membrane through the milled central chamber, before being collected via the outlet in either layer (Figure 4.12).

Figure 4.12 Direction of the fluid flow through the main PC body of optimised cell culture device. Fluid flow depicted by arrows, complete DMEM flows into device via inlet, passes over the PET membrane via the milled central chamber before flowing out via the outlet.

4.2.2.2 Optimised Cell Culture Device Operation

A549 cells were seeded at a density of $2x10^5$ on a 12µm thick, 0.4µm pore size, transparent PET membrane chloroform bonded to a PMMA wafer and incubated at 37°C, 5% CO_2 overnight to allow cells to adhere. After overnight incubation, the wafer was transferred to the central chamber of the PC device (CCD3), secured and manually perfused to prime the device. The device was subsequently transferred to dark, humidified, 37°C egg incubator for the duration of the culture period. The device was perfused at a rate of 1µl/min with HEPES buffered complete DMEM via platinum cured silicon tubing (2.4mm OD, 0.8mm ID) through the two inlets feeding the apical and basal surfaces of the membrane. Effluent was collected every 24 hours for 72 hours post transfer to device via two outlets pooled into a single centrifuge tube. To check cell viability both on and off the device, the PMMA wafer/membrane layer was also cultured in standard culture condition in a 37°C, 5% CO_2 incubator for 72 hours, thus enabling a direct comparison between the methods used.

4.2.3 Determining Effectiveness of Cell Culture Microfluidic Device

4.2.3.1 Cell Culture Microfluidic Device Viability Assessment

Initial viability assessments of the three microfluidic cell culture devices were based on trypan blue exclusion and resazurin staining. CCD1 membranes cultured in both a standard CO_2 incubator and on a microfluidic device were removed from the device and cut in half. Each half was then mounted on a glass microscope slide and orientated to ensure both 1N1 P2X3 cells and A549 cells were placed upward facing. Membranes were stained with 20µl of 0.2% resazurin solution (Sigma Aldrich) and viewed on a light box. This method allowed colour changes to be observed through the reduction of the blue resazurin dye to pink resorufin by viable cells, whilst non-viable cells retain the blue colouration (O'Brien *et al*, 2000). To confirm resazurin results, a second set of membranes was processed in the same manner by cutting the membrane in half and orienting the cells accordingly, these membranes were stained with 20µl of 0.4% trypan blue solution and view under a light microscope. Viability assessment could be made by the extent of blue stained non-viable cells compared to unstained viable cells. For CCD2 and CCD3 membranes were stained with either trypan blue to estimate the extent of viable and non-viable cells or with Kwik Diff™ staining solution (see 2.2.1.6) to visualise the extent of cell growth across the membrane.

4.2.3.2 Cell Culture Microfluidic Device LDH Assay

Cell cytotoxicity using LDH analysis was conducted on A549 cells cultured on CCD3 only as cells could be cultured more consistently on this device compared to previous iterations. Cells were lysed 72 hours post transfer to the device or culture in a standard incubator, by removing membranes from the wafers and placing them in a 6 well plate containing 500µl of completed DMEM with 50µl of 10% (v/v) lysis buffer (Triton X-100). Membranes were incubated at 37°C, 5% CO_2 for 45 minutes, agitated briefly to slough off any cells and to ensure effluent was evenly mixed before a sample was taken for LDH analysis. LDH assay was conducted as outlined in 2.2.9.7 and absorbance was measured on a Tecan Infinite M200 multimode plate reader at 490 and 690nm all values were adjusted to account for the media.

4.2.3.3 Cell Culture Microfluidic Device SRB Assay

SRB assays were conducted on cells cultured on CCD3 only as cells could be cultured more consistently on this device compared to previous iterations. Membranes were removed from wafers 72 hours post transfer to the device or culture in a standard incubator, transferred to a 24 well plate, fixed with 1ml of ice cold (4^{o}C) 25% TCA on ice for 1 hour, washed 4 times with distilled water, the supernatant discarded and the membranes dried. Fixed cells were stained using 250µl of 0.4% sulforhodamine B in 1% acetic acid per well for 30 minutes at room temperature, excess stain removed, the membranes washed 4 times with 1% acetic acid, the supernatant discarded and the membranes dried. Subsequently the membranes were transferred to new wells, the stain dissolved in 500µl 10mM Tris base at pH10 on a gyro-rocker for 5 minutes to ensure even distribution of the stain across the well and the empty membrane disposed of. Absorbance was measured on a Tecan Infinite M200 multimode plate reader at 540nm, with 21 points measured per well.

4.2.4 PCLS Microfluidic Device Optimisation

4.2.4.1 Optimisation of PCLS Device Overview

Two different devices were optimised for use with PCLS, these being a modified version of the CCD3 PMMA/PC device outlined in 4.2.4.2 and 4.2.4.3 (referred to as PCLS device Ai and PCLS device Aii respectively) and the second being the polyether ether ketone (PEEK) device outlined in 4.2.4.4 and 4.2.4.5 (referred to as PCLS device Bi and PCLS device Bii respectively). PCLS device Ai and Aii were designed and manufactured by Dr Alex Iles (Department of Chemistry, University of Hull). PCLS device Bi and Bii were designed and manufactured by Dr Dmitriy Kuvshinov (Department of Chemical Engineering, University of Hull), with PCLS device Bi on loan from the Greenman Laboratory (University of Hull) (Kennedy *et al,* 2019).

4.2.4.2 PCLS Device A Iteration One (Ai)

CCD2 was modified for use with PCLS through the removal of the membrane and wafer from the device's central chamber, to create PCLS device Ai. PCLS device Ai was designed and manufactured by Dr Alex Iles (Department of Chemistry, University of Hull) for use in

tissue culture. The device comprised of two identical PMMA sides measuring 80mm x 50mm x 10mm milled using a CNC machine and drilled in four corners to enable the device to be sealed. Each half comprised of a 3mm diameter inlet and outlet tapering to 0.8mm at the fluid delivery/collection point and a milled central chamber approximately 25mm x 10mm x 0.2mm, surrounded by a 1mm deep channel to hold a silicone O-ring to improve the seal between the two halves (Figure 4.13).

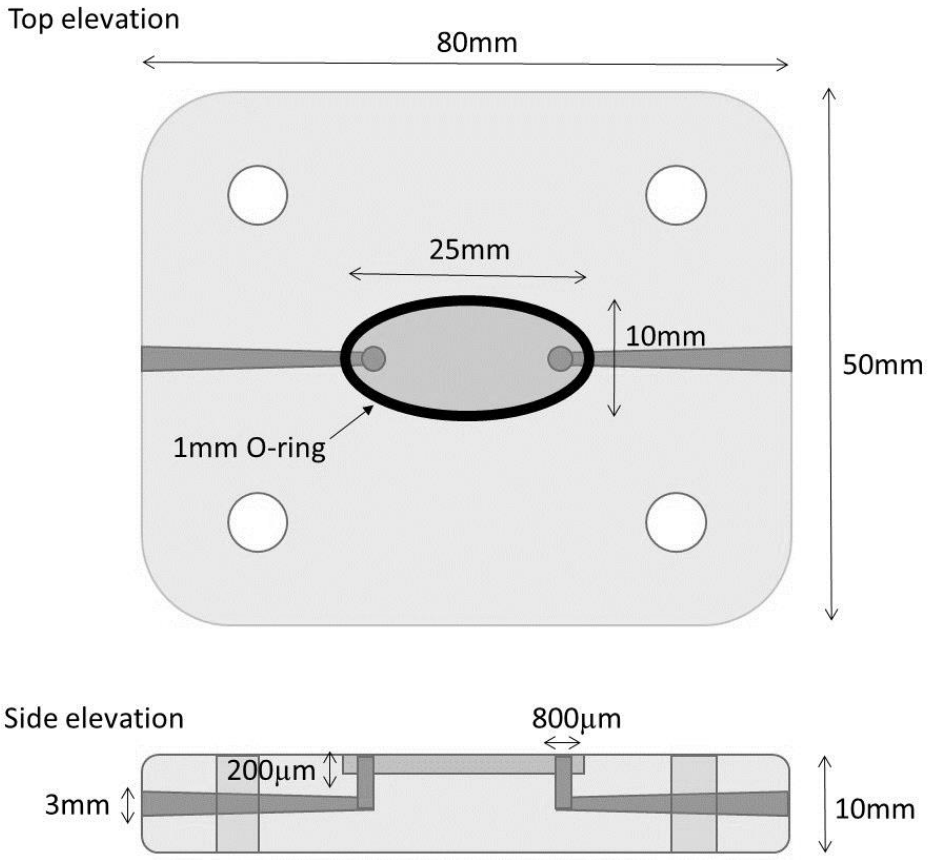

Figure 4.13 Microfluidic PCLS device A iteration one schematic showing the top and side elevations of the main PMMA body of the device.

Fluid was delivered/collected from the device through platinum cured tubing (2.4mm OD, 0.8mm ID) (Advanced Fluid Solutions), connected to the device by a polypropylene push fit elbow luer connector (Thistle Scientific). Direction of tissue DMEM flow was via the inlet in either layer, passing across the tissue through the milled central chamber, before being collected via the outlet in either layer (Figure 4.14). Tissue DMEM was flowed through both

inlets and effluent pooled together from both outlets, due to chambers no longer being separated through the presence of a membrane.

Figure 4.14 Direction of the fluid flow through the main PMMA body of microfluidic PCLS device A iteration one. Fluid flow depicted by arrows, tissue DMEM flows into device via inlet, passes over the tissue via the milled central chamber before flowing out via the outlet.

500µm PCLS were produced as previously explained (see 3.2.1.2) and 8mm biopsy punched discs were removed from the slices. The PCLS was placed in the central chamber with 100µl of tissue DMEM, sealed and perfused manually applying gentle pressure to the filled 20ml plastic syringes (Fisher Scientific), with pre-warmed tissue DMEM, buffered with 25mM HEPES. The device was subsequently incubated at 37^{o}C in an egg incubator for a period of 6 days with effluent samples collected every 24 hours (initial 2 hour effluent collected from 12 well plate (Sarstedt) where slices are held prior to device setup). Continuous perfusion was achieved through the use of an infusion syringe pump (Harvard Apparatus UK) running with an initial media flow rate of 50µl/min for 10 minutes to remove any bubbles inadvertently added to the system during setup and to ensure the entire system was perfused effectively, before being reduced to 2µl/min for the duration of the culture period (Figure 4.15). Effluent collection throughout the culture period was stored at 4^{o}C for later analysis.

Figure 4.15 Microfluidic PCLS device Ai configuration showing arrangement on infusion syringe pump **(A)** (only one inlet shown connected for clarity of position) and placement of PCLS within the device and position of inlets and outlets **(B)**.

Similar issues to those discussed 4.2.1.3 became apparent during the optimisation of PCLS device Ai, these being the leakage of media from the inlets of the device which was resolved by the use of PTFE tape and the problem relating to sterilising the device which was rectified by moving from a PMMA to PC based device. Additionally, this device also leaked from the outlets and between the two layers, as a consequence of the absence of the membrane and wafer coupled with the presence of the PCLS in the central chamber, thus affecting the flow of the tissue DMEM through the device. The lack of the wafer and membrane resulted in an incomplete seal at the O-rings, whilst the thickness of the PCLS at 500µm was slightly larger than that of the central chamber at around 400µm. Thus this created further pressure forcing tissue DMEM to leak in the manner outlined and preventing effective perfusion of the PCLS during the culture period.

4.2.4.3 PCLS Device A Iteration Two (Aii)

To overcome the issues outlined with PCLS device Ai, CCD3 was utilised alongside a modified PMMA wafer. PCLS device Aii was designed and manufactured by Dr Alex Iles (Department of Chemistry, University of Hull) for use in tissue culture. The device comprised of two identical PC sides measuring 80mm x 50mm x 10mm milled using a CNC machine and drilled in four corners to enable the device to be sealed. Each half comprised of a 3mm diameter inlet and outlet tapering to 0.8mm at the fluid delivery/collection point

and a milled central chamber approximately 25mm x 10mm x 0.5mm, surrounded by a 1mm deep channel to hold a silicone O-ring to improve the seal between the two halves. Tissue was cultured on a modified PMMA wafer that was laser cut measuring approximately 25mm x 10mm x 0.3mm with a 6mm diameter laser cut central circular aperture, with the 500µm PCLS suspended on a chloroform bonded 70µm cell strainer. The wafer was secured in the central chamber (500µm depth per side) which was sealed with O-rings and screws to minimise leakages from the cell culture area (Figure 4.16).

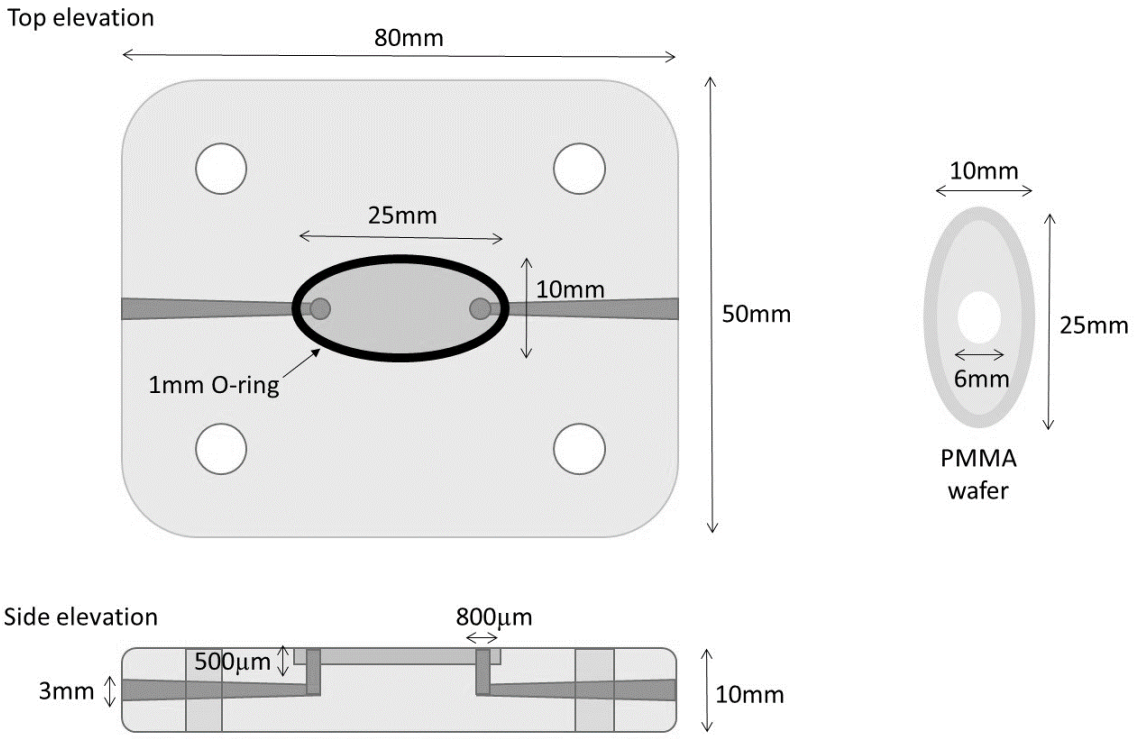

Figure 4.16 Microfluidic PCLS device A iteration two schematic showing the top and side elevations of the main PC body of the device **(A)** and the PMMA wafer for use as a tissue culture surface **(B)**.

Fluid was delivered/collected from the device through platinum cured tubing (2.4mm OD, 0.8mm ID) (Advanced Fluid Solutions), connected to the device by a polypropylene push fit elbow luer connector (Thistle Scientific) wrapped in PTFE tape to create a secure fitting. Direction of tissue DMEM flow was via the inlet in either layer, passing across the tissue in the top or and the cell strainer in the bottom of the milled central chamber, before being collected via the outlet in either layer. Tissue DMEM was flowed through both inlets and

effluent pooled together from both outlets as the tissue DMEM from both inlets mixed during the culture period, owing to the tissue DMEM being able to pass through the cell strainer (Figure 4.17).

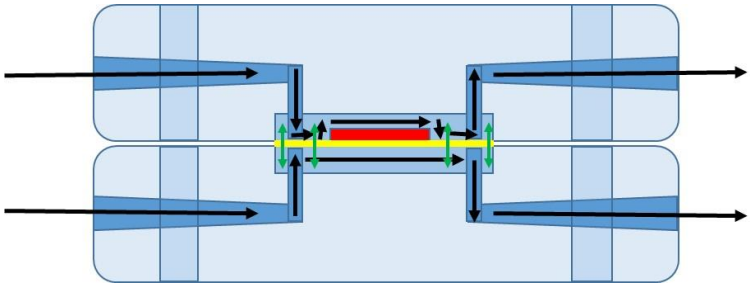

Figure 4.17 Direction of the fluid flow through the main PC body of microfluidic PCLS device A iteration two. Fluid flow depicted by arrows, tissue DMEM flows into device via inlet, passing across the tissue (represented in red) in the top or and the cell strainer (represented in yellow) in the bottom of the milled central chamber before flowing out via the outlet. Green arrows represent the fluid flow across the cell strainer between the two halves of the device.

The modified PMMA wafer was designed with a central circular aperture that could hold a 6mm biopsy punched disc from a 500µm PCLS, suspended on a chloroform bonded 70µm cell strainer (Figure 4.18).

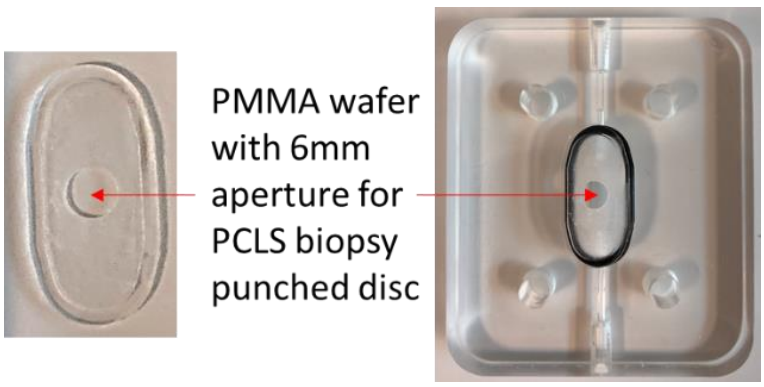

Figure 4.18 Microfluidic PCLS device Aii configuration showing modified PMMA wafer and position on the O-ring over central chamber.

Once in place the PCLS was covered with 200µl of tissue DMEM and the device seal and manually perfused as described previously (4.2.4.2). The device was subsequently incubated at 37^{o}C in an egg incubator for a period of 6 days with effluent samples collected every 24 hours (2 and 24 hour effluent was collected from a 12 well plate where slices were held prior to device setup). Continuous perfusion was achieved through the use of an infusion syringe pump running at 2µl/min for the duration of the culture period. Effluent collection throughout the culture period was stored at 4^{o}C for later analysis.

4.2.4.4 PCLS Device B Iteration One (Bi)

PCLS device Bi (Figure 4.21) having been previously used for head and neck cancer studies (Kennedy *et al*, 2019; on loan from Greenman Laboratory, University of Hull) required less optimisation beyond modifications in the procedure to suit the lung tissue being used. PCLS device Bi was originally designed and manufactured by Dr Dmitriy Kuvshinov (Department of Chemical Engineering, University of Hull) for use in culturing head and neck squamous cell carcinomas and here was utilised to culture 500µm PCLS. The device comprised of two identical PEEK sides measuring 30mm diameter by 10mm depth milled using a CNC machine, with four holes to enable the device to be sealed. Each half comprised of a 1mm diameter inlet and outlet and a milled central chamber measuring approximately 10mm diameter by 4mm, into which a 10mm diameter by 4mm porous Pyrex® sintered disc, pore size 160 – 250mm (The Lab Warehouse, Grays, UK) was placed. A seal between the two halves was provided by a 1mm thick silicon gasket with a 6mm diameter central hole in which the PCLS slice is placed (Figure 4.19).

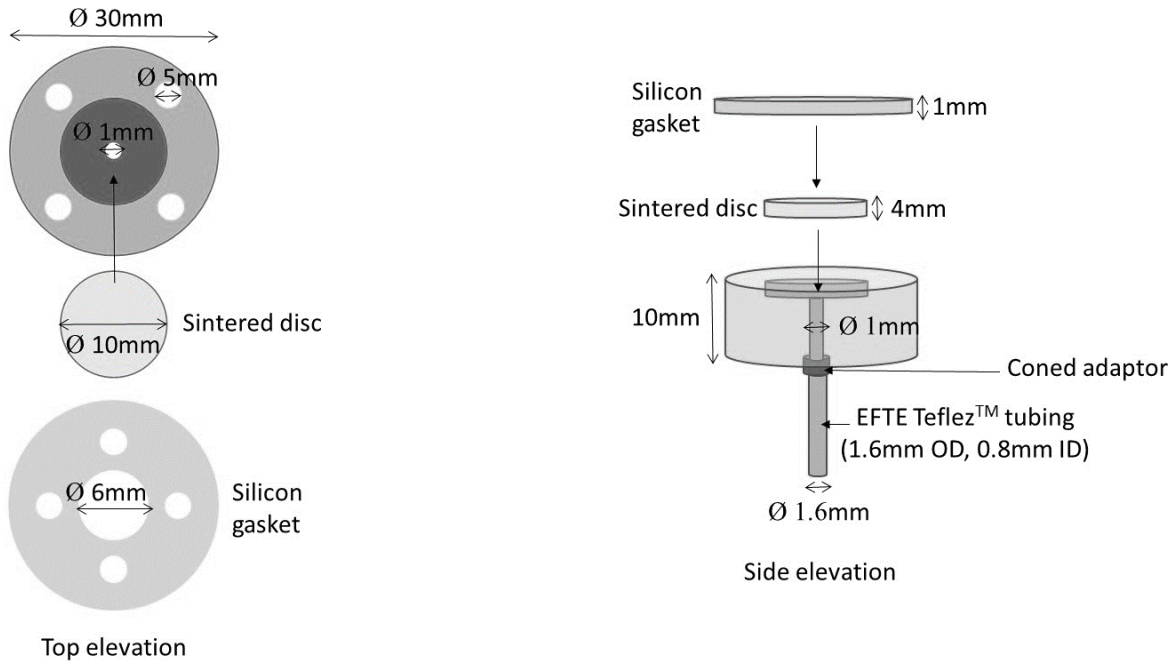

Figure 4.19 Microfluidic PCLS device B iteration one schematic showing the top and side elevations of the device.

Ethylene-tetrafluoroethylene (ETFE Teflez®) tubing (1.6mm OD, 0.8mm ID) was secured to each side via a coned adaptor (LabSmith, Mengel Engineering, Denmark) to create a since inlet and outlet. Direction of tissue DMEM flow was via the inlet, pooling in the first sintered disc before passing around and through the tissue and the cell strainer into the second sintered disc, finally being collected via the outlet. Tissue DMEM flowed through the single inlet at an initial rate of 50µl/min for 10 minutes and then at a slower rate of 2µl/min, with effluent collected via the single outlet at 24 hour intervals and stored at 4°C. (Figure 4.20).

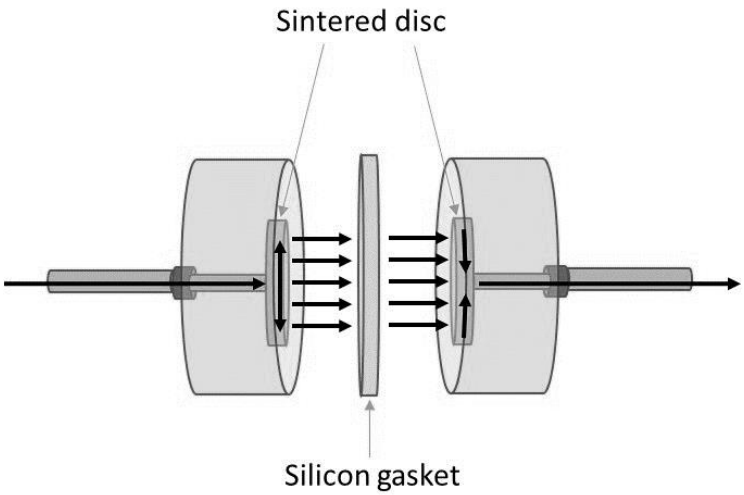

Figure 4.20 Direction of the fluid flow through the main PEEK body of microfluidic PCLS device B iteration one. Fluid flow depicted by black arrows, tissue DMEM flows into device via inlet, pooling in the first sintered disc before passing around and through the tissue and the cell strainer into the second sintered disc, finally being collected via the outlet.

Due to design differences compared to PCLS device Ai, this device required the application of a 6mm biopsy punched disc of 500µm PCLS into the centre of the silicone gasket, which was separated from the sintered disc by a section of 70µm cell strainer to prevent the tissue from adhering to the sintered disc, thus enabling removal from the device after the culture period for further analysis. The presence of the depression and sintered disc enabled tissue DMEM to pool and provide continuous perfusion around the entire PCLS, ensuring even distribution of nutrients across the tissue. Once the tissue was in place, the device was screwed together to create a complete seal and perfused using the aforementioned media and method (4.2.4.2) (Figure 4.21).

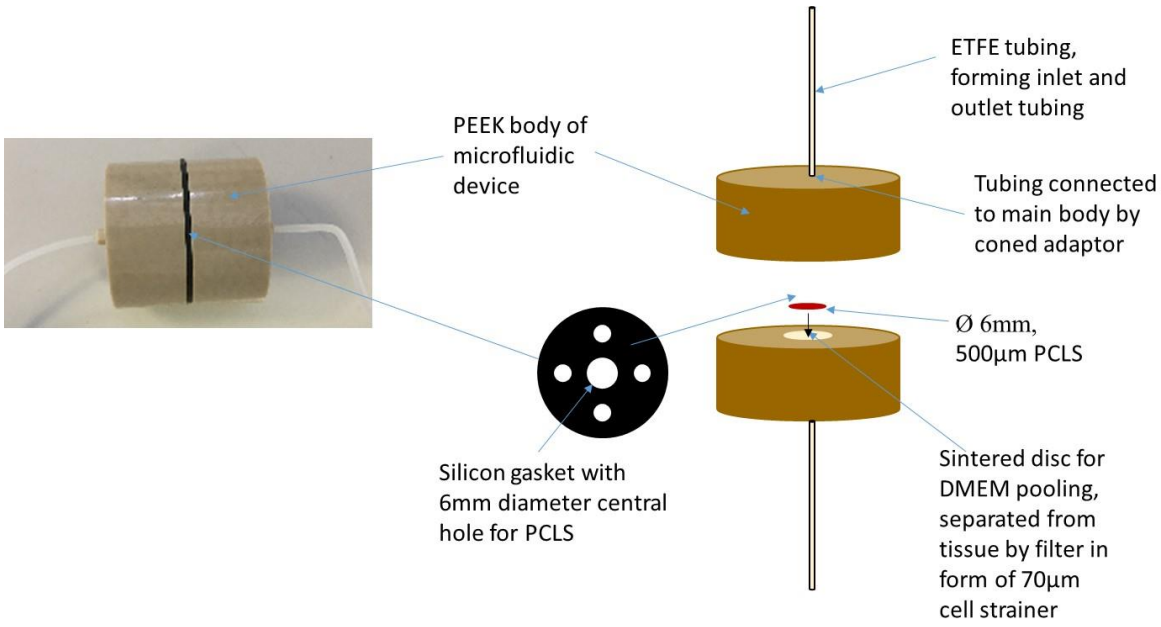

Figure 4.21 Microfluidic PCLS device Bi schematic showing different elements of the device and the configuration of the constructed device.

4.2.4.5 PCLS Device B Iteration Two (Bii)

Whilst PCLS device Bi functioned effectively the central hole in the silicone gasket and the size of the sintered disc limited the size of the PCLS disc to 6mm diameter, to enable a large PCLS to be utilised a modified device was produced. PCLS device B iteration two was designed and manufactured by Dr Dmitriy Kuvshinov (Department of Chemical Engineering, University of Hull) for use in culturing 500µm PCLS. The device comprised of two identical PEEK sides measuring 35mm diameter by 12mm depth milled using a CNC machine, with four holes to enable the device to be sealed. Each half comprised of a 1.8mm diameter inlet and outlet and a milled central chamber measuring approximately 20mm diameter by 4mm, into which a 20mm diameter by 4mm Pyrex® sintered disc, pore size 160 – 250mm (The Lab Warehouse) was fitted. A seal between the two halves was provided by a 3mm thick silicon gasket with a 14mm diameter central hole in which the PCLS is placed (Figure 4.22).

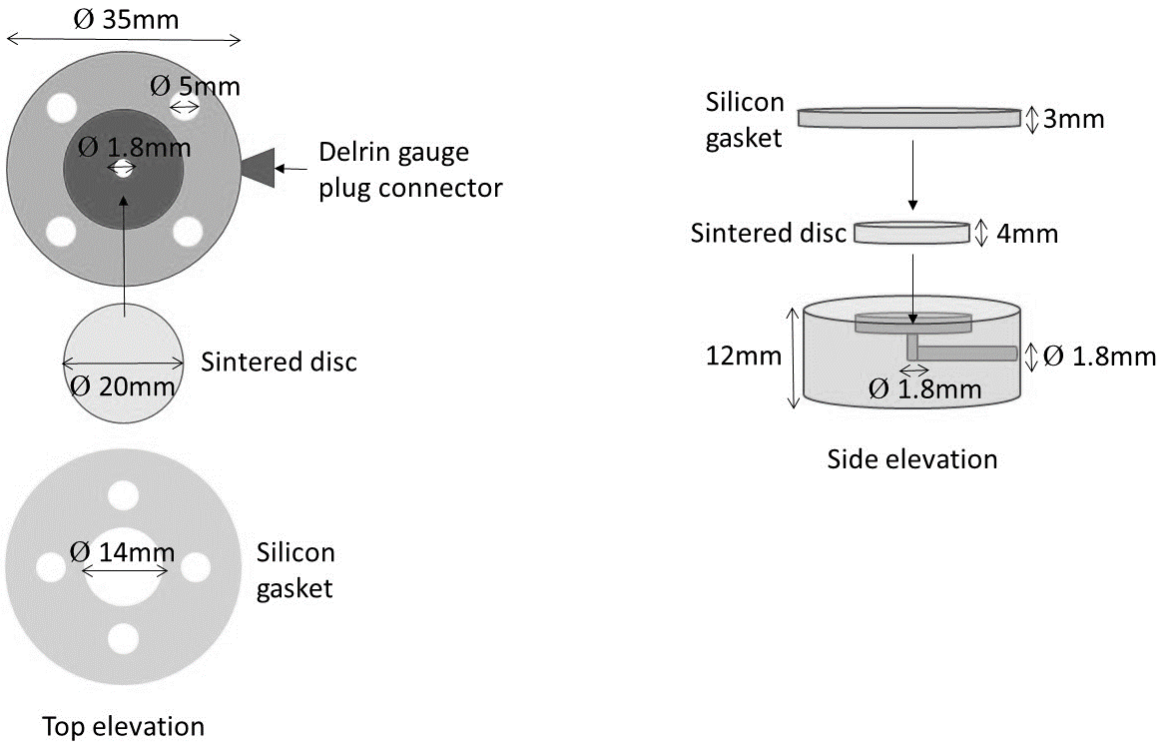

Figure 4.22 Microfluidic PCLS device B iteration two schematic showing the top and side elevations of the device.

Although the 6mm PCLS disc was reproducible, the small diameter made it difficult to handle and reduced the area of tissue available for exposure to test compounds to 28mm^2 compared to 50mm^2 if a 8mm diameter disc was utilised. The creation of PCLS device Bii addressed this issue whilst working on the same principle as PCLS device Bi with some minor modifications. These modification included a change to a silicon gasket with a 14mm central hole and the use a larger depression and sintered disc (diameter 20mm, depth 4mm) in the central region of each half of the device (Figure 4.23).

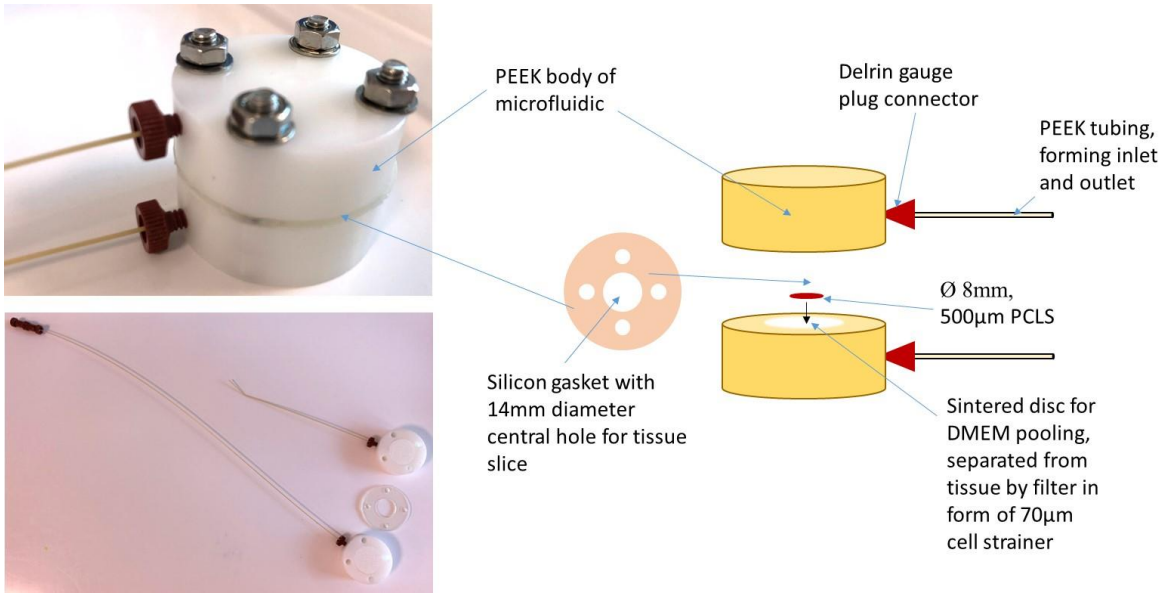

Figure 4.23 Microfluidic PCLS device Bii schematic showing different elements of the device and the configuration of the constructed device.

8mm biopsy punched PCLS discs were placed in the centre of the silicon gasket, separated from the sintered disc by a section of 70µm cell strainer as previously discussed (4.2.4.4). Once the tissue was in place, the device was sealed and perfused using the aforementioned media and method (4.2.4.2) (Figure 4.24).

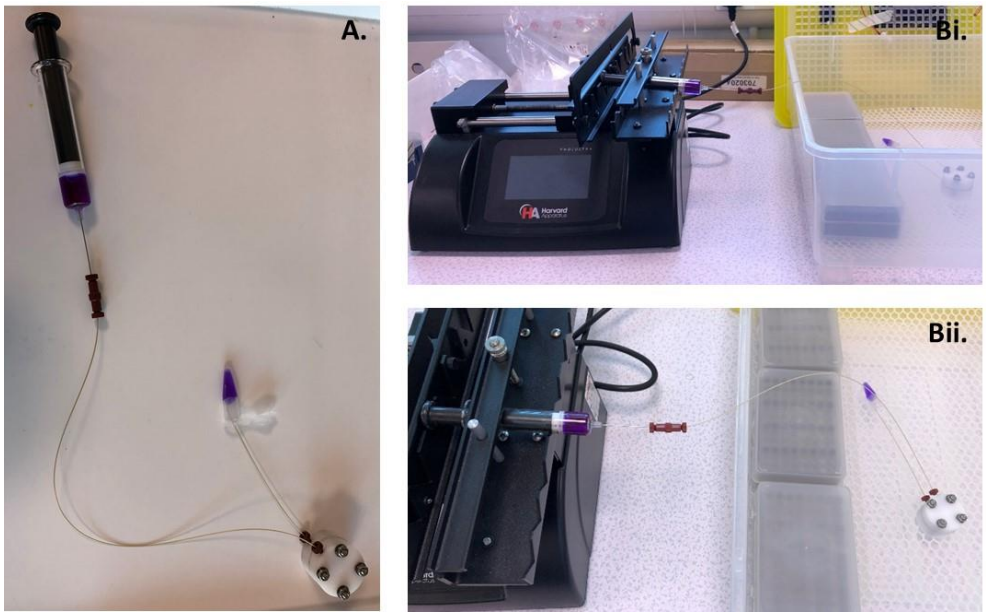

Figure 4.24 Microfluidic PCLS device Bii configuration showing arrangement of constructed device **(A)** and showing arrangement on infusion syringe pump **(Bi and Bii)**.

PEEK tubing (0.8mm OD, 0.4mm ID) was secured to the device via a delrin microtight gauge plug, 6-32 coned connector (Kinesis) screwed into a thread milled into the side of the device at the inlet/outlet site, to create a since inlet and outlet. Direction of tissue DMEM flow was via the inlet, pooling in the first sintered disc before passing around and through the tissue and the cell strainer into the second sintered disc, finally being collected via the outlet. Tissue DMEM flowed through the single inlet at an initial rate of 2µl/min, with effluent collected via the single outlet at 24 hour intervals and stored at 4^{o}C (Figure 4.25).

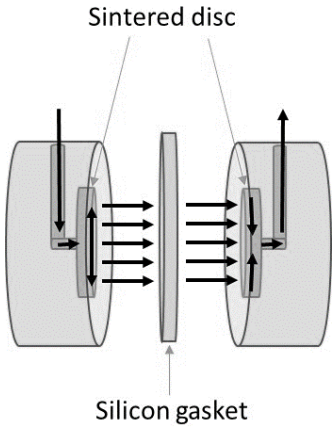

Figure 4.25 Direction of the fluid flow through the main PEEK body of microfluidic PCLS device B iteration two. Fluid flow depicted by black arrows, tissue DMEM flows into device via inlet, pooling in the first sintered disc before passing around and through the tissue and the cell strainer into the second sintered disc, finally being collected via the outlet.

4.2.4.6 Justification for Chosen PCLS Device Based on Preliminary Observations

Prior to conducting any experimental analysis, obvious differences in two devices was apparent which directly influenced the decision to further utilise and develop a device for conducting experiments with PCLS. The most noticeable observation was the variation in the effluent colour, which indicated a potential variation in viability between the devices. The effluent being collected from PCLS device A had changed from the normal reddish-orange colour to a pinkish-purple colour indicating that the pH of the media had become more alkaline (Pick and Keisari, 1980) even with the additional buffering provided by HEPES in the solution (Halldorsson *et al*, 2015), whilst the effluent from PCLS device B retained the normal colour. Furthermore, PCLS device A also repeatedly leaked, became blocked or

stopped collecting effluent, thus meaning the tissue was not always continuously perfused and would likely factor in any noticeable difference which might be observed in experimental data. As a consequence of these observations PCLS device B became the main focus for developing a suitable PCLS device.

4.2.5 PCLS Device Design

4.2.5.1 Optimised Device Design for PCLS

A microfluidic device was designed and manufactured by Dr Dmitriy Kuvshinov (Department of Chemical Engineering, University of Hull) for use in culturing 500µm PCLS. The device comprised of two identical PEEK sides measuring 35mm diameter by 12mm depth milled using a CNC machine, with four holes to enable the device to be sealed. Each half comprised of a 1.8mm diameter inlet and outlet and a milled central chamber measuring approximately 20mm diameter by 4mm, into which a 20mm diameter by 4mm Pyrex® sintered disc, pore size 160 – 250mm (The Lab Warehouse, Grays, UK) was placed. A seal between the two halves is provided by a 3mm thick silicon gasket with a 14mm diameter central hole in which the PCLS was placed (Figure 4.26).

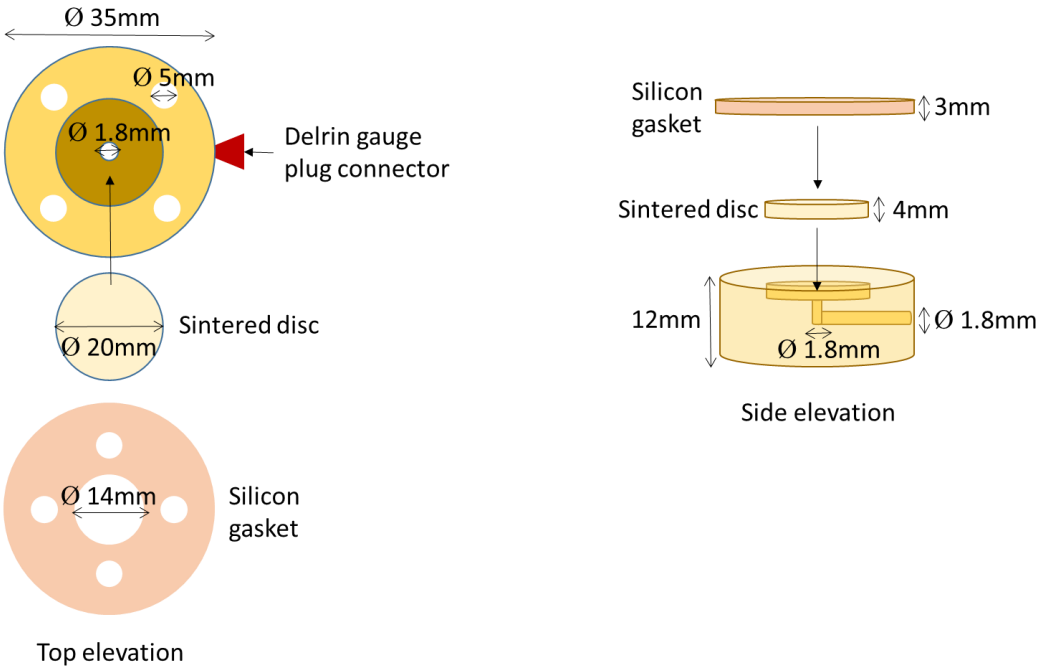

Figure 4.26 Optimised PCLS microfluidic device schematic showing the top and side elevations of the device.

Fluid was delivered/collected from the device through PEEK tubing (0.8mm OD, 0.4mm ID), connected to the device by a delrin microtight gauge plug, 6-32 coned connector (Kinesis) screwed into a thread milled into the side of the device at the inlet/outlet site. Direction of tissue DMEM flow was via the inlet, pooling in the first sintered disc before passing around and through the tissue and the cell strainer into the second sintered disc, finally being collected via the outlet (Figure 4.27).

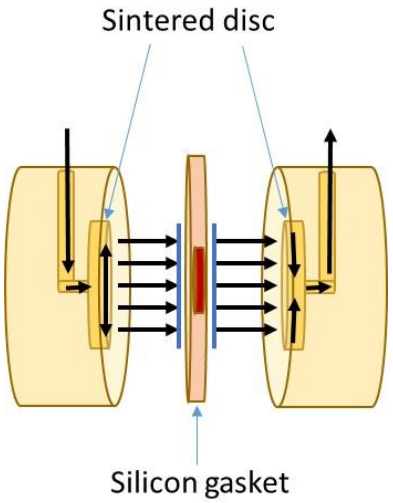

Figure 4.27 Direction of the fluid flow through the main PEEK body of optimised microfluidic PCLS device. Fluid flow depicted by black arrows, tissue DMEM flows into device via inlet, pooling in the first sintered disc before passing around and through the tissue (represented in red) and the cell strainer (represented in blue) into the second sintered disc, finally being collected via the outlet.

4.2.5.2 Optimised PCLS Device Operation

The PEEK microfluidic device was soaked in 70% ethanol overnight prior to use, the entire system perfused with 70% ethanol for 10 minutes and rinsed with 1x PBS for 10 minutes before the addition of any human tissue. Lung tissue was inflated and slices at 500µm as previously describe (see 3.2.1.1 and 3.2.1.2), from each slice a minimum of one 8mm biopsy punched disc was removed and placed in a 12 well plate with 500µl of tissue DMEM until required. A 70µm cell strainer was place on the sintered disc inside the device prior to the placement of the silicon gasket, once positioned the PCLS was placed in the central hole of

the silicon gasket and the device secured via four screws. The device was manually perfused with tissue DMEM to prime the system prior to subsequent automatic perfusion with tissue DMEM at a rate of 2µl/min via an infusion/withdrawal syringe pump. Effluent was collected at 2 and 24 hours from the 12 well plate and then every 24 hours from the device, effluent was stored at 4^{o}C until analysed. After a culture period of 6 days tissue was removed and either lysed (see 3.2.2.1) for LDH analysis (see 3.2.2.2) or alternatively snap frozen (3.2.4.1) for morphological analysis via H&E (3.2.4.3 and 3.2.4.5).

4.3 Microfluidic Device Results

4.3.1 Cell Culture Viability on a Microfluidic Device

4.3.1.1 Cell Culture Device Iteration One Observations on Viability

Membranes were collected after 72 hours in culture in a standard CO_2 incubator or on CCD1, cut in half and the membranes orientated so both 1N1 P2X3 cells and A549 cells were upward facing. Membranes were stained with 0.2% resazurin solution and viewed on a light box. Figure 4.28 provides representative images of stained membranes indicating the presence of pink resorufin staining as a consequence of the reduction of the resazurin stain, with both A549 and 1N1 P2X3 cells cultured in standard culture condition and thus viable cells, whilst cells cultured in CCD1 remained blue indicating non-viable cells under these culture conditions.

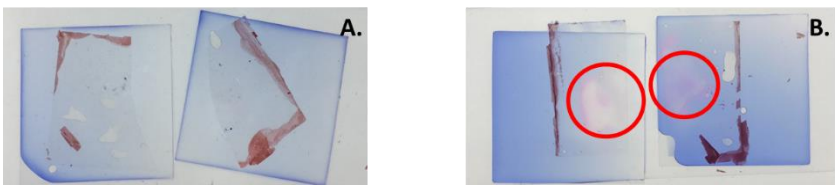

Figure 4.28 Resazurin stained membranes cultured on CCD1 **(A)** and in a standard incubator **(B)**. A549 cells were present on the membranes situated to the left of each image and 1N1 P2X3 cells were present on the membranes situated to the right of each image. Red circles indicate patches on membranes where blue resazurin dye has been reduced to pink resorufin in the presence of viable cells. Data represents three independent experiments (n=3).

To confirm resazurin results, a second set of membranes was processed in the same manner as above and stained with 0.4% trypan blue solution and view under a light microscope, to enable a comparison of the extent of viable unstained and non-viable stained cells to be assessed. Figure 4.29 provides representative images of trypan blue stained membranes, showing both stained (non-viable) and unstained (viable) A549 and 1N1 P2X3 cells from standard culture condition and predominantly stained (non-viable) A549 and 1N1 P2X3 cells cultured on CCD1.

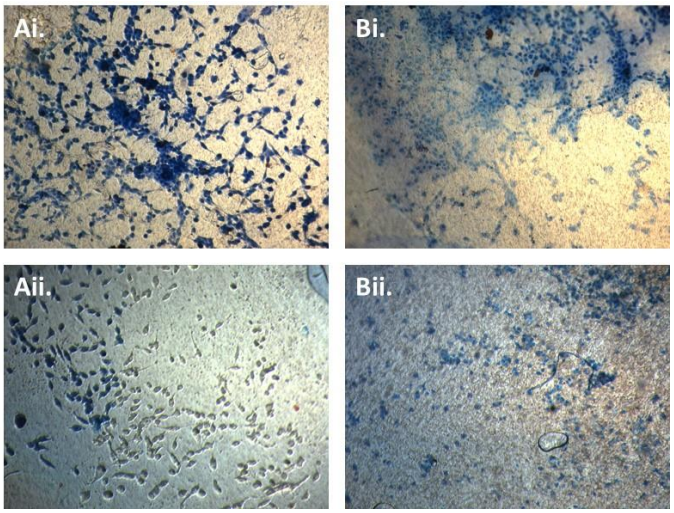

Figure 4.29 1N1 P2X3 cells **(Ai – Aii)** and A549 cells **(Bi – Bii)** stained with 0.4% trypan blue solution and viewed under a light microscope at 100x magnification 72 hour post culture on CCD1 **(Ai – Bi)** and 72 hour post culture in a standard CO_2 incubator **(Aii – Bii)**. Data represents three independent experiments (n=3).

Both viability assays indicate that the cells cultured on CCD1 were non-viable whilst the cells cultured in the standard CO_2 incubator remained predominately viable. These issues with viability supported the problems encountered during optimisation due to leakage and device design which supported the move towards the use of CCD2.

4.3.1.2 Cell Culture Device Iteration Two Observation on Viability and Cell Growth

Membranes were removed from the PMMA wafer after 72 hours in culture in a standard CO_2 incubator or on CCD2, stained with 0.4% trypan blue solution and viewed under a light

microscope, to enable a comparison of the extent of viable unstained and non-viable stained cells to be assessed. Figure 4.30 provides representative images of trypan blue stained membranes, showing both stained (non-viable) and unstained (viable) A549 and 1N1 P2X3 cells from standard culture condition and predominantly stained (non-viable) A549 and 1N1 P2X3 cells cultured on CCD2.

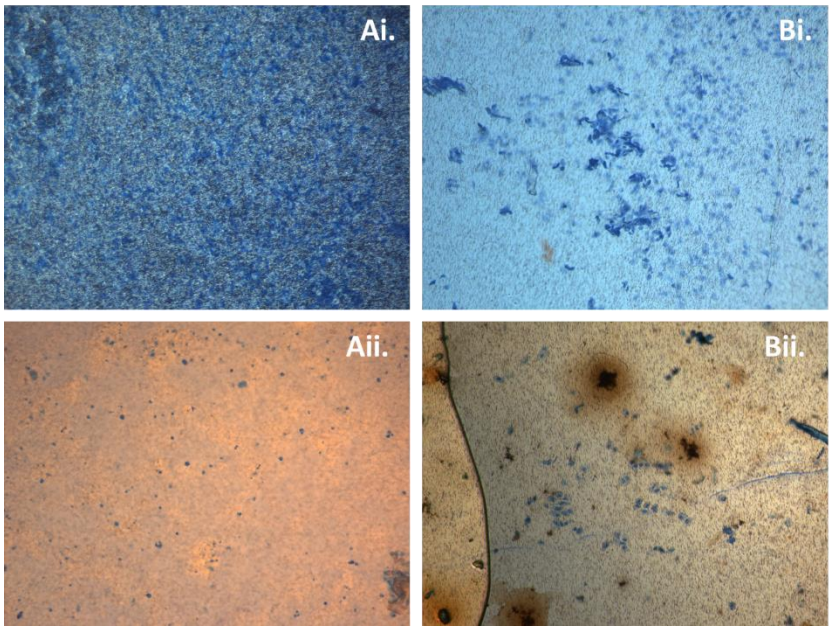

Figure 4.30 A549 cells **(Ai – Aii)** and 1N1 P2X3 cells **(Bi – Bii)** stained with 0.4% trypan blue solution and viewed under a light microscope at 100x magnification 72 hour post culture on CCD2 **(Ai – Bi)** and 72 hour post culture in a standard CO_2 incubator **(Aii – Bii)**. Data represents three independent experiments (n=3).

To better understand the development of the monolayer across the membrane in response to the lower viability of cells cultured on CCD2, membranes seeded with A549 cells cultured on CCD2 and in a standard CO_2 incubator for 72 hours were stained with Kwik Diff™ staining solution. Figure 4.16 shows sparse coverage of the membrane with A549 cells when cultured on CCD2, with evidence of limited cellular growth in the regions of the membrane where the inlet and outlet are positioned (Figure 4.31) and bubble formation during perfusion of the device. Conversely, when A549 cells were cultured in a standard CO_2 incubator the cells formed a confluent monolayer across the useable region of the membrane and covered the majority of the available surface.

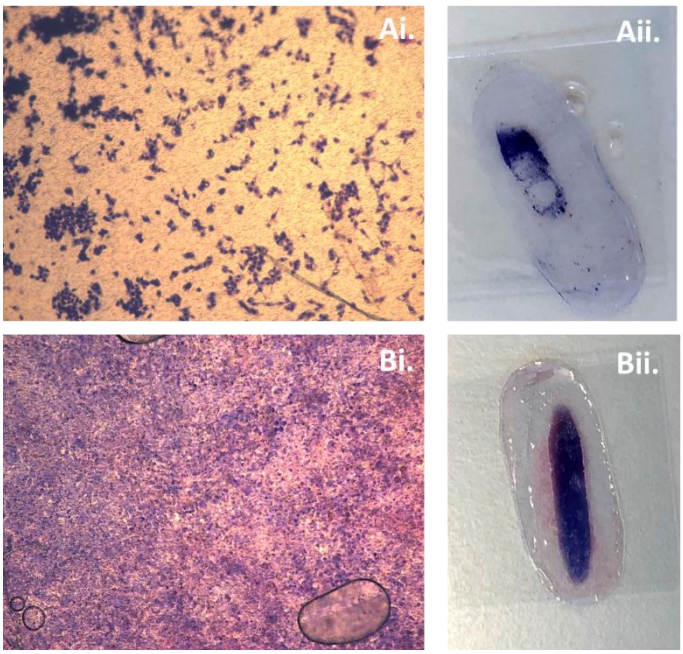

Figure 4.31 A549 cells stained using Kwik Diff™ stain solution viewed under a light microscope at 100x magnification 72 hour post culture on CCD2 **(Ai)** and cells 72 hour post culture in a standard CO_2 incubator **(Bi)**. Entire stained membrane removed from the PMMA wafer of cells cultured on CCD2 **(Aii)** and in a standard CO_2 incubator **(Bii)**. Data represents three independent experiments (n=3).

Both assays indicated that the cells cultured on CCD2 displayed improved growth compared to CCD1 however, the cells remained predominantly non-viable when cultured on the device when compared to cells cultured in the standard CO_2 incubator.

4.3.1.3 Cell Culture Device Iteration Three Observations on Viability and Cell Growth

Membranes were removed from the PMMA wafer after 72 hours in culture on CCD3, stained with 0.4% trypan blue solution and viewed under a light microscope, to enable the extent of viable unstained and non-viable stained cells to be assessed. Additionally, membranes cultured on CCD3 were also stained with Kwik Diff™ staining solution after a 72 hour culture period, to assess the development of the monolayer across the membrane during culture. Figure 4.32 provides representative images of trypan blue stained membranes, showing both stained (non-viable) and unstained (viable) A549 after 72 hours

culture on CCD3 and the extent of cell growth creating a confluent monolayer across the useable area of the membrane.

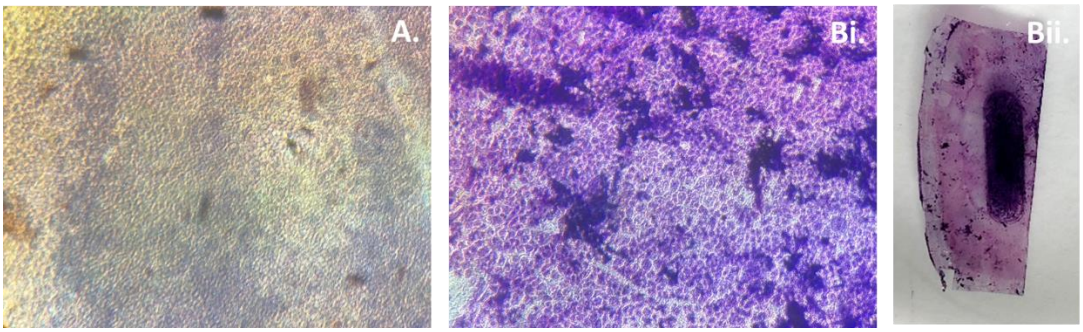

Figure 4.32 A549 cells stained with 0.4% trypan blue solution and viewed under a light microscope at 100x magnification 72 hour post culture on CCD3 **(A).** A549 cells stained using Kwik Diff™ stain solution viewed under a light microscope at 100x magnification 72 hour post culture on CCD3 **(Bi)** and the entire stained membrane removed from the PMMA wafer of cells cultured on CCD3 **(Bii)**. Data represents three independent experiments (n=3).

Both assays indicate that the cells cultured on CCD3 had improved growth compared to CCD2 and showed better viability than that observed on previous iterations of the device. Whilst there was still evidence of non-viable cells in some areas of the membrane, there was a greater number of viable cells compared to previous iterations of the device. Similarly, there was also an improvement in the formation of a confluent monolayer of cells, with the majority of the membrane being covered.

4.3.1.4 A549 Cells Cultured on Cell Culture Device Three have Reduced Viability

To support the observations made around cell viability the extent of cellular cytotoxicity was determined by measuring the extent of LDH in effluent collected during the 72 hour culture period and after complete lysis of A549 cells cultured on the microfluidic device membranes (using CCD3) as described in 4.2.3.2. When comparing the effluent there is no significant difference ($P>0.05$) between the amount of LDH released by cells cultured on CCD3 compared to those cultured in a standard CO_2 incubator. Whilst after complete lysis

of cells there was a 46% reduction in LDH released from A549 cells cultured on CCD3 compared to those cultured in a standard CO_2 incubator (P<0.005) (Figure 4.33).

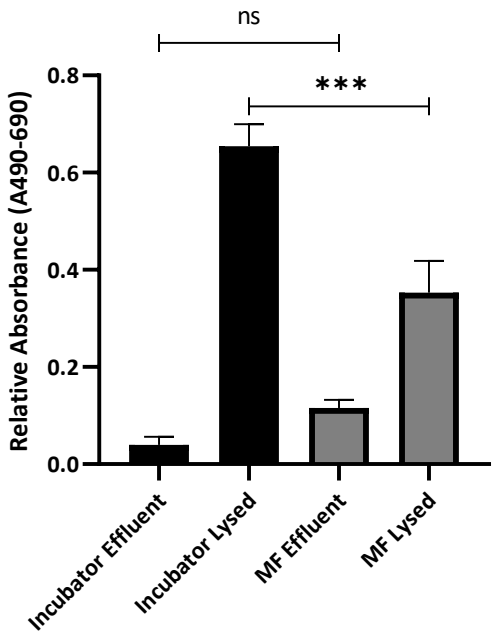

Figure 4.33 LDH analysis of A549 cells cultured on CCD3 compared to A549 cells cultured in a standard CO_2 incubator. LDH measurements were based on absorbance reading (490 – 690nm) accounting for media blank, for effluent collected 72 hours post culture and after cell were completely lysed. Results are displayed as mean ± SEM (n=3). Statistical analysis was conducted using a two-way ANOVA with multiple comparison by Tukey analysis. P<0.005***

4.3.1.5 A549 Cells Cultured on Cell Culture Device Three have Reduced Cell Proliferation

To support the observation made around cell growth, the extent of cellular proliferation was measured by the extent of SRB dye binding to the A549 cells cultured on the microfluidic device membranes (using CCD3) as described in 4.2.3.3. Comparison on absorbance of dye binding between A549 cells cultured on CCD3 to those cultured in a standard CO_2 incubator showed no significant difference however, there was a 39% reduction in absorbance and thus equivalent cell mass and number for cells cultured on CCD3 compared to a standard incubator (Figure 4.34).

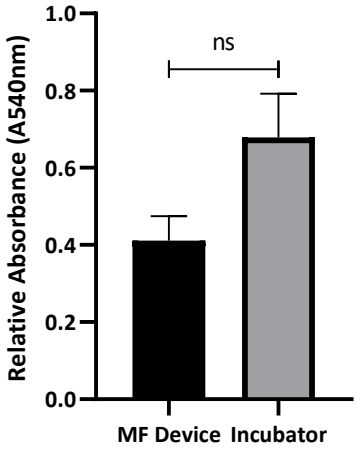

Figure 4.34 SRB analysis of A549 cells cultured on CCD3 compared to A549 cells cultured in a standard CO_2 incubator. SRB measurements were based on absorbance reading (540nm) accounting for media blank, of cells stained after 72 hours in culture. Results are displayed as mean ± SEM (n=3). Statistical analysis was conducted using a paired t-test.

4.3.2 Healthy Tissue LDH Cytotoxicity Analysis on a Microfluidic Device

4.3.2.1 Human PCLS Cultured on PCLS Device A Iteration One (Ai) have Reduced Viability

The extent of cellular cytotoxicity was determined by measuring the level of LDH in effluent collected during the 6 day culture period and after complete lysis of 8mm diameter 500µm PCLS, cultured on PCLS device Ai (3.2.2.1 and 3.2.2.2). When comparing the effluent there was no significant difference ($P>0.05$) between the amount of LDH released by the tissue cultured on PCLS device Ai compared to tissue cultured in a static multi-well plate in a standard CO_2 incubator. Whilst after complete lysis of cells there was a 68% difference in LDH released from tissue cultured on PCLS device Ai compared to those cultured on a static multi-well plate in a standard CO_2 incubator ($P<0.001$) (Figure 4.35).

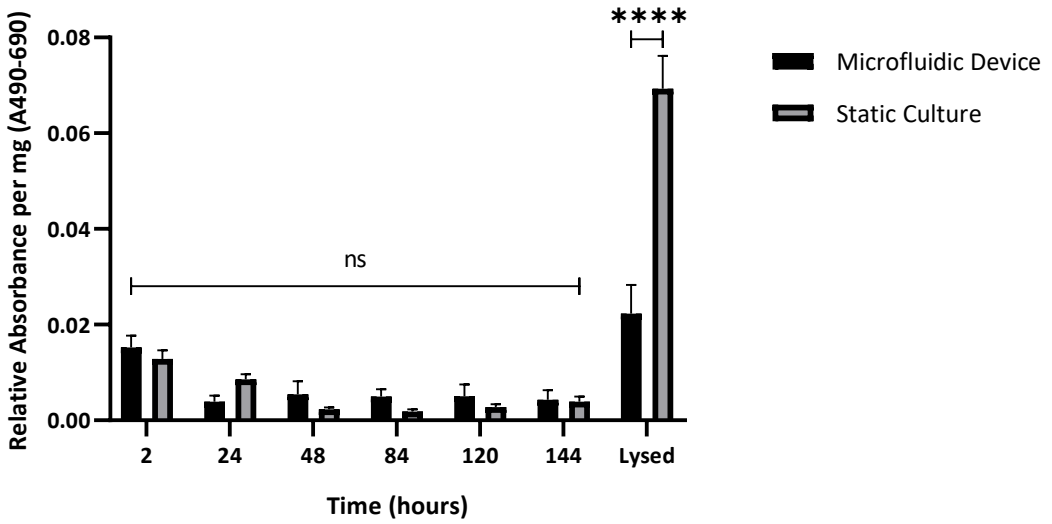

Figure 4.35 LDH analysis of 8mm diameter, 500µm PCLS cultured on PCLS device Ai compared to 8mm diameter, 500µm PCLS cultured on a static multi-well plate in a standard CO_2 incubator. LDH measurements were based on absorbance reading (490 – 690nm) accounting for media blank, for effluent collected between 2 – 144 hours post culture and after PCLS was completely lysed. Results are displayed as mean ± SEM (N=5, n=6). Statistical analysis was conducted via multiple t-test using the Holm-Sidák method. $P<0.001^{****}$

4.3.2.2 Human PCLS Cultured on PCLS Device A Iteration Two (Aii) have Reduced Viability

To identify whether the extent of cellular cytotoxicity had improved between PCLS device Ai and Aii, the LDH assay was conducted in the same manner as 4.3.2.1 on the effluent and lysed 6mm diameter 500µm PCLS cultured on PCLS device Aii. The LDH released by the effluent was minimal, barely registering as an absorbance measurement in either culture method. After complete lysis of cells there was a 96% difference in LDH released from tissue cultured on PCLS device Aii compared to those cultured on a static multi-well plate in a standard CO_2 incubator however, due to limited number of experimental replicates statistical analysis was not possible (Figure 4.36).

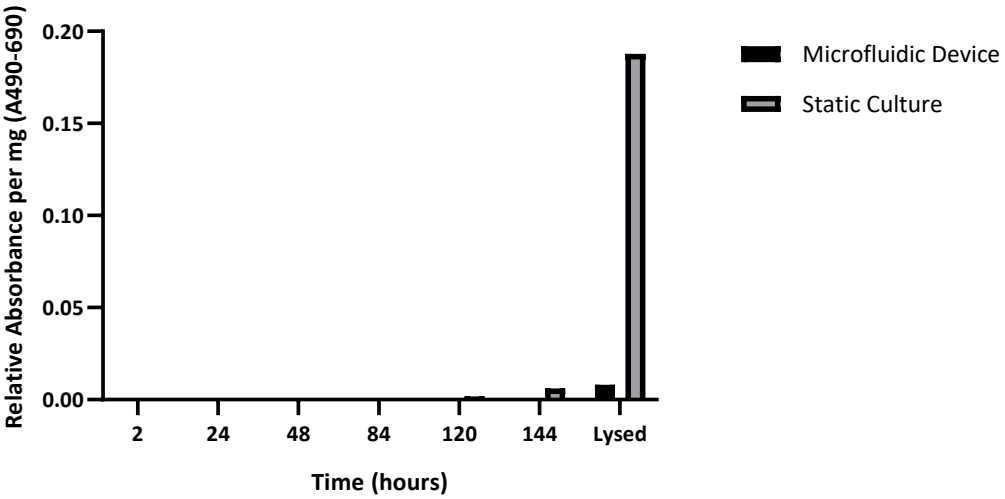

Figure 4.36 LDH analysis of 6mm diameter, 500µm PCLS cultured on PCLS device Aii compared to 6mm diameter, 500µm PCLS cultured on a static multi-well plate in a standard CO_2 incubator. LDH measurements were based on absorbance reading (490 – 690nm) accounting for media blank, for effluent collected between 2 – 144 hours post culture and after PCLS was completely lysed. Results are displayed as mean values (N=1, n=2). Statistical analysis could not be conducted due to insufficient replicates of the experiment.

4.3.2.3 Human PCLS Cultured on PCLS Device B Iteration One (Bi) does not have Reduced Viability

Due to the difference in design it was necessary to determine how effectively each device functioned, thus to identify whether the extent of cellular cytotoxicity differed between PCLS device A iteration and Bi, the LDH assay was conducted in the same manner as 4.3.2.1 on the effluent and lysed 6mm diameter 500µm PCLS cultured on PCLS device Bi. When comparing the effluent there is no significant difference ($P>0.05$) between the amount of LDH released by the tissue cultured on PCLS device Bi compared to tissue cultured on a static multi-well plate in a standard CO_2 incubator. Similarly, after complete lysis of cells there was a 34% difference in LDH released from tissue cultured on PCLS device Bi compared to those cultured on a static multi-well plate in a standard CO_2 incubator ($P>0.05$) (Figure 4.37).

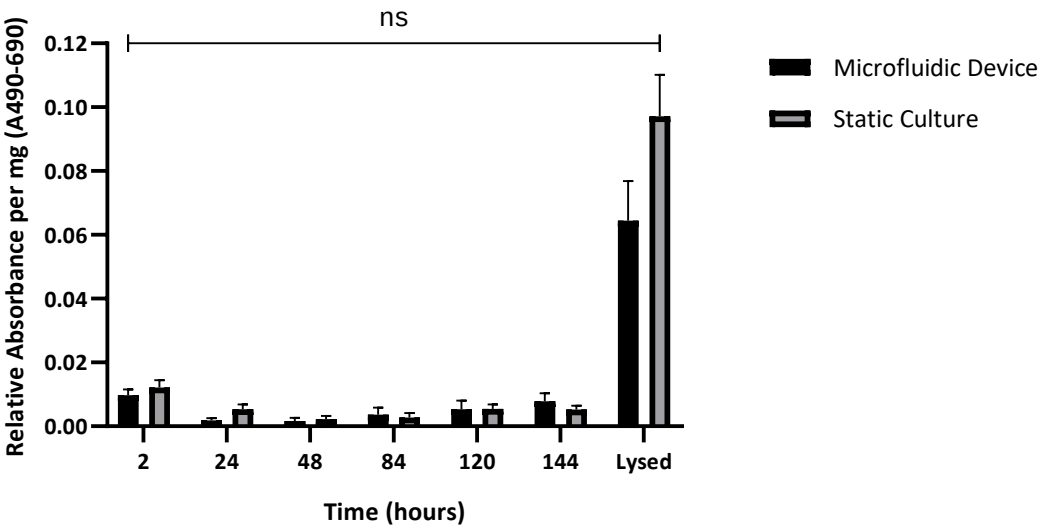

Figure 4.37 LDH analysis of 6mm diameter, 500µm PCLS cultured on PCLS device Bi compared to 6mm diameter, 500µm PCLS cultured on a static multi-well plate in a standard CO_2 incubator. LDH measurements were based on absorbance reading (490 – 690nm) accounting for media blank, for effluent collected between 2 – 144 hours post culture and after PCLS was completely lysed. Results are displayed as mean ± SEM (N=3, n=6). Statistical analysis was conducted via multiple t-test using the Holm-Sidák method.

4.3.2.4 Human PCLS Cultured on PCLS Device B Iteration Two (Bii) have Reduced Viability

To identify whether the extent of cellular cytotoxicity had improved between PCLS device Bi and Bii, the LDH assay was conducted in the same manner as 4.3.2.1 on the effluent and lysed 8mm diameter 500µm PCLS cultured on PCLS device Bii. When comparing the effluent there was little observable difference between the LDH released by the tissue cultured on PCLS device Bii compared to tissue cultured on a static multi-well plate in a standard CO_2 incubator. After complete lysis of cells there was an 89% difference in LDH released from tissue cultured on PCLS device Bii compared to those cultured on a static multi-well plate in a standard CO_2 incubator however, due to limited number of experimental replicates statistical analysis was not possible (Figure 4.38).

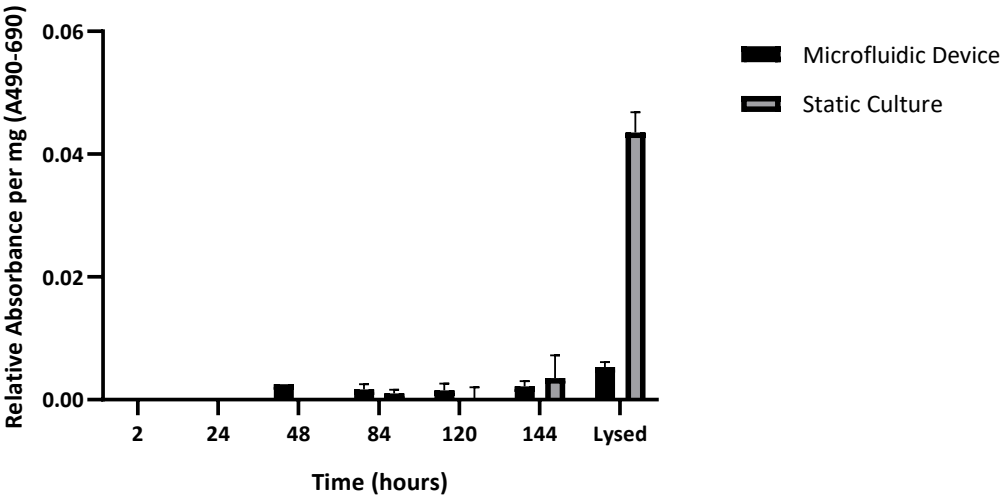

Figure 4.38 LDH analysis of 8mm diameter, 500µm PCLS cultured on PCLS device Bii compared to 8mm diameter, 500µm PCLS cultured on a static multi-well plate in a standard CO_2 incubator. LDH measurements were based on absorbance reading (490 – 690nm) accounting for media blank, for effluent collected between 2 – 144 hours post culture and after PCLS was completely lysed. Results are displayed as mean ± SEM (N=2, n=2). Statistical analysis could not be conducted due to insufficient replicates of the experiment.

4.3.3 Morphological Assessment of Healthy PCLS on a Microfluidic Device

4.3.3.1 Cellular Morphology of Human PCLS is not Altered when Cultured on PCLS Device B Iteration One (Bi)

To demonstrate that culturing PCLS on a microfluidic device had limited impact on the cellular morphology of the tissue. Cryosections (8µm thickness) were taken of 6mm diameter 500µm PCLS, cryopreserved 6 days post culture on PCLS device Bi or in a multi-well plate and stained with H&E (3.2.4.1, 3.2.4.2 and 3.2.4.3). Although no airways are clearly observable in these sections, the lung parenchyma structure appears largely unaffected by the continuous perfusion of tissue DMEM through the PCLS. The section taken from the microfluidic device appears to have a more honeycomb structure when compared to the section taken from the multi-well plate however, this may be a reflection on the structure of the tissue rather than a consequence of the perfusion (Figure 4.39). As such it appears that culturing PCLS on a microfluidic device does not detrimentally affect the cellular morphology of the tissue and provides a suitable alternative to static culture condition in a multi-well plate.

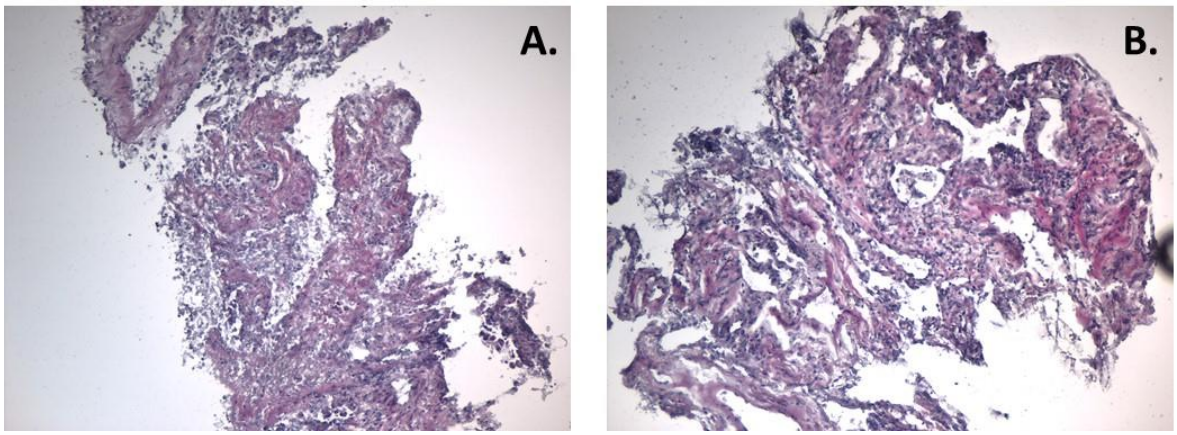

Figure 4.39 Microscopy images (x100 magnification) of H&E stained cryosections of 6mm diameter 500µm PCLS, 6 days post culture on PCLS device Bi in a 12 well plate, cultured in a standard CO_2 incubator.

4.4 Discussion

4.4.1 Microfluidic Device for Cell Culture

Given there is currently a shift towards a more extensive use of microfluidic devices to create organ-on-a-chip models which enable 2D and 3D cell culture to better recapitulate the *in vivo* environment (Zhang and Radisic, 2017), the aim was to create a microfluidic device which could successfully support the growth of two independent cell lines which mimic those found in the airways. Furthermore, this device aimed to allow interaction between the cell lines to take place in a manner akin to the *in vivo* environment and as had been performed using traditional cell culture techniques in chapter 2 whilst, having the advantage of providing continuous perfusion of the cells as would occur *in vivo*. Huh *et al* (2010) have previously described a lung-on-a-chip model which could maintain an epithelial and endothelial cell line culture, with an air-liquid interface and cyclic stretching mechanism to reproduce breathing patterns experienced *in vivo*, this pre-existing model formed the basis from which our, albeit less complex, model was designed and fabricated.

The first iteration of the device (CCD1) demonstrated that A549 and 1321N1 P2X3 cells could be successfully cultured on the purchased PET membranes and on opposing sides of the membrane. However, when compared to cells cultured under standard cell culture conditions the extent of cell growth was noticeably reduced and the majority of cells

cultured in the device were non-viable. The main issue relating to cell culture technique with this iteration was the formation of bubbles within the central chamber due to the depth of the PDMS layer, this resulted in cells receiving insufficient nutrients and thus preventing the formation of a confluent monolayer. Furthermore, this deep PDMS layer effectively created a large amount of dead space, which although continuously perfused was unlikely to have created a continual replenishment of nutrients, as complete DMEM was only forced into the device and not actively withdrawn, so nutrient turnover had the potential to be reduced as complete DMEM appeared to pool next to the membrane rather than continuously flow over it. This dead space may also have been subjected to turbulent flow as the inlet/outlet were positioned directly above the membrane, which has the potential to increase the sheer stress placed on the cells and thus could reduce the likelihood of cells growing evenly across the membrane. As a consequence of the poor fluid dynamics and thus poor perfusion, the device required a complete redesign to create a device which could better support the cell lines whilst maintaining similar design principles. Furthermore, this device provided an opportunity to consider the suitability of adhesives and fixings to ensure continuous perfusion could be achieved on a device. The very simplistic nature of securing the device with binder clips led to almost inevitable leakages from between each of the layers of the device, thus although the device could be successfully perfused, the large loss of complete DMEM through the device further impacted the growth of the cell lines and influenced the next iteration of the cell culture device.

Having previously shown that cell lines could be cultured on the membranes, the major issues of bubble formation and leakages throughout the device needed rectifying. The second iteration of the device (CCD2) overcame the major issue of securing the two sides of the device through the incorporation of screw fixings and the presence of an O-ring to create a better seal with the membrane. Additionally, the inlet position on the new design reduced the likelihood of bubble formation directly above the membrane as there was less dead space present and the complete DMEM naturally flowed across the membrane rather than pooling next to it. Furthermore, the addition of the PMMA wafer and a reduced depth in the central chamber also reduced bubble formation thus enabling cells to grow more effectively on the membrane, as nutrients were delivered evenly across the membrane.

Whilst, the leakages between the two layers of the device had been overcome, there was still a reduction in cell viability when cultured on CCD2 compared to those cultured in a standard incubator. The reduced viability can be linked to the problems encountered with leakages at the device inlet/outlet, thus there was a failure to deliver sufficient nutrients to the cells, resulting in reduced cell growth and increased cell death. Of further note, is the limited growth of 1N1 P2X3 cells, this is probably indicative of the less adherent nature of this cell line, resulting in an increased likelihood of cells being detached from the membrane whilst moving the PMMA wafer into the incubator and subsequently the sheer stress introduced through the continuous perfusion of the device whilst in culture. Coating the membrane in poly-D-lysine prior to seeding of cells may have aided in the adherence of the 1N1 P2X3 cells, as it does in static culture. However, due to time constraints and the complexity of trying to optimise the device, a single culture was opted for at this stage, with A549 cells being more adherent in nature, the logical choice at this developmental stage was to switch to optimising with a single cell line with the intention of expanding to a second once the cell growth issues had been rectified. Although A549 cells were more adherent and could the retained on the membrane when under continuous perfusion, the extent of coverage of A549 cells across the membrane was also reduced when cells were cultured on CCD2 compared to in static culture. This was most noticeable on the sections of the membrane which were positioned directly under the inlet/outlet points of the main body of the device. This difference in cell growth would suggest that the position of the inlet/outlets resulted in an increase in shear stress as the complete DMEM passed over the cells. Although this device is designed to have laminar flow, there is the potential for some turbulent flow occurring as the complete DMEM exits the inlet onto the membrane, this coupled with the continuous perfusion has the potential to increase sheer stress which caused cells to be sloughed off the membrane in this area during the culture period.

Whilst the problem of leakage at the device inlet could easily be rectified with the use of PTFE tape around the push fittings to better secure the tubing, the position of the inlet/outlet in relation to the membrane required a further iteration to the device to adjust the size of the PMMA wafer. The improvement in both cell viability and growth of cells cultured on CCD3, observed through trypan blue exclusion and Kwik Diff™ staining respectively, are a reflection of the revised positioning of the inlet/outlet over the PMMA

wafer rather than the membrane adhered to it. This revised position of the inlet/outlet prevented the cells being sloughed off as readily, enabling cells to grow evenly across the entire membrane, which when stained showed cell growth which was more in line with that observed in static culture. In addition to the revised inlet/outlet position, the resolution of problems pertaining to leakage also helped ensured cells received sufficient nutrients during in culture however, there were still some differences in the extent of cell viability across the membrane. The trypan blue exclusion assay still indicates more non-viable regions on the CCD3 membrane compared to those cultured in a standard incubator. However, unlike in previous iterations these were small patches of non-viable cells spread over the entire membrane, rather than being small regions of viable cells in the central region of the membrane amongst mostly non-viable cells, thus suggesting cells are growing more effectively across the entire membrane rather than just central locations.

This is further supported by the LDH measurements, which indicate that cells are less viable when cultured on CCD3 compared to those cultured in a standard incubator. When cells cultured on CCD3 are compared to those cultured in a static culture there is a slight increase in the level of LDH evident in the effluent and a significant reduction in the level released from lysed cells cultured on CCD3. This reduction in LDH from lysed cells suggests there are fewer viable cells present on the membrane at the end of the culture period when cultured on a microfluidic device compared to a standard incubator in static culture. The increased LDH in effluent and reduced LDH in lysed cells is indicative of cell undergoing apoptosis, resulting in membrane damage and the leakage of LDH (Fotakis and Timbrell, 2006) whilst in culture on CCD3. Whilst there was a significant difference in LDH released from lysed cells, there was also a slight reduction in cell proliferation and consequently cell mass of cells cultured on CCD3 compared to in static culture, when measured using the SRB assay. The reduction in cell proliferation and consequently cell mass when grown in CCD3 compared to a standard incubator, may reflect the sloughing of dead cells away from the membrane whilst under continuous perfusion, while cells were retained in static culture. Furthermore, this reduction in cell proliferation could partially account for the lower LDH measurements rather than cell viability being the only factor involved. It should be noted, that the SRB assay is unable to distinguish between viable and non-viable cells (Vichai and Kirtikara, 2006), thus any non-viable cells which are retain will also be stained, thereby

increasing the absorbance measurement obtained and indicating a higher cell density than would be seen if non-viable cells are removed from the culture system. Thus the decreased cell mass may be a consequence of continuous perfusion rather than solely due to a lack of proliferation which is more akin to the *in vivo* environment whereby there is a continuous replenishment of nutrients, waste removal and sloughing of dead cells at the basal membranes ensuring only viable cells are retained (Goral *et al*, 2013). Given this question regarding cell mass, it would be beneficial to conduct further analysis on the cell culture effluent to determine whether there is an increased cell count in the effluent from CCD3 compared to static culture.

Whilst several limitations pertaining to viability, cell proliferation and leakages were overcome with the iterations made to the device design, one of the main limitation is the ease of use of the final device (CCD3). Although not as small as some microfluidic devices, this device is awkward to construct due to the number of parts, furthermore it is relatively time consuming due to the nature of assembly. For example while placement of the PMMA wafer is simple, it sits directly on top of the O-ring thus when the two sides are fitted together it is easy to dislodge the wafer preventing the device from sealing completely leading to leakages between the two sides. Similarly, the fitting of the inlet/outlet tubing is problematic, in CCD1 the tubing had to be permanently fixed which made any adjustments at a later stage impossible, this was offset somewhat in CCD2/3 by the use of push fittings. However, the push fitting did not create a tight enough seal and so tended to leak, this was overcome by wrap a small piece of PTFE tape around the fitting. Whilst this prevented the leaks, it was awkward to perform due to the size of the fitting and was further complicated due to assembly being completed in a sterile environment, both of which increased the risk of introducing contaminates to the device, having the potential to create an infection in the cell culture environment. The use of screw fittings for the inlet and outlet tubing would be the ultimate design for this aspect of the device, as this would not only remove the need to secure the inlet/outlet tubing with PTFE tape but would also keep the fittings secure in the side of the device, reducing the likelihood of leaks and helping improve the viability of the cells in culture. The final issue pertaining to construction is the prevention of cells drying during assembly, as although a small volume of complete DMEM was added to the membrane, the application of the second side of the device resulted in displacement of the

complete DMEM, which further impacts the sealing of the device and risks the cells drying if manual perfusion is not performed quickly. The timely assembly of this device is important to ensure cell viability is maintained and could potentially be overcome through seeding of membranes in a fully constructed device. However, the adherent nature of the cell lines used could lead to potential blockages in the inlet/outlet channels within the device as the cells require several hours to adhere so could not be flushed through the system without complete loss from the device. With this in mind there is a need to develop further iterations to streamline the assembly of the device with subsequent optimisation until a single cell line can be cultured effectively prior to the addition of a second cell line on the opposing side of the membrane.

It is also worth noting that whilst the majority of data has a low n number, typically around 3 or 4 replicates, this does not truly reflect the number of attempts made in order to get the devices to work to any extent. When CCD1 is considered it took around 10 attempts to create a sufficient seal to between the membrane and the PDMS to enable cells to be seeded onto the membrane without complete leakage of the complete DMEM and cells from the membrane. Having determined that CCD1 could be discounted as a potential candidate for the final cell culture device, the same process had to be followed for CCD2/3. In this instance the seeding of cells onto the membrane was less problematic as the PMMA wafer floated on the complete DMEM, thus only a couple of attempts were needed to successfully seed cells. However, the leakage from the device created a new set of problems, which took around 5 attempts to overcome before PTFE tape was tried creating a sufficient seal allowing recordable data could be collected.

Although further iterations and optimisation of the cell culture microfluidic device are required to enable multiple cell lines to be successfully cultured, the observations made indicate that A549 cells can successfully be maintained on a microfluidic device for a minimum of 72 hours and that cells can proliferate at a rate similar to that observed in the standard culture environment in not only this chapter but in the basal cells used in the latter half of chapter 2. The ultimate aim of this model was to recreate the co-culture model optimised in chapter 2, in which two different cell lines could be cultured simultaneously

and any interactions between these cell lines measured. This microfluidic device also has the potential to enable cells to be cultured at an air-liquid interface, in this model airway epithelial cells would be cultured on the side of membrane at the air interface, whilst receiving nutrients via the membrane at the liquid interface. Thus this model has the potential to better recapitulating the *in vivo* environment as epithelial cells lining the airways are not continuously bathed in bodily fluids as occurs in standard culture techniques. Although only one cell line was successfully cultured in this instance, the morphology of the cells cultured on the microfluidic device was retained and were comparable to the morphology observed in chapter 2. In addition to using this model for the co-culture method to look at the TRPV4 – ATP – P2X3 pathway interactions in basal cells challenged with TRPV4 agonists, this microfluidic device could also be used to culture cells infected with RV16. Utilising this model to investigate RV16 infection, would enable effluent to be collected from either side of a membrane, potentially enabling viral shedding to be model in a manner which is more akin to the *in vivo* environment. Alternatively, cells could be cultured with an air-liquid interface during the RV16 infection, enabling cytokine response to be study in effluent from the liquid interface. In additional the introduction of a second cell line at the liquid interface (such as endothelial cells or nerve cells) would enable interactions between RV16 infected airway epithelial cells and other cells in the respiratory tract to be investigate. Furthermore, the continuous perfusion provides an *in vitro* environment which is more akin to the *in vivo* environment, which is evident through the sloughing of dead cells away from the culture membrane as is observed at the basal membrane.

4.4.2 Microfluidic Device for PCLS Culture

As with cell culture, there is also a similar drive towards the use of microfluidic devices for culturing *ex vivo* tissue sample to not only mimic the *in vivo* environment but also to increase the extent of work which can be conducted on each tissue sample (McLean *et al*, 2018). As such the aim was to create a microfluidic device which could successfully maintain a PCLS for 7 days without any detrimental effect on the morphology or physiology of the tissue sample when compared to standard tissue culture techniques in chapter 3. This is the first time PCLS has been cultured on a microfluidic device, therefore the iterations utilised are based on modelling of fluidic dynamics conducted within the

University of Hull Microfluidics Group and the previously optimised device used in the culture of precision cut head and neck tumour slices (Bower *et al,* 2017; Kennedy *et al*, 2019).

The first iteration of device A (Ai) demonstrated that PCLS has the potential to be maintained on a microfluidic device due to there being no significant difference between the amount of LDH measured in the tissue effluent from both the device and standard culture conditions. However, when the characteristic spike from lysed tissues was considered, the LDH measured was significantly lower from PCLS cultured on the device compared to that observed in standard culture. This spike in LDH release when PCLS was lysed indicates that the tissue in microfluidic culture is viable, albeit not as viable as PCLS in standard tissue culture, as LDH is only released from cells when membranes lyse during cell death (Fotakis and Timbrell, 2006). Thus if there was no spike in LDH release after lysis, the tissue could be considered non-viable having already released any LDH as the cells died, but given that there is not a noticeable increase in LDH released into the effluent in this instance, this does not appear to be the case. The reason for this observed difference between PCLS cultured on a microfluidic device and using standard culture techniques is unlikely to be due to a single factor however, given that tissue appears to some extent to retain a certain level of viability the fluid flow within the device is potentially a reason for the reduced viability. The initial iteration (Ai) lacked a PMMA wafer to hold the PCLS within the central chamber and the overall depth of the chamber was slightly smaller (approximately 400µm) than the thickness of the PCLS (approximately 500µm). Thus it is likely that the tissue DMEM flowing through the system was passing around rather than flowing over the PCLS. This poor fluid flow is likely to have reduced the delivery of nutrients to the centre of the PCLS and as a consequence increased cytotoxicity within the tissue. Further compounding the issue of fluid flow was the likelihood of the device leaking. Leakages occurred by two main routes, one being by the problems discussed in 4.4.1 whereby tissue DMEM leaked from the inlet/outlet, the second was due to the lack of a PMMA wafer. Without the presence of the PMMA wafer between the O-ring on either side of the device, the seal created was insufficient to prevent leakage of tissue DMEM between the two layers. Both issues impacted tissue viability in a similar manner to the cell viability

discussed in 4.4.1, as tissue did not received sufficient tissue DMEM to maintain viability throughout the tissue for the duration of the culture period.

Iteration two of device A (Aii) was produced in response to the aforementioned problems regarding fluid flow within the central chamber of device Ai. By including a PMMA wafer, the seal created between the wafer and O-rings was more secure, preventing leakage of tissue DMEM between the two layers of the device, helping ensure sufficient nutrient delivery to the tissue. In addition the deeper central chamber ensured that there was sufficient depth to accommodate a 500μm PCLS. This deeper central chamber prevented the PCLS from being squashed into the space and enabled better flow of tissue DMEM throughout the device, as the tissue DMEM in this device could flow not only around but also over the tissue, thus improving nutrient delivery to the tissue. The initial LDH measurements suggest that when lysed the PCLS cultured in the microfluidic device was non-viable after 6 days in culture, when compared to PCLS in standard culture, as there is no characteristic peak in LDH release. This being said, there is also no apparent release of LDH into the effluent throughout the duration of the culture period, which is in itself noteworthy, as this was not observed in any other LDH assay in either chapter 3 or 4. Typically, a higher level of LDH would be measured at 2 hours, as a consequence of the damage caused during tissue slicing however, in this case this is also absent from the data. The reason for the apparent lack of LDH in the effluent is not clear, especially for the PCLS in standard culture however, given the lack of replicates it may represent a piece of tissue which has high viability. Alternatively it could represent a missed step in the LDH assay, in some but not all wells, as multiple reagents were added to each well, thus increasing the risk of missing some wells and causing the apparent lack of LDH. Furthermore, when the microfluidic device is consider, this lack of LDH may reflect the amount of effluent collected in a 24 hour time period, which is approximately 2.5ml compared to 500μl in the static culture, thus any LDH is likely to be diluted to some extent. Although a higher volume of effluent is typically collected from the microfluidic devices, there is a risk that the outlet can become blocked, as small pieces of tissue are dislodged due to the continuous flow of tissue DMEM, such blockages can result in insufficient effluent samples volumes, outlet leakages and consequently missed LDH measurements. In addition, the effluent collected from this device had changed from the normal reddish-orange colour to a pinkish-purple

colour indicating that the pH of the media had become more alkaline (Pick and Keisari, 1980) even with the additional buffering provided by HEPES in the solution (Halldorsson *et al*, 2015), further indication that there may be some variation in viability when compared to standard culture. This being said, the lack of optimisation and the limited number of replicates conducted on this device makes it difficult to form any conclusions about how successful this device is for the culture of PCLS.

Having previously been shown to be able to maintain head and neck cancer slices on a microfluidic device (Kennedy *et al*, 2019) iteration one of device B (Bi) had the added advantage of being designed for the sole purpose of culturing precision cut tissue slices when compared to device A, which was a dual purpose device, as such device B (Bi) could be easily adapted to suit PCLS. The ability to maintain PCLS on a microfluidic device was confirmed by the LDH measured from both tissue effluent and lysed tissue whereby there is no significant difference between the values measured from tissue cultured on the device compared to in standard culture. Whilst the amount of LDH released post lysis from the microfluidic device is lower than that released by the tissue in standard culture, at 144 hours there is a slight increase in the amount measured in the effluent, suggesting that some changes to viability may have occurred during the culture period of the tissue on the device compared to in standard culture and may account for some of the differences at the point of lysis. Although the recorded measurement was slightly lower for PCLS cultured on the device, the relatively limited number of repeats (n=3) is also likely to account for some of the difference, as although the device had been previously optimised, the minor adjustments made for the culture of PCLS, such as a difference in slice thickness here 500µm is used instead of 350µm, plus the difference in tissue morphology between lung tissue and head and neck cancer tissue could have impacted the overall viability of the tissue on the device. The suitability of this device was also confirmed through the comparison of the cellular morphology of the tissue, as there is little observable difference between the sections, thus the fluid flow through the device does not cause noticeable damage the tissue structure and as a consequence the viability.

Whilst iteration one of device B (Bi) functioned effectively for PCLS culture further modifications were made with the long term aim of producing a microfluidic device which would enable on device microscopy to make further measurements such as bronchoconstriction, ATP analysis and calcium signalling. Iteration two of device B (Bii) was the first step in this device development, hence the similar initial design with changes to accommodate larger diameter PCLS (8mm rather than 6mm as used in device B (Bi)). The initial LDH measurements suggest that when lysed this PCLS was barely viable after 6 days in culture owing to a large difference in LDH released by the tissue in standard culture compared to that cultured on the device. Although, there is no large peak in LDH post lysis for the tissue cultured on the microfluidic device, there is also no large increase seen in the extent of LDH released into the effluent, suggesting that there was no sudden loss of viability during the culture period and rather potentially reflecting an inherent issue with either the device or tissue sample utilised. This is a similar observation to that made with device A (Aii) which also exhibited limited LDH in the effluent, interestingly the same observation around changes to the colour of the tissue DMEM were also seen in this device, suggesting that the fluid flow through the device needs to be modified to ensure sufficient nutrients are being delivered to the tissue. However, the main limiting factor is the number of replicates performed using this particular device. Having only received a single prototype of the device it was not possible to perform a number of technical replicates for each biological replicate received, thus given that the ratio of tissue to agarose in any given PCLS can vary within a single donor, there is the potential for a large extent of variation in data collected. As such the opportunity to conduct any beneficial optimisation on this device was limited by not only tissue availability but also the limited number of replicates performed (N=2, n=2) thus, it makes it difficult to form any conclusions about how successful this device is for the culture of PCLS without further optimisation.

The major limitation in the development of a PCLS-on-a-chip model is the availability of tissue samples and the number of devices available to conduct each experimental procedure in either duplicate or triplicate. While multiple devices can be fabricated the length of time from initial design to fabricated product cannot only be quite lengthy but also expensive. Therefore a decision had to be made regarding the initial measurement of tissue viability, owing to the reproducibility and accessibility of LDH, this made a logical first

choice as a method to provide an initial indication of cytotoxicity. The use of LDH provided an opportunity to determine if an iteration was suitable before having multiple devices fabricated, but the indeterminate length of time between tissue samples delayed this fabrication further hence making the formation of conclusions about the effectiveness of a device difficult. Another limitation which needs further consideration is the variability of results, as large standard deviations are a common observance in PCLS data. Whilst these do not necessarily reduce with a greater number of tissue samples acquired as seen in chapter 3, increased number of replicates makes the standard deviations more consistent between the differing test conditions. The potential cause of this variability is multi-faceted and is likely to be a combination of variations between donors, differing volume of agarose throughout an inflated tissue sample and the extent of connective tissue in an individual PCLS. It is impossible to account for any of these factors thus variability in PCLS will continue to exist however, it highlights the need to increase the number of replicates conducted in order to form valid conclusions regarding the use of PCLS-on-a-chip as an *ex vivo* model.

Although, the viability of the PCLS when cultured on the microfluidic device is slightly lower than PCLS cultured in standard conditions, this difference is not significant, thus the data collected suggests that this is a valid model for continuing the work started in chapter 3, especially in relation to PCLS infection with RV16. Furthermore, the microfluidic device concept has a number of additional benefits compared to standard culture, including providing continuous perfusion, reducing reagent volumes and enabling on device testing. Given that there is little difference in viability and morphology of the PCLS cultured on device, the infection technique and sampling methods used in chapter 3 could be replicated on a microfluidic device with the benefit of having the potential to be fully automated, which could remove some of the variability observed between samples. In addition, the continuous perfusion of the tissue is more akin to the *in vivo* environment, which may alter the response observed in the tissue during infection. The microfluidic device concept used in device Ai/Aii also provides an opportunity to create a system which can provide an air-liquid interface, thus PCLS could be cultured at this interface recreating the *in vivo* environment more closely, as the airways within the PCLS would not typically be submerged in bodily fluids, as is done in standard culture when PCLS is placed tissue DMEM. Moreover, the incorporation of an air-liquid interface within this method could also

presents an opportunity to infect tissue in a similar manner to that which is observed *in vivo*, as hRV infects cells which are at the air-liquid interface rather than those bathed in bodily fluids. The extent of flexibility which microfluidic devices can provide makes them a very attractive concept to further develop the PCLS infection model used in chapter 3, as a way to not only investigate the mechanisms used in hRV infection but also to replace the limited animal models which currently exist.

Disregarding the latter iterations on both devices due to the limited number of replicates, comparison of the LDH data allows a decision to be formulated about the suitability of device Ai and Bi. The characteristic spike observed from the lysed tissue was noticeably smaller in PCLS device A compared to PCLS device B, thus suggesting that PCLS device B would be more appropriate for the PCLS culture on a microfluidic device, as the higher LDH release from lysed tissue is indicative of a greater tissue viability. With this in mind, device B would provide a better starting point from which to develop further iterations and hopefully achieve the long term aim of conducting experimental analysis on the device rather than off the device as is currently done. Furthermore, although preliminary, the data collected thus far indicates that PCLS-on-a-chip is a viable and alternative method of utilising this existing *ex vivo* PCLS model.

5 Chapter 5: General Discussion

5.1 General Conclusions

The mechanisms of cough are not fully understood, although the neuromodulation via P2X receptors in response to ATP continues to show promise in studies aimed at attenuating the P2X3 response and reducing cough frequency (Abdulqawi *et al*, 2015; Song and Morice, 2017). Much of the work pertaining to the attenuation of P2X3 receptors have been conducted *in vivo* (Abdulqawi *et al*, 2015), as such chapter 2 utilised this existing theory to create a co-culture calcium signalling model which aimed to measure the interactions of the TRPV4 – ATP – P2X3 pathway *in vitro*. Although the commercially available P2X3 antagonists lack both specificity and potency (Bölcskei and Farkas, 2014), the use of a P2X3 antagonist NF110 demonstrated that small reductions in calcium flux from P2X3 receptors after stimulation with extracellular ATP could be achieved in both the co-culture and mixed culture methods utilised. Although the co-culture method has a number of limitations, including the limited movement of ATP across the membrane (Azarashvili *et al*, 2011; Durnin *et al*, 2016), the lack of agonists and antagonists with high specificity and potency (Thorneloe *et al*, 2008; Jin *et al*, 2011; Zhang *et al*, 2012; Bölcskei and Farkas, 2014; Bonvini *et al*, 2016) and cell lines models which do not truly reflect the cells involved in cough (Albright *et al*, 1990; Swain *et al*, 2010; Park *et al*, 2015; Srinivasan *et al*, 2015), this model has the potential to enable cell to cell interactions to be investigated and suggests that the hypothesised TRPV4 – ATP – P2X3 pathway has the potential to be part of the mechanism involved in cough.

Whilst the aim of utilising the co-culture model to investigate the role of hRV infection in post viral cough and inflammatory response did not come to fruition, chapter 2 provided a foundation for the subsequent infection of PCLS with hRV by providing a baseline indication of the impact RV16 has on alveolar (A549) and bronchial (Beas-2b) cell lines, which are similar cells to those present in human lung tissue samples. Infection of A549 and Beas-2b cell lines showed a difference in response, with A549 cells exhibiting a more limited response to RV16 infection in terms of cell cytotoxicity and mass compared to Beas-2b cells. This observation is in line with a number of existing studies which identified hRV infection as having a limited impact on cell cytotoxicity (Griego *et al*, 2000; Ghildyal *et al*, 2005; Lötzerich *et al*, 2018). Furthermore, this difference in response reflects the widely accepted observation that lower respiratory tract infections with hRV occur much less frequently

than upper respiratory tract infections, whereby bronchial cells are more likely to be infected than alveolar cells (Papadopoulos and Johnston, 2000; Hayden, 2004; Gualano *et al*, 2006; Aponte *et al*, 2015). The TEER findings also mirror existing research demonstrating reduced tight junction integrity (Lopez-Souza *et al*, 2004; 2009) whereby TEER measurements decrease and fluorescein leakage increases in response to RV16 infection in both cell lines. Whilst the changes in MMP-2 and MMP-9 expression post infection with RV16, although minimal, demonstrate some similarities to the MMP-2 and MMP-9 upregulation proposed in other studies (Gualano *et al*, 2006; Tacon *et al*, 2010). Although, there are some inconsistences in the data collected, on the whole the data reflects a number of previous studies and whilst no novel findings were made, this data provided a suitable set of baseline measurements which could be utilised in the development of the PCLS infection model.

Given that *in vitro* studies do not provide the sample level of complexity as the *in vivo* environment (Torisawa *et al*, 2014) and owing to the lack of animal models available for the study of hRV infection (Newcomb *et al*, 2008; del Vecchio *et al*, 2015), PCLS was utilised as an *ex vivo* technique to explore the observations made *in vitro* in chapter 2 in a manner more akin to the *in vivo* environment. PCLS is a widely used and accepted model for the study of respiratory diseases and toxicology of chemicals in the respiratory system (Martin *et al*, 1996; Seehase *et al,* 2012; Neuhaus *et al*, 2013; Lauenstein *et al*, 2014; Sun *et al*, 2015; Ghosh *et al*, 2016; Alsafadi *et al,* 2017; Temann *et al*, 2017). Furthermore, the use of human PCLS increases the number of experiments which can be performed on a single sample and aids in reducing reliance on animal tissue (Fisher *et al*, 1994; Wohlsen *et al*, 2003; Switalla *et al*, 2010). Prior to determining whether PCLS could be successfully infected with RV16, optimal PCLS thickness and culture period were determined. Initially chapter 3 considered whether any specific thickness of PCLS that had greater viability compared to any other, as numerous studies suggest the use of 200 – 300µm (Sturton *et al*, 2008; Schlepütz *et al*, 2012; Bai *et al*, 2016; Alsafadi *et al*, 2017; Zmora *et al*, 2017) however, the work in this chapter indicates there is little difference between thicknesses of 300 – 700µm or small tissue lumps. Whilst this is somewhat contradictory given the extensively used thickness of 200 – 300µm, there are examples of other studies which utilise PCLS of 400 – 750µm (Nave *et al*, 2008; An *et al*, 2012; Temann *et al*, 2017) and small lump tissue (Nicholas *et al*, 2015)

effectively, thus indicating this deviation from the more commonly used thicknesses is not completely unprecedented. This increased range of thicknesses affords the use of PCLS with even greater flexibility than the technique currently provides, as the thickness of the PCLS can be determined based on the requirements of any given experiment rather than solely on the concerns relating to viability. In addition, this chapter also demonstrated that PCLS and small tissue lumps can be maintained in culture for 7 days without any significant impact on tissue viability or cytotoxicity, which approximately doubles the typically used period of approximately 3 days (Bergner and Sanderson, 2002b; Wohlsen *et al*, 2003; Ressmeyer *et al*, 2006; Neuhaus *et al*, 2013) and enables tissue to be maintained for sufficiently long enough to be infected with RV16 and the effect measured over a number of days.

Chapter 3 also aimed to demonstrate the successful infection of PCLS and small lump tissue with RV16 for the first time using excess human tissue collected during thoracic surgery. Utilising the data collected from A549 and Beas-2b cells as a reference point, alongside the work of Kennedy *et al* (2018) with RV39 infection of PCLS and Nicholas *et al* (2015) with influenza, successful infection of PCLS and small tissue lumps was achieved. Infection of human *ex vivo* tissue with RV16 has limited impact on viability and cytotoxicity of the tissue which was in line with the observations made in chapter 2 and is also indicative of the pathogenesis of hRV, whereby cells do not reach a cytolytic stage (Ghildyal *et al,* 2005; Thacker *et al*, 2019) or undergo apoptosis and necrosis, with cell death instead occurring via a caspase independent pathway (Lötzerich *et al*, 2018). In addition, the infection of PCLS with RV16 suggests a slight reduction in TEER measurements compared to uninfected tissue, whilst this aligns with the observations in A549 and Beas-2b cell infection and supports the notion that hRV reduces tight junction integrity and provides a route for opportunistic bacterial pathogens to cause subsequent secondary infections (Sajjan *et al*, 2008; Rezaee *et al*, 2011), it is unclear how much of this effect is due to the virus and how much is a consequence of the morphology of the tissue or presence of agarose. Whilst hRV infections are widely shown to have limited impact on cytotoxicity, other effects have also been proposed, for example it is hypothesised that hRV infection increases hypersensitivity in the airways, particularly in individuals with underlying respiratory conditions (Aponte *et al*, 2015). This increased hypersensitivity is linked to increased hyperresponsiveness and

bronchoconstriction (Grünberg *et al*, 1997), an observation which was made in this chapter, as infected PCLS demonstrated an increased responsiveness to potent bronchoconstrictive agents, although a similar response was also identified in sham infection which may indicate that the response is not virus specific. Moreover, this chapter also showed upregulation in ICAM-1 protein expression in *ex vivo* human tissue for the first time, which is in line with previous *in vitro* and *in vivo* observations (Terajima *et al*, 1997; Yamaya *et al*, 1999; Grünberg *et al*, 2000; Winther *et al*, 2002; Othumpangat *et al*, 2012). Similar upregulation of Muc5AC and TRPV4 protein expression was also observed, which supports previous studies that identified increased mucus production as a common symptom in hRV infection, due to increased cell permeability and for use in mucociliary clearance (Groneberg *et al*, 2002; Inoue *et al*, 2006) and the increased TRP channel expression in facilitating the viral replication process (Chen *et al*, 2020). Cytokine and chemokine upregulation was also shown to occur to some extent, which reflects the activation of numerous proinflammatory mediators observed in hRV infections and the potential role play by the cytokine cascade in the pathophysiological effect of the virus (Griego *et al*, 2000; Kaul *et al*, 2000; Bosco *et al*, 2016). Whilst, some of this data is preliminary in nature and would benefit from a greater number of replicates being conducted, the majority of findings align to the observations made in chapter 2. Generally, the premise of this model appears sound, infection of the tissue can be done successfully and with further optimisation and development of the methods used to investigate viral response could provide a good model to study the mechanisms of hRV infections.

The intention of chapter 4 was to go beyond the scope of culturing cells and PCLS in a traditional manner and demonstrate whether data could be replicated on a microfluidic device. Working on the premise that the continual perfusion of a microfluidic device better recapitulates the *in vivo* environment than standard culture techniques (Shaw *et al*, 2011; Esch *et al*, 2015), there has been a shift towards the more extensive use of microfluidic devices to develop an array of organ-on-a-chip models (Zhang and Radisic, 2017). Focused on two main elements, this chapter aimed to develop a lung-on-a-chip model to replicate elements of the work undertaken in previous chapters, two devices were created the first based on the co-culture method used in chapter 2 and the second based on the PCLS culture methods used in chapter 3. After testing multiple iterations of cell culture devices,

the last iteration used (CCD3) showed promising early indications that A549 cells could be cultured successfully on a microfluidic device, with a similar rate of cell viability and proliferation to that observed in standard culture conditions for up to 72 hours and has the potential to be developed to provide the growth of multiple cell lines, both with and without an air-liquid interface as has been conducted in other studies (Huh *et al*, 2007; 2012; Tavana *et al*, 2011; Stucki *et al*, 2015; Benam *et al*, 2015; 2016). Additionally, a PCLS-on-a-chip model was devised and tested on multiple iterations of a tissue culture device as part of this chapter. After initial tests, the chosen pre-existing device (PCLS device Bi) was utilised and showed that after minor modifications to enable PCLS to be cultured on the device, it was possible to maintain the tissue on device for up to 6 days, with minimal impact on tissue viability or morphology, mirroring existing findings by Kennedy *et al* (2019). Based on these initial observations both the cell culture and tissue culture microfluidic devices provide a promising start in the development of a lung-on-a-chip model, which in the long term may provide a way to culture cells and tissue in an environment which better recapitulates the *in vivo* environment, than current *in vitro* culture techniques can offer.

When considered together, these findings suggest that there are multiple methods which can be employed to develop further understanding of hRV infections in a manner which better recapitulates the *in vivo* environment and in doing so further reduces the reliance on animal models and the use of controlled infection to create suitable *in vivo* models.

5.2 General Limitations and Recommendations

Whilst, the aforementioned methods were on the whole successful in achieving the desired outcome, a range of limitations exist which need to be consider and accounted for, should any further research be undertaken. When the co-culture calcium signalling model and hRV infection techniques are considered, the first limitation to address is the cell line models chosen, as although widely accepted in the study of respiratory diseases, there is a need to consider the cell type represented, the position within the respiratory tract and model of immortalisation. The reduced response in A549 cells compared to Beas-2b cells likely reflects both the difference in cell type and the relative position in the respiratory tract, with A549 representing alveolar cells in the lower respiratory tract compared to Beas-2b

representing bronchial cells in the upper respiratory tract. Thus whilst lower respiratory tract infections with hRV can occur, these are less frequent (Hayden, 2004) and may explain the differences in the observations made. In terms of immortalisation, A549 cells originate from adenocarcinoma cells, therefore the architecture, expression of specific markers and barrier properties differ from the primary alveolar type II cells they represent (Swain *et al*, 2010). Conversely, Beas-2b cells are non-cancerous in origin, instead immortalisation is achieved through infection with Ad12-SV40 virus, so although these cells retain wild type properties (Park *et al*, 2015) the ability to differentiate into different epithelial cell types is reduced compared to primary bronchial epithelial cells (Albright *et al*, 1990). The immortalisation process thus may go some way to explain the differences observed between cell lines, with Beas-2b cells retaining more of the primary cell phenotype compared to A549 cells. Thus although Beas-2b cells provide a slightly better model than A549 cells in regards to the cell types involved in hRV infections, use of cell lines means that the cells do not truly reflect those found *in vivo*. To overcome this issue the use of primary cells isolated from bronchial tissue would form a better model however, this is not without difficulties due to variations between donors, complexities in isolating cells and longevity in culture, which makes the use of this cell type less favourable in long term studies (Forbes, 2000). The second limitation relates to the complexities of the co-culture method, whilst the cell lines used grows rapidly, there is a need to overestimate the required seeding density to prevent excessive loss of cells when the orientation of the Thincerts™ is changed part way through the culture process. This means that although the same seeding densities are used in all experiments, there is no guarantee that the same number of cells will be lost, which may lead to variations in results. Furthermore, over time the cell monolayer became unstable and detached from the culture surface which prevented some experiments being conducted for the desired time period. Given these issues, increasing the number of replicates would help to reduce inconsistences and account for the loss of cell numbers.

Limitations also exist within the PCLS model and similarly need to be considered if the model is to be further developed to continue the study of hRV in *ex vivo* human tissue. The first limitation to consider is the variations observed between donors and the impact this has on the analysis of data. Given that tissue is collected from individuals undergoing lung resection surgery, typically for lung cancer removal, there is always going to a large degree

of variations between donors. In order to mitigate for these variations increasing the number of replicates would help to improve the reliability of the findings. However, this in itself can be problematic due to the limited and at times sporadic tissue supply, hence the low number of replicates in some experiments. Whilst, this is not an ideal situation given the variations seen when working with tissue samples, it allowed for a number of different techniques to be utilised to provide as complete a picture as possible of the way hRV effected the tissue. In addition, although the tissue collected is deemed to be healthy, due to its proximity to the distal region of the lung, away from the tumour margin, there is a high likelihood that comorbidities will be present. Underlying respiratory conditions such as COPD are linked to exacerbations during hRV infection (Griego *et al*, 2000; Jacobs *et al*, 2013) and may impact the data collect, thus, if suitable amendments could be made to the ethics approval held, collection of comorbidity information relating to underlying respiratory diseases may help determine whether anomalies in the data are a direct consequence of the underlying diseases. Furthermore, the tissue type collected has other inherent problems being predominately alveolar in nature, which does not strictly reflect the cell types which would typically be exposed to a hRV infection, due to the position in the lower rather than upper respiratory tract (Hayden, 2004). This being said, the use of human PCLS from alveolar tissue is likely to be more akin to the *in vivo* environment in which hRV infection occur, due to the retention of lung parenchyma which cannot be achieved through cell based studies. Another limitation which needs some consideration is the length of time tissue is cultured for post infection with RV16. The 5 day period used resulted in some changes and falls within the typical disease progression and longevity of approximately 2 weeks (Atkinson *et al*, 2016) however, some changes were minimal. Given that peak responses may have been missed or alternatively not reached, repetition of experiments utilising various end points may help to identify at which stage during the infective period optimal measurements can be made. The final limitation which needs to be considered is the persistence of agarose in tissue throughout the duration of the culture period, which makes tissue processing difficult and could have the potential to affect the data collected. However, it should be noted that the use of agarose is important in creating an environment which maintains open airways whilst stretching lung tissue to near total capacity (Dandurand *et al*, 1993; Brook *et al*, 2010) and being inert is unlikely to have any noticeable impact on tissue viability or interact with the tissue in anyway (Ulrich *et al*, 2011). The use of low agarose concentrations helps to address this limitation to some extent, so

whilst not completely eradicating it, it provides enough rigidity to the tissue for slicing with hopefully negligible impact on the experimental data.

Some of the limitations discussed previously regarding suitability of cell lines and variations between tissue samples, also apply here, so will not be discussed again however, other limitations also apply to the microfluidic devices used. One of the major issues with all of the devices was the development of blockages and/or leakages, which arise as a side effect of the continuous perfusion of the system. Whilst blockages are somewhat unavoidable as cells and tissues become dislodged by the continual movement of DMEM, the application of PTFE tape to leaky connectors, alongside periodic tightening of fixings, reduced the extent of leakages. Further developments to the device to use screw rather than push connectors would further reduce the likelihood of leaks occurring. Additionally, the lengthy fabrication process limited the number of devices available for use at any given time, as such CCD3 and PCLS device Aii being one and the same, could be used for either cell culture or tissue culture, but not simultaneously, which made planning for use difficult, especially due to the sporadic nature of tissue samples. The final limitation relates to the extent of gas exchange in the device, compared to a standard incubator. Although DMEM was buffered with HEPES to account for the absence of CO_2 during incubation (Halldorsson *et al*, 2015), the effluent collected from all devices except PCLS device Bi was a pinkish-purple colour rather than the normal reddish-orange colour, indicating the pH of the DMEM has become more alkaline and suggesting the absence of CO_2 may have had some role to play. All devices have relatively large central chambers where turnover of DMEM was likely to be relatively slow, thus without continued CO_2 buffering of the DMEM the pH is altered, an observation that can also been made in small volume of unused DMEM which have been opened for prolonged periods. Whether this has any impact on viability is not clear from the current data, thus further iterations of the device may benefit from changes to the size of the central chamber and/or type of tubing used to alter the extent of gas exchange and increase the turnover of DMEM in the device.

5.3 Future Work

Although the research undertaken in this thesis has provided little in terms of novel findings relating to the mechanisms involved in hRV infection or cough, it has provided an opportunity to create and commence the optimisation of a number of models which have the potential to be utilised in future studies, to further develop the existing knowledge relating to hRV and cough. As with most research, the main limiting factors in this piece of research was both finances and time. As such the plans discussed below reflect ideas which are impacted by neither factor.

Further research using the co-culture model would incorporate the method developed here and the *in vitro* modelling of hRV. With cough identified as one of the major symptoms of hRV and currently having no effective treatment, being able to infect an airway epithelial cell line and subsequently look at the interactions with non-airway cells that are situated in the respiratory system (for example nerve cells and endothelial cells), may aid in determining how the infection leads to symptoms such as a cough. Given that hRV infections have little cytotoxic effect on the infected cells and that much of the pathogenesis is thought to be linked to the inflammatory response, co-culturing of cells would enable specific receptors to be targeted in airway epithelial cells and the downstream inflammatory response measured in the chosen cell line, using techniques such as calcium signalling, patch clamping, cytokine arrays and ELISA. If such interactions can be elicited and downstream receptors identified, subsequent testing of new or existing antagonists could be conducted to identify if the downstream response can be attenuated. This model could also have the potential to be used to study the role of secondary bacterial infections in hRV infection as a consequence of tight junction dysregulation, for instance primary airway epithelial cells could be infected with hRV and subsequently exposed to common secondary bacteria, enabling downstream responses to be compared to when no secondary infection is present. Furthermore, whilst the P2X3 receptor is currently a major candidate in the cough pathway, this model allows for other receptor combinations to be considered and a range of potential treatments to be tested.

Although the co-culture model has benefits for *in vitro* modelling of hRV and cough, the use of cell lines has its own range of disadvantages. As such further development of the *ex vivo* PCLS and small tissue lump model would be beneficial as it provides a model which is more akin to the *in vivo* environment. PCLS using human tissue has a multitude of benefits in respiratory research however, for the study of hRV it is of particular importance owing to the lack of suitable animal models. Human PCLS ensures the relevant receptors for hRV binding are present, maintains lung architecture and provides a near *in vivo* response whilst retaining the flexibility of an *in vitro* model. In addition to extending the number of replicates of existing experiments, further development of the cytokine array data through the use of ELISAs would be useful to determine which cytokines are upregulated in response to infection. Furthermore, the western blot analysis suggested that some changes to global protein expression of some receptors occurred post infection, thus it would be beneficial to explore this further and to extend this analysis to include immunohistochemistry to identify where in the tissue these changes occur. To extend the scope of the study further, having shown no cytotoxic effect can be observed, exploration of whether a caspase-independent cell death pathway is involved in infection, via western blot analysis, seems a logical next step in trying to elicit the mechanisms involved in infection and how this results in the observed symptoms. Moreover, other responses which have been identified as part of the pathogenesis of hRV could be studied, such as the role of ROS is barrier dysfunction and the influence of this on secondary bacterial infections. Given that PCLS remains viable in culture for a number of days, it would be worth considering whether tissue could be infected with hRV and/or exposed to oxidative stress, prior to introducing a secondary bacterial infection, in order to identify whether any changes to cytokine response occurs as part of the proinflammatory pathway during primary and secondary infection. The PCLS model has the potential to enable investigations of changes in cytokine and chemokine release, protein expression and the pathway involved in the pathogenesis of infection, which may give rise to targets for drug development, enabling new and existing drugs to be used to target specific symptoms with the aim of alleviating them to some extent.

Whilst, a cure for the common cold caused by hRV is unlikely to be achievable owing to the vast number of serotypes which exist, the development of a treatment to reduce major

symptoms would be a valuable alternative. As such, the ultimate aim of this future research would be the development of a treatment for rhinovirus infection and post viral cough, which could aid in the reduction of hRV related chronic respiratory disease exacerbations and has the potential to also treat chronic cough suffers. The development of such a treatment could help to reduce the significant morbidity levels of rhinovirus infection and in doing so would also reduce the significant economic burden it creates.

Reference List

AAT Bioquest Inc. (2020). Quest Graph™ EC50 Calculator. (online) available at http://www.aatbio.com/tools/ec50-calculator [accessed 24/02/20].

Abdelaal H.M., Kim H.O., Wagstaff R., Sawahata R., Southern P.J. and Skinner P.J. (2015). Comparison of Vibratome and Compresstome sectioning of fresh primate lymphoid and genital tissues for *in situ* MHC-tetramer and immunofluorescence staining. *Biological Procedures Online*. **17** (2).

Abdullah H., Heaney L.G., Cosby S.L. and McGarvey L.P.A. (2013). Rhinovirus upregulates transient receptor potential channels in a human neuronal cell line: implications for respiratory virus-induced cough reflex sensitivity. *Thorax*. **69**, p46 – 54.

Abdulqawi R., Dockry R., Holt K., Layton G., McCarthy B.G., Ford A.P. and Smith J.A. (2015). P2X3 receptor antagonist (AF-219) in refractory chronic cough: a randomised, double-blind, placebo-controlled phase 2 study. *Lancet*. **385**, p1198 – 1205.

Achten N.B., Wu P., Bony L., Blanken M.O., Gebretsadik T., Chappell J.D., Wang L., Yu C., Larkin E.K., Carroll K.N., Anderson L.J., Moore M.L., Sloan C.D. and Hartert T.V. (2017). Interference between respiratory syncytial virus and human rhinovirus infection in infancy. *The Journal of Infectious Diseases*. **215**, p1102 – 1106.

Adan A., Kiraz Y. and Baran Y. (2016). Cell proliferation and cytotoxicity assays. *Current Pharmaceutical Biotechnology*. **17**, p1213 – 1221.

Adriaensen D., Brouns I. and Timmermans J-P. (2015). Sensory input to the central nervous system from the lungs and airways: a prominent role for purinergic signalling via P2X2/3 receptors. *Autonomic Neuroscience: Basic and Clinical*. **191**, p39 – 47.

Albright C.D., Jones R.T., Hudson E.A., Fontana J.A., Trump B.F. and Resau J.H. (1990). Transformed human bronchial epithelial cells (Beas-2b) alter the growth and morphology of normal human bronchial epithelial cells *in vitro*. *Cell Biology and Toxicology*. **6** (4), p379 – 398.

Alder A., Cowley E.A., Bates J.H.T. and Eidelman D.H. (1998). Airway-parenchymal interdependence after airway contraction in rat lung explants. *Journal of Applied Physiology*. **85** (1), p 231 – 237.

Alsafadi H.N., Staab-Weijnitz C.A., Lehmann M., Lindner M., Peschel B., Königshoff M. and Wagner D.E. (2017). An ex vivo model to induce early fibrosis-like changes in human precision-cut lung slices. *American Journal of Physiology: Lung Cellular and Molecular Physiology.* **312** (6), L896 – 902.

Amineva S.P., Amine A.G., Gern J.E. and Palmenberg A.C. (2011). Comparison of rhinovirus A infection in human primary epithelial and HeLa cells. *Journal of General Virology*. **92**, p2549 – 2557.

An S.S., Wang W.C.H., Koziol-White C.J., Ahn K., Lee D.Y., Kurten R.C., Panettieri Jr. R.A. and Liggett S.B. (2012). TAS2R activation promotes airway smooth muscle relaxation despite β_2-adrenergic receptor tachyphylaxis. *American Journal of Physiology: Lung Cellular and Molecular Physiology*. **303**, L304 – 311.

Andersson D.A., Gentry C., Moss S. and Bevan S. (2008). Transient receptor potential A1 is a sensory receptor for multiple products of oxidative stress. *The Journal of Neuroscience*. **28** (10), p2485 – 2494.

Aponte F.E., Taboada B., Espinoza M.A., Arias-Ortiz M.A., Monge-Martinez J., Rodriguez-Vázquez R., Diaz-Hernández F., Zárate-Vidal F., Wong-Chew R.M., Firo-Reyes V., del Rio-Almendárez C.N., Gaitán-Meza J., Villaseñor-Sierra A., Martinez-Aguilar G., Garcia-Borjas M., Noyoal D.E., Pérez-Gónzalez L.F., López S., Santos-Preciado J.I. and Arias C.F. (2015). Rhinovirus is an important pathogen in upper and lower respiratory tract infections in Mexican children. *Virology Journal*. **12** (31).

Astolfi M., Péant B., Lateef M.A., Rousset N., Kendall-Dupont J., Carmona E., Monet F., Saad F., Provencher D., Mes-Masson A-M. and Gervais T. (2016). Micro-dissected tumor tissues on chip: an *ex vivo* method for drug testing and personalized therapy. *Lab on a Chip*. **16**, p312 – 325.

Atac B., Wagner I., Horlan R., Lauster R., Marx U., Tonevitsky A.G., Azar R.P. and Linder G. (2013). Skin and hair on-a-chip: *in vitro* skin model versus *ex vivo* tissue maintenance with dynamic perfusion. *Lab on a Chip*. **13**, p3555 – 3561.

Atkinson S.K. (2019). The effect of human rhinovirus-16 on thermo-TRP channels, hypotonic activation and ATP activation. PhD thesis. Hull York Medical School, Hull.

Atkinson S.K., Sadofsky L.R. and Morice A.H. (2016). How does rhinovirus cause the common cold cough? *BMJ Open Respiratory Research*. **3**, e000118.

Azarashvili T.S., Odinokova I.V., Krestinina O.V., Baburina Y.L., Grachev D.E., Teplova V.V. and Holmuhamedov E.L. (2011). Role of phosphorylation of Porin (VDAC) in regulation of mitochondrial outer membrane under normal conditions and alcohol intoxication. *Biochemistry (Moscow) Supplementary Series A: Membrane and Cell Biology*. **5** (1), p11 – 20.

Babcock H. P., Chen C. and Zhuang X. (2004). Using Single-Particle Tracking to Study Nuclear Trafficking of Viral Genes. *Biophysical Journal*. **87** (4), p2749 – 2758.

Bach P.H., Vickers A.E.M., Fisher R., Baumann A., Brittebo E., Carlile D.J., Koster H.J., Lake B.G., Salmon F., Sawyer T.W. and Skibinski G. (1996). The use of tissue slices for pharmacotoxicology studies. *Alternative to Laboratory Animals*. **24**, p893 – 923.

Bai Y., Krishnamoorthy N., Patel K.R., Rosas I., Sanderson M.J. and Ai X. (2016). Cryopreserved human precision-cut lung slices as a bioassay for live tissue banking: a viability study of bronchodilation with bitter-taste receptor agonists. *American Journal of Respiratory Cell and Molecular Biology.* **54** (5), p656 – 663.

Baker M. (2011). A living system on a chip. *Nature*. **471**, p661 – 665.

Baldini F., Carloni A., Giannetti A., Porro G. and Trono C. (2009). An optical PMMA biochip based on fluorescence anisotropy: application to C-reactive protein assay. *Sensor and Actuators B: Chemical.* **139**, p64 -68.

Banerjee A., Trivedi C.M., Damera G., Jiang M., Jester W., Hoshi T., Epstein J.A. and Panettieri R.A. Jr. (2012). Trichostatin A abrogates airway constriction, but not inflammation, in murine and human asthma models. *American Journal of Respiratory Cell and Molecular Biology*. **46** (2), p132 – 138.

Barbosa A.I. and Reis N.M. (2017). A critical insight into the development pipeline of microfluidic immunoassay devices for sensitive quantitation of protein biomarkers at point-of-care. *Analyst*. **142**, p858 – 882.

Barnard D.L. (2009). Animal models for the study of influenza pathogenesis and therapy. *Antiviral Research.* **82** (2), A110 – 122.

Bartlett N.W., Walton R.P., Edwards M.R., Aniscenko J., Caramori G., Zhu J., Glanville N., Choy K.J., Jourdan P., Burnet J., Tuthill T.J., Pedrick M.S., Hurle M.J., Plumpton C., Sharp N.A., Bussell J.N., Swallow D.M., Schwarze J., Guy B., Almond J.W., Jeffery P.K., Lloyd C.M., Papi A., Killington R.A., Rowlands D.J., Blair E.D., Clarke N.J. and Johnston S.L. (2012). Mouse models of rhinovirus-induced disease and exacerbation of allergic airway inflammation. *Nature Medicine*. **14** (2), p199 – 204.

Bedke N., Sammut D., Green B., Kehagia V., Dennison P., Jenkins G., Tatler A., Howarth P.H., Holgate S.T. and Davies D.E. (2012). Transforming growth factor-beta promotes rhinovirus replication in bronchial epithelial cells by suppressing the innate immune response. *PLoS ONE*. **7** (9), e44580.

Behringer E.J. and Segal S.S. (2015). Membrane potential governs calcium influx into microvascular endothelium: integral role for muscarinic receptor activation. *The Journal of Physiology*. **593** (20), p4531 – 4548.

Belvisi M.G. and Bolser D.C. (2002). Summary: animal models for cough. *Pulmonary Pharmacology and Therapeutics.* **15**, p249 – 250.

Belvisi M.G., Dubuis E. and Birrell M.A. (2011). Transient receptor potential A1 channels: insights into cough and airway inflammatory disease. *Chest*. **140** (4), p1040 – 1047.

Benam K.H., Villenave R., Lucchesi C., Varone A., Hubeau C., Lee H-H., Alves S.E., Salmon M., Ferrante T.C., Weaver J.C., Hamilton G.A. and Ingber D.E. (2015). Small airway-on-a-chip enables analysis of human lung inflammation and drug responses *in vitro*. *Nature Methods*. **13** (2), p151 – 157.

Benam K.H., Novak R., Naworth J., Hirano-Kobayashi M., Ferrante T.C., Choe Y., Prantil-Baun R., Weaver J.C., Bahinski A., Parker K.K. and Ingber D.E. (2016). Matched-comparative modelling of normal and diseased human airway responses using a microengineered breathing lung chip. *Cell Systems*. **3**, p456 – 466.

Bergner A. and Sanderson M.J. (2002a). Acetylcholine-induced calcium signalling and contraction of airway smooth muscle cells in lung slices. *Journal of General Physiology*. **119** (2), p187 – 198.

Bergner A. and Sanderson M.J. (2002b). ATP stimulates Ca^{2+} oscillations and contraction in airway smooth muscle cells and mouse lung slices. *American Journal of Physiology: Lung Cellular and Molecular Physiology*. **283**, L1271 – 1279.

Bertino J.S. (2002). Cost burden of viral respiratory infections: issues for formulary decision makers. *American Journal of Medicine*. **112** (6A), S42 – 49.

Bhatia S.N. and Ingber D.E. (2014). Microfluidic organs-on-chips. *Nature Biotechnology*. **32** (8), p760 – 772.

Bhattacharyya A. and Klapperich C.M. (2007). Design and testing of a disposable microfluidic chemiluminescent immunoassay for disease biomarkers in human serum samples. *Biomedical Microdevices*. **9**, p245 – 251.

Biau D.J., Kernéis S. and Porcher R. (2008). Statistics in brief: the importance of sample size in the planning and interpretation of medical research. *Clinical Orthopaedics and Related Research*. **466** (9), p2282 – 2288.

Bible K.C. and Kaufmann S.H. (1996). Flavopiridol: a cytotoxic flavone that induces cell death in noncycling A549 human lung carcinoma cells. *Cancer Research*. **56**, p4856 – 4861.

Black G., Ard D., Smith J. and Schibik T. (2010). The impact of the Weibull distribution on the performance of the single-factor ANOVA model. *International Journal of Industrial Engineering Computations*. **1** (2), p185 – 198.

Blackshaw L.A., Brierley S.M. and Hughes P.A. (2010). TRP channels: new targets for visceral pain. *Gut*. **59**, p126 – 135.

Blake A.J., Rodgers F.C., Bassuener A., Hippensteel J.A., Pearce T.M., Pearce T.R., Zarnowska E.D., Pearce R.A. and Williams J.C. (2010). A microfluidic brain slice perfusion chamber for multisite recording using penetrating electrodes. *Journal of Neuroscience Methods*. **189** (1), p5 – 13.

Blanca M.J., Alarcón R., Arnau J., Bono R. and Bendayan R. (2018). Effect of variance ratio on ANOVA robustness: might 1.5 be the limit? *Behaviour Research and Therapy*. **50**, p937 – 962.

Blanco J.C.G., Core S., Pletneva L.M., March T.H., Boukhvalova M.S. and Kajon A.E. (2014). Prophylactic antibody treatment and intramuscular immunization reduce infectious human rhinovirus 16 load in the lower respiratory tract of challenged cotton rats. *Trials in Vaccinology*. **3**, p52 – 60.

Bochkov Y.A., Watters K., Ashrafa S., Griggs T.F., Devries M.K., Jackson D.J., Palmenberg A.C. and Gern J.E. (2015). Cadherin-related family member 3, a childhood asthma susceptibility gene product, mediates rhinovirus C binding and replication. *Proceedings of the National Academy of Science of the United States of America (PNAS)*. **112** (17), p5485 – 5490.

Bochkov Y.A. and Gern J.E. (2016). Rhinoviruses and Their Receptors: Implications for Allergic Disease. *Current Allergy and Asthma Reports*. **16** (30).

Bölcskei H. and Farkas B. (2014). P2X3 and P2X2/3 receptor antagonist. *Pharmaceutical Patent Analysis*. **3** (1), p53 – 64.

Bonham A.C., Kott K.S., Ravi K., Kappagoda C.T. and Joad J.P. (1996). Substance P contributes to rapidly adapting receptor responses to pulmonary venous congestion in rabbits. *Journal of Physiology*. **493** (1), p229 – 238.

Bonner K., Pease J.E., Corrigan C.J., Clark P. and Kay B. (2013). CCL17/thymus and activation-regulated chemokine induced calcitonin gene-related peptide in human airway epithelial cells through CCR4. *Journal of Allergy and Clinical Immunology*. **132**, p942 – 950.

Bonvini S.J., Birrell M.A., Grace M.S., Maher S.A., Adcock J.J., Wortley M.A., Dubuis E., Ching Y-M., Ford A.P., Shala F. Miralpeix M., Tarrason G., Smith J.A. and Belvisi M.G. (2016). Transient receptor potential cation channel, subfamily V, member 4 and airway sensory afferent activation: role of adenosine triphosphate. *Journal of Allergy and Clinical Immunology*. **138** (1), p249 – 261.

Bonvini S.J. and Belvisi M.G. (2017). Cough and airway disease: the role of ion channels. *Pulmonary Pharmacology and Therapeutics*. **47**, p21 – 28.

Bonvini S.J., Birrell M.A., Dubuis E., Adcock J.J., Wortley M.A., Flajolet P., Bradding P. and Belvisi M.G. (2020). Novel airway smooth muscle-mast cell interactions and a role for the TRPV4-ATP axis in non-atopic asthma. European Respiratory Journal. 56 (1), 1901458.

Booth J.L., Coggeshall K.M., Gordon B.E. and Metcalf J.P. (2004). Adenovirus type 7 induces interleukin-8 in a lung slice model and required activation of Erk. *Journal of Virology*. **78** (8), p4156 – 4164.

Bosco A., Wiehler S. and Proud D. (2016). Interferon regulatory factor 7 regulates airway epithelial cell responses to human rhinovirus infection. *BMC Genomic*. **17** (76).

Bothwell P.J., Kron C.D., Wittke E.F., Czerniak B.N. and Bode B.P. (2018). Targeted Suppression and Knockout of ASCT2 or LAT1 in Epithelial and Mesenchymal Human Liver Cancer Cells Fail to Inhibit Growth. *International Journal of Molecular Sciences.* **19** (7), 2093.

Bower R., Green V.L., Kuvshinova E., Kuvshinov D., Karsai L., Crank S.T., Stafford N.D. and Greenman J. (2017). Maintenance of head and neck tumor on-chip: gateway to personalized treatment? *Future Science OA*. **3** (2), FSO174.

Braman S.S. (2006). Postinfectious cough: ACCP evidence-based clinical practice guidelines. *Chest*. **129**, p138S – 146S.

Brendel K., Gandolfi A.J., Krumdieck C.L. and Smith P.F. (1987). Tissue slicing and culturing revisited. *Trends in Pharmacological Sciences*. **8** (1), p11 – 15.

Brierley S.M., Page A.J., Hughes P.A., Adam B., Liebregts T., Cooper N.J., Holtmann G., Liedtke W. and Blackshaw L.A. (2008). Selective role for TRPV4 ion channels in visceral sensory pathways. *Gastroenterology*. **134**, p2059 – 2069.

Brockman-Schneider R.A., Pickles R.J. and Gern J.E. (2014). Effects of vitamin D on airway epithelial cell morphology and rhinovirus replication. *PLoS ONE*. **9** (1), e86755.

Brook B.S., Peel S.E., Hall I.P., Politi A.Z., Sneyd J., Bai Y., Sanderson M.J. and Jensen O.E. (2010). A biomechanical model of agonist-initiated contraction in the asthmatic airway. *Respiratory Physiology and Neurobiology*. **170**, p44 – 58.

Brown S.M., Koarai A., Sturton R.G., Nicholson A.G., Barnes P.J. and Donnelly L.E. (2013). A role for M_2 and M_3 muscarinic receptors in the contraction of rat and human small airways. *European Journal of Pharmacology*. **702**, p109 – 115.

Bryson K.J., Garrido D., Esposito M., McLachlan G., Digard P., Schouler C., Guabiraba R., Trapp S. and Vervelde L. (2020). Precision cut lung slices: a novel versatile tool to examine host-pathogen interaction in the chicken lung. *Veterinary Research*. **51** (1), 2.

Cadieux A., Monast N.P., Pomerleau F., Fournier A. and Lanoue C. (1999). Bronchoprotector properties of calcitonin gene-related peptide in guinea pig and human airways. *American Journal of Respiration and Critical Care Medicine*. **159**, p235 – 243.

Cairns J.T., Habgood A., Edwards-Pritchard R.C., Joseph C., John A.E., Wilkinson C., Stewart I.D., Leslie J., Blaxall B.C., Susztak K., Alberti S., Nordheim A., Oakley F., Jenkins G. and Tatler A.L. (2020). Loss of ELK1 has differential effects on age-dependent organ fibrosis. *The International Journal of Biochemistry and Cell Biology*. **120**, 105668.

Came P.E., Schafer T.W. and Silver G.H. (1976). Sensitivity of Rhinoviruses to Human Leukocyte and Fibroblast Interferons. *The Journal of Infectious Diseases.* **133** (2), A136 – 139.

Carr 3rd R., Koziol-White C., Zhang J., Lam H., An S.S., Tall G.G., Panettieri R.A. Jr. and Benovic J.L. (2016). Interdicting Gq Activation in Airway Disease by Receptor-Dependent and Receptor-Independent Mechanisms. *Molecular Pharmacology.* **89** (1), p94 – 104.

Carr S.D., Green V.L., Stafford N.D. and Greenman J. (2014). Analysis of radiation-induced cell death in head and neck squamous cell carcinoma and rat liver maintained in microfluidic devices. *Otolaryngoly – Head and Neck Surgery*. **150** (1), p73 – 80.

Catterton M.A., Dunn A.F. and Pompano R.R. (2018). User-defined local stimulation of live tissue through a movable microfluidic port. *Lab on a Chip*. **18** (14), p2003 – 2012.

Cauwe B., Van den Steen P.E. and Opdenakker G. (2007). The biochemical, biological and pathological kaleidoscope of cell surface substrates processed by matrix metalloproteinases. *Critical Reviews in Biochemistry and Molecular Biology*. **42**, p113 – 185.

Chandran S., Watkins J., Abdul-Aziz A., Shafat M., Calvert P.A., Bowles K.M., Flather M.D., Rushworth S.A. and Ryding A.D. (2017). Inflammatory differences in plaque erosion and rupture in patients with ST-segment elevation myocardial infarction. *Journal of the American Heart Association*. **6**, e005868.

Chapman D.G., Tully J.E., Nolin J.D., Jansen-Heininger Y.M. and Irvin C.G. (2014). Animal Models of Allergic Airways Disease: Where Are We and Where to Next? *Journal of Cellular Biochemistry*. **115** (12), p2055 – 2064.

Cheah L.T., Dou Y.H., Seymour A.M., Dyer C.E., Haswell S.J., Wadhawan J.D. and Greenman J. (2010). Microfluidic perfusion system for maintaining viable heart tissue with real-time electrochemical monitoring of reactive oxygen species. *Lab on a Chip*. **10** (20), p2720 – 2726.

Chen X., Cao R. and Zhong W. (2020). Host calcium channels and pumps in viral infections. *Cell*. **9** (1), 94.

Chen Y., Fang Z., Merritt B., Strack D., Xu J. And Lee S. (2016). Onset of particle trapping and release via acoustic bubbles. *Lab on a Chip*. **16**, p3024 – 3032.

Cheow L.F., Viswanathan R., Chin C-S., Jennifer N., Jones R.C., Guccione E., Quake S.R. and Burkholder W.F. (2014). Multiplexed analysis of protein-ligand interactions by fluorescence anisotropy in microfluidic platform. *Analytical Chemistry*. **86**, p9901 – 9908.

Chiu D.T., de Mello A.J., Carlo D.D., Doyle P.S., Hansen C., Maceiczyk R.M. and Wootton R.C.R. (2017). Small but perfectly formed? Successes, challenges, and opportunities for microfluidics in the chemical and biological sciences. *Chem*. **2**, p201 – 223.

Cho M-H., Niles A., Huang R., Inglese J., Austin C.P., Riss T. and Xia M. (2008). A bioluminescent cytotoxicity assay for assessment of membrane integrity using a proteolytic biomarker. *Toxicology in Vitro*. **22** (4), p1009 – 1106.

Christensen D., Foged C., Rosenkrands I., Lundberg C.V., Andersen P., Agger E.M. and Nielsen H.M. (2010). CAF01 liposomes as a mucosal vaccine adjuvant: *in vitro* and *in vivo* investigations. *International Journal of Pharmaceutics*. **390** (1), p19 – 24.

Clark L.C. and Lyons C. (1962). Electrode systems for continuous monitoring in cardiovascular surgery. *Annuals of the New York Academy of Science*. **102**, p29 – 45.

Collins A.M., Rylance J., Wootton D.G., Wright A.D., Wright A.K.A., Fullerton D.G. and Gordon S.B. (2014). Bronchoalveolar lavage (BAL) for research; obtaining adequate sample yield. *Journal of Visualized Experiments*. **85**, e4345.

Comstock A.T., Ganesan S., Chattoraj A., Faris A.N., Margolis B.L., Hershenson M.B. and Sajjan U.S. (2011). Rhinovirus-induced barrier dysfunction in polarized airway epithelial cells is mediated by NADPH oxidase 1. *Journal of Virology*. **85** (13), p6795 – 6808.

Cooper J.R., Abdullatif M.B., Burnett E.C., Kempsell K.E., Conforti F., Tollet H., Collins J.E. and Davies D.E. (2016) Long term culture of the A549 cancer cell line promotes multilamellar body formation and differentiation towards an alveolar type II pneumocyte phenotype. *PLoS ONE*. **11** (10), e0164438.

Cooper P.R. and Panettieri R.A. Jr. (2008). Steroids completely reverse albuterol-induced β_2-adrenergic receptor tolerance in human small airways. *The Journal of Allergy and Clinical Immunology.* **122** (4), p734 – 740.

Cooper P.R., Kurten R.C., Zhang J., Nicholls D.J., Dainty I.A., and Panettieri R.A. (2011a). Formoterol and salmeterol induce a similar degree of β2-adrenoceptor tolerance in human small airways but via different mechanisms. *British Journal of Pharmacology*. **163** (3), p521 – 532.

Cooper P.R., Zhang J., Damera G., Hoshi T., Zopf D.A. and Panettieri R.A. Jr. (2011b). C-027 inhibits IgE-mediated passive sensitization bronchoconstriction and acts as histamine and serotonin antagonist in human airways. *Allergy and Asthma Proceedings*. **32** (5), p359 – 365.

Corne J.M. and Holgate S.T. (1997). Mechanisms of virus induced exacerbations of asthma. *Thorax*. **52**, p380 – 389.

Daham K., James A., Balgoma D., Kupczyk M., Billing B., Lindeberg A., Henriksson E., Fitzgerald G.A., Wheelock C.E., Dahlén S-E. and Dahlén B. (2014). Effects of selective COX-2 inhibition on allergen-induced bronchoconstriction and airway inflammation in asthma. *Journal of Allergy and Clinical Immunology*. **134**, p306 – 313.

Dakhama A., Kanehiro A., Mäkelä M.J., Loader J.E., Larsen G.L. and Gelfand E.W. (2002). Regulation of airway hyperresponsiveness by Calcitonin gene-related peptide in allergen sensitized and challenged mice. *American Journal of Respiration and Critical Care Medicine.* **165**, p1137 – 1144.

Damera G., Druey K.M., Cooper P.R., Krymskaya V.P., Soberman R.J., Amrani Y., Hoshi T., Brightling C.E. and Panettieri R.A. Jr. (2012). An RGS4-mediated phenotypic switch of bronchial smooth muscle cells promotes fixed airway obstruction in asthma. *PLoS ONE*. **7** (1), e28504.

Dandurand R.J., Wang C.G., Phillips N.C. and Eidelman D.H. (1993). Responsiveness of individual airways to methacholine in adult rat lung explants. *Journal of Applied Physiology*. **75** (1), p364 – 372.

Davidovich N., Chhour P. and Margulies S.S. (2013a). Uses of remnant human lung tissue for mechanical stretch studies. *Cellular and Molecular Bioengineering*. **6** (2), p175 – 182.

Davidovich N., Huanh J. and Margulies S.S. (2013b). Reproducible uniform equibiaxial stretch of precision-cut lung slices. *American Journal of Physiology: Lung Cellular and Molecular Physiology.* **304**, L210 – 220.

Dawson A., Dyer C., Macfie J., Davies J., Karsai L., Greenman J. and Jacobsen M. (2016a). A microfluidic chip based model for the study of full thickness human intestine using dual flow. *Biomicrofluidics*. **10**, 064101.

Dawson A., Green V., Bower R. and Greenman J. (2016b). Microfluidics: the fur-free way towards personalised medicine in cancer therapy. *Drug Target Review*. **3**, p12 – 17.

de Graft I.A.M. and Koster H.J. (2003). Cryopreservation of precision-cut tissue slices for application in drug metabolism research. *Toxicology in Vitro*. **17** (1), p1 – 17.

de Oliveira J.R.J.M., Otuki M.F., Cabrini D.A., Brusco I., Oliveira S.M., Ferreira J. and André (2016). Involvement of the TRPV1 receptor in plasma extravasation in airways of rats treated with an angiotensin-converting enzyme inhibitor. *Pulmonary Pharmacology and Therapeutics*. **41**, p25 – 33.

de Winter J.F.C. and Dodou D. (2010). Five-point likert items: t test versus Mann-Whitney-Wilcoxon. *Practical Assessment, Research, and Evaluation*. **15** (11).

del Vecchio A.M., Brangian P.J., Barnathan E.S., Flavin S.K., Silkoff P.E. and Turner R.B. (2015). Utility of animal and *in vivo* experimental infection of humans with rhinovirus in the development of therapeutic agents for viral exacerbations of asthma and chronic obstructive pulmonary disease. *Pulmonary Pharmacology and Therapeutics*. **30**, p32 – 43.

Dick E.C., Jenning L.C., Mink K.A., Wartgow C.D. and Inhorn S.I. (1987). Aerosol transmission of rhinovirus colds. *The Journal of Infectious Diseases*. **156** (3), p442 – 448.

Dicpinigaitis P.V., Tibb A.S., Ramsey D.L., Carr A.N. and Poore C.L. (2014). Stability of cough reflex sensitivity during viral upper respiratory tract infection (common cold). *Pulmonary Pharmacology and Therapeutics*. **28**, p154 – 157.

Diemert S., Dolga A.M., Tobaben S., Grohm J., Pfeifer S., Oexler E. and Culmsee C. (2012). Impendance measurement for real time detection of neuronal cell death. *Journal of Neuroscience Methods*. **203** (1), p69 – 77.

Dinno A. (2015). Nonparametric pairwise multiple comparisons in independent groups using Dunn's test. *The Stata Journal*. **15** (1), p292 – 300.

Dodson K.H., Echevarria F.D., Li D., Sappington R.M. and Edd J.F. (2015). Retina-on-a-chip: a microfluidic platform for point access signalling studies. *Biomedical Microdevices*. **17** (6), 114.

Douville N.J., Zamankhan P., Tung Y-C., Li R., Vaughan B.L., Tai C-F., White J., Christensen P.J., Grotberg J.B. and Takayama S. (2011). Combination of fluid and solid mechanical stresses contribute to cell death and detachment in microfluidic alveolar model. *Lab on a Chip*. **11** (4), p557 – 760.

Duffy D.C., McDonald J.C., Schueller O.J.A. and Whitesides G.M. (1998). Rapid prototyping of microfluidic systems in poly(dimethylsiloxane). *Analytical Chemistry*. **70**, p4974 – 4984.

Duncombe T.A., Tentori A.M. and Herr A.E. (2015). Microfluidics: reframing biological enquiry. *Nature Reviews Molecular Cell Biology*. **16**, p554 – 567.

Durnin L., Moreland N., Lees A. and Mutafova-Yambolieva V.N. (2016). A commonly used ecto-ATPase inhibitor, ARL-67156, blocks degradation of ADP more than the degradation of ATP in murine colon. *Neurogastroenterol and Motility*. **28**, p1370 – 1381.

Eccles R. (2005). Understanding the symptoms of the common cold and influenza. *Lancet Infectious Disease*. **5**, p718 – 725.

Eddings M.A., Johnson M.A. and Gale B.K. (2008). Determining the optimal PDMS-PDMS bonding technique for microfluidic devices. *Journal of Micromechanics and Microengineering*. **18**, 067001.

Ehrhardt C., Kneuer C, Fiegel J., Hanes J., Schaefer U.F., Kim K-J., Lehr C-M. (2002) Influence of apical fluid volume on the development of functional intercellular junctions in the human epithelial cell line 16HBE14o-: implications for the use of this cell line as an in vitro model for bronchial drug absorption studies. *Cell Tissue Research*. **308**, p391 – 400.

El-Hashim A.Z. and Amine S.A. (2005). The role of substance P and bradykinins in the cough reflex and bronchoconstriction in guinea-pigs. *European Journal of Pharmacology*. **513**, p125 – 133.

Erickson D. and Li D. (2004). Integrated microfluidic devices. *Analytica Chimica Acta*. **507**, p11 – 26.

Esch E.W., Bahinski A. and Huh D. (2015). Organs-on-ships at the frontiers of drug discovery. *Nature Reviews Drug Discovery*. **14** (4), p248 – 260.

Esch M.B., Mahler G.J., Stokol T. and Shuler M.L. (2014). Body-on-a-chip simulation with gastrointestinal tract and liver tissues suggests that ingested nanoparticles have the potential to cause liver injury. *Lab on a chip*. **14**, p3081 – 3092.

Etemadi M.R., Ling H-W., Abidin S.Z., Chee H-Y. and Sekawi Z. (2017). Gene expression patterns induced at different stages of rhinovirus infection in human alveolar epithelial cells. *PLoS ONE*. **12** (5), e176947.

Ettinger A. and Wittmann E. (2014). Fluorescence Live Cell Imaging. *Methods in Cell Biology*. **123**, p77 – 94.

Fagerland M.W. (2012). T-tests, non-parametric tests, and large studies – a paradox of statistical practice? *BMC Medical Research Methodology*. **12** (78).

Farne H., Jackson D.J. and Johnston S.L. (2016). Are emerging PGD2 antagonists a promising therapy class for treating asthma? *Expert Opinion on Emerging Drugs*. **21** (4), p359 – 364.

Fay M.P. and Proschan M.A. (2010). Wilcoxon-Mann-Whitney or t-test? On assumptions for hypothesis tests and multiple interpretations of decision rules. *Statistics Surveys*. **4**, p1 – 39.

Fendrick A.M., Monto A.S., Nightengale B. and Sarnes M. (2003). The economic burden of non-influenza-related viral respiratory tract infection in the United States. *Archives of Internal Medicine*. **163**, p487 – 494.

Fisher R.L., Smith M.S., Hasal S.J., Hasal K.S., Gandolfi A.J. and Brendel K. (1994). The use of human lung slices in toxicology. *Human and Experimental Toxicology*. **13**, p466 – 471.

Fixe P. and Praloran V. (1998). M-CSF: haematopoietic growth factor or inflammatory cytokine? *Cytokine*. **10** (1), p32 – 37.

Flaherty R.A., Borges E.C., Sutton J.A., Aronoff D.M., Gaddy J.A., Petroff M.G. and Manning S.D. (2019). Genetically distinct group B *Streptococcus* strains induce varying macrophage cytokine response. *PLoS ONE*. **14** (9), e0222910.

Fleige S. and Pfaffl M.W. (2006). RNA integrity and the effect on the real-time qRT-PCR performance. *Molecular Aspects of Medicine*. **27**, p126 – 139.

Forbes B. (2000). Human airway epithelial cell lines for *in vitro* drug transport and metabolism studies. *Pharmaceutical Science and Technology Today*. **3** (1), p18 – 27.

Forbes B., Shah A., Martin G.P., Lansley A.B. (2003). The human bronchial epithelial cell line 16HBE14o- as a model system of the airways for studying drug transport. *International Journal of Pharmaceutics*. **257**, p161 – 167.

Fotakis G. and Timbrell J.A. (2006). In vitro cytotoxicity assays: comparison of LDH, neutral red, MTT and protein assay in hepatoma cell lines following exposure to cadmium chloride. *Toxicology Letters*. **160** (2), p171 – 177.

Franco-Bocanegra D.K., McAuley C., Nicoll J.A.R. and Boche D. (2019). Molecular mechanisms of microglial motility: changes in ageing and Alzheimer's disease. *Cells*. **8** (639).

Gallo-Oller G., Ordoñez R. and Dotor J. (2018). A new background subtraction method for Western blot densitometry band quantification through image analysis software. *Journal of Immunological Methods*. **457**, p1 – 5.

Gelderblom W.C.A., Semple E., Marasas W.F.O. and Farber E. (1992). The cancer-initiating potential of the fumonisin B mycotoxins. *Carcinogenesis*. **13** (3), p433 – 437.

Gelman A., Hill J. and Yajima M. (2012). Why we (usually) don't have to worry about multiple comparisons. *Journal of Research on Educational Effectiveness*. **5** (2), p189 – 211.

Georas S.N. and Rezaee F. (2014). Epithelial barrier function: at the front line of asthma immunology and allergic airway inflammation. *Journal of Allergy and Clinical Immunology*. **134**, p509 – 520.

Gern J.E., Lee W.M., Swenson C.A., Nakagome K., Lee I., Wolff M., Grindle K., Sigelman S., Liggett S.B., Togias A., Evans M., Denlinger L., Gangnon R., Bochkov Y.A. and Crisafi G. (2019). Development of a rhinovirus inoculum using a reverse genetics approach. *The Journal of Infectious Diseases*. **220** (2), p187 – 194.

Ghildyal R., Dagher H., Donninger H., de Silva D., Li X., Freezer N.J., Wilson J.W. and Bardin P.G. (2005). Rhinovirus infects primary human airway fibroblasts and induced a neutrophil chemokine and a permeability factor. *Journal of Medical Virology*. **75**, p608 – 615.

Ghosh A., Koziol-White C.J., Asosingh K., Cheng G., Ruple L., Groneberg D., Friebe A., Comhair S.A., Stasch J.P., Panettieri R.A. Jr., Aronica M.A., Erzurum S.C. and Stuehr D.J. (2016). Soluble guanylate cyclase as an alternative target for bronchodilator therapy in asthma. *Proceedings of the National Academy of Science of the United States of America (PNAS).* **113** (17), E2355 – 2362.

Goral V.N., Zhou C., Lai F. and Yuen P.K. (2013). A continuous perfusion microplate for cell culture. *Lab on a Chip*. **13**, p1039 – 1043.

Goris K., Uhlenbruck S., Schwegmann-Wessels C., Köhl W., Niedorf F., Stern M., Hewicker-Trautwein M., Bals R., Taylor G., Braun A., Bicker G., Kietzmann M. and Herrier G. (2009). Differential sensitivity of differentiated epithelial cells to respiratory viruses reveals different viral strategies of host infection. *Journal of Virology*. **83** (4), p1962 – 1968.

Grace M.S., Dubuis E., Birrell M.A. and Belvisi M.G. (2013). Pre-clinical studies in cough research: role of transient receptor potential (TRP) channels. *Pulmonary Pharmacology and Therapeutics*. **26**, p498 – 507.

Greiff D. and Kelly R.T. (1966). Cryotolerance of enzymes: I. Freezing of lactic dehydrogenase. *Cryobiology*. **2** (6), p335 – 341.

Griego S.D., Weston C.B., Adams J.L., Tal-Subger R. and Dillon S.B. (2000). Role of p38 mitogen-activated protein kinase in rhinovirus-induced cytokine production by bronchial epithelial cells. *The Journal of Immunology*. **165**, p5211 – 5220.

Greiller C.L., Suri R., Jolliffe D.A., Kebadze T., Hirsman A.G., Griffiths C.J., Johnston S.L. and Martineau A.R. (2019) Vitamin D attenuates rhinovirus-induced expression of intercellular adhesion molecule-1 (ICAM-1) and platelet-activating factor receptor (PAFR) in respiratory epithelial cells. *Journal of Steroid Biochemistry and Molecular Biology*. **187**, p152 – 159.

Grivel J-C. and Margolis L. (2009). Use of human tissue explants to study human infectious agents. *Nature Protocols*. **4** (2), p256 – 269.

Groneberg D.A., Eynott P.R., Lim S., Oates T., Wu R., Carlstedt I., Roberts P., McCann B., Nicholson A.G., Harrison B.D. and Chung K.F. (2002). Expression of respiratory mucins in fatal status asthmaticus and mild asthma. *Histopathology*. **40** (4), p367 – 373.

Grünberg K., Kuijpers E.A., de Klerk E.P., de Gouw H.W., Kroes A.C., Dick E.C. and Sterk P.J. (1997). Effects of experimental rhinovirus 16 infection on airway hyperresponsiveness to bradykinin in asthmatic subjects in vivo. *American Journal of Respiratory and Critical Care Medicine.* **155** (3), p833 – 838.

Grünberg K., Sharon R.F., Hiltermann T.J.N., Brahim J.J., Dick E.C., Sterk P.J. and Van Krieken J.H.J.M. (2000). Experimental rhinovirus 16 infection increases intercellular adhesion molecule-1 expression in bronchial epithelium of asthmatics regardless of inhaled steroid treatment. *Clinical Experimental Allergy*. **30** (7), p1015 – 1023.

Gualano R.C., Vlahos R. and Anderson G.P. (2006). What is the contribution of respiratory viruses and lung proteases to airway remodelling in asthma and chronic obstructive pulmonary disease? *Pulmonary Pharmacology & Therapeutics*. **19** (1), p18 – 23.

Guo M.T., Rotem A., Heyman J.A. and Weitz D.A. (2012). Droplet microfluidics for high-throughput biological assays. *Lab on a Chip*. **12**, p2146 – 2155.

Gwaltney Jr. J.M. and Jordan Jr. W.S. (1964). Rhinoviruses and respiratory disease. *Bacteriology Reviews*. **28** (4), p409 – 422.

Hadfield A.T., Lee W., Zhao R., Oliveira M.A., Minor I., Rueckert R.R. and Rossmann M.G. (1997). The refined structure of human rhinovirus 16 at 2.15 Å resolution: implications for the viral life cycle. *Structure*. **5** (3), p427 – 441.

Halldorsson S., Lucumi E., Gómez-Sjöberg R. and Fleming R.M.T. (2015). Advantages and challenges of microfluidic cell culture in polydimethylsiloxane devices. *Biosensors and Bioelectronics*. **63**, p218 – 231.

Hammarström S. (1983). Leukotrienes. *Annual Review of Biochemistry*. **52**, p355 – 377.

Hammond C., Kurten M. and Kennedy J.L (2015). Rhinovirus and asthma: a storied history of incompatibility. *Current Allergy and Asthma Reports*. **15** (2).

Han M., Rajut C., Ishikawa T., Jarman C.R., Lee J. and Hershenson M.B. (2018). Small animal models of respiratory viral infection related to asthma. *Viruses*. **10** (12), 682.

Han X., Na T., Wu T. and Yuan B-Z. (2020). Human lung epithelial Beas-2b cells exhibit characteristics of mesenchymal stem cells. *PLoS ONE.* **15** (1), 30227174.

Haniu H., Saito N., Matsuda Y., Tsukahara T., Maruyama K., Usui Y., Aoki K., Takanashi S., Kobayashi S., Nomura H., Okamoto M., Shimizu M. and Kato H. (2013). Culture medium type affects endocytosis of multi-walled carbon nanotubes in BEAS-2B cells and subsequent biological response. *Toxicology in Vitro*. **27** (6), p1679 – 1685.

Harris 2nd J.M. ad Gwaltney Jr J.M. (1996). Incubation periods of experimental rhinovirus infection and illness. *Clinical Infectious Diseases*. **23**, p1287 – 1290.

Hart A. (2001). Mann-Whitney test is not just a test of medians: differences in spread can be important. *British Medical Journal.* **323**, p391 – 393.

Hattersley S.M., Dyer C.E., Greenman J. and Haswell S.J. (2008). Development of a microfluidic device for the maintenance and interrogation of viable tissue biopsies. *Lab on a Chip*. **8**, p1842 – 1846.

Hattersley S.M., Sylvester D.C., Dyer C.E., Stafford N.D., Haswell S.J. and Greenman J. (2012). A microfluidic system for testing the responses of head and neck squamous cell carcinoma tissue biopsies to treatment with chemotherapy drugs. *Annals of Biomedical Engineering*. **40** (6), p1277 – 1288.

Hayden F.G. (2004). Rhinovirus and the lower respiratory tract. *Reviews in Medical Virology*. **14**, p17 – 31.

Henares T.G., Mizutani F. and Hisamoto H. (2008). Current development in microfluidic immunosensing chip. *Analytica Chimica Acta*. **611**, p17 – 30.

Henjakovic M., Martin C., Hoymann H.G., Sewald K., Ressmeyer A.R., Dassow C., Pohlmann G., Krug N., Uhlig S. and Braun A. (2008a). *Ex vivo* lung function measurements in precision-cut lung slices (PCLS) from chemical allergen-sensitized mice represent a suitable alternative to *in vivo* studies. *Toxicological Sciences*. **106** (2), p444 – 453.

Henjakovic M., Sewald K., Switalla S., Kaiser D., Müller M., Veres T.Z., Martin C., Uhlig S., Krug N. and Braun A. (2008b). *Ex vivo* testing of immune responses in precision-cut lung slices. *Toxicology and Applied Pharmacology*. **231**, p68 – 76.

Henry C.O., Dalloneau E., Pérez-Berezo M., Plata C., Wu Y., Guillon A., Morello E., Aimar R., Potier-Cartereau M., Esnard F., Coraux C., Börnchen C., Kiefmann R., Vandier C., Touqui L., Valverde M.A., Cenac N. and Si-Tahar M. (2016). In vitro and in vivo evidence for an inflammatory role of the calcium channel TRPV4 in lung epithelium: Potential involvement in cystic fibrosis. *American Journal of Physiology: Lung Cellular and Molecular Physiology*. **311**, L664 – 675.

Herbert J., Thiermann H., Worek F., Wille T. (2017). Precision cut lung slices as test system for candidate therapeutics in organophosphate poisoning. *Toxicology*. **398**, p94 – 100.

Hewson C.A., Haas J.J., Bartlett N.W., Message S.D., Laza-Stanca V., Kebadze T., Caramori G., Zhu J., Edbrooke M.R., Stanciu L.A., Kon O.M., Papi A., Jeffery P.K., Edwards M.R. and Johnston S.L. (2010). Rhinovirus induced MUC5AC in human infection model and *in vitro* via NF-κB and EGFR pathways. *European Respiratory Journal*. **36**, p1425 – 1435.

Higuchi Y. (2015). Observation of environmental stress cracking in polymethylmethacrylate by using the chemiluminescence method. *Materials Sciences and Applications*. **6**, p1084 – 1088.

Hillyer P., Shepard R., Uehling M., Krenz M., Sheikh F., Thayer K.R., Huang L., Yan L., Panda D., Luongo C., Buchholz U.J., Collins P.L., Donnelly R.P. and Rabin R.L. (2018). Differential responses by human respiratory epithelial cell lines to respiratory syncytial virus reflect distinct patterns of infection control. *Journal of Virology*. **92** (15), e02202-17.

Hocke A.C., Becher A., Knepper J., Peter A., Holland G., Tönnies M., Bauer T.T., Schneider P., Neudecker J., Muth D. and Wendtner C.M. (2013). Emerging human Middle East respiratory syndrome coronavirus causes widespread infection and alveolar damage in human lungs. *American Journal of Respiratory and Critical Care Medicine.* **188** (7), p882 – 886.

Hofer F., Gruenberger M., Kowalski H., Machat H., Huettinger M., Kuechler E. and Blaas D. (1994). *Proceedings of the National Academy of Science of the United States of America (PNAS)*. **91**, p1839 – 1842.

Hofmann O., Voirin G., Niedermann P. and Manz A. (2002). Three-dimensional microfluidic confinement for efficient sample delivery to biosensor surfaces. Application to immunoassays on planar optical waveguides. *Analytical Chemistry*. **74**, p5243 – 5250.

Holzer P. (1998). Neurogenic vasodilatation and plasma leakage in the skin. *General Pharmacology: The Vascular System*. **30** (1), p5 – 11.

Houikian P. and Raoult D. (2002). Traditional and molecular techniques for the study of emerging bacterial diseases: one laboratory's perspective. *Emerging Infectious Diseases*. **8** (2), p122 – 131.

Houle J.C., Chen A.V., Brenna A.C., Mealey K.L. and Kiszonas A.M. (2015). Determination of optimal storage temperature and duration for analysis of total and isoenzyme lactate dehydrogenase activities in canine serum and cerebrospinal fluid. *Veterinary Clinical Pathology*. **44** (2), p253 – 261.

Huh D., Fujioka H., Tung Y-C., Futai N., Ill R.P., Grotberg J.B. and Takayama S. (2007). Acoustically detectable cellular-level lung injury induced by fluid mechanical stresses in microfluidic airway systems. *Proceedings of the National Academy of Sciences of the United States of America (PNAS)*. **104** (48), p18886 – 18891.

Huh D., Matthews B.D., Mammoto A., Montoya-Zavala M., Hsin H.Y. and Ingber D.E. (2010). Reconstituting organ-level lung functions on a chip. *Science*. **328** (5986), p1662 – 1668.

Huh D., Hamilton G.A. and Ingber D.E. (2011). From 3D cell culture to organs-on-chips. *Trends in Cell Biology*. **21** (12), p745 – 754.

Huh D., Leslie D.C., Matthews B.D., Fraser J.P., Jurek S., Hamilton G.A., Thorneloe K.S., McAlexander M.A. and Ingber D.E. (2012). A human disease model of drug toxicity-induced pulmonary edema in a lung-on-a-chip microdevice. *Science Translational Medicine.* **4** (159), 159ra147.

Imura Y., Sato K. and Yoshimura E. (2010). Micro total bioassay system for ingested substances: assessment of intestinal absorption, hepatic metabolism and bioactivity. **82**, p9983 – 9988.

Inci I. (2017). Donors after cardiocirculatory death and lung transplantation. *Journal of Thoracic Disease*. **9** (8), p2660 – 2669.

Inoue D., Yamaya M., Kubo H., Sasaki T., Hosoda M., Numasaki M., Tomioka Y., Yasuda H., Sekizawa K., Nishimura H. and Sasaki H. (2006). Mechanisms of mucin production by rhinovirus infection in cultured human airway epithelial cells. *Respiratory Physiology and Neurobiology*. **154**, p484 – 499.

Irwin R.S., Baumann M.H., Bolser D.C., Boulet L-P., Braman S.S., Brightling C.E., Brown K.K., Canning B.J., Chang A.B., Dicpinigaitis P.V., Eccles R., Glomb W.B., Goldstein L.B., Graham L.M., Hargreave F.E., Kvale P.A., Lewis S.Z., McCool D., McCrory D.C., Prakash U.B.S., Pratter M.R., Rosen M.J., Schulman E., Shannon J.J., Smith Hammond C. and Tarlo S.M. (2006). Diagnosis and management of cough executive summary: ACCP evidence-based clinical practice guidelines. *Chest*. **126** (1S), p1S – 23S.

Iwane M.K., Prill M.M., Lu X., Miller E.K., Edwards K.M., Hall C.B., Griffin M.R., Staat M.A., Anderson L.J., Williams J.V., Weinberg G.A., Ali A., Szilagyi P.G., Zhu Y. and Erdman D.D. (2011). Human rhinovirus species associated with hospitalizations for acute respiratory illness in young US children. *The Journal of Infectious Diseases*. **204**, p1702 – 1710.

Jaccard J., Becker M.A. and Wood G. (1984). Pairwise multiple comparison procedures: a review. *Psychological Reviews*. **96** (3), p589 – 596.

Jacobs E., Hissin P.J., Propper W., Mayer L. and Sarkozi L. (1986). Stability of lactate dehydrogenase at different temperatures. *Clinical Biochemistry*. **19**, p183 – 188.

Jacobs S.E., Lamson D.M., St. George K. and Walsh T.J. (2013). Human rhinoviruses. *Clinical Microbiology Reviews*. **26** (1), p135 – 162.

Jan S-L and Shieh G. (2014). Sample size determinations for Welch's test in one-way heteroscedastic ANOVA. *British Journal of Mathematical and Statistical Psychology*. **67**, p72 – 93.

Jang Y.J., Kwon H-J. and Lee B-J. (2006). Effect of clarithromycin on rhinovirus-16 infection in A549 cells. *European Respiratory Journal*. **27**, p12 – 19.

Jennings L.C., Anderson T.P., Beynon K.A., Chua A., Laing R.T.R., Werno A.M., Young S.A., Chambers S.T. and Murdoch D.R. (2008). Incidence and characteristics of viral community-acquired pneumonia in adults. *Thorax*. **63**, p42 – 48.

Jia X., Zhang H., Cao X., Yin Y. and Zhang B. (2014). Activation of TRPV1 mediates thymic stromal lymphopoietin release via the Ca^{2+}/NFAT pathway in airway epithelial cells. *FEBS Letters*. **588**, p3047 – 3054.

Jiang X. and Kopp-Schneider A. (2015). Statistical strategies for averaging EC50 from multiple dose-response experiments. *Archives of Toxicology*. **89**, p2119 – 2127.

Jin M., Wu Z., Chen L., Jaimes J., Collins D., Walters E.T. and O'Neil R.G. (2011). Determinants of TRPV4 activity following selective activation by small molecule agonist GSK1016790A. *PLoS ONE*. **6** (2), e16713.

Johnston S.L. (2005). Overview of virus-induced airway disease. *Proceedings of the American Thoracic Society*. **2**, p150 – 156.

Johnston S.L., Papi A., Bates P.J., Mastronarde J.G., Monick M.M. and Hunninghake G.W. (1998). Low grade rhinovirus induces a prolonged release of IL-8 in pulmonary epithelium. *The Journal of Immunology*. **160**, p6172 – 6181.

Joos G.F., Germonpre P.R., Kips J.C., Peleman R.A. and Pauwels R.A. (1994). Sensory neuropeptides and the human lower airways: present state and future directions. *European Respiratory Journal*. **7**, p1161 – 1171.

Kamei J., Takahashi Y., Yoshikawa Y. and Saitoh A. (2005). Involvement of P2X receptor subtypes in ATP-induced enhancement of the cough reflex sensitivity. *European Journal of Pharmacology*. **528**, p158 – 161.

Kang M-J., Choi J-M., Kim B.H., Lee C-M., Cho W-K., Choe G., Kim D-H., Lee C.G. and Elisa J.A. (2012). IL-18 induced emphysema and airway and vascular remodelling via IFN-γ, IL-17A, and IL-13. *American Journal of Respiration and Critical Care Medicine*. **185** (11), p1205 – 1217.

Katsares V., Petsa A., Felesakis A., Paparidis Z., Nikolaidou E., Gargani S., Karbounidou I., Ardelean K-A., Grigoriadis N., and Grigoriadis J. (2009). A rapid and accurate method for the stem cell viability evaluation: the case of the thawed umbilical cord blood. *Lab Medicine*. **40** (9), p557 – 560.

Kaul P., Biagioli M.C., Singh I. and Turner R.B. (2000). Rhinovirus-induced oxidative stress and interleukin-8 elaboration involves p47-*phox* but is independent of attachment to intracellular adhesion molecule-1 and viral replication. *The Journal of Infectious Diseases*. **181**, p1885 – 1890.

Kennedy J.L., Turner R.B., Braciale T., Heymann P.W. and Borish L. (2012). Pathogenesis of rhinovirus infection. *Current Opinion in Virology*. **2**, p287 – 293.

Kennedy J.L., Koziol-White C.J., Jeffus S., Rettiganti M.R., Fisher P., Kurten M., Eze A., House S., Sikes J.D., Askew E., Putt C., Panettieri R.A., Jones S.M. and Kurten R.C. (2018). Effects of rhinovirus 39 infection on airway hyperresponsiveness to carbachol in human airways precision cut lung slices. *Journal of Allergy and Clinical Immunology*. **141** (5), p1887 – 1890.

Kennedy R., Kuvshinov D., Sdrolia A., Kuvshinova E., Hilton K., Crank S., Beavis A.W., Green V. and Greenman J. (2019). A patient tumour-on-a-chip system for personalised investigation of radiotherapy based treatment regimens. *Scientific Reports*. **9**, 6327.

Khinda V.I.S., Kaur G., Brar G.S., Kallar S. and Khurana H. (2017). Clinical and Practical Implications of Storage Media used for Tooth Avulsion. *International Journal of Clinical Pediatric Dentistry*. **10** (2), p158 – 165.

Kicic A., Stevens P.T., Sutanto E.N., Kicic-Starcevich E., Ling K-M., Looi K., Martinovich K.M., Garratt L.W., Iosifidis T., Shaw N.C., Buckley A.G., Rigby P.J., Lannihan F.J., Knight D.A. and Stick S.M. (2016). Impaired airway epithelial cell responses from children with asthma to rhinoviral infection. *Clinical and Experimental Allergy.* **46** (11), p1441 – 1455.

Kim L., Vahey M.D., Lee H-Y. and Voldman J. (2006). Microfluidic arrays for logarithmically perfused embryonic stem cell culture. *Lab on a Chip*. **6**, p394 – 406.

Kim L., Toh Y-C., Voldman J. and Yu H. (2007). A practical guide to microfluidic perfusion culture of adherent mammalian cells. *Lab on a Chip*. **7**, p681 – 694.

Kim H.J., Huh D., Hamilton G. and Ingber D.E. (2012). Human gut-on-a-chip inhabited by microbial flora that experiences intestinal peristalsis-like motions and flow. *Lab on a Chip*. **12**, p2165 – 2174.

Kim H.J. and Ingber D.E. (2013). Gut-on-a-chip microenvironment induces human intestinal cells to undergo villus differentiation. *Integrative Biology*. **5**, p1130 – 1140.

Kowal K., Gielicz A. and Sanak M. (2017). The effect of allergen-induced bronchoconstriction on concentration of 5-oxo-ETE in exhaled breath condensate of house dust mite-allergic patients. *Clinical Mechanisms in Allergic Disease.* **47**, p1253 – 1262.

Koziol-White C.J., Jia Y., Baltus G.A., Cooper P.R., Zaller D.M., Crackower M.A., Sirkowski E.E., Smock S., Northrup A.B., Himes B.E., Alves S.E. and Panettieri R.A. Jr. (2016a). Inhibition of spleen tyrosine kinase attenuates IgE-mediated airway contraction and mediator release in human precision cut lung slices. *British Journal of Pharmacology*. **173** (21), p3080 – 3087.

Koziol-White C.J., Yoo E.J., Cao G., Zhang J., Papanikolaou E., Pushkarsky I., Andrews A., Himes B.E., Damoiseaux R.D., Liggett S.B., Di Carlo D., Kurten R.C. and Panettieri R.A. Jr. (2016b). Inhibition of PI3K promotes dilation of human small airways in a rho kinase-dependent manner. *British Journal of Pharmacology*. **173** (18), p2726 – 2738.

Krumdieck C.L. (2013). Development of a live tissue microtome: reflections of an amateur machinist. *Xenobiotica*. **43**: 1, p2 – 7.

Krumdieck C.L., Dos Santos J.E. and Ho K-J (1980). A new instrument for the rapid preparation of tissue slices. *Analytical Biochemistry*. **104**, p118 – 123.

Kuo C., Lim S., King N.L.C., Bartlett N.W., Walton R.P., Zhu J., Glanville N., Aniscenko J., Johnston S.L., Burgess J.K., Black J.L. and Oliver B.G. (2011). Rhinovirus infection induces expression of airway remodelling factors in vitro and in vivo. *Respirology*. **16**, p367 – 377.

Kurai D., Saraya T., Ishii H. and Takizawa H. (2013). Virus-induced exacerbations in asthma and COPD. *Frontiers in Microbiology*. **4** (293).

Lamberti A., Marasso S.L. and Cocuzza M. (2014). PDMS membranes with tunable gas permeability for microfluidic applications. *RSC Advances*. **4**, p61415 – 61419.

Lantz B. (2013). The impact of sample non-normality on ANOVA and alternative methods. *British Journal of Mathematical and Statistical Psychology*. **66**, p224 – 244.

Lauenstein L., Switalla S., Prenzler F., Seehase S., Pfennig O., Förster C., Feiguth H., Braun A. and Sewald K. (2014). Assessment of immunotoxicity induced by chemicals in human precision-cut lung slices (PCLS). *Toxicology in Vitro*. **28**, p588 – 599.

Lavoie T.L., Krishnan R., Siegel H.R., Maston E.D., Fredberg J.J., Solway J. and Dowell M.L. (2012). Dilatation of the constricted human airway by tidal expansion of lung parenchyma. *American Journal of Respiratory and Critical Care Medicine.* **186** (3), p225 – 232.

Lazarowski E.R., Boucher R.C. and Harden T.K. (2000). Constitutive release of ATP and evidence for major contribution of ecto-nucleotide pyrophosphatase and nucleoside diphosphokinase to extracellular nucleotide concentrations. *Journal of Biological Chemistry*. **275** (40), p31061 – 31068.

Le D.D., Rochlitzer S., Fischer A., Heck S., Tschernig T., Sester M., Bals R., Welte T., Braun A. and Dinh Q.T. (2014). Allergic airway inflammation induced the migration of dendritic cells into airway sensory ganglia. *Respiratory Research*. **15** (73).

Lee S. and Lee D.K. (2018). What is the proper way to apply the multiple comparison test? *Korean Journal of Anesthesiology*. **71** (5), p353 – 360.

Lee W-M., Lemanske R.F., Evans M.D., Vang F., Pappas T., Gangnon R., Jackson D.J. and Gern J.E. (2012). Human Rhinovirus Species and Season of Infection Determine Illness Severity. *American Journal of Respiratory and Critical Care Medicine*. **186** (9), p886 – 891.

Leoni L., Serai S.D., Haque M.E., Magin R.L. and Roman B.B. (2010). Functional MRI characterization of isolated human islet activation. *NMR in Biomedicine*. **23** (10), p1158 – 1165.

Levy S.E. and Harvey E. (1974). Effect of tissue slicing on rat lung metabolism. *Journal of Applied Physiology*. **37** (2), p239 – 240.

Liang H-J., Li J-L., Di Y-L., Zhang A-S. and Zhu F-X. (2015). Logarithmic transformation is essential for statistical analysis of fungicide EC50 values. *Journal of Phytopathology*. **163**, p456 – 464.

Lin C-C., Wang J-H., Wu H-W. and Lee G-B. (2010). Microfluidic immunoassays. *Journal of Laboratory Automation*. **15** (3), p253 – 274.

Lin Y-J., Hsu H-H., Ruan T. and Kou Y.R. (2013). Mediator mechanisms involved in TRPV1, TRPA1 and P2X receptor-mediated sensory transduction of pulmonary ROS by vagal lung C-fibers in rats. *Respiratory Physiology and Neurobiology*. **189**, p1 – 9.

Lopez-Souza N., Dolganov G., Dubin R., Sachs L.A., Sassina L., Sporer H., Yagi S., Schnurr D., Boushey H.A. and Widdicombe J.H. (2004). Resistance of differentiated human airway epithelium to infection by rhinovirus. *American Journal of Physiology: Lung Cellular and Molecular Physiology*. **286**, L373 – 381.

Lopez-Souza N., Favoreto S., Wong H., Ward T., Yagi S., Schnurr D., Finkbeiner W.E., Dolganov G.M., Widdicombe J.H., Boushey H.A. and Avila P.C. (2009). Greater *in vitro* susceptibility to rhinovirus infection of bronchial than nasal airway epithelial cells in human subjects. *Journal of Allergy and Clinical Immunology*. **123** (6), p1384 – 1390.

Lötzerich M., Roulin P.S., Boucke K. Witte R., Georgiev O. and Greber U.F. (2018). Rhinovirus 3C protease suppresses apoptosis and triggers caspase-independent cell death. *Cell Death and Disease*. **9**, 272.

Lu C., Li S. and Liu Y. (2020). Role of immunosuppressive therapy in rheumatic diseases concurrent with covid-19. *Annals of the Rheumatic Diseases*. **79** (6), p737 – 739.

Luo Y., Yu F. and Zare R.N. (2008). Microfluidic device for immunoassays based on surface plasmon resonance. *Lab on a Chip*. **8**, p694 – 700.

Lyons-Cohen M.R., Thomas S.Y., Cook D.N. and Nakano H. (2017). Precision-cut mouse lung slices to visualize pulmonary dendritic cells. *Journal of Visualized Experiments*. **112**, e55465.

Maes M., Vanhaecke T., Cogliati B., Yanguas S.C., Willebrords J., Rogiers V. and Vinken M. (2015). Measurement of apoptotic and necrotic cell death in primary hepatocyte cultures. *Methods in Molecular Biology*. **1250**, p349 – 361.

Mallia P., Footitt J., Sotero R., Jepson A., Contoli M., Trujillo-Torralbo M-B., Kebadze T., Aniscenko J., Oleszkiewicz G., Gray K., Message S.D., Ito K., Barnes P.J., Adcock I.M., Papi A., Stanciu L.A., Elkin S.L., Kon O.M., Johnson M. and Johnston S.L. (2012). Rhinovirus infection induces degradation of antimicrobial peptides and secondary bacterial infection in chronic obstructive pulmonary disease. *American Journal of Respiratory and Critical Care Medicine.* **186** (11), p1117 – 1124.

Mansbach J.M. and Carmargo C.A. (2009). Respiratory viruses in bronchiolitis and their link to recurrent wheezing and asthma. *Clinics in Laboratory Medicine*. **29** (4), p741 – 755.

Manz A., Harrison D.J., Verpoorte E.M.J., Fettinger J.C., Paulus A., Lüdi H. and Widmer H.M. (1992). Planar chips technology for miniaturisation and integration of separation techniques into monitoring systems. *Journal of Chromatography*. **593**, p253 – 258.

Markov D.A., Lillie E.M., Garbett S.P. and McCawley L.J. (2014). Variation in diffusion of gases through PDMS due to plasma surface treatment and storage conditions. **16** (1), p91 – 96.

Martin B.C., Minner E.J., Wiseman S.L., Klank R.L. and Gilbert R.J. (2008). Agarose and methylcellulose hydrogel blends for nerve regeneration applications. *Journal of Neural Engineering*. **5**, p221 – 231.

Martin C., Uhlig S. and Ullrich V. (1996). Videomicroscopy of methacholine-induced contraction of individual airways in precision-cut lung slices. *European Respiratory Journal*. **9**, p2479 – 2487.

Martin N.C., Pirie A.A., Ford L.V., Callaghan C.L., McTurk K., Lucy D. and Scrimger D.G. (2006). The use of phosphate buffered saline for the recovery of cells and spermatozoa from swabs. *Scientific Justice*. **46** (3), p179 – 184.

Maschmeyer I., Lorenz A.K., Schimek K., Hasenberg T., Ramme A.P., Hübner J., Lindner M., Drewell C., Bauer S., Thomas A., Sambo N.S., Sonntag F., Lauster R. and Marx U. (2015). A four-organ-chip for interconnected long-term co-culture of human intestine, liver, skin and kidney equivalents. *Lab on a Chip*. **15** (12), p2688 – 2699.

Mathias N.R., Timoszyk J., Stetsko P.I., Megill J.R., Smith R.L. and Wall D.A. (2002). Permeability characteristics of Calu-3 human bronchial epithelial cells: *in vitro – in vivo* correlation to predict lung absorption in rats. *Journal of Drug Targeting*. **10** (1), p31 – 40.

Mauleon G., Lo J.F., Peterson B.L., Fall C.P. and Eddington D.T. (2013). Enhanced loading of Fura-2/AM calcium indicator dye in adult rodent brain slices via a microfluidic oxygenator. *Journal of Neuroscience Methods*. **216** (2), p110 – 117.

Mazutis L., Gilbert J., Ung W.L., Weltz D.A., Griffiths A.D. and Heyman J.A. (2013). Single-cell analysis and sorting using droplet-based microfluidics. *Nature Protocols*. **8** (5), p870 – 891.

McClain M.T., Henao R., Williams J., Nicholson B., Veldman T., Hudson L., Tsalik E.L., Lambkin-Williams R., Gilbert A., Mann A., Ginsburg G.S. and Woods C.W. (2016). Differential evolution of peripheral cytokine levels in symptomatic and asymptomatic response to experimental influence virus challenge. *Clinical and Experimental Immunology*. **183** (3), p441 – 451.

McDonald J.C., Duffy D.C., Anderson J.R., Chiu D.T., Wu H., Schueller O.J.A. and Whitesides G.M. (2000). Fabrication of microfluidic systems in poly(dimethylsiloxane). *Electrophoresis*. **21**, p27 – 40.

McHugh M.L. (2011). Multiple comparison analysis testing in ANOVA. *Biochemia Medica*. **21** (3), p203 – 209.

McLean G.R. (2014). Developing a vaccine for human rhinovirus. *Journal of Vaccines and Immunology*. **2** (3), p16 – 20.

McLean I.C., Schwerdtfeger L.A., Tobet S.A. and Henry C.S. (2018). Powering *ex vivo* tissue models in microfluidic systems. *Lab on a Chip.* **10**, p1399 – 1410.

Merchant N., Nagaraju G.P., Rajitha B., Lammata S., Jella K.K., Buchwald Z.S., Lakka S.S. and Ali A.N. (2017). Matrix metalloproteinases: their functional role in lung cancer. *Carcinogenesis*. **38** (8), p766 – 780.

Message S.D., Laza-Stanca V., Mallia P., Parker H.L., Zhu J., Kebadze T., Contoli M., Sanderson G., Kon O.M., Papi A., Jeffery P.K., Stanciu L.A. and Johnston S.L. (2008). Rhinovirus-induced lower respiratory illness is increased in asthma and related to virus load and Th1/2 cytokine and IL-10 production. *Proceedings of the National Academy of Sciences of the United States of America (PNAS)*. **105** (36), p13562 – 13567.

Mihara H., Uchida K., Koizumi S. and Moriyama Y. (2018). Involvement of VNUT-exocytosis in transient receptor potential vanilloid 4-dependent ATP release from gastrointestinal epithelium. *PLoS ONE*. **13** (10), e0206276.

Mishra P., Singh U., Pandey C.M., Mishra P. and Pandey G. (2019). Application of student's t-test, analysis of variance, and covariance. *Annals of Cardiac Anaesthesia*. **22**, p407 – 411.

Moe N., Pedersen B., Nordbø S.A., Skanke L.H., Krokstad S., Smyrnaios A. and Døllner H. (2016). Respiratory virus detection and clinical diagnosis in children attending day care. *PLoS ONE*. **11** (7), e0159196.

Mok J., Mindrinos M.N., Davis R.W. and Javanmard M. (2014). Digital microfluidic assay for protein detection. *Proceedings of the National Academy of Sciences of the United States of America (PNAS)*. **111** (6), p2110 – 2115.

Morice A.H. (2010). The cough hypersensitivity syndrome: a novel paradigm for understanding cough. *Lung*. **188** (1S), S87 – 90.

Morice A.H., Kastelik J.A. and Thompson R. (2001). Cough challenge in the assessment of cough reflex. *British Journal of Clinical Pharmacology*. **52**, p365 – 375.

Morin J-P., Fouquet F., Monteil C., Le Prieur E., Vaz E. and Dionnet F. (1999). Development of a new *in vitro* system for continuous *in vitro* exposure of lung tissue to complex atmospheres: application to diesel exhaust toxicology. *Cell Biology and Toxicology*. **15**, p143 – 152.

Morin J-P., Baste J-P., Gay A., Crochemore C., Corbière C. and Monteil C. (2013). Precision cut lung slices as an efficient tool for in vitro lung physio-pharmacotoxicology studies. *Xenobiotica*. **43** (1), p63 – 72.

Morgan K., Sadofsky L.R., Crow C., and Morice A.H. (2014). Human TRPM8 and TRPA1 pain channels, including a gene variant with increased sensitivity to agonists (TRPA1 R797T), exhibit differential regulation by SRC-tyrosine kinase inhibitor. *Bioscience Reports*. **34** (4), e00131.

Mosser A.G., Brockman-Schneider R., Amineva S., Burchell L., Sedgwick J.B., Busse W.W. and Gern J.E. (2002). Similar frequency of Rhinovirus-infectible cells in upper and lower epithelium. *The Journal of Infectious Diseases*. **185**, p734 – 743.

Mosser A.G., Vrtis R., Burchell L., Lee W-M., Dick C.R., Weisshaar E., Bock D., Swenson C.A., Cornwell R.D., Meyer K.C., Jarjour N.N., Busse W.W. and Gern J.E. (2005). Quantitative and qualitative analysis of rhinovirus infection in bronchial tissues. *American Journal of Respiratory and Critical Care Medicine*. **171**, p645 – 651.

Münker T.J.A.G., van de Vihfeijken S.E.C.M., Mulder C.S., Vespasiano V., Becking A.G., and Kleverlaan C.J., On behalf of the CranioSafe Group (2018). Effects of sterilization on the mechanical properties of poly(methyl methacrylate) based personalized medical devices. *Journal of the Mechanical Behavior of Biomedical Material*. **81**, p168 – 172.

Mutou Y., Ibuki Y., Terao Y., Kojima S. and Goto R. (2006). Chemical change of chlorinated biphenol A by ultraviolet irradiation and cytotoxicity of their products on Jurkat cells. *Environmental Toxicology and Pharmacology*. **21**, p283 – 289.

Nagashima J.B., El Assal R., Songsasen N., Demirci U. (2018). Evaluation of an ovary-on-a-chip in large mammalian models: Species specificity and influence of follicle isolation status. *Journal of Tissue Engineering and Regenerative Medicine*. **12** (4), e1926 – 1935.

Nave R. and McCracken N. (2008). Metabolism of ciclesonide in the upper and lower airways: review of available data. *Journal of Asthma and Allergy*. **7** (1), p11 – 18.

NCBI Molecular Modelling Database (MMDB) (2007). 1AYM – Human Rhinovirus 16 coat protein at high resolution, biological unit. (online) available at https://www.ncbi.nlm.nih.gov/Structure/mmdb/mmdbsrv.cgi?dps=0&uid=1AYM [accessed 24/05/18].

Neuhaus V., Schwarz K., Klee A., Seehase S., Förster C., Pfennig O., Jonigk D., Fieguth H-G., Koch W., Warnecke G., Yusibov V., Sewald K. and Braun A. (2013). Functional testing of an inhalable nanoparticle based influenza vaccine using a human precision cut lung slice technique. *PLoS ONE*. **8** (8), e7172B.

Neuhaus V., Schaudien D., Golovina T., Temann U.A., Thompson C., Lippmann T., Bersch C., Pfennig O., Jonigk D., Braubach P., Fieguth H.G., Warnecke G., Yusibov V., Sewald K. and Braun A. (2017). Assessment of long-term cultivated human precision-cut lung slices as an ex vivo system for evaluation of chronic cytotoxicity and functionality. *Journal of Occupational Medicine and Toxicology*. **12** (13).

Newcomb D.C., Sajjan U.S., Nagarkar D.R., Wang Q., Nanua S., Zhou Y., McHenry C.L., Hennrick K.T., Tsai W.C., Bentley J.K., Lukacs N.W., Johnston S.L. and Hershenson M.B. (2008). Human rhinovirus 1B exposure induced phosphatidylinositol 3-kinase-dependent airway inflammation in mice. *American Journal of Respiratory and Critical Care Medicine.* **177**, p1111 – 1121.

Ng A.H.C., Uddayasanker U. and Wheeler A.R. (2010). Immunoassays in microfluidic systems. *Analytical and Bioanalytical Chemistry.* **397**, p991 – 1007.

Nichol K.L., D'Heilly S. and Ehlinger E. (2005). Colds and influenza-like illnesses in university students: impact on health, academic and work performance, and health care use. *Clinical Infectious Diseases*. **40**, p1263 – 1270.

Nicholas B., Staples K.J., Moese S., Meldrum E., Ward J., Dennison P., Havelock T., Hinks T.S.C., Amer K., Woo E., Chamberlain M., Singh N., North M., Pink S., Wilkinson T.M.A. and Djukanovic R. (2015). A novel lung explant model for the ex vivo study of efficacy and mechanisms of anti-influenza drugs. *The Journal of Immunology*. **194**, p6144 – 6154.

Nie Y., Huang C., Zhong S., Wortley M.A., Luo Y., Lou W., Xie Y., Lai K. and Zhong N. (2016). Cigarette smoke extract (CSE) induced transient receptor potential Ankyrin 1 (TRPA1) expression via activation of HIF1α in A549 cells. *Free Radical Biology and Medicine*. **99**, p498 – 507.

Nonaka M., Ogihara N., Fukumoto A., Sakanushi A., Kusama K., Pawankar R. and Yagi T. (2010). Combined stimulation with poly(I:C), TNF-α and Th2 cytokines induces TARC production by human fibroblasts from the nose, bronchioles and lungs. *International Archives of Allergy and Immunology*. **152** (4), p327 – 341.

O'Brien J., Wilson I., Orton T. and Pognan F. (2000). Investigation of the Alamar Blue (resazurin) fluorescent dye for the assessment of mammalian cell cytotoxicity. *European Journal of Biochemistry*. **267**, p5421 – 5426.

Ojiaku C.A., Coa G., Zhu W., Yoo E.J., Shumyatcher M., Himes B.E., An S.S. and Panettieri R.A. Jr. (2018). TGF-β1 evokes airway smooth muscle cell shortening and hyperresponsiveness via Smad3. *American Journal of Respiratory Cell and Molecular Biology*. **58** (5), p575 – 584.

Oliver B.G.G., Johnston S.L., Baraket M., Burgess J.K., King N.J.C., Roth M., Lim S. and Black J.L. (2006). Increased proinflammatory responses from asthmatic human airway smooth muscle cells in response to rhinovirus infection. *Respiratory Research*. **7** (71).

Oliver B.G.G., Lim S., Wark P., Laza-Stanca V., King N., Black J.L., Burgess J.K., Roth M. and Johnston S.L. (2008). Rhinovirus exposure impairs immune responses to bacterial products in human alveolar macrophages. *Thorax.* **63**, p519 – 525.

O'Neill J.D., Anfang R., Anandappa A., Costa J., Javidfar J.J., Wobma H.M., Singh G., Freytes D.O., Bacchetta M.D., Sonett J.R. and Vunjak-Novakovic G. (2013). Decellularization of human and porcine lung tissues for pulmonary tissue engineering. *Annals Thoracic Surgery*. **96** (3), p1046 – 1056.

Orellana E.A. and Kasinski A.L. (2016). Sulforhodamine B (SRB) Assay in Cell Culture to Investigate Cell Proliferation. *Bio-protocol*. ***6*** (21), e1984.

Othumpangat S., Reiger M. and Piedimonte G. (2012). Nerve growth factor modulates human rhinovirus infection in airway epithelial cells by controlling ICAM-1 expression. *American Journal of Physiology – Lung Cellular and Molecular Physiology*. **302**, L1057 – 1066.

Paddenberg R., Mermer P., Golderberg A. and Kummer W. (2014). Videomorphometric analysis of hypoxic pulmonary vasoconstriction of intra-pulmonary arteries using murine precision cut lung slices. *Journal of Visualized Experiments*. **83**, e50970.

Paine 3rd R., Christensen P., Toews G.B. and Simon R.H. (1994). Regulation of alveolar epithelial cell ICAM-1 expression by cell shape and cell-cell interactions. *American Journal of Physiology – Lung Cellular and Molecular Physiology*. **266** (4 Pt1), L476 – 484.

Pang L., Yuan X., Shao C., Li M., Wang Y., Wang H., Xie G., Xie Z., Yuan Y., Zhou D., Sun X., Zhang Q., Xin Y., Li D. and Duan Z. (2017). The suppression of innate immune response by human rhinovirus C. *Biochemical and Biophysical Research Communications*. **490**, p22 – 28.

Papi A. and Johnston S.L. (1999). Rhinovirus infection induces expression of its own receptor intercellular adhesion molecule 1 (ICAM-1) via increased NF-κB-mediated transcription. *The Journal of Biological Chemistry.* **274** (14), p9707 – 9720.

Papi A., Papadopoulos N.G., Stanciu L.A., Degitz K., Holgate S.T. and Johnston S.L. (2001). Effect of desloratadine and loratadine on rhinovirus-induced intercellular adhesion molecule 1 upregulation and promoter activation in respiratory epithelial cells. *Journal of Allergy and Clinical Immunology*. **108** (2), p221 – 228.

Papadopoulos N.G., Bates P.J., Bardin P.G., Papi A., Leir S.H., Fraenkel D.J., Meyer J., Lackie P.M., Sanderson G., Holgate S.T. and Johnston S.L. (2000). Rhinoviruses infect the lower airways. *The Journal of Infectious Diseases*. **181**, p1875 – 1884.

Papadopoulos N.G. and Johnston S.L. (2000). Rhinovirus as pathogens of the lower respiratory tract. *Canadian Respiratory Journal*. **7** (5), p409 – 414.

Park Y., Kim D., Dai J. and Zhang Z. (2015). Human bronchial epithelial BEAS-2B cells, an appropriate in vitro model to study heavy metals induced carcinogenesis. *Toxicology and Applied Pharmacology*. **287** (3), p240 – 245.

Parrish A.R., Gandolfi A.J. and Brendal K. (1995). Precision-cut tissue slices: Applications in pharmacology and toxicology. *Life* Sciences. **57** (21), p1887 – 1901.

Patel M.C., Pletneva L.M., Boukhvalova M.S., Vogel S.N., Kajon A.E. and Blanco J.C.G. (2017). Immunization with live human rhinovirus (HRV) 16 induces protection in cotton rats against HRV14 infection. *Frontier in Microbiology*. **8**, 1646.

Patra B., Peng C-C., Liao W-H., Lee C-H. and Tung Y-C. (2016). Drug testing and flow cytometry analysis on a large number of uniform sized tumor spheroids using a microfluidic device. *Scientific Reports*. **6**, 21061.

Pégorier S., Wagner L.A., Gleich G.J. and Pretolani M. (2006). Eosinophil-derived cationic proteins activate the synthesis of remodelling factor by airway epithelial cells. *The Journal of Immunology*. **177**, p4861 – 4869.

Pelleg A., Schilman E.S. and Barnes P.J. (2016). Extracellular adenosine 5'-triphosphate in obstructive airway diseases. *Chest*. **150** (4), p908 – 915.

Pelon W. (1961). Classification of the "2060" virus as ECHO 28 and further study of its properties. *American Journal of Hygiene*. **73**, p36 – 54.

Pelon W., Mogabgab W.J., Philips I.A. and Pierce W.E. (1957). A cytopathogenic agent isolated from naval recruits with mild respiratory illnesses. *Experimental Biology and Medicine*. **94** (2), p262 – 267.

Pereira S.V., Raba J. and Messina G.A. (2010). IgG anti-gliadin determination with an immunological microfluidic system applied to the automated diagnostic of the celiac disease. *Analytical and Bioanalytical Chemistry.* **396**, p2921 – 2927.

Piccinini F., Tesei A., Arienti C. and Bevilacque A. (2017). Cell counting and viability assessment of 2D and 3D cell cultures: expected reliability of the trypan blue assay. *Biological Procedures Online*. **19** (8).

Pick E. and Keisari Y. (1980). A simple colorimetric method for the measurement of hydrogen peroxide produced by cells in culture. *Journal of Immunological Methods*. **38** (1-2), p161 – 170.

Placke M.E. and Fisher G.L. (1987). Adult peripheral lung organ culture – a model for respiratory tract toxicology. *Toxicology and Applied Pharmacology*. **90**, p284 – 298.

Pomfret R., Sillay K. and Miranpuri G. (2013). Investigation of the electrical properties of agarose gel: characterization of concentration using nyquist plot phase angle and the implications of a more comprehensive *in vitro* model of the brain. *Annals of Neurosciences*. **20** (3), p99 – 107.

Poria D.K. and Ray P.S. (2017). RNA-protein UV-crosslinking Assay. *Bio-protocol*. ***7*** (6), e2193.

Power P., Loughran S. and Johnson P. (2009). Modelling the effect of infection on asthma. *Drug Discovery Today: Disease Models*. **6** (4), p107 – 112.

Price R.J., Ball S.E., Renwick A.B., Barton P.T., Beamand J.A. and Lake B.G. (1998). Use of precision-cut rat liver slices for studies of xenobiotic metabolism and toxicity: comparison of Krumdieck and Brendel tissue slicers. *Xenobiotica*. **28** (4), p361 – 371.

Price W.H. (1956). The isolation of a new virus associated with respiratory clinical disease in humans. *Proceedings of the National Academy of Science of the United States of America (PNAS)*. **42** (12), p892 – 896.

Protti A., Andreis D.T., Milesi M., Iapichino G.E., Monti M., Comini B., Pugni P., Melis V., Santini A., Dondossola D., Gatti S., Lombardi L., Votta E., Carlesso E. and Gattinoni L. (2015). Lung anatomy, energy load and ventilator-induced lung injury. *Intensive Care Medicine Experimental*. **3** (34).

Proud D., Turner R.B., Winther B., Wiehler S., Tiesman J.P., Reichling T.D., Juhlin K.D., Fulmer A.W., Ho B.Y., Walanski A.A., Poore C.L., Mizoguchi H., Jump L., Moore M.L., Zukowski C.K. and Clymer J.W. (2008). Gene expression profiles during *in vivo* human rhinovirus infection. *American Journal of Respiratory and Critical Care Medicine*. **178**, p 962 – 968.

Public Health England (2012). European Catalogue of Authenticated Cell Cultures (ECACC) cell line profile A549. (online) available at https://www.phe-culturecollections.org.uk/media/126404/a549-cell-line-profile.pdf [accessed 11/11/2019].

Public Health England (2016). European Catalogue of Authenticated Cell Cultures (ECACC) cell line profile 1321N1. (online) available at https://admin.phe-culturecollections.org.uk/media/125051/1321n1-cell-line-profile.pdf [accessed 11/11/2019].

Public Health England (ND). European Catalogue of Authenticated Cell Cultures (ECACC) general cell collection BEAS-2B. (online) available at https://www.phe-culturecollections.org.uk/products/celllines/generalcell/detail.jsp?refId=95102433&collection=ecacc_gc [accessed 11/11/2019].

Punyadarsaniya D., Liang C-H., Winter C., Petersen H., Rautenschlein S., Hennig-Pauka I., Schwegmann-Wessels C., Wu C-L., Wong C-H. and Herrier G. (2011). Infection of differentiated porcine airway epithelial cells by influenza virus: differential susceptibility to infection by porcine and avian viruses. *PLoS ONE*. **6** (12), e28429.

Qiao Y., Dong Q., Li B., Obaid S., Miccile C., Yin R.T., Talapatra T., Lin Z., Li S., Li Z. and Efimov I.R. (2018). Multiparametric slice culture platform for the investigation of human cardiac tissue physiology. *Progress in Biophysics and Molecular Biology*. **144**, p139 – 150.

Ramachandran R., Morice A.H. and Compton S.J. (2006). Proteinase-activated receptor$_2$ agonists upregulate granulocyte colony-stimulating factor, IL-8, and VCAM-1 expression in human bronchial fibroblasts. *American Journal of Respiratory Cell and Molecular Biology*. **35** (1), p133 – 41.

Ramakrishnan M.A. (2016). Determination of 50% endpoint titer using a simple formula. *World Journal of Virology*. **5** (2), p85 – 86.

Rambani K., Vukasinovic J., Glezer A. and Potter S.M. (2009). Culturing thick brain slices: an interstitial 3D microperfusion system for enhanced viability. *Journal of Neuroscience Methods*. **180** (2), p243 – 254.

Rasmussen A.L. and Racaniello V.R. (2011). Selection of rhinovirus 1A variants adapted for growth in mouse lung epithelial cells. *Virology*. **420**, p82 – 88.

Ravin K.A. and Loy M. (2016). The eosinophil in infection. *Clinical Reviews in Allergy and Immunology*. **50** (2), p 214 – 227.

Razali N.M. and Wah Y.B. (2011). Power comparison of Shapiro-Wilk, Kolmogorov-Smirnov, Lilliefors and Anderson-Darling test. *Journal of Statistical Modeling and Analytics.* **2** (1), p21 – 33.

RCSB Protein Data Bank (PDB) (2011). 1AYM – Human Rhinovirus 16 coat protein at high resolution, biological assembly 1. (online) available at https://www.rcsb.org/structure/1AYM [accessed 24/05/18].

Reichard A. and Asosingh K. (2019). Best practices for preparing a single cell suspension from solid tissues for flow cytometry. *Journal of Quantitative Cell Science*. **95A**, p216 – 226.

Reiger A.M., Neslon K.L., Konowalchuk J.D. and Barreda D.R. (2011). Modified annexin V/propidium iodide apoptosis assay for accurate assessment of cell death. *Journal of Visualized Experiments.***50**, e2597.

Ressmeyer A.R., Larsson A.K., Vollmer E., Dahlèn S.E., Uhlig S. and Martin C. (2006). Characterisation of guinea pig precision-cut lung slices: comparison with human tissues. *European Respiratory Journal*. **28**, p603 – 611.

Ressmeyer A.R., Bai Y., Delmotte P., Uy K.F., Thistlethwaite P., Fraire A., Sato O., Ikebe M. and Sanderson M.J. (2010). Human airway contraction and formoterol-induced relaxation is determined by Ca2+ oscillations and Ca2+ sensitivity. *American Journal of Respiratory Cell and Molecular Biology*. **43** (2), p179 – 191.

Rezaee F., Meednu N., Emo J.A., Saatian B., Chapman T.J., Naydenov N.G., de Benedetto A., Beck L.A., Ivanov A.I. and Georas S.N. (2011). Polyinosinic:polycytidylic acid induces protein kinase D-dependent disassembly of apical junctions and barrier dysfunction in airway epithelial cells. *Journal of Allergy and Clinical Immunology*. **128** (6), p1216 – 1224.

Rider C.F., Miller-Larsson A., Proud D., Giembycz M.A. and Newton R. (2013). Modulation of transcriptional responses by poly(I:C) and human rhinovirus: Effect of long-acting β2-adrenoceptor agonists. *European Journal of Pharmacology.* **708** (1-3), p60 – 67.

Robinett K.S., Koziol-White C.J., Akoluk A., An S.S., Panettieri R.A. Jr. and Liggett S.B. (2014). Bitter taste receptor function in asthmatic and nonasthmatic human airway smooth muscle cells. *American Journal of Respiratory Cell and Molecular Biology*. **50** (4), p678 – 683.

Rochon J., Gondan M. and Kieser M. (2012). To test or not to test: preliminary assessment of normality when comparing two independent samples. *BMC Medical Research Methodology*. **12** (81).

Roestenberg M., Hoogerwerf M-A., Ferreira D.M., Mordmüller B. and Yazdanbakhsh M. (2018). Experimental infection of human volunteers. *The Lancet Infectious Diseases*. **18** (10), E312 – 322.

Rogers C.S., Abraham W.M., Brogden K.A., Engelhardy J.F., Fisher J.T., McCray Jr. P.B., McLennan G., Meyerholz D.K., Namati E., Ostedgaard L.S., Prather R.S., Sabater J.R., Stoltz D.A., Zabner J. and Welsh M.J. (2008). The porcine lung as a potential model for cystic fibrosis. *American Journal of Physiology – Lung Cellular and Molecular Physiology*. **295**, L240 – 263.

Rosner S.R., Ram-Mohan S., Paez-Cortez J.R., Lavoie T.L., Dowell M.L., Yuan L., Ai X., Fine A., Aird W.C., Fredburg J.J. and Krishnan R. (2014). Airway contractibility in the precision-cut lung slices after cryopreservation. *American Journal of Respiratory Cell and Molecular Biology*. **50** (5), p876 – 881.

Ross A.E., Belanger M.C., Woodroof J.F. and Pompano R.R. (2017). Spatially resolved microfluidic stimulation of lymphoid tissue *ex vivo*. *Analyst*. **142**, p649 – 659.

Roumane A., Berthenet K., El Fassi C. and Ichim G. (2018). Caspase-independent cell death does not elicit a proliferative response in melanoma cancer cells. *BMC Cell Biology*. **19**, 11.

Rountree A., Karkamkar A., Khalil G., Folch A., Cook D.L. and Sweet I.R. (2016). BaroFuse, a novel pressure-driven, adjustable-throughput perfusion system for tissue maintenance and assessment. Heliyon. **2** (12), e00210.

Rowe R.K. and Gill M.A. (2015). Asthma: the interplay between viral infections and allergic diseases. *Immunology and Allergy Clinics of North America*. **35** (1), p115 – 127.

Royston L. and Tapparel C. (2016). Rhinovirus and respiratory enteroviruses: not as simple as ABC. *Viruses*. **8** (16).

Sackmann E.K., Fulton A.L. and Beebe D.J. (2014). The present and future role of microfluidics in biomedical research. *Nature*. **507** (7491), p181 – 189.

Sajjan U., Wang Q., Zhao Y., Gruenert D.C. and Hershenson M.B. (2008). Rhinovirus disrupts the barrier function of polarized airway epithelial cells. *American Journal of Respiratory and Critical Care Medicine*. **178**, p1271 – 1281.

Sanderson M.J. (2011). Exploring lung physiology in health and disease with lung slices. *Pulmonary Pharmacology and Therapeutics*. **24**, p452 – 465.

Sanfilippo S., Canis M., Ouchchane L., Botchorishvili R., Artonne C., Janny L. and Brugnon F. (2011). Viability assessment of fresh and frozen/thawed isolated human follicles: reliability of two methods (trypan blue and calcein AM/ethidium homodimer-1). **28**, p1151 – 1156.

Schlepütz M., Uhlig S. and Martin C. (2011). Electric field stimulation of precision-cut lung slices. *Journal of Applied Physiology*. **110**, p545 – 554.

Schlepütz M., Rieg A.D., Seehase S., Spillner J., Perez-Bouza A., Braunschwieg T., Schroeder T., Bernau M., Lambermont V., Schlumbohm C., Sewald K., Autschbach R., Braun A., Kramer B.W., Uhlig S. and Martin C. (2012). Neurally Mediated Airway Constriction in Human and Other Species: A Comparative Study Using Precision-Cut Lung Slices (PCLS). *PLoS ONE*. **7** (10), e47344.

Schmider E., Ziegler M., Danay E., Beyer L. and Bühner M. (2010). Is it really robust? Reinvestigating the robustness of ANOVA against violations of the normal distribution assumption. *Methodology*. **6** (4), p147 – 151.

Schroth M.K., Grimm E., Frindt P., Galagan D.M., Konno S-I., Love r. and Gern J.E. (1999). Rhinovirus replication causes RANTES production in primary bronchial epithelial cells. *American Journal of Physiology: Lung Cellular and Molecular Physiology.* **20** (6), p1220 – 1228.

Seehase S., Lauenstein H.D., Schlumbohm C., Switalla S., Neuhaus V., Förster C., Fieguth H.G., Pfennig O., Fuchs E., Kaup F.J., Bleyer M., Hohlfeld J.M., Braun A., Sewald K. and Knauf S. (2012). LPS-induced lung inflammation in marmoset monkeys – an acute model for anti-inflammatory drug testing. PLoS ONE. **7** (8), e43709.

Seymour M.L., Gilby N., Bardin P.G., Fraenkel D.J., Sanderson G., Penrose J.F., Holgate S.T., Johnston S.L. and Sampsin A.P. (2002). Rhinovirus infection increases 5-lipoxygenase and cyclooxygenase-2 in bronchial biopsy specimens from nonatopic subjects. *The Journal of Infectious Diseases*. **185**, p540 – 544.

Shabram P. and Aguilar-Cordova E. (2000). Multiplicity of infection/multiplicity of confusion. *Molecular Therapy*. **2** (5), p420 – 421.

Shaw K.J., Birch C., Hughes E.M., Jakes A.D., Greenman J. and Haswell S.J. (2011). Microsystems for personalised biomolecular diagnostics. *Engineering in Life Sciences.* **11** (2), p121 – 132.

Shimokawa K., Katayama M., Matsuda Y., Takahashi H., Hara I., Sato H. and Kaneko S. (2002). Matrix metalloproteinase (MMP)-2 and MMP-9 activities in human seminal plasma. *Molecular Human Reproduction.* **8** (1), p32 – 36.

Shin S-H., Ye M-K. and Kim J-K. (2014). Effects of fungi and eosinophils on mucin gene expression in rhinovirus-infected nasal epithelial cells. *Allergy Asthma and Immunology Research*. **6** (2), p149 – 155.

Shukla S.D., Mahmood M.Q., Weston S., Latham R., Muller H.K., Sohal S.S. and Walters E.H. (2017). The main rhinovirus respiratory tract adhesion site (ICAM-1) is upregulated in smokers and patients with chronic airflow limitation (CAL). *Respiratory Research*. **18** (6).

Silva P.N., Green B.J., Altamentova S.M. and Rocheleau J.V. (2013). A microfluidic device designed to induce media flow throughout pancreatic islets while limiting shear-induced damage. *Lab on a Chip*. **13**, p4374 – 4384.

Siminski J.T., Kavanagh T.J., Chi E. and Raghu G. (1992). Long-term maintenance of mature pulmonary parenchyma cultured in serum-free conditions. *American Journal of Physiology: Lung Cellular and Molecular Physiology*. **262** (1), L105 – 110.

Simintiras C.A., Fröhlich T., Sathyapalan T., Arnold G.J., Ulbrich S.E., Leese H.J. and Sturmey R.G. (2017). Modelling aspects of oviduct fluid formation *in vitro*. *Reproduction*. **153** (1), p22 – 33.

Sin A., Baxter G. and Shuler M. (2001). Animal on a chip: a microscale cell culture analog device for evaluating toxicological and pharmacological profiles. *Proceedings of SPIE – Microfluidics and BioMEMS*. **4560**, p98 – 101.

Sinclair J.K., Taylor P.J. and Hobbs S.J. (2013). Alpha level adjustments for multiple dependent variable analyses and their applicability – a review. *International Journal of Sports Science and Engineering.* **7** (1), p17 – 20.

Smith P.F., Gandolfi A.J., Krumdieck C.L., Putnam C.W., Zukoski C.F., Davis W.M. and Brendel K. (1985). Dynamic organ culture of precision liver slices for *in vitro* toxicology. *Life Sciences*. **36**, p1367 – 1375.

Smith P.F., Krack G., McKee R.L., Johnson D.G., Gandolfi A.J., Hruby V.J., Krumdieck C.L. and Brendel K. (1986). Maintenance of adult rat liver slices in dynamic organ culture. *In Vitro Cellular and Developmental Biology*. **22** (12), p706 – 712.

Smith S.M., Wunder M.B., Norris D.A. and Shellman Y.G. (2011). A simple protocol for using a LDH-based cytotoxicity assay to assess the effects of death and growth inhibition at the same time. *PLoS ONE*. **6** (11), e26908.

Solari E., Marcozzi C., Bistoletti M., Baj A., Giaroni C., Negrini D. and Moriondo A. (2020). TRPV4 channels' dominant role in the temperature modulation of intrinsic contractility and lymph flow of rat diaphragmatic lymphatics. *The American Journal of Physiology: Heart and Circulatory Physiology*. **319**, H507 – 518.

Sollier E., Go D.E., Che J., Gossett D.R., O'Byrne S., Weaver W.M., Kummer N., Rettig M., Goldman J., Nickols N., McCloskey S., Kulkarni R.P. and Carlo D.D. (2014). Size-selective collection of circulating tumor cells using Vortex technology. *Lab on a Chip*. **14**, p63 – 67.

Song W-J. and Morice A.H. (2017). Cough hypersensitivity syndrome: a few more steps forward. *Allergy, Asthma and Immunology Research*. **9** (5), p394 – 402.

Sonntag F., Schilling N., Mader K., Gruchow M., Klotzbach U., Lindner G., Horland R., Wagner I., Lauster R., Howitz S., Hoffmann S. and Marx U. (2010). Design and prototyping of a chip-based multi-micro-organoid culture system for substance testing, predictive to human (substance) exposure. *Journal of Biotechnology*. **148**, p70 – 75.

Spina D. and Page C.P. (2013). Regulating cough through modulation of sensory nerve function in airways. *Pulmonary Pharmacology and Therapeutics*. **26**, p486 – 490.

Srinivasan B., Kolli A.R., Esch M.B., Abaci H.E., Shuler M.L. and Hickman J.J. (2015). TEER measurement techniques for in vitro barrier model systems. *Journal of Laboratory Automation*. **20** (2), p107 – 126.

Staal-van den Brekel A.J., Dentener M.A., Buurman W.A. and Wouters E.F. (1995). Increased resting energy expenditure and weight loss are related to a systemic inflammatory response in lung cancer patients. *Journal of Clinical Oncology*. **13** (10), p2600 – 2605.

Stefaniak M.S., Krumdieck C.L., Spall R.D., Gandolfi A.J. and Brendel K. (1992). Biochemical and histological characterization of agar-filled precision cut rat lung slices in dynamic organ culture as an *in vitro* tool. *In Vitro Toxicology*. **5** (1), p7 – 19.

Stewart C.E., Torr E.E., Jamili N.H.M., Bosquillon C. and Sayers I. (2012). Evaluation of differentiated human bronchial epithelial cell culture system for asthma research. *Journal of Allergy*. **2012**.

Stöckl J., Vetr H., Majdic O., Zlabinger G., Kuechler E. and Knapp W. (1999). Human major group rhinoviruses downmodulate the accessory function of monocytes by inducing IL-10. *The Journal of Clinical Investigation*. **104** (7), p957 – 965.

Stone H.A., Stroock A.D. and Ajdari A. (2004). Engineering flows in small devices: microfluidics towards a lab-on-a-chip. *Annual Review of Fluid Mechanics*. **36**, p381 – 411.

Strober W. (2015). Trypan blue exclusion test of cell viability. *Current Protocols in Immunology*. **111**: A3.B.1 – A3.B.3.

Stucki A.O., Stucki J.D., Hall S.R.R., Felder M., Mermoud Y., Schmid R.A., Geiser T. and Guenat O.T. (2015). A lung-on-a-chip array with an integrated bio-inspired respiration mechanism. *Lab on a Chip*. **15**, p1302 – 1310.

Sturton R.G., Trifilieff A., Nicholson A.G. and Barnes P.J. (2008). Pharmacological characterization of indacaterol, a novel once daily inhaled β_2 adrenoreceptor agonist, on small airways in human and rat precision-cut lung slices. *The Journal of Pharmacology and Experimental Therapeutics.* **324** (1), p270 – 275.

Subauste M.C., Jacoby D.B., Richard S.M. and Proud D. (1995). Infection of a human respiratory epithelial cell line with rhinovirus. *Journal of Clinical Investigation.* **97** (2), p421 – 430.

Sun Y., Jain D., Koziol-White C.J., Genoyer E., Gilbert M., Tapia K., Panettieri R.A. Jr., Hodinka R.L. and López C.B. (2015). Immunostimulatory defective viral genomes from respiratory syncytial virus promote a strong innate antiviral response during infection in mice and humans. *PLoS Pathogens*. **11** (9), e1005122.

Sung J.H., Kam C. and Shuler M.L. (2010). A microfluidic device for a pharmacokinetic-pharmacodynamic (PK-PD) model on a chip. *Lab on a chip*. **10**, p446 – 455.

Swain R.J., Kemp S.J., Goldstraw P., Tetley T.D. and Stevens M.M. (2010). Assessment of cell line models of primary human cells by Raman Spectral Phenotyping. **98** (8), p1703 – 1711.

Switalla S., Lauenstein L., Prenzler F., Knothe S., Förster C., Feiguth H-G., Pfennig O., Schaumann F., Martin C., Guzman C.A., Ebensen T., Müller M., Hohlfeld J.M., Krug N., Braun A. and Sewald K. (2010). Natural innate cytokine response to immunomodulators and adjuvants in human precision-cut lung slices. *Toxicology and Applied Pharmacology*. **246**, p107 – 115.

Tacon C.E., Wiehler S., Holden N.S., Newson R., Proud D. and Leigh R. (2010). Human rhinovirus infection up-regulates MMP-9 production in airway epithelial cells via NF-κB. *American Journal of Respiratory Cell and Molecular Biology*. **43** (2), p201 – 209.

Takai E., Tsukimoto M., Harada H. and Kojima S. (2014). Autocrine signalling via release of ATP and activation of P2X7 receptor influences motile activity of human lung cancer cells. *Purinergic Signalling*. **10** (3), p487 – 497.

Tamimi A., Serdarevic D. and Hanania N.A. (2012). The effects of cigarette smoke on airway inflammation in asthma and COPD: therapeutic implications. *Respiratory Medicine.* **106**, p319 – 328.

Tang F.S.M., Hansbro P.M., Burgess J.K., Ammit A.J., Baines K.J. and Oliver B.G. (2016). A novel immunomodulatory function of neutrophils on rhinovirus-activated monocytes *in vitro*. *Thorax.* **71** (11), p1039 – 1049.

Tarn M.D. and Pamme N. (2011). Microfluidic platforms for performing surface-based clinical assays. *Expert Review of Molecular Diagnostics*. **11** (7), p711 – 720.

Tatler A.L., Barnes J., Habgood A., Goodwin A., McAnulty R.J. and Jenkins G. (2016). Caffeine inhibits TGFβ activation in epithelial cells, interrupts fibroblast responses to TGFβ, and reduces established fibrosis in *ex vivo* precision-cut lung slices. *Thorax*. **71**, p565 – 567.

Tavana H., Zamankhan P., Christensen P.J., Grotberg J.B. and Takayama S. (2011). Epithelium damage and protection during reopening of occluded airways in a physiologic microfluidic pulmonary airway model. *Biomedical Microdevices*. **13**, p731 – 742.

Taylor A.L., Schwiebert L.M., Smith J.J., King C., Jones J.R., Sorscher E.J., Schwiebert E.M. (1999). Epithelial P2X purinergic receptor channel expression and function. *The Journal of Clinical Investigation*. **104**, p875 – 884.

Taylor G. (2017). Animal models of respiratory syncytial virus infection. *Vaccine*. **35**, p469 – 480.

Taylor-Clark T.E. (2016). Role of reactive oxygen species and TRP channels in the cough reflex. *Cell Calcium*. **60**, p155 – 162.

Tedjo W., Nejad J.E., Feeny R., Yang L., Henry C.S., Tobet S. and Chen T. (2018). Electrochemical biosensor system using a CMOS microelectrode array provides high spatially and temporally resolved images. Biosensors and Bioelectronics. **114**, p78 – 88.

Temann A., Golovina T., Neuhaus V., Thompson C., Chichester J.A., Braun A. and Yusibov V. (2017). Evaluation of inflammatory and immune responses in long-term cultured human precision-cut lung slices. *Human Vaccines and Immunotherapeutics*. **13** (2), p351 – 358.

Terajima M., Yamaka M., Sekizawa K., Okinaga S., Suzuki T., Yamada N., Nakayama K., Ohrui T., Oshima T., Numazaki Y. and Saski H. (1997). Rhinovirus infection of primary cultures of human tracheal epithelium: role of ICAM-1 and IL-1β. *American Journal of Physiology – Lung Cellular and Molecular Physiology*. **273** (4), L749 – 759.

Thaker S.K., Ch'ng J. and Christofk H.R. (2019). Viral hijacking of cellular metabolism. *BMC Biology*. **17** (59).

Thorneloe K.S., Sulpizio A.C., Lin Z., Figueroa D.J., Clouse A.K., McCafferty G.P., Chendrimada T.P., Lashinger E.S.R., Gordon E., Evans L., Misajet B.A., DeMarini D.J., Nation J.H., Casillas L.N., Marquis R.W., Votta B.J., Sheardown S.A., Xu X., Brooks D.P., Laping N.J. and Westfall T.D. (2008). N-((1S)-1- -3-hydroxypropanoyl)-1-piperazinyl]carbonyl}-3-methylbutyl)-1-benzothiophene-2-carboxamide (GSK1016790A), a novel and potent transient receptor potential vanilloid 4 channel agonist induces urinary bladder contraction and hyperactivity: part I. *Journal of Pharmacology and Experimental Therapeutics*. **326** (2), p432 –442.

Tian C., Tu Q., Liu W. and Wang J. (2019). Recent advances in microfluidic technologies for organ-on-a-chip. *Trends in Analytical Chemistry*. **117**, p146 – 156.

Tomarken A.J. and Serlin R.C. (1986). Comparison of ANOVA alternatives under variance heterogeneity and specific noncentrality structures. *Psychological Bulletin*. **99** (1), p90 – 99.

Tomassini J.E., Graham D., DeWitt C.M., Lineberger D.W., Rodkey J.A. and Colonno R.J. (1989). cDNA cloning reveals that the major group rhinovirus receptors on HeLa cells is intercellular adhesion molecule 1. *Proceedings of the National Academy of Science of the United States of America (PNAS)*. **86**, p4907 – 4911.

Torisawa Y., Spina C.S., Mammoto T., Mammoto A., Weaver J.C., Tat T., Collins J.J. and Ingber D.E. (2014). Bone marrow-on-a-chip replicates hematopoietic niche physiology *in vitro*. *Nature Methods*. **11** (6), p663 – 669.

Tsaloglou M-N., Jacobs A. and Morgan H. (2014). A fluorogenic heterogeneous immunoassay for cardiac muscle troponin cTnI on a digital microfluidic device. *Analytical and Bioanalytical Chemistry*. **406**, p5967 – 5976.

Tsao C-W. (2016). Polymer microfluidics: simple, low-cost fabrication process bridging academic lab research to commercialized production. *Micromachines*. **7** (12), 225.

Turner R.B., Woodfolk J.A., Borih L., Steinke J.W., Patrie J.T., Muehling L.M., Lahtinen S. and Lehtinen M.J. (2017). Effect of probiotic on innate inflammatory response and viral shedding in experimental rhinovirus infection – a randomised controlled trial. *Beneficial Microbes*. **8** (2), p207 – 215.

Tyrrell D.A.J. (1965). A collaborative study of the aetiology of acute respiratory infections in Britain 1961 – 4: a report of the Medical Research Council working party on acute respiratory virus infections. *The British Medical Journal*. **2** (5457), p319 – 326.

Tyrrell D.A.J. and Chanock R.M. (1963). Rhinovirus: a description. *Science*. **141** (3576), p152 – 153.

Ulrich T.A., Lee T.G., Shon H.K., Moon D.W. and Kumar S. (2011). Microscale mechanisms of agarose-induced disruption of collagen remodeling. *Biomaterials*. **32** (24), p5633 – 5642.

Umachandran M., Howarth J. and Joannides C. (2004). Metabolic and structural viability of precision-cut rat lung slices in culture. *Xenobiotica*. **34** (8), p771 – 780.

Unger B.L., Ganesan S., Comstock A.T., Faris A.N., Hershenson M.B. and Sajjan U.S. (2014). Nod-like receptor X-1 is required for rhinovirus-induced barrier dysfunction in airway epithelial cells. *Journal of Virology*. **88** (7), p3705 – 3718.

van der Meer A.D. and van den Berg A. (2012). Organs-on-chips: breaking the *in vitro* impasse. *Integrative Biology*. **4**, p461 – 470.

van der Zalm M.M., Wilbrink B., van Ewijk B.E., Overduin P., Wolfs T.F.W. and van der Ent C.K. (2011). Highly frequent infections with human rhinovirus in healthy young children: a longitudinal cohort study. *Journal of Clinical Virology*. **52**, p317 – 320.

van Hecke T. (2012). Power study of anova versus Kruskal-Wallis test. *Journal of Statistics and Mathematical Systems.* **15** (2 – 3), p241 – 247.

van Midwoud P.M., Groothuis G.M.M., Merema M.T. and Verpoorte E. (2009). Microfluidic biochip for the perifusion of precision-cut rat liver slices for metabolism and toxicology studies. *Biotechnology and Bioengineering*. **105** (1), p184 – 194.

van Rijt S.H., Bölükbas D.A., Argyo C., Datz S., Lindner M., Eickelbery O., Königshoff M., Bein T. and Meiner S. (2015). Protease-mediated release of chemotherapeutics from mesoporous silica nanoparticles to *ex vivo* human and mouse lung tumors. *ACS Nano*. **9** (3), p2377 – 2389.

Velalopoulou A., Chatterjee S., Pietrofesa R.A., Koziol-White C., Panettieri R.A., Lin L., Tuttle S., Berman A., Koumenis C. and Christodifou-Solomindou M. (2017). Synthetic Secoisolariciresinol Diglucoside (LGM2605) Protects Human Lung in an Ex Vivo Model of Proton Radiation Damage. *International Journal of Molecular Science*. **18** (12), E2525.

Viana F. (2016). TRPA1 channels: molecular sentinels of cellular stress and tissue damage. *The Journal of Physiology*. **594** (15), p4151 – 4169.

Vichai V. and Kirtikara K. (2006). Sulforhodamine B colorimetric assay for cytotoxicity screening. *Nature Protocols*. **1** (3), p1112 – 1116.

Vietmeier J., Niedorf F., Bäumer W., Martin C., Deegen E., Ohnesorge B. and Kietzmann M. (2007). Reactivity of equine airways – a study on precision-cut lung slices. *Veterinary Research Communications*. **31**, p611 – 619.

Wagner I., Materne E.M., Brincker S., Süssbier U., Frädrich C., Busek M., Sonntag F., Sakharov D.A., Trushkin E.V., Tonevitsky A.G., Lauster R. and Marx U. (2013). A dynamic multi-organ-chip for long-term cultivation and substance testing proven by 3D human liver and skin tissue co-culture. *Lab on a Chip*. **13** (18), p3538 – 3547.

Wang J.H., Kwon H.J. and Jang Y.J. (2009). Rhinovirus upregulates matrix metalloproteinase-2, matrix metalloproteinase-9, and vascular endothelial growth factor expression in nasal polyp fibroblasts. *Laryngoscope*. **119** (9), p1834 – 1838.

Wang X., Wolf M.P., Keel R.B., Lehner R. and Hunziker P.R. (2012). Polydimethylsiloxane embedded mouse aorta ex vivo perfusion model: proof-of-concept study focusing on atherosclerosis. *Journal of Biomedical Optics*. **17** (7), 076006.

Wark P.A.B., Johnston S.L., Bucchieri F., Powell R., Puddicombe S., Laza-Stanca V., Holgate S.T. and Davies D.E. (2005). Asthmatic bronchial epithelial cells have a deficient innate immune response to infection with rhinovirus. *The Journal of Experimental Medicine*. **201** (6), p937 – 947.

Wark P.A.B., Grissell T., Davies B., See H. and Gibson P.G. (2009). Diversity in the bronchial epithelial cell response to infection with different rhinovirus strains. *Respirology*. **14**, p180 – 186.

Waris M., Österback R., Lahti E., Vuorinen T., Ruuskanen O. and Peltola V. (2013). Comparison of sampling methods for the detection of human rhinovirus RNA. *Journal of Clinical Virology*. **58**, p200 – 204.

Watson C.Y., Damiani F., Ram-Mohan S., Rodrigues S., de Moura Queiroz P., Donaghey T.C., Rosenblum Lichtenstein J.H., Brain J.D., Krishnan R. and Molina R.M. (2016). Screening for chemical toxicity using cryopreserved precision cut lung slices. *Toxicological Sciences*. **150** (1), p225 – 233.

Waymouth C. (1970). Osmolality of mammalian blood and of media for culture of mammalian cells. *In Vitro*. **8** (2), p109 – 127.

Weibel D.B. and Whitesides G.M. (2006). Applications of microfluidics in chemical biology. *Current Opinion in Chemical Biology*. **10**, p584 – 591.

Weinheimer V.K., Becher A., Tönnies M., Holland G., Knepper J., Bauer T.T., Schneider P., Neudecker J., Rückert J.C., Szymanski K., Temmesfeld-Wollbrueck B., Gruber A.D., Bannert N., Suttorp N., Hippenstiel S., Wolff T. and Hocke A.C. (2012). Influenza A viruses target type II pneumocytes in the human lung. *The Journal of Infectious Diseases*. **206** (11), p1685 – 1694.

West P.W., Canning B.J., Merlo-Pich E., Woodcock A.A. and Smith J.A. (2015). Morphologic characterization of nerves in whole-mount airway biopsies. *American Journal of Respiratory and Critical Care Medicine*. **192** (1), p30 – 39.

Wilkinson T.M.A., Aris E., Bourne S., Clarke S.C., Peeters M., Pascal T.G., Schoonbroodt S., Tuck A.C., Kim V., Ostridge K., Staples K.J., Williams N., Williams A., Wootton S., Devaster J-M. (2017). A prospective, observation cohort study of the seasonal dynamics of airway pathogens in the aetiology of exacerbations in COPD. *Thorax*. **72** (10), p911 – 927.

Winther B., Arruda E., Witek T.J., Marlin S.D., Tsianco M.M., Innes D.J. and Hayden F.G. (2002). Expression of ICAM-1 in nasal epithelium and levels of soluble ICAM-1 in nasal lavage fluid during human experimental rhinovirus infection. *Archives of Otolaryngology – Head and Neck Surgery*. **128**, p131 – 136.

Whitesides G.M. (2006). The origins and the future of microfluidics. *Nature*. **442**, p368 – 373.

Wohlsen A., Martin C., Vollmer E., Brandscheid D., Magnussen H., Beker W-M., Lepp U. and Uhlig S. (2003). The early allergic response in small airways of human precision-cut lung slices. *European Respiratory Journal*. **21**, p1024 – 1032.

Wolters T.L.C., Netea M.G., Hermus A.R.M.M., Smit J.W.A. and Netea-Maier R.T. (2017). IGF1 potentiates the pro-inflammatory response in human peripheral blood mononuclear cells via MAPK. *Journal of Molecular Endocrinology*. **59** (2), p129 – 139.

Wujak L., Hesse C., Sewald K., Jonigk D., Braubach P., Warnecke G., Fieguth H.G., Braun A., Lochnit G., Markart P., Schaefer L. and Wygrecka M. (2017). FXII promotes proteolytic processing of the LRP1 ectodomain. *Biochimica et Biophysica Acta*. **1861** (8), p2088 – 2098.

Xatzipsalti M. and Papadopoulos N.G. (2007). Cellular and animals models for rhinovirus infection in asthma. *Model of Exacerbations in Asthma and COPD*. **14**, p31 – 41.

Xiao S., Coppeta J.R., Rogers H.B., Isenberg B.C., Zhu J., Olalekan S.A., McKinnon K.E., Dokic D., Rashedi A.S., Haisenleder D.J., Malpani S.S., Arnold-Murray C.A., Chen K., Jiang M., Bai L., Nguyen C.T., Zhang J., Laronda M.M., Hope T.J., Maniar K.P., Pavone M.E., Avram M.J., Sefton E.C., Getsios S., Burdette J.E., Kim J.J., Borenstein J.T. and Woodruff T.K. (2017). A microfluidic culture model of the human reproductive tract and 28-day menstrual cycle. Nature Communications. **28** (8), 14584.

Yamaya M., Sekizawa K., Suzuki T., Yamada N., Furukawa M., Ishizuka S., Nakayama K., Terajima M., Numazaki Y. and Sasaki H. (1999). Infection of human respiratory submucosal glands with rhinovirus: effects of cytokine and ICAM-1 production. *American Journal of Physiology*. **277**, L362 – 371.

Yang K.S., Kim H.J., Ahn J.K. and Kin D.H. (2009). Microfluidic chip with porous anodic alumina integrated with PDMS/glass substrate for immune-diagnosis. *Current Applied Physics*. **9**, e60 – 65.

Yasotharan S., Pinto S., Sled J.G., Bolz S-S. and Günther A. (2015). Artery-on-a-chip platform for automated, multimodal assessment of cerebral blood vessel structure and function. *Lab on a Chip*. **15**, p2660 – 2669.

Yim P.D., Gallos G., Perez-Zoghbi J.F., Trice J., Zhang Y., Siviski M., Sonett J. and Emala C.W. Sr. (2013). Chloride channel blockers promote relaxation of TEA-induced contraction in airway smooth muscle. *Journal of Smooth Muscle Research*. **49**, p112 – 124.

Yin F.H. and Lomax N.B. (1986). Establishment of a mouse model for human rhinovirus infection. *Journal of General Virology*. **67**, p2335 – 2340.

Yissachar N., Zhou Y., Ung L., Lai N.Y., Mohan J.F., Ehrlicher A., Weitz D.A., Kasper D.L., Chiu I.M., Mathis D. and Benoist C. (2017). An Intestinal Organ Culture System Uncovers a Role for the Nervous System in Microbe-Immune Crosstalk. *Cell*. **168** (6), p1135 – 1148.

Yoo E.J., Cao G., Koziol-White C.J., Ojiaku C.A., Sunder K., Jude J.A., Michael J.V., Lam H., Pushkarsky I., Damoiseaux R., Di Carlo D., Ahn K., An S.S., Penn R.B. and Panettieri R.A. Jr. (2017). Gα12 facilitates shortening in human airway smooth muscle by modulating phosphoinositide 3-kinase-mediated activation in a RhoA-dependent manner. *British Journal of Pharmacology*. **174** (23), p4383 – 4395.

Yu L., Chen M.C.W. and Cheung K.C. (2010). Droplet-based microfluidic system for multicellular tumor spheroid formation and anticancer drug testing. *Lab on a Chip*. **10**, p2424 – 2432.

Yu L., Lui Y. and Xu F. (2019). Comparative transcriptome analysis reveals significant difference in the regulation of gene expression between hydrogen cyanide- and ethylene-treated *Arabidopsis thaliana*. *BMC Plant Biology*. **19** (92).

Zaheer R.S. and Proud D. (2010). Human rhinovirus-induced epithelial production of CXCL10 is dependent upon IFN regulatory factor-1. *American Journal of Respiratory Cell and Molecular Biology*. **43**, p413 – 421.

Zambon A., Zoso A., Gagliano O., Magrofuoco E., Fadini G.P., Avagaro A., Foletto M., Quake S. and Elvassore N. (2015). High temporal resolution detection of patient-specific glucose uptake from human ex vivo adipose tissue on-chip. *Analytical Chemistry*. **87**, p6535 – 6543.

Zimmermann M., Lampe J., Lange S., Smirnow I., Königrainer A., Hann-von-Weyhern C., Fend F., Gregor M., Bitzer M. And Lauer U.M. (2009). Improved reproducibility in preparing precision-cut liver tissue slices. *Cytotechnology*. **61**, p145 – 152.

Zhang B. and Radisic M. (2017). Organ-on-a-chip devices advance to market. *Lab on a Chip*. **17**, p2395 – 2420.

Zhang Y., Catalán M.A. and Melvin J.E. (2012). TRPV4 activation in mouse submandibular gland modulates Ca^{2+} influx and salivation. *American Journal of Physiology: Gastrointestinal and Liver Physiology*. **303**, G1365 – 1372.

Zhao F. and Klimecki W.T. (2015). Culture conditions profoundly impact phenotype in Beas-2b, a human pulmonary epithelial model. *Journal of Applied Toxicology*. **35** (8), p945 – 951.

Zhao L., Sullivan M.N., Chase M., Gonzales A.L. and Earley S. (2014). Calcineurin/nuclear factor of activated T cells-coupled vanilloid transient receptor potential channel 4 Ca^{2+} sparklets stimulate airway smooth muscle cell proliferation. *American Journal of Respiratory Cell and Molecular Biology*. **50** (6), p1064 – 1075.

Zhong S., Nie Y., Gan Z., Liu X., Fang Z., Zhong B., Tian J., Huang C., Lai K. and Zhong N. (2015). Effects of *Schisandra chinensis* extracts on cough and pulmonary inflammation in a cough hypersensitivity guinea pig model induced by cigarette smoke exposure. *Journal of Ethnopharmacology*. **165**, p73 – 82.

Zhu J., Message S.D., Qiu Y., Mallia P., Kebadze T., Contoli M., Ward C.K., Barnathan E.S., Mascelli M.A., Kon O.M., Papi A., Stanciu L.A., Jeffery P.K. and Johnston S.L. (2014). Airway inflammation and illness severity in response to experimental rhinovirus infection in asthma. *Chest*. **145** (6), p1219 – 1229.

Zhu L., Lee P., Lee W., Zhao Y., Yu D. and Chen Y. (2009). Rhinovirus-induced major airway mucin production involves a novel TRL3-EGFR-dependent pathway. *American Journal of Respiratory Cell and Molecular Biology*. **40**, p610 – 619.

Zhu Y., Chidekel A. and Shaffer T.H. (2010). Cultured human airway epithelial cells (Calu-3): a model of human respiratory function, structure and inflammatory responses. *Critical Care Research and Practice*. **394578**.

Zhu Z., Tang W., Ray A., Oskar E., Landry M.L., Gwaltney Jr. J. and Elias J.A. (1996). Rhinovirus stimulation of interleukin-6 *in vivo* and *in vitro*: evidence for nuclear factor κB-dependent transcriptional activation. *The Journal of Clinical Investigation*. **97** (2), p421 – 430.

Zmora P., Molau-Blazejewska P., Bertram S., Walendy-Gnirß K., Nehlmeier I., Hartleib A., Moldenhauer A-S., Konzok S., Dehmel S., Sewald K., Brinkmann C., Curths C., Knauf S., Gruber J. Mätz-Rensing K., Dahlmann F., Braun A. and Pöhlmann S. (2017). Non-human primate orthologues of TMPRSS2 cleave and activate the influenza virus hemagglutinin. *PLoS ONE*. **12** (5), e0176597.

Appendices

Appendix A1

General Reagents

HBSE

Reagent	Mass/Volume	Final Concentration
HEPES	596mg	10mM
EDTA	2.26g	1.71mM
NaCl	124mg	155mM

Made up to a final volume of 250ml with dH_2O

200mM Tris Buffer

Reagent	Mass/Volume	Final Concentration
Tris HCl	22.2g	140mM
Tris base	10.6g	87mM

Made up to a final volume of 1 litre with dH_2O, pH8

LDH Assay Mixture

Reagent	Mass/Volume	Final Concentration
Phenazine methosulfate (PMS)	0.9mg	0.9%
Iodonitrotetrazolium (INT)	3.3mg	3.3%
Nicotinamide adenine dinucleotide (NAD)	8.6mg	3.7%

The LDH assay mixture was prepared in the following manner:

0.9mg PMS was dissolved in 100µl dH_2O

3.3mg INT was dissolved in 100µl DMSO

8.6mg NAD was dissolved in 2.3ml dH_2O

PMS, INT and NAD were mixed (total volume 2.5ml) and stored in the dark

10x TAE Buffer

Reagent	**Mass/Volume**	**Final Concentration**
Tris	48.5g	40mM
Glacial acetic acid	11.4ml	20mM
EDTA	20ml of 0.5M stock	1mM

Made up to a final volume of 1 litre of dH_2O

Diluted to 1x running buffer, 100ml of 10x running buffer added to 900ml dH_2O

Appendix A2

Reagents for Western Blotting

4x Laemmli Buffer

Reagent	Mass/Volume	Final Concentration
Sodium dodecyl sulfate	0.8g	8%
Glycerol	4ml	40%
Bromophenol blue	4mg	0.04%
Tris HCl pH6.8	2.4ml	240mM
β-mercaptoethanol	500µl	5%

Made up to a final volume of 10ml with dH_2O

5x Non-reducing Buffer

Reagent	Mass/Volume	Final Concentration
Sodium dodecyl sulfate	10g	4%
Glycerol	50ml	20%
Bromophenol blue	25mg	0.01%
Tris HCl pH6.8	4.91g	125mM

Made up to a final volume of 250ml with dH_2O

10x Running Buffer

Reagent	Mass/Volume	Final Concentration
Sodium dodecyl sulfate	10g	0.1%
Glycine	144g	192mM
Tris base	30g	25mM

Made up to a final volume of 1 litre of dH_2O

Diluted to 1x running buffer, 100ml of 10x running buffer added to 900ml dH_2O

TBS

Reagent	Mass/Volume	Final Concentration
NaCl	4.14g	1.5M
Tris base	1.21g	200mM

Made up to a final volume of 500ml with dH_2O, pH7.6

Buffer 1 for Resolving Gel

Reagent	Mass/Volume	Final Concentration
Sodium dodecyl sulfate	4g	0.04%
Tris base	181.1g	1.5M

Made up to a final volume of 1 litre with dH_2O, pH8.8

Buffer 2 for Stacking Gel

Reagent	Mass/Volume	Final Concentration
Sodium dodecyl sulfate	4g	0.04%
Tris base	60.5g	0.5M

Made up to a final volume of 1 litre with dH_2O, pH6.8

Appendix A3

Reagents for Zymograph

5x Non-reducing Buffer

Reagent	Mass/Volume	Final Concentration
Sodium dodecyl sulfate	10g	4%
Glycerol	50ml	20%
Bromophenol blue	25mg	0.01%
Tris HCl pH6.8	4.91g	125mM

Made up to a final volume of 250ml with dH_2O

10x Running Buffer

Reagent	Mass/Volume	Final Concentration
Sodium dodecyl sulfate	10g	0.1%
Glycine	144g	192mM
Tris base	30g	25mM

Made up to a final volume of 1 litre of dH_2O

Diluted to 1x running buffer, 100ml of 10x running buffer added to 900ml dH_2O

Washing Buffer

Reagent	Mass/Volume	Final Concentration
Triton X-100	6.25ml	2.5%
Tris HCl pH7.5	12.5ml of 1M stock	50mM
$CaCl_2$	625µl of 2M stock	5mM
$ZnCl_2$	2.5µl of 0.1M stock	1µM

Made up to a final volume of 250ml with dH_2O

Incubation Buffer

Reagent	Mass/Volume	Final Concentration
Triton X-100	2.5ml	1%
Tris HCl pH7.5	12.5ml of 1M stock	50mM
$CaCl_2$	625µl of 2M stock	5mM
$ZnCl_2$	2.5µl of 0.1M stock	1µM

Made up to a final volume of 250ml with dH_2O

Staining Solution

Reagent	Mass/Volume	Final Concentration
Methanol	40ml	40%
Acetic acid	10ml	10%
Coomassie blue	0.5g	0.5%

Made up to a final volume of 100ml with dH_2O

Destaining Solution

Reagent	Mass/Volume	Final Concentration
Methanol	400ml	40%
Acetic acid	100ml	10%

Made up to a final volume of 1 litre with dH_2O